Université de Liège

Faculté des Sciences

Inorganic carbon dynamics and air-ice-sea CO_2 fluxes in the open and coastal waters of the Southern Ocean

Dynamique du carbone inorganique et flux air-glace-mer de CO_2 dans l'Océan Austral ouvert et côtier

Dissertation présenté par

Bruno Delille

en vue de l'obtention du grade de Docteur en Sciences

Juin 2006

à Miche…

Down in the South, by the waste without sail on it—
Far from the zone of the blossom and tree—
Lieth, with winter and whirlwind and wail on it,
Ghost of a land by the ghost of a sea.
Weird is the mist from the summit to base of it;
Sun of its heaven is wizened and grey;
Phantom of light is the light on the face of it—
Never is night on it, never is day!
Here is the shore without flower or bird on it;
Here is no litany sweet of the springs—
Only the haughty, harsh thunder is heard on it,
Only the storm, with a roar in its wings!

Shadow of moon is the moon in the sky of it—
Wan as the face of a wizard, and far!
Never there shines from the firmament high of it
Grace of the planet or glory of star.
All the year round, in the place of white days on it—
All the year round where there never is night—
Lies a great sinister, bitter, blind haze on it:
Growth that is neither of darkness nor light!
Wild is the cry of the sea in the caves by it—
Sea that is smitten by spears of the snow;
Desolate songs are the songs of the waves by it—
Down in the South, where the ships never go.

Beyond Kerguelen – Henry Kendall
(selected stranzas)

.

Remerciements

Ce travail est dédié à mon promoteur et ami, Michel Frankignoulle, parti trop tôt sans avoir pu tenir ce travail entre ses mains. J'espère que sa conception de la science, en particulier le désir de sortir des sentiers battus et de viser l'excellence, transparaît, au moins un peu, dans ce manuscrit.

Je remercie le Pr Jean-Marie Bouquegneau, Doyen de la Faculté des Sciences, d'avoir accepté d'être le président du jury. Je tiens également à le remercier d'avoir soutenu notre groupe, l'Unité d'Océanographie Chimique, après le décès de Michel et d'avoir contribué à assurer la pérennité de ce dernier. Mes remerciements vont dans le même sens au Pr Jean-Claude Gérard, président du Département d'Astrophysique, Géophysique et Océanographie.

Un des autres grands artisans de la pérennité de notre groupe et qui a accompagné ce travail est le Pr François Ronday, co-promoteur de ce travail, malgré ses responsabilités en tant qu'Administrateur de l'Université. Sa probité, sa proximité, son engagement à nos cotés et ses encouragements dans des périodes critiques ont été déterminants pour assurer la continuité de notre travail et la finalisation de ce manuscrit.

J'ai également rencontré certains chercheurs qui ont eu une influence déterminante sur mon travail; je pense en particulier à Jean-Marie Beckers, Anja Engel, Michel Fiala, Jean-Pierre Gattuso, Andrey Kostianoy, Michèle Loijens, Anne Mouchet, Nicolas Metzl, Guy Munhoven, Emilien Pelletier, Ulf Riebesell, Emma Rochelle-Newal, Bronte Tilbrook, et Ingrid Zondervan. Je les remercie tous et toutes sincèrement.

Je remercie également chaleureusement les équipages des *N.O. Astrolabe, Aurora Australis*, *Marion Dufresne, Polarstern* et du plus petit, du plus ardu, mais aussi de celui auquel je me sens le plus attaché, le *N.O. La Curieuse* (et notamment ses capitaines Denis Rochard et Jean-Marc Guédé avec qui j'ai eu quelques cours de matelotage). Point de départ de ce travail, j'ai une pensée émue en repensant à ceux qui en sus des membres d'équipage de la Curieuse on fait mon quotidien lors de la 46ème mission à Kerguelen et dont la plupart m'ont accompagné durant ces journées sans soleils et nuits sans sommeil passées à échantillonner les fjords des Iles de la Désolation. Je pense en particulier à Beb's, Biniou, Caro, Damien, DDT, Elie, les Frédéric, Gildas, Guillaume, Le bib, Le génér, Jérôme, Mouf, P'tit gars, Thierry et Yannick ainsi que les hivernants de la 47ème et 49ème missions impliqués dans le programme MICROBIOKER (Cédric Prevost et Fabien Gleizon).

Il existe en Belgique une expertise certaine dans la biogéochimie océanique, mais au-delà de cela, un remarquable esprit de collaboration qui se développe finalement dans une ambiance cordiale quoique le terme "amicale" me semble s'imposer de lui-

même. Ce sont deux piliers qui m'amènent à pouvoir espérer beaucoup de nos recherches tant au niveau de l'excellence qu'au niveau du réel plaisir de faire partie de cette communauté. Les animateurs de cette communauté sont entre autres les Pr Luc André, Lei Chou, Frank Dehairs, Hugues Goosse, Christiane Lancelot et Jean-Louis Tison. Qu'il soit dit ici, ce qui n'est jamais dit en réunion: merci pour vos compétences, votre engagement, votre confiance et l'esprit de travail que vous avez su construire en Belgique. C'est sur cette base qu'ont pu s'épanouir quelques biogéochimistes en herbe, voire confirmés qui continuent à développer l'esprit de leurs aînés et avec qui j'ai la chance de pouvoir travailler, voire courir les mers: Sylvie Becquevort, Damien Cardinal, Stéphanie Jacquet, Jeroen de Jong, et Véronique Schoemann. Est il est nécessaire d'écrire que je les remercie tous très sincèrement ?

Du Nord au Sud, sur le terrain ou par e-mail, j'ai toujours pu compter sur le support d'un trio de techniciens de l'Université de Liège: Renzo Biondo, Nadine Darchambeau et Jean-Marie Théate. Je n'oublie pas que leur support les a parfois éloignés de long mois de chez eux.

Au cours de ce travail, j'ai côtoyé au sein de notre équipe quelques compagnons de thèse avec lesquels j'ai pu tisser des liens parfois étroits. Je pense à Gwenaël Abril, Frédéric Gazeau, Yéfanlan Mathieu Koné et Laure-Sophie Schiettecatte.

En mer, à l'étranger, sur la glace, la complicité, l'amitié, est souvent venue en renfort de la science, notamment avec Delphine Lannuzel, Jérôme Harlay, Emile Libert et Jean-Louis Tison.

La complicité scientifique, très forte, s'efface parfois devant la simple intimité affective. Je partage cela avec Alberto et mon père, Daniel. Il va sans dire que ce manuscrit porte leurs traces à chaque page.

Moins impliqués dans l'élaboration de ce manuscrit, mais néanmoins très présents dans mon esprit: Didi et Simone et ma mère Elisabeth, ainsi que leurs petits-enfants Ioen et Solène. Enfin ma dernière pensé va à celle qui à défaut de m'avoir déjà épousé, à dû malgré tout épouser toute cette "science" et les contraintes qui lui sont inhérentes, Cécile.

Ce travail a été réalisé grâce au soutien de la Politique Fédérale Scientifique (et notamment de Maaike Vancauwenberghe) à travers les projets BELCANTO I, II et III (contrats: AA/DD/B14, EV/12/7E, SD/CA/03A) ainsi que le projet CANOPY (EV/12/20C), de l'Institut Paul-Emile Victor à travers le programme MICROBIOKER, de la communauté Français de Belgique à travers le projet SIBCLIM (ARC-contract 02/07-287) et du FNRS. Certains organismes internationaux ont supporté la -lourde- logistique: l'Australian Antarctic Division, l'Alfred-Wegener-Institut et l'Institut Paul-Emile Victor (je tiens à remercier notamment deux de leurs responsables: Alain Lamalle et Pierre David pour leur confiance et leur enthousiasme pour mon travail).

Les co-promoteurs de ce travail sont Alberto Borges et le Pr François Ronday.

Les membres du jury sont les Pr J.-M. Bouquegneau (Président), Dr N.Metzl, Pr F.Dehairs, Pr C.Lancelot, Pr. J.-L.Tison, Pr F.Ronday, et le Dr A.V.Borges.

Abstract

Despite the fact that the Southern Ocean (S.O.) is a high nutrients-low chlorophyll area (HNLC), it acts as a significant sink for atmospheric CO_2. We addressed the temporal and spatial variations of the frontal system of the Indian sector of the S.O. using remote sensing measurements of sea surface temperature (SST) and we present the first synoptic partitioning of the main physical-biogeochemical provinces. In the Crozet basin, if the signature of the fronts is well marked in the mesoscale distribution of the partial pressure of CO_2 (pCO_2), this latter hardly reflects the chlorophyll a (Chl *a*) distribution during the summer post-bloom period. Scaling in situ pCO_2 measurements using remote sensing measurements of SST and Chl *a*, we assessed spring and summer air-sea flux of CO_2 per physical-biogeochemical province. Spring and summer air-sea CO_2 fluxes in the Indian sector of the S.O. ranges from -0.048 PgC, to -0.057 PgC and -0.04 PgC in the North Subantarctic, South Subantarctic and Polar Frontal zones, respectively. A further collaborative effort was carried out applying a similar approach to the western Pacific sector of the S.O.. Integrating CO_2 fluxes over the year shows that this area acts as a sink for atmospheric CO_2 of 0.08 PgC yr^{-1}. Both studies provide lower estimates than the Takahashi et al. (Takahashi et al., 2002; Takahashi, 2003) climatology but corroborate (Metzl et al., 1999; Takahashi et al., 2002) the conclusions of inverse models, indicating that this climatology overestimates the CO_2 sink in the S.O. (Gurney et al., 2004; Jacobson et al., 2005).

We present a three years survey of pCO_2 in Subantarctic coastal waters surrounding the Kerguelen Archipelago, with a particular attention on the role of *Macrocystis* giant kelp beds. Primary production of *Macrocystis* lasts from early spring to late autumn and is tightly linked to solar irradiance. Maximum net kelp community production can be as high as 15 gC m^{-2} d^{-1} at the solar irradiance climax. Such production strongly affects pCO_2 within kelp bed. Coastal waters of the archipelago experience earlier and more intense phytoplanktonic blooms than offshore waters, which markedly affect pCO_2. However, over the year near-shore waters of the archipelago act as a source of CO_2 of 0.32TgC yr^{-1}.

The role of sea ice cover in the budgets of exchanges of CO_2 between the S.O. and the atmosphere has been neglected, since it was assumed as an impermeable and inert cover that prohibited air-sea fluxes of gases. We report the first direct measurements of pCO_2 within first year pack ice, multi-year pack ice and land fast sea ice, and corresponding CO_2 fluxes at the air-sea ice interface. Internal spring and summer sea ice specific processes (dilution with ice crystals, dissolution of carbonate minerals and primary production), drive drastic decreases of pCO_2 and lead to marked undersaturation of CO_2 with respect to the atmosphere. Despite its thinness, the Antarctic sea ice cover thus appears to sustain a significant uptake of atmospheric CO_2. We scaled measurements CO_2 fluxes over bare sea ice using remote sensing measurement of sea ice surface temperature: in spring and summer, the Antarctic sea ice cover acts as a sink of atmospheric CO_2 ranging from 0.015 PgC to 0.024 PgC which represents 6% to 9% of the annual uptake of the S.O. south of 50°S (0.27 PgC yr^{-1}). However, we surmise that the present evaluation of the sea ice CO_2 sink is an underestimate, since it does not account for the uptake of CO_2 by biologically active sea ice surface communities. Eddy-covariance measurements of air-sea ice CO_2 fluxes over slush - a mixture of melting snow, ice and flooding seawater covering sea ice - which hosts abundant surface communities showed 4-fold higher fluxes than over bare sea ice. On the whole, sea ice represents an additional significant CO_2 sink that should be taken into account when budgeting exchanges of CO_2 fluxes between the S.O. and the atmosphere.

Résumé

Nonobstant que l'Océan Austral (O.A.) est une zone de forte concentration en nutriments-faible concentration en chlorophylle, il se comporte comme un puits de CO_2 atmosphérique. Nous avons étudié les variations spatio-temporelles du système de fronts dans le secteur Indien de l'O.A. à l'aide de mesures satellitaires de la température des eaux de surface et présentons la première partition synoptique des principales provinces hydrologiques. Si la signature des fronts est bien marquée dans la distribution de la pression partielle en CO_2 (pCO_2) dans le bassin de Crozet, cette dernière reflète peu la distribution de la chlorophylle a dans cette période estivale post-efflorescence. En extrapolant des données de pCO_2 in situ en utilisant des mesures satellitaires de température des eaux de surface et de concentration chlorophylle a, nous avons estimés les flux air-mer printaniers et estivaux par province hydrologique. Ces derniers varient de -0.048 à -0.057 et -0.04 PgC an^{-1} pour respectivement les zones Nord Subantarctique, Sud Subantarctique et du Front Polaire. Une approche similaire a été mené en collaboration avec d'autres groupes pour la secteur Ouest-Pacifique de l'O.A.. L'intégration des flux de CO_2 sur l'année montre que cette zone se comporte comme un puits de CO_2 atmosphérique à hauteur de 0.08 PgC yr^{-1}. Ces deux études convergent vers des estimations moins élevées que la climatologie de Takahashi et al. (2002,2003), mais corroborent les conclusions des modèles atmosphériques inverses qui indiquent que cette climatologie surestime probablement les flux de CO_2 dans l'O.A. (Gurney et al., 2004).

Nous présentons un suivi de trois ans dans les eaux côtières subantarctiques qui ceinturent l'Archipel de Kerguelen avec une attention particulière portée au rôle des herbiers de Macrocystis, des algues géantes. La production primaires des ces dernières s'étend depuis le début du printemps jusqu'à la fin de l'automne et est étroitement liée à l'insolation. La production nette maximale à l'échelle de la communauté peut atteindre 15 gC m^{-2} j^{-1} au maximum annuel de l'insolation. En corollaire, une telle production affecte fortement la pCO_2. En outre, les eaux côtières de l'archipel sont marquées par une efflorescence de phytoplancton plus précoce et plus intense que les eaux au large, ce qui affecte la pCO_2. Toutefois, intégrée sur l'année, les eaux situées à proximité immédiate des côtes de l'archipel se comportent comme une source de CO_2 de 0.32 TgC an^{-1}.

Le rôle de la banquise dans les budgets de CO_2 de l'O.A. a été négligée du fait qu'elle été considérée comme une couverture imperméable et inerte qui empêche les échanges air-mer de gaz. Nous rapportons les premières mesures de la pCO_2 dans la glace de l'année, multi-annuelle, et rattachée au continent, avec des mesures de flux à l'interface air-glace. Les processus internes propres à la glace de mer (dilution par les cristaux de glace, dissolution des carbonates et production primaire) sont responsables d'une forte décroissance de la pCO_2 et conduisent à une sous-saturation marquée du CO_2 par rapport à la concentration atmosphérique. En dépit de sa faible épaisseur, la banquise Antarctique apparaît donc soutenir une forte absorption de CO_2 atmosphérique. Nous avons extrapolé les mesures de flux de CO_2 au-dessus de la glace de mer nue en utilisant des mesures satellitaires de température de surface. Au printemps et en été, la banquise Antarctique se comporte comme un puits de CO_2 atmosphérique compris entre 0.015 et 0.024 PgC qui

représente 6 à 9 de l'absorption annuelle de CO_2 par l'O.A. au sud de 50°S (0.27 PgC an^{-1}). Toutefois, nous estimons que cette évaluation du puits de CO_2 par la banquise est sous estimée du fait qu'elle ne tient pas en compte l'absorption par les communauté de surface. Les mesures de flux turbulent de CO_2 air-glace de mer au dessus du slush – un mélange de neige fondante, de glace et d'eau de mer infiltrée – qui abrite d'abondantes communautés de surface, présente des valeurs 4 fois plus importantes qu'au dessus de la glace de mer nue. Dans l'ensemble, la glace de mer représente un puits de CO_2 additionnel qui doit être pris en compte dans les budgets de flux de CO_2 de l'O.A..

Contents

List of abbreviations

AABW: Antarctic Bottom Water
AADW: Antarctic Deep Water
AAIW: Antarctic Intermediate Water
AD: Antarctic Divergence
CAZ: Coastal Antarctic Zone
CFC : Chlorofluorocarbons
Chl *a*: Chlorophyll *a*
DIC: Dissolved Inorganic Carbon
DMS: Dimethylsulfide
DMSP: Dimethylsulphoniopropionate
HNLC: High Nutrient – Low Chlorophyll
IronEx: Iron Experiment
LGM: Last Glacial Maximum
PF: Polar Front
PFZ: Polar Frontal Zone
pCO_2: Partial Pressure of Carbon Dioxide
fCO_2: Fugacity of Carbon Dioxide
MIZ: Marginal Ice Zone
NADW: North Atlantic Deep Water
NSAF: North Subantarctic Front
NSAZ: North Subantarctic Zone
SSAF: South Subantarctic Front
SSAZ: South Subantarctic Zone
PFR: Polar Frontal Region
PFZ: Polar Frontal Zone
PIC: Particulate Inorganic Carbon
POC: Particulate Organic Carbon
POOZ: Permanently Open Ocean zone
SACCF: Southern Antarctic Circumpolar Current Front
SAF: Subantarctic Front
SAM: Southern Annular Mode
SAMW: Subantarctic Mode Waters

SAZ: Subantarctic Zone

SEAWIFS: SEA-viewing Wide Field-of-view Sensor

SIZ: Seasonal Ice zone

SO: Southern Ocean

SOFeX: Southern Ocean Iron Experiment

SOIREE: Southern Ocean Iron Enrichment Experiment

SST: Sea Surface Temperature

SSTZ: South Subtropical Frontal Zone

STC: Subtropical Convergence

STF: Subtropical Front

STZ: Subtropical Zone

TA: Total Alkalinity

TEP: Transparent Exopolymeric Particles

VGPM: Vertically Generalized Production

WRR: Weddell-Ross Region

1 Introduction

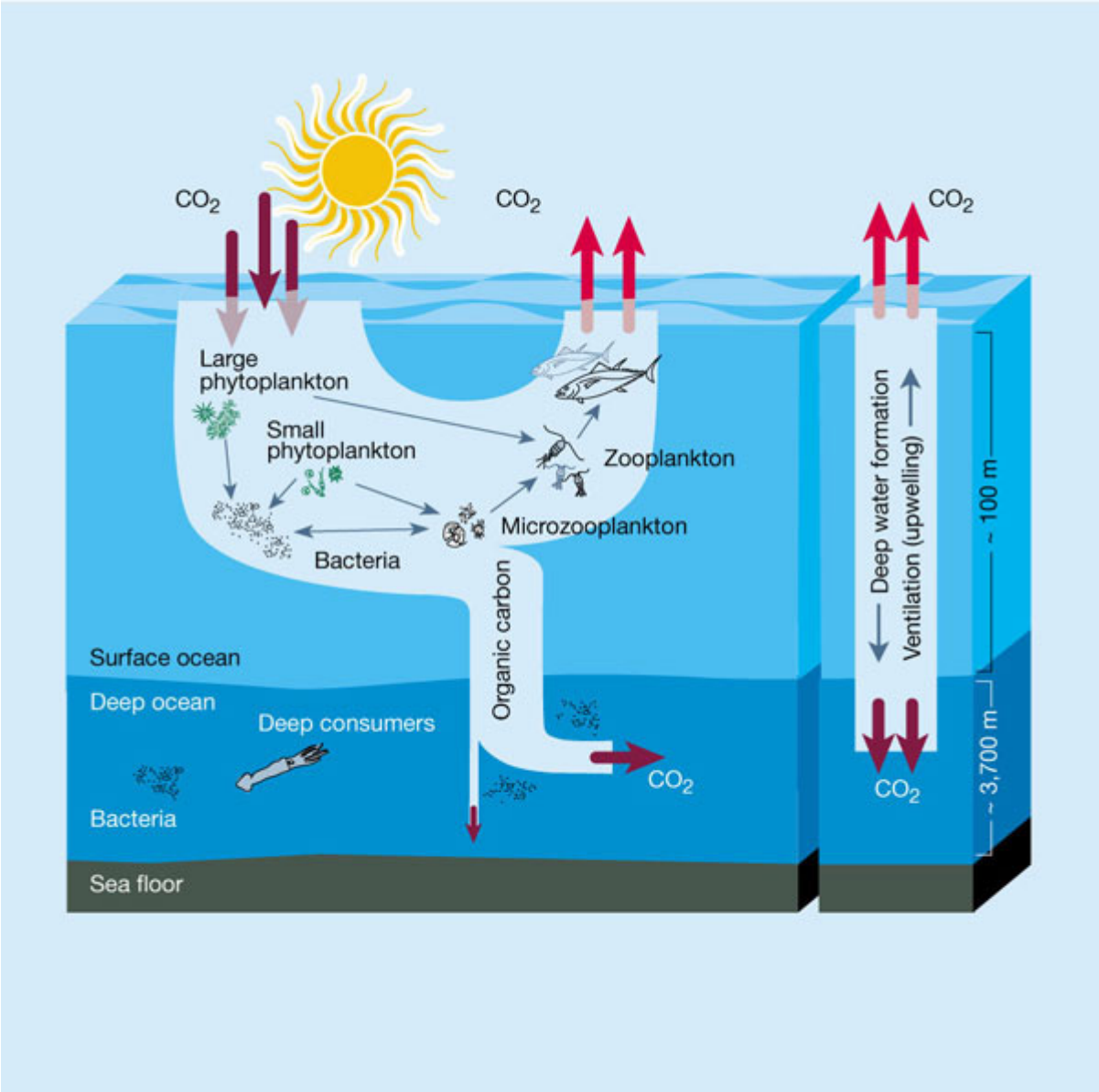

The biological pump after Chisholm (2000) modified from Johnson

1.1 Chemistry of the carbonate system

If the theory of di-acids as carbonic acid is learnt in high school, it is still worth to say that the chemistry of CO_2 in seawater raises numerous subtleties that can be bewildering at first. Even the well-known notion of pH is intrinsically linked in seawater to the CO_2 system but is "for many people, a confused and mysterious topic" (Dickson, 1993). Which modeller, biologist or student has not ever been a little confused by the four different pH scales used by marine chemists?

1.1.1 Dissociation of the carbonic acid and equilibrium constants

The carbonate system represents the different dissociated species encountered in seawater of the carbonic acid H_2CO_3. This di-acid is dissociated in several species: carbon dioxide (CO_2), bicarbonate (HCO_3^-) and carbonate (CO_3^{2-}) whose concentrations depend on thermodynamical equilibriums which are related to salinity, temperature and pressure.

In seawater the two electrically forms H_2CO_3 and aqueous carbon dioxide CO_2(aq) are analytically indistinguishable and H_2CO_3 concentration is much lower than that of CO_2 (aq). General use combines therefore these two species according to:

$$[CO_2] = [CO_2(aq)] + [H_2CO_3] \quad (1)$$

In standard seawater conditions CO_2 dissociates according to:

$$H_2CO_3 \leftrightarrow CO_2(aq) + H_2O \xleftrightarrow{K_1} HCO_3^- + H^+ \xleftrightarrow{K_2} CO_3^{2-} + 2H^+ \quad (2)$$

where K_1 and K_2 are the thermodynamic equilibrium constants (first and second dissociation constants of the carbonate system):

$$K_1 = \frac{a_{H^+} \times a_{HCO_3^-}}{a_{CO_2}} \quad (3)$$

and

$$K_2 = \frac{a_{H^+} \times a_{CO_3^{2-}}}{a_{HCO_3^-}} \quad (4)$$

expressed in terms of activities and are while CO_2 refers to both CO_2 (aq) and H_2CO_3 accordingly to (2).

Since only the activity of H^+ can be directly measured, and that for the other quantities it is only analytically possible to measure the total concentrations, empirically determined apparent equilibrium constants refer to molal concentrations rather than activities. They can be used for media with a constant, high ionic strength

such as seawater. These apparent equilibrium constants K_1^* and K_2^* are valid only for the pH scale, concentration scale and ionic strength for which they were determined (Millero, 1995):

$$K_1^* = \frac{\left[H^+\right] \times \left[HCO_3^-\right]}{\left[CO_2\right]} \tag{5}$$

and

$$K_2^* = \frac{\left[H^+\right] \times \left[CO_3^{2-}\right]}{\left[HCO_3^-\right]} \tag{6}$$

The condition of a constant high ionic strength is not followed when pH measurements in seawater (a high ionic strength media) are calibrated on the infinite dilution scale with U.S. National Bureau of Standard (NBS) standards produced with freshwater. Mixed equilibrium constants (K_1' and K_2') which contain both activities and molal concentrations are used on the NBS scale:

$$K_1' = \frac{a_{H^+} \times \left[HCO_3^-\right]}{\left[CO_2\right]} \tag{7}$$

and

$$K_2' = \frac{a_{H^+} \times \left[CO_3^{2-}\right]}{\left[HCO_3^-\right]} \tag{8}$$

a_H is operationally defined under the infinite dilution convention (e.g. (Skirrow and Whitfield, 1975; Dickson, 1984)).

First and second apparent dissociation constants of the carbonic acid (K_1' and K_2') are given in mol kg^{-1} according to Mehrbach et al. (1973) refitted by Dickson and Millero (1987) on the total pH scale.

$$pK_1^* = \frac{3670.7}{T_{(K)}} - 62.008 + 9.7944 \times \ln(T_{(K)}) - 0.0118 \times S + 0.000116 \times S^2 \tag{9}$$

and

$$pK_2^* = \frac{1394.7}{T_{(K)}} + 4.777 - 0.0184 \times S + 0.000118 \times S^2 \quad (10)$$

in mol kg^{-1}, and where $T_{(K)}$ is the absolute temperature (K) and S salinity.

The apparent dissociation constants from Mehrbach et al. (1973) refitted by Dickson and Millero (1987) have been determined to be the optimal apparent dissociation constants for the carbonate system computations (Wanninkhof et al., 1999; Lueker et al., 2000; Lee et al., 2000) among others sets from Hansson (1973) refitted by Dickson and Millero (1987), Peng et al. (1987), Goyet and Poisson (1989) and Roy et al. (1993). An alternative formulation of the dissociation constants from the Mehrbach et al. (1973) data set has been proposed by Lueker et al. (2000).

On the NBS scale, the mixed dissociation constant are given according to Mehrbach et al. (1973) refitted by Millero (1979):

$$\ln(K_1') = 290.9097 - \frac{14554.21}{T_{(K)}} - 45.0575 \ln(T_{(K)}) + \left(0.0221 + \frac{34.02}{T_{(K)}}\right) \times \sqrt{S} \quad (11)$$

and

$$\ln(K_2') = 207.6548 - \frac{11843.79}{T_{(K)}} - 33.6485 \ln(T_{(K)}) + \left(0.9805 - \frac{92.65}{T_{(K)}}\right) \times \sqrt{S} \quad (12)$$

in mol kg^{-1}, and where $T_{(K)}$ is the absolute temperature (K) and S salinity.

Other relevant formulations are provided in the annexes:

- 8.1.1.1 Alternative carbonic acid dissociation constants (page 295)
- 8.1.1.2 Effect of pressure on carbonic acid dissociation constants (page 295)
- 8.1.1.3 Dissociation constant of boric acid (page 296)
- 8.1.1.4 Dissociation constant of HSO_4^- (page 297)

1.1.2 Bjerrum plot

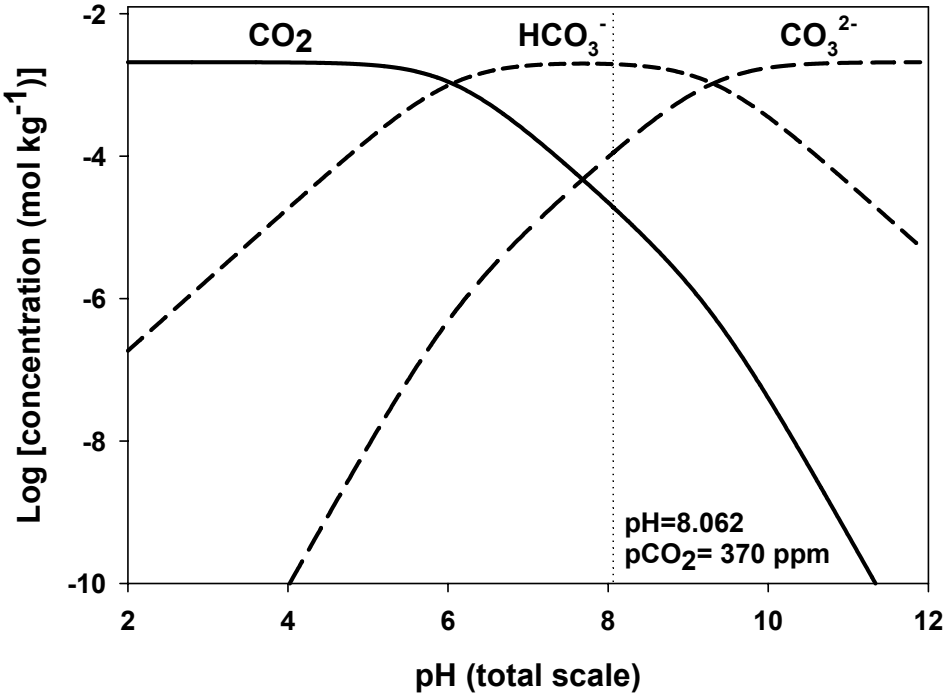

Figure 1.1-1 : Bjerrum plot showing the changes of CO_2, HCO_3^- and CO_3^{2-} in standard condition of Antarctic surface waters (T°=5°, salinity=34, P= 1 atm, DIC=2100 µmol kg^{-1}). The horizontal dotted line corresponds to the equilibrium with the atmosphere.

The plot of logarithm of the concentrations of CO_2, HCO_3^- and CO_3^{2-} versus pH, the so-called Bjerrum plot, is represented on Figure 1.1-1. At equilibrium with the atmosphere (pCO_2=370 ppm, pH=8.062), the concentration of CO_2, HCO_3^- and CO_3^{2-} accounts for, respectively, 0.9%, 93.8% and 5.3 % of the total pool of inorganic carbon, the so-called dissolved inorganic carbon (DIC, also denoted TCO_2 and ΣCO_2). In standard conditions, DIC is mainly present as HCO_3^-. According to the Bjerrum plot, in standard seawater conditions the changes between the different species can be represented, in first approximation, by the equilibrium:

$$2HCO_3^- \leftrightarrow CO_2 + CO_3^{2-} + H_2O \qquad (13)$$

This is a useful and easy representation of the dynamics of the carbonate system in the standard condition of seawater.

While salinity, temperature and pressure allow to compute the dissociation constants, the complete computation of the speciation of the carbonate system

requires to solve a system of 2 equations ((5) and (6) for example) with 4 unknowns. Two additional equations that do not introduce additional unknowns are required to solve the system, which are provided by a couple from the four parameters which can be analytically determined: pH, total alkalinity (TA), DIC and the partial pressure of CO_2 (pCO_2).

DIC is generally expressed in µmol kg^{-1} of seawater:

$$DIC = [CO_2] + [HCO_3^-] + [CO_3^{2-}] \quad (14)$$

1.1.3 Partial pressure and fugacity of CO_2

The pCO_2 of a seawater sample refers to the partial pressure of CO_2 in the gas phase that is in equilibrium with that sample. The concentration of CO_2 in seawater is given by Henry's law:

$$[CO_2] = K_0 \times pCO_2 \quad (15)$$

where K_0 is the solubility coefficient of CO_2 in seawater given after Weiss (1974):

$$\begin{aligned} \ln(K_0) = & -60.2409 + 93.4517 \times \frac{100}{T_{(K)}} + 23.3585 \times \ln(0.01 \times T_{(K)}) \\ & + S \times \left[0.023517 - 0.00023656 \times T_{(K)} + 0.0047036(0.01 \times T_{(K)})^2\right] \end{aligned} \quad (16)$$

in mol kg^{-1} atm^{-1} and $T_{(K)}$ and S denote the absolute temperature (K) and the salinity, respectively.

Accordingly to Dalton's law, the partial pressure of an ideal gas is defined as the pressure of a single ideal gas in the mixture as if that gas alone occupied the container. For real gases Dalton's law is an approximation, and fugacity should be preferred. Fugacity is the pressure value needed at a given temperature to make the properties of a non-ideal gas satisfies the equation for an ideal gas, i.e.

$$fCO_2 = \nu \times pCO_2 \quad (17)$$

where fCO_2 is the fugacity of CO_2 and ν is the fugacity coefficient. For an ideal gas ν=1 and $\nu \to 1$ in the limit of infinitely dilute mixture. The relationship between fugacity and partial pressure is analogous to the relationship between activity and concentration of ions in aqueous solutions.

For CO_2 ν is given by :

$$\nu = \exp\left(p \times \frac{B + 2\delta}{RT_{(K)}}\right) \quad (18)$$

where p denotes the total pressure is given in Pa (1 atm=101325 Pa), B is the first virial coefficient of CO_2 , δ is the cross virial coefficient, R is the ideal gas constant (R=8.314 J K^{-1} mol^{-1}), T is the absolute temperature (K).

B (in m^3 mol^{-1}) is given by Weiss (1974):

$$B = \left(\begin{array}{l} -1636.75 + 12.0408 \times T_{(K)} - 3.27957.10^{-2} \times T_{(K)}^2 \\ +3.16528.10^{-5} \times T_{(K)}^3 \end{array} \right).10^{-6} \quad (19)$$

and δ (in m^3 mol^{-1}) is given by:

$$\delta = \left(57.7 - 0.118 \times T_{(K)}\right).10^{-6} \quad (20)$$

pCO_2 in seawater can be measured by equilibration in a dried air stream, and atmospheric pCO_2 data are by convention expressed in dry air. This requires the conversion of pCO_2 in dry air to pCO_2 in wet air (saturated in water vapour):

$$pCO_{2\ in\ wet\ air} = pCO_{2\ in\ dry\ air}\ x\ (1 - VP(H_2O)) \quad (21)$$

where $VP(H_2O)$ is the water vapour pressure in atm.

DOE (1994) provides a very accurate but rather complex procedure to compute the water vapour pressure that for the purpose of the conversion and required accuracy can also be computed from the Weiss and Price (1980) relationship as recommended by Körtzinger et al. (2000)

$$\ln(VP(H_2O)) = 24.4543 - 67.4509\ x\ (\frac{100}{T_{(K)}}) - 4.8489\ x\ \ln(\frac{T_{(K)}}{100}) - 0.000544\ x\ S \quad (22)$$

where $VP(H_2O)$ is the water vapour pressure in atm, T is the absolute temperature (K) and S salinity.

1.1.4 pH scales

The conventional definition of pH is given by:

$$pH=-\log[H^+] \quad (23)$$

This equation is not useful while studying seawater since free protons are not present in significant amounts in this media (Dickson, 1984) as protons are bounded to water molecules, forming H_3O^+ among other hydrates. Furthermore, protons are also complexed with other ions, mainly sulphate ions (SO_4^{2-}) and fluroride ions (F^-).

Thereafter, it comes that the proton activity (a_{H^+}) should be used instead of concentration:

$$pH_a = -\log a_{H^+} \quad (24)$$

However, it is not always possible to determine experimentally activities, since the concentration of a single ion cannot vary independently since electroneutrality is required. Hence, as for most other chemical quantities in oceanography (salinity, carbonic acid dissociation constants,…), operational definitions of pH were proposed. Four operational definitions of pH in seawater are used. In some studies, the pH scale is not always clearly stated, yielding confusion. Furthermore, misuse of pH scales brings substantial errors in the computation of the speciation of the carbonate system.

NBS scale

The first operational pH scale, the so-called NBS scale, was proposed by the U.S. National Bureau of Standards and aimed to give access to the proton activity:

$$pH_{NBS} \approx pH_a \tag{25}$$

This pH scale involves the use of the mixed carbonic dissociation constants (K_1' and K_2' ; (7) and (8)) which contain proton activity and the molal concentrations of the other species of the carbonate system and (Mehrbach et al., 1973).

The reference state for pH_a and pH_{NBS} is a infinite dilute solution, i.e. as we dilute a solution, the distance between solutes increases and in the limit of infinite dilution, the solutes are infinitely far apart. The activity coefficient ν_{H^+} approaches 1 – i.e. activity approaches concentration - when $[H^+]$ approaches zero in pure water.

The NBS scale applies for low ionic strength solutions, and the corresponding standards (buffers) have a very low ionic strength. NBS buffers are inadequate for high ionic strength solutions like seawater while using combined electrodes, since in order to overcome the error due to the junction potential (a superimposed potential, proportional to the ionic strength, which cannot be determined analytically) it is required to use buffers of the same ionic strength of the samples.

On the whole the use of NBS scale is not recommended for seawater measurements, but it is appropriate for pH measurements in fresh and brackish waters, in particular in estuarine systems (Frankignoulle and Borges, 2001a).

Three other pH scale have been developed for seawater based on the use of buffers made from artificial seawater, that largely overcome the problem of the junction potential, since buffers and samples have similar ionic strengths and compositions. These pH scales imply the use of apparent dissociation constants (K_1^* and K_2^* ; (5) and (6)). The three scales differ in the way protonation encountered in seawater is accounted in the definition of the pH (Table 1-1)

Table 1-1 : Definition of pH valid for seawater

Free scale	$pH_F = -\log\left[H^+\right]_F$	(26)
Total Scale	$pH_T = -\log\left(\left[H^+\right]_F + \left[HSO_4^-\right]\right)$	(27)
Seawater scale	$pH_{SWS} = -\log\left(\left[H^+\right]_F + \left[HSO_4^-\right] + [HF]\right)$	(28)

The free scale is probably the more intuitive as it only takes into account “free” protons. However, in seawater, protons interact with sulphate ions according to:

$$HSO_4^- \xleftrightarrow{K_S^*} H^+ + SO_4^{2-} \tag{29}$$

so that the “total” hydrogen ion concentration is:

$$\left[H^+\right]_T = \left[H^+\right]_F + \left[HSO_4^-\right] \quad (30)$$

and only $[H^+]_T$ can be determined analytically (Dickson, 1993). The use of the "free" sale requires therefore to know $\left[HSO_4^-\right]$ which is difficult to determine.

Total Hydrogen ion scale

The total hydrogen ion scale or total scale is probably the pH scale most widely used for pH measurements in seawater. This scale includes the effect of protonation by sulfate ions in its definition and therefore does not require the experimental determination of $\left[HSO_4^-\right]$. A useful set of buffer standards was proposed in artificial seawater containing sulphate ions (Dickson, 1993), whose assigned pH values was accurately determined on the "total scale" (Dickson, 1993; DelValls and Dickson, 1998). Furthermore, a set of consistent apparent dissociation constants (Roy et al., 1993) were accurately determined on this pH scale based on similar artificial sweater composition as the buffers proposed by Dickson (1993).

Dissociation constants of sulfate ion is provided in the annexes (8.1.1.4)

Seawater scale

A more accurate pH scale takes into account the protonation with fluoride ions:

$$HF \xleftrightarrow{K_F^*} H^+ + F^- \quad (31)$$

The total hydrogen ion concentration in this pH scale is therefore:

$$\left[H^+\right]_{SWS} = \left[H^+\right]_F + \left[HSO_4^-\right] + [HF] \quad (32)$$

The difference between the total and the seawater scale lies is the fact whether the medium on which the scale is based contains fluoride or not. However, the difference between the two pH scales is small (typically 0.001) since $\left[HSO_4^-\right]$ is much larger than $[HF]$ in seawater. A set of apparent dissociation constants consistent with this scale was determined by Goyet and Poisson (1989).

Choice of pH scale and dissociation constants

Conversion formulae between different pH scales, together with the conversion of acidity constants between different pH scales have been proposed (Dickson and Millero, 1987; Dickson, 1993). However, the best approach is to avoid such conversion and to use consistent sets of pH scale, buffers, and dissociation constants. In fresh and brackish waters, it is preferable to use the NBS pH scale (which require to use NBS buffers) and mixed dissociations constants of Merhabch et al (Mehrbach et al., 1973) refitted by Millero (1979). In seawater, it is preferable to use the "total" pH scale (using buffers proposed by (Dickson, 1993)) with apparent dissociation constants from Mehrbach et al. (1973) refitted by Dickson and Millero

(1987) since they have been estimated to be the optimal apparent dissociation constants for seawater (Wanninkhof et al., 1999; Lee et al., 2000).

1.1.5 Total Alkalinity

1.1.5.1 Definition of total alkalinity

The currently accepted definition of total alkalinity (TA) was proposed by Dickson ((Dickson, 1981; DOE, 1994)): the number of moles of hydrogen ion equivalent to the excess of proton acceptors (bases formed from weak acids with a dissociation constant pK ≥4.5, at 25°C and zero ionic strength) over proton donors (acids with pK < 4.5) in one kilogram of sample.

For seawater, such definition yields:

$$\begin{aligned} TA = &\left[HCO_3^-\right] + 2\left[CO_3^{2-}\right] + \left[B(OH)_4^-\right] + \left[OH^-\right] + \left[HPO_4^{2-}\right] + 2\left[PO_4^{3-}\right] + \left[H_3SiO_4^-\right] \\ &+ \left[NH_3\right] + \left[HS^-\right] - \left[H^+\right]_F - \left[HSO_4^-\right] - \left[HF\right] - \left[H_3PO_4\right] \end{aligned} \quad (33)$$

where $[H^+]_F$ is the free concentration of protons.

TA relates readily to the titration of seawater with a strong acid, usually HCl, in which the equivalence point is determined by following the decrease of pH. Total alkalinity is therefore sometimes referred as titration alkalinity. During this work, the equivalence point of was determined using the Gran function (Gran, 1952). The equivalence point of the titration generally occurs at around pH=4.3 and corresponds to the endpoint of the titration of the carbonic acid, as carbonic acid is the dominant weak acid-base system in seawater (Fig. 1.1-1). This leads to the consistent choice by Dickson (1981) of the pK value of 4.5 to distinguish proton donors and acceptors. The extended Bjerrum plot of the figure 1-2 provides an overview of the main acid-base systems present in seawater and in addition gives an idea of their relative concentrations in the course of the titration. It can also be used to distinguish which compounds are accounted in TA, and are either considered as proton acceptors (bases formed from weak acids with pK ≥4.5) or proton donors (acids with pK < 4.5).

According to figure 1-2, carbonic acid and boric acid (in addition to water itself) are the most important acid-base systems in seawater. A good approximation of TA, namely the practical alkalinity (PA) is therefore given by accounting only the contribution of carbonic acid, boric acid, and water.

The contribution of carbonic acid is denoted as carbonate alkalinity (CA) which is a useful and simple approach of alkalinity:

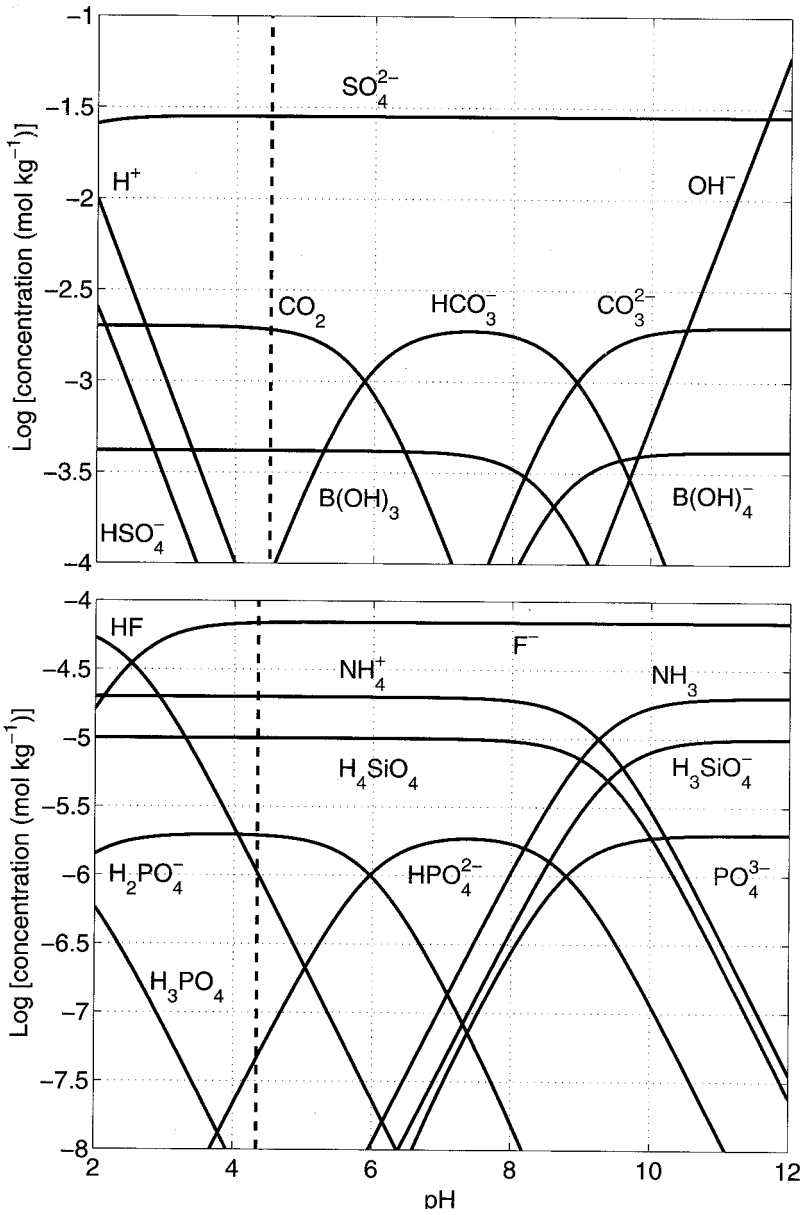

Figure 1-2 : Bjerrum plot with main acid-base systems present in standard seawater after Zeebe and Wolf-Gladrow {Zeebe & Wolf-Gladrow 2001 2044 /id/d}

$$CA = \left[HCO_3^-\right] + 2\left[CO_3^{2-}\right] \tag{34}$$

The contribution of boric acid to PA, the borate alkalinity, is:

$$\text{Borate alkalinity} = \left[B(OH)_4^-\right] \tag{35}$$

It can be derived from the following equation:

$$B(OH)_3 + H_2O \xleftrightarrow{K_B} B(OH)_4^- + H^+ \tag{36}$$

where K_B is the dissociation constant of boric acid that is a function of salinity and temperature. The concentration of total borate (B_t) is conservative and a function of salinity (Culkin, 1965).

$$B_t = [B(OH)_3] + [B(OH)_4^-] \quad (37)$$

It comes:

$$[B(OH)_4^-] = \frac{B_t * K_B}{[H^+] + B_t} \quad (38)$$

This expression can be readily computed from temperature, pH and salinity.

The contribution of water to PA can be expressed as:

Water Alkalinity= $[OH^-] - [H^+]_F$

Hence the definition of the practical alkalinity (PA) can be expressed as:

$$PA = [HCO_3^-] + 2[CO_3^{2-}] + [B(OH)_4^-] + [OH^-] - [H^+]_F \quad (39)$$

1.1.5.2 Conservation of total alkalinity

As every solution, the principle of electroneutrality applies to seawater. Hence, it comes:

$$\begin{aligned} &[Na^+] + 2[Mg^{2+}] + 2[Ca^{2+}] + [K^+] + ... + [H^+]_F \\ &- [Cl^-] - 2[SO_4^{2-}] - [NO_3^-] - [HCO_3^-] - 2[CO_3^{2-}] - [B(OH)_4^-] - [OH^-] - ... = 0 \end{aligned} \quad (40)$$

Seawater is a complex solution, and only the most abundant ions appear in this equation. If we place on the left part of the equation the strong cations and anions (completely dissociated and whose concentration is therefore not affected by pH), it comes:

$$\begin{aligned} &[Na^+] + 2[Mg^{2+}] + 2[Ca^{2+}] + [K^+] + ... - [Cl^-] - 2[SO_4^{2-}] - [NO_3^-] - ... \\ &= [HCO_3^-] + 2[CO_3^{2-}] + [B(OH)_4^-] + [OH^-] - [H^+]_F + / - [\text{minor compounds}] = TA \end{aligned} \quad (41)$$

The left part of the equation gathers the ions originating from strong bases and acids. Hence, their relative concentrations do not depend on equilibrium constants, and they are not affected by pH, temperature, salinity or pressure. Indeed, the relative concentration of major ions in seawater is constant (Dittmar's principle) and mainly depend on salinity. Their concentrations are in fact conservative, and the left member of the equation is therefore conservative. Corollary the right member, which represents the most important contribution to TA, and is very similar, neglecting the term 'minor compounds' to the definition of the Practical Alkalinity (PA), is also conservative.

The conservative property of the TA is useful since it can be used as a water mass tracer in addition to salinity. This approach was used to investigate distribution of Barium in the Crozet Basin (Jacquet et al., 2002).

1.1.6 Buffer factor

The response of the oceanic reservoir to increasing atmospheric carbon dioxide has three aspects: (1) the kinetics of the exchange processes of CO_2 between atmosphere and ocean, (2) as well as within the water masses; and (3) the uptake capacity of seawater for additional CO_2, a thermodynamic property.

Item (1) that relates to air-sea exchange is discussed in section 1.1.8 while item (2) is discussed in the section 1.4.1. The other important factor controlling the uptake capacity of the oceanic reservoir (item 3) is the buffer factor, which relates the changes of pCO_2 to the changes of the overall pool of inorganic carbon, namely DIC. The homogeneous Revelle factor was introduced by Sundquist and Plummer (1981):

$$\beta = \frac{d\ln(pCO_2)}{d\ln(DIC)} = \frac{\Delta pCO_2}{pCO_2} \times \frac{DIC}{\Delta DIC} \qquad (42)$$

It describes the change in pCO_2 relative to the DIC change induced by an input/output of dissolved CO_2. It results from equilibrium dissociation reactions of the carbonate system and is a function of several physico-chemical conditions, among them on the pCO_2 itself.

.

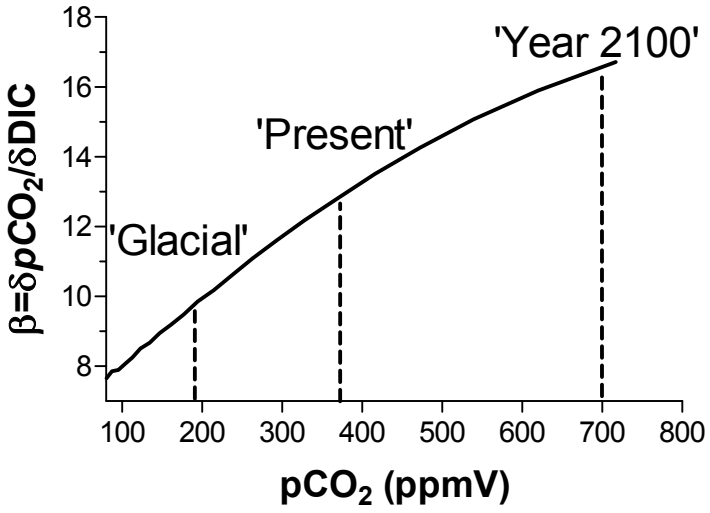

Figure 1.1-4: Buffer factor of the carbonate system for increasing partial pressure of CO_2 in the following conditions: salinity of 31.3, temperature of 10.0°C and TA of 2150 mmol kg^{-1}. Glacial conditions correspond to the pCO_2 of last glacial period (pCO_2 = 180 ppmV), 'present' denotes the present pCO_2 (pCO_2 = 370 ppmV) and 'year 2001l' denotes the predicted pCO_2 accordingly to the Intergovernmental Panel on Climate Change ''business as usual'' scenario IS92a, after Delille et al. (2005)

In the context of raising atmospheric pCO_2 and consequently in the ocean, the buffer factor of the ocean increases with the increase of pCO_2, which means that the capacity of the ocean to buffer the increase of atmospheric pCO_2 will be reduced.

The evolution of the buffer factor from glacial to future atmospheric pCO_2 values is given in the figure 1.1-4.

β increases from 9.6 in the 'glacial' conditions (pCO_2 = 180 ppmV) to 12.8 in the 'present' conditions (pCO_2= 370 ppmV) and to 16.6 in the 'year 2100' conditions (pCO_2 = 700 ppmV, accordingly to the Intergovernmental Panel on Climate Change ‘‘business as usual’’ scenario IS92a). For the same removal of CO_2 by primary production, the corresponding decrease of pCO_2 is 6 times higher in the 'year 2100' conditions (ΔpCO_2 = 116 ppmV for ΔDIC= 20 µmol kg^{-1} and β= 16.6 at pCO_2 = 700 ppmV, and DIC= 2000 µmol kg^{-1}) than under the 'glacial' conditions (ΔpCO_2 = 20 ppmV for ΔDIC= 20 µmol kg^{-1} and β= 9.6 at pCO_2 = 180 ppmV and DIC= 1740 µmol kg^{-1}). Hence, in the future CO_2 rich world, other processes - temperature oscillations, upwelling of CO_2 rich waters or precipitation of calcium carbonate (Frankignoulle et al., 1994) among others - will also contribute to the thermodynamic enhancement of the amplitude of pCO_2 changes from daily to seasonal time-scales. In the same way, a higher spatial heterogeneity of pCO_2 can be expected from local to global scales.

β is also a useful tool for identifying the biogeochemical processes that mainly affect the inorganic carbon dynamics, such as primary production, calcification or water mass mixing. It can be obtained by plotting ln(pCO_2) versus ln(DIC), and when dissolved CO_2 is the only inorganic species involved in the carbon exchange (e.g. air-sea exchange, primary production) or in other words when TA remains constant, β corresponds to the Revelle factor (Revelle and Suess, 1957) and its about 10 for average present day seawater conditions. However, β also depends on other processes that modify the inorganic species involved in the CO_2 system speciation. Thus, if organic matter production/respiration by organic metabolism has no effect on β, this value can decrease down to -7 under the influence of inorganic metabolism (e.g. uptake or release of bicarbonates and/or carbonates by calcifying organisms). When organic and inorganic carbon metabolisms occur simultaneously, one can use the relation β=-7.02+0.186×%C_{org} (Frankignoulle, 1994) where ×%C_{org} is the percentage of change in inorganic carbon concentration due to organic metabolism compared to inorganic carbon metabolism.

Using this approach, Robertson et al. (1994) studied a coccolithophorid bloom in the North Atlantic, while Wanninkhof and Feely (1998) discussed the influence of aging water masses from the Atlantic to the South Indian and South Pacific Oceans. Furthermore, the homogeneous buffer factor may provide substantial help in understanding inorganic carbon dynamics even in coastal waters where complex and intense biogeochemical processes co-occur (Frankignoulle et al., 1996a; Frankignoulle et al., 1996b).

1.1.7 Inorganic carbon dynamics

1.1.7.1 Temperature changes

By influencing both the solubility coefficient K_0 and the speciation of the carbonate system through the dissociation constant K_1 and K_2, temperature readily affects pCO_2. This effect can be easily computed from the algorithms of Copin-Montégut

(1988,1989). These algorithms are used for corrections in pCO_2 measurements, or to remove temperature effect on temporal/spatial changes of pCO_2.

It comes:

$$\ln(pCO_2) = \frac{a(t)}{a(t_i)} \ln \frac{(pCO_{2i})}{b(t_i)} + \ln(b(t)) \quad (43)$$

with:

$$a(t) = 1 - ((1090 + 7S) \times 10^{-6}) \times t \quad (44)$$

$$b(t) = 1 - ((3695 + 9S) \times 10^{-5}) \times t + ((389 + 2.2S) \times 10^{-6}) \times t^2 + ((0.34 - 0.124S) \times 10^{-6}) t^3 \quad (45)$$

where t is the temperature (°C) and S the salinity.

1.1.7.2 Salinity changes

Evaporation/precipitation by concentrating/diluting DIC and TA, and through the changes on the equilibrium constants affects pCO_2 and the speciation of the carbonate system. This effect can be enhanced in the marginal ice zone while sea ice growing/melting affects salinity of the water column, but this in sea ice itself that the effect of salinity have a tremendous effect on the inorganic carbon dynamics in line with the huge variations of salinity and the formations of brines. Effect of salinity changes on the carbonate system can be readily estimated since both TA and DIC are proportional to salinity. While discussing the relative effect of physical and biogeochemical processes n inorganic carbon dynamics, the effects of salinity changes can be “removed” through the use of DIC and TA normalized at a constant salinity (denoted as DIC_{35} and TA_{35}, respectively) accordingly to:

$$DIC_{35} = DIC \times \frac{35}{S} \quad (46)$$

and

$$TA_{35} = TA \times \frac{35}{S} \quad (47)$$

where DIC and TA are given at the salinity S.

In the present work, equations (46) and (47) were used for normalization purposes, although they assume a zero value for both DIC and TA in freshwater, which is un-realistic. This has lead to a more complex normalization procedure by Friis et al. (2003). However, this procedure can only be applied when DIC and TA are conservative, hence, when normalization is of little use.

1.1.7.3 Water masses mixing

Water masses mixing, advection, upwelling, vertical mixing significantly affect significantly pCO_2 and the carbonate system speciation. They can be estimated from DIC and TA which are conservative through mixing processes (cf 1.1.5.2).

1.1.7.4 CO_2 exchanges at the air-sea interface

The effect of the CO_2 exchanges at the air-sea interface on the pCO_2 and speciation of the carbonate system generally does not appear clearly since it is a rather slow processes compared to immediate effects as temperature changes (cf 1.1.7.1) or fast processes as CO_2 fixation through biosynthesis (cf 1.1.7.6). They can be more obvious during autumn and winter, when the effects from the other processes on pCO2 are less marked. It can be assessed by iterations using k-wind relationships (cf 1.1.8.2) although prone to large uncertainties.

1.1.7.5 Precipitation/dissolution of $CaCO_3$

Precipitation of calcium carbonate ($CaCO_3$) in standard seawater conditions is described by:

$$Ca^{2+} + 2\,HCO_3^- \rightarrow CaCO_3 + CO_2 + H_2O \qquad (48)$$

The precipitation of one mole of $CaCO_3$ produces CO_2 and decrease DIC by one mole and TA by two moles. Such precipitation can be biologically mediated by calcifying organisms like coccolithophores or occurs spontaneously, for instance within sea ice, as a result of large increases of $CaCO_3$ saturation owing to salinity increase.

Dissolution of $CaCO_3$, in standard seawater conditions, corresponds to the reverse of equation (48).

1.1.7.6 Photosynthesis/respiration

According to the classical Redfield-Ketchum-Richards (RKR) reaction of biosynthesis (Redfield et al., 1963; Richards, 1965)

$$106\,CO_2 + 16\,NO_3^- + H_2PO_4^- + 17\,H^+ + 122\,H_2O \rightarrow (CH_2O)_{106}(NH_3)_{16}H_3PO_4 + 138\,O_2 \qquad (49)$$

one mole of H^+ is consumed for each mole of NO_3^- or $H_2PO_4^-$ consumed through biosynthesis, increasing TA by one mole. Thus, photosynthesis decreases DIC and pCO_2 and increases TA (H^+ consumption). Aerobic respiration involving a complete recycling of nitrogen in first instance corresponds to the reverse of the equation (49) and then increases DIC and pCO_2 and decreases TA.

Photosynthesis as predicted by the RKR equation involves the assimilation of nitrate. If the assimilation of NH_4^+ occurs instead of assimilation of NO_3^-, photosynthesis decreases TA (H^+ production):

$$R-OH + NH_4^+ \leftrightarrow R-NH_2 + H^+ + H_2O \qquad (50)$$

where R- represents organic matter. The equation (50) is the reverse equation to ammonification which then increases TA (H^+ consumption):

$$R-NH_2+H^+ +H_2O \leftrightarrow R-OH+NH_4^+ \quad (51)$$

Nitrification on the other hand decreases TA (H^+ production) according to:

$$NH_4^+ +2O_2 \leftrightarrow R-NO_3^- +2H^+ +H_2O \quad (52)$$

The complete recycling of nitrogen involves both ammonification and nitrification and leads to a net production of H^+ and decrease of TA and eventually corresponds to the equation (49).

1.1.7.7 Anoxic processes

After the exhaustion of O_2, organic matter decay by bacteria involves a series of anoxic reactions which occur depending of the availability of electron acceptors and the energy efficiency of the corresponding oxidation reactions. The following reactions are listed accordingly to their decreasing free enthalpy, the first equation having the highest free enthalpy and then occur preferentially. The term CH_2O represents the organic matter.

Denitrification:

$$5CH_2O+4NO_3^- +4H^+ \rightarrow 5CO_2+7H_2O+2N_2 \quad (53)$$

Manganese (IV) reduction:

$$CH_2O+2MnO_2+4H^+ \rightarrow CO_2+3H_2O+2Mn^+ \quad (54)$$

Iron (III) reduction:

$$CH_2O+2Fe_2O_3+8H^+ \rightarrow CO_2+5H_2O+4Fe^{2+} \quad (55)$$

Sulfatoreduction:

$$2CH_2O+SO_4^{2-}+2H^+ \rightarrow 2CO_2+2H_2O+H_2S \quad (56)$$

Methanogenesis:

$$2CH_2O \rightarrow CO_2+CH_4 \quad (57)$$

With the exception of methanogenesis (57), all processes (53)-(56) consume H^+ and therefore increase TA. These processes occur mainly in the sediments, and due to the much larger abundance in seawater of SO_4^{2-}, sulphate-reduction is the main anaerobic diagenetic organic matter degradation pathway. In presence of O_2, H_2S is oxidized producing proton. Hence, a net flux of TA from the sediment to the water

column should not occur unless reduced sulfur is permanently trapped, namely as pyrite, which only significantly occurs in iron rich sediments which are not abundant. However, the acidification related to the production of protons from the oxidation of H_2S in sub-oxic and oxic layers of the sediment can lead to the dissolution of $CaCO_3$ and a net TA production (e.g. Ku et al. (1999); Barrón et al. (2006)).

Table 1-2. Main physical and biogeochemical processes and their interactions with pCO_2 and the carbonate system. The quantitative examples of processes were chosen arbitrary. pCO_2 changes were computing for standard S.O. conditions (temperature of 5°C, salinity of 34, TA= 2400, DIC= 2233.5) using CO_2 speciation was calculated using the CO2sys.xls package (Pelletier et al., 1998) the CO_2 acidity constants of Mehrbach et al. (1973) refitted by Dickson and Millero (1987), the CO_2 solubility coefficient of Weiss (1974), the SO_4^{2-} dissociation constant of Dickson (1990a), the borate acidity constant of Dickson (1990b) while the total borate molality was calculated using the Uppström (1974) ratio to chlorinity. pCO_2 changes related to water masses mixing involves mechanisms beyond the scope of the table. Last column provides the theoretical slope of the processes in DIC_{35} vs TA_{35} plots.

		Processes	Opposite processes	Relevant paragraph/ equation	Quantitative example	ΔDIC	ΔTA	ΔpCO2	$\Delta DIC_{35}/\Delta TA_{35}$
Abiotic		Temperature increase	Temperature decrease	1.1.7.1	Decrease of temperature of 1°C	**0**	**0**	-17.3	no changes
		Evaporation, ice growth	Precipitation, ice melting.	1.1.7.2 (46)(47)	Increase of salinity of 0.5	35.3	32.8	8.4	no changes
		Mixing, upwelling, deep mixing, brine melting		1.1.7.3		conservative	conservative	-	conservative
		Uptake of atmospheric CO_2	Release of atmospheric CO_2	1.1.7.4	Equilibrium of seawater with pCO_2 of 348 µatm with atmo. (PCO_2=370 µatm)	10.0	**0**	21.9	0 (horizontal displacement)
Biological		$CaCO_3$ precipitation	$CaCO_3$ dissolution	1.1.7.5 (48)	Precipitation of 10 µmol of $CaCO_3$	-10.0	-20.0	18.4	2.0
		Photosynthesis (NO_3^- assimilation)	Respiration (full recycling of nitrogen)	1.1.7.6 (49)	Synthesis of "10 µmol" of organic matter	-10.0	1.6	-24.9	-0.2
		Photosynthesis (NH_4^+ assimilation)		1.1.7.6 (50)	Synthesis of "10 µmol" of organic matter	-10.0	-1.4	-19.3	0.1
		Ammonification		1.1.7.6 (51)	Ammonification involving "10 µmol" of organic matter	**0**	1.4	-2.8	vertical displacement
		Nitrification		1.1.7.6 (52)	Nitrification of 10 µmol of NH_4^+	**0**	-2.8	5.8	vertical displacement
	Anoxic	Denitrification		1.1.7.7 (53)	Degradation of "10 µmol" of organic matter	10.0	8.0	2.1	0.8
		Manganese (IV) reduction		1.1.7.7 (54)	Degradation of "10 µmol" of organic matter	10.0	40.0	10.5	4.0
		Iron (III) reduction		1.1.7.7 (55)	Degradation of "10 µmol" of organic matter	10.0	80.0	21.1	8.0
		Sulfatoreduction		1.1.7.7 (56)	Degradation of "10 µmol" of organic matter	10.0	10.0	2.6	1.0
		Methanogenesis		1.1.7.7 (57)	Degradation of "10 µmol" of organic matter	5.0	**0**	0.0	0 (horizontal displacement)

1.1.8 Air-sea exchange

1.1.8.1 Theoretical considerations

It is possible to determine nowadays the speciation of the carbonic system with a high accuracy, compared to the spatial and temporal variability. While studying CO_2 issues and related CO_2 fluxes, generally the main uncertainties lie in the lack of pCO_2 data and poor assessment of CO_2 fluxes. To overcome the under sampling issue, several solutions have been developed, from autonomous pCO_2 measurements units deployed on buoys and moorings, to the increasing use of Volunteer Observing Ships (VOS), and the use of relationships between pCO_2 and variables that can be derived from remote sensing (mainly chlorophyll *a* and sea surface temperature) to interpolate at larger temporal and spatial scales from satellite imagery. Even if the implementation of some of these solutions is hardly achievable in remote/ice covered areas as the Southern Ocean, it is worth noting that an increasing number of time-series are available. Then, one of the main sources of uncertainty is the assessment of CO_2 fluxes from the air-water CO_2 concentration gradient measurement, i.e. the poor constrain of the gas transfer velocity of CO_2.

A good starting point to understand CO_2 gas transfer velocity issues, is the mass transfer equation of molecular diffusion given by the Fick's law:

$$J = -D\frac{\partial C}{\partial x} \tag{58}$$

where J (mol m^{-2} s^{-1}) is the diffusion flux, D is molecular diffusion coefficient (m^2 s^{-1}), $\frac{\partial C}{\partial x}$ is the concentration gradient of a given solute (mol m^{-2}).

If we consider the air-sea exchange of CO_2, this equation written according to:

$$F = k(C_w - \lambda C_a) \tag{59}$$

where F is the air-sea flux of CO_2 (mol m^{-2} s^{-1}), k is the gas transfer velocity (m s^{-1}), C_w is the concentration of CO_2 in the bulk of water near the interface (mol m^{-3}, λ is the dimensionless Ostwald solubility coefficient defined as the volume of gas (at T and P) dissolved per unit volume of solvent and C_a is the concentration of gas in the air phase near the interface. Indeed, λC_a can be expressed as αPCO_2 where α is the solubility coefficient (mol m^{-3} µatm^{-1}) and PCO_2 denotes conventionally the partial pressure of CO_2 in air (while pCO_2 denotes the partial pressure of CO_2 in water). α corresponds to K_0 of the equation (15) provided in unit of volume rather than in unit of mass. The flux can be written:

$$F = k \times \alpha\ (pCO_2 - PCO_2) \tag{60}$$

where k denotes the gas transfer velocity

or

$$F = K\,(pCO_2 - PCO_2) \tag{61}$$

where K denotes the gas exchange coefficient (Etcheto and Merlivat.L, 1988). Equations (60) and (61) hold true if fugacity is used instead of partial pressure.

The main resistance of the transfer across the air-water interface for sparingly soluble gases such as CO_2 lies in the water phase, through a micro-layer of water where the transfer depends on molecular diffusion (e.g. Liss and Slater (1974)). Under low turbulent conditions, the micro-layer thickens and the resistance to air-sea exchange increases, while under turbulent conditions, the micro-layer is eroded and the resistance to air-sea exchange decreases. Hence, k depends on water turbulence, which is introduced as the kinematic viscosity of water through the Schmidt number. Schmidt number is dimesionless and describes the ratio of transfer coefficient for momentum and mass, i.e. the ratio of kinematic viscosity of water ν ($m^2 s^{-1}$), and the molecular diffusion coefficient D ($m^2 s^{-1}$) of a given gas in water:

$$Sc = \frac{\nu}{D} \tag{62}$$

The Schmidt number depends on the nature of the gas, salinity and temperature. For CO_2, it ranges from 600 in freshwater to 660 in seawater at 20°C (e.g. (Wanninkhof, 1992)). A function to compute the Schmidt number at salinity of 35 from temperature is given by Wanninkhof (1992):

$$Sc = 2073.1 - 125.62T + 3.6276T^2 - 0.043219T^3 \tag{63}$$

where T is temperature (°C)

The concept of a resistive diffusive sub-layer provides the base for the models of gas transfer at water surfaces. If this layer is stretched or eroded in some way the result will be an increase of the gas flux, at least locally. Different models have been proposed which differ in the way in which turbulence produced outside the layer acts to erode it or to mix it altogether. The turbulence may be produced by interaction of water currents with the bottom, as in rivers and estuaries; by the breakdown of the wind-driven shear layer; by the rupture of the surface caused by breaking waves or the return of bubbles to the surface; or by the interaction of injected momentum from wave breaking into the relatively vorticity free environment beneath the waves. The choice of appropriate model depends on which of these agents for thinning or rupturing the diffusive sub-layer is considered to be dominant. How turbulence is taken into account is reflected in the way these models take the Schmidt number into account. Three general models have been proposed hitherto.

Film model

In the film model, air-sea exchange of gas is mainly limited by molecular diffusion through a stagnant layer or film water at the air-water interface with a constant thickness which depends on given circumstances (Whitman, 2006). The gas transfer velocity is therefore proportional to molecular diffusion:

$$k \propto D \quad \propto Sc^{-1} \tag{64}$$

Boundary layer model for rigid and rough surfaces

If the source of turbulence is the breakdown of the shear flow imposed by a tangential stress at the surface, turbulent diffusivity can be used. It relates mixing

length (linked to the distance from the boundary) and the local velocity gradient (shear) and leads to:

$$k \propto D^{2/3} \propto Sc^{-2/3} \quad (65)$$

Surface renewal models

Surface renewal models, introduced by Higbie (1935) and Danckwert (2006) are based on the concept that turbulent eddies bring fluid from the bulk to the surface periodically and it is this "renewal rate", *r*, that determines the rate of gas exchange rather than the thickness of the diffusive layer. The renewal events are assumed to occur randomly with a frequency and intensity that are related to the turbulence properties in the bulk or to the degree of wave breaking.

In these models:

$$k \propto D^{0.5} \propto Sc^{-0.5} \quad (66)$$

The film model is applicable to a limited number of cases. Boundary layer model appears to represent better air-sea gases exchange across smooth liquid interfaces, while for an interface with waves, surface renewal models are more reliable. However, it must keep in mind that the Schmidt number exponent (Sc^{-n}) varies substantially with the transfer regime, tending to increase (becoming less negative) for more turbulent regime (Wanninkhof et al., 1993) and n ranges from 0.2 to 1 have been reported (Jähne and Haussecker, 1998; Jean-Baptiste and Poisson, 2000)

Other factors not explicitly accounted in these conceptual models, also affect gas air-sea exchange (Fig. 1.1-5).

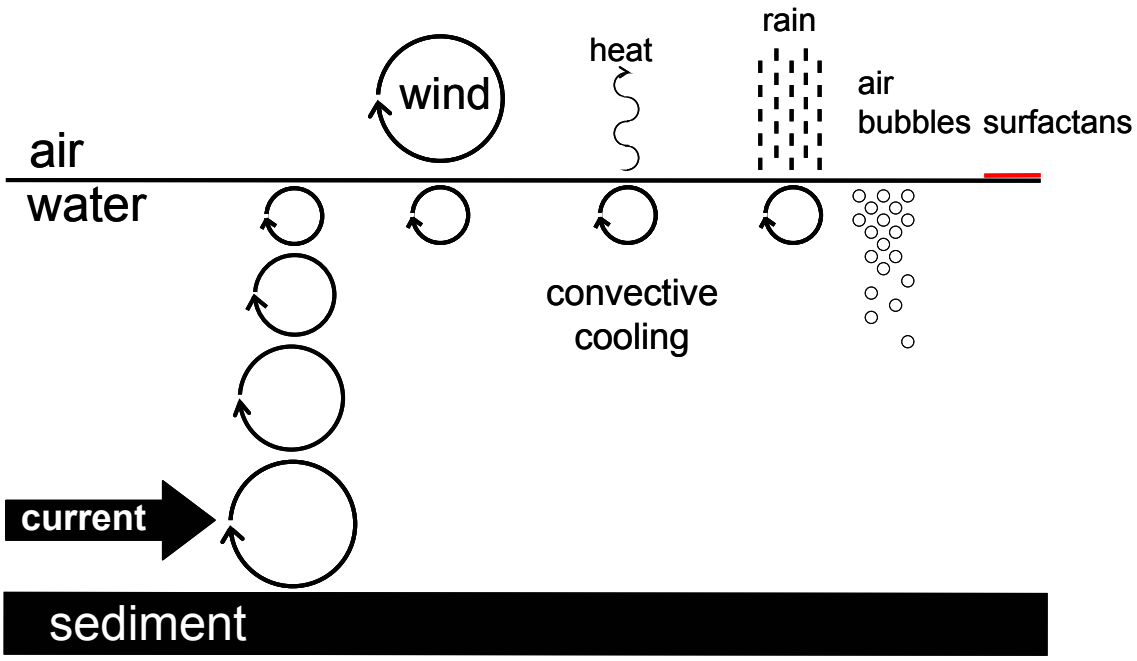

Figure 1.1-5. Processes influencing air-sea gas.

Surfactants

Surfactants can affect air-water gas fluxes in several ways. At high concentrations, surfactants can act as a third medium, in which case an added boundary layer has to be taken into account, since gases will have to transfer through the water boundary layer, surfactant, and air boundary layer. The solubility of the gas in the, often heterogeneous, surfactant materials will affect the rate of transfer. This condition seldom occurs in open ocean waters. More often, the surfactant layer is not continuous or little more than a mono-molecular layer such that most of its effect is related to decreasing the gas transfer velocity rather than influencing the chemical gradient. Surfactants damp waves and decrease near-surface turbulence. This effect is pronounced even with slightly soluble surfactants and in cases where surfactant concentrations are less than required to create a mono-molecular surface. Most experimental investigations on surfactant effects have been carried out in laboratory conditions, and there is little at sea evidence of the applicability of the conclusions derived from these experiments. An elegant laboratory study of the effect of surfactants on k is provided by Frew (1997). Water was collected along a transect from Narragansett to Bermuda, covering coastal waters to open oceanic waters, and was studied for k in large tanks with variable and adjusted turbulent conditions (with stirrers). Significant decreases in k were linearly correlated to Chl *a*, dissolved organic carbon (DOC) and surfactant concentrations. However, during IronEX 2, chlorophyll *a* concentrations increased from 0.3 to 3.0 µg L^{-1} and a reduction of 60% in k would have been expected if the laboratory results of Frew (1997) were applicable to real oceans. However, k remained constant throughout the experiment as did wind speed (Nightingale et al., 2000a). Wanninkhof et al. (2004) report k values during SOFex that are consistent with previously published k-wind relationships. During the course of this experiment, a shift from low to high Chl *a* concentrations was also observed, without inducing a significant effect on k values.

Chemical enhancement

Chemical reactions of the gas in micro-layer can enhance air-sea gas exchange, especially under calm condition, since as the gas molecules react in the boundary layer, their concentration is affected and thereafter the concentration gradient across the interface. Such chemical enhancement depends on the gas, the chemical characteristics of the medium and the chemical reaction time relative to the diffusion time and thereafter to the turbulence conditions. For CO_2, chemical enhancement is mainly ascribed to the first dissociation of CO_2 acid into bicarbonates (2) and hydration with H_2O. This may enhance the air-sea exchange of CO_2 by 2 to 3% under low turbulent conditions (Liss and Slater, 1974; Wanninkhof, 1992; Wanninkhof and Knox, 1996).

Breaking waves and bubbles

k increases non-linearly with increasing wind speed and sea state (Fig.1.1-6) and part of this increase is likely to be related to breaking waves and the injection of bubbles. Wave breaking injects bubbles into the upper layer of the ocean. Ambient air is therefore injected below the interface where diffusion occurs between the gases in the bubble and those dissolved in adjacent water. Bubbles can surface (disrupting the micro-layer and enhancing turbulence) and release therefore their final content or

they can dissolve completely. Some attempts have been made to describe the gas transfer due to breaking waves and bubbles (e.g. Asher et al. (1996), Woolf (1997), Asher and Wanninkhof (1998), Woolf et al. (2006)), but there are limited data with which to test each model.

Convective cooling

Cole and Caraco (1998) show an enhancement of k at low wind speeds (<2 m s^{-1}) in Lake Mirror that they attributed to convective cooling. Diurnal heat fluxes generate daytime surface ocean stratification and subsequent large nighttime buoyancy fluxes, leading to enhanced water turbulence, independently from wind stress. GasEx-2001 in the equatorial Pacific shows that this process is also significant in open ocean waters under low wind speed conditions (McGillis et al., 2004).

Water currents

In streams, the interaction of the gravity flow and bottom topography generates, due to bottom shear, turbulence that is frequently considered to be the main factor controlling k of sparingly soluble gases, in these sheltered systems where wind is usually very low. This has led to various parameterizations of the gas transfer velocity as a function of water current and depth based on empirical or conceptual approaches, reviewed by Bansal (1973) and more recently by Melching et al. (1999) and Gualtieri et al. (2006). The frequently referenced conceptual relationship of O'Connor and Dobbins (1958) relates k to water currents and depth :

$$k = 1.719 w^{0.5} h^{-0.5} \quad (67)$$

in cm h^{-1}, where *w* is the water current in cm s^{-1} and *h* is the depth in m.

This relationship has been shown to satisfactorily predict k at low wind speeds in estuarine environments based on measurements using the gradient flux technique and floating domes (respectively, Zappa et al. (2003); Borges et al. (2004a)). Borges et al. (2004b) showed that in the Scheldt estuary tidal currents can contribute up to 30% to k besides wind stress.

Rain

The relationship between rain and k has been examined in a series of laboratory experiments, in both freshwater (Ho et al., 1997) and seawater (Ho et al., 2004). Recent field measurements in a tropical reservoir confirm the conclusions and parameterizations from these laboratory experiments (Guérin et al., 2006). Raindrops falling on the water surface can significantly enhance the rate of gas exchange across the air-water interface and k increases systematically with the kinetic energy flux to the water surface supplied by the raindrops. Additionally, raindrops entrain bubbles also enhancing gas exchange. However, rain-induced air-water gas

exchange is mainly caused by turbulence-driven exchange processes (Ho et al., 2000). Recently laboratory experiments show that rain and wind combine linearly to influence air-water gas exchange (Ho et al., 2006).

On the whole, wind speed is recognised as the main factor on k, as its intensity determines the model to be used, the relative importance of additional processes (chemical enhancement, the ability surfactants to form a mono-molecular surface) and drives some additional processes such as wave breaking and bubbles. Hence, numerous studies aimed to constrain air-sea exchanges as function of wind speed. Besides making some sense theoretically, such relationships are very useful since wind speed is a variable that is easily measured on ships, can be modelled from pressure fields or derived from radar backscatter satellite imagery. Other predictors of water turbulence and hence k such as significant wave height show the same among of scatter than k-wind relationships (e.g. Nightingale et al. (Nightingale et al., 2000b)).

1.1.8.2 Empirical gas transfer relationships

Several methods have been used to estimate air-water gases exchanges, namely direct field measurement using the chamber method, eddy covariance, eddy accumulation methods, vertical gradient flux technique, gas mass balance in wind tunnels, assessment from natural and/or bomb produced ^{14}C, carbon mass balance, ^{222}Rn deficiency method and deliberate tracers (sulphur hexafluoride (SF_6) and tritium (^3He)).

We describe herewith some experiments which led to the most used k-wind relationships. It is worth noting that it is not the wind itself which drives gas exchanges across the interface, but wind-related effects on the interface - wind-generated turbulence and bubbles injection among others-. A k-wind relationship constrains the interaction between wind and wind-related effects of importance for gas exchange, turbulence for instance. However, numerous factors affect these interactions, as, fetch, bottom depth, surfactants,…, so that a k-wind relationship is, strictly speaking, only valid in the conditions it has been established. As pointed out by Wanninkhof (1992) wave fields over the open ocean “grow” over distances of hundreds of kilometers off shore suggesting that surface turbulence over the ocean influencing gas transfer might be fetch dependent. If we consider a k-wind relationship established in the open ocean, it intrinsically constrains the effect of wind stress on waves in the area where it has been established, and such interaction depends on the fetch for instance. In a sheltered coastal area with limited fetch, the effect of wind on waves will be different from the open ocean area, and corollary the effect of wind on gas transfer will be different. The reliability of the open-ocean k-wind relationship is then questionable. The same applies for the effect on wind on turbulence and waves as a function of bottom depth, for instance. Besides, non wind-dependent factors, thus hardly included in k-relationship, are of importance, like tidal currents in estuaries, stream currents in rivers, rain, occurrence of surfactants which depends in part of biological processes, etc. This explains in part the reason why

different k-wind relationship exist, and underline that while choosing which k-wind relationship to be applied to compute air-water gas exchanges in an area, attention must be paid to use a relationship established in comparable conditions to this area, if possible.

Liss and Merlivat (1986) relationship

This relationship is derived from a deliberate tracer experiment with SF_6 in a lake (Wanninkhof et al., 1985) for wind speeds up to 13 m s^{-1} and extended to higher wind speeds based on wind tunnel experiments (Broecker et al., 1978; Broecker and Siems, 1984). This relationship reflects some of the considerations of the models described above (especially in the way Sc is taken into account) and distinguishes three regimes: a smooth surface regime (68), a rough surface regime, i.e. capillary waves (69) and a breaking wave regime (70):

$$k = 0.17\, u_{10}\left(\frac{Sc}{600}\right)^{-2/3} \quad \text{for} \quad u_{10} \le 3.6 \tag{68}$$

$$k = (2.85u_{10} - 9.65)\times\left(\frac{Sc}{600}\right)^{-0.5} \quad \text{for } 3.6 < u_{10} \le 13 \tag{69}$$

$$k = (5.9u_{10} - 49.3)\times\left(\frac{Sc}{600}\right)^{-0.5} \quad \text{for } 13 < u_{10} \tag{70}$$

in cm h^{-1}, where 600 is the Schmidt number in fresh water at 20°C and u_{10} denotes wind speed at a height of 10 m (m s^{-1}). Wind speed depends on the height and can be converted using the drag coefficient (e.g. Hwang (2005)). This relationship is probably an underestimate as noted by Wanninkhof (1992) since SF_6-derived measurements carried out in a lake are strongly effected by fetch limitation.

Wanninkhof (1992) relationship

It is an elegant theoretical fit to the bomb derived ^{14}C inventory at global scale (Broecker et al., 1985) and in the Red Sea (Cember, 1989). This quadratic relationship was favorably compared with dual tracer experiment (Wanninkhof and Thoning, 1993; Wanninkhof et al., 1997). Wanninkhof (1992) pointed out that k is not linear with wind speed. The variability of wind speed and its time scale are therefore important in calculating the gas transfer. He then proposed two relationships, one for short term (71) measurements of steady wind as provided by shipboard anemometers or remote sensing data and one to be used for long term (72) averages of wind speed. Both relationship are linked by the global ocean wind speed frequency distribution which can be approximated using the Rayleigh probability distribution function (Hennessey, 1977; Wentz et al., 1984):

$$k_{(\text{short term})} = 0.31\, u_{10}^2 \times\left(\frac{Sc}{660}\right)^{-0.5} \tag{71}$$

$$k_{(\text{long term})} = 0.39\, u_{10}^2 \times \left(\frac{Sc}{660}\right)^{-0.5} \quad (72)$$

in cm h^{-1}, where 660 is the Schmidt number in seawater water at 20°C.

Wanninkhof and McGillis (1999) relationship

This relationship is derived form a SF_6 and ^3He dual tracers experiment carried out in the North Atlantic that compared favorably with covariance measurements carried out during Gas Ex-98. A short-term (73) and a long-term (74) cubic relationship were proposed:

$$k_{(\text{short term})} = 0.0283\, u_{10}^3 \times \left(\frac{Sc}{660}\right)^{-0.5} \quad (73)$$

$$k_{(\text{long term})} = \left(1.09\, u_{10} - 0.333\, u_{10}^2 + 0.078\, u_{10}^3\right) \times \left(\frac{Sc}{660}\right)^{-0.5} \quad (74)$$

where 660 is the Schmidt number in seawater water at 20°C.

Wanninkhof and McGillis (1999) k-wind relationship was fitted to the data to constrain the global ocean inventory of bomb ^{14}C of DIC given by Broecker et al. (1985). It has been claimed that the bomb radiocarbon ocean inventory of Broecker et al. (1985) is an over-estimate, hence the Wanninkhof (1992) and Wanninkhof and McGillis (1999) parameterizations would over-estimate k (Hesshaimer et al., 1994; Peacock, 2004).

Nightingale et al. (2000b) relationship

This relationship is based on part on previous tracer experiments (Wanninkhof et al., 1993; Wanninkhof et al., 1997) and in particular revised Watson et al. (1991) SF_6 and ^3H North Sea experiment plus additional experiments in the North Sea involving a third non-volatile tracer, the spores of the bacterium *Bacillus globigii var. Niger.* The following relationship was proposed:

$$k = (0.22u_{10}^2 + 0.33\, u_{10}) \times \left(\frac{Sc}{660}\right)^{-0.5} \quad (75)$$

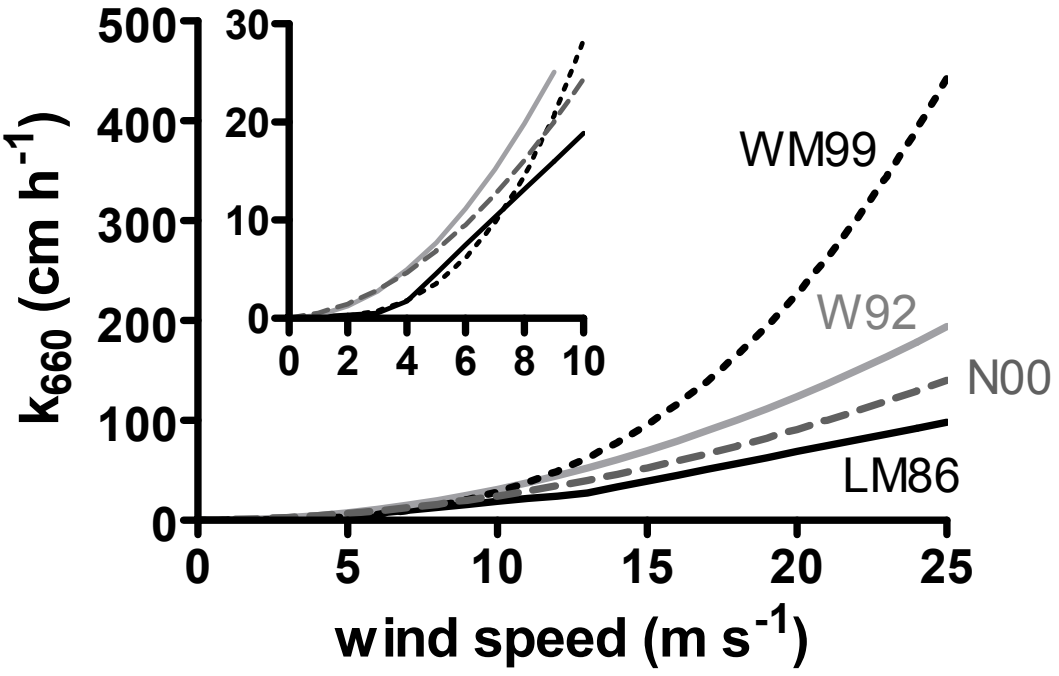

Figure 1.1-6 Summary of short-term relationships between k660 and u10. Black solid line (LM86): Liss and Merlivat (1986)- eqs.(68)(69)(70), medium grey dashed line (N00): Nightingale et al (2000)-eq.(75), light grey solid line (W92): Wanninkhof (1992)-eq.(71), black dotted line (WM99): Wanninkhof and McGillis (1999)-eq.(73).

It is worth noting that high wind speeds are regularly encountered in the Southern Ocean, while the different k-wind relationships greatly differ at high speed (Fig. 1.1-6). This leads to significant differences of k_{660} values obtained with the 4 k-wind relationships, especially for wind speed above 15 m s^{-1}. Indeed, there are very few measurements carried out at high wind speed which would allow to constrain k-wind relationships at high wind speed. In order to fill this gap, two experiments were carried out in the Southern Ocean area. The experiment of Jean-Baptiste and Poisson (2000), despite the remoteness of the site, conducted out a SF_6 and ^3H release experiment in the Lake Suisse of the Kerguelen Archipelago, which at some points is comparable with a natural wind tunnel which would be submitted to high wind stress. Their measurements agree with the experiment of Wanninkhof et al. (1993) while k-wind relationship from Liss and Merlivat (1986) underestimate k by 40%. However, they also observed a large range (from 0.9 up to 0.2) of the Sc exponent and questioned the validity of the normalization method for k_{CO2} from gas transfer experiments based on dual tracers, especially in high-wind regimes. Wanninkhof et al. (2004) carried out some air-sea gas transfer measurements with dual deliberate tracers (SF_6 and ^3H) during the Southern Ocean Iron Fertilization experiment (SOFex) carried out in the Pacific sector of the Southern Ocean. Due to uncertainties in the measurements, it was difficult to definitely determine if a quadratic or cubic k-wind relationship was the best fit of their results, yet the cubic relationships tended to provide better results. On the whole, both experiments, lead us to conclude that both Wanninkhof (1992) and Wanninkhof and McGillis (1999) k-

wind relationships should be used to derive CO_2 fluxes from pCO_2 measurements in the S.O. but it is worth noting that these issue deserves further investigations.

1.2 The Southern Ocean

A "barren" ocean full of paradoxes…

For decades, the Southern Ocean was considered as a somewhat "barren" area, yet quite full of paradoxes. The persistence of high concentration of macronutrients (nitrate and phosphate) and relatively low chlorophyll a concentrations raised several long-lived intriguing questions. First striking feature, the low productivity of surface waters despite the persisting high concentration of macronutrients was most commonly referred as the "Antarctic Paradox", yet indeed this corresponds to High Nutrient-Low Chlorophyll (HNLC) definition. Corollary, this first paradox comes to a second one; primary production was, at first sight, insufficient to support the population of Southern Ocean grazers, including krill, copepods, microzooplancton, etc, (whose biomass is high enough to provide enough food resources to the largest animal on earth, the blue whale). Finally, another striking feature was the discrepancy observed between the low rate of production of diatoms in the surface waters of the Southern Ocean, and the opal abundance in the sedimentary deposits in Antarctica, which was known as the "opal paradox".

Improvement of measurement techniques allowed to resolve the two last paradoxes. New measurements of biogenic silica production rates, opal rain rates in the water column and opal sediment burial rates for the Indian Ocean sector of the Southern Ocean showed that the assumed opal paradox is a result of underestimated opal production rates and overestimated opal accumulation rates (Pondaven et al., 2000). Furthermore, up scaling of primary production derived from remote sensing yield to a significant increase in the estimate of primary production for the Southern Ocean consistent to grazer biomass (Arrigo et al., 1998). Work of Martin et al. (1990), was the beginning of an active research on the role of the iron as the limitating micronutrient of primary production of the HNLC waters of the southern ocean which make the notion of "Antarctic paradox" somewhat obsolete.

1.2.1 Ocean dynamic and zonation of the Southern Ocean

1.2.1.1 General considerations

Ocean dynamic has been described in details by Tomczac and Godfery (1994). Briefly, even if the S.O. is not strictly speaking recognized by the International Hydrographic Bureau which generally delimits sea and ocean with geographical criteria - boundaries are related to continent or referenced with regard to land positions -. However, the S.O. connects three main ocean basins (Pacific, Atlantic and Indian) and its unique features are repeated in each basin; on this ground the Southern Ocean undoubtedly deserves its own name. Its most conventional definition is the region south of the Subtropical Front (STF). If we refer to ocean dynamics, a classical definition of this definition is the line where the tropical/temperate dynamics - a balance between three dynamic regions, the ocean interior, the surface boundary of Elkman Layer and the western boundary region – break downs. This occurs where the permanent thermocline reaches the surface, i.e. at the Subtropical Convergence. Its southern limit is marked by a frontal region of limited width known as the Subtropical Front (STF). It is worth noting the northern limit of the S.O. is not a well defined line, but a broad zone of transition between tropical/temperate and polar ocean dynamics. This limitation given, the surface are of the S.O. represents approximately 77 10^6 km², corresponding to 22% of the surface of the world ocean. It encompasses several seas, some of them being permanently ice covered: Ross Sea, the Bellingshausen Sea, the Scotia Sea and the Weddell Sea.

Among its particular features, Tomczac and Godfery (1994) pointed out that the S.O. is the only region where the flow of water can continue all around the globe – the circumpolar flow - nearly unhindered and the circulation therefore comes closest to the situation in the atmosphere. Furthermore, the permanent thermocline reaches the surface in the Subtropical Convergence and does not extend into the polar regions. Indeed, temperature differences between the sea surface and the ocean floor close to the continent are below 1°C and generally do not exceed 5°C. In the same way, density variations with depth are small and the pressure gradient force is more evenly distributed over the water column. As a result, currents are not restricted to the upper few hundred meters of the ocean but extend to great depth. Observation in Drake Passage show mean current speeds of 0.01 – 0.04 m s^{-1} at 2500 m depth, or 10-30% of the speeds observed at the 500 m level. The Circumpolar Current has the largest mass transport of all ocean currents, as it moves a 2000 m thick layer of water with speed comparable to other surface currents.

Taking into account that circumpolar current is present at all depth, the bottom topography (figure 1.2-1) has a much larger impact on the current and in the hydrology in general than in the any ocean. Garaboato et al. (2004) reported that turbulent mixing over rough topography in the Southern Ocean is remarkably intense and widespread. Mixing rates exceeding background values by a factor of 10 to 1000 are common above complex bathymetry over a distance of 2000 to 3000 km at depths greater than 500 to 1000 m. Some interactions between sea floor topography and ocean dynamics (in particular frontal patterns) are discussed in the chapter 2.1.

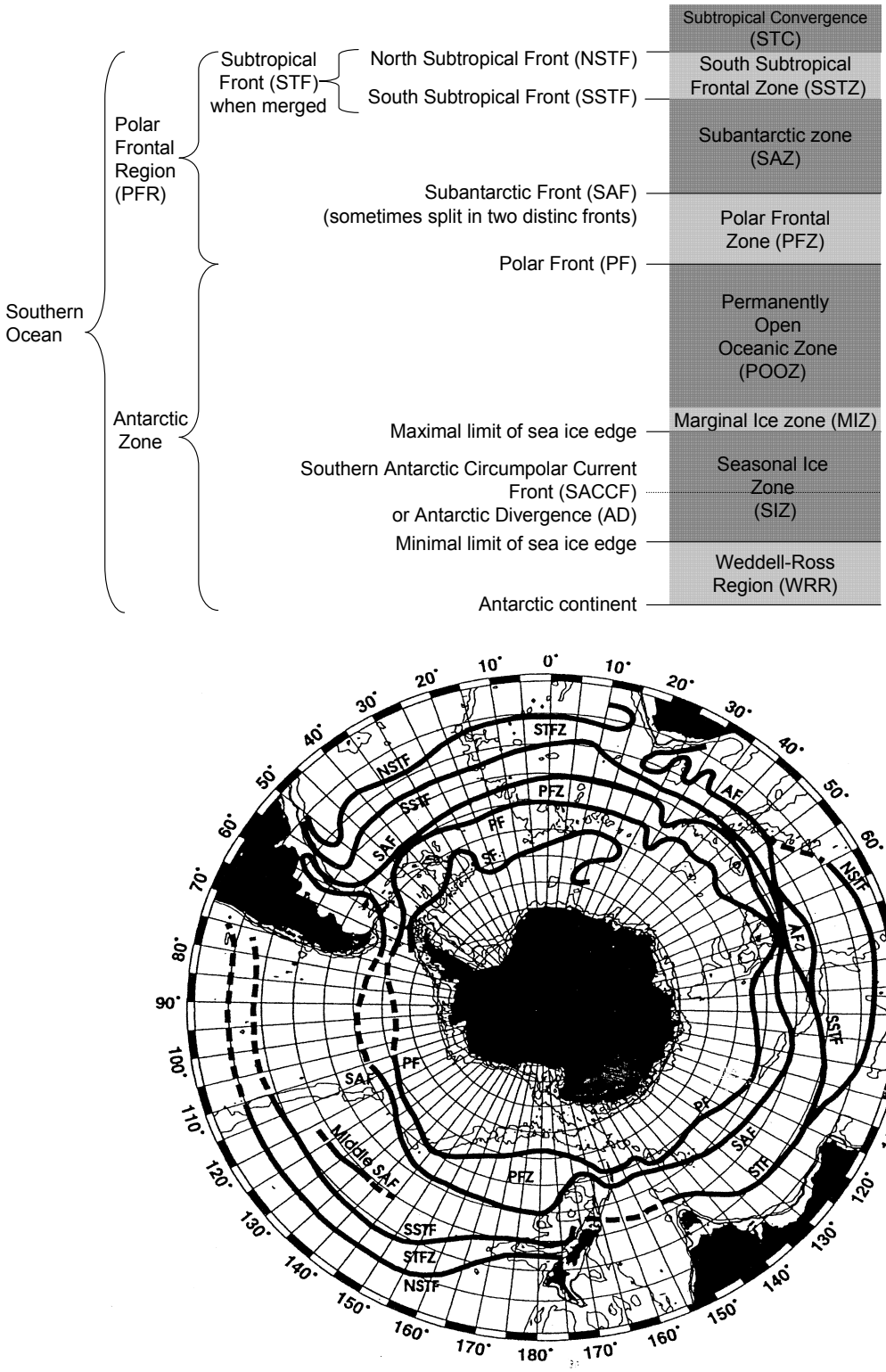

Figure 1.2-1 Top - Main frontal systems encountered in the S.O. (from north to south). The fronts or the sea ice edge determine discriminate the different provinces of the S.O.. Bottom, S.O. frontal scheme based on salinity and temperature profiles after Belkin and Gordon (Belkin and Gordon, 1996). The Antarctic Zone (AZ) denotes the region south of the PF. Dashed lines show poorly defined frontal positions. Sometimes the PFR refers as a narrow band surrounding the PFZ (Moore and Abbott, 2002).

Wind regime in the S.O. is largely dominated by a circumpolar belt of geostrophic winds dominated by frequent storms which start in the north and angle south-eastwards to die near 65°S where the winds turn into easterlies. Close to the

Antarctic continent wind direction is reversed from eastward to westward. Polar easterlies blows along the coast which drive the East Wind Drift, a narrow coastal current which flows westwards against the dominant eastward flowing Circumpolar Current.

The combined effect of consistently large wind speeds with little variation in wind direction, and no land barriers lead to the build-up of a fully developed sea. The combination of infinite fetch around Antarctica and high average wind stress makes the Southern Ocean the region with the largest average wave height.

1.2.1.2 Fronts and zonation of the Southern Ocean

The Southern Ocean is characterized by a latitudinal succession of circumpolar frontal structures which delimit different zones. The Subtropical Convergence is of some 1000 km meridional extent and is the subduction region for Central Water. It corresponds to a narrow band around Antarctica where the salinity changes rapidly between 35.0 and 34.5 from north to south and temperature drops rapidly as well. Its Southern limit is the STF. This STF can split in two fronts the North Subtropical Front (NSTF) and South Subtropical Front (SSTF). The area between these two fronts is then called the Subtropical Zone (STZ). Southwards, two other frontal structures are encountered: the Subantarctic Front and the Polar Front. These frontal structures together with sea ice edge delimit several zones whose terminology is provided in the figure 1.2-1. Map of the front of this figure have been determined form salinity and temperature profiles. However remote sensing data allow a synoptic approach using distribution of sea surface temperature (Moore et al. (1999), chapter 2.1) or altimetry (Park and Gambéroni, 1995; Kostianoy et al., 2003).

The figure 1.2-2 provides a hydrological section through the S.O.. It describes the different water masses and relates sharp gradients in temperature and salinity to frontal structures. It is worth noting that the ranges of values associated to the frontal structures vary in time and the fonts generally refer to the maximum of the horizontal gradient (chapter 2.1). Frontal structures also include meanders, convolutions and eddies of various sizes (section 2.2.5.1). They can merge (section 2.2.5.1) or split (chapter 2.1).

The positions of the fronts present large longitudinal differences which are partly due to the interaction with bottom topography while, large shifts in the latitudinal positions occurs (chapter 2.1), probably in response to variations in the wind stress. How this variability in the atmospheric conditions translates into variability of the oceanic conditions is not known, but it can reasonably be argued that variations in the position of the Subtropical Front might be larger in regions of strong meridional shifts of the boundary between the Trades and the Westerlies than elsewhere.

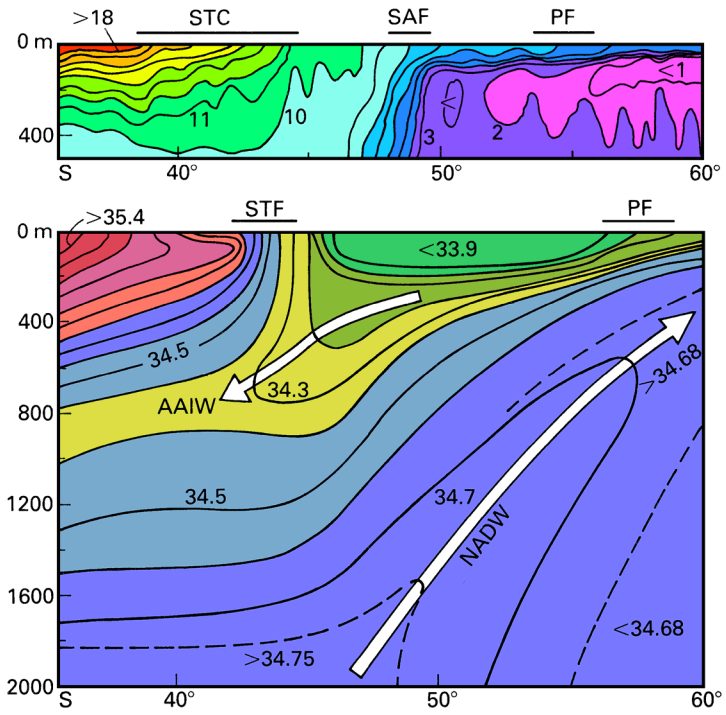

Figure 1.2-2 Hydrological sections through the S.O. (summer conditions). Top: temperature section in the eastern Indian sector. The Polar Frontal Zone is indicated by the 3-9°C isotherms and the split into the Subantarctic (SAF) and Polar (PF) Fronts by the crowding of isotherms at the surface around 7-9°C and 5-6°C. The Subtropical Front (STF) is indicated by the crowding of isotherms near 13-15°C within the Subtropical Convergence (STC). From Ewdards and Emery (1982). Bottom: salinity section in the eastern Atlantic sector. Crowding of isohalines near 34.5 indicates the STF. The Antarctic Divergence (or Southern Antarctic Circumpolar Front – SSACF) is located poleward of the section; near 65°S its salinity maximum is found just below 150 m.upwelling of North Atlantic Deep Water (NADW) towards the divergence is indicated by the rise of the salinity maximum and sinking of Antartcic Intermdiate Water (AAIW) from the Polar Front by the associated salinity minimum. Based on Bainbridge (1980). From Tomczak & Godfrey (1994)

The zones delimited by the frontal structures are provided in the figure 1.2-2. Their surface area are provided in the table 1-3

Zone	Surface area (km²)
SAZ and PFZ	$3\ 10^6$
POOZ	$14\ 10^6$
SIZ	$16.\ 10^6$
WRR	$0.9.\ 10^6$

Table 1-3. Surface area of the zones of the Southern Ocean. After (JGOFS Synthesis group, 2001).

1.2.1.3 Water masses and circulation

The Antarctic Divergence or Southern Antarctic Circumpolar Current Front mark the southern limit of Circumpolar Current and is produced by upwelling of water in the transitional zone between Westerlies and Easterlies. It corresponds to a latitudinal salinity maximum. At the surface the maximum is masked by low salinity from high

precipitation and additional melting of ice, but it is clearly discernible below 150 m (figure 1.2-2, bottom). The upwelling is unique in that the water reaching the surface comes from great depths; in the Atlantic Ocean, it is lifted from between 2500 m and 4000 m. The deep upwelling occurs for two reasons. Firstly, there is equatorward movement in the intermediate water (Antarctic Interemedate Water -AAIW) and above, and again in the bottom water (Antarctic Bottoma Water (AABW) below 4000m m depth. Poleward movement must therefore occur in the intermediate depth range due to the mass conservation, and this water must be lifted to the surface somewhere, to replace the water which sinks to form the Intermediate and Bottom Waters. The general southward and upward movement of high salinity North Atlantic Deep Water from depths below 2000 m is reflected in the shape of the isohalines. A substantial portion of this water comes to within 200 m of the surface at the Antarctic Divergence where it warms the surface water, melting the sea ice and the snow that falls on it, and sinks again at the PF. By the time it is subducted it can no longer be recognized as Deep Water, having been warmed and diluted by rain and snow on its northward passage, and is then known as the low salinity Antarctic Intermediate Water. In the S.O. the effect of precipitation on sea surface salinity is augmented by the loss of salt from the surface in winter, as brine rejected by sea ice sinks to great depth, and the melting of ice in summer; this explains the low salinity of near-surface water in the Antarctic region.

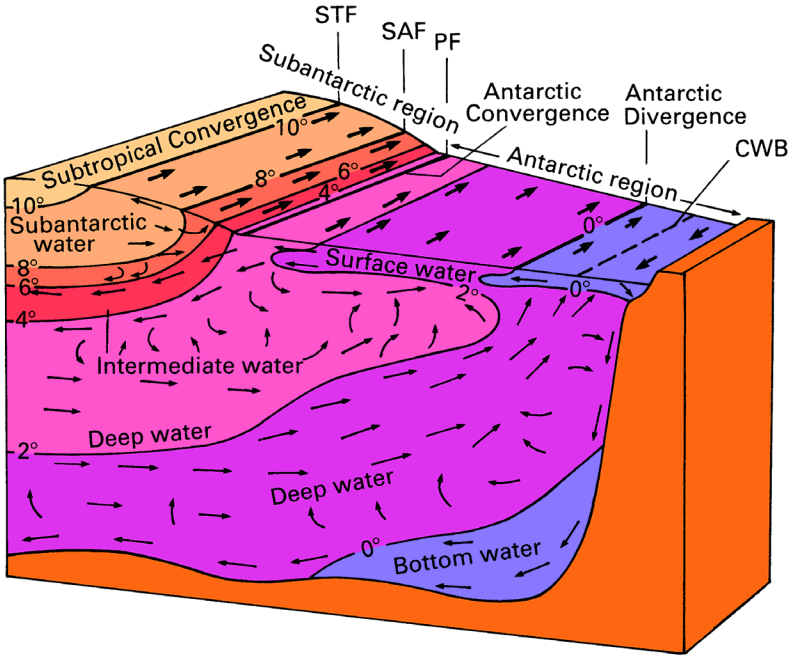

Figure 1.2-3 Interplay of strong zonal currents, meridional flow caused by deep convection, convergences and divergences, and water mass formation and spreading in the Southern Ocean. This is a long-lived block diagram adapted from Sverdrup et al. (1942). Names of the zones slightly differ with current accepted ones from the figure 1.2-1. CWB: Coastal Water Boundary).

Modification of properties in the vicinity of the fronts is particularly strong during winter when convection creates a deep surface layer with water of uniform temperature and salinity in a region of usually strong horizontal and vertical gradients. Water in such layers is often called Mode Water and the winter water in the SAZ referred to as Subantarctic Mode Water (SAMW). This water contributes to

the Central Water of the southern hemisphere. In some areas it is responsible for the formation of Antarctic Intermediate Water (AAIW). In the Antarctic zone, water at the surface has very low temperatures, ranging down to the freezing point of -1.9°C, and low salinities as a result of ice melting in summer. This water is called Antarctic Surface Water. In the Subantarctic zone, surface water has a larger temperature and salinity range since seasonal variations of solar heating, rainfall, and evaporation become more important. The temperature range of this Subantarctic Upper Water spans 4 - 10°C in winter and 4 - 14°C in summer, with a salinity varying between 33.9 and 34.9 and reaching as low as 33.0 in summer as the ice melts. This produces a shallow surface layer of low salinity and an intermediate salinity maximum between 150 m and 450 m depth.

The transformation of North Atlantic Deep Water into Antarctic Intermediate Water occurs as a mixing process between the deeper waters and surface water at the Antarctic Divergence. South of Australia Intermediate Water consists of some 60% Subantarctic Upper Water and 40% Circumpolar Water. Antarctic Circumpolar Water is formed through the missing of NADW and Antarctic Bottom Water.

1.2.1.4 Deep water formation

Origin of Antarctic Bottom Water lies in deep convection at the continental shelf driven by the freezing of sea ice but its final properties are shaped during intense mixing with the water of the Circumpolar Current (Circumpolar Water) while sinking to the bottom. The areas where convective sinking occurs are believed to be relatively

limited in size. With the exception of the Bransfield Strait, the sinking occurs underneath the ice (Weddell Sea, Ross Sea, and along the Adélie Coast and Enderby Land). When sea ice forms, it freezes freshwater and leaves most of the salt behind in the ocean water, resulting in an increase in salinity of the ocean water. Sea ice takes up only about 10~15% of the seawater salt. Above shelves, this can increase the density of the surface waters to the point where they flow off the shelf and into deep waters. The Antarctic Bottom Water (AABW) is the general name for the deep water formed over the continental shelf or in deeper water in the Antarctic.

The Weddell Sea probably contributes most to Bottom Water formation. The water as it sinks underneath sea ice flows westward under the influence of the Coriolis force, forming a thin layer of extremely cold water above the continental slope. It mixes with the overlying water, which is recirculated with the large cyclonic eddy in the central Weddell Sea to form the Weddell Deep Water.

Above the shelf surface waters freezes and forms either the Weddell Sea Winter Water or the Eastern Shelf Water, which subsequently flows either down the continental slope or southwards under the ice shelf. Under the Ice, this water melts the shelf ice, and due to the high pressure under the ice shelf, the water becomes fresher and supercooled, and forms Ice Shelf Water (ISW). ISW flows northwards again and its density becomes higher than the surrounding water. When the ISW descends along the continental margin it attains high velocity and consequently entrains ambient water, to form Weddell Sea Deep Water and Weddell Sea Bottom Water. On reaching 65°S some of the water gets injected into the Circumpolar Current, where it continues to mix with the Circumpolar Water. The further path of Antarctic Bottom Water surrounds Antarctica and receives significant input from the

Adélie Shelf and the Ross Sea where cold and saline water is injected from the surface. Eventually, the water spreads from the Circumpolar Current (i.e. with the properties of Circumpolar Water) into all three oceans. Estimates of northward flow of Antarctic Bottom Water range from 2.5 to 5 Sv.

1.2.2 The biological pump of the Southern Ocean.

The biological pump is the suite of biologically-mediated processes that transform CO_2 to biogenic carbon and transport it from the euphotic zone to the mesopelagic and bathypelagic regions, where long term circulation prevent the release to the atmosphere of the CO_2 issued from remineralization, at the time scale of ocean overturning (about 1000 yr). In the euphotic layer, CO_2 is taken up by photosynthesising organisms which require for their growth light, inorganic nutrients (phosphate, ammonium or/and nitrate, and dissolved silica) and inorganic micronutrients (like iron). Depending on the phytoplankton assemblages and associated food-web, the organic carbon fixed through photosynthesis is either released as CO_2 in the mixed layer by microbial respiration or exported below the pycnocline as phytoplankton cells, plankton detritus or zooplankton faecal pellets. In the latter case, a larger fraction of carbon is retained within the ocean rather than released back to the atmosphere.

The net uptake of carbon through the biological pump depends on:

- light conditions, availability of macro- and micronutrients and top-down control by grazers, that set net primary production rates, ecosystem structure and sedimentation rates
- mineralization of the exported carbon throughout its descent toward the ocean floor, mineralization in the sediments and final burial rate in the sediments.

Nowadays, the crucial role of iron in fostering primary production in the HNLC Southern Ocean is well documented (section 1.2.2.2). Low concentrations of iron, a micronutrient involved in the fixation of nitrogen/nitrate by phytoplankton, hampers large primary production. In addition, light limitation, silicate limitation and grazing also control primary production and the succession of phytoplankton assemblages. This succession leads to changes in primary production rates, food web structure, sedimentation rates and overall organic carbon export, with an overall impact on the efficiency of the carbon pump. We review hereafter the contribution of primary and secondary producers to the carbon pump of the S.O. and the role of iron in the limitation of phytoplankton growth. Such review should not overcome the fact that the effficiency of the biological pump does not rely only on the overall primary production, but also on organic carbon export to the deep waters and mesotrophic processes.

1.2.2.1 Primary producers and their impact on the biological pump

Microbial network and related regenerated production

Pasquer et al. (2005) point out that there is a background plankton ecosystem of pico/nano phytoplankton, which recycles within the euphotic zone most of the available chemical elements (C, N, P, Fe), and acts as an efficient retention system (e.g. (2000)). Sedimentation rates of pico/nano phytoplankton are low, owing to their small size, and their abundance is limited by protozoans grazing pressure. As a consequence, pico/nano phytoplankton do not export much carbon. On the whole, such microbial network and related regenerated production regime do not export significant amount of organic carbon and constitute a low-efficiency biological pump. Microbial network regenerated production based ecosystems are ubiquitious and dominate in iron-poor and deep mixed areas like the POOZ. In such ecosystems the major form of nitrogen is ammonia which is easily utilised by the phytoplankton cells, as opposed to nitrate which must be reduced by the iron-rich enzymes nitrate- and nitrite reductase.

Major phytoplankton groups of productive regions-New production

When growth conditions including light, major macronutrients (N, P, Si) and micronutrients (Fe) concentrations are more favourable, intense blooms of generally larger-sized phytoplanktoners which are able to use nitrate as the primary N source, provided sufficient iron availability. Such ecosystems result in new production. In favourable conditions, four main taxonomic groups are able to support significant C export: diatoms, Phaeocystis sp., N_2-fixing diazotrophs, and coccolithophorids. diatoms, Phaeocystis sp account for most of the biological pump in the S.O.. They do not bloom together and are found in different biogeochemical zones of the S.O..

Diatoms

Diatoms account for about one third of the annual primary production in the global ocean (Nelson et al., 1995; Sarthou et al., 2005). In the S.O. diatoms are abundant and can represent at the peak of the bloom as much as 80% of the total phytoplankton biomass. However, the larger iron requirements of nitrate using diatoms place them at a competitive disadvantage with the smaller size classes of phytoplankton at low iron concentrations. Timmermans et al. (2006) reported that half-saturation constants (K_m) for growth of 4 S.O. diatoms species were low (0.19–1.14 nmol L^{-1} Fe_{diss}), and close to the ambient Fe_{diss} concentrations of 0.2 nmol L^{-1}. However, the range in K_m varied with the size of diatom, being larger for large species. Hence iron concentration affects diatoms assemblages, low concentration hampering the growth of the large species.

At the end of the bloom, large diatoms usually sink massively. Along the melt-water regions of the Antarctic Peninsula, biomass of diatoms can be 10 to100-fold higher than those of average oceanic regions, being the main food for the abundant larval forms of the krill *Euphausia superba* (Capella et al., 1992; Nelson et al., 1995).

On the whole, diatoms blooms are an efficient pathway for biologically-mediated CO_2 sequestration, owing to their high sedimentation rates or the grazing by large zooplankton.

Phaeocystis

Although characterized by a complex life cycle involving free flagellated cells, the most striking feature of *Phaeocystis sp.* blooms is the occurrence of large (100 –1000 µm) colonies. These are composed of mucus-like polysaccharides, which form TEP, that may potentialyl lead to particule aggregation at the end of the bloom (Hong et al., 1997; Engel et al., 2004b; Schoemann et al., 2005). Such aggregates significantly enhance sedimentation of organic carbon (Passow, 1991). Within wind-driven, nutrient-rich surface mixed layers (SML) of 80 m depth of the Southern Ocean, pelagic light-adapted phytoplankton as diatoms require meltwater-induced stability of the water column to provide sufficient light for initiation of their spring- summer blooms in coastal waters. Populations of *Phaeocystis antarctica*, a shade-adapted colonial prymnesiophyte, may dominate in the more deeply mixed waters because of their ability to maintain near-maximal photosynthetic rates at much lower irradiance levels than diatoms as proposed by Arrigo et al. (1999). *P. antarctica* bloom first in spring within coastal Antarctic waters (Perrin et al., 1987; Moline et al., 1997) succeeded by the other major functional groups of diatoms and cryptophytes (Smetacek et al., 1990; Jacques and Panouse, 1991) as sea ice melting drives enhanced stratification. DiTullio et al. (2000) reported the early and rapid carbon export of *P. antarctica* blooms to deep water and sediments of the Ross Sea, and suggest that senescence may not be a prerequisite for *P. antarctica* carbon export. By comparing C:P ratio of diatoms and *P. Antarctica,* Arrigo et al. (1999) suggested that *P. antarctica* can be potentially more efficient than diatoms in fixing atmospheric CO_2. These authors also pointed out that predicted enhanced upper ocean stratification (in response to an increase of temperature) may favour light-adapted diatoms and then reduce the ability of the ecosystem to absorb CO_2. However, Walsh et al. (2001) pointed out that the decrease of sea ice extent could lead to deeper surface mixed layers. This should drive a shift of the food web, from diatoms grazed by euphausiids to smaller shade-adapted flagellates consumed by salps.

Diazotrophs

Diazotrophs such as the colony-forming cyanobacteria *Trichodesmium sp.* play an unique role in the nitrogen global cycle due to their ability to fix atmospheric N_2. Cyanobacteria known as “nitrogen fixers” accomplish this energetically-expensive process to produce biologically available nitrogen to meet their N requirements. This newly “fixed” nitrogen makes its way through the microbial network into other organisms and the environment (LaRoche and Breitbarth, 2005). Nitrogen fixation provides a source of new nitrogen from the atmosphere rather than from the deep ocean and enhances new production and fixation of atmospheric CO_2. However, growth of *Trichodesmium sp.* is iron limited (Rueter, 1988; Rueter et al., 1990; Berman-Frank et al., 2001) as nitrogen fixation relies on the nitrogenase enzyme, which contains iron. Temperature also controls the growth of cyanobacteria is the temperature has reported by (Murphy and Haugen, 1985).

Coccolithophore

The production of CO_2 through calcification is superimposed to the uptake of CO_2 by photosynthesis by coccolithophores but these organisms generally lead to net sink of CO_2. Blooms of *Emiliania huxleyi* may be more efficient carbon sinks than other phytoplankton blooms, as a result of the higher sedimentation of coccolithophore cells and zooplankton feacal pellets, due to the high density of calcite (Buitenhuis et al., 2001). This is supported by sediment trap data below 1000 m which show that ballast minerals, and in particular $CaCO_3$, drive the sinking of organic carbon to the bathypelagic zone (Armstrong et al., 2001; Klaas and Archer, 2002). Besides the ballast effect, C export by coccolithophores is favoured by production of TEP (Engel et al., 2004a; Delille et al., 2005). However, even if coccolithophores have been observed in the Weddell Sea as a consequence of oceanic transport from Agulhas Current (Winter et al., 1999), blooms of these organisms are concentrated in sub-polar and temperate latitudes (Iglesias-Rodriguez et al. 2002, chapter 2.2). The S.O. south of the polar front is the only major oceanic regions with the high Arctic Ocean where coccolithophores are very rare or absent (Davidson and Marchant, 1992). Coccolithophores develop preferentially in highly stratified water, due to high light requirement (Dower and Lucas, 1993), while open Southern Ocean waters are characterized by very deep mixed layers. Furthermore, coccolithophores are sensitive to micronutrients limitation, in particular iron and zinc (Schulz et al., 2004; Xu et al., 2005). Conversely, it should be noted that the inventory of particulate inorganic carbon (PIC) inferred from remote sensing (Brown and Yoder, 1994; Balch et al., 2005) exhibits huge amounts of PIC in the whole S.O. during the phytoplankton blooming season. Hence, the abundance of calcifying organisms in the S.O. certainly deserves further investigation.

1.2.2.2 High nutrients - low chlorophyll, the role of iron

"Give me a half tanker of iron, and I will give you an ice age." John H. Martin

In the 1930s, Joseph Hart speculated that HNLC areas might be due to an iron deficiency. Some decades later, J.H. Martin investigated the presence of iron in plankton and highlighted that the concentration of iron in the oceans was overestimated due to analytical flaws (mainly contamination). By developing and applying clean trace metal analytical techniques, J.H. Martin and co-workers evidenced that metal concentrations in the ocean were orders of magnitude lower than previously thought that in the HNLC regions iron concentration was exceedingly low or non-existent. They then hypothesised that iron acts as a micronutrient for phytoplankton production, and therefore the lack of iron was the sole cause for such low phytoplankton levels in HNLC waters. J.H. Martin tested this hypothesis in the late eighties in the north-east Pacific subarctic waters and showed that iron enrichment strongly stimulates phytoplankton growth (1988). He also tested this hypothesis in the Drake Passage, and claimed that iron levels could in part be responsible for past glacial periods (Martin et al., 1990; Martin, 1990). The impact of trace metals on phytoplankton growth was also investigated in the Weddell Sea

(DeBaar et al., 1990; Buma et al., 1991) that lead an intense research effort on iron fertilization issues in the Southern Ocean (Boyd et al., 2000; De Baar et al., 2005).

The assimilation of nitrate by microalgae is mediated by a group of enzymes called assimilatory reductases, which come in both nitrite- and nitrate-reducing varieties. Butler (1998) pointed out that many essential life processes, besides nitrogen fixation, such as photosynthesis, respiration, proteolysis, and the enzymatic equilibration of carbon dioxide and bicarbonate involve multi-electron transformations or hydrolytic transformations. The essential steps in all of these processes are catalyzed by metalloenzymes which contain iron and other transition metals.

Iron-enrichment experiments (both shipboard and in situ) and survey of naturally iron-enriched regions suggest that iron fosters large class of phytoplankton (DeBaar et al., 1990; Martin et al., 1990; Buma et al., 1991; Boyd and Abraham, 2001) mainly chain diatoms (de Baar et al., 1995; De Baar et al., 2005; Lancelot et al., 2006). However, nanoplankton or picoplankton such as *Trichodesmium* can be also be iron limited (section 1.2.2.1).

Since the first in situ iron fertilization experiment IronEx-1 (Iron Experiment -1) - (Martin et al., 1994; Coale et al., 1996a; Coale et al., 1996b) nine other have been conducted so far. All these experiments have shown a strong stimulation of primary production by iron addition. However, the impact on the carbon pump does not only rely on enhanced primary production. The comparison of the nine experiment by de Baar et al. (2005) shows that the efficiency of iron fertilization in terms of CO_2 uptake is inversely correlated with the depth of the mixed layer that controls the light availability for phytoplankton growth. In addition to light conditions, temperature and grazing affect the overall primary production in the mixed layer. Even if large diatoms, which are generally associated to strong downwards fluxes of biogenic matter, benefit from iron addition, the efficiency of iron addition in terms of export of organic carbon remains to be firmly proven (De Baar et al., 2005). For instance, during the Southern Ocean Iron Enrichment Experiment (SOIREE) (Boyd et al., 2000), there was no significant increase in the vertical export flux of biogenic particules (Charette and Buesseler, 2000; Trull and Armand, 2001; Nodder and Waite, 2001) while during Southern Ocean Iron Experiment (SOFeX), Buesseler et al. (2004) reported carbon fluxes similar in magnitude to those of natural occurring blooms in the Southern Ocean.

Recently, Dehairs et al. (2006) observed on cultures of *Phaeocystis antarctica* (Haptophyceae) and *Thalassiosira gravida* (diatoms), two widespread phytoplankton species of the Southern Ocean, that there was no effect of iron enrichment on the saturating light intensity. This underlines that light limitation remains a crucial factor for phytoplankton growth even in iron-replete areas, as also suggested by de Baar et al. (2005). In contrast, iron addition affects the morphological forms, enhancing the presence of the colonial form compared to the free-living cells for *P. antarctica*, and increasing the occurrence of long chains of diatoms versus free living cells for *Thalassiosira gravida*. This is relevant for the efficiency of the biological carbon pump since the morphological forms of primary producers determines its fate and cycling in the planktonic food web. Free-living cells lead to carbon retention within the microbial food-web. Larger structures (colonies or chains) also participate in the microbial food web by liberating single cells, or lead to C export through aggregates. On the whole, higher sedimentation rates were measured under iron enriched condition.

It has also been suggested that iron could be a limiting factor for bacterial growth in the S.O. (Tortell et al., 1996). Dehairs et al. (2006) pointed out that the extent to which iron regulates bacterial dynamics in the HNLC areas remains unresolved. They observed in cultures that the bacterial activitiesare not directly enhanced by iron addition, but rather by the improved quality of the phytoplankton-derived organic matter.

Iron is not the only limiting micro-nutrient of phytoplankton growth. For instance, Peers et al. (2005) suggest that Cu may be an important micronutrient for phytoplankton growth in low iron regions because of its role in iron acquisition. Phytoplankton growth can be co-limitated by iron and light (Armstrong, 1999; Boyd et al., 2000; Boyd et al., 2001) . Silicic acid has also been suggested to be a limiting nutrient, but some experiments have shown that iron is the primary nutrient limiting phytoplankton over much of the Subantarctic Southern Ocean (Sedwick et al., 1999; Boyd et al., 2001). Silicic acid nevertheless plays an important role in structuring phytoplankton natural assemblages (Hutchins et al., 2001).

1.2.2.3 Primary production of the Southern Ocean waters

Table 1-4 provides an overview of the estimates of annual primary production in the Southern Ocean. Annual primary production (south of 50°S) scaled from satellite data and simulated by models ranges from 2900 Tg C yr^{-1} to 4414 Tg C yr^{-1}. Primary production peaks in December to reach 816 Tg C yr. However, such assessments do not account for the productive area located north of 50°S (mainly PFR).

A less restrictive definition of the extent of the Southern Ocean can lead to much higher primary production estimates. The estimate of primary production in the 30°S-50°S band from Moore and Abbott (2000) is 5-fold higher than the one south of 50°S. Smith and Gordon (1997) pointed out the hyper-productivity of the Ross Sea with maximum measured rates of primary production exceeding 6 g C m^{-2} d^{-1} in the Ross Sea polynya. In the same way, Arrigo et al. (1998) computed that the Ross Sea contributes for 28% of the annual production of the S.O. south of 50°S. However, this estimate was challenged by Moore & Abbott (2000), these authors considered a larger northwards extent of the S.O. and pointed out that the northern regions like the STFZ are highly productive.

Antarctic sea ice is also characterized by high rates of primary production, and its integrated primary production ranges from 36 TgC yr^{-1} to 70 TgC yr^{-1}. This corresponds to about 10%-28% of the annual primary production of ice covered regions and 1%-2% of the whole Southern Ocean south of 50°S. In the same way, the MIZ exhibits markedly higher primary production rates than the POOZ, but its relative contribution to the primary production of the Southern Ocean is relatively small, owing to its size.

Region	Net primary production ($gC\ m^{-2}\ yr^{-1}$)	Integrated primary production ($TgC\ yr^{-1}$)	Zone	References
PFZ	73.2	385	All	(Moore and Abbott, 2000)
PPOZ		2942	All	(Arrigo et al., 1998)
POOZ	58.5	509	All	(Moore and Abbott, 2000)
POOZ (Coastal)	45-290		South Orkney Islands	(Horne et al., 1969); (Whitaker, 1982); (Clarke and Leakey, 1996)
Coastal (POOZ & SIZ & WRR)		80	All	(Arrigo et al., 1998)
PPOZ/SIZ	10-175		Bransfield Strait	(von Bodungen, 1986; Holm-Hansen and Mitchell, 1991; Wefer and Fisher, 1991)
POOZ/SIZ	25-65		Between South Shetlands and Peninsula	(El-Sayed and Taguchi, 1981; von Brockel, 1985); (von Bodungen et al., 1988)
MIZ		422	All	(Arrigo et al., 1998)
MIZ	54.2	96	All	(Moore and Abbott, 2000)
MIZ		180	All	(Legendre et al., 1992)
Under-Ice		44	All	(Legendre et al., 1992)
WRR		55	All	(Moore and Abbott, 2000)
Sea ice cover		63-70	All	(Legendre et al., 1992)
Sea ice cover		36	All	(Arrigo et al., 1997)
Open Ocean	10			(El-Sayed and Turner, 1977; Holm-Hansen et al., 1977)
Open Ocean		11270	30-50°S band	(Moore and Abbott, 2000)
Whole S.O.		4414	South of 50°S	(Arrigo et al., 1998)
Open Ocean south of 50°S	62.4	2900	South of 50°S	(Moore and Abbott, 2000)
Whole S.O. south of 30°S	131	14170	South of 30°S	(Moore and Abbott, 2000)

Table 1-4. Annual primary production from nutrient budgets, sediment trap estimates ^{14}C measurements (Horne et al., 1969; El-Sayed and Turner, 1977; Holm-Hansen et al., 1977; Whitaker, 1982; von Bodungen, 1986; Clarke and Leakey, 1996), Sea-viewing Wide Field-of-view Sensor (SEAWIFS) data (Arrigo et al., 1998), sea ice model outputs (Arrigo et al., 1997) and vertically generalized production model (VGPM) constrained by remote sensing outputs (Moore and Abbott, 2000).

	C_{sat} (mg m^{-3})
Oligotrophic	≤0.1
Mesotrophic	0.1≥ and <1.0
Eutrophic	≥1.0

Table 1-5 : Classification of waters based on satellite derived pigment concentrations (C_{sat}) according to Antoine et al. (Antoine et al., 1996) and Berenfeld and Falkowski (Behrenfeld and Falkowski, 1997)

Considering the classification of table 1-5, Arrigo et al. (1998) estimated that less than 0.1 % of the Southern Ocean waters can be classified as oligotrophic, and that primary production occurs mostly in mesotrophic waters (68% of the total), while 32% occurs in eutrophic waters.

1.2.2.4 Secondary producers and their impact on the biological pump.

As pointed out in section 1.2.2.1, when light or iron availability limits algal growth which, in many areas may be for most of the year, the Southern Ocean is dominated by the microbial network in winter and the microbial food web in summer. In winter heterotrophic bacteria are grazed by flagellates, which are in turn prey to ciliates. Flagellated and ciliates release dissolved organic matter which is used by bacteria. In summer, small pico/nano phytoplankton are grazed by protozoan, nano-flagelates and micro-zooplankton. In such microbial food webs, much of the grazed material is retained and recycled in the upper mixed layer, and not vertically exported.

The key secondary producers in the Southern Ocean are large microphagous zooplankton (salps, krill and some large copepods) (Le Fevre et al., 1998; Voronina, 1998). They are of crucial importance in regulating the efficiency of the biological pump, especially in large areas of the Southern Ocean where the microbial network predominates. They provide an efficient pathway to organic carbon export as they ingest microbial-size particles and repackage small, non-sinking particles into both metazoan biomass and large, rapidly sinking faeces. In the wide areas, where the microbial network predominates, large zooplankton that are omnivorous or able to ingest small particles have a competitive advantage over herbivorous zooplankton. Krill efficiently transfer carbon to apex predators while their faecal pellets are vertically exported during transient spring sedimentation events (von Bodungen et al., 1987; Bathmann et al., 1991). The exoskeletons of krill are relatively fast-sinking, while the contribution of their faecal pellets to downwards biogenic flux depends on size, packing index and diet. Less documented, salps prefer warmer waters than krill (Foxton, 1966; Le Fevre et al., 1998; Nicol, 2000; Pakhomov et al., 2002), and oceanic regions with lower food concentrations than krill (Le Fevre et al., 1998; Pakhomov et al., 2002) . Salps therefore tend to occupy the extensive lower-productivity regions of the Southern Ocean. Salps may be a significant direct link towards some fish and indirectly to other apex predators. At some locations, especially in offshore waters, they may account for most of the downward flux of biogenic carbon (Huntley et al., 1989; Le Fevre et al., 1998) owing to their ability to rapidly multiply in response to sudden increase of phytoplankton productivity, and to the sinking rate of their large and dense faecal pellets that are both resistant to bacterial degradation and are among the fastest-sinking of all zooplankters (Fortier et

al., 1994). Unregulated filtration of all particles entering the branchial cavity of salps, makes them prone to fatal clogging at high particles and phytoplankton abundance, and probably restricts them to oligotrophic offshore waters.

Finally, large copepods are a trophic link towards fish and their grazing activity generally impedes the vertical export of organic particles. Copepods contribute to the termination of phytoplankton blooms, but are relatively poor contributors to the downwards organic matter flux (Bathmann et al., 1987; Lampitt et al., 1990; Ayukai and Hattori, 1992), due to the generally low sinking rate of their faecal pellets. Furthermore, copepods can ingest their own faecal pellets and mechanically break them into smaller-slower-sinking particles.

On the whole, biogenic carbon is channelled mainly towards apex predators and episodically into the deep ocean. Without these original interactions, Antarctic waters might be dominated by microbial components and recycling processes instead of active export of carbon produced by small phytoplankton towards the meso- and bathypelagic zones or apex predators (Le Fevre et al., 1998).

1.2.2.5 A simple tentative schematic of the carbon pump in the Southern Ocean

Using the ability of the ecological model SWAMCO to take into account complex interplay ranging from physical conditions to limitation of phytoplankton growth by micro-nutrients and grazing pressure, Lancelot et al. (Lancelot et al., 2000) pointed out that limitation by a single factor can be invoked in the Southern Ocean. These authors also pointed out that the impact of physical condition and availability of micro-nutrients on the natural assemblages and their repercussions on the biological pump. We propose a tentative conceptual frame of the carbon pump in the Southern Ocean which aim to present a simplified overview showing how light conditions, and silicate and iron concentrations impact phytoplankton assemblages, subsequently zooplankton assemblages, and finally carbon export. The aim of this tentative schematic is to be as simple as possible, and we recognize that the system is more complex, and is characterized by both spatial and temporal variability. We present only light, silicate and iron concentrations as bottom-up controls since strong control by micro-nutrient is a peculiarity of the Southern Ocean. But this should not overshadow the fact that other more conventional factors such as temperature also control the distribution of phytoplankton (e.g; chapter 2.2). Furthermore, processes in the mesopelagic realm that strongly impact the efficiency of the biological pump were ignored in this conceptual frame. Finnaly, the distribution of the primary producers or second producers with repect to export efficiency is still prone to significant uncertainties and need better constrains, through modelling experiment for instance.

The Southern Ocean is a so-called HNCL zone where the concentrations of inorganic macronutrients (nitrate and phosphate) are relatively high and, generally, are not a critical limiting factor for phytoplankton growth. However, while the SIZ and POOZ present elevated concentration of silicate, the northern part of the Southern Ocean can be depleted, affecting the growth of diatoms.

Light availability exerts a strong control on phytoplankton growth (Nelson and Smith, 1991). Some areas of the S.O. experience exceptionally favourable light

conditions, like the MIZ in early summer, where strong stratification owing to ice melt is intrinsically associated to continuous and elevated solar irradiance. The POOZ and the PFR experience deep mixing (Heywood et al., 2002; Garabato et al., 2004) together with low solar irradiance owing to persistent cloudiness, limiting primary production (Holm-Hansen et al., 1977; Smith Jr and Nelson, 1985). Hence, depending on the light conditions and stratification, phytoplankton assemblages can shift from sun-adapted diatoms to shade-adapted prymesiophytes (especially in the MIZ, section 1.2.2) or to nanoflagelattes, if light rather than grazing is the most important limiting factor.

If both iron concentrations and light conditions are unfavourable to the growth of large diatoms or prymesiophytes, as it can occur in the POOZ, then the trophic network predominantes. In such a system, nutrients are recycled internally and it is characterized by low new production and carbon export. In the microbial network, nano-flagellate are strongly controlled by grazers (top-down control).

The shift in the dominant phytoplankton population induces changes in the upper trophic levels and eventually on the organic matter export. For instance, shift from diatom-grazing euphausiids to ephemeral flagellate consuming salps will influence the sinking fluxes of zooplankton feacal pellets and phytoplankton debris and eventually carbon export. In the MIZ. Walsh et al. (2001) and Atkinson et al. (2004) observed a marked transition from krill to salps in the course of the past eight decades closely related to the decrease of the ice cover extent. Walsh et al. (2001) observed in the period (1975-1996) induced 100-fold variations of both *E. superba* and *Salpa thompsoni* adult populations. This highlights a strong bottom-up control which can have cascading repercussions throughout the first trophic levels. However, Lancelot et al. (Lancelot et al., 1993) noted that in some ice-free areas, algal biomass is regulated by episodic passage of krill swarms that track algal blooms (top-down control).

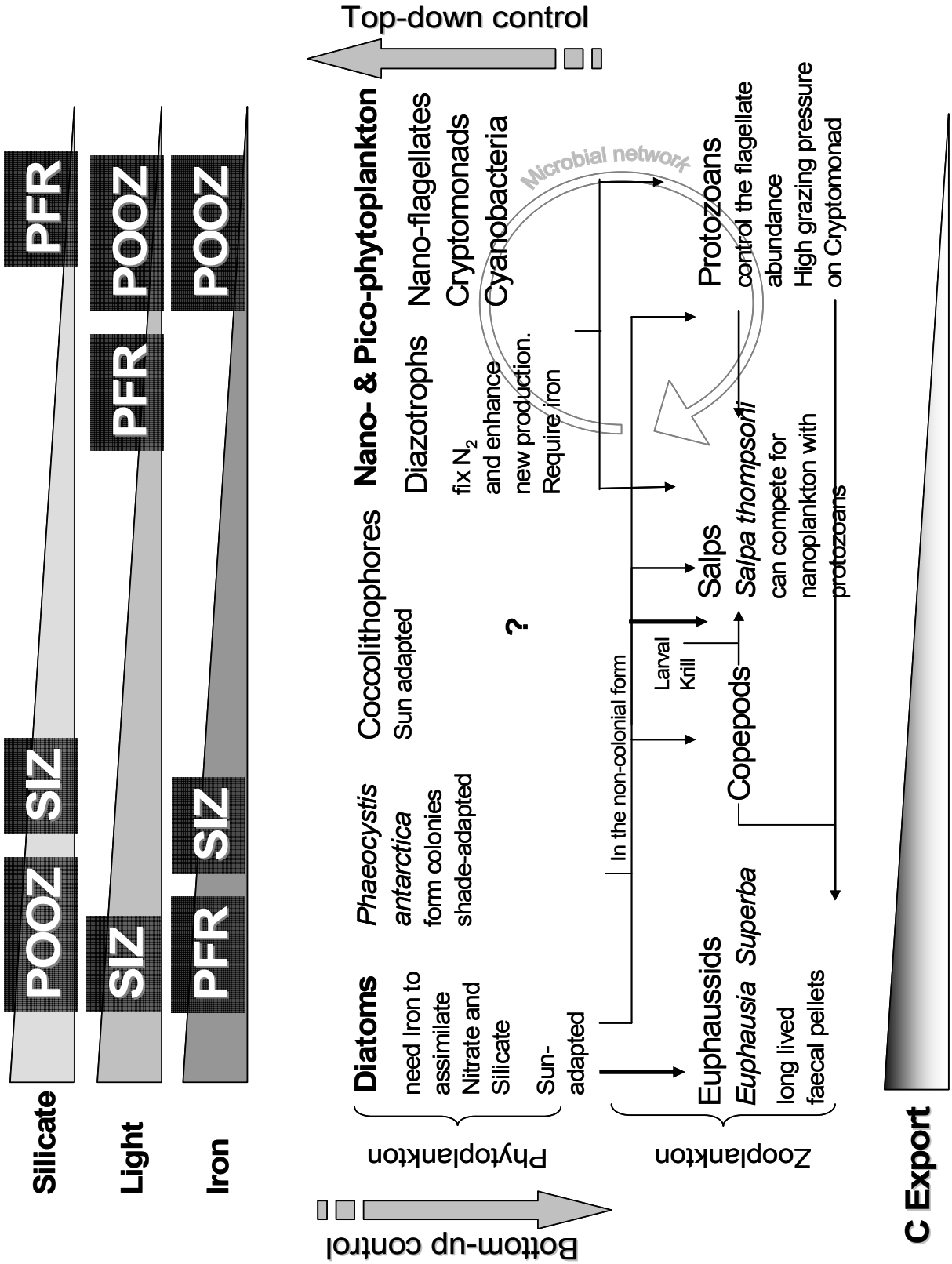
Top-down control
Bottom-up control
Silicate
Light
Iron
POOZ
SIZ
PFR
Phytoplankton
Zooplankton
Diatoms
need Iron to assimilate Nitrate and Silicate
Sun-adapted
Phaeocystis antarctica
form colonies
shade-adapted
Coccolithophores
Sun adapted
?
Nano- & Pico-phytoplankton
Diazotrophs
fix N2 and enhance new production. Require iron
Nano-flagellates
Cryptomonads
Cyanobacteria
Microbial network
Protozoans
control the flagellate abundance
High grazing pressure on Cryptomonad
Salps
Salpa thompsoni
can compete for nanoplankton with protozoans
Copepods
Larval Krill
In the non-colonial form
Euphausiids
Euphausia Superba
long lived faecal pellets
C Export

Figure 1.2-4: Conceptual frame of the carbon pump in the Southern Ocean. From left to right, silicate and iron concentrations, and C export are decreasing, light conditions (both light irradiance and mixed layer depht) are less favourable to phytoplankton growth, and the system shifts from top-down control to bottom-up control. POOZ, SIZ, PFR denote the main biogeochemical provinces of the S.O. and distributed according to predominant spring/summer conditions. This is a simplified representation of the carbon pump, and we acknowledge the occurrence of large variations in the conditions with regards to the considered area, and their impact on the ecosystem. Zooplankton trophic network partly adapted from Walsh et al. (2001).

1.2.3 The Indian sector

Limitation of phytoplankton growth west of Kerguelen archipelago is still a mater a debate. Fasham et al (2006) suggest, from modelling simulation, that underwater light levels have a more limiting effect on phytoplankton growth than iron supply at Kerfix station. However, in the Crozet basin, Sedwick et al (2002b) argue that nutrients were the primary limitation. They distinguished three distinct regimes of resources limitations of phytoplankton growth. In the PFZ, iron availability exerts the primary limitation on nitrate drawdown and biomass accumulation, thus community growth, with silicic acid availability exerting a secondary limitation on diatom growth and biogenic silica production. In the STZ macronutrients (nitrate/phosphate) are the primary limitation on community growth iron deficiency imposed a significant secondary limitation on community growth, particularly diatom growth, such that the algal community was poised close to co-limitation by macronutrients and iron. Within the SAF/STF, iron deficiency is the primary limitation on algal community growth; however, they observed evidence of secondary limitation of nitrate drawdown and biomass accumulation by silicic acid deficiency, via control of algal community structure--such that iron addition preferentially stimulated the growth of non-diatom nanoplankton--suggesting that the algal community was poised close to co-limitation by iron and silicic acid. This conclusion converges with observations of Hutchins et al (2001) in the SAZ, south of Tasmania, who suggested that iron is the proximate limiting nutrient for chlorophyll production, photosynthetic efficiency, nitrate drawdown, and diatom growth, but that Si also exerts considerable control over algal growth and species composition. Both nutrients together are needed to reach a maximum growth response, suggesting that both Fe and Si play important roles in structuring the subantarctic phytoplankton community.

1.2.4 Interannual variability of primary production: the role of the Southern Annular Mode

Physics and biology of the S.O. are affected by several oscillations. For instance, some part of the Indian sector are affected by the subtropical southern Indian Ocean dipole (section 1.3.1.5) while the influence spread over El-Nino Southern Oscillation extend over the S.O. Currently, the Southern Annular Mode (SAM), receives a growing attention. The SAM or the Antarctic Oscillation, is the leading mode of climate variability on timescales from intraseasonal to interannual over the entire Southern Ocean (Thompson and Wallace, 2000). It is characterized by a large-scale

alternation of atmospheric mass between the mid- and high-latitudes, and is associated with a meridional shift in the atmospheric westerly winds (Hartmann and Lo, 1998). Wind shifts associated with the SAM alter Southern Ocean circulation patterns substantially (Watterson, 2000; Hall and Visbeck, 2002; Oke and England, 2004). The SAM Index is defined by the leading principal component of the 700 mb geopotential height south of 20°S in the atmosphere. Positive SAM is associated with negative pressure anomalies over Antarctica, positive pressure anomalies over the mid-latitudes and a strengthening of the longitdinal atmospheric gradient. The anomalously strong pressure gradient during positive SAM acts to significantly strengthen the westerly wind at ~55°S and to weaken westerly winds (easterly anomaly) at 35°S by as much as 9 m s^{-1} (Hartmann and Lo, 1998; Hope et al., 2004; Chierici et al., 2005).

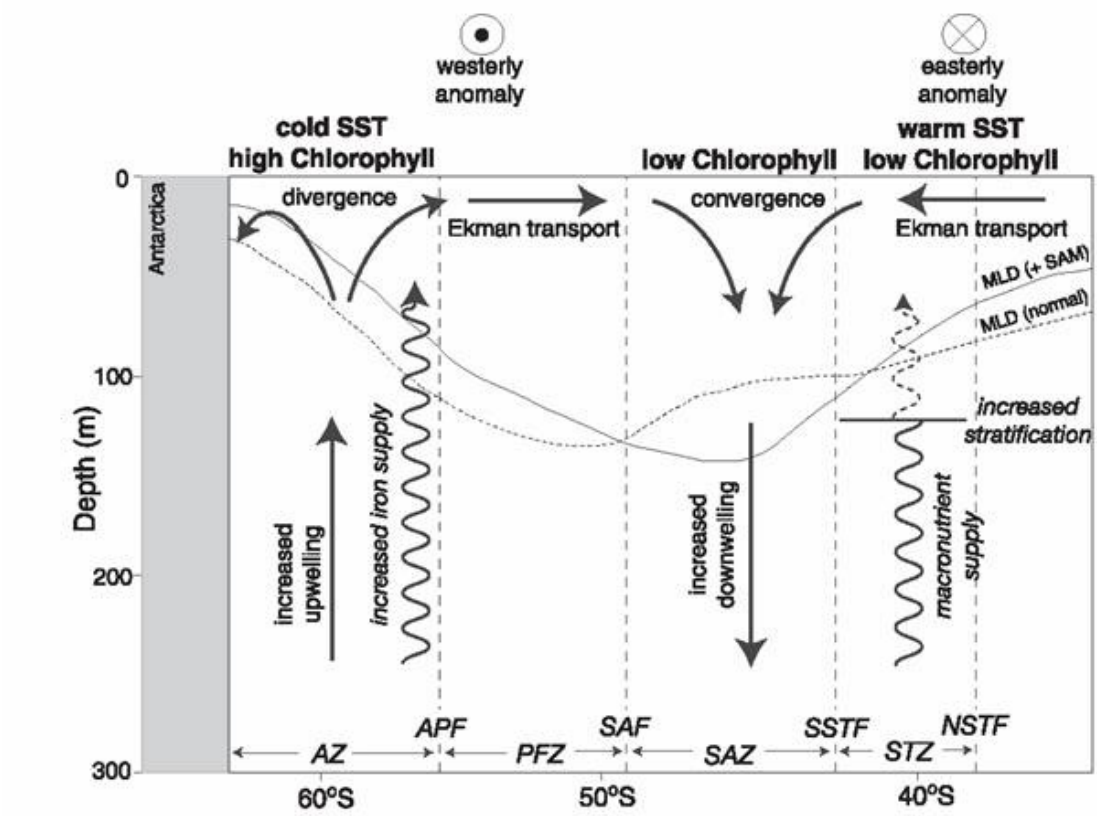

Figure 1.2-5 Shematic illustration of the upper ocean response to a positive phase of the SAM (after Lovenduski and Gruber 2005)

By correlating surface chlorophyll concentration (SEAWIFS) with sea surface temperature (AVHRR Ocean pathfinder) and wind speed (QuikSCAT) Lovenduski and Gruber (2004) evidenced the influence of SAM on biology and proposed the following mechanisms. Surface westerly wind anomalies generate northward Ekman transport anomalies in the region south of the Polar Front (PF) around 55°S and in the Polar Frontal Zone (Figure 1.2-5), enhancing the divergence, driving increasing upwelling of iron-rich deep water and generating negative Sea Surface Temperature (SST) anomalies in the PFZ and south of the PF. By driving anomalous upwelling of iron, such positive SAM events enhance chlorophyll concentration in this region where primary production is limited by micronutrients. Further north in the Subtropical Zone (STZ), surface easterly wind anomalies produce southward Ekman transport

anomalies, yielding to positive anomalies in both the STZ and SAZ. This acts to enhance stratification and reduce macronutrient supply and chlorophyll abundance in the STZ. As a result of northward Ekman transport south of the PF and southward transport in the STZ, increased convergence of water in the Subantarctic Zone (SAZ) increases downwelling of water and deepen mixed layer, increasing light limitation in a region limited by light and decreasing chlorophyll abundance.

1.3 pCO_2 and related CO_2 fluxes in the Southern Ocean

1.3.1.1 An overview: the Takahashi's climatology

In order to provide an overview of the seasonal and latitudinal variability of ΔpCO_2 (difference of partial pressure of CO_2 between surface seawater and the atmosphere), we derived the figure 1.3-1 from the ΔpCO_2 and air-sea CO_2 fluxes climatology of Takahashi et al. (2002; 2003).

We present here the longitudinally averaged values of ΔpCO_2 and of air-sea CO_2 fluxes. It is worth noting that large longitudinal variation of pCO_2 exits in the southern ocean (Murphy et al., 1991a; Murphy et al., 1991b). However, due to the general circumpolar circulation, and the strong latitudinal temperature gradient, the Southern Ocean physical and biogeochemical processes generally exhibit circumpolar patterns with strong latitudinal variations compared to longitudinal ones, which are reproduced in each ocean basin. For instance, the succession of fronts has a general circumpolar pattern which is reproduced in each ocean basin and discriminates biogeochemical provinces.

In order to decipher the impact of biological activity and water masses mixing on ΔpCO_2 from the effect of temperature changes, we used the ΔpCO_2 seasonal anomaly corrected from the temperature variability. It accounts for the difference of ΔpCO_2 corrected from the variations of temperature, with ΔpCO_2 in August, that generally corresponds to the period at which the highest ΔpCO_2 values are observed in the S.O.. It comes:

$$\Delta pCO_{2\ anomaly} = \Delta pCO_2@SST_{Augsut} - \Delta pCO_{2\ August} \quad (76)$$

where $\Delta pCO_{2\ anomaly}$, $\Delta pCO_2@SST_{August}$ and $\Delta pCO_{2\ August}$ stand for ΔpCO_2 seasonal anomaly, ΔpCO_2 linearized at the sea surface temperature (SST) of August, and ΔpCO_2 in August, respectively.

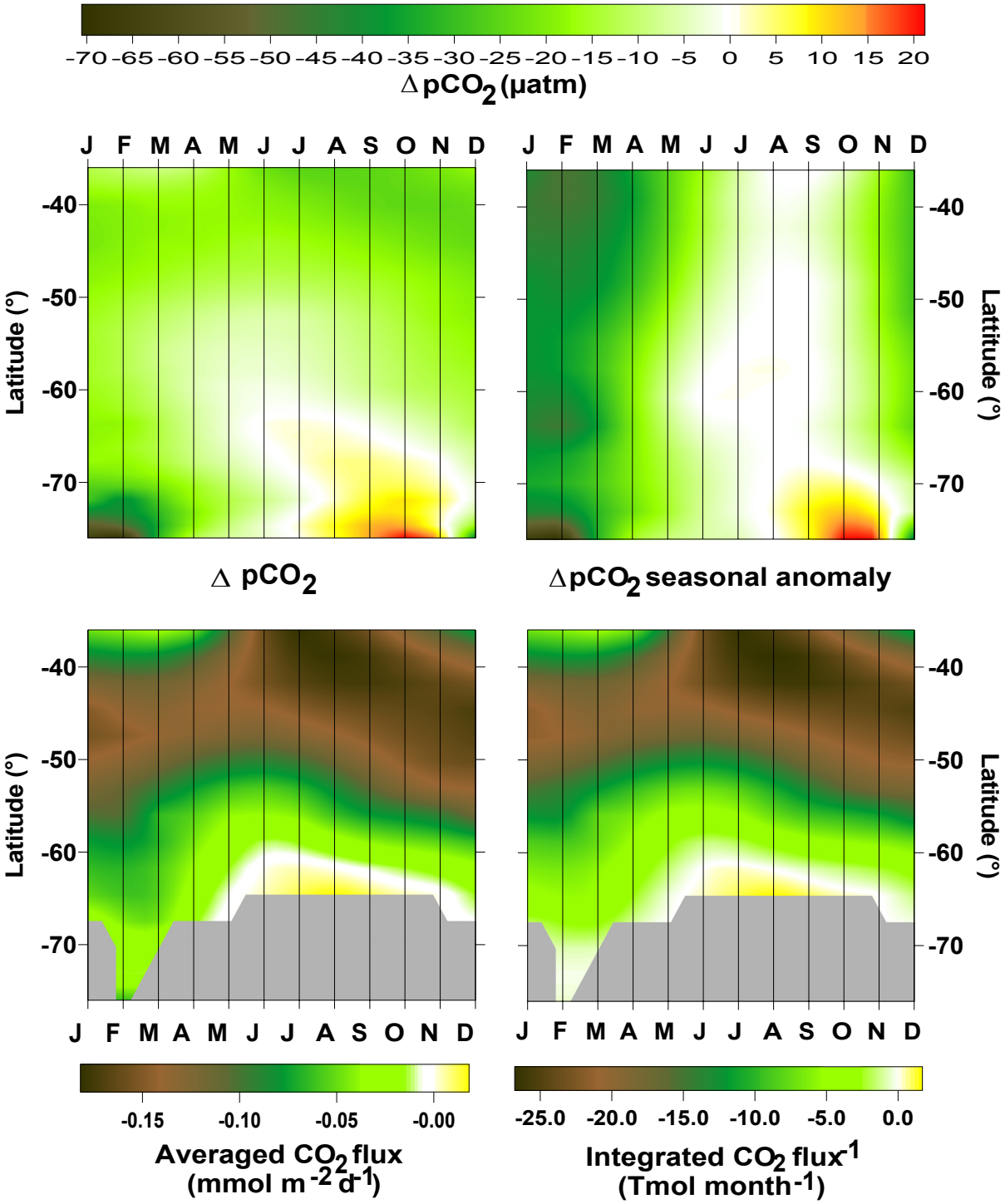

Figure 1.3-1: Seasonal and latitudinal variability of dpCO2, seasonal dpCO2 anomaly and related averaged and integrated air-sea CO2 fluxes in the Southern Ocean derived from the climatology of Takahashi et al. (2002; 2003). Air-sea CO_2 flux was computed using the Wanninkhof (1992) k-wind relationship. Integrated fluxes are provided in Tmol month^{-1} and are integrated on areas of 4 degree latitude by 360 degree longitude. Grey areas represent the sea ice cover.

ΔpCO_2 seasonal anomaly is computed at each latitude. It provides an idea of how all processes, deduced from the effect of temperature changes, affect ΔpCO_2. Indeed this figure aims to distinguish the effect of biological activity and water mixing (among other processes) on ΔpCO_2. As this figures aims to exhibits seasonal variations

rather than spatial variation, we removed the latitudinal variation of ΔpCO_2 base level through the use of the anomaly compared to the ΔpCO_2 in August (when the impact of biological activity and vertical mixing on pCO_2 are probably at their weakest).

ΔpCO_2 distribution shows, while considering longitudinal averages, that surface waters of the S.O. are under saturated with regards to atmospheric CO_2 almost all year round and almost everywhere. Only the southernmost part of the seasonal ice zone appears to be CO_2 over saturated from July to November. At 40°S, the seasonal variability is weak at with ΔpCO_2 ranging from -17 µatm to -25 µatm during the year. ΔpCO_2 is more variable southwards: at 76°S, ΔpCO_2 ranges from -64 µatm in January to 21 µatm in October. Strong CO_2 under saturation and over saturation observed in the SIZ does not translate into significant CO_2 fluxes and highest (absolute values) air-sea CO_2 fluxes are observed northward. The general decrease (absolute values) of air-sea CO_2 fluxes southwards is enhanced while considering integrated CO_2 fluxes, owing to the decrease of the surface area. Hence, frontal area appears to be the largest contributor to the uptake of atmospheric CO_2 in the Southern Ocean.

While seasonal variability of ΔpCO_2 is weakest in the frontal area, this region exhibits strong variations of the ΔpCO_2 seasonal anomaly, which is only exceeded in the southernmost part of the SIZ. Increase of ΔpCO_2 seasonal anomaly (absolute values) from October to February can be ascribed to phytoplankton photosynthetic activity which would appear to be enhanced and to last for a longer period in the band comprised between 40°S and 50°S compared to the one comprised between 50°S and 65°S. Such enhanced northward biological activity can potentially support enhanced air-sea CO_2 fluxes in summer. However, in the northernmost part of the S.O. the highest CO_2 fluxes are observed in winter as a probable consequence of superimposed thermal effect.

In the 60°S-75°S latitudinal band which roughly corresponds to the SIZ, mean and integrated air-sea CO_2 fluxes are weak and the summer uptake of CO_2 is partly compensated by the winter efflux. The patches of CO_2 over saturated waters observed in figure 1.3-1 correspond to marginal ice zones or sea ice covered areas. In winter and early spring, SIZ waters are generally CO_2 over-saturated, yet the related CO_2 fluxes are weak.

Figure 1.3-1 presents longitudinal monthly average values composed from data obtained in different years. This masks local and short term ΔpCO_2 variability together with long term and large scale (longitudinal) variability. For instance, transient over saturation of CO_2 occurs in all the zones of the Southern Ocean, while it is not depicted in the figure 1.3-1. Local, short term and long term variability are described hereafter.

1.3.1.2 Variability

As the Takahashi et al. (2002) climatology averages both latitudinaly and longitudinally a huge number of data, it tends to smooth seasonal variations and local spatial variations. Here we present briefly some areas and seasons that experience particular variability.

The polar frontal zone

The strong variability of pCO_2 in the polar frontal zone have been repeatedly documented. Hence the signature of the frontal structures appears conspicuously in the latitudinal distribution of pCO_2 with drastic drop of pCO_2 corresponding to the frontal jets. Besides this variability the PFZ and the SAZ generally exhibit strong under-saturation owing to enhanced biological activity, cooling of subtropical waters advected southwards, and formation of Antarctic Intermediate Water (AAIW) (Metzl et al., 1991; Metzl et al., 1995; Bakker et al., 1997).Mesoscale frontal structure can be reflected in the pCO_2 distribution as meanders of the Polar Frontal jet and associated mesoscale eddy promotes phytoplankton growth (Bakker et al.(1997), chapter 2.2) .

Winter oversaturation

Hence while no over-saturation appeared in the figure 1.3-1 north of 65°S. Winter oversaturation extend north to the SIZ, in the POOZ and last from autumns to spring. Indded, It is worth noting that CO_2 over-saturation have been repeatedly reported as in autumn in the Pacific (Murphy et al., 1991a; Murphy et al., 1991b), thoroughout winter in the Indian sector of the S.O. between 42°S and 49°S in July 1984 (Goyet et al., 1991), between 47 and 57°S in August 1993 and August 2000 (Metzl et al., 1999; Metzl et al., 2006) or in the eastern part of the Indian sector during early summer(Inoue and Sugimura, 1986; Inoue and Sugimura, 1988). This winter over-saturation is due to strong winter mixing (mixed layer down to 500 m have been reported in the S.O.) that outweighs the effect of temperature increase.

Longitudinal variations

The figure 1.3-1 by providing longitudinal averages of pCO_2 and related air-sea CO_2 fluxes intrinsically masks the longitudinal variations. These longitudinal variation are poorly documented compared t the latitudinal variations as Southern Ocean survey often consist in latitudinal transect. However, Murphy et al. (Murphy et al., 1991a; Murphy et al., 1991b) reported marked longitudinal changes of pCO_2 in the South Pacific during autumn, with western surface water under-saturated by up to 60 µatm and eastern water over-saturated by up to 20 µatm. Hence, South Pacific Ocean shift from a sink in the western part to a source in the eastern part. This shift has been ascribed to the dominance of biologically activity over physical effect on pCO_2 in the southwest pacific, owing to the increase of phytoplankton biomass east of Australia, while physical controls dominate over biological effects in the remote southeast Pacific. Westward enhanced primary production may be due to aeolian or bottom iron fertilization from Australia and New Zealand.

Other specific area or processes related to sea ice cover lead to strong variability and can contribute significantly to the CO_2 budgets of the S.O.: sea ice formation (Anderson et al., 2004), seasonal and permanently ice covered zones (Anderson et al., 1991; Hoppema et al., 1998; Hoppema, 1999; Stoll et al., 1999; Hoppema et al., 2000; Hoppema et al., 2001; Sweeney, 2003; Hoppema, 2004a; Hoppema, 2004b), polynya (Yager et al., 1995; Bates et al., 1998) and marginal ice zones (Bellerby et al., 1995; Bakker et al., 1997).

1.3.1.3 Budgets of air-sea CO_2 fluxes

By compiling 940000 pCO_2 measurement in surface open oceanic waters, Takahashi et al. (2002; 2003) proposed a monthly climatology of $\Delta pCO_2$and using k-relationship of Wanninkhof(1992) and NCEP/NCAR 41-year mean monthly wind speeds, they derived air-sea CO_2 fluxes. They estimated that the global open ocean absorbs 1.6 PgC yr^{-1} and that the Southern Ocean (south of 50°S account for -0.35 PgC yr^{-1}). However, the arbitrary limit of 50°S to define the Southern Ocean might correspond to its northward limit (i.e. the Subtropical Front) and is somewhat restricted. Such limit excludes the SAZ in the Atlantic sector and in a large part of the Indian sector, and some parts in the Pacific sector (Orsi et al., 1995; Belkin and Gordon, 1996; Moore et al., 1999; chapter 2.1) . This is of importance as the SAZ is probably one of the most productive regions of the S.O. and acts as a significant sink of atmospheric CO_2 (Metzl et al., 1999)-section 1.3.1.1. For instance, if we budget CO_2 fluxes of the Takahashi et al. (2002; 2003) climatology south of 50°S, 44°S and 40°S, the corresponding Southern Ocean CO_2 sink is, 0.35 PgC yr^{-1}, 0.71 PgC yr^{-1} and 0.98 PgC yr^{-1}, respectively.

The open ocean global CO_2 sink of 1.6 PgC yr^{-1} derived from the Takahashi et al. (2002; 2003) climatology compares well with the values given by global circulation models (GCM) which are comprised between 1.2 PgC yr^{-1} and 1.8 PgC yr^{-1}. On the whole, the Southern Ocean generally accounts for between 20% and 45% of the global ocean sink of CO_2. Average fluxes south of 40°S from *in situ* pCO_2 measurement (items 9 to 12 on Table 1-6) account for 66% of the global CO_2 fluxes derived from the Takahashi et al. (2002) climatology.

Assements of CO_2 fluxes based on *in situ* pCO_2 like the latter climatology, are prone to some uncertainty due to the poor winter data coverage. McNeil (2005) proposed a climatology of TA and DIC to overcome this caveats, since in poorly covered areas or seasons, these quantities can be extrapolated from five common hydrographic measurements which benefit of a better coverage: - temperature, salinity, nitrate, silicate and oxygen concentration (Feely et al., 2002). After corrections of the anthropogenic CO_2 signal using the CFC-age method, multi-parameter regressions of DIC and TA against temperature, salinity, nitrate, silicate and oxygen concentration were established, and the pCO_2 fields computed. CO_2 fluxes were calculated from pCO_2 fields using NCEP 10m wind speeds and the Wanninkhof (1992) k-wind relationship. This approach yields a moderate CO_2 sink in the whole Southern Ocean south of the STF at 40°S (0.19 PgC yr^{-1}; table 1-6) but the

region of the S.O. south of 50°S acts as a CO_2 source (0.24 PgC yr^{-1}) contrasting with the results derived from the other methods.

To assess the overall air-sea CO_2 fluxes at basin scale, an alternative method to the interpolation of pCO_2 field measurements is the use of biogeochemical models, either 1D model (Metzl et al., 2006) or extended GCM (Matear and Hirst, 1999). Such models are constrained by hydrographic data and validated against pCO_2 measurements. The model of Matear and Hirst (1999) is consistent with the Takahashi et al. (2002) climatology, giving confidence in the outputs of the model. In contrast to the other assessments of the table 1-6, the 1D model of Metzl et al. (2006) provides CO_2 fluxes per oceanographic zone, rather than by latitudinal bands. This is a useful approach to compare air-sea CO_2 fluxes with other processes such as carbon export, which are specific to oceanographic zones rather than latitudinal bands.

In parallel to the above bottom-up scaling approaches, carbon sources and sinks can be estimated from resulting patterns of variability in atmospheric CO_2. The observed atmospheric CO_2 concentration field results surface fluxes of CO_2 and air mass transport of CO_2. The atmospheric transport is simulated by numerical models, and surface fluxes are determined by inversion from the observational atmospheric data. This kind of analysis can be applied at a number of scales of space and time, depending on the type and spatial density of atmospheric data. Global inverse calculations are based on flask samples of air collected weekly at sites around the world, and can resolve annual and seasonal net carbon sources and sinks for regions the size of continents and ocean basins. They provide independent estimates of net sources and sinks over large areas, without giving details on the finer-scale variability or the underlying processes. Results results from Roy et al. (2003) inversion model provide encouraging results consistent with the Takahashi et al. (2002; 2003) climatology and the Matear and Hirst (1999) GCM outputs.In this frame, 2 intercomparaison of atmospheric inversion models converges, and assess that the mean CO_2 sink south of 44°S is about 0.43 PgC yr^{-1} (Gruber et al., 2005). However, this modelling approachs brings inconsistent results at smaller scale. Inversion modelling based on dissolved inorganic carbon yeld some consistent results (0.4 PgC yr^{-1})(Mikaloff Fletcher et al., 2006), while combined oceanic/atmospheric inversion modelling brings a modest CO_2 sink of 0.14 PgC yr^{-1}. On the whole, according to the compilation of the table 1-6, estimates of the S.O. CO_2 sink converges towards 0.27PgC y^{-1} south of 50°S and 0.45 PgC y^{-1} south of 44°S. This latter estimate take into account the higly productive northern part of the S.O. and appears to be more comprehensive.

Table 1-6. Assessment of the annual air-sea CO_2 fluxes in the Southern Ocean (in PgC yr^{-1}). The assessments of Metzl et al. (1999; 2006) are formally provided for the oceanographic provinces: SAZ, POOZ and SIZ. Conversion of this province into latitudinal band is only valid for the western part of the Indian sector of the S.O. .

Methodology	Reference		Latitude (°S)								Global	Accuracy
			36	**40**	44	47	**50**	58	**60**	**70**		
Atmospheric inverse modelling												
Atmospheric Inversion	Roy et al., 2003	(1)					-0.28					
Oceanic Inversion	Gloor et al. 2003	(2)	-0.48						-0.06		-1.80	
Oceanic Inversion	Mikaloff Fletcher et al. 2006	(3)			-0.12				-0.28			
TRANSCOM-2 Atmospheric Inversions	Gurney et al. 2002	(4)				-0.47					-1.18	
TRANSCOM-3 Atmospheric Inversions	Gurney et al. 2004	(5)				-0.55					-1.34	
TRANSCOM-3 Atmospheric Inversions	after Gruber 2005	(6)			-0.36				-0.10			± 0.26 PgC yr^{-1}
Mean 10 Inversion models	after Gruber 2005	(7)			-0.07				-0.33			± 0.35 PgC yr^{-1}
Oceanic/Atmospheric Inversion	Jacobson et al. 2005	(8)			-0.14							
Ocean carbon cycle modelling												
Ocean General Circulation Model	Matear & Hirst 1999	(9)					-0.30				-1.35	
Ocean General Circulation Model (MOM3)	Jacobson et al. 2005	(10)			-0.58							
1D biogeochemical model	Metzl et al. 2005	(11)					-0.05	-0.12				
Oceanic pCO2, DIC, TA measurements												
Oceanic pCO2 climatology -NCEP 10m winds	Takahashi et al. 2002	(12)	-0.21	-0.63			-0.30		-0.05	-0.0016	-1.64	± 0.22 %
Summer/winter pCO2 measurements	Metzl et al. 1999	(13)		-1.05								
Oceanic DIC/TA climatology - NCEP 10m winds	McNeil et al. 2005	(14)		-0.47			0.16		0.12			± 0.25, ± 0.08, ± 0.08
					-0.19							± 0.26 PgC yr^{-1}
Average (58-70°S)	Mean of (2),(3),(6),(7),(12)							-0.16				
(50-70°S)	Mean of (1),(9),(11),(12)						-0.27					
(44-70°S)	Mean of (3)(6),(7),(8),(10),(12)				-0.45							
(40-70°S)	Mean of (11),(12),(13),(14)			-0.94								

1.3.1.4 Anthropogenic CO_2

During the Anthropocene (the period elapsed since the industrial revolution in the early 18th century), the ocean absorbed about 19 PgC of anthropogenic CO_2 , i.e. ~48% of the overall anthropogenic CO_2 emissions (Sabine et al., 2004b). This would represent only one third of the long term-potential, as the long turnover of the global ocean (of the order of several centuries) hampers a rapid equilibration of deep waters with the atmosphere. On the whole the ocean has the potential to take up approximately 85 percent of the anthropogenic CO_2 that is released to the atmosphere (Sabine et al., 2004a).

Most efficient areas for anthropogenic CO_2 sequestration are convergence zones, where waters with relatively high anthropogenic concentrations are moving into the ocean's interior. Conversely, regions of upwelling, where waters with low anthropogenic concentrations are brought near the surface, are modest contributor to the anthropogenic CO_2 sequestration.

According to Sabine et al. (2004b), the S.O. accounts for a large part of the anthropogenic CO_2 uptake by the global ocean owing to the formation of large volumes of intermediate (Antarctic Intermediate Water – AAIW) and mode water (Subantarctic Mode Water) (e.g. section 1.2.1.3), while the formation of deep water in the high-latitudes appears to be a modest contributor. Water masses precursors of AAIW and SAMW, while at the surface, appear to take up large amounts of anthropogenic CO_2 from the atmosphere as a result of both high wind speeds (enhancing gas transfer) and low anthropogenic content. AAIW and SAMW therefore contain high concentration of anthropogenic CO_2 which are transported equatorward and downward in large volume (McNeil et al., 2001; Sabine et al., 2004b). On the whole the contribution of the S.O. mode and intermediate water to the oceanic anthropogenic CO_2 inventory is estimated to exceed 20 PgC (Sabine et al., 2004b) and related penetration of anthropogenic CO_2 down to 2000 have been reported (Lo Monaco et al., 2005b).

Deep water formation in the Southern Ocean have been thought being potentially an efficient mechanism for anthropogenic CO_2 sequestration south of 50° owing to the cold temperature (and enhanced solubility of CO_2) and large volumes of water entertained towards the very deep layers of the ocean. However, early studies (Weiss et al., 1979; Chen, 1982; Poisson and Chen, 1987) contradicted this hypothesis and suggested a weak penetration of anthropogenic CO_2 related to Antarctic Deep Water (AADW) formation. Low transport of anthropogenic CO_2 was ascribed to winter sea ice cover which prevents the ventilation of upwelled circumpolar water prior to sinking. Since then, data based and model estimate confirmed these views and Sabine et al. (2004b) estimated that the S.O. south of 50°s contributes a modest 9% to the global inventory. These authors stressed that, in addition to the sea ice cover barrier, high Revelle factor of this cold water, time-limited contact with the surface before sinking, and mixing during sinking with old, anthropogenic CO_2-poor waters, acts to impede high transport of anthropogenic CO_2 into the ocean interior through AADW formation. However, these authors noticed that a robust estimate of the anthropogenic CO_2 concentration associated to the Antarctic Bottom Water (AABW) is hampered by the limited data available. In addition Sabine

et al. showed a significant accumulation of anthropogenic CO_2 near the Adélie Land coast

However, more recently, Lo Monaco et al. (2005a; 2005b) and McNeil et al. (2001), challenged previous conclusions. They pointed out that a low penetration of anthropogenic CO_2 was inconsistent with the significant injection of chlorofluorocarbons (CFC) along Antarctic continental slope and in AADW and AABW. Hence recent inventory of anthropogenic CO_2 estimated using a multiparametric linear regression approach (McNeil et al., 2001), by taking into-account oxygen disequilibrium under ice (Lo Monaco et al., 2005b) or using newly developed back-calculation method (Lo Monaco et al., 2005a), suggest that deep and bottom water formation in the S.O. is a key process in the natural sequestration of anthropogenic CO_2 and that the inventory of anthropogenic CO_2 in the S.O. could be much larger than what is currently accepted (McNeil et al., 2001; Lo Monaco et al., 2005a).

1.3.1.5 Inter-annual variability

Bousquet et al. (2000) used atmospheric inverse global modelling to show that the Southern Ocean (south of 50°S) and the equatorial zone are the two ocean basins that present the highest inter-annual variability. Metzl et al. (2006), Conway et al. (Conway et al., 1994) reported that the CO_2 sink in the southern hemisphere, which is mainly covered by oceans, exhibits rapid and highly significant changes for year to year (e.g. -0.5 PgC yr^{-1} in 1988 against -1.5 PgC yr^{-1} in 1989). However, there are too few pCO_2 data sets in the S.O. to allow to study long term variability of pCO_2 and related CO_2 fluxes.

Measurements carried out in the framework of MINERVE and OISO programs provide the longest consistent pCO_2 time-series S.O., in the western part of the Indian sector. Based on these data sets, Jabaud-Jan et al. (2004) by comparing the year 1998 and 2000 showed that large scale climatic oscillation can significantly affect the distribution of pCO_2 and related CO_2 fluxes. Hence, the subtropical southern Indian Ocean dipole is characterized by warm SST anomalies in the southwestern part of the southern subtropical region, south of Madagascar (Saji et al., 1999). Such event was detected during summer 1998 when the ocean was warmer from 20°S to 60°S. While high mesoscale variability in the SAZ and PFZ hampered the detection of long term variability, larger variability in the sources and sinks of CO_2 was observed south of the PF. In the POOZ, enhanced primary production was associated to the increase of temperature. The decrease of pCO_2 due to enhanced primary production outweighed the increase of pCO_2 related to temperature increase (+0.5°C) to lead to the doubling of the summer oceanic sink in 1998 compared to 2000. Conversely, surface waters in the SIZ turns from a CO_2 sink in 2000 to a source of CO_2 as a consequence of a stronger increase of temperature in 1998 (+1.1°) associated to a 40% decrease in chl *a* concentration. In the eastern part of the Indian sector, high biological activity event observed in 2002 in the POOZ and SIZ (Savoye et al., 2004) strongly decreases pCO_2 (Yoshikawa-Inoue and Ishii, 2005). In the same area, by comparing a transect carried out in summer 1997 and 2003, Brévière et al. (Brévière et al., 2005) showed that the POOZ shifted from a negligible in 1997 to a major CO_2 sink in 2003, while the SIZ turned from a CO_2 sink

to a CO_2 source, the sink in the Coastal Antarctic Zone (CAZ) increased fourfold, and CO_2 sink in SAZ remained unchanged.

In the light of previous observations, assessing long term variability is prone to some uncertainties. Accordingly, while comparing CO_2 fluxes assessed from pCO_2 measurements, ocean models and atmospheric inverse models, Metzl (2004) points out that all methods show marked inter-annual variability, but inconsistently from each other.

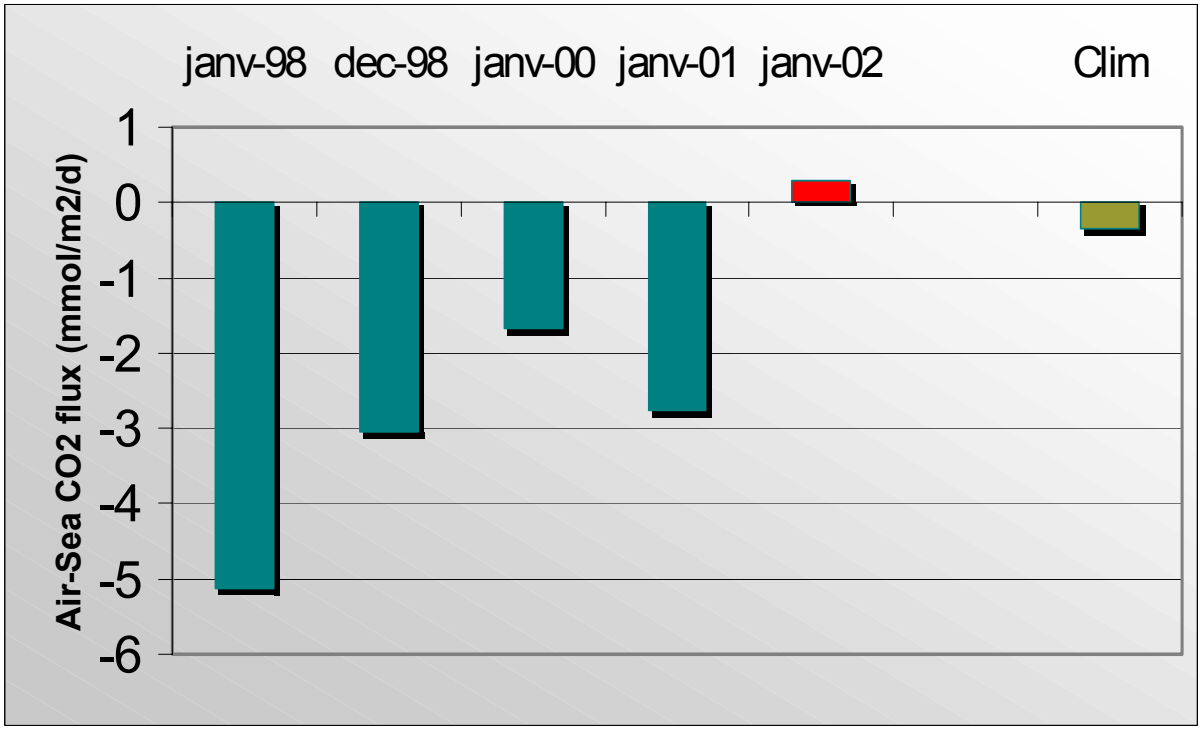

Figure 1.3-2. Interannual variability of summer CO_2 fluxes in the of the 50°S-57°S band of the western part Indian sector of the S.O derived from surface water pCO_2 measurement using the Wanninkhof (1992) k-wind relationship. "Clim" represent the CO_2 fluxes cderived from climatology of Takahashi (2002; 2003); from (Metzl, 2005).

While compiling summer CO_2 fluxes estimates derived from pCO_2 measurements carried out in the western part of the Indian sector of the S.O., Metzl (2004) showed that the summer CO_2 fluxes strongly vary, with, potentially, a decreasing trend of the CO_2 sink from 1998 to 2001, and shifting to a CO_2 source in 2002.

However, in the eastern part of the Indian sector, Yoshikawa-Inoue and Ishii (2005) observed that over the period 1969-2002, pCO_2 in surface waters increased at a slower rate than PCO_2 in the atmosphere, yet with also some large differences between the zones. In the POOZ, the water pCO_2 increased faster than PCO_2 in the atmosphere. On the whole, this should lead to an increase of the CO_2 sink (if we assume that wind speed does not present significant long-term changes). They also pointed out that in the SAZ the increase of ΔpCO_2 owing to biological activity outweighs the effect of the increase of temperature.

Hence, inter-annual variability of pCO_2 and related CO_2 fluxes need further investigations.

1.4 The Southern Ocean in a globally changing Earth system

"We are conducting a great geochemical experiment, unlike anything in human history and unlikely to be repeated again on Earth. Within a few centuries we are returning to the atmosphere and oceans the concentrated organic carbon stored in sedimentary rocks over hundred of millions of years" (Revelle and Suess, 1957).

The comparison of the present atmospheric concentration of CO_2 with the ice core record reveals that we have left the domain that defined the Earth system for the 650,000 years before the Industrial Revolution. Atmospheric CO_2 concentration is now nearly 100 ppmv higher, and has risen to that level at a rate at least 10 and possibly 100 times faster than at any other time in the past 650 kyr (Falkowski et al., 2000; Siegenthaler et al., 2005). We have therefore driven the Earth system away from the tightly bounded domain glacial-interglacial dynamics (Falkowski et al., 2000). The assessment of socio-economic repercussions of greenhouse-gas-induced climate changes remains challenging. However, perspectives are worrying enough to trigger the implementation of the Kyoto protocol aiming to stabilize the concentration of greenhouse gas in the atmosphere.

Among the major naturally occurring atmospheric greenhouse gases (excluding water vapour), carbon dioxide (CO_2) has a dominant role since it currently contributes about 55% of anthropogenic greenhouse forcing. The ocean plays a dominant role in the sequestration of anthropogenic CO_2. Human activities presently release about 7.7 Petagrams of carbon per year (PgC yr^{-1}) to the atmosphere, by fossil fuel burning and change in land; it is well established that 3.3 PgC yr^{-1} remain in the atmosphere; the ocean behaves as a sink estimated to 2.0 PgC yr^{-1} and the terrestrial biosphere is assumed to trap the remaining 2.4 PgC yr^{-1}. The global ocean is a major sink of anthropogenic CO_2, which accounts for 48% of the total fossil-fuel and cement-manufacturing emissions of the anthropocene. Furthermore, the current fraction of total anthropogenic CO_2 emissions stored in the ocean appears to be about one-third of the long-term potential (Sabine et al., 2004b).

1.4.1 Role of CO_2 and the Southern Ocean on the transition from glacial to interglacial times

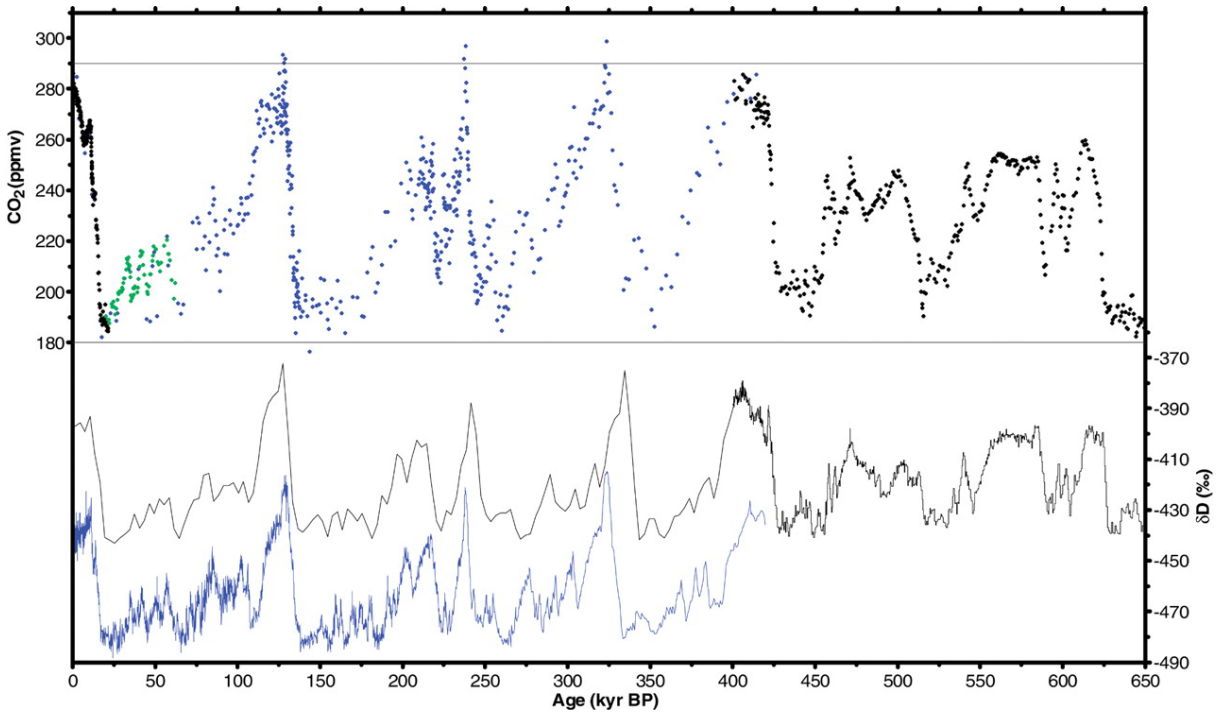

Figure 1.4-1. Composite CO_2 and δD records over six and a half ice age cycles, back to 650,000 years B.P. From Siegenthaler et al. (2005). Black, blue and green dots and lines indicates data measurements from Dome C, Vostok and Taylor Dome, respectively. The ratio of deuterium to hydrogen in ice (expressed as the term δD) provides a record of temperature over Antarctica with more δD negative values corresponding to colder conditions. Black line: Dome C, blue line: Vostok.

About 21 kyr ago, the Earth was at the last glacial maximum (LGM), the peak of the latest of a succession of glaciations alternating with shorter warm periods (interglacials) at intervals of about 100 kyr. The Earth's surface conditions at LGM were considerably different from today's. Huge ice-sheets, possibly up to several kilometres thick, covered large part of the Northern Hemisphere continents while sea level was about 120m lower than now (Project Members Climap, 1976). Figure 1.4-1 presents a composite record of CO_2 concentration and δD (a proxy of temperature, figure 1.4-1) in ice back to 650 kyr reconstructed from ice-cores drilled at various places in Antarctica. Several crucial statements for the understanding of the Earth's climate can be deduced from the figure 1.4-1. First, the concentration of CO_2 and temperature are thightly linked. Second, at any time in the past 650 kyr, the atmospheric CO_2 concentrations were considerably lowerr than they are today (378 ppmV). Interglacial maxima were about 280-300 ppmV during the past 430 kyr, before that, they were only 240-260 ppmV. Glacial minima were consistently in the range of 180-200 ppmV (Siegenthaler et al., 2005). Sea level and sea ice extent are also tightly linked to the evolution of CO_2 concentration and δD (e.g. Sigman and Boyle (2000) and Wolff et al. (2006)). It is worth noting that the cause of the timing and magnitude of these patterns has been a matter of intense over the past. Still, as

yet, there is no broadly accepted explanation for this difference. Besides, recent measurements carried out at Dome C (Siegenthaler et al., 2005) show that a decrease of the magnitude of the changes before 430 kyr B.P. and that long interglacial with stable conditions are not exceptional. Also, the reasons for such observations remain unresolved.

Several reasons have been invoked to explain the glacial-interglacial cycles. This oscillation are statistically linked to cyclic changes in the orbital parameters of the Earth, with characteristic frequencies of roughly 100, 41 and 23 yrs (Hays et al., 1976; Berger et al., 1984). However, related variations of solar irradiance, know as the 'Milankovitch cycles', cannot account for the large amplitude of the glacial cycles of temperature and rapid climate transitions. Positive feedback within the Earth's climate system must amplify the orbital forcing to produce glacial-interglacial cycles.

It is now well established that the evolution of the concentration of the so-called greenhouse gases in the atmosphere is one of the main forcing of glacial cycles (Houghton et al., 2001). Complete review of the different explanations of the variations of atmospheric CO_2 concentration that have been proposed so far go beyond the scope of this introduction. We will present some of them related to potential changes of the circulation and biological pump in the Southern Ocean mostly based on the works of Sigman and Boyle (2000) and Munhoven (Munhoven, 1997). The proposed list is not exhaustiven, and other alternative explanations may be just as valid.

The continental reservoir of organic carbon (figure 1.4-2) most probably decreased during the last age, and thus led to a transfer of CO_2 to the ocean/atmosphere system. This reservoir was therefore acting as a source of CO_2 atmosphere, not a sink, during the glaciation and represented therefore a negative feedback to decreasing CO_2.

Paleo-records and models focus on the atmospheric concentration of CO_2 that exert a significant constrain on the radiation budget of the Earth, however the oceans play a major role in regulating atmospheric CO_2 concentration (Archer et al., 2000; Sigman and Boyle, 2000). The oceans are by far the largest reservoir of carbon on Earth (figure 1.4-2) that exchange large amounts of CO_2 with the atmosphere on the times scales of 10 kyr and less.

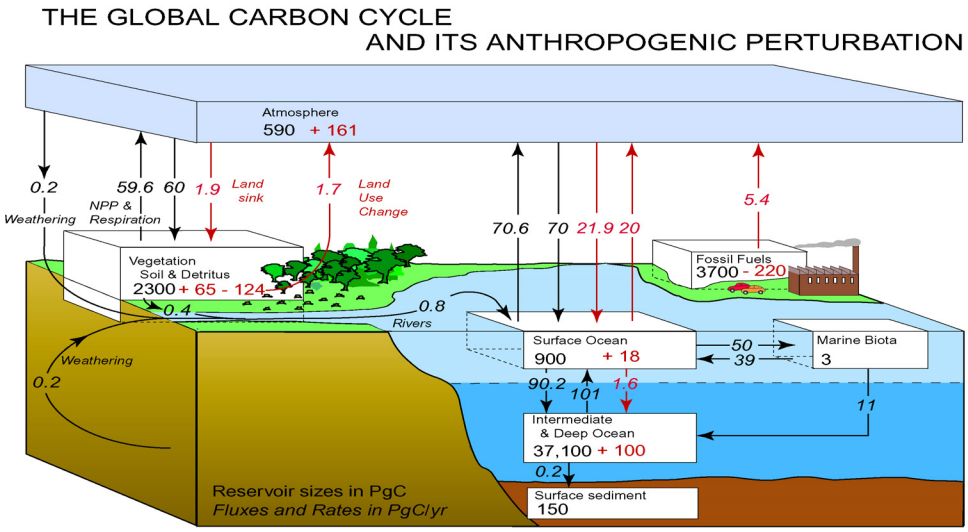

Figure 1.4-2. The preindustrial global carbon cycles an its anthropogenic perturbation. Arrows show the fluxes (in PgC yr^{-1}) between the atmosphere and its two primary sinks, the land and the ocean, averaged over the 1980s. Natural fluxes are in black, anthropogenic fluxes are in red. The net flux between reservoirs is balanced for natural processes but not for the anthropogenic fluxes. Within the boxes, black numbers give the preindustrial times. For the land sink, the first red number is an inferred terrestrial land sink whose origin is speculative; the second one is the decreases due to deforestation. Numbers are slight modifications of those published by the Intergovernmental Panel on Climate Change (Houghton et al., 2001). NPP is net primary production. (From Sarmiento and Gruber (2002))

Hence, most proposed explanations of the dynamics of atmospheric CO_2 call upon changes in thermodynamics, chemistry and biology of the oceans.

The exchange of CO_2 between the atmosphere and the surface ocean is achieved relatively rapidly (6 m to 10 yrs) but the pCO_2 of surface waters is continuously reset by its interaction with the deep ocean reservoir of inorganic carbon which is 25 times that of the atmosphere and surface ocean combined. On the whole, at times scales of interest for paleoclimatology it is considered that the ocean and atmosphere are close to steady state with respect to CO_2 exchange.

Changes of sea surface temperature and salinity

During glaciations, decrease of temperature led to a higher solubility of CO_2 in surface waters. Considering a sea surface temperature decrease of 5°C at low and 2.5° at high latitudes (Guilderson et al., 1994), Sigman and Boyle (2000) estimated that this increased solubility could be responsible for a CO_2 decrease of about 30 ppmV. In parralel, the ocean was about 3% saltier than it is today owing to the 120 m sea level depression at the LGM. This in turn induces an increase of pCO_2 in the atmosphere, estimated to 6.5 ppmV (Broecker, 1982; Sigman and Boyle, 2000).

Ocean alkalinity

The alkalinity of the ocean exerts a strong constrain on the oceanic inorganic carbon reservoir. Numerous issues have arisen regarding to the links between ocean alkalinity, processes affecting the alkalinity, buffer effect of the carbonate system, repercussion on the depth of the lysocline and related burial/dissolution of $CaCO_3$ in the sediments and the feedback on atmospheric CO_2. Briefly, the input of alkalinity from the continents and the removal of alkalinity in sediments should remain in close balance. Perturbation of the surface alkalinity by some changes in weathering of emergent carbonates on land or changes in precipitation and burial of $CaCO_3$ in pelagic waters (changes in the ratio of calcium carbonate to organic carbon in the biogenic particles downward flux, i.e. the so-called rain ratio,) (Broecker, 1982) or in shallow coral reefs and carbonate banks (Berger, 1982; Opdyke and Walker, 1992) affect alkalinity of the surface waters and may therefore induce significant CO_2 fluxes between the atmosphere and the surface water. However, these changes in surface alkalinity are partly compensated by changes in calcite saturation depth and subsequently in the depth of the lysocline. Such changes of the lysocline affect the overall burial of $CaCO_3$ in the oceanic sediments and then act as a negative feedback on the alkalinity - the alkalinity compensation -. In turn, this affect the CO_2 fluxes related to the primary effect on surface alkalinity.

Sigman and Boyle (2000) point out that the average lysocline depth indicates that no such significant alteration of the rain ratio that can solely explain glacial/interglacial change occurred. In the frame, despite $CaCO_3$ dynamics and their repercussion of the glacial-interglacial cycles are not fully resolved, the authors argue that there are reasons to doubt the role of whole ocean alkalinity changes as the sole driver of glacial/interglacial CO_2 changes. However, most biological pump mechanisms for lowering atmospheric CO_2 affects the total alkalinity of the ocean, and this contribute significantly to their capacity to lower atmospheric CO_2

The ocean nutrient reservoir and low-latitude productivity

Broecker (1982) suggested that lower glacial CO_2 levels might be ascribed to a strengthening of the oceanic biological pump. Broecker (1982) and McElroy (1983) suggested that such strengthening could be driven by an increase of the oceanic nitrate and phosphate reservoirs which would allow enhanced low-latitude biological production. However, large - and unrealistically - changes of nutrients are required to affect PCO_2 in the ranges observed in the course of glacial cycles. Alternative scenarios calling upon changes in the C:P ratio in the global ocean, better utilization of nutrients or constant production but reduced mixing and ventilation in conjunction with reduced mixinh between surface and deep ocean at high latitude have also been proposed (e.g. (1997)).

Iron hypothesis

Evidence of the low iron concentration in the Southern Ocean as a limitation of phytoplanktonic growth led Martin (1990) to suggest that changes of aeolian iron flux to the S.O. might be the cause of glacial-interglacial changes, via the change in the efficiency of the S.O. biological pump. Indeed Antarctic ice core records previously suggested that glacial increases in S.O. macronutrient utilization and in the export of particulate organic carbon (POC) to the deep ocean may be attributed to increases in aeolian iron flux (Martin, 1990; Kumar et al., 1995; Watson et al., 2000). However,

this hypothesis is challenged by some models (Bopp et al., 2003) and recent sedimentary records (Kohfeld et al., 2005) and data from Dome C ice cores (Rothlisberger et al., 2004; Wolff et al., 2006). Instead, the initiation of glacial cycles could be ascribed to increased stratification of the glacial ocean (Toggweiler, 1999; Sigman and Boyle, 2000), reduced ventilation of CO_2-rich deep water as a result of more extended sea ice cover (Stephens and Keeling, 2000) that is remarkably well linked to temperature and CO_2 concentration (Wolff et al., 2006), and changes in the location and mechanisms of deep-water formation that alter deepwater composition (Toggweiler et al., 2003a; Toggweiler et al., 2003b).

Silicic acid leakage

An additional explanation to glacial cycles, the so called “silicic acid leakage” hypothesis, has arisen recently (Brzezinski et al., 2002; Matsumoto et al., 2002). SAMW supply 75% of the nutrients necessary to the biota north of 30°S (Sarmiento et al., 2004). The ‘‘silicic acid leakage’’ hypothesis states that the nitrate to silicic acid ratio (NO_3^-:$Si(OH)_4$) of SAMW is therefore important in controlling low latitude productivity. During interglacial times, NO_3^-:$Si(OH)_4$ is high and SAMW mainly supply nitrate to low latitudes favouring the development of carbonated organisms. Laboratory experiments show that the NO_3^-:$Si(OH)_4$ uptake ratio of diatoms increases with iron concentration (Brzezinski et al., 2002). It may therefore be expected NO_3^-:$Si(OH)_4$ was lower due to the higher aeolian iron input. Thereafter, glacial SAMW exported more silicic acid compared to nitrate to low-latitude regions, stimulating the growth of siliceous organisms in those areas. This decreases the rain ratio at low latitudes, which in turn reduces atmospheric CO_2 concentration (Archer and Johnson, 2000). This hypothesis have recently received some support from sedimentary records (Crosta et al., 2005) and assigns a supplementary role to the S.O. with respect to CO_2 and climate at glacial-interglacial timescale.

Finally, Wolff et al. (2006) indicate that sulfur compounds had no significant role in climate feedback. The lack of changes in sulphur compound concentrations in Dome C ice, suggests that the abundance and production of DMS-planktonic producers as *P. Antarctica* have hardly changed in the course of glacial-interglacial cycles.

1.4.2 The Southern Ocean in the Anthropocene

1.4.2.1 Global warming and thermohaline circulation

The central role of the S.O. in the global circulation implies that any changes occurring there would have global impacts. Some coupled ocean-atmosphere models predict that changes in the circulation of the S.O. under global warming will be very profound, with major reduction in the depth and extent of convective mixing occuring by the time of atmospheric CO_2 concentration doubling, with near-cessation of convection by the time of tripling (Hirst, 1999). Similarly significant reduction in the downwelling adjacent to Antarctica associated with Antarctic Bottom Water formation

is to be expected, which also nearly ceases by the time of atmospheric CO_2 tripling. These changes are associated with such strong reductions in surface density and salinity that the pycnocline and the halocline south of 60°S might intensify by about a factor of four.

However, there remains considerable uncertainty regarding the behaviour of Antarctica in future climate change scenarios (Oppenheimer and Alley, 2004). Changes in the freshwater flux to the North Atlantic Ocean act as the pacemaker of oceanic thermohaline circulation changes (Bryan, 1986; Stocker et al., 1992; Manabe and Stouffer, 1997). However, recent studies suggest that the oceanic thermohaline circulation is more sensitive to the freshwater flux to the S.O. than to the North Atlantic (Seidov et al., 2001). One scenario outlined by Oppenheimer (1998) is that the Ross Ice Shelf could disintegrate within 20 yr - 50 yr. The resulting discharge of freshwater into the surface layers of the Southern Ocean could affect the global thermohaline circulation and the global climate. Weaver and Hillaire-Marcel (2004) proposed that a large meltwater pulse from Antarctica triggered a sudden warming during the last deglaciation. They added in their model freshwater to specific areas known to be formation sites of AAIW and AABW. As the density of AAIW and AABW decreased, the formation of NADW intensified. After 500 yr, the North Atlantic region had warmed by up to 5°C, while large areas of the southern hemisphere had cooled, by as much as 7°C. Other studies predicted that salinity perturbations in the S.O. would lead to significant temperature anomalies at the equator, (Ivchenko et al., 2004) and a global impact within 10 yr (Richardson et al., 2005).

Finnaly, the S.O. circulation is also intimately linked to sea ice cover. Any changes in the latter can therefore have major impact on the oceanic thermohaline circulation (Goosse and Fichefet, 1999). Recent model studies suggest that the main forcing for driving changes of the thermohaline circulation is the changing Antarctic sea ice cover (Shin et al., 2003; Liu et al., 2005)

1.4.2.2 Impact of raising sea surface temperature on marine communities

A large data set on pelagic communities of the North Sea showed that climate changes induce shifts in the phenology from primary producers to tertiary producers, including diatoms and dinoflagellates, copepods, (among other, e.g. (2004)) and fish (Both et al., 2006). The main drivers of these changes are likely to be the increase of annual average SST (+ 0.9°C from 1958 to 2002), and the resulting intensification and/or earlier onset of stratification. Regarding to the evolution of the blooming period, the effect of raising SST appears to affect more dinaflogellates. This community appears to respond not only physiologically to temperature but also to stratification, and bloomed earlier during the seasonal cycle. Diatoms were less affected because the blooming of these organisms depends on the photoperiod that controls diatom spore growth and germination (Eilersten et al., 1995). This can have significant implications on secondary and tertiary producers. Indeed, there is not only the fact that pelagic organism are responding to global warming, but also the variability of the intensity of the response amongst the pelagic assemblages. The different extent to which functional groups are evolving in response to warming lead

to a mismatch between successive trophic levels and a change in the synchrony of timing between primary, secondary and tertiary production. Because efficient transfer of marine pelagic production to higher trophic levels, and its implication for the biological pump, is largely dependent on the temporal synchronysation between successive trophic production peaks, it is suggested that marine trophodynamics may have already been radically altered (notwithstanding some species adaptations). For instance, the decline in the abundance of key planktonic prey and shifts in their seasonality, in addition to over-fishing, have enhanced the decline in North Sea cod stocks (Beaugrand et al., 2003). Also, in the North Sea nearly two-thirds of species have shifted in mean latitude and/or depth over 25 yr (Perry et al., 2005; Both et al., 2006). Species with shorte life cycles and smaller body sizes are more subject to changes. Such differences in shifting rates are a matter of concern since this could alter spatial overlap among species, thereby disrupting interactions and potentially compounding the decoupling effects of climate-driven changes in phenology. Presenty, S.O. records do not allow to conduct such studies. However, this raises some concern for the S.O. food web.

1.4.2.3 Reduced sea ice extent

The past and future evolution of the sea ice cover was conducted using the ORCA2-LIM and ECBILT-CLIO 3D ice-ocean models (Dehairs et al., 2006). Over the past 250 years, the annual mean ice coverage has decreased in response to both natural and anthropogenic forcing. The latter forcing has become stronger over the past 150 years. Nowadays, the decrease of ice cover is more acute in the northern than in the southern hemisphere. This different behaviour is due to the thermal inertia of the S.O. However, model outputs predict a more abrupt decrease of S.O. sea ice extent in the future Annual mean sea ice extents in both hemispheres would therefore become comparable by the end of the century. In parallel, the seasonal amplitude of sea ice extent will increase.

Reduced ice extents such such as those predicted would lead to deeper surface mixed layers in the S.O.. As a consequence, the future decline of ice melt-induced stability of the water column may lead to a shift in the dominant food web, from larger, sun-adapted diatoms to smaller, shade-adapted fagellates (Walsh et al., 2001). This would impact the biological pump and the sequestration of atmospheric CO_2. In addition, as a consequence of this shift in the natural assemblages of phytoplankton, a marked transition from krill to salps has been ascribed to reduced sea ice extent (Nicol, 2000; Walsh et al., 2001; Atkinson et al., 2004). As pointed out by Atkinson et al. (2004), such changes among key species would have profound implications for the S.O. higher trophic organisms such as penguins, albatrosses, seals and whales that rely on krill for food.

1.4.2.4 Sensitivity of the carbon pump to global change

Bopp et al. (2001) point out that raising temperature and related increase of stratification induce a reduction in nutrient supply and an increase in light efficiency. By the time atmospheric CO_2 concentrations doubling, superimposition of these two effects will have lead to a global reduction of the global marine export production by 6%. However large regionally variability has to be expected, e.g. an increase of 10%

of marine export production is predicted in the S.O.. Bopp et al. (2001) also stressed the need for a better representation of ocean dynamics in the S.O. and ifor mproved sea-ice models.

SWAMCO is a suite of 1D models of the marine planktonic system calculating C, N, P, Si, Fe cycling within the upper ocean, the export production and the exchange of CO_2 (Lancelot et al., 2000; Hannon et al., 2001; Pasquer et al., 2005). SWAMCO-4 is constrained by physical, chemical and biological (grazing, lysis) controls, and explicitly details the dynamics of four relevant phytoplankton functional groups (diatoms, pico/nano phytoplankton, coccolithophorids, and *Phaeocystis spp*.) with respect to C, N, P, Si, Fe cycling and climate change. It allows to investigate the response of the S.O. carbon pump (among other) to raising PCO_2. By running SWAMCO-4 at different latitudes, Pasquer et al. (2005) showed that raising PCO_2 over the last decade should have enhanced the carbon uptake by the ocean at all latitudes. However the amplitude of the predicted atmospheric CO_2 sinks displays large regional and inter-annual variations. This holds for the marginal ice zone of the Ross Sea where the magnitude of the predicted annual CO_2 sink positively corelates with the length of the surface ocean ice-cover period which determines the iron surface concentration at the time of ice melting.

By coupling SWAMCO-4 to the 3D ice-ocean ORCA-LIM model, Dehairs et al. (2006) point out the dual effect of available light (combination of latitudinal and ice coverage effects) and Fe limitation in controlling primary production, and stress the need to better constrain iron sources in the Southern Ocean and mesozooplankton grazing in the MIZ.

1.4.2.5 Ocean acidification

Current model projections predict that surface ocean pCO_2 levels will double over their pre-industrial values by the middle of this century. The concomitant surface ocean pH changes will be 3 times higher than those experienced during the transition from glacial to interglacial periods (Falkowski et al., 2000). *In vitro* experiments suggest that the repercussions of such an acidification could be significant for phytoplanktonic communities and the carbon cycle. Indeed, despite some studies having shown that marine autotrophic communities are often insensitive to pCO_2 changes, several studies have at the countrary shown that some seagrass (Zimmerman et al., 1997), macroalgae (Gao et al., 1993), diatom (Riebesell et al., 1993; Chen and Durbin, 1994), coccolithophorid (Nimer and Merrett, 1993; Hiwatari et al., 1995; Riebesell et al., 2000; Zondervan et al., 2001; Delille et al., 2005; Engel et al., 2005) and cyanobacteria (Qiu and Gao, 2002) species exhibit higher photosynthesis rates under CO_2 enrichment. In mesocosm experiments, raising CO_2 levels enhance the carbon export of coccolithophorids mainly due to the increase of TEP production and affects rain ratio (inorganic:organic carbon ratio of exported matter) in coccolithophorids (Delille et al., 2005; Engel et al., 2005). It has also been shown that phytoplanktonic assemblages can experience marked changes (Tortell et al., 2002; Martin-Jezequel et al., 2004) under elevated pCO_2. While few studies investigating the impact of high CO_2 levels on bacteria have not reported conspicuous effects (Rochelle-Newall et al., 2004), pelagic and benthic calcifying organisms are affected by the increase of CO_2. These include corals (Gattuso et al., 1998a; Kleypas et al., 1999; Langdon et al., 2003) coralline algae, foraminifers and

pteropods (Orr et al., 2005). Even fish and other water-breathing animals might be as they are probably more sensitive to hypercania - too elevated levels of CO_2 in the blood - than terrestrial animals (Ishimatsu et al., 2005).

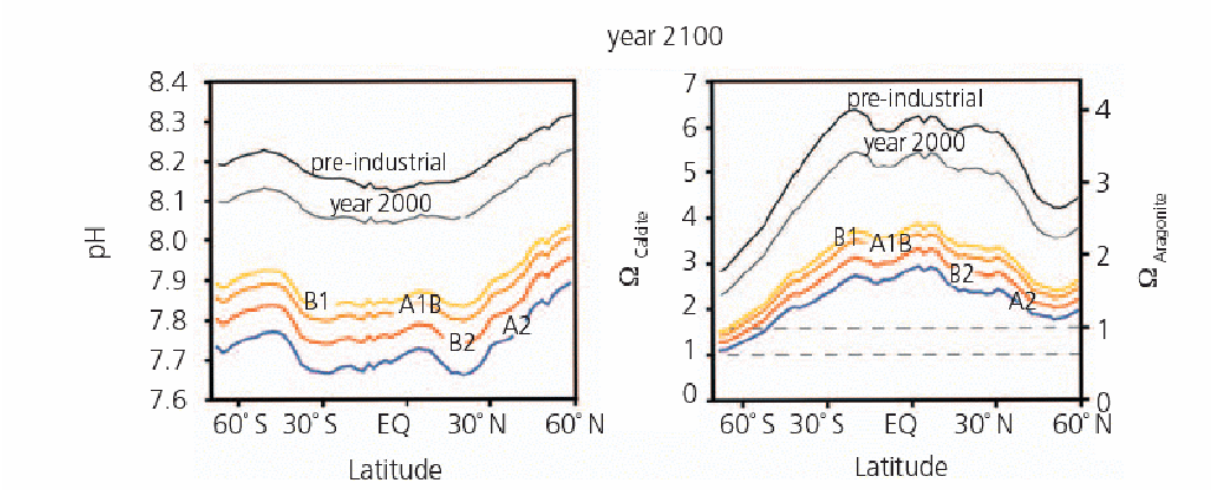

Figure 1.4-3. Modelled variations in pH and Calcite and Aragonite saturation state in the surface oceans modelled for various IPPC scenarios for future emissions in 2100. Dashed lines show calcite and aragonite saturation horizons where a saturation state of less than 1 corresponds to under-saturation. (from Raven et al. (2005) after Caldeira and Wickett (2005)).

In the Southern Ocean, growth of marine calcifying organisms would be dramatically affected by the fall of the calcite and aragonite saturation state resulting from the decrease of pH (Fig. 1.4-3), as some projections predict that aragonite saturation state of the surface waters south of Australia will cross the threshold of saturation by 2100 (Caldeira and Wickett, 2005). Decrease of saturation state would not only affect coccolithophorids, but also pteropods which form a key link in the food chain throughout the Southern Ocean (Orr et al., 2005).

It has also been suggested that the speciation and subsequent mobilization of micronutrients may also be affected (Kester, 1986; Morel et al., 2005) with both beneficial (e.g., Co, Fe) and inhibitory consequences (e.g., Cu) which are of interest in HNLC areas such as the Southern Ocean. For the time being, large scale impacts of this ocean acidification on phytoplanktonic communities and on the carbon cycle remain to be investigated (Gruber et al., 2004).

1.5 Sea Ice

1.5.1 Physical properties

Sea ice physical and biological processes have been described in details by Thomas and Dieckmann (2003) and Arrigo and Thomas (2004). In the course of the year, Southern Ocean, Arctic Ocean, Baltic and other seas such as Caspian and Okhotsk seas experience a cycle of freezing and melting. In the Arctic region, the ice cover doubles its size from summer to winter (Table 1-7), while in the S.O., the corresponding value is five-fold, so that total sea ice extent at anyone time range

between 19 × 10^6 km² to 27.5 × 10^6 km² (Fig. 1.5-1). Thus, sea ice at its maximum seasonal extent covers about 7% of the Earth surface, representing one of the largest biomes on Earth (Arrigo et al., 1997; Lizotte, 2001).

	Ice extent					Ice area	
	Arctic region		Southen Ocean		Both hemispheres	Arctic	Southen Ocean
Min	7.5	(September)	3.8	(February)	19	6	3
Max	15.5	(March)	19	(September)	27.5	14.5	15.5

Table 1-7. Minimum and maximal ice extent (corresponding month within brackets) and ice area (× 10^6 km²) averaged over the 1979-2000 period compiled after (Comiso, 2003).

As the surface seawater cool down to temperature close to -1.86° C (freezing point of seawater with a salinity of 34) frazil ice (Fig. 1.5-2) can develop rapidly under turbulent conditions as strong wind events drive air-sea transfer of large quantities of heat that that triggers sea ice growth (e.g. (Haas, 2003; Eicken, 2003)). When wind speed decreased and sea surface calms, ice crystals floating at the sea surface can coalesce into semi-consolidated grease ice, and eventually, into thicker nilas and pancake ice (Sarmiento and Gruber, 2002). Ice pancakes fuses together to form a continuous ice pack. Subsequent ice growth develops vertically beyond the consolidated pancake stage vertically as heat is extracted from the sea ice surface by the cold atmosphere, to form the columnar ice (Fig. 1.5-2).

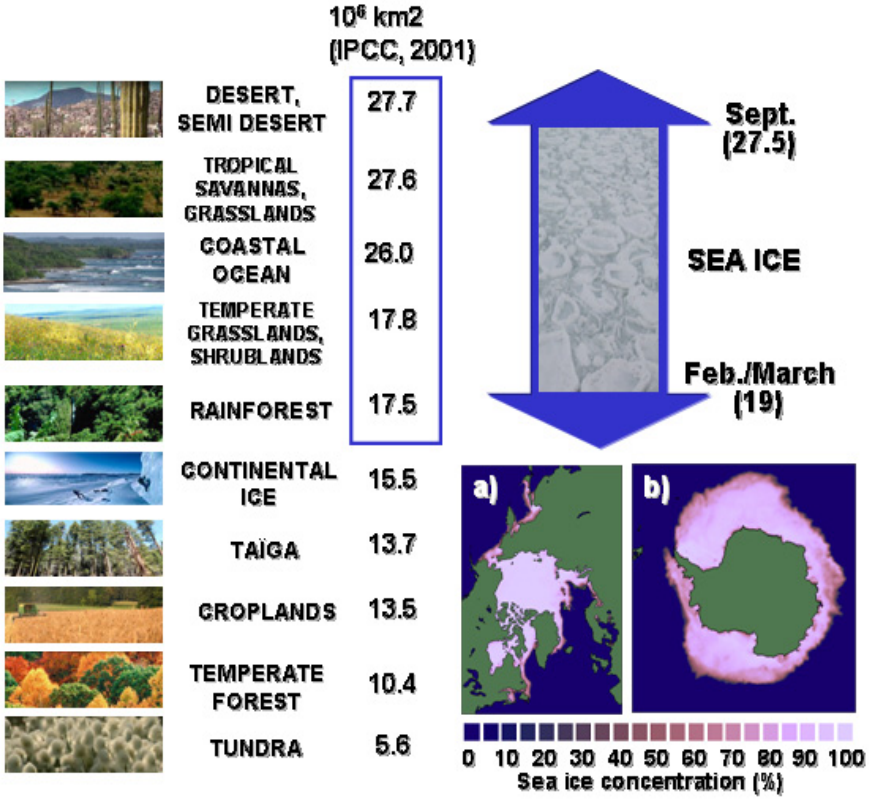

Figure 1.5-1. Surface area covered by sea ice compared to other biomes after - a) sea ice concentration in the Arctic Region in February 2005 (total extent: 14.4 × 10^6 km^2), b) sea ice concentration in the Southern Ocean in September 2005 (total extent: 19.2 × 10^6 km^2) from sea ice index products delivered by the National Snow and Ice Data Centre (http://nsidc.org/data/seaice_index/). After Tison et al. (2005).

Such columnar ice constitutes most of the land-fast sea ice, where the frazil ice stage is limited. Columnar ice extends vertically into the water column. Rafting of ice floes, as sea ice is moved by the wind and tides, causes breakage and occasionally forces parts of the floe below freeboard, flooding the ice surface with seawater (Fig. 1.5-2). This is an important process which can trigger growth of surface communities as an efficient pathway for nutrient supply (section 1.5.2.1).

Physical and chemical processes at the interface of the growing columnar ice with water is of importance as they constrains the properties, chemical composition and biological abundance of the ice. The lamellar ice-water interface, referred as the skeletal layer (Fig. 1.5-3), is a relatively open system where develop a boundary layer which experience supercooling and enhanced impurities concentration owing to impurities expulsion from the ice.

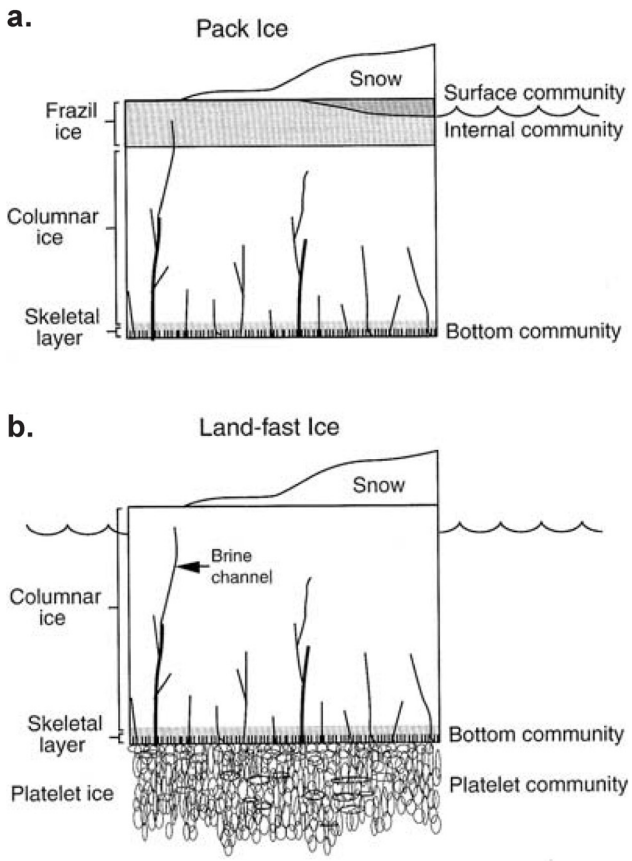

Figure 1.5-2 Schematic illustration of pack ice (a) and land-fast (b) sea ice showing the major physical features and locations of microbial habitats. From Arrigo (2003).

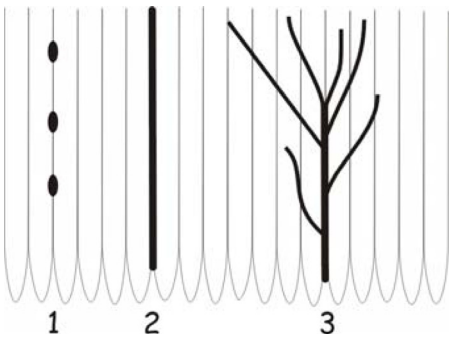

Figure 1.5-3. Schematic illustration of skeletal layer and most common brines inclusions: 1 : brine pockets, 2: brine layers and 3: brine channels. From Verbeke (2005).

During sea ice growth, most of the impurities (solutes, gases, particulate matter) are expelled from the pure ice crystals at the ice-water interface. However, a small fraction of impurities (~10%) remains trapped in bubbles, brine pockets, tubes or channels (Fig. 1.5-3) that contribute to the overall sea ice porosity and host active auto- and hetero-trophic microbial communities (Arrigo et al., 1997; Lizotte, 2001; Thomas and Dieckmann, 2002a; Arrigo, 2003). Expelled impurities can remain trapped in the brines inclusions that experienc therefore high concentration of dissolved and particulate matter. Salinities over 150 are common in these intrusions and temperature can be less than -20°C.

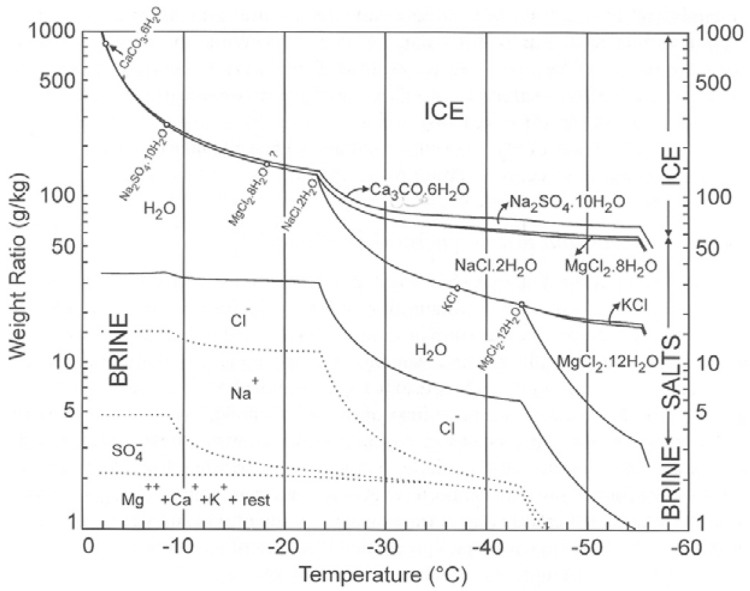

Figure 1.5-4 Phase diagram of sea ice. The different curves indicate the mass fraction of solid ice (top), salts (middle) and liquid (bottom) present in closed volume of ideal sea water at different temperature. Open circles indicate the temperature at which the salts precipitate. From Assur (1958).

As a consequence, chemical equilibriums within the brines are strongly affected and precipitation of salts can occurs (Fig. 1.5-4). Precipitation of $CaCO_3$ is of particular importance for CO_2 dynamics and is detailed in the chapters 4.1 and 4.3. As showed by the (Fig. 1.5-4), $CaCO_3$ is potentially the first salt to precipitate during sea ice growth.

Further depletions occur via processes such as brine expulsion, migration, drainage or convection, that are mainly controlled by the history of the thermal regime of the ice (Weeks and Ackley, 1986; Wettlaufer et al., 1997; Eicken, 2003) while brine volume and salinity also depend on thermodynamic equilibrium reactions (Cox and Weeks, 1983).

A 5% relative brine volume is a threshold above which sea ice permeability increases drastically (Golden et al., 1998) and is also likely to represent a threshold above which air-ice gas exchange increases (Buckley and Trodahl, 1987). This permeability threshold would occur at a temperature of -10°C for a bulk ice salinity of 10, corroborating the observation that sea ice is a highly permeable medium for gases (Gosink et al., 1976) and consistent with the reported uptake of atmospheric CO_2 over ice covered waters (Semiletov et al., 2004).

1.5.2 Sea ice biota

Algal communities, especially diatoms, flourish within the distinct micro-habitats which are created when sea ice forms and ages (Fig. 1.5-2). Primary production by

this community can be significant (section 1.2.2.3). The primary advantage afforded by sea ice is that is provides a platform from which sea ice algae can remain suspended in the upper ocean where light is sufficient for net growth. Growth of the algae will be partly limited by the supply of nutrient, especially in the columnar ice. This latter is driven, if sea ice is permeable to liquids, by internal convection or brine drainage which supply nutrient-rich underlying seawater to the upper layer of the ice (Weeks and Ackley, 1986; Ackley and Sullivan, 1994; Golden et al., 1998).

The initial stage of sea ice formation generally begins in the autumn when there are still substantial microbial populations left over in surface waters from the preceding spring blooms. As a result, during early frazil ice formation, particles such as microalgae, heterotrophic protists, and bacteria are often scavenged from the water column as the newly-formed frazil ice crystals rise to the surface (Garrison et al., 1989). In some cases, enrichment factors for Chl *a* calculated from the ratio between the concentrations in ice and underlying water have been reported to be as high as 53, with the incorporation of large diatoms being observed most commonly (Weissenberger and Grossmann, 1998). Hence while most of the inorganic impurities are expelled from sea ice, a significant fraction of organic matter can be concentrated within the sea ice. These concentration of biogenic particulate matter is a pathway to concentrate macro and micro-nutrients as iron, that otherwise would have been expelled. This macro and micro-nutrients, released during organic matter decay, can be either recycled internally within sea ice ore released in the brines, then to seawater. Recently, it has be shown that iron inputs to surface waters from melting sea ice would represent 70% of the estimated daily total flux when taking into account available data on dust deposition, extraterrestrial iron, vertical diffusion and upwelling, being a paramount contribution to Fe biogeochemical cycle in the water column (Lannuzel et al., 2006) .

Details of two specific communities are provided below (sections 1.5.2.1 and 1.5.2.2) as their interactions with CO_2 dynamics are investigated in the chapters 4.2 and 4.3.

1.5.2.1 Surface communities

Surface communities require a particular attention reagarding to air-sea ice CO_2 fluxes issues. Surface communities are situated at the air-sea ice interface and they can exchange CO_2 directly with the atmosphere without hampering by low ice permeability. Furthermore they can be highly productive and therefore uptake of CO_2 related to surface community primary production can potentially overcome air-sea ice fluxes.

Sea ice surface communities benefit from high light levels and from nutriments from seawater flooding as snow loading or sea ice rafting depress the ice surface below the freeboard. Such surface flooding occurs over 15-30% of the ice pack in Antarctica (Wadhams et al., 1987). Slush – a mixture of melting snow, ice and flooding seawater covering sea ice - is known to berth highly productive algae community (Legendre et al., 1992).These surface communities exhibit photosynthetic rates comparable to those of open ocean Antarctic phytoplankton (Lizotte and

Sullivan, 1992) and might be responsible for the majority of sea surface productivity in Antarctic sea ice (Legendre et al., 1992).

Semiletov et al. (2004) reported significant CO_2 fluxes over arctic sea ice edge and ascribed their origin to both open brine channels and sea-ice melt ponds. Sea ice melt ponds are liquid water mostly originating from melted snow that lies at the surface of sea ice and occurs usually in the spring. Melt pond are common in the arctic but less in the Antarctic. Biollgical activity within melt pond is poorly documented. Carstens (2002) stated that "low salinity and low ion levels as well as its ultraoligotrophic character and exposure to high levels of irradiance seem to act as limiting factors regarding the colonization" of melt ponds in the North East Greenland Current. Conversely, Gradinger et al. (2005) reported Chl *a* concentrations in melt pond ranging from (1 to 7 µg L^{-1}), similar to concentration in ice surface and in the same range than concentration of bottom ice. This communities would be fuelled in nutrients by marine infiltration or atmospheric deposition (Granskog et al., 2003). Such Chl *a* concentration suggest that primary production in melt ponds may deserves investigation, but to our best knowledge, no estimates are available yet.

Surface snow communities can be high within snow algal patches. The concentrations of snow algae, in coloured snow patches from different locations on earth vary between 6 and 530. 10^3 cells mL^{-1} (Gradinger and Nürnberg, 1996). They pointed out that species composition within snow algal patches is highly variable, but diatoms are absent. They gives significant gross estimate of primary production ranging from 12 to 476 mg C m^{-2} d^{-1} in algae-rich red snow patches, but, again, no up scaling of primary production within snow above sea ice is available.

1.5.2.2 Platelet ice

Platelet ice is a semi-consolidated layer of ice ranging from a few cm to several meters in thickness which is commonly observed beneath land-fast ice like in Adélie land or in regions adjacent to floating ice shelves where surface waters can become supercooled (Fig. 1.5-2 b). Platelet ice is the most porous of all sea ice types, being composed of approximately 20% ice and 80% seawater by volume. As a consequence, platelet ice provides approximately five times more surface for algal attachment than the skeletal layer where most of the biomass is usually concentrated. Furthermore, high porosity allows a rapid nutrient exchange with surrounding seawater, which fuel algae growth. This contrasts with congelation ice where algae growth is often limited by the availability of nutrients which are mostly supplied (if there are no top-down seawater infiltrations) to the upper sea ice layer through internal physical processes (internal convection and brine drainage). As a consequence of its high surface area and high porosity, platelet ice harbours some of the highest accumulations of sea ice algae found anywhere on Earth, sometimes exceeding 1000 mg Chl *a* m^{-2} (e.g. (Arrigo, 2003) for a review).

1.6 Aims

Open ocean

When we started our work, the spatial and temporal variability of pCO_2 in the open waters of the S.O. was still poorly documented due to the recurrent under-sampling of the S.O.. Corollary, no overall assessment of air-sea CO_2 fluxes derived from in situ pCO_2 measurements was available in the Southern Ocean. We therefore aimed to:

- Investigate mesoscale spatial and temporal variability of pCO_2 in the open waters of the S.O.
- Assess air-sea CO_2 fluxes at the ocean basin scale by first compiling extended data set, then scaling using remote sensing data. This required to focus our study on one ocean basin (the Indian sector of the S.O.) in order to compile a comprehensive data set of pCO_2 measurements.
- Produce air-sea CO_2 fluxes estimates per hydrological province rather than per latitudinal band. This required delimiting these areas. To achieve this objective, we derived the position of the frontal structure from the distribution of the sea surface temperature inferred from remotes sensing data.

Subantarctic coastal area

With the exception of the studies of Metzl et al. (1991), Poisson et al. (1993) and Louanchi et al. (1996) which investigated pCO_2 dynamics above the Kerguelen Plateau, coastal area have been largely ignored in CO_2 budgets of the S.O. We conducted a three years survey - which was the first annual survey with weekly to monthly frequency to be carried out in the S.O. – to investigate CO_2 dynamics and related CO_2 fluxes in the subantarctic waters surrounding the Kerguelen Archipelago. Furthermore, Kerguelen shores host forests of the giant kelp *Macrocystis pyrifera.* While a few studies investigated CO_2 dynamics above seagrass (*Posidonia*) meadows in the Mediterranean Sea, no study of pCO_2 was conducted in productive and dense *Macrocystis* kelp bed. Hence, our survey was a unique opportunity to estimate the CO_2 fluxes related to these kelp forests. We therefore aimed

- To investigate the seasonal evolution of pCO_2 in near-shore shallow waters occupied by Macrocystis kelp bed
- To assess the primary productivity of the kelp throught DIC measurement carried out during diel cycles
- Explore spatial and seasonal variability of pCO_2 and related air-sea CO_2 fluxes in the deeper waters surrounding the archipelago.

Sea ice

For decades, sea ice has been considered by the scientific community and biogeochemical modellers involved in assessing oceanic CO_2 uptake as an inert and impermeable barrier to air-sea exchange of gases. However, this assumption is not supported by studies of the permeability of ice to gases and liquids, which show that sea ice is permeable at temperatures above -10°C (Gosink et al., 1976; Golden et al., 1998). Furthermore, sea ice hosts microbial communities which may potentially uptake CO_2. With the exception of the work of Gleitz et al. (1995), to out best knowledge, no study investigated inorganic carbon dynamics within natural sea ice. Furthermore these authors did not measure or compute pCO_2. Hence, we aim to:

- Verify the assertion of the impermeability of sea ice, by measuring CO_2 fluxes at the air-sea ice interface using several methods (chamber method, eddy covariance and CO_2 profiles).
- Investigate pCO_2 dynamics within sea ice brines. Due to the uncertainties in the inorganic carbon chemistry at subzero temperatures and high salinity, we wanted to measure pCO_2 directly rather than to compute it from TA and pH measurement which require to use the dissociation constants of carbonic acid which might not be valid in the range of temperature and salinity encountered in sea ice brines. We developed therefore an autonomous system to measure pCO_2 in the field using the equilibration method.
- Determine the interaction between sea ice and the underlying layer with regards to dissolved inorganic carbon. We therefore measured pCO_2 underneath the ice.

2 Open Ocean

Clouds over the Southern Ocean (picture taken during the ISPOL cruise in November 2005)

2.1 Fronts in the Southern Ocean as inferred from satellite sea surface temperature data

2.1.1 Foreword

Much of the work presented in this manuscript was carried out in the framework of the projects BELCANTO I, II and III. The backbone of these projects is the integrated approach to study the biogeochemistry of the Southern Ocean and in particular the vertical fate of carbon, from the exchange of CO_2 at the air-sea interface to the export to the mesopelagic and bathypelagic zones. We therefore aimed to evaluate how air-sea CO_2 fluxes translate to carbon storage in deep waters through C export. Carbon export is assessed from multiproxies for the different biogeochemical regions of the Southern Ocean, making awkward the comparison with air-sea CO_2 exchanges which are conventionally given per latitudinal bands. We therefore aimed to provide an assessment of air-sea CO_2 fluxes per biogeochemical region. To achieve this, the first step was to map these biogeochemical regions, using remote sensing tools. We provide in this chapter the first synoptic description of the zonation of the Indian Sector of the Southern Ocean, together with the temporal evolution of the frontal structures.

This chapter has been published in Journal of Marine Systems: "Kostianoy A.G., A.I. Ginzburg, M. Frankignoulle & B. Delille, 2004. Fronts in the Southern Indian Ocean as inferred from satellite sea surface temperature data *Journal of Marine Systems* 45(1-2): 55-73. doi:10.1016/j.jmarsys.2003.09.004 ".

Another publication dealing with the subject "Kostianoy A.G., A.I. Ginzburg, M. Frankignoulle & B. Delille, 2003. Fronts and Mesoscale Variability in the Southern Indian Ocean as Inferred from the TOPEX/POSEIDON and ERS-2 Altimetry Data. Oceanology 43(5):632-642" is available as an annex; the abstract is given below:

Charts of sea level anomalies based on the combined altimetry data from the*TOPEX/POSEIDON* and *ERS-2* satellites, as well as the corresponding charts of the sea surface dynamic heights (constructed by the superposition of SLA distributions over the climatic dynamic topography) and the temperature gradients at the ocean surface on the basis of the satellite Multi-Channel Sea Surface Temperature data, were used to study the mesoscale variability related to the fronts in the Southern Indian Ocean (30°–60°S, 20°–150°E). An analysis of these three types of satellite information for the central weeks of each month during the period from 1997 to 1999 allowed us to distinguish zones of enhanced meandering (eddy formation) within the basin under study, as well as the contributions of individual fronts and their interaction to the regional mesoscale variability. The problems of the correlation between the intensity of mesoscale variability and peculiarities of the local bottom topography and seasonal/interannual variability of mesoscale dynamics are addressed.

Available online at www.sciencedirect.com
SCIENCE DIRECT®
Journal of Marine Systems 45 (2004) 55–73
JOURNAL OF MARINE SYSTEMS
www.elsevier.com/locate/jmarsys

Fronts in the Southern Indian Ocean as inferred from satellite sea surface temperature data

Andrey G. Kostianoy[a,*], Anna I. Ginzburg[a], Michel Frankignoulle[b], Bruno Delille[b]

[a] *P.P. Shirshov Institute of Oceanology, Russian Academy of Sciences, Moscow, Russia*
[b] *Unité d'Océanographie Chimique, MARE, University of Liège, Belgium*

Received 4 April 2002; accepted 8 September 2003

Abstract

Sea surface temperature (SST) derived from the weekly measurements made by the Advanced Very High Resolution Radiometers (AVHRR) of NOAA satellites was used to investigate the structure and space-time variability of large-scale fronts in the Southern Indian Ocean (30–60°S and 20–150°E) during the period of 1997–1999. Monthly SST gradient maps provided an overall view of five basic fronts: the North and South Subtropical fronts (NSTF and SSTF, respectively), the Agulhas Front (AF), the Subantarctic Front (SAF), and the Polar Front (PF). Mean location of the fronts and associated SST and SST gradients with corresponding standard deviations were calculated at each 10°-spaced longitude. A double structure of the NSTF, SAF, and PF was demonstrated as well as the meandering of all fronts with amplitudes of 2–5° in latitude and wavelength of several degrees in longitude. Convergence and transient interaction between neighboring fronts appear to occur not only in the Crozet and Kerguelen regions, but in other regions as well. The mean locations and SST range of every front are in good agreement with previous work based on hydrographic surveys [J. Geophys. Res. 101 (1996) 3675], although some details are different (in particular, the larger zonal extent of the NSTF and the wider frontal SST ranges than previously observed). A good correspondence of the measurements made during two hydrographic surveys in the Kerguelen region (22 January–3 February 1999) and in the Tasmania region (3–22 March 1998) with satellite SST and SST gradient maps was found.

Keywords: Remote sensing; Sea surface temperature; Oceanic fronts; Polar fronts; Southern Ocean; Indian sector (30–60°S and 20–150°E)

1. Introduction

Investigations of large-scale circulation and related frontal features in the Southern Ocean, including the Indian sector, have begun in the 1920s to 1950s (Sarukhanian and Smirnov, 1986; Belkin and Gordon, 1996). However, most studies of the Southern Indian Ocean fronts were carried out during 1980s to 1990s (Lutjeharms, 1981; Deacon, 1982, 1983; Gambéroni et al., 1982; Edwards and Emery, 1982; Colton and Chase, 1983; Lutjeharms and Valentine, 1984; Belkin, 1989a,b; Park et al., 1991, 1993, 2001; Tomczak and Godfrey, 1994; Orsi et al., 1995; Park and Gambéroni, 1995, 1997; Rintoul et al., 1997; Neiman et al., 1997; Holliday and Read, 1998; Smythe-Wright et al., 1998; Rintoul and Bullister, 1999; Pakhomov et al., 2000; Pollard and Read, 2001; Rintoul and Sokolov, 2001;

* Corresponding author. Tel.: +7-095-124-8810; fax: +7-095-124-5983.
E-mail address: kostianoy@online.ru (A.G. Kostianoy).

0924-7963/$ - see front matter

Rintoul and Trull, 2001). A comprehensive review of all available meridional hydrographic sections across the fronts located in the region between Greenwich meridian and Tasmania together with published papers, with consideration of the criteria for determination of different fronts, has been made by Belkin and Gordon (1996). The Southern Indian Ocean was shown to feature a complicated frontal system of quasi-zonal fronts with remarkable regional differences determined by peculiarities of bottom topography (Fig. 1). Five basic fronts are recognized there: the Agulhas Front (AF) associated with the Agulhas Retroflection, the North and South Subtropical fronts (NSTF and SSTF, respectively) as the northern and southern boundaries of the Subtropical Frontal Zone, and the Subantarctic and Polar fronts (SAF and PF, respectively) as the northern and southern boundaries of the Polar Frontal Zone. Three of the latter fronts have a circumpolar character related to the jets of the Antarctic Circumpolar Current; the NSTF is supposed to have wind-driven nature (Belkin and Gordon 1996).

Complicated frontal features arise from the merg ing of neighboring fronts in the regions correspondin to pronounced bottom topography peculiarities, as i the Crozet region (triple AF/SSTF/SAF front name the "Crozet Front") and in the Kerguelen Basin (AF SSTF/SAF or AF/SSTF/SAF/PF frontal structures (Belkin and Gordon, 1996). However, Holliday an Read (1998), according to their continuously sample surface temperature and salinity data, supposed tha these features could result from wide spacing (abou 100 km usually) between hydrographic stations Moreover, in the cases of high space-time variabilit of a front (for example, the "Crozet Front"), even section made in a few days cannot be considere synoptic (Park and Gambéroni, 1997). Furthermore the hydrographic data coverage of the Southern Indian Ocean is rather irregular, with data sparse areas in th regions west of the Crozet Plateau, east of the Ker

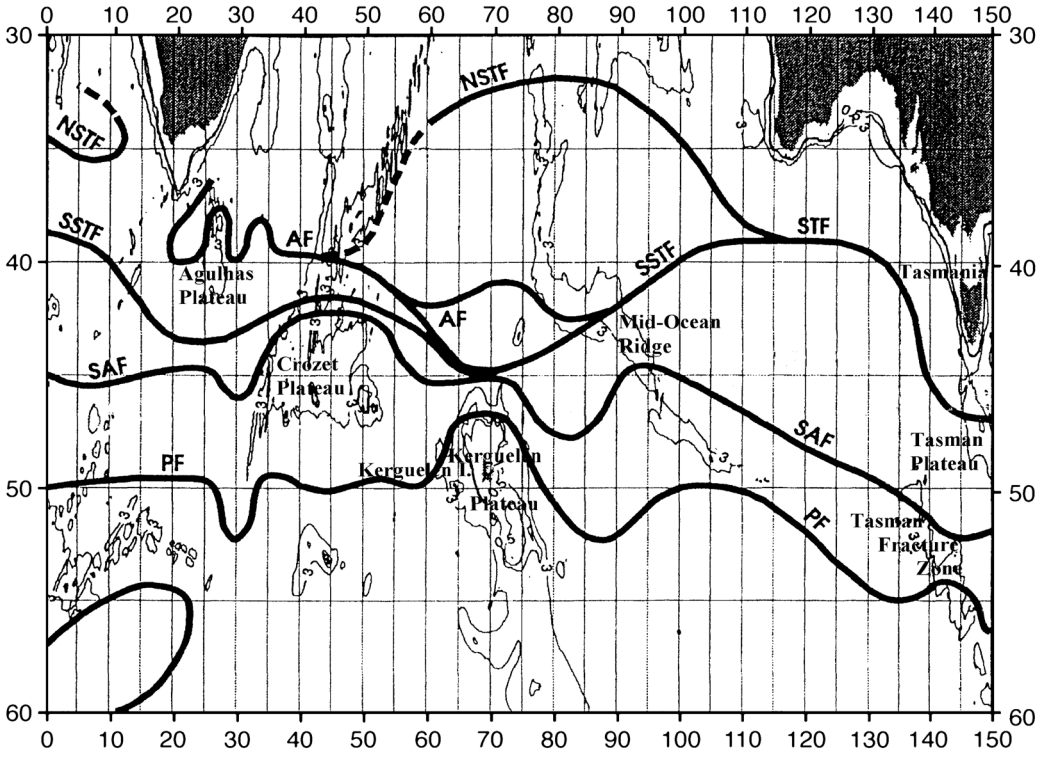

Fig. 1. Study area with frontal paths according to Belkin and Gordon (1996, Fig. 4). Notation: NSTF and SSTF—North and South Subtropica fronts, respectively; AF—the Agulhas Front; SAF—Subantarctic Front; PF—Polar Front.

guelen Plateau, and north of 37°S (Belkin and Gordon, 1996). Hence, detailed and regular synoptic surveys are needed—especially in the regions where fronts are merging and splitting—to have a comprehensive picture of the frontal structure at the basin scale.

Because all five fronts in the Southern Indian Ocean have surface temperature signatures (Belkin and Gordon, 1996), reliable satellite sea surface temperature (SST) data with high spatial and temporal resolution can be used to investigate the variability of the positions of the fronts and their intensity as well. Satellite SST maps have already been used to study dynamics of the PF (Moore et al., 1997, 1999), while Kazmin and Rienecker (1996) used satellite SST data to obtain a global picture and reveal seasonal variability of the main large-scale oceanic frontal zones.

This paper represents the first investigation of the structure and space-time variability of the complete frontal system of the Southern Indian Ocean (30°–60°S, 20°–150°E) based on satellite weekly SST data set for the period of 1997–1999, with an emphasis on poorly known or unknown aspects of location or behavior of different fronts. Furthermore, some examples of nearly synchronous field and satellite observations of fronts in the Kerguelen region (January–February 1999) and in the Tasmania region (March 1998) are considered.

2. Data and methods

The weekly mean Multichannel Sea Surface Temperature (MCSST) data of 1/6 × 1/6° (approximately

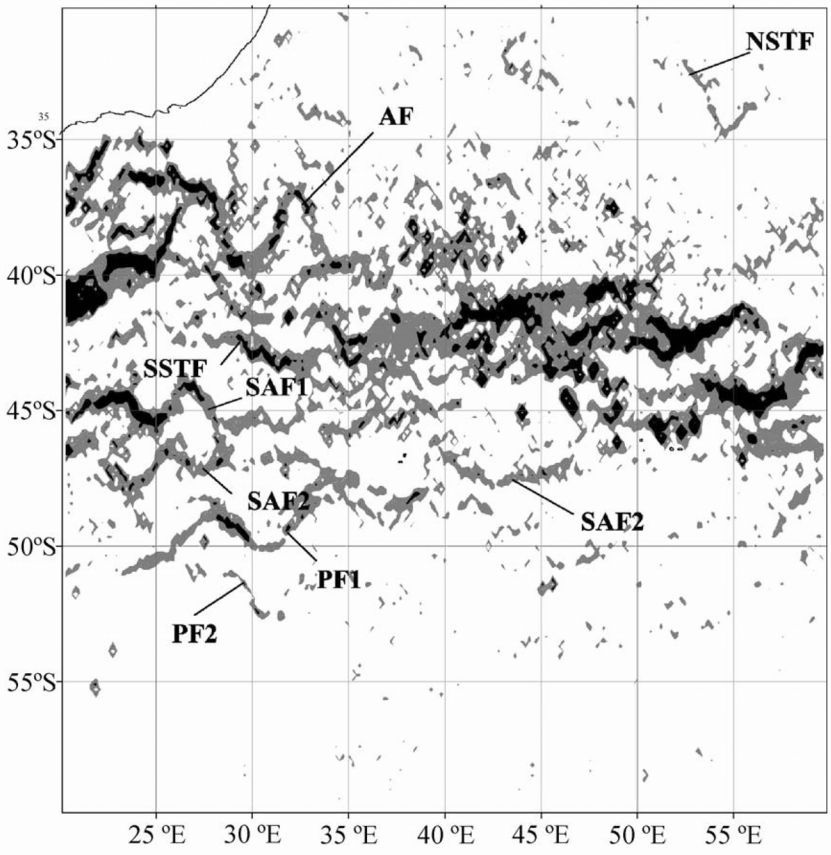

Fig. 2. Sea surface temperature (SST) gradient map for the mid-February 1997 (western region). Hereinafter (unless otherwise stated), grey tone corresponds to SST gradients of 0.02–0.04 °C/km, black tone—to SST gradients equal or higher than 0.04 °C/km.

18 km) resolution were used in this study. The SST data were derived from the Advanced Very High Resolution Radiometers (AVHRR) mounted on the satellites of the National Oceanic and Atmospheric Administration (NOAA). These data are produced in the Jet Propulsion Laboratory (JPL, USA) since 1981 with the temperature resolution of about 0.1 °C. For each grid point, the SST value is computed as the average of all MCSST measurements available for 1 week. Furthermore, JPL provides "interpolated" data sets in which the areas void of measurements (basically due to cloudiness) are filled using the Laplacian interpolation technique. For the present analysis, we used the nighttime interpolated MCSST data for the period 1997–1999 from the area between 30–60°S and 20–150°E. It should be noted that because subsurface measurements (mainly drifters data) are widely used as ground-truth data to calibrate SST values from AVHRR, the MCSST data correspond in fact to the temperature of the surface layer and can be compared with field measurements without any correction for the temperature drop in the skin layer (Fedorov and Ginsburg, 1992).

In order to retain the maximal spatial resolution of the data, the analysis was based not on the monthly averaged data, as it was made in the study of Kazmin and Rienecker (1996), but on the weekly averaged data for the weeks in the middle of each month of the 3 years. Thus, the data set used in this study comprised 36 SST maps (36 mid-month weeks) of 170 × 739 pixels. In order to obtain a picture of main fronts in the Southern Indian Ocean, the SST maps have been converted to SST gradient maps. The SST gradient was calculated for each grid point using a two-dimensional gradient operator that computes the SST difference between two adjacent points along latitude and longitude. Some examples of the SST gradient maps obtained for the western (20–60°E), central (60–100°E), and eastern (100–150°E) regions of the basin in different years are given in Figs. 2–10. In order to obtain a clear frontal pattern and to avoid "noise" in the SST gradient distribution,

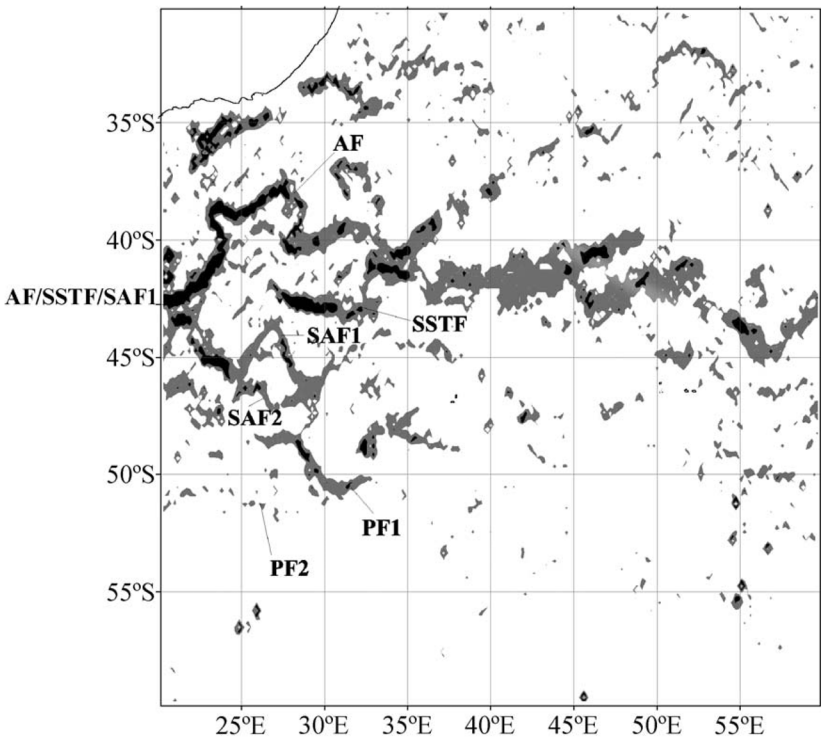

Fig. 3. Sea surface temperature gradient map for the mid-March 1997 (western region).

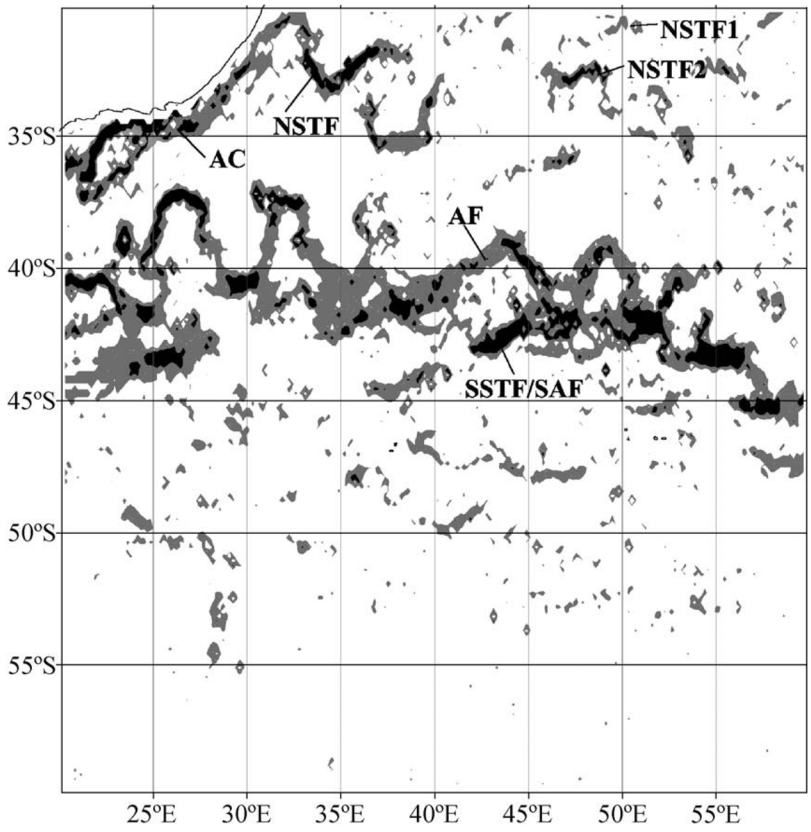

Fig. 4. Sea surface temperature gradient map for the mid-April 1998 (western region).

attention had to be paid to map only the values that were higher than 0.02 °C km^{-1}. The lowering of the threshold of the SST gradient mapping highlights the less detectable fronts south of 45°S (in the western region), but increases the "noise" of the rest of the area. However, we kept the same minimum threshold (0.02 °C km^{-1}) for all SST gradients maps of the three regions to allow the comparison of the different parts of the Southern Indian Ocean. Two gradations of shading of SST gradients were used in SST gradient maps: one in the range 0.02–0.04 °C km^{-1} and another equal or higher than 0.04 °C km^{-1}. Such kind of analysis has been already applied to the Northeast Atlantic Ocean (5–45°N) in order to detect the Azores Frontal Zone, the Northwest African upwelling front, and the Cape Verde Frontal Zone (Djenidi et al., 2000).

The digital files of the SST gradients obtained were used to determine positions of the NSTF, AF, SSTF, SAF, and PF according to the location of the appropriate maximum gradient at fixed longitudes starting from 20°E with a regular 10°-longitude interval (the interval was chosen to reduce the huge amount of data). In uncertain cases, for instance, when fronts lost their spatial coherence due to local low gradients, the appropriate SST files were used to trace the fronts. Furthermore, maps, sections, and SST characteristics of fronts presented in Belkin and Gordon (1996) were used as a reference to control the position and SST of poorly defined fronts in such cases. The same criteria were used in the cases where two or three fronts tended to merge. As a result, mean position (latitude), SST at this latter position, and SST gradient with corresponding standard deviations as well as mini-

mum and maximum values have been calculated for every front at each 10° of longitude.

Data collected during two hydrographic surveys carried out in the Southern Indian Ocean during the period under consideration were also analyzed. One of the survey was carried out during 3–22 March 1998 in the Tasmania region (about 40–55°S, 141–145°E) during the SAZ cruise (*R.S.V. Aurora Australis*) (see also (Rintoul and Trull, 2001)) and another during 22 January–3 February 1999 in the Kerguelen region (43.5–45.5°S, 61–65°E) in the course of Antares 4 cruise (*R.S.V. Marion Dufresne*). Concurrent spatial distributions of SST were obtained during both cruises, with a Sea Bird® SBE21 thermosalinograph during the SAZ cruise and with a FSI® TSG thermosalinograph during Antares 4 cruise. For both cruises, SST has been measured every minute and averaged over 5-min intervals. Thus, the distance between consecutive measurements ranged from 0.5 to 2 km depending on the ship speed.

3. Frontal pattern

3.1. Manifestation of the fronts in SST gradient maps

The set of weekly SST gradient maps for 36 mid-month weeks (for example, Figs. 2–10) gives a general indication of the structure, extent, variability, and intensity of the Southern Indian Ocean fronts. It appears obviously that the fronts in the western part of the basin (20–60°E) are marked by higher SST gradients than those situated in the central and eastern parts (Fig. 11c) where SST gradients are more diffuse and basic fronts are hardly seen in accordance to the general eastwards decrease of SST gradients generally observed in the Indian Basin (Kazmin and Rienecker, 1996). The general observed eastward decrease of frontal SST gradients can be ascribed to the decrease of overall SST latitudinal gradients across the whole investigated region (around 1.2 °C/°lat and 0.8 °C/°lat at 40°E and 140°E, respectively; Fig. 11). The AF and SSTF (37–44°S) are the best-defined fronts in the western region (Figs. 2–6 and 11) due to their high intensity (Fig. 11c), while as the intensity of frontal features decreases northward and southward, the NSTF (30–35°S), SAF (44–46°S), and PF (49–52°S) are progressively less distinguishable. In the central region (60–100°E), the most pronounced frontal system is located north of the Kerguelen Plateau, where the AF, SSTF, SAF, and PF usually merge, and southeast of the Plateau, where high SST gradients are associated with the PF (Figs. 7, 8, and 11). In the eastern region (100–150°E), some increases of SST gradients can be observed between 45°S and 55°S and are related to the SAF and PF, while between 35°S and 40°S and also south of Tasmania, some relatively marked SST gradients are associated with the NSTF and SSTF (Figs. 9–11). The northernmost front located just south of Australia, with marked seaward offshoots at about 124°E, is likely to correspond to the Leeuwin Current (Legeckis and Cresswell, 1981; Griffiths and Pearce, 1985). Basic statistics shows that in average, the strongest fronts are the AF with SST gradient of 0.037 ± 0.013 °C km^{-1} and the SSTF with SST gradient of 0.035 ± 0.013 °C km^{-1}. SST gradient was 0.030 ± 0.003 °C km^{-1} for the SAF, 0.027 ± 0.003 °C km^{-1} for the NSTF, and 0.025 ± 0.005 °C km^{-1} for the PF which appears to be the least "intense" front. Furthermore, the less intense fronts (NSTF, SAF, and PF) exhibit weak changes of the magnitude of SST gradients.

3.2. Overall frontal patterns

Fig. 11a presents the mean positions of the fronts together with the associated standard deviations at every 10° of longitude that represent both seasonal variability of the fronts location and their meandering (unfortunately, because of the meridional shifts of the fronts, their clear seasonal changes cannot be defined). The overall patterns correspond to the frontal structures presented by Belkin and Gordon (1996) (Fig. 1). In first instance, the merging of the AF, SSTF, and SAF between 50°E and 60°E which gives rise to the Crozet Frontal Zone—which is justified by the crossing of the standard deviation bars at 60°E—and the proximity of the SSTF, SAF, and PF at 70°E (the Kerguelen Frontal Zone) appear obviously in Fig. 11a. However, the frequently observed southern location of the AF when AF and SSTF/SAF are practically merged is not shown here. Furthermore, the proximity of boundaries of standard deviation ranges in the region between 20°E and 40°E could indicate a

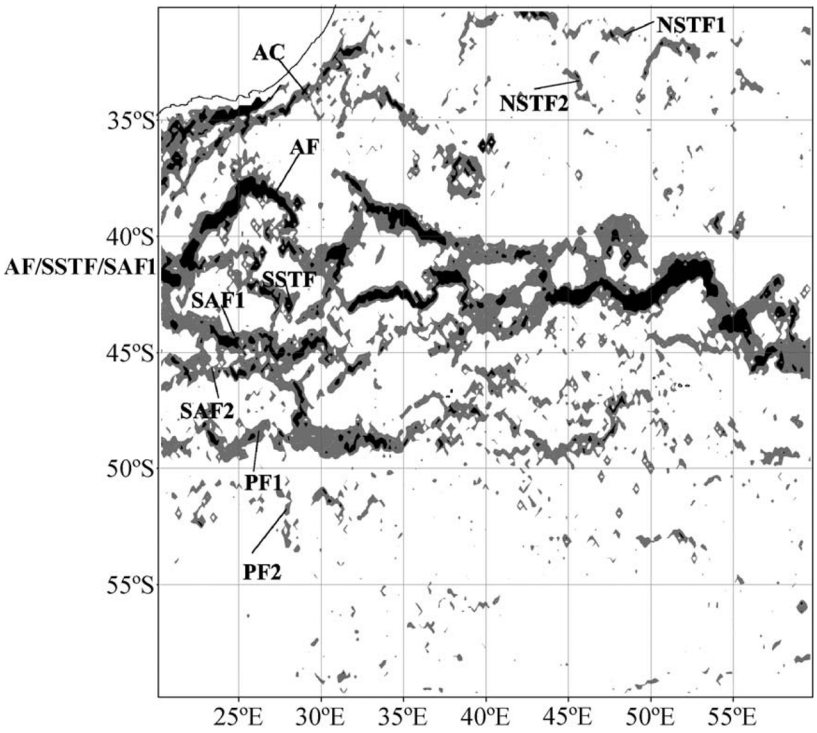

Fig. 5. Sea surface temperature gradient map for the mid-June 1999 (western region).

possible transient interaction of the AF, SSTF, and SAF there (see Section 3.3). Moreover, the poleward meanders of the SAF and PF east of the Kerguelen Plateau (90°E), the slight decrease of the distance between the SAF and PF at about 110°E after the crossing by the SAF of the Southeast Indian Ridge (Fig. 11a), as well as the location of the PF north of Kerguelen archipelago are some characteristics which can be found in the frontal patterns proposed by Belkin and Gordon (1996) (Fig. 1). This northern position of the PF is in agreement with previous studies (Fig. 102 in Sarukhanian and Smirnov, 1986; Park et al., 1991). However, some weekly maps show the PF to split in two branches rounding the Kerguelen archipelago northward and southward as it was mentioned by Belkin and Gordon (1996), and finally, the front was also observed sometimes south of the archipelago (Park and Gambéroni, 1997; Moore et al., 1999).

The satellite data analysis presents, however, some differences with regard to the work of Belkin and Gordon (1996). Both the quasi-stationary AF meanders located at 26–27°E and at 32–33°E (Grundlingh, 1978; Lutjeharms, 1981; Lutjeharms and van Ballegooyen, 1984, 1988), which appear obviously in Figs. 2–6, are not represented in Fig. 11a because they are located between the 10°-spaced longitudes chosen for the analysis. Poleward meanders of the SAF and PF at 30°E are also absent in Fig. 11a since though these meanders appear in some SST gradient maps (e.g., in Figs. 2 and 3), this is not a statistically significant and persistent feature. The extent of the NSTF in Fig. 11a is noticeably larger than previously found by Belkin and Gordon (1996) (Fig. 1) since the authors assessed that the front diverged from the AF east of about 45°E to coalesce with the SSTF at about 115°E. In Fig. 11a, the NSTF is shown from 40°E and far away from the AF. Typically, the part of the front west of 40°E is unclear due to the low SST gradients observed. However, sometimes, frontal features with enhanced SST gradients can be traced in the latitude range 30–35°S farther westward, where

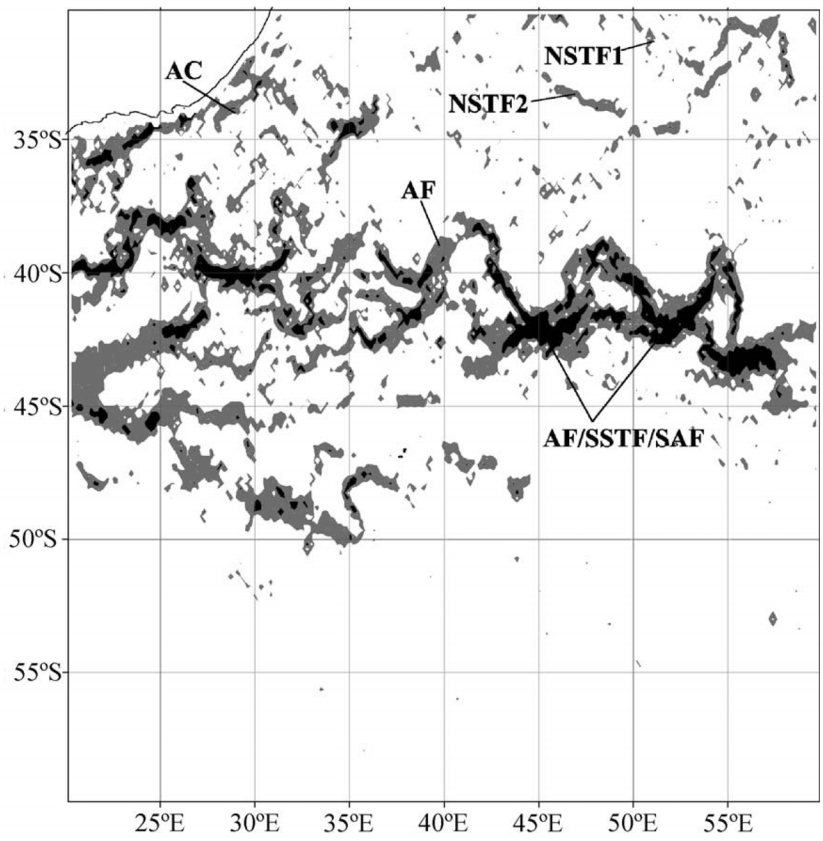

Fig. 6. Sea surface temperature gradient map for the mid-November 1998 (western region).

they reach the Agulhas Current (AC) rounding the coast of Africa. In most cases, the merging of the fronts with the AC occurs at about 30–33°E (Figs. 4–6). It is not excluded that in some cases, the westernmost part of such features in the vicinity of the AC (e.g., eddy-like structure centered at 31.5°S and 32°E in Fig. 4) is associated with a meander of the current, the so-called Natal Pulse (Lutjeharms and Roberts, 1988). However, in the general case, the frontal features within 30–35°E aligned in the seemingly zonal direction might be the westward extent of the NSTF. The question on the nature of these features has to be investigated in the future; however, in this study, they are designated as NSTF (Figs. 4–6). In the eastern region, the NSTF and SSTF are traced as different frontal structures up to about 140°E, although the close proximity and the crossing of standard deviation bars of both fronts between 110°E and 140°E could indicate a transient merging. Furthermore, the fronts probably coalesce east of 140°E to form the subtropical front (STF). Finally, the seasonal shift of the NSTF up to 5° latitude, which could be expected in accordance with the corresponding seasonal shift of the wind convergence between westerlies and easterlies (Belkin and Gordon, 1996), was not observed.

Standard deviations of the frontal zones position were made possible to compare the degree of variability between all frontal zones at each longitude (Fig. 11a). Remarkable difference in the variability is seen between longitudes 20–30°E, where the frontal zones are more stable (0.8–1.4°lat.), and the rest of the region, where they exhibit larger northward and southward displacements (1.0–2.5°lat.). Between 20°E and 60°E, the PF is constrained northward by the Crozet Plateau and southward by the Ob-Lena

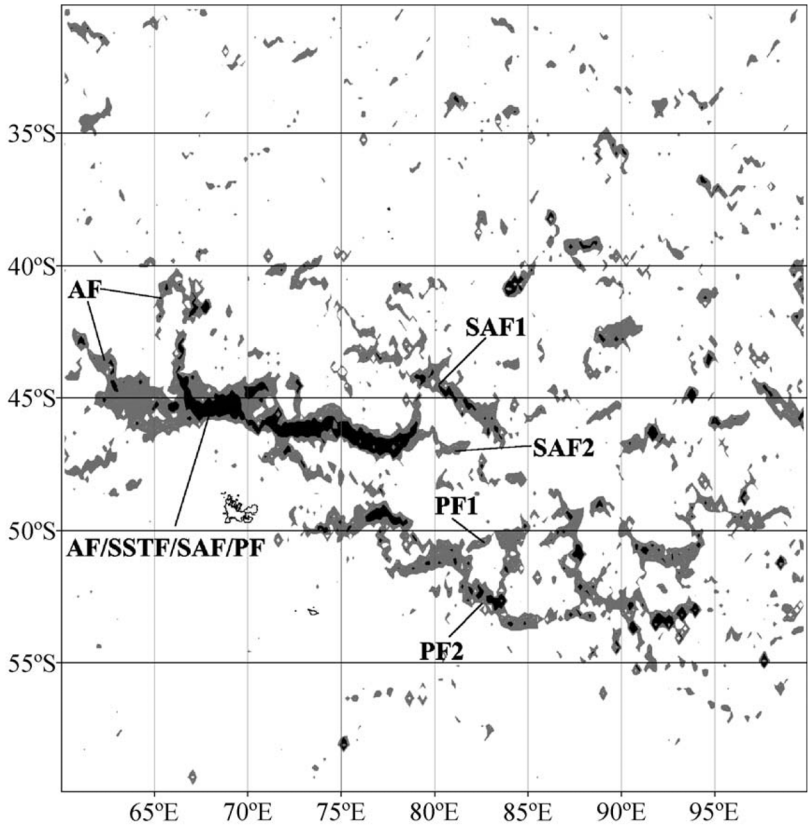

Fig. 7. Sea surface temperature gradient map for the mid-April 1997 (central region).

Rise, and thereafter exhibit a weak standard deviation. At 50°E and 60°E, since the PF is not constrained southward, the PF exhibits large latitudinal variation. As PF rounds the Kerguelen Plateau, it is constrained northward by the merging SAF/SSTF and southward by the Kerguelen archipelago so that the magnitude of latitudinal change decreases to reach a minimum at 80°E (Fig. 11a). Between 90°E and 140°E, as the PF is not constrained by peculiar bottom topography, its latitudinal movements increase. The same behaviour is observed for the SSTF which shows weak latitudinal change as it is constrained by Crozet Plateau and the AF between 40°E and 50°E or as it passes between the Kerguelen and Amsterdam plateaus (70–80°E), while its latitudinal change increases in the eastern region highlighting the role of bottom topography constraints on the latitudinal variations of the fronts positions.

3.3. Fine spatial structure of frontal zones

The weekly SST gradient maps reveal an intense spatial and temporal variability of the fronts position and configuration. All the fronts meander with a wavelength of about 3–5° in longitude and amplitude of about 2–4° in latitude. In addition to the two quasi-stationary meanders of the AF over the Agulhas Plateau (26–27°E) and at 32–33°E (Grundlingh, 1978; Lutjeharms and van Ballegooyen, 1984, 1988; Belkin and Gordon, 1996), four cyclonic meanders of the front can be episodically observed between 35°E and 55°E, where the AF crosses the Southwest Indian Ridge (Fig. 11a). Such meanders located at about 37°E, 42–44°E, 48–49°E, and 54–55°E are observed in Figs. 4 and 6. In addition, two more meanders of the AF can be formed at about 62°E and 66°E, west of the Kerguelen Plateau (Fig. 7).

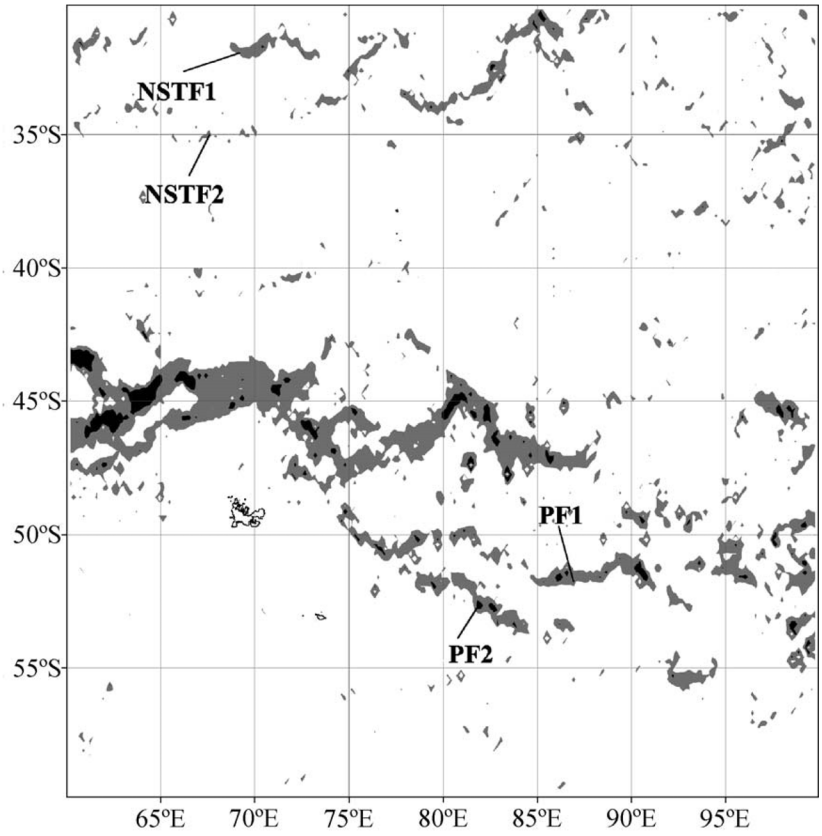

Fig. 8. Sea surface temperature gradient map for the mid-July 1997 (central region).

Hence, the Agulhas Return Current meanders from 25°E to about 66°E. It should be mentioned that similar northward excursions of the current could be expected from the trajectory of a drifting buoy in the region presented by Grundlingh (1978).

It follows from Figs. 2–6 that the amplitudes, the shapes, and the locations of the AF meanders are variable. If we compare Figs. 2 and 3, the variability timescale seems to be less than 1 month. The maximum amplitude of the meanders is about 3–4° in latitude, and wavelength is about 5–7° in longitude. Numerous patches of the increased SST gradients with diameters about 100 km or less as well as marked rings of around 200–300 km in diameter arise from the separation of the meanders from the Agulhas Return Current and are observed north of the AF in the SST gradient maps. One of such rings centered at 37.5°S and 39°E is well distinguished in Fig. 5. Similar rings were observed in the region from about 36°S to 40°S and from 25°E to 56°E in all seasons during the 3 years considered.

Because of the meandering of the fronts, the "instant" distance between neighboring fronts in the western part of the Southern Indian Ocean might be very different than the average presented in Fig. 11a. For example, southward displacement of the AF at 20°E can result in a situation where three fronts (the AF, SSTF, and SAF) are close (Figs. 3 and 5). A similar complicated frontal system can be formed at 35°E and 30°E (the AF/SSTF in Figs. 3 and 5, respectively). In the Crozet Basin (35–60°E), the AF, SSTF, and SAF can episodically converge (at 47°E in Fig. 5, at 45°E and 52°E in Fig. 6). But in other cases, especially in an area corresponding to an AF cyclonic meander, the distance between the AF and SSTF/SAF can increase up to 3° in

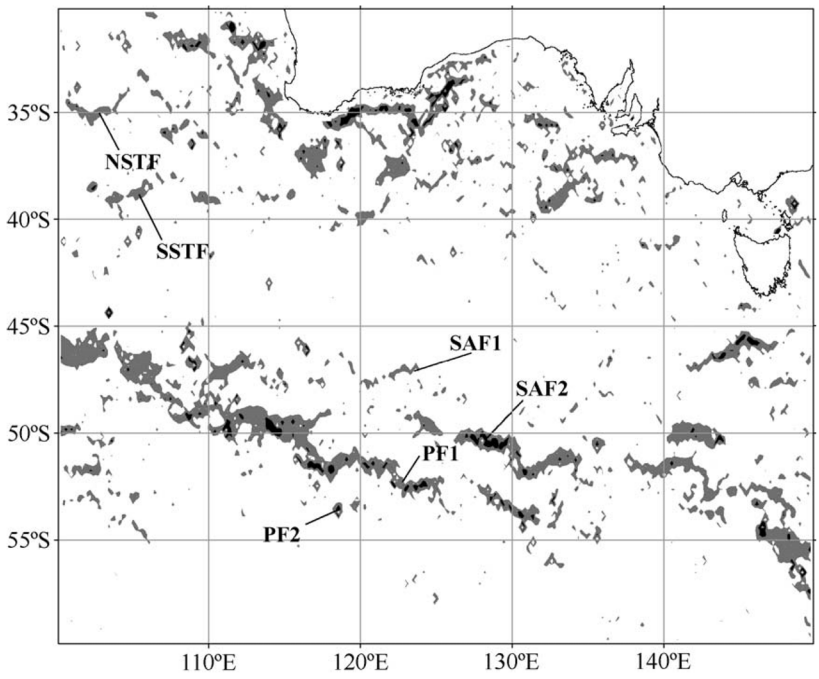

Fig. 10. Sea surface temperature gradient map for the mid-August 1998 (eastern region).

taneously (Fig. 2). The maximum separation between the fronts is observed at about 37.5°E, one front being located north of the Prince Edward Islands and another south of them. A marked northward meander of the SAF2 can be seen at about 39°E. The front rounds the Crozet Plateau from the south (a similar episodic behavior of the SAF has been mentioned by Moore et al., (1999)). At two locations (at about 47.5°S and 34°E, and 48.5°S and 38°E), the SAF2 is in the vicinity of the meandering PF1. Similar patterns of the SAF and PF have also been observed at about 35–36°E (Pakhomov et al., 2000; Pollard and Read, 2001) and between 30°E and 34°E (Read and Pollard, 1993; Belkin and Gordon, 1996; Holliday and Read, 1998). Besides, the close look at the section along 30°E in Fig. 7 of the work of Belkin and Gordon (1996) reveals two branches of the SAF, one at about 44–45°S and another one at 48.5–49°S which merges with the PF. Thus, the simultaneous existence of two subantarctic fronts and the interaction of the SAF and PF east of 30°E influenced by bottom topography appear to be repeatedly observed (see also Park et al., 2001).

Moreover, the double structure of the SAF between 20°E and 30°E appears obviously in (Figs. 2, 3, and 5). Since the phase difference between the meanders of SAF1 and SAF2 reaches 180° between 25°E and 28°E, the distance between the fronts ranges from a rather small distance at 25°E to about 3° in latitude at 27°E (Figs. 2 and 3). This double frontal structure persists for 1 month. In other cases, the southward meander of the SAF2 merges with the PF, as it occurred at 28°E in Fig. 5.

In the same way, the PF appears to have also a bimodal structure in the western part of the basin, with mean locations situated at about 49–50°S and 52°S (Figs. 2 and 5). In Fig. 2, both PF1 and PF2 have poleward meanders at about 30°E. East of the Kerguelen Plateau, at least between 75°E and 95°E, the PF has also a double structure that is well marked in Figs. 7 and 8 (PF1 and PF2 with mean positions at about 50–51°S and 53–54°S). Some SST gradient maps suggest that two branches of the SAF might exist there (for example, SAF1 and SAF2 at 79–85°E in Fig. 7). The double SAF also appears

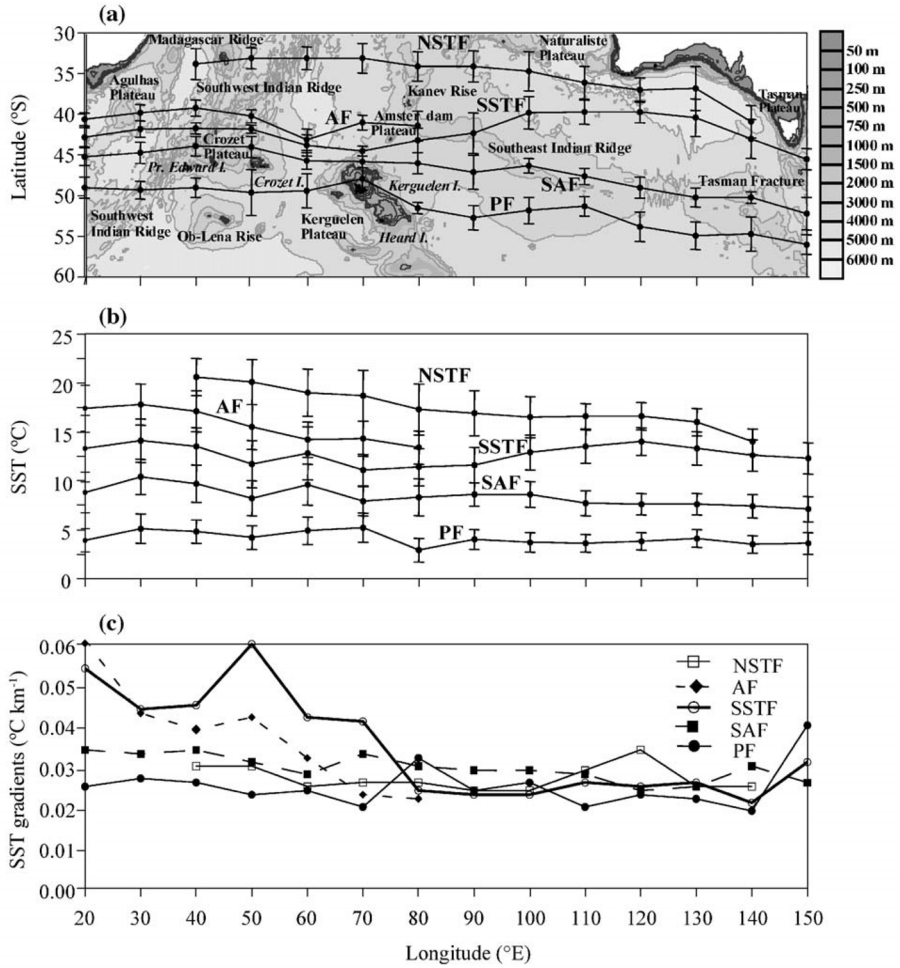

Fig. 11. (a) Bathymetry of the Southern Indian Ocean with average positions and standard deviations of the fronts, (b) average sea surface temperature (SST) and standard deviations and (c) SST gradients of the North and South Subtropical fronts (NSTF and SSTF), the Agulhas Front (AF), Subantarctic Front (SAF); and Polar Front (PF) in the Southern Indian Ocean as inferred from Multichannel SST data (1997–1999).

in the eastern part of the Southern Indian Ocean at 120–143°E in Fig. 10. It was already observed by Belkin and Gordon (1996) and its pattern is detailed in Section 3.4. Furthermore, considering the SST gradient pattern in Fig. 10, we feel that a double structure of the PF in the eastern region could exist as it has been repeatedly observed by Rintoul and Sokolov (2001) with branches at 53–54°S and 59°S. Finally, some SST maps imply that the SSTF can also have a bimodal path in the western part of the basin (for example, between 25°E and 35°E in Fig. 2).

3.4. Near-synchronous hydrographic and satellite observations of fronts in the Crozet Basin and Tasmania region

Two hydrographic surveys (SAZ and Antares 4 cruises) allow us to compare the results of field measurements near Tasmania (3–22 March 1998) and in the Crozet Basin (22 January–3 February 1999) (Dehairs et al., 2001) with near-concurrent SST gradient maps for the period of mid-February 1999 and mid-March 1998 (Figs. 12 and 13, respectively).

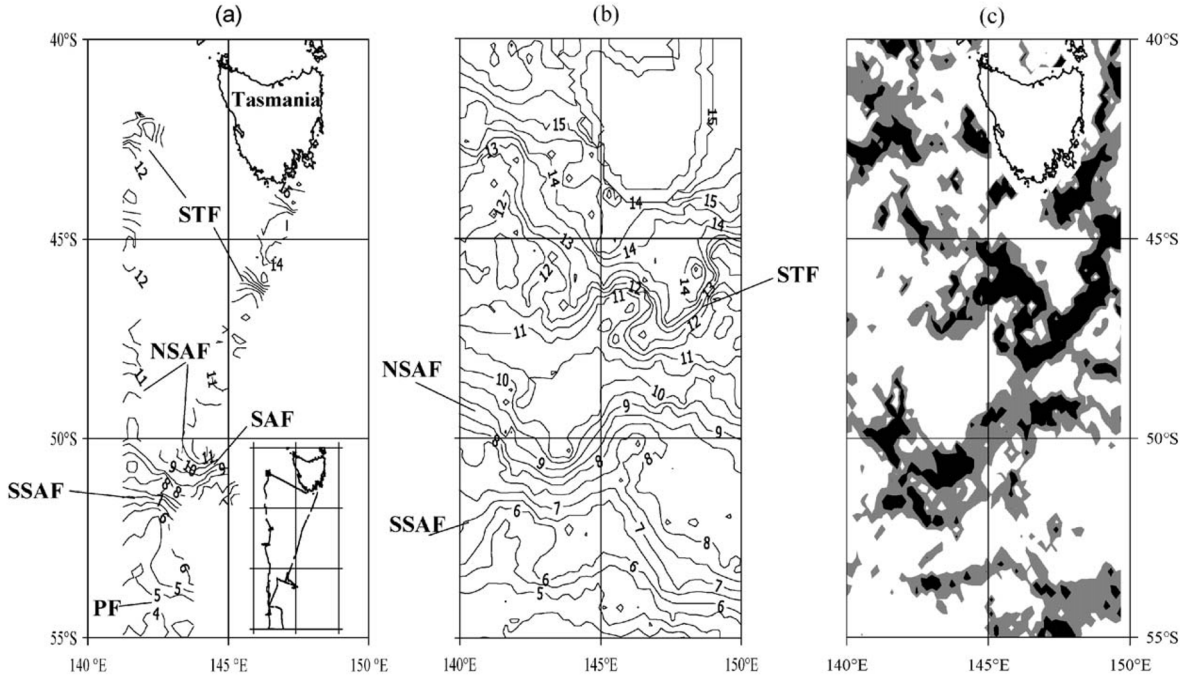

Fig. 13. Fronts in the Tasmania region in the austral summer of 1998: (a) sea surface temperature (SST) field from CTD survey during 3–22 March 1998 (*R.S.V. Aurora Australis*) (the ship route is shown in the insert map); (b) satellite SST map for the region of field measurements in the mid-March 1999; (c) corresponding satellite SST gradient map (grey tone corresponds to SST gradients of 0.012–0.02 °C/km; black tone—to higher gradients).

terized by a temperature change from 14 to 16 °C can be observed north of the STF. This additional frontal structure merges with the STF at about 142°E, 146°E, and 149°E. One can notice that the best-developed meander of the STF and subsequent convergence towards the NSAF were observed over the Tasmania Plateau. The southward meander of the NSAF and its confluence with the northward meander of the SSAF at about 143°E occurred in the vicinity of the Tasman Fracture Zone (Fig. 11a). The meanders of the NSAF and SSAF appear obviously in a sea surface height map based on TOPEX/Poseidon data for the mid-March 1998, whereas the STF with a weak density signature is not manifested in the map (Rintoul and Trull, 2001, Fig. 2).

The cyclonic eddy-like structure or meander which is observed between the two SAF branches at about 50°S and 146°E in Fig. 13c is also seen in a sea surface height map for the mid-March 1998 (Rintoul and Trull, 2001, Fig. 2). Interestingly, the similar cold-core cyclonic eddy or meander was repeatedly found on XBT sections at about the same location throughout the 1993–1994 austral summer by Rintoul et al. (1997). This implies a correlation between the feature and the bottom topography. Our analysis of SST maps for the period 1997–1999 has shown that a clear correlation between surface manifestation of the bottom-controlled meander (eddy) and season is absent. The feature was observed in May–September and December 1997, in March and October–November 1998, and in February–July and September–November 1999.

The examples considered above suggest that the available satellite SST data supply reliable information on the structure of frontal zones, their dynamics, and absolute values of the surface layer temperature.

4. SST ranges of the fronts in the Southern Indian Ocean (20–150°E)

Fig. 11b gives an indication of the variation of SST along the fronts. The temperature changes for the PF,

SAF, and SSTF are small. Minimum mean value of the PF SST at 80°E may be associated with the southward meander of the front at this longitude (Fig. 11a). It is possible that the minimum mean SST values of the SAF and SSTF observed at 50°E and 70°E (the regions of the Crozet and Kerguelen Plateaus, respectively) are due to the close approach and interaction of several fronts in these regions (Fig. 11a). The overall decrease of the mean SST of both AF and NSTF eastwards may be attributed to their moving away from the Agulhas Current that is the origin of warm water. The standard deviation of the mean SST of each front at each longitude is conditioned by both their seasonal variations and north–south displacement resulting from their meandering or interaction with neighboring fronts (Fig. 11a,b). Standard deviations of the frontal zones SST show that their SST is much variable (1.0–3.5 °C) in the western region (where frontal zones are more stable in term of position) in comparison with their SST (1.0–1.5 °C) in the eastern region (where frontal zones are more variable). Generally, the amplitude of the SST standard deviation is larger at the NSTF and is lower at the PF.

Mean SST and latitude ranges of each front in the Southern Indian Ocean are presented in Fig. 14. The SST ranges for the whole basin as well as for its

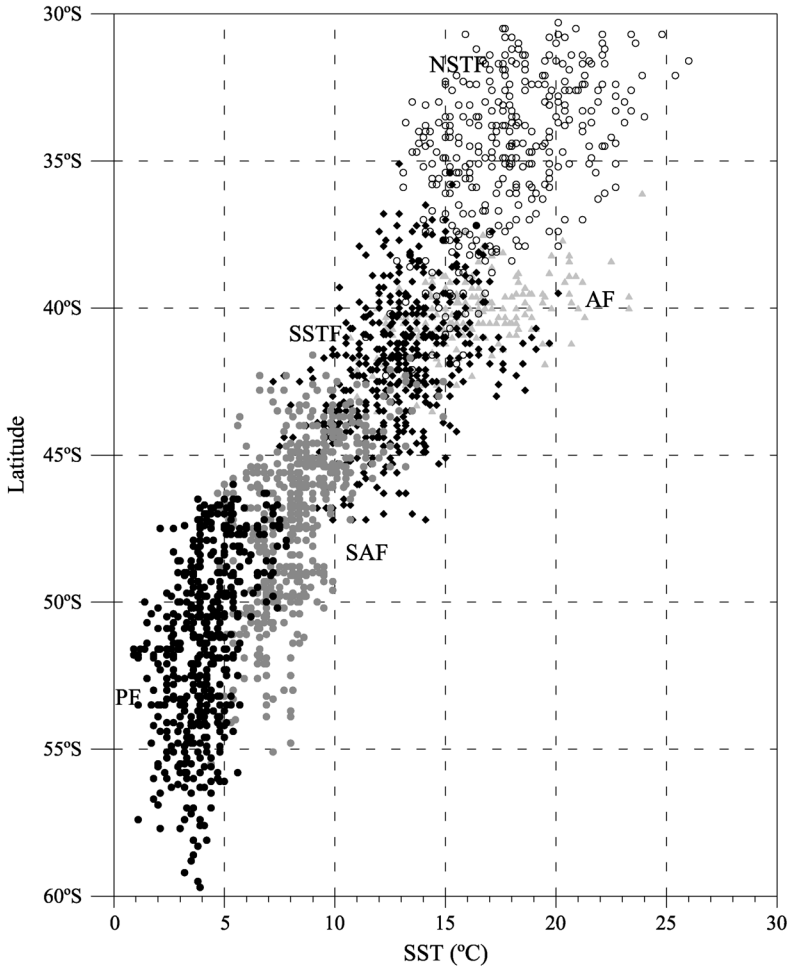

Fig. 14. Latitude-frontal sea surface temperature diagram in the Southern Indian Ocean based on satellite multichannel sea surface temperature data (1997–1999).

western (20–60°E), central (60–100°E), and eastern (100–150°E) parts are detailed in Table 1. For comparison purposes, the SST ranges for every front inferred from hydrographic sections and tables from Belkin and Gordon (1996) are given in Table 1 as well (the right-hand column). When a double structure of the fronts is encountered, SST of both fronts are taken into consideration in the corresponding SST ranges based on in situ measurements.

SST ranges as well as their boundary values obtained by two methods differ to some extent, the lowest differences being for the SAF and PF and largest for the NSTF, AF, and SSTF. On one hand, the difference can be accounted for by objective factors like interannual and seasonal temperature variability, north–south displacement of the fronts, and their interactions. For instance, the minimum SST values of the AF (10.7 °C) and SSTF (7.2 °C) correspond to September 1999 at 50°E, where the merging of the AF, SSTF, and SAF was observed at that time. The unusually wide range of the PF is associated with the frequently observed double structure of the front, when one front with surface temperature of about 3–5 °C is typically located at 50–52°S and another one either northward (6–9 °C at 46–48°S and 45°E in Fig. 9 in Belkin and Gordon, 1996) or southward (e.g., frontal surfacing isotherms 1.5–3 °C at about 59°S and 150°E in Fig. 19 in the same paper). In addition, different methods were used to determine SST ranges from satellite and field data: in the former case, the SST value at the point of maximum SST gradient was taken as a frontal SST, whereas in the latter case, both low and high boundary isotherms of a front were considered. Discrepancy may rise from the fact that in situ CTD measurements do not cover homogeneously all the regions of the Southern Indian Ocean, all the seasons at the same time, and usually have worse spatial resolution. On the other hand, a subjective factor can influence the boundary values of the frontal SST ranges based on satellite data. For example, in the cases of double structure of the SAF, it is impossible to distinguish the SAF from the PF on the base of satellite data alone. However, in most cases, the SST ranges of fronts determined from satellite data are in good agreement with those based on in situ measurements.

5. Concluding remarks

This study has demonstrated the efficiency and consistency of the analysis of satellite SST data in an investigation of the structure and both spatial and temporal variability of the position, intensity, and temperature ranges of the main fronts of the Southern Indian Ocean. The main advantage of this method is related to the use of regular SST data set with a relatively high resolution (1/6 of degree) and relatively high frequency (1 week), which provides the pattern of all fronts and frontal zones over the whole basin simultaneously.

To our best knowledge, for the first time, all five fronts have been mapped in the Southern Indian Ocean during 3 years (1997–1999) from a regular set of weekly satellite SST data, and for the first time, the intensity of each front in terms of SST gradients was calculated and compared for different regions. In general, the overall diagram of mean locations of the fronts corresponds to the structures previously observed through hydrographic data, but some details have been found to be different. In particular, the double structure of the NSTF, SAF, and PF in the

Table 1
Sea surface temperature ranges (SST) of fronts in the Southern Indian Ocean (20–150°E) inferred from satellite multichannel SST data (present study) and hydrographic in situ data by Belkin and Gordon (1996)

Fronts	SST ranges (°C)				
	Multichannel SST (present study)				In situ data (Belkin and Gordon, 1996)
	20–60°E	60–100°E	100–150°E	Total	
NSTF	14.6–26.0	13.1–24.8	11.4–22.1	11.4–26.0	16.0–23.0
AF	10.7–23.9	11–19.5	–	10.7–23.9	12.0–21.7
SSTF	7.2–20.1	7.7–18.6	9.2–17.1	7.2–20.1	9.0–17.0
SAF	4.8–14.9	4.4–13.5	4.8–11.4	4.4–14.9	5.0–14.0
PF	1.2–7.8	0.9–7.8	1.1–6.2	0.9–7.8	1.5–9.0

western, central, and eastern sectors of the Southern Indian Ocean was pointed out as well as the meandering of all fronts with amplitudes of 2–5° in latitude and wavelength of several degrees in longitude. Note that the conclusion about wavelike oscillations of the Antarctic Circumpolar Current jets, with wavelength up to 400 km, have been pointed out by Kort (1981) using the analysis of drifters trajectories. Furthermore, the variability of the fronts location and related SST values due to the meandering of the fronts, their splitting into two branches, or their merging into a single structure appears to exceed the seasonal variability of the frontal position and SST. At large scale, overall frontal position and their latitudinal changes appear to be strongly constrained by bottom topography.

On the whole, it is worth to note that the observed complicated internal structure of the fronts, which might comprise several frontal features with enhanced SST gradients, implies that they should be seen as "frontal zones" rather than "fronts" (Fedorov, 1986; Rodionov and Kostianoy, 1998; Kostianoy and Lutjeharms, 1999).

Satellite data showed that the close approach and transient interaction of the AF, SSTF, and SAF can occur not only in the Crozet and Kerguelen basins, but at 20–30°E as well. Moreover, the formation of the northward meander of the AF in the Kerguelen Basin results in the increase of the distance between the AF and the SSTF/SAF. It should be pointed out that both the present satellite data set with a spatial resolution of 18 km and hydrographic surveys with a resolution around 1–2 km might be inadequate for an accurate analysis of the merged fronts in the Crozet Basin whose main goal is to distinguish individual fronts among this complex structure.

The analysis of SST of the fronts have pointed out the decoupling between frontal position and SST of the fronts so that it appears hazardous to determine frontal positions in terms of strictly defined temperature ranges.

The SST ranges inferred from satellite data (1997–1999) for each front are broader than those previously reported in the literature. This discrepancy between the SST ranges based on in situ measurements and satellite data can be explained by the interannual and seasonal variability of SST, the larger spatial and temporal coverage of satellite data, the north–south displacements of the fronts, and finally by the different methods for the determination of SST ranges. On the other hand, satellite-derived SST ranges can be slightly overestimated because of the possible errors in the identification of a front when two or more fronts are closely spaced. Synchronous satellite and field observations could resolve these discrepancies.

Acknowledgements

This research was supported by the Belgian Federal Office for Scientific, Technical and Cultural Affairs (SSTC) through the Belgian Scientific Program on the Antarctic (contract A4/DD/B14 and EV/7/12E). The work was performed mostly at the Chemical Oceanography Unit and GeoHydrodynamics and Environment Research (GHER) of the Liege University where A.G.K. held the Belgian SSTC Research Fellowship in 2000 and 2002. This opportunity and the hospitality of the Chemical Oceanography Unit and GHER are greatly appreciated. The support by the SSTC is gratefully acknowledged. This is MARE contribution no. 31. The authors would like to thank anonymous reviewers for comments and suggestions that much improved the original manuscript.

2.2 Mesoscale distribution of pCO_2 and related parameters across the frontal zone of the Southern Ocean.

2.2.1 Foreword

The ANTARES IV cruise, carried out in the framework of the French contribution to Southern Ocean – Joint Global Ocean Flux Study (S.O.-JGOFS), offered the opportunity to study at mesoscale the surface pCO_2 distribution across a frontal zone. This study was carried out in the Crozet Basin in a particular region where bottom topography leads to the merging of the Polar Frontal Zone with the Aghulas Front. This region is therefore characterized by complex and highly dynamic physical structures which promote biological activity and subsequent uptake of atmospheric CO_2.

This chapter was been presented at the third SO-JGOFS Symposium held in Brest (France) in July 2000 and has been published in Marine Ecology Progress Series:

Fiala M., B. Delille, C. Dubreuil, E. Kopczynska, K. Leblanc, J. Morvan, B. Quéguiner, S. Blain, C. Cailliau,P. Conan, R. Corvaisier, M. Denis, M. Frankignoulle, L. Oriol, S. Roy. 2003. Mesoscale surface distribution of biogeochemical characteristics associated with a frontal system in the Crozet Basin (Southern Indian Ocean) during austral summer 1999. Marine Ecology Progress Series 249, 1–14

Also, some data of the study carried out during the ANTARES IV cruise have been used to trace water masses and investigate the fate of dissolved Barium in the water column. This complementary study has been published:

Jacquet S.H.M., F. Dehairs, D.B. Cardinal, J. Navez & B. Delille**,** 2005. Barium distribution controlled by hydrological and biogeochemical processes: results from a Southern Ocean Frontal System [Crozet-Kerguelen Basin], *Marine Chemistry* 95(3-4): 149-162

This article is available as an annex; the abstract is given below:

We investigated the dissolved and excess particulate Ba distribution (Ba_{xs}, an estimate of biogenic Ba considered to consist mainly of barite [$BaSO_4$]) across the complex frontal system of the Crozet–Kerguelen Basin (Southern Ocean; 42–47°S, 62–65°E). Baxs profiles show the characteristic mesopelagic maximum (depth range between 150 and 400 m) reaching up to 1000 pM in the Subantarctic Zone and Subtropical Front, the highest value observed for Southern Ocean mesopelagic waters. Dissolved Ba (concentrations between 38 and 104 nM) correlates with silicate and alkalinity, but the regression is not perfect, reflecting the involvement of different biogenic carriers in the control of the water column distribution of these compounds. Dissolved Ba in the upper 500 m appears strongly influenced by cross-frontal exchanges, involving both northward and southward transport of water masses. In the mesopelagic waters (150–400 m) of the Polar Front Zone, a dissolved Ba depletion faces the Ba_{xs} maximum. This depletion appears mainly maintained by cross-frontal advection of waters containing less Ba and originating north of the Subantarctic Front. Overall, no clear evidence that precipitation of barite reflected by the occurrence of Ba_{xs} maxima does measurably influence the distribution of dissolved Ba was found.

Vol. 249: 1–14, 2003 | MARINE ECOLOGY PROGRESS SERIES
Mar Ecol Prog Ser | Published March 10

Mesoscale surface distribution of biogeochemical characteristics in the Crozet Basin frontal zones (South Indian Ocean)

M. Fiala[1,*], B. Delille[2], C. Dubreuil[3], E. Kopczynska[4], K. Leblanc[3], J. Morvan[5], B. Quéguiner[3], S. Blain[6], C. Cailliau[6], P. Conan[1], R. Corvaisier[6], M. Denis[3], M. Frankignoulle[2], L. Oriol[1], S. Roy[3]

[1]Laboratoire Arago, Université P & M Curie, UMR-CNRS 7621, 66651 Banyuls-sur-mer Cedex, France
[2]Unité d'Océanographie Chimique, Institut de Physique, Université de Liège, 4000 Sart Tilman, Belgium
[3]Laboratoire d'Océanographie et de Biogéochimie, Université de la Méditerranée, UMR-CNRS 6535, Parc Scientifique et Technologique de Luminy, Case 901, 13288 Marseille Cedex 9, France
[4]Department of Antarctic Biology, Polish Academy of Sciences, Ustrzycka 10, 02141 Warszawa, Poland
[5]Ecole Normale Supérieure de Chimie de Rennes, Avenue du Général Leclerc, 35700 Rennes-Beaulieu, France
[6]Laboratoire des Sciences de l'Environnement Marin, Institut Universitaire Européen de la Mer, Université de Bretagne Occidentale, UMR-CNRS 6539, 29280 Plouzané, France

ABSTRACT: A mesoscale study was conducted in January and February 1999 in the Crozet Basin frontal zones (43° 50′ to 45° 20′ S, 61° 00′ to 64° 30′ E) within the southernmost and easternmost convergence area of the Antarctic Circumpolar Current (ACC) and the Agulhas Return Current (ARC). Distribution of biogeochemical parameters was strongly linked to the merged Subtropical (STF) and Subantarctic (SAF) Fronts which mark the border between the cold and less saline subantarctic waters and the warm and more saline subtropical waters. This survey took place during a post-bloom period. Chlorophyll *a* concentrations were low throughout the study area ranging from 0.2 µg l^{-1} in the Polar Frontal Zone (PFZ) to 0.4 µg l^{-1} in the Subtropical Zone (STZ). Maximum chlorophyll *a* values (0.8 µg l^{-1}) associated with an increase in biogenic silica concentration (from 0.03 to 0.34 µM) and a diatom peak (1.2×10^5 cells l^{-1}) were encountered in the northeastern part of the STF edge. Despite northwardly decreasing concentrations of nitrates from 14 µM in the PFZ to 6 µM in the STZ, they were not the main factor limiting phytoplankton growth. Low silicic acid (mean = 0.6 µM) could have limited diatom development in the PFZ and the STZ where diatom numbers were low. In STZ waters, where average diatom numbers were highest, various species of *Nitzschia* and *Thalassiothrix* were common, but *Pseudonitzschia* spp. were dominant. Throughout the survey area, pico- and nano-sized cells dominated the phytoplankton assemblage, and their number was the highest in the STZ. Cyanobacteria, only present in subtropical waters >12.5°C, were the major component of the picoplankton size-fraction. While dinoflagellate numbers were low in the Subantarctic Zone (SAZ), their abundance and species numbers increased in the STZ, where *Oxytoxum laticeps* became dominant and several further large-size species of *Prorocentrum*, *Ceratium* and *Gymnodinium* appeared in addition to those at the STF. The distribution of different biogeochemical parameters suggests that the Crozet Basin frontal region is a non-exporting system at the end of summer. During this post-bloom period, biological activity is low and phytoplankton growth severely limited. This is evidenced by the weak dependence of the partial pressure of carbon dioxide (pCO_2) on biological activity and the importance of the air-sea exchange in maintaining pCO_2 close to saturation.

KEY WORDS: Frontal zones · Nutrients · Biogenic silica · Chlorophyll *a* · pCO_2 · Phytoplankton · Bacteria

INTRODUCTION

The Southern Ocean is characterized by the occurrence of several permanent circumpolar frontal systems that form the eastward flowing Antarctic Circumpolar Current (ACC). The Subtropical Front (STF) represents the northern border of the ACC. It separates the warm and saline subtropical waters from the cool

*Email: mfiala@obs-banyuls.fr

and less saline subantarctic waters. Southwards, the Subantarctic Front (SAF) and the Polar Front (PF) mark the transition between subantarctic and Antarctic waters. The fronts mark the boundaries between different zones of the ACC: the Subantarctic Zone (SAZ) between the STF and the SAF, and the Polar Frontal Zone (PFZ) between the SAF and PF (Nowlin & Klinck 1986). Although this structure is circumpolar, the position of the different fronts is determined by the spatial pattern of the wind field, bottom topography and seasonal variability (Deacon 1982, Gamberoni et al. 1982, Piola et al. 1987). The Crozet Basin shows a complex circulation pattern in contrast to other frontal regions of the ACC. Due to the northwards bend of the ACC across the Crozet Plateau, the SAF and STF are tightly coalesced and form a concentrated jet merging with the Agulhas Return Current (ARC) (Park et al. 1991, 1993).

The Southern Ocean is considered, together with the subarctic and equatorial Pacific Ocean, to be a high-nutrient, low-chlorophyll (HNLC) region. However, *in situ* studies and satellite observations indicate higher productivity and chlorophyll biomass in a variety of disparate regions. Phytoplankton blooms have been observed in the marginal ice zone (Smith & Nelson 1990, Sullivan et al. 1993), around islands (Perissinotto et al. 1992, 2000, Pakhomov & Froneman 1999, Blain et al. 2001) and along frontal zones (Laubscher et al. 1993, Bathmann et al. 1997). Fronts are regions of strong horizontal temperature and/or salinity gradients that may occur in lakes, rivers and oceans (Franks 1992). Phytoplankton blooms are closely related to fronts in the oceans. Like other oceanic frontal regions, the Crozet Basin exhibits high levels of chlorophyll concentration during summer (Weeks & Shillington 1996, Metzl et al. 1991). The biomass enhancement is generally associated with low pCO_2 values (Metzl et al. 1999). This strong sink of atmospheric CO_2, considered one of the most important in the Southern Ocean, may result from physical mechanisms and biological processes (Metzl et al. 1998).

Previous studies have mainly focused on the PF (El-Sayed & Weber 1982, Fiala et al. 1998a,b, Hense et al. 2000). In contrast, little is known about the STF in spite of its importance as an efficient hydrodynamical barrier for various organisms (Clementson et al. 1998, Bradford-Grieve et al. 1999, Froneman et al. 1999). The STF is characterized by a sharp horizontal gradient in temperature and salinity which separates water masses of different physico-chemical properties. It exhibits dramatic changes in the diversity and distribution of phytoplankton, zooplankton (Furuya et al. 1986, Froneman et al. 1995, Barange et al. 1998), fishes (Roberts 1980) and birds (Pakhomov & McQuaid 1996). The STF also exhibits biomass and production enhancements (Weeks & Shillington 1996, Gall & Hawes 1999, Read et al. 2000). Because of its large circumpolar extension, it is a major contributor to the global ocean production (Dower & Lucas 1993). Several factors could explain the biomass enhancement in the vicinity of fronts, including increased *in situ* production resulting from strong water stratification due to the mixing of the warm subtropical water with the cold subantarctic water (Laubscher et al. 1993, Bradford-Grieve et al. 1997) and a passive transport of cells (Van Ballegooyen et al. 1994). Biomass enhancement can also result from the formation of eddies that move across the STF transporting heat, salt and nutrients into the surrounding environment (Froneman et al. 1999, Read et al. 2000). The Crozet Basin frontal zone corresponds to one of the strongest eddy activity areas of the Southern Ocean. SeaWiFS images have revealed the omnipresence of isolated eddies each side of the Agulhas Front (AF) (Park et al. 2002).

The present study focused on the fine spatial distribution of a large set of parameters in the surface waters of the Crozet Basin in an area crossed by the ACC and encompassing the transition from cold subantarctic to warm subtropical waters. Our purpose was to gain information about the influence of hydrological fronts on the distribution of the biogeochemical parameters and the phytoplankton community during late austral summer.

MATERIALS AND METHODS

Study area. A mesoscale study was conducted over 15 d (22 January to 5 February 1999) in the Crozet Basin frontal zone during the 'Antares 4' cruise on board the RV 'Marion Dufresne 2'. The survey area lay within the southernmost and easternmost convergence zone of the ACC and the ARC. The investigated region was delimited by a fine grid bounded by a parallelogram of 1.5° latitude × 2° longitude (~200 × 200 km) between 43° 50′ and 45° 20′ S and between 61° 00′ and 64° 30′ E. The grid was composed of 9 SW-NE parallel transects separated by distances of ~20 km (see Fig. 1).

Sampling. Surface seawater was sampled from the ship's continuous flow-through system (~7 m depth bow inlet) during the deployment of an undulating TowYo vehicle (Prieur & Sournia 1994). The vehicle was towed at ~4 knots and surface samples were collected along the grid from the flow-through system at regular intervals: 7.4 km for partial pressure of carbon dioxide (pCO_2), nutrients concentration and flow cytometry measurements, 14.8 km for chlorophyll *a* (chl *a*) concentration and 29.6 km for optical microscopy cell counting.

Methods. Salinity and temperature were recorded at 7.4 km intervals using a Seabird thermosalinograph

and a Falmouth Scientific Instruments temperature sensor.

Nitrate and silicic acid were determined on board via a standard automated method (Tréguer & Le Corre 1975).

For particulate silica analysis, 1 l samples were filtered onto 0.6 µm Nuclepore polycarbonate filters. Filters were then oven-dried (60°C) on board, stored in plastic petri dishes, and returned to the laboratory for further analysis. Biogenic silica (BSi) was measured by the hot NaOH digestion method of Paasche (1973) as modified by Nelson et al. (1989) (blanks: 0.006 ± 0.005 µm; precision: <±10% in the range 0 to 20 µm). After NaOH extraction, filters were assayed for lithogenic silica (LSi) by fluorhydric acid addition according to the method described by Ragueneau & Tréguer (1994) (blanks: 0.011 ± 0.006 µm; precision: <±10% in the range 0 to 20 µm).

pCO_2 was measured using an equilibrator coupled to a non-dispersive infrared gas analyzer (Li-Cor, LI-6262). The equilibrator consists of a Plexiglas cylinder (height: 80 cm; diameter: 10 cm) filled with marbles to increase the exchange surface area (Frankignoulle et al. 2001). Seawater runs (3 l min^{-1}) from the top to the bottom of the equilibrator and air is pumped upward (3 l min^{-1}). The temperature at the outlet of the equilibrator was monitored using a platinum resistance thermometer (Metrohm). pCO_2 values were corrected for the temperature difference between seawater *in situ* and in the equilibrator using the algorithm proposed by Copin-Montégut (1988, 1989). The Li-Cor analyzer was calibrated once a day with 2 gas standards of 0 and 345.4 ppm, respectively.

Chl *a* concentrations were measured on board after filtration of 1 l seawater onto a 47 mm Whatman GF/F glass-fibre filter at a vacuum differential of <20 cm Hg. Filters were ground manually in 100% acetone (water retention in the filter brought the final concentration to 90%) and extraction was carried out in the dark for 24 h at 5°C. The fluorescence of the acetone extract was measured on a Perkin Elmer MPF 66 spectrofluorometer (Neveux & Panouse 1987).

For flow cytometry analysis, prefiltered samples (100 µm mesh-size net) were fixed with 2% paraformaldehyde (Trousselier et al. 1995) and frozen in liquid nitrogen until later analysis in the laboratory. Just before analysis, samples were rapidly thawed in a 30°C water bath and fluorescent beads of 1 or 10 µm diameter were added to normalize the flow cytometer setting and to provide a reference for concentration calculations. Samples were analysed using a Cytoron Absolute (Ortho Diagnostic Systems) flow cytometer, with a 488 nm air-cooled argon laser. Each cell was characterized by 5 optical parameters: forward-scatter (linked to cell size) and right-angle scatter (linked to cell structure) and red (>620 nm), orange (565 to 592 nm) and green (515 to 530 nm) fluorescences. Counting varied by <3.7% SD (n = 23) over a range of concentrations covering 1 order of magnitude. Data were collected and stored in list-mode with the Immunocount software (Ortho Diagnostic Systems). Analyses were run with the Winlist software (Verity Software House). The flow cytometric analysis was restricted to <10 µm phytoplanktonic cells. Heterotrophic bacteria were counted after staining. For this purpose, 1 ml of seawater was supplemented with 10 µl SybrGreen II (from the molecular probes solution diluted 10×) and incubated for 10 min in the dark before analysis.

Aliquots of 100 ml seawater were sampled for taxonomic analysis and enumeration of phytoplankton communities. They were preserved with formalin (final concentration 0.4%) and stored in the dark at room temperature until laboratory analysis. Cells were counted using an Olympus inverted microscope according to procedures described by Utermöhl (1958). Due to sample preservation and optical resolution, the inverted microscope counting technique underestimates the pico-size species.

Statistical analysis. To determine the importance of hydrological features in structuring the planktonic community, we used 2 connected statistical methods. In a first step, ordination by principal components analysis (PCA; Statgraphics Plus software) was used to define hydrographic regions based on similarities in temperature, salinity, pCO_2 and nutrients (nitrates and silicates). The values of the variables were standardised by subtracting their means and dividing by their standard deviations. In a second step, hierarchical cluster analysis in the space of the first principal components was used to gather hydrologically similar stations. The dissimilarity between clusters was calculated using average values. The average distance was calculated from the distance between each point in a cluster and all other points in another cluster. Euclidean distances between values were measured.

RESULTS

Frontal structure within area investigated

The different front locations (Fig. 1) were determined using temperature and salinity measurements from 200 m depth (Park et al. 2002). These fronts can be considered representative of the surface hydrological structure although some slight deviations occur (i.e. the more southwards direction of the SAF/STF in the eastern part of the survey area). A detailed description of the large-scale frontal circulation within the entire Crozet Basin during this cruise has been given by Park

et al. (2002), but can be summarized thus: at the entrance to the Crozet Basin at 50°E, the ACC and ARC merged to form a frontal system composed of the SAF, STF and AF. Moving eastwards the SAF and STF shifted southwards. They reconverged most strongly at 63° 30′ E, due to a sharp meandering northwards (Fig. 1). A number of mesoscale meanders and eddies were superimposed on the main basin circulation. Meanders show an irregular configuration, continually evolving with time. Cyclonic and anticyclonic eddies with a diameter of 150 to 200 km were present at regular intervals of 300 to 500 km. The survey grid was bordered by the edge of 2 cyclonic eddies in its southwestern and eastern corners and by the southern edge of an anticyclonic eddy to the north (Park et al. 2002).

The northern part of the survey grid intercepted the AF, whereas its south-east domain encompassed the SAF and STF (Fig. 1). The fronts defined the boundaries between 3 relatively homogeneous zones: (1) the PFZ located southwards, between the SAF and PF; (2) the STZ located north of the STF and AF; (3) the SAZ which was reduced to a narrow band in the investigated region due to the coalescence of the SAF and STF.

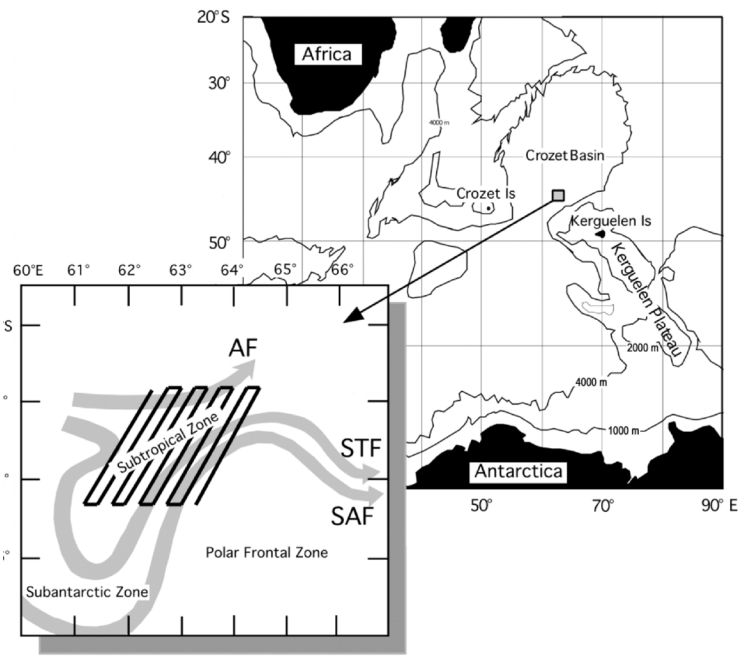

Fig. 1. Location of survey grid (9 parallel SW-NE transects) along which surface-water samples were collected during Cruise 'Antares 4' (January to February 1999). Positions of the different fronts are shown (identified at 200 m depth: Park et al. 2002). SAF: Subantarctic Front; STF: Subtropical front; AF: Agulhas Front

Surface temperature and salinity distributions

The SE-NW transition between the PFZ and STZ was marked by a sharp increase in temperature and salinity. Temperature (T) of the surface water increased from 10 to 16.5°C over a distance of 170 km and salinity (S) increased from 33.8 to 35.2 over the same distance (Fig. 2a,b). The PFZ surface water, south of the SAF-STF, was colder (11.2°C) and less saline (<33.8) than the northern subtropical surface water (12.5°C < T < 15.5°C and 34.3 < S < 35.0) (Table 1).

Surface nutrient distribution

Nitrate concentrations mirrored the frontal structure. They followed a negative gradient from south to north, decreasing sharply from 16 µM in the southeast to <1 µM in the northwest (Fig. 2c). Nitrate values were >16 µM in PFZ waters and between 2 and 9 µM in STZ waters. The frontal region (SAF/STF) exhibited concentrations between 7 and 15 µM. North of the AF, surface waters showed nitrate depletion (Table 1).

In contrast, silicic acid concentrations did not show a well-defined gradient (Fig. 2d). The concentrations were low over the study area, with values from 0.1 to 1.4 µM. South of the AF the surface concentrations were between 0.2 and 0.9 µM; north of the AF, the values increased slightly, with a maximum of >1 µM.

Biogenic and lithogenic silica distribution

Biogenic silica (BSi) concentrations were low throughout the study area (Fig. 3a). BSi distribution more or less matched the position of the frontal structure. Very low values (0.02 to 0.15 µmol l^{-1}) were observed in the northern area that corresponded to the occurrence of warmer and more saline subtropical waters. In the subantarctic waters, BSi concentrations increased northwards from 0.02 to 0.34 µmol l^{-1} (Table 1). The maximum value was recorded at the eastern boundary of the study area in the coalescent SAF and STF.

Lithogenic silica (LSi) was less abundant than BSi in the whole study area. The distribution pattern was also closely related to the frontal structure (Fig. 3b). LSi values were at the detection limit in

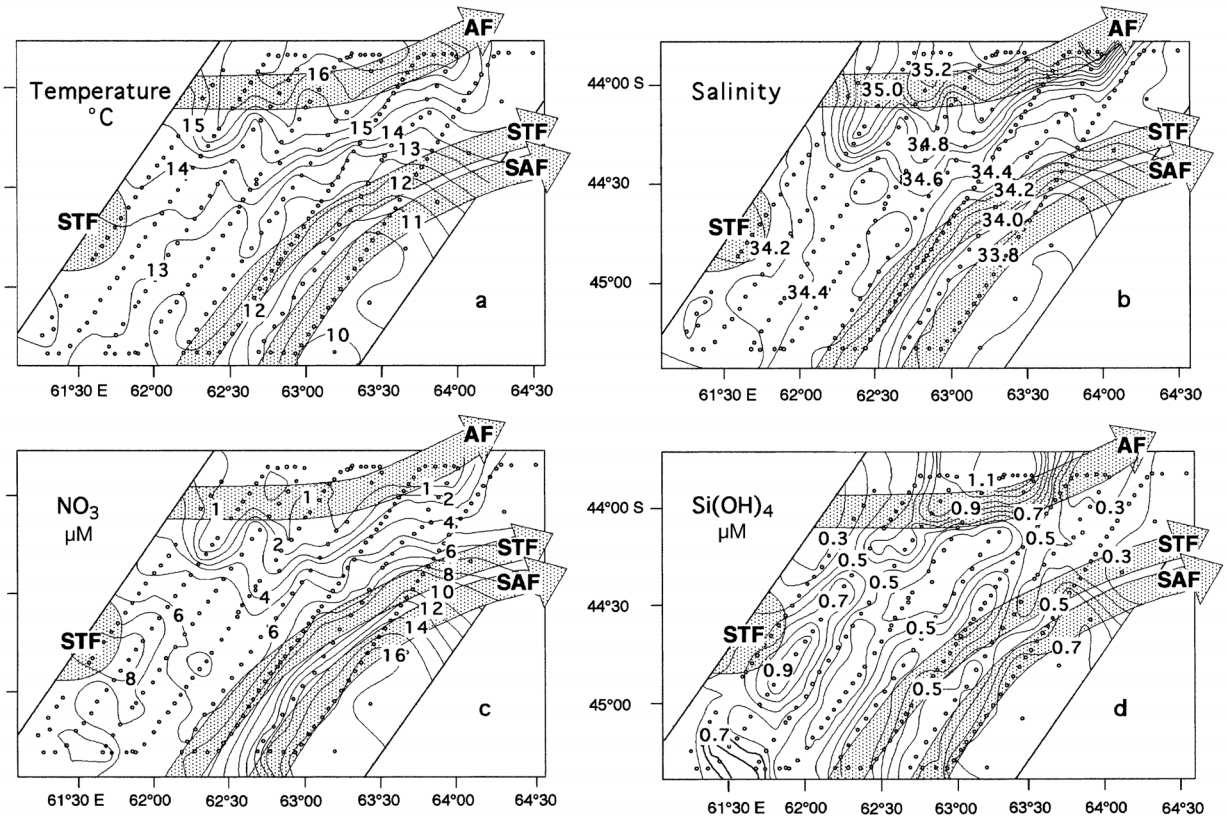

Fig. 2. Surface distribution of (a) temperature, (b) salinity, (c) nitrate concentration and (d) silicic acid concentration in the Crozet Basin during late summer. Here and in Figs. 3 to 5, sampling stations are indicated by dots, and abbreviations are as in Fig. 1; shaded arrows indicate direction of fronts

Table 1. Temperature, salinity, nitrate, silicic acid (Si), biogenic silica (BSi), lithogenic silica (LSi), chlorophyll *a* (chl *a*) and pCO_2 in the 4 hydro-chemical clusters determined by statistical analysis. PFZ: Polar Frontal Zone; STZ: Subtropical Zone; AF: Agulhas Front

Cluster	Temperature (°C)	Salinity	Nitrate (µM)	Si (µM)	BSi (µmol l^{-1})	LSi (µmol l^{-1})	Chl *a* (µg l^{-1})	pCO_2 (µatm)
Cluster 1 (PFZ)								
Mean (±SD)	11.22 ± 0.59	33.80 ± 0.06	14.42 ± 1.90	0.58 ± 0.18	0.06 ± 0.07	0.02 ± 0.02	0.17 ± 0.08	351.5 ± 12.5
Range	9.87–12.6	33.76–33.98	10.4–17.1	0.2–0.9	0.02–0.30	0.00–0.07	0.08–0.37	329.0–371.3
Sample no.	39	39	39	39	13	13	22	39
Cluster 2 (STZ)								
Mean (±SD)	13.81 ± 0.85	34.38 ± 0.14	6.11 ± 1.66	0.55 ± 0.19	0.11 ± 0.05	0.02 ± 0.01	0.41 ± 0.10	318.7 ± 7.2
Range	12.51–15.85	34.09–34.70	2.4–9.4	0.2–1.0	0.03–0.34	0.00–0.06	0.2–0.81	305.3–344.7
Sample no.	170	170	170	170	44	44	90	170
Cluster 3 (AF)								
Mean (±SD)	16.47 ± 0.51	35.05 ±0.16	0.62 ± 0.94	0.43 ± 0.19	0.07 ± 0.02	0.01 ± 0.01	0.38 ± 0.12	304.3 ± 3.8
Range	14.98–16.96	34.72–35.28	0.00–3.40	0.1–0.8	0.04–0.10	0.00–0.02	0.21–0.65	298.9–313.5
Sample no.	34	34	34	34	10	10	17	34
Cluster 4 (North AF)								
Mean (±SD)	17.03 ± 0.39	±0.12	0.33 ± 0.45	1.12 ± 0.14	0.05 ± 0.01	0.10 ± 0.0	0.27 ± 0.05	310.9 ± 4.6
Range	16.06–17.37	35.00–35.43	0.0–1.7	0.9–1.4	0.05–0.06	0.00–0.01	0.19–0.34	303.3–315.7
Sample no.	18	18	18	18	4	4	8	18

western subtropical waters. Higher values were observed in eastern subantarctic waters, but they did not exceed 0.07 µmol l^{-1} (Table 1).

Chl *a* distribution

Like other parameters, chl *a* distribution was strongly influenced by the frontal structure. The southern waters of the PFZ were poor in chl *a*, with concentrations of <0.4 µg l^{-1} (Fig. 3c). Northwards, the concentrations increased to 0.30–0.50 µg chl *a* l^{-1} in the central part of STZ (Table 1). At the northeastern border of the STF, chl *a* values reached a maximum of 0.81 µg l^{-1}.

pCO_2 distribution

Over the study area, surface-water pCO_2 ranged from a slight supersaturation (>360 µatm, the equilibrium value) to a net undersaturation (<300 µatm). The pCO_2 distribution was closely related to the frontal structure (Fig. 3d). The merged SAF and STF marked the boundary between the saturated PFZ waters (360 to 370 µatm) and the northern undersaturated STZ waters (310 to 330 µatm). The lowest values (~300 µatm) were observed in the warm and saline subtropical waters (Table 1). In the southeastern part of the grid, the pCO_2 increase was associated with the STF meander covered by the grid.

Phytoplankton abundance determined by flow cytometry (FCM)

Three phytoplankton groups were identified by FCM analysis with regard to size and fluorescence characteristics (Li 1994): picoeukaryotes (<3 µm), nanoeukaryotes (3 to 10 µm) and cyanobacteria (<1.5 µm).

Picophytoplankton cells were present throughout the area investigated (Fig. 4a). The highest abundance was observed in the STZ (from 4 to 10×10^6 cells l^{-1}) with a peak (12×10^6 cells l^{-1}) in the southwestern part. At the

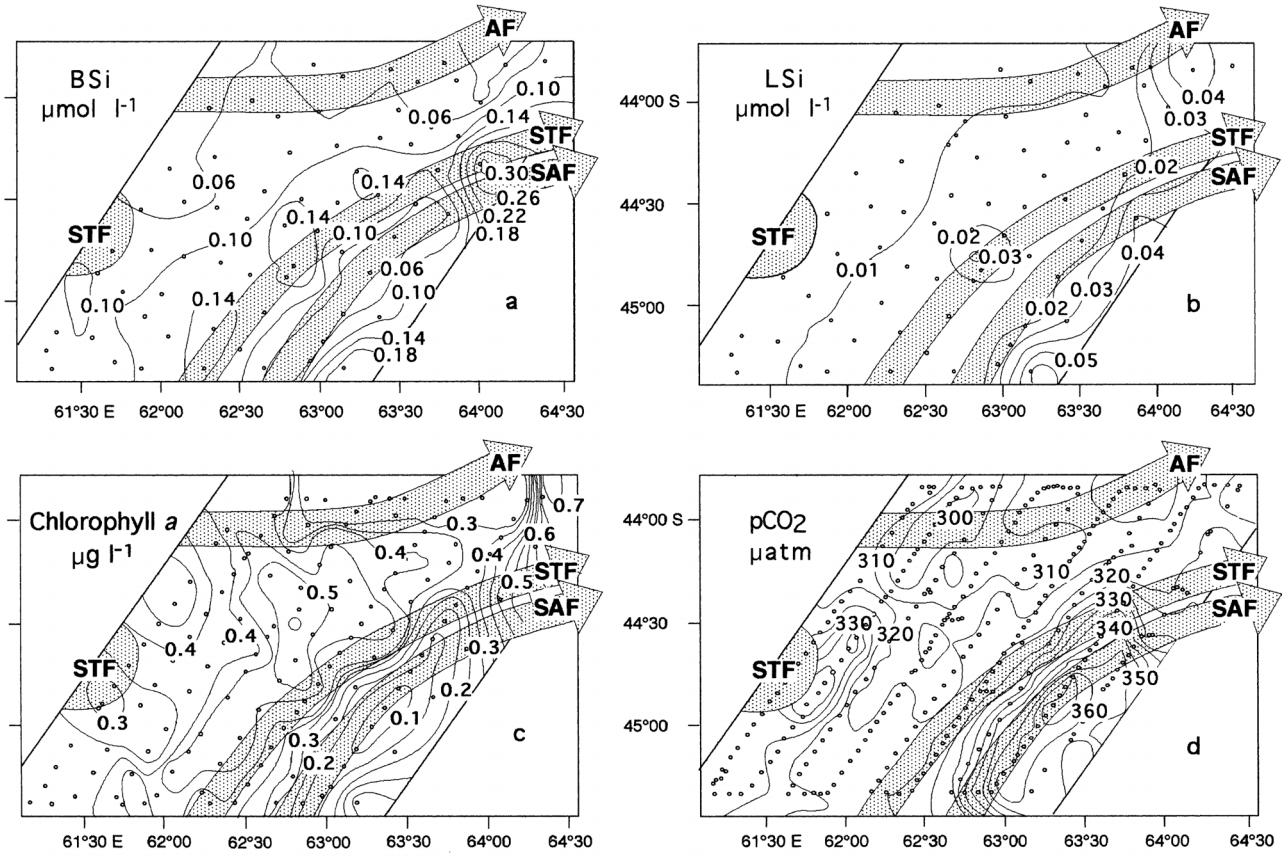

Fig. 3. Surface distribution of (a) biogenic silica concentration, (b) lithogenic silica concentration, (c) chl *a* concentration and (d) pCO_2

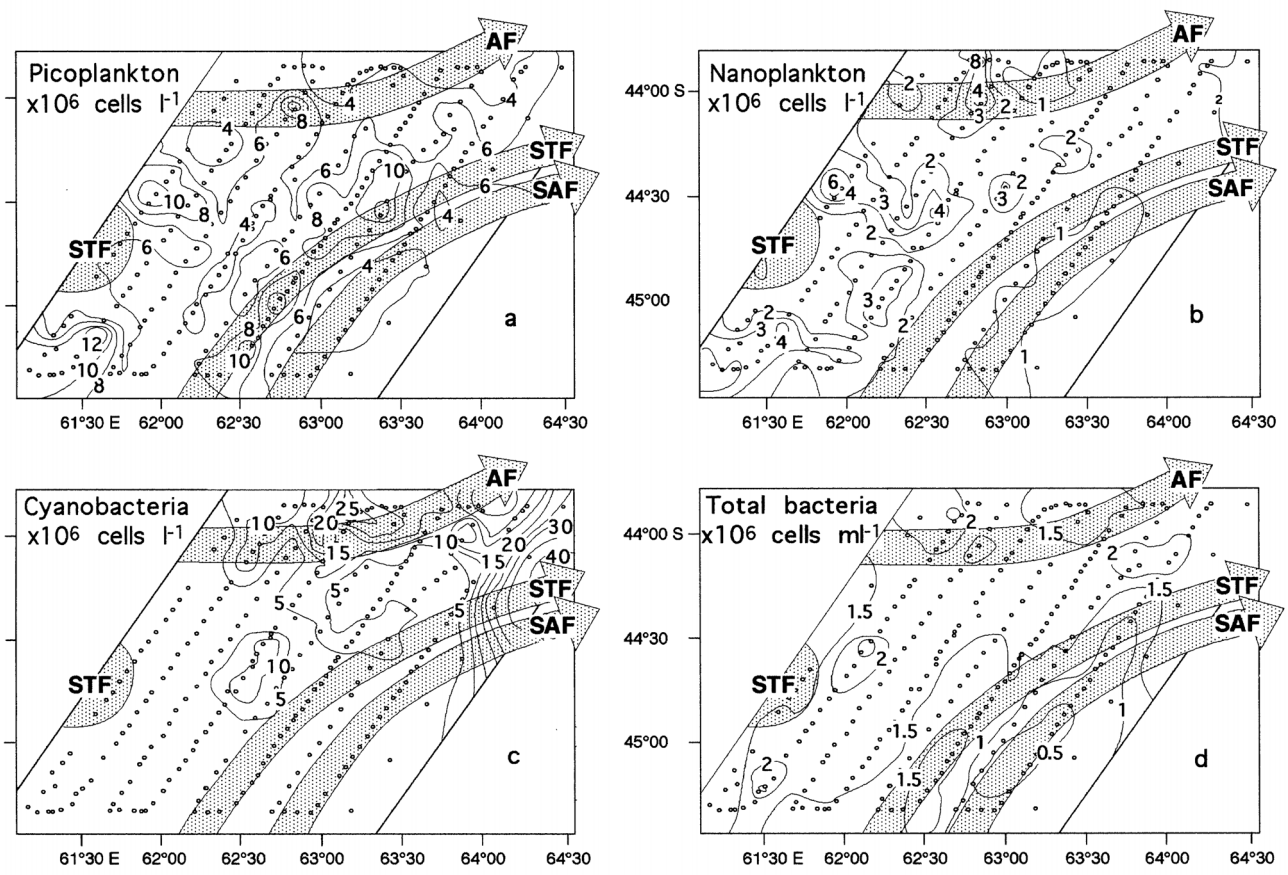

Fig. 4. Surface distribution of (a) picoplankton, (b) nanoplankton, (c) cyanobacteria and (d) total bacteria as measured by flow cytometry (FCM)

STF, picoplankton cells were also abundant (6 to 10×10^6 cells l^{-1}) whereas the SAF and the PFZ had the lowest concentrations (Table 2). Surface distribution of nanophytoplankton (Fig. 4b) was similar to that of picoplankton except at the STF, where they did not exhibit any special feature. Nanoplankton abundance (up to 8×10^6 cells l^{-1}) was about half that of picoplankton. In subantarctic waters, their abundance was low (~10^6 cells l^{-1}) (Table 2). Cyanobacteria were only present in subtropical waters (>12.5°C) (Fig. 4c) and their peaks of abundance (2 to 5×10^7 cells l^{-1}) occurred in the warmer waters of the STZ and in the AF (Table 2). In the northern subtropical waters, cyanobacteria were dominant and contributed 68% to total phytoplankton numbers, whereas picoeukaryotes only contributed 23%. On the other hand, in the southern STZ, picoeukaryotes were dominant (61%). In the cold and low-salinity waters of the PFZ, picoplanktonic cells were dominant; they contributed 76% to total phytoplankton abundance compared to 15% for nanoplankton.

Heterotrophic bacteria

Heterotrophic bacteria concentrations ranged from 0.5×10^6 to $>2 \times 10^6$ cells ml^{-1} (Fig. 4d). They were present throughout the entire area investigated. However, their abundance remained at $<1.2 \times 10^6$ cells ml^{-1} south of the STF. Peak abundance (up to 2.5×10^6 cells ml^{-1}) was observed in the STZ (Table 2).

Microscope analysis of the phytoplankton community

Phytoplankton populations were composed, in order of decreasing abundance, of picoplankton (~2 µm) and naked nanoflagellates (3 to 20 µm), dinoflagellates (8 to 300 µm), coccolithophorids (5 to 30 µm) and diatoms (5 to 600 µm). Variations in cell numbers of the major phytoplankton groups in surface waters were

Table 2. Picoplankton, nanoplankton, pico- and nanoflagellates, dinoflagellates, cyanobacteria, coccolithophorids, diatoms and total bacteria in the 4 hydrochemical clusters determined by statistical analysis. Region abbreviations as in Table 1

Cluster	Picoplankton ($\times 10^6$ cells l^{-1})	Nanoplankton ($\times 10^6$ cells l^{-1})	Pico- + nano-flagellates ($\times 10^6$ cells l^{-1})	Dinoflagellates ($\times 10^3$ cells l^{-1})	Cyano-bacteria ($\times 10^6$ cells l^{-1})	Coccolitho-phorids ($\times 10^3$ cells l^{-1})	Diatoms ($\times 10^3$ cells l^{-1})	Total bacteria ($\times 10^6$ cells l^{-1})
Cluster 1 (PFZ)								
Mean (±SD)	3.7 ± 1.3	0.8 ± 0.3	0.25 ± 0.12	41.9 ± 29.8	0.6 ± 1.3	136.1 ± 62.6	19.9 ± 9.8	0.6 ± 0.3
Range	1.3–6.5	0.2–1.5	0.09–0.50	10.5–110.0	0.0–6.6	13.1–265.3	6.6–36.8	0.3–1.9
Sample no.	37	37	14	14	38	14	14	38
Cluster 2 (STZ)								
Mean (±SD)	4.9 ± 1.8	2.1 ± 1.2	0.8 ± 0.7	232.0 ± 119.4	4.8 ±7.9	164.4 ± 73.0	69.3 ± 71.2	1.6 ± 0.4
Range	0.9 –12.0	0.6–6.3	0.04–5.01	50.2–519.3	0.0–52.1	59.6–337.3	2.1–399.5	0.7–0.3
Sample no.	162	162	40	40	161	40	40	137
Cluster 3 (AF)								
Mean (±SD)	3.1 ± 1.4	1.4 ± 0.3	1.0 ± 0.5	144.3 ± 81.2	11.7 ± 9.6	171.6 ± 77.7	30.5 ± 16.8	1.7 ± 0.4
range	1.4–7.5	0.7–2.2	0.27–1.93	37.9–307.7	0.4–40.3	97.3–307.7	15.5–68.4	0.7–2.7
Sample no.	32	32	10	10	34	10	10	25
Cluster 4 (North AF)								
Mean (±SD)	3.1 ± 1.4	1.7 ± 2.1	1.70 ± 1.76	58.5 ± 1.6	23.5 ± 11.9	153.5 ± 77.8	22.9 ± 2.6	1.4 ± 0.2
Range	1.1–6.6	0.6–8.8	0.46–3.70	57.3–59.6	0–52	98.5–208.6	6.9–38.9	1.1–1.8
Sample no.	16	16	2	2	18	2	2	15

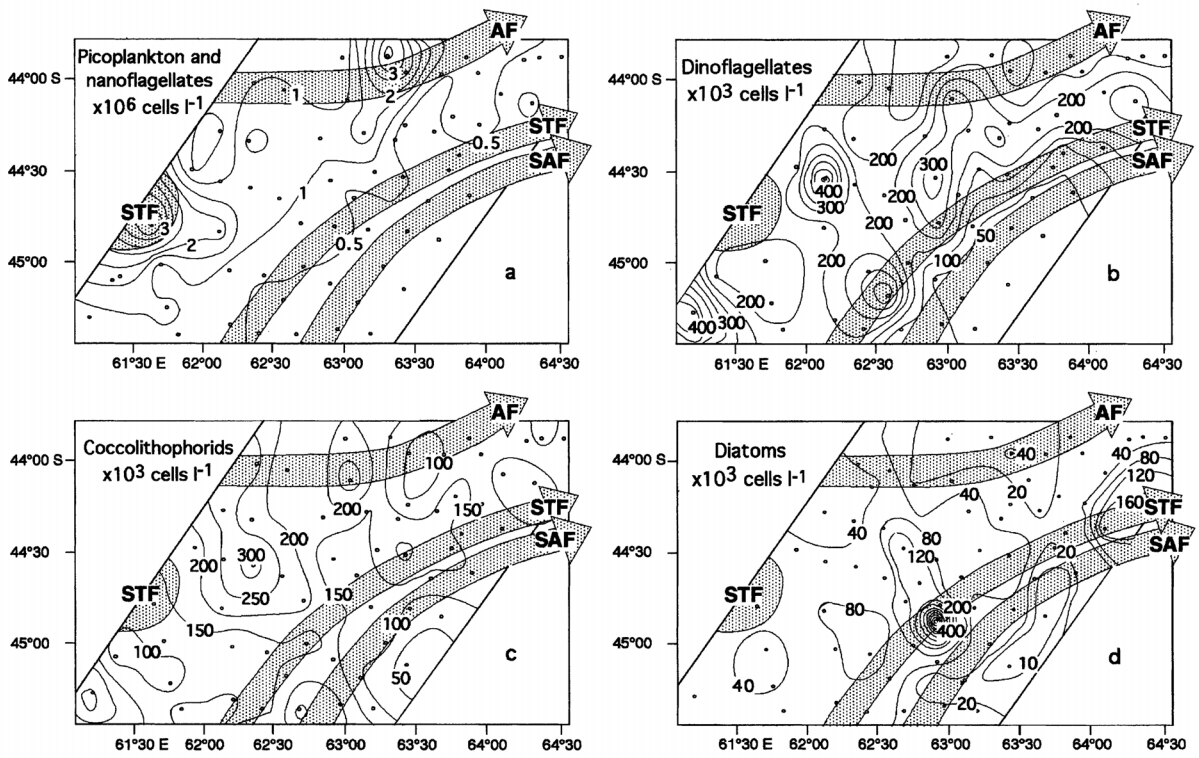

Fig. 5. Surface distribution of (a) picoplankton plus nanoflagellates (<20 µm), (b) dinoflagellates, (c) coccolithophorids and (d) diatoms measured by microscope counting

generally associated with changes in the frontal structure. A SE-NW positive gradient was observed in cell abundance. The combined groups of picoplankton plus naked nanoflagellates were remarkably similar south and north of the STF edge (cell numbers averaged $<2 \times 10^5$ l^{-1}: Fig. 5a). Maxima of 2.0 to 5.0 $\times$ 10^6 cells l^{-1} were noted in the STZ and north of the AF (3.7×10^6 l^{-1}) (Table 2). Nanoflagellates comprised prymnesiophytes, prasinophytes, cryptophytes and deflagellated, oval-shaped monads.

In the STZ, dinoflagellates varied between 2.0×10^5 l^{-1} and ca. 4.0×10^5 l^{-1} (Table 2). Maxima were recorded near the western STF meander and the northern part of the STF, with concentrations of 5.2 and 4.3×10^5 cells l^{-1}, respectively (Fig. 5b). South of the SAF, dinoflagellate numbers were lower than 5×10^4 l^{-1} and consisted mainly of small gymnodinioid cells (<18 µm) and *Prorocentrum* spp. A great change occurred within the STF, where both cell abundance and species numbers increased. *Oxytoxum laticeps*, present in very small quantities south of the STF, became dominant (3×10^4 l^{-1}), and was followed by *O. variabile*, *O. parvum*, several species of *Gonyaulax*, larger (>20 µm) *Gyrodinium* spp., *Gymnodinium* spp., *Prorocentrum* spp., and *Ceratium fusus*. In the STZ, further new species appeared in addition to those at the STF: various *Prorocentrum* spp. (*P. rostratum*, *P. magnum*, *P. dentatum*, *P. triestinum*), *Ceratium lineatum*, *C. pentagonum*, and large (40 to 70 µm) *Gymnodinium*/*Gyrodinium* spp. *Oxytoxum laticeps* and small gymnodinioid cells also remained dominant in this area. Quite a similar dinoflagellate species composition was observed at the AF.

Southwards in the PFZ, the numbers of coccolithophorids (max. 2.7 cells $\times$ 10^5 l^{-1}) were 4- to 5-fold greater than those of dinoflagellates. Northwards they were generally outnumbered by dinoflagellates at the STF and in the STZ (Fig. 5c). Maxima (3.4×10^5 cells l^{-1}) were observed in the central part of the STZ (Table 2). *Emiliania huxleyi* was the dominant species throughout the entire area of the study. Other frequently found species, with numbers increasing in the STZ, included *Gephyrocapsa* sp., *Dactylethra* sp., *Halopappus* sp., whereas species such as *Syracosphaera* sp. and *Calyptrosphaera* sp. were common north of the STF.

Diatoms were the least abundant group in the area investigated (Fig. 5d). Average cell numbers ranged between 2×10^4 l^{-1} in the PFZ to 7×10^4 l^{-1} in the STZ (Table 2). The highest cell numbers (8 to 12 $\times$ 10^4 l^{-1}) were found in the central STZ, with a maximum of 1.2×10^5 l^{-1} north of the STF edge. Another peak was encountered within the STF (4×10^5 l^{-1}). Within the AF, cell numbers were lower (average 3.0×10^4 l^{-1}). Diatoms were represented mainly by a few species of *Pseudonitzschia* (e.g. *P. turgidula*, *P. heimii*, *P. delicatissima*) which reached a peak in subtropical waters. Various species of *Nitzschia* (*N. longissima*, *N. closterium*, *N. bicapitata*) and *Thalassiothrix* spp. were also common in the STZ.

During the survey, *Phaeocystis antarctica* was only observed in a few samples from the northern SAF–STF edge, with highest counts of 6×10^4 l^{-1} north of the STF (data not shown).

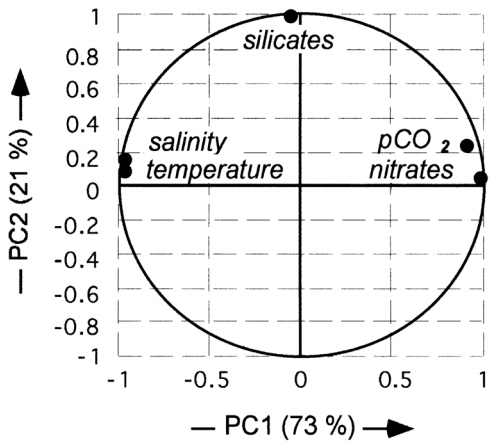

Fig. 6. Principal components analysis: plots of component weights

Statistical analysis

PCA was used to determine the influence of physical and chemical parameters (temperature, salinity, nitrates, silicic acid and pCO_2) on phytoplankton community distribution in the study area. Two principal components were extracted which account for 95.0 % of the variability in the original data. The first principal component (PC1) accounts for 73.6 % of the variance and gives positive weighting to nitrates and pCO_2, and negative weighting to salinity and temperature (Fig. 6). The second principal component (PC2) accounts for 21.4 % of the variance and gives general positive weights to all parameters, with the highest weight to silicates.

A hierarchical cluster analysis applied with the 2 first principal components as variables distinguished 4 clusters. Clusters 1, 2 and 3 are well separated along the PC1 axis, and PC2 allows the discrimination between Clusters 3 and 4. (Fig. 7). The correspondence between clusters and hydrological structures clearly appears in Fig. 8. Cluster 1 regroups stations located in the PFZ; Cluster 2 is occupied by stations located in the STZ; Cluster 3 gathers stations located in the AF region. Cluster 4, located north of the AF, is characterized by the highest concentrations of silicates (1 to 1.4 µM).

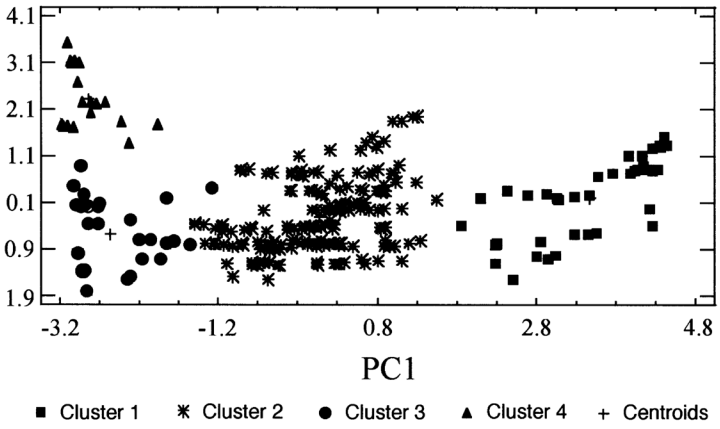

7. Two-dimensional scatterplot of the clustered observations (261 sampled ions) versus the 2 variables: first principal component (PC1) and second principal component (PC2)

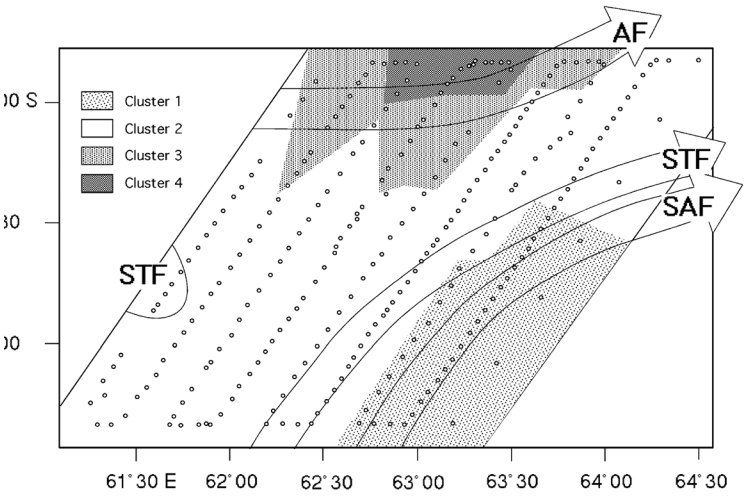

Fig. 8. Clustering of sample stations derived from statistical analysis

DISCUSSION

One major point of interest in the investigated area is that it covers the zone in which 3 oceanic fronts (SAF, STF and AF) converge. It therefore encompasses large gradients of temperature (10.0 to 16.5°C) and salinity (33.6 to 35.2) over a short distance (~170 km) in the northwards transition from subantarctic to subtropical waters. Statistical analysis confirms that physicochemical parameters were determinant in the distinction of 2 main regions, the southern PFZ and the northern STZ separated by a merged frontal system.

In the PFZ (Cluster 1) chl *a* concentrations were low (<0.3 µg l^{-1}) despite the presence of large amounts of nitrate (>15 µM). However, low concentrations of silicic acid were detected (0.7 µM). This situation is typical of the PFZ waters during late summer (Dafner & Mordasova 1994, Fiala et al. 1998a, Kopczynska et al. 2001). Particulate biogenic silica concentration in the surface waters was low and never exceeded 0.2 µmol l^{-1}, reflecting a weak diatom contribution to phytoplankton biomass. Data collected during the same cruise (Leblanc et al. 2002) suggested that the BSi accumulation could be the result of a bloom preceding the cruise period and/or an allochtonous input by lateral advection. Phytoplankton cell numbers were low and picoplankton was dominant, a general feature observed in different seasons in the Southern Ocean (Fiala et al. 2002). Picoplankton, nanoflagellates and coccolithophorids exceeded dinoflagellates and diatoms in numbers. This is consistent with data recorded during late summer to the south of Africa in the northern part of the PFZ (Kopczynska et al. 1986). In the PFZ, where temperature and salinity were comparatively low, pCO_2 was close to equilibrium (~360 µatm). As phytoplankton biomass was low and the upper mixed layer was shallow (Sedwick et al. 2002), pCO_2 was weakly influenced by biological activity or by a CO_2 supply from deep water. Therefore, it was the air–sea CO_2 exchange, enhanced by strong winds encountered in the region, that played an important role in pCO_2 dynamics by maintaining pCO_2 close to saturation.

Field experiments conducted during the cruise (Blain et al. 2002, Sedwick et al. 2002) indicated that dissolved iron availability was the primary limiting factor to nitrate drawdown and phytoplankton growth in the PFZ. On the other hand, low silicic acid availability exerted a secondary limitation on the diatom growth rate. Recent studies have shown that iron and/or silicate are limiting phytoplankton growth in different regions of the Southern Ocean (Sedwick et al. 1999, Boyd & Law 2001, Hutchins et al. 2001).

The confluence of the SAF and STF reduced the SAZ to a very narrow band. The general trend of the merging SAF/STF front was southwest to northeast. The convergent front marked the transition between warm subtropical waters and cold subantarctic waters. A drastic drop in the nitrate values from southeast to northwest within the STF and in the STZ was ob-

served, and suggested an active nutrient uptake by the preceding phytoplankton bloom reported about a month earlier from SeaWiFS images (Park et al. 2002). In the STZ surface waters, chl *a* concentrations increased slightly (<0.4 µg l^{-1}), but remained lower than those observed during other seasons (Weeks & Shillington 1996, Bradford-Grieve et al. 1997). Despite low concentrations, nitrates were not the main factor limiting primary production. As in the PFZ waters, dissolved iron availability associated with low orthosilicic acid concentrations limited phytoplankton growth (Sedwick et al. 2002). Low BSi concentrations reflected the low contribution of diatoms to phytoplankton biomass. Pico- and nano-size cells dominated the phytoplankton assemblage. Their distribution was patchy and the maximum counts (measured by flow cytometry analysis) of pico- and nanoplankton cells were 10^7 and 5×10^6 cells l^{-1}, respectively. Dominance of the small phytoplankton size fractions in the subtropical waters was also observed by Bradford-Grieve et al. (1997), Fouilland et al. (1999) and Froneman et al. (2001). Cyanobacteria dominated the pico-size fraction. Their distribution appeared to be mainly controlled by temperature, as they grew preferentially in warm (>15°C) water masses where they constituted the dominant population. This is consistent with observations of Murphy & Haugen (1985), who reported that decreases in cyanobacteria abundance correlate with decreasing temperature in the North Atlantic Ocean. The cyanobacteria abundance observed in the STZ was of the same order of magnitude as that reported for the North Atlantic (Murphy & Haugen 1985, Veldhuis et al. 1993). The absence of prochlorophytes at the latitudes sampled was consistent with observations showing their disappearance at latitudes >43° S (Fouilland et al. 1999). The STF is the scene of a dramatic northwards increase in cell quantities and species number of dinoflagellates. This change is probably attributable to an increase in water temperature which promotes the development of warm-water dinoflagellate species. Chl *a* concentrations were generally low within the STZ, but they increased to a maximum of 0.8 µg l^{-1} at the northeast border of the STF where the AF and the STF/SAF were in close proximity. This value, although high, was lower than values observed by Weeks & Shillington (1996) and Read et al. (2000) in the Southwest Indian Ocean frontal region. The chl *a* peak is attributable to the development of diatoms and cyanobacteria. Peak chl *a* concentration and cell abundance were most probably due to the presence of a cyclonic eddy located northeast of the study grid which had recently detached from the SAF, as revealed by SeaWiFS images (Park et al. 2002). These images also showed that chl *a* concentrations were higher in the eddy edge than in the eddy core. This is consistent with previous studies conducted in the STF south of Africa (Dower & Lucas 1993, Froneman et al. 1999).

Phytoplankton assemblages found in the Crozet Basin show similarities with regard to major groups and species composition to phytoplankton communities observed in late summer in the subantarctic region south of Africa (Kopczynska et al. 1986) and south of Australia (Kopczynska et al. 2001). In the present study and the 2 previous studies of Kopczynska et al. (1986, 2001), nanoflagellates and dinoflagellates increased both in cell densities and species numbers north of the PF towards the STZ. Diatoms were the least abundant group. Representatives of the genus *Pseudonitzschia*, dominant among diatoms in the Crozet Basin, have been previously reported to be typical north of the PF (Hasle 1969, Steyaert 1973, Kopczynska et al. 1986). Dinoflagellates were dominated everywhere by the nano-sized (<20 µm) genera *Gymnodinium*, *Gyrodinium* and *Prorocentrum*. The highest differences in the species composition of this group were observed between the STZ of the Indian Ocean and south of Australia, and are attributable to the larger micro-sized (>20 µm) species (Kopczynska et al. 2001). Also common to the present study and previous studies (Kopczynska et al. 1986, McKenzie & Cox 1991, Kopczynska et al. 2001) is the observation that several species of diatoms (e.g. *Nitzschia bicapitata*, *N. subpacifica*, *Thalassiothrix delicatula*) and dinoflagellates (*Ceratium pentagonum*, *C. lineatum*, *Oxytoxum* spp.) were only encountered north of the PF. The rich flora of dinoflagellates and coccolithophorids found in the present study is typical of warm waters of the South Indian Ocean (Taylor 1976, Heimdal 1997).

Summer bacterial abundances (0.5 to 2.5×10^6 cells ml^{-1}) observed in the Crozet Basin were in a range of those (1.2 to 2×10^6 cells ml^{-1}) reported by Lochte et al. (1997) for the Atlantic sector of the PF during spring 1990, but were larger than abundances (0.2 to 0.5×10^6 cells ml^{-1}) recorded near the Kerguelen Islands during the 'Antares 3' cruise in October 1995 (M. Denis unpubl. data). Such differences could result from an uncoupling or time-lag between phytoplankton and bacterioplankton development. In line with this explanation, Billen & Becquevort (1991) observed, in Prydz Bay and the Weddell Sea, a time-lag of about 15 to 30 d between the maxima of phytoplankton and bacterial biomasses. Similarly, bacterial numbers reached maximum values approximately 1 mo after blooms of *Phaeocystis pouchetii* in Antarctic coastal waters (Gibson et al. 1990, Davidson & Marchant 1992).

Such an uncoupling can be explained in several ways, either by extremely low exudation of dissolved organic carbon, by phytoplankton, by low bacterial uptake or conversion of organic material, by repression of the bacterial metabolism due to low temperatures, or

by high grazing pressure (Lochte et al. 1997). The present study was conducted during a post-bloom period in a region where phytoplankton growth is stimulated by the frontal hydrodynamics. This would explain the fact that bacterial concentrations were larger than those observed south of the Kerguelen Islands in January to March 1994 (0.1 to 0.6×10^6 cells ml^{-1}, Talbot 1995) or south of Tasmania in February 1999 (2 to 4×10^5 cell ml^{-1}, Hall & Safi 2001).

The surface signatures of the fronts are clearly distinguishable in the pattern of pCO_2. The distribution of pCO_2 mirrored remarkably the meso-scale salinity distribution rather than temperature distribution. This was expected because in the PF area, cold and warm core eddy-like features show up more clearly in salinity than in temperature, as the latter is modified by atmospheric heat exchanges (Read et al. 2000). During the cruise, this phenomenon was likely to have been enhanced as a consequence of the narrowness of the frontal band. Furthermore, atmospheric heat exchange influences the pCO_2 through the effect of temperature on thermodynamic equilibrium constants of the carbonate system. Taking into account the overall distribution of pCO_2 during the cruise, atmospheric heat exchange enhanced the gradients of pCO_2 at the fronts. As the northern warm and CO_2-undersaturated waters approached the fronts, they tended to cool with a concomitant decrease in pCO_2. On the other hand, the southern cold and slightly supersaturated waters tended to warm up and, conversely, pCO_2 increased in the vicinity of the fronts. The large northwards drop in pCO_2 is linked to the overall positive S-N gradient of chl *a*. However, at the mesoscale, no significant drops in pCO_2 were associated with the chl *a* maximum.

Furthermore, in the northeastern part of the survey area, the lowest pCO_2 values were associated with both a minimum in nutrients concentration and a maximum in bacteria abundance, while chl *a* did not exhibit significant changes. The minimum concentration of nutrients and maximum number of bacteria were probably the consequence of a development of strong primary production prior to the cruise that led to the pCO_2 minimum. Thereafter, the distribution of pCO_2 generally appears to have reflected the impact of the bloom period preceding the cruise, indicating that the signature of the CO_2 system distribution bloom remained for several weeks to months.

From the distribution of different biogeochemical parameters, the Crozet Basin frontal region appears to be a non-exporting system at the end of summer. This conclusion is particularly supported by the low contribution of large cells as well as the low contribution of siliceous organisms to the total phytoplankton. Biological activity was very low at that time of the year, as evidenced by the stronger dependence of pCO_2 on hydrological structures. These results are also confirmed by the low primary production rates measured during the cruise (Leblanc et al. 2002). The present study period (January–February) marked the end of a productive period in that area, phytoplankton production being hindered by a combination of limiting resources including iron and silicic acid (Sedwick et al. 2002). Our results compare very well with the situation observed in the same season in the same sub-systems in the Australian sector, where phytoplankton were dominated by non-siliceous organisms (Kopczynska et al. 2001) and exhibited the same kind of limitation by iron and silicic acid (Sedwick et al. 1999, Quéguiner 2001).

Acknowledgements. This work is a French contribution to the SO-JGOFS program. It was supported by the French Polar Institute (IPEV) and the INSU-CNRS. This research was partly financed by the Polonium Program of scientific cooperation between Poland and France. It was also partly conducted under grants A4/DD/B14 and EV/12/7E within the Scientific Research on the Antarctic supported by the Belgian Office for Scientific, Technical and Cultural Affairs. We thank the captain, officers and crew of RV 'Marion Dufresne 2' and B. Ollivier for outstanding on board support. Special thanks to G. Grégori for stimulating discussions, Y. H. Park for constructive comments and C. Bangy for her help in running the flow cytometer. The comments of 2 anonymous reviewers greatly assisted in improving this manuscript.

2.3 Variability of the net air–sea CO_2 flux inferred from shipboard and satellite measurements in the Southern Ocean south of Tasmania and New Zealand.

2.3.1 Foreword

It is intrinsically difficult to study synoptically dissolved inorganic carbon spatial distributions at the ocean basin scale, or to resolve adequately the seasonal changes. Synoptic at sea measurements of any oceanographic variable over large areas are logistically impossible, and long continuous ship based time-series are not achievable in remote areas as the Southern Ocean. To encompass these under sampling issues, several solutions have been developed, from autonomous pCO_2 measurements units deployed on drifting buoys or fixed platforms, to the increasing use of Volunteer Observing Ships (VOS). However, these recently developed tools are hardly implemented in the Southern Ocean. Indeed, the sea ice cover hampers the use of drifting boys or fixed platforms, while VOS tracks are somewhat illusive due to the lack of commercial ship lines in the S.O.. Thus, most of pCO_2 measurements are provided using conventional oceanographic surveys. Regular surveys are carried out in the frame of LDEO-NSF (Lamont-Doherty Earth Observatory – National Science Fundation) and CARAUS (CARbone AUStral) projects, but they suffered from the lack of data in winter due to logistical constrains. One project provides regular winter surveys, the OISO observatory (Océan Indien Service d'Observation), but, only two surveys are scheduled per year in the framework of this project.

To encompass under-sampling, one alternative is to take advantage of remote sensing tools to extrapolate in situ measurements. We attempted to do so in the S.O. sector south of the Tasmania and New Zealand using a dual approach which involved the gathering of data sets and extrapolation based on remote sensing data (Sea Surface Temperature and Chlorophyll a concentration). This approach is prone to some caveats, but allowed us to improve current budgets of CO_2 fluxes derived from simple compilations of pCO_2 measurements (Takahashi et al., 2002).

This study was conducted in collaboration with the Laboratoire d'Océanographie Dynamique et de Climatologie/Institut Pierre Simon Laplace (France), the Lamont-Doherty Earth Observatory (USA), and the School of Environmental Sciences/ University of East Anglia (U.K.), and was published in Journal of Geophysical Research:

Rangama Y., J. Boutin,.J. Etcheto, L. Merlivat, T. Takahashi, B. Delille, M. Frankignoulle, & D.C.E. Bakker, 2005. Variability of net air-sea CO2 flux inferred from in situ and satellite measurements in the Southern Ocean south of Tasmania and New Zealand, Journal of Geophysical Research, 110(C9), C09005, doi:10.1029/2004JC002619.

Variability of the net air–sea CO_2 flux inferred from shipboard and satellite measurements in the Southern Ocean south of Tasmania and New Zealand

Y. Rangama,[1] J. Boutin,[1] J. Etcheto,[1] L. Merlivat,[1] T. Takahashi,[2] B. Delille,[3] M. Frankignoulle,[3,4] and D. C. E. Bakker[5]

Received 23 July 2004; revised 27 March 2005; accepted 18 May 2005; published 8 September 2005.

[1] We determine the distribution of oceanic CO_2 partial pressure (pCO_2) with respect to remotely sensed parameters (sea surface temperature (SST) and chlorophyll (Chl)) in order to gain an understanding of the small-scale (10–100 km) pCO_2 variability and to estimate the net air–sea CO_2 flux in the region (125°E–205°E; 45°S–60°S), which represents 22% of the Southern Ocean area between 45°S and 60°S. We split the study area into several biogeochemical provinces. In chlorophyll-poor regions, pCO_2 is negatively correlated with SST, indicating that pCO_2 is mostly controlled by mixing processes. For Chl > 0.37 mg m^{-3}, pCO_2 is negatively correlated with Chl, indicating that pCO_2 variability is mostly controlled by carbon fixation by biological activity. We deduce fields of pCO_2 and of air–sea CO_2 fluxes from satellite parameters using pCO_2-SST, pCO_2-chlorophyll relationships and air–sea gas exchange coefficient, K, from satellite wind speed. We estimate an oceanic CO_2 sink from December 1997 to December 1998 of −0.08 GtC yr^{-1} with an error of 0.03 GtC yr^{-1}. This sink is approximately 38% smaller than that computed from the Takahashi et al. (2002) climatological distribution of ΔpCO_2 for the 1995 year but with the same K (−0.13 GtC yr^{-1}). When we correct ocean pCO_2 for the interannual variability between 1995 and 1998, the difference is even larger, and we cannot reconcile both estimates in February–March and from June to November. This strengthens the need of new in situ measurements for validating extrapolation methods and for improving knowledge of interannual pCO_2 variability.

Citation: Rangama, Y., J. Boutin, J. Etcheto, L. Merlivat, T. Takahashi, B. Delille, M. Frankignoulle, and D. C. E. Bakker (2005), Variability of the net air–sea CO_2 flux inferred from shipboard and satellite measurements in the Southern Ocean south of Tasmania and New Zealand, *J. Geophys. Res.*, *110*, C09005, doi:10.1029/2004JC002619.

Introduction

[2] In situ measurements of sea surface CO_2 partial pressure indicate that the Southern Ocean may be a large oceanic sink for atmospheric CO_2. Actually, the climatological net air–sea flux of CO_2 reconstructed from such measurements by *Takahashi et al.* [2002] shows strong sinks between 40°S and 60°S; compiling measurements from several campaigns in the subantarctic zone (SAZ) of the Southern Ocean, *Metzl et al.* [1999] estimated that the absorbed flux of CO_2 might be up to 1 GtC yr^{-1} in the whole SAZ. However, the air–sea CO_2 fluxes estimated in the Southern Ocean using atmospheric inversions [*Gurney et al.*, 2004], ocean biogeochemical models and oceanic inversions [*Gloor et al.*, 2003] are smaller than that deduced from in situ measurements. Recently, *Gloor et al.* [2003] estimated an uptake of −0.3 GtC yr^{-1} between 36°S and 58°S in the Indian and Pacific sectors of the Southern Ocean using an inverse oceanic model. The fluxes for the same region were estimated as −0.4 GtC yr^{-1} from atmospheric transport models, while the CO_2 sink in the Takahashi climatology is close to −0.8 GtC yr^{-1}.

[3] The air–sea CO_2 flux is classically estimated from ocean-surface measurements as the product of the local air–sea CO_2 exchange coefficient (K) and partial pressure difference (ΔpCO_2). The regional flux is derived by the integration of the local flux over a given region. The main unknown when dealing with the spatial distribution and the temporal variability of the air–sea flux comes from the ΔpCO_2 variability which is poorly known, due to the complex physical and biogeochemical processes governing the sea surface partial pressure (pCO_2) and to the scarcity of in situ measurements in these remote and rough waters. Although the absolute value of K is not well fixed, its spatial and temporal variability is relatively well known as

[1] Laboratoire d'Océanographie Dynamique et de Climatologie/Institut Pierre Simon Laplace, Université Pierre et Marie Curie, Paris, France.
[2] Lamont-Doherty Earth Observatory of Columbia University, Palisades, New York, USA.
[3] Unité d'Océanographie Chimique, MARE, Université de Liège, Liège, Belgium.
[4] Deceased 13 March 2005.
[5] School of Environmental Sciences, University of East Anglia, Norwich, UK.

0148-0227/05/2004JC002619$09.00

Table 1. List of Shipboard Campaigns

Cruise Area	Cruise Name	Start Cruise	End Cruise	Season	Ship Name
East of New Zealand	NBP 97 8	06/11/1997	11/11/1997	spring	R/V *Nathaniel B. Palmer*
(AESOPS campaigns)	RR KIWI 8 first transect	08/01/1998	13/01/1998	summer	R/V *Roger A. Revelle*
	RR KIWI 8 second transect	03/02/1998	07/02/1998	summer	
	RR KIWI 9 first transect	13/02/1998	26/02/1998	summer	
	RR KIWI 9 second transect	07/03/1998	18/03/1998	fall	
	NBP 98 2	25/03/1998	02/04/1998	fall	R/V *Nathaniel B. Palmer*
South of Tasmania	dta 99	22/10/1999	28/10/1999	spring	R/V *Astrolabe*
(Astrolabe campaigns)	rta 99	21/12/1999	26/12/1999	summer	
South of New Zealand and Tasmania	first SOIREE transect	02/02/1999	09/02/1999	summer	R/V *Tangaroa*
(SOIREE campaigns)	second SOIREE transect	22/02/1999	28/02/1999	summer	

a result of the good coverage of satellite wind speed measurements.

[4] Main processes controlling the variability of pCO_2 are oceanic circulation, thermodynamical effects, biological carbon uptake and air–sea gas exchange. Schematically, oceanic circulation promotes pCO_2 variations by mixing and transport of water masses with different properties (dissolved inorganic carbon, temperature, salinity, etc.); the thermodynamical effect is caused by the dependence of the CO_2 solubility and dissociation constants on temperature; biological activity is responsible for carbon fixation and release.

[5] The objective of our paper is to determine the spatial distribution of the air–sea CO_2 flux and its seasonal variation over a region of the Southern Ocean south of Tasmania and New Zealand.

[6] Our study was limited to 1.5 years in order to minimize uncertainties from possible interannual variations in surface ocean pCO_2. Specifically, the effect of the increase of the atmospheric CO_2 concentration on pCO_2 in the Southern Ocean is poorly known and it may reach 3 μatm over 2 years. Therefore we choose to limit our study to less than 2 years and to a region for which both satellite chlorophyll and in-situ campaigns in several seasons are available. This study focuses on the area south of Tasmania and New Zealand (125°E–205°E; 45°S–60°S) from December 1997 to December 1998, where several shipboard campaigns were carried out at a time when the Advanced Very High Resolution Radiometer (AVHRR) and the Sea-viewing Wide-Field-of view Sensor (SeaWiFS) satellites were making measurements of sea surface temperature (SST) and of ocean color, respectively.

[7] In section 2, we present the data; in section 3, we analyze observed pCO_2 variability and in section 4 we describe pCO_2 extrapolation and associated errors. In section 5, we present air–sea fluxes and comparison with the *Takahashi et al.* [2002] climatological mean estimates. The results are discussed in section 6.

Data

In Situ pCO_2

[8] We study oceanic pCO_2 measurements made in the area south of Tasmania and southeast of New Zealand during various campaigns. We only use data after September 1997 when the chlorophyll content extracted from SeaWiFS chlorophyll images is available: two Astrolabe campaigns conducted in the course of opportunistic logistical cruises by the University of Liege during spring and summer south of Tasmania and four Antarctic Environment and Southern Ocean Process Study (AESOPS) campaigns conducted during spring, summer, and fall south east of New Zealand (P.I: T. Takahashi) (see Table 1 for more details and Figure 1a for the location of the transects). In addition, data collected during two Southern Ocean Iron Release Experiment (SOIREE) transects are used to validate the extrapolation method. Even though we use AESOPS campaigns conducted during a restricted period, it can be seen in the work of *Morrison et al.* [2001] that these data are consistent with those from other years at the southern edge of the studied area; it is also true at lower latitudes. Hence we consider that our analysis is based on a representative year.

[9] We eliminate data collected over the continental shelves (water depth less than 500m), using the same criteria as *Moore and Abbott* [2000], retaining only pCO_2 measurements made in the open ocean. This correction is applied to three AESOPS transects (NBP 97 8, RR KIWI 9, and NBP 98 2), which cross the Bounty plateau at about 180°E, 48°S.

Astrolabe Campaigns

[10] A complete description of the experimental set-up is given by *Frankignoulle et al.* [2001]. xCO_2 accuracy is estimated to be 2ppm, the precision on the order of ±0.5 ppm. The estimation of pCO_2 from CO_2 concentration measurements is described in Appendix A. Given uncertainties linked to the atmospheric pressure correction, we estimate pCO_2 precision to be about ±2 μatm.

AESOPS Campaigns

[11] The method for measuring pCO_2 in surface water during the AESOPS campaigns is described by *Takahashi et al.* [2000]; the overall pCO_2 precision is estimated to be ±1.5 μatm. We use data available on http://www1.whoi.edu/southern.html that are shown in the work of *Rubin* [2003]. We do not use the pCO_2 measurements collected during the RR KIWI 8 campaign (first leg from 8 January 1998 to 13 January 1998) between 49°S and 45°S, since there are wide gaps in the data.

SOIREE Campaigns

[12] We use pCO_2 measured during two SOIREE transects conducted during February 1999 south of Australia. Figure 2 shows the location of these transects superimposed on the monthly SeaWiFS chlorophyll distribution for February 1999 south of Australia. The transects cross the center of the study area, between 142°E and 170°E, a region not explored by AESOPS and Astrolabe campaigns, thus allowing us to check the ability of our regression method to reproduce pCO_2 at different locations. The method of the

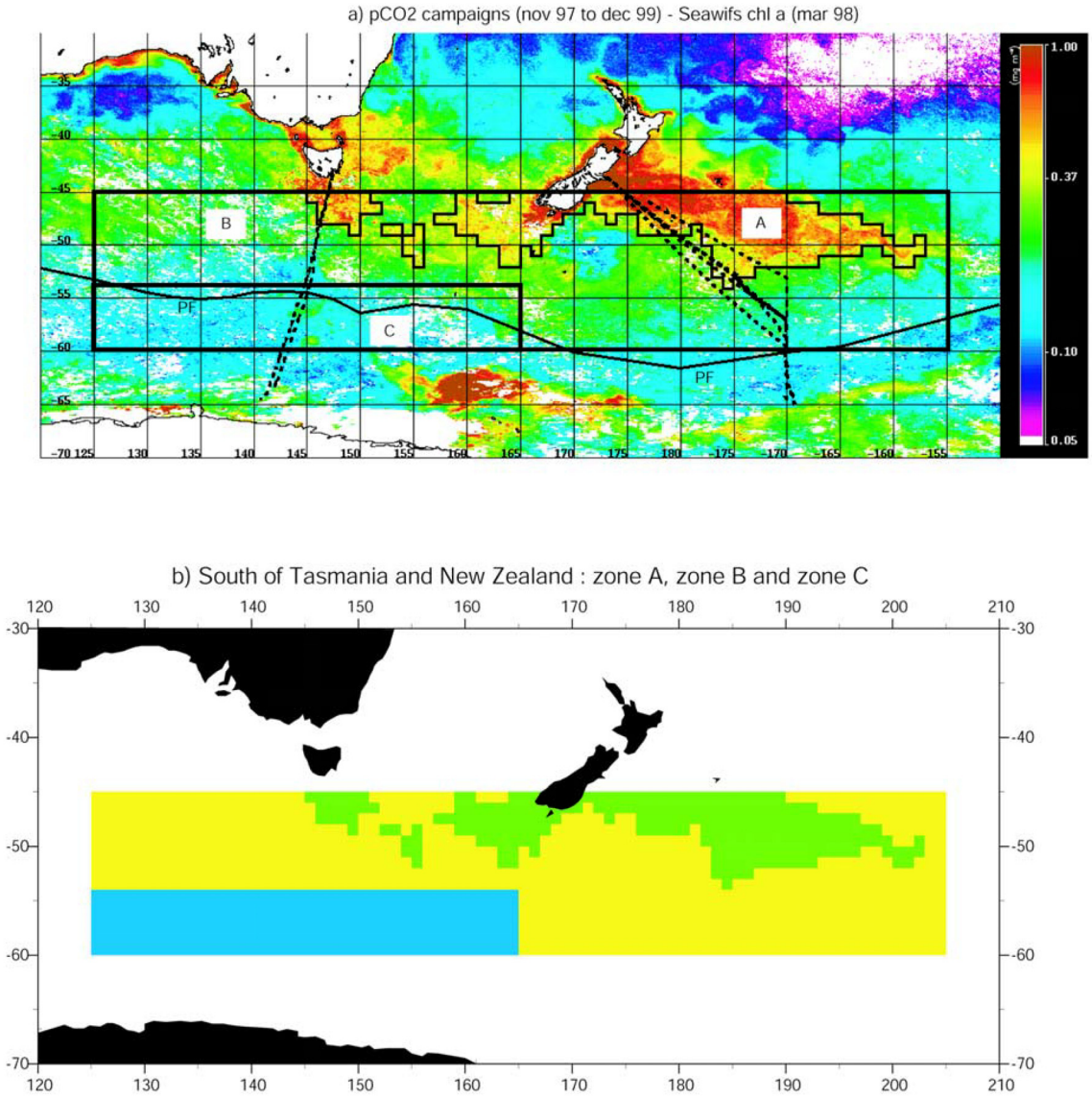

Figure 1. (a) Tracks of the campaigns (dashed lines; AESOPS campaigns in the eastern part, Astrolabe campaigns in the western part) superimposed on a SeaWiFS chlorophyll map (March 1998). The climatological Polar Front (PF) from *Belkin and Gordon* [1996] and the boundaries between zones A, B, and C are indicated in solid lines. (b) Zone A (chlorophyll-rich region; green), B (yellow), and C (blue) for March 1998.

surface water pCO_2 measurements is described by *Watson et al.* [2000] and by *Bakker et al.* [2001]. The accuracy and precision of the measurements are estimated to be 1.0 and 0.6 μatm, respectively.

Satellite Parameters

[13] We use SST derived by the National Meteorological Center (NMC) from in situ and AVHRR data using the *Reynolds and Smith* [1994] objective interpolation analysis and level 3 SeaWiFS chlorophyll data (version 3) distributed by the Physical Oceanography Distributed Active Archive Center (PODAAC). Reynolds SST data grids have a 1 × 1 degree resolution and SeaWiFS chlorophyll (Chl) data grids have a 9 × 9 km resolution. We use weekly 9 km SeaWIFS Chl to develop the extrapolation scheme. Monthly grids of SST and Chl are used to extrapolate pCO_2.

[14] We use level 2 ERS-2 wind products (instantaneous; 25 km resolution) delivered by the Institut Français de Recherche pour l'Exploitation de la Mer (IFREMER)/Centre ERS d'Archivage et de Traitement (CERSAT) in Brest, France, to derive the gas exchange coefficient, K. K is derived from Reynolds SST, ERS-2 satellite wind speed (U) data and a K–U relationship. The air–sea flux differences induced by the use of different K-U parameterizations were already documented by *Boutin et al.* [2002]. We do

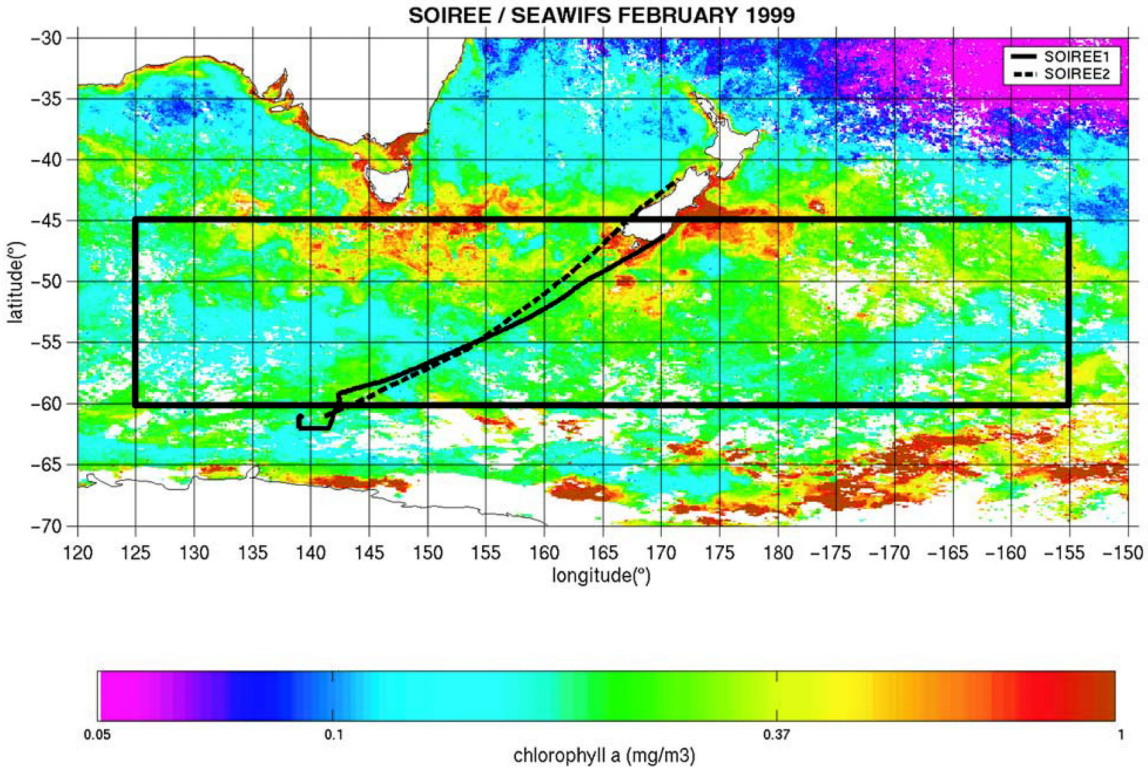

Figure 2. SOIREE transects superimposed on the SeaWiFS chlorophyll map for February 1999.

not consider here a cubic relationship, as proposed by *Wanninkhof and McGillis* [1999] as the cubic dependency has not been firmly confirmed on recent experiments: analysis of measurements in the Southern Ocean by [*Wanninkhof et al.*, 2004] does not allow to distinguish between a cubic and a quadratic relationship; *Frew et al.* [2004] found that the best fit to the CoOP97 measurements follow a quadratic K-U relationship close to the [*Nightingale et al.*, 2000] relationship. In our study area, K derived from the *Liss and Merlivat* [1986] and *Nightingale et al.* [2000] parameterizations are systematically lower than the one deduced from the *Wanninkhof* [1992] U^2 formulation by a factor 1.8 and 1.2 respectively (Figure 3). Whatever the relationship is used, K varies seasonnaly by a factor 1.4 between winter and summer. In the following we will use the *Wanninkhof* [1992, relation 3] K–U relationship for short-term wind speed as it is the most widely used in the literature; using other K-U parameterization would lead to different absolute values of air–sea CO_2 flux as discussed by *Boutin et al.* [2002], but the relative differences between fluxes deduced from various Δp fields would remain in the same proportions as K shown in Figure 3. In particular, according to recent studies by *Peacock* [2004] and *Sweeney et al.* [2004], ^{14}C inventory used to calibrate *Wanninkhof* [1992] relationship could be overestimated by 15 to 25% so that absolute values of our flux estimates could be over-estimated as well. To take into account small-scale variability of wind speed, K values are computed for each ERS-2 measurement (instantaneous, 25 km resolution). Then, K

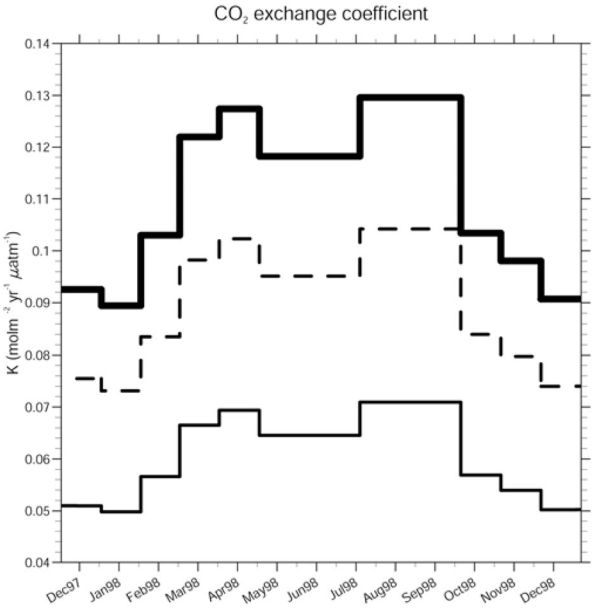

Figure 3. CO_2 exchange coefficient averaged over the study area and derived from *Wanninkhof* [1992] relationship (thick line), *Nightingale et al.* [2000] relationship (dashed line) and *Liss and Merlivat* [1986] relationship (thin line) for the year 1998.

Table 2. Summary of the Relations[a]

Zones	Seasons or Months	Fits or $\langle pCO_2 \rangle$ *Chl* in mg.m^{-3}, *SST* in °C and pCO_2 in µatm	Std[e] in µatm	Stdfit[e] in µatm	Number of Data
Zone A: chl-"rich" area	spring, summer, fall and winter[b]	$pCO_2 = -33.04 \times Chl. + 347.89$	11.3	7.9	209
chl-"rich" area in the southwestern area (region C)	December and January only	$pCO_2 = -33.04 \times Chl. + 363.$	...	...	...
Zone B: chl-"poor" area	spring	$pCO_2 = -2.69 \times SST + 370.80$	8.2	5.7	1155
	summer December	$pCO_2 = -1.23 \times SST + 352.50$	5.8	4.8	368
	summer January	$pCO_2 = \langle pCO_2 \rangle = 334$	9.3	...	1205
	summer February	$pCO_2 = \langle pCO_2 \rangle = 348$	9.2	...	3083
	fall	$pCO_2 = -2.06 \times SST + 362.63$	4.2	2.6	3042
	winter	$pCO_2 = -2.38 \times SST + 366.72$[c]	...	...	...
Zone C: southwestern area	spring	$pCO_2 = \langle pCO_2 \rangle = 357$	4.0	...	365
	summer	$pCO_2 = \langle pCO_2 \rangle = 357$	6.5	...	298
	fall	$pCO_2 = \langle pCO_2 \rangle = 350$	2.3	...	1167
	winter	$pCO_2 = \langle pCO_2 \rangle = 354$[d]	...	...	...

[a]Used to extrapolate pCO_2 and statistics of the residuals to the fits.
[b]No winter data: the same fit is used for winter.
[c]The pCO_2–SST fit in spring and in fall are averaged to compute this new linear fit.
[d]Here $pCO_2 = \frac{\langle pCO_2 \rangle in\ spring + \langle pCO_2 \rangle in\ fall)}{2}$.
[e]Here stdfit, standard deviation of pCO_2 with respect to the fits; std, standard deviation of pCO_2 measurements.

values are interpolated over a 1 × 1 degree grid using an objective analysis described by *Boutin et al.* [1995].

Atmospheric pCO_2

[15] In order to deduce maps of ΔpCO_2 from maps of extrapolated pCO_2, we use atmospheric concentration of CO_2 in dry air (atmospheric xCO_2) provided by *Globalview–CO_2* [2003, available via anonymous FTP at ftp.cmdl.noaa.gov, path: ccg/co2/GLOBALVIEW] at Cape Grim station in Tasmania (144.68°E; 40.68°S) and we assume that this value is equal to the atmospheric xCO_2 mean value over the area (125°E–205°E; 60°S–45°S). We estimate monthly maps of atmospheric pCO_2, pCO_{2a}, at 1° × 1° resolution using equation (A1), monthly atmospheric xCO_2, ECMWF maps of atmospheric pressure, Patm, and saturated water pressure, pH_2O. pH_2O is computed from Reynolds SST grids (monthly, 1 × 1 degree resolution) using the formulation of *Weiss and Price* [1980]. ECMWF Patm maps represent the field at sea level, originally at 2.5° × 2.5° resolution that we subsampled to 1° × 1° resolution.

Correlation of Oceanic pCO_2 With Chlorophyll and SST

[16] First, we look for biogeochemical provinces inside which in situ pCO_2 measurements appear to have a similar behavior with respect to SST and chlorophyll. Next, inside each zone, we look for a relationship between pCO_2 and SST or chlorophyll. The pCO_2–SST relationships take into account pCO_2 variability induced by mixing and thermodynamic effects. In addition, the use of chlorophyll data enables the biological effect to be taken into account.

[17] We use different combinations of in situ data (campaign by campaign, seasonal, annual, etc.) in various regions. pCO_2 is expected to have a seasonal variation but this could not be shown from the measurements themselves because of large spatial variations. We decide to arbitrarily split the measurements by seasons as defined by *Moore and Abbott* [2000]: summer (December to February), fall (March to May), winter (June to August), and spring (September to November).

[18] Given the large scatter of data we only test linear fits between pCO_2 and SST and between pCO_2 and chlorophyll. We do not use multiparametric fits between pCO_2-SST-Chl because in such fits, the variability of pCO_2 is split in two parts, one coming from SST variability and one coming from the chlorophyll variability. Therefore this division of pCO_2 variability is quite artificial because SST and Chl are correlated; on the other hand, the residuals of the pCO_2-Chl fits are not correlated with SST (see below).

[19] We analyze the quality of the fits using the standard deviation of the difference between measured pCO_2 and pCO_2 predicted by the fit, stdfit. When stdfit is not significantly smaller than the standard deviation of pCO_2 measurements, std, our fit does not improve the pCO_2 prediction compared to taking a constant value for pCO_2. In that case or in case the correlation coefficient is less than 0.5, we take a constant pCO_2 value.

The pCO_2 Variability Correlated With Chlorophyll

[20] To get pCO_2 at a resolution close to that of SeaWiFS level 3 data (9 × 9 km), we average pCO_2 for areas 0.08° in latitude and in longitude, hereafter called pCO_2(9 km). Then, we collocate pCO_2(9km) measurements with weekly 9 km SeaWiFS chlorophyll maps. The weekly SeaWiFS data are chosen as a compromise between minimizing data gaps due to cloud coverage (very frequent on daily images) and maintaining the temporal evolution of the chlorophyll content inside one month (we observe significant temporal changes from one week to the next).

[21] We always find a chlorophyll-rich zone in the northern part of each transect. Its mean southern limit is 49°S and 48°S on the eastern and western campaigns, respectively. When comparing collocated chlorophyll and pCO_2 measurements campaign by campaign, we observe a negative correlation between the two parameters in the chlorophyll-rich zone. We empirically derive a chlorophyll threshold equal to 0.37 mg m^{-3} to define the chlorophyll-rich zone in which such a correlation is observed. This limit is adopted because the accuracy of the chlorophyll content retrieved from SeaWiFS measurements decreases for low

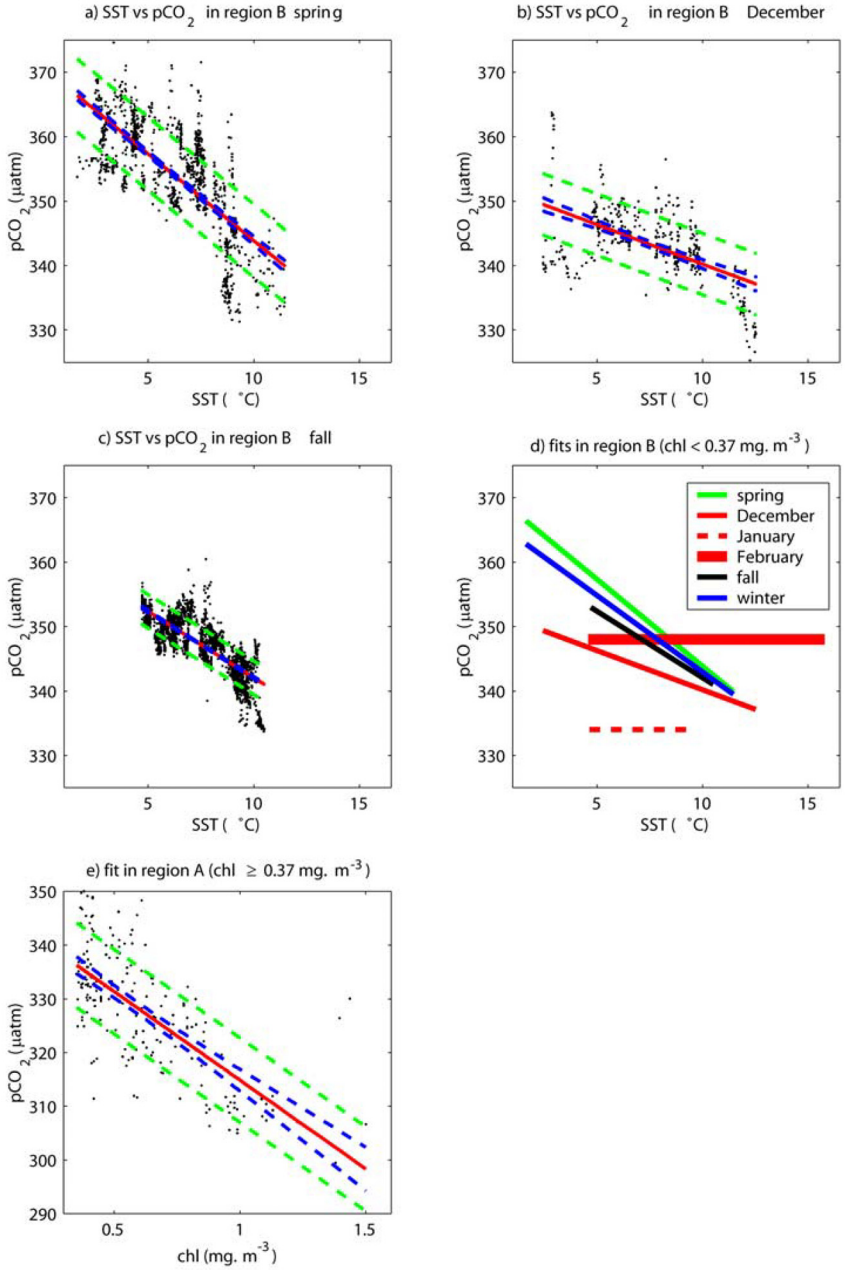

Figure 4. Linear fit (red), its 95% confidence interval (blue dashed line), and the pCO_2 residuals with respect to the fits (±stdfit) (green dashed line) superimposed on the pCO_2–SST scatterplot for zone B in (a) spring, (b) December and (c) fall; (d) Summary of pCO_2–SST relationships used in the paper (including mean values) plotted over the SST ranges covered by the measurements. (e) Same as (a) for a yearly pCO_2–chlorophyll fit in zone A (for chl $\geq$ 0.37 mg m^{-3}).

values, thus hampering the comparison in chlorophyll-poor regions. The chlorophyll-rich zone will be referred to as zone A from here on. Its limit is found from monthly 1 × 1 degree SeaWiFS images rather than from weekly 9 × 9 km images, in order to avoid data gaps due to cloud coverage, and this varies from month to month with changes in chlorophyll. An example is given in Figures 1a and 1b for March 1998. Zone A includes a southern part of the subtropical frontal zone (not shown in Figure 1a) and a northern part of the subantarctic zone.

[22] The best pCO_2–chlorophyll fit in zone A is obtained when all data for spring, summer and fall are pooled; it is

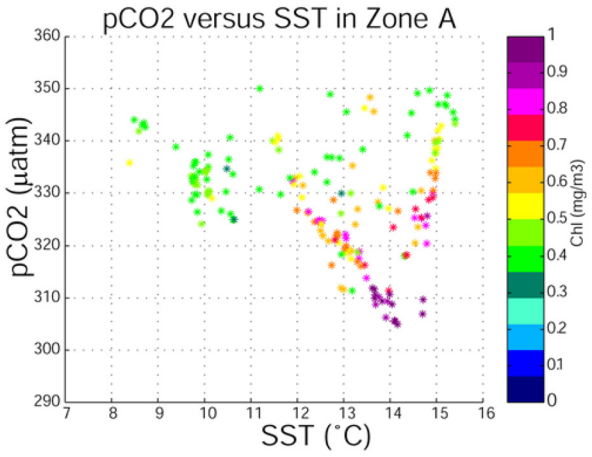

Figure 5. The pCO_2 versus SST for AESOPS and Astrolabe campaigns in Zone A; Chl is color coded. High chlorophyll values corresponding to low pCO_2 values are only observed at high SST. Nevertheless, pCO_2-SST fit is of lower quality than pCO_2-Chl fit.

indicated in Table 2 and Figure 4e. High chlorophyll are only observed for high SST so that chlorophyll and SST appears to be correlated (r = 0.65); low pCO_2 also appears for high SST (Figure 5), but the corresponding pCO_2-SST fit is of poorer quality (stdfit = 8.6 µatm) and not used in the following. In addition, the residuals of pCO_2-Chl fits are not correlated with SST (r = 0.1).

The pCO_2 Variability Correlated With SST

[23] In the rest of the study area (Chl < 0.37mg m^{-3}), we find a sharp latitudinal SST and pCO_2 gradient at about 54°S on the Astrolabe measurements corresponding to the position of the Polar Front (PF) (see Figure 1a). We divide the remaining area into two zones; schematically zone B north of the Polar Front and zone C south of the Polar Front (see Figure 1a). We do not find any clear latitudinal pCO_2 and SST gradient corresponding to the climatological Subantarctic Front (SAF) derived either from *Orsi et al.* [1995] or from *Belkin and Gordon* [1996] (not shown in Figure 1a). Hence we keep data from the SAZ and from the polar zone together.

[24] For zone B, in spring and fall, we establish seasonal negative correlations between pCO_2 and SST (see Table 2 and Figure 4a, 4c, and 4d). These fits are similar, but their 95% confidence intervals do not overlap indicating that they are statistically different. In addition, we test a pCO_2–SST fit from spring and fall data together: in that case, stdfit is much larger (4.1 µatm) than stdfit for fall data only (2.6 µatm), so we decide to keep one fit for each season. In summer, we find a significant negative correlation only for December. For January and February, the pCO_2–SST correlation coefficient is less than 0.5, so we do not take into account the pCO_2 changes due to the SST variations but use an average pCO_2 value. Since no measurement is available for winter, a winter pCO_2–SST relationship is derived by averaging the coefficients of the pCO_2–SST fit for spring and fall.

[25] In zone C, we do not find any correlation between pCO_2 and SST; consequently we use the seasonal pCO_2 average derived from the Astrolabe measurements in spring and summer. In fall, since we have no data for zone C, we take the average of the AESOPS pCO_2 measurements in the same latitude range. In winter, pCO_2 is assumed to be equal to the average of the spring and fall values.

Interpretation of Observed pCO_2 Relationships With Chl and SST

[26] Finding a pCO_2–chlorophyll or a pCO_2–SST fit does not mean that only biological or physical mechanisms are at work, but rather that a particular mechanism dominates the small-scale (10–100 km) variability. In fact, a biological contribution may be included in an SST fit since the biological activity tends to be higher in warm water. A physical contribution may be included in a chlorophyll fit as well since mixing affects biology.

[27] We find that the ocean is undersaturated in most of the study area, implying that biology is decreasing the average pCO_2 even in zone B. However, in this zone, we could not show any short-scale pCO_2–chlorophyll correlation. There are several reasons for this absence of correlation: biological export involves slow and weakly variable mechanisms that may be hiden by more variable processes; a strong carbon fixation may have occurred outside of our study area and the waters with reduced CO_2 may have been advected in zone B; subsurface chlorophyll may be different from the surface chlorophyll visible from space. However, a quantitative study of the processes responsible for this undersaturation would require more data in order to describe the historic of water masses. Conversely in zone A where chlorophyll gives the best fit, it means that the thermodynamical and mixing effects more or less compensate each other, at small-scale, leaving a dominant short-term biological signature.

[28] This coupling between physical and biological effects is illustrated by the test described below. Instead of comparing pCO_2 at measured SST to chlorophyll, we used pCO_2 at constant temperature, correcting for the thermodynamical effect using the formulation of *Takahashi et al.* [2002, relation 1] (isochemical conditions are assumed here):

$$(pCO_2 \text{ at } T_{cst}) = (pCO_2)_{obs} \cdot \exp[0.0423(T_{cst} - T_{obs})] \quad (1)$$

where T is the sea surface temperature in °C and the subscript "cst" and "obs" indicate constant and observed values, respectively. Here pCO_2 at constant temperature is taken as a proxy for the total carbon content.

[29] In all cases, the correlation coefficient is higher when using pCO_2 normalized at constant temperature. However, this does not mean that the fit of (pCO_2 at T_{cst}) is better suited for the simulation of (pCO_2 at T_{obs}) than the fit obtained from pCO_2 at T_{obs}. Actually, the correlation coefficient is defined as $r = \sqrt{1 - (stdfit^2/std^2)}$ and stdfit for the fit of (pCO_2 at T_{cst}) and for the fit of (pCO_2 at T_{obs}) are similar while std of (pCO_2 at T_{cst}) is much larger than std of (pCO_2 at T_{obs}) (more than 30 and 10 µatm respectively). In fact, when (pCO_2 at T_{cst}) regressions are used to predict pCO_2 at measured SST using the inverse of equation (1), the standard deviation of the predicted minus

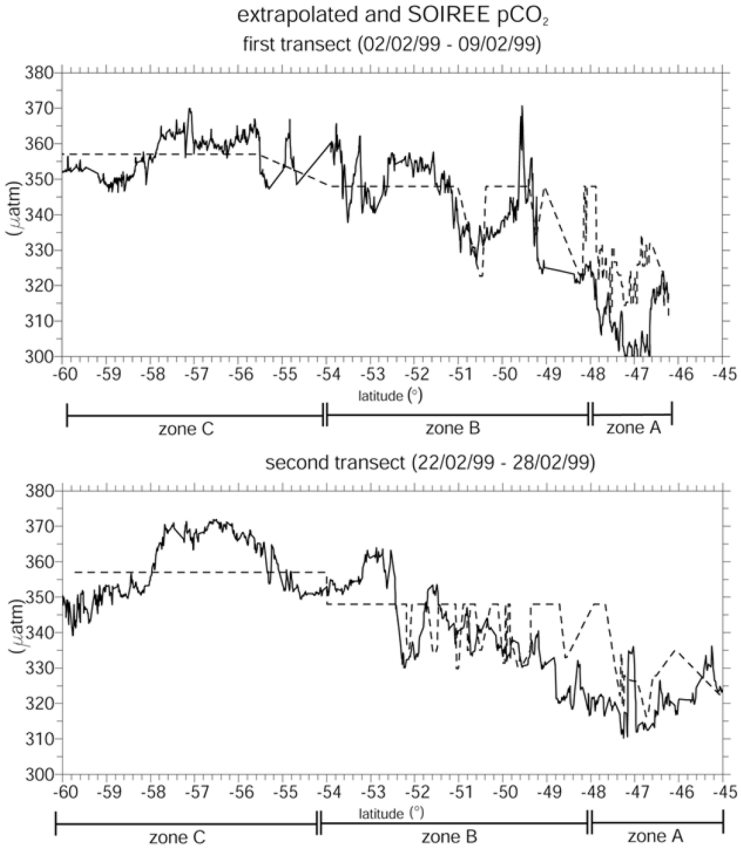

Figure 6. Variation in pCO_2 measurements (solid line) and extrapolated pCO_2 (dashed line) along SOIREE transects in February 1999 (first leg; top, second leg; bottom).

measured pCO_2 at T_{obs} becomes larger than the observed variability. This can be explained as the correction for the temperature effect does not take into account water mixing for which SST is also a tracer, thus worsening our representation of physical mechanisms and our prediction.

[30] The importance of mixing in zone B is shown by the pCO_2–SST regressions: the slope of these regressions is always negative or zero, contrary to what is expected for thermodynamical effect alone. In zone B, the mixing effect usually dominates the thermodynamical effect. It is likely that it also plays an important role in zone A.

Extrapolation of pCO_2

Summary of pCO_2-Chl and pCO_2-SST Fits (Standard Extrapolation Method)

[31] We keep fits between pCO_2 and SST during three periods in zone B and a yearly fit between pCO_2 and chlorophyll in zone A. The corresponding scatterplots are displayed on Figures 4a, 4b, 4c and 4e together with the fits. We also indicate the 95% confidence interval for the fits, that represents the interval in which the fit is expected to fall given the number and the scatter of the points, and the fit ± stdfit, that quantifies the scatter of the individual measurements around the fit. Figure 4d summarizes the pCO_2–SST relationships applied in the paper (including pCO_2 constant values); coefficients of the fits are reported in Table 2.

[32] Hereafter, since this method gives the best results among those tested (see below), it will be called the "standard" extrapolation method.

Quality of Extrapolated pCO_2

Comparison of Extrapolated pCO_2 With Independent SOIREE Measurements

[33] The drawback of the method is that it is based on a limited number of measurements and that only a few independent measurements are available for validation. We test the fits used for extrapolating pCO_2 using independent measurements from two pCO_2 SOIREE transects located between the Astrolabe and AESOPS transects. We apply the pCO_2 fits (standard scheme) using in situ SST and weekly SeaWiFS chlorophyll to compute extrapolated pCO_2 in each zone (A, B, and C) crossed by the ship's route during the Febuary 1999 SOIREE cruise. On the two transects, extrapolated and in situ pCO_2 follow the same main trends (Figure 6). South of 48°S, extrapolated pCO_2 values agree well with the measurements although, at the local-scale, differences of up to 20 µatm occur. Most of the time, differences are less than 10 µatm. North of 48°S, high-chlorophyll (zone A) are correlated with low pCO_2 values. pCO_2 drawdown in these areas is relatively well simulated (on the first leg, differences are smaller than 10 µatm). When averaged zone by zone, (see Table 3), extrapolated pCO_2 and in situ pCO_2 are very close, especially in zone B

Table 3. Comparison of Measured and Extrapolated pCO_2 Along SOIREE Transects

	Zone A			Zone B			Zone C		
	In Situ pCO_2, μatm	Predicted pCO_2, μatm	Std of Difference, μatm	In Situ pCO_2, μatm	Predicted pCO_2, atm	Std of Difference, μatm	In Situ pCO_2, μatm	Predicted pCO_2, μatm	Std of Difference, μatm
Transect 1	311	324	10.6	347	348	10.3	358	357	5.6
Transect 2	329	330	10.2	343	348	11.6	360	357	8.2

and C. The standard deviation of the difference between measured and predicted pCO_2 (6 to 12 μatm) is consistent with the precision of our regressions (2 to 9 μatm) or mean values considered in our extrapolation method in February 1999 (Table 2). This gives credibility to our extrapolation method. Even though more independent measurements at other seasons are needed for a complete validation, this result is encouraging, especially as the SOIREE transects crossed a zone where we have no measurement to develop our extrapolation method.

"Statistical" Error on Extrapolated pCO_2 Fields

[34] Since we do not get independent measurements at all seasons, we estimate an order of magnitude of the error on our extrapolated fields in each biogeochemical province and at seasonal scale from stdfit. Although this error estimate is not based on independent measurements, it quantifies the scatter of the measurements around the fit which is likely to be due to physical and biogeochemical processes that are not completely taken into account by the pCO_2–SST and pCO_2–chlorophyll fits.

[35] We use Reynolds SST to compute extrapolated pCO_2 maps. Then we introduce an error on pCO_2 that comes from differences between Reynolds SST and in situ SST that are used to develop pCO_2–SST fits. To quantify this error, we collocate weekly 1 × 1 degree satellite SST with SST measured during the AESOPS and Astrolabe campaigns: the mean bias is 0.03°C, and the standard deviation of the difference is 0.78°C (15 355 data points). Using the equations in Table 2, this SST uncertainty leads to an uncertainty in extrapolated pCO_2, error_from_SST, between 1.0 and 2.1 μatm.

[36] Therefore we estimate the precision of the pCO_2 extrapolated maps for zones A, B, and C as the root mean square of the quadratic sum of stdfit (Table 2) and of error_from_SST. In the following we call it statistical precision. It is always less than 8 μatm (Figure 7, top) and is smallest in fall and spring in zones B and C.

Alternative Extrapolation Methods Used to Determine "Methodological Error"

[37] To evaluate the sensitivity of the extrapolated pCO_2 to the biogeochemical provinces boundaries and to the variables used to fit pCO_2, we also compare results obtained with two alternative extrapolation methods derived from the same set of measurements. The difference in pCO_2 extrapolated using the standard method and the alternative methods will be referred as methodological error.

[38] In both alternative schemes, fits are derived separately for the eastern and western campaigns, assuming that the processes at play in both regions may be different, and the study area is divided at 165°W into two parts: eastern and western. This separation was not useful in the standard extrapolation method, because the chlorophyll threshold allows getting the same method valid for both transects.

[39] In the first alternative scheme (scheme I), we define province boundaries using SST thresholds (instead of Chl) and use only pCO_2-Chl fits. We define three provinces bound by north–south SST spatial gradients (larger than 1°C per 0.5° latitude) which have marked pCO_2 signatures (typically more than 10 μatm). The SST thresholds corresponding to the zones' boundaries are defined seasonally from in situ measurements, campaign by campaign, and vary from 6°C to 8°C and from 10°C to 11.5°C, respectively. In each zone, we use pCO_2–chlorophyll fits, assuming that in each zone the main effect controlling variability of pCO_2 is biological carbon uptake or water mixing and that chlorophyll is a tracer for both processes. In this scenario, we average SeaWiFS chlorophyll maps over 3 to 7 weeks centered on the corresponding cruise to minimize the number of cloudy pixels. To remove spatial variations in SeaWiFS chlorophyll that could occur at a small spatial scale, we apply a running filter over 0.5° in latitude on pCO_2 and collocated chlorophyll measurements. This scenario cannot be applied in winter because of too many cloudy pixels on SeaWiFS chlorophyll images in this season. Results obtained with this scenario are described by *Boutin et al.* [2001].

[40] The second scheme (scheme II) is very similar to the standard extrapolation method except that (1) the boundary between zones A and B is fixed (at 48°S between 140°E and 165°E and at 49°S between 165°E and 155°W), thus neglecting the variability in the spatial extent of the chlorophyll-rich zone, and (2) fits are different in the eastern and western parts.

[41] A summary of the standard deviation of the difference between pCO_2 values measured and reconstructed using each method is given in Table 4. It shows that the standard scheme better matches the measurements except in spring. This improves slightly if eastern and western campaigns are separately treated. However, this improvement may be due to the limited number of campaigns considered here. In summary we retain the standard extrapolation scheme because it allows pooling the data from the eastern and western campaigns based on biological and physical criteria, while giving similar or even lower residuals of the measurements with respect to the fits.

[42] We compare pCO_2 fields extrapolated using the standard extrapolation method with the ones obtained using alternative schemes. The maximum difference between pCO_2 fields obtained with the standard scheme and alternative schemes (Figure 7, middle) is less than 10 μatm almost everywhere in different seasons. Only in the northern part of the study area the differences between the worst performing scheme (here scheme 1) and the standard scheme are larger due to a drawback of scheme I in which low pCO_2 measurements were incorrectly interpreted as being regional instead of being caused by local high biological activity. For instance, in March the pCO_2–chlorophyll relation for the northern region of scheme I,

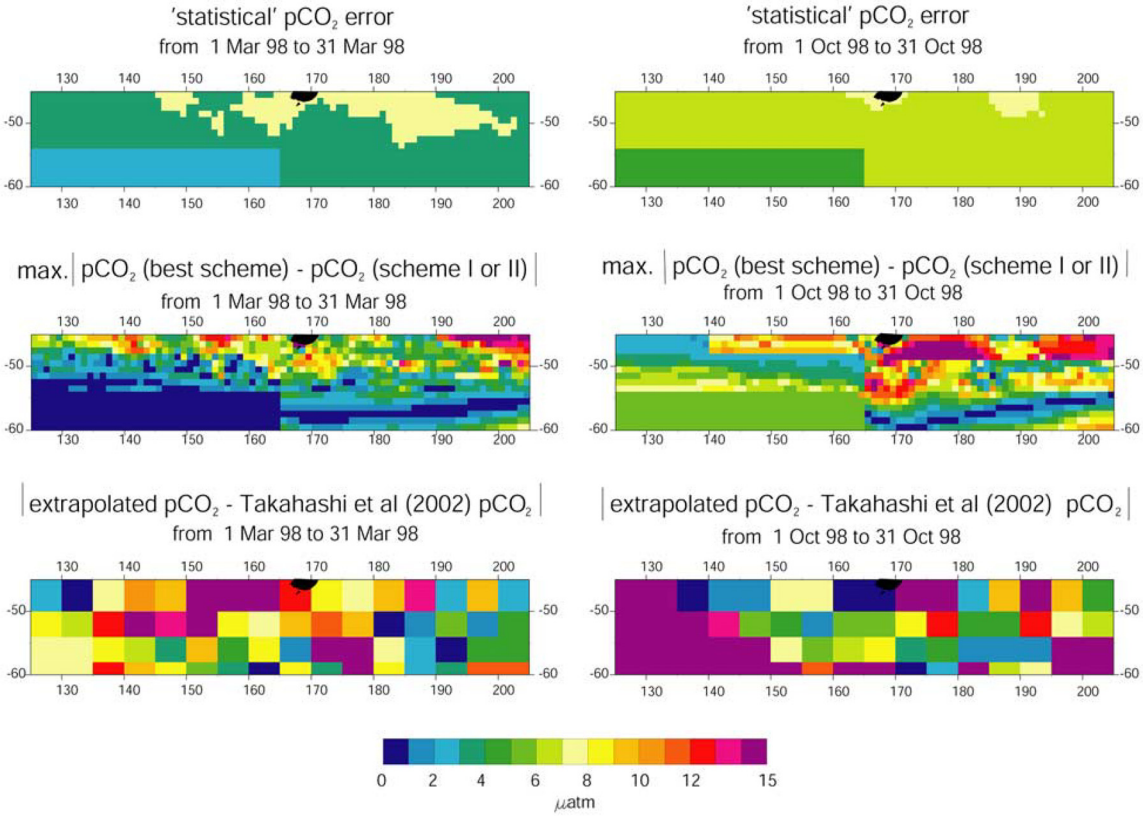

Figure 7. (top) Statistical error on pCO_2 derived with the standard scheme (see text). (middle) Maximum absolute value of the difference between pCO_2 extrapolated with the standard scheme and with one of the alternative schemes (methodological error). (bottom) Absolute difference in absolute value between extrapolated pCO_2 and *Takahashi et al.* [2002] corrected pCO_2 in March and in October 1998.

derived from AESOPS measurements made in region of high chlorophyll content, is used in regions where the chlorophyll content is low and the relation invalid.

[43] In summary, the statistical error and the methodological error are the largest in Zone A, up to 10 µatm, and minimum in zone C, up to 6 µatm; in most zones, statistical error is slightly lower than methodological error (except in zone C). The order of magnitude of statistical error and methodological error is similar to the error deduced from the comparison with SOIREE measurements.

Extrapolated pCO_2 Maps

[44] We use the standard method summarized in 4.1 to derive regional fields of ocean pCO_2 over the study area (125°E–205°E; 45°S–60°S) from December 1997 to December 1998. We choose December 1997 as the beginning of this period because summer begins in December (see definition of seasons above).

[45] Since the fits are linear, we use Reynolds SST and SeaWiFS chlorophyll data at low resolution (1 month and 1 × 1 degree) to compute monthly 1 × 1 degree extrapolated pCO_2 maps. We find a chlorophyll-rich zone (zone A) from December 1997 to April 1998 and from October 1998 to December 1998, so that from May 1998 to September 1998, the study area is composed of the zones B and C without zone A.

[46] On SeaWiFS images in December 1997 and January 1998, chlorophyll-rich areas are found in parts of the southwestern region (zone C) too. In this case, we assume that the pCO_2 decrease due to biological activity is the same as in zone A: we take a pCO_2–chlorophyll relationship with the same slope (a) as in zone A and a zero ordinate (b′) adjusted in the continuity of mean pCO_2 values in the low-chlorophyll area in zone C, $\langle pCO_2 \rangle$, as follows: the continuity is computed at ordinate (chlorophyll threshold)/2 because this is more or less the point where the fits in zone A and B join each other (except in February):

$$b' = (\langle pCO_2 \rangle \text{in zone C without chlorophyll}) - a \cdot (\text{chlorophyll threshold})/2.$$

We find b′ equal to 363 µatm in summer. Although we could not check the validity of this approach, possible errors should not have large consequences since this concerns only a few points.

[47] Monthly extrapolated pCO_2 maps for March 1998 (the beginning of fall) and for October 1998 (spring) are shown in Figure 8. In March 1998, low pCO_2 regions (less than 330 µatm) occur south of Tasmania, south and east of New Zealand. These areas are associated with chlorophyll-rich regions. In the whole study area, we find a north–south pCO_2 gradient due to negative correlation between SST and

Table 4. Standard Deviation of the Differences Between pCO_2 Measurements and Predicted Values[a] in the Whole Study Area, for Different Extrapolation Schemes

Seasons	Scheme I	Scheme II	"Standard" Scheme
Spring	6.1	4.6	5.3
Summer	10.6	11.4	9.6
Fall	6.4	5.6	4.8
Spring, summer, and fall	8.5	8.5	7.4

[a]Values are stdfit, in μatm.

pCO_2: in the northern part, pCO_2 is about 330 μatm (northeast) to 340 μatm (northwest), while in the southern part, pCO_2 is about 350 μatm (southwest) to 355 μatm (extreme southeast). Thus spatial pCO_2 variation is about 10–25 μatm from north to south and less than 10 μatm from east to west. In October 1998, pCO_2 values are higher than in March due to lower biological activity and to lower SST in October than in March. Again, low pCO_2 regions occur south and east of New Zealand, but the low pCO_2 region south of Tasmania disappears. Zone A is smaller than in March, because of lower biological activity. In the northern part, pCO_2 is relatively homogeneous (about 345 μatm) except in the chlorophyll-rich zone south and east of New Zealand. The pCO_2 value increases from north to south and is more or less homogeneous in the southern part (about 355 μatm in the southwest to 360 μatm in the southeast).

Monthly ΔpCO_2 and Air–Sea Fluxes Maps Deduced From Our Extrapolation and From *Takahashi* [2002] ΔpCO_2 Fields

Monthly Atmospheric pCO_2

[48] Monthly 1 × 1 degree maps of pCO_{2a} are shown in Figure 9 for March 1998 and for October 1998. We find a north–south pCO_{2a} gradient up to 10 μatm, which is stronger in March than in October. The spatial variation of pCO_{2a} is mainly due to north–south gradient of the ECMWF atmospheric pressure: in March, average Patm varies from about 1008 mbar at 45°S to 985 mbar at 60°S; in October it varies from about 1003 mbar to 986 mbar. It should be noticed that the north–south gradient of oceanic pCO_2 is positive, while the pCO_{2a} gradient is negative. Hence the north–south ΔpCO_2 gradient is enhanced by nearly 40% with respect to the gradient in oceanic pCO_2. For October, we reach to a similar conclusion. However, the north–south gradient in pCO_{2a} is weaker, about 5 μatm.

[49] Low values observed in coastal area near New Zealand are an artefact of the subsampling of ECMWF Patm maps and are due to low Patm value over New Zealand. Given the small number of rasters affected by this drawback, this does not affect significantly regionally and temporally averaged ΔpCO_2 and air–sea fluxes.

Monthly ΔpCO_2

[50] ΔpCO_2 maps are deduced as the difference between pCO_{2a} and extrapolated pCO_2 and are shown in Figure 10 (top) for March and October 1998. Because of the anti-correlation between the north–south variations of pCO_2 and pCO_{2a}, the north–south gradient of ΔpCO_2 is large (about 20 μatm). In the northern part, we observe regions with a strongly negative ΔpCO_2 between −15 and −30 μatm, because of high atmospheric pCO_2 values (about 354–358 μatm) and low oceanic pCO_2 (in the range 330–340 μatm). These areas are roughly correlated with chlorophyll-rich regions. In the southern part, oceanic pCO_2 is slightly larger than pCO_{2a}; therefore ΔpCO_2 is close to equilibrium in March and slightly positive in October.

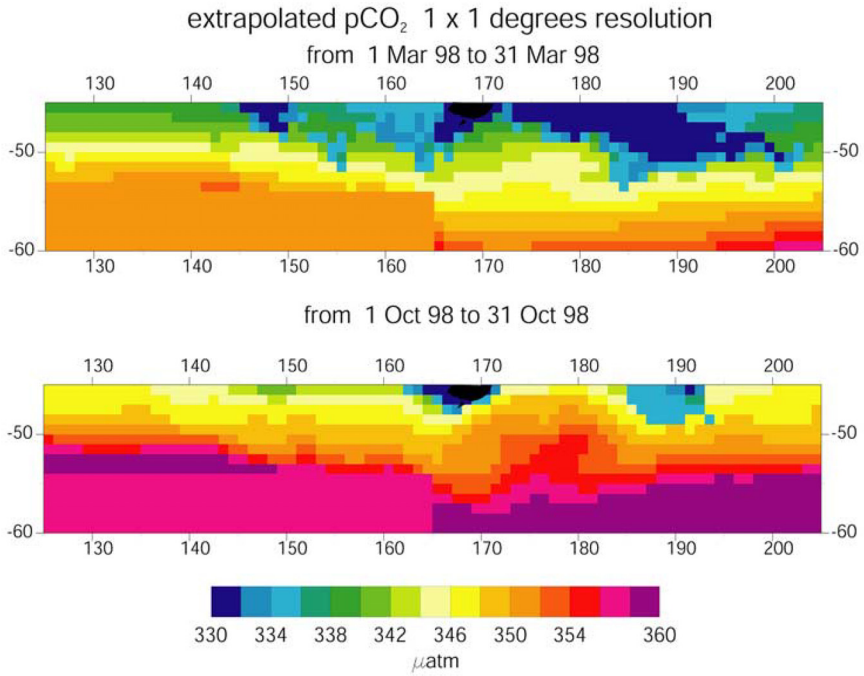

Figure 8. Extrapolated pCO_2 maps (top) in March 1998 and (bottom) in October 1998.

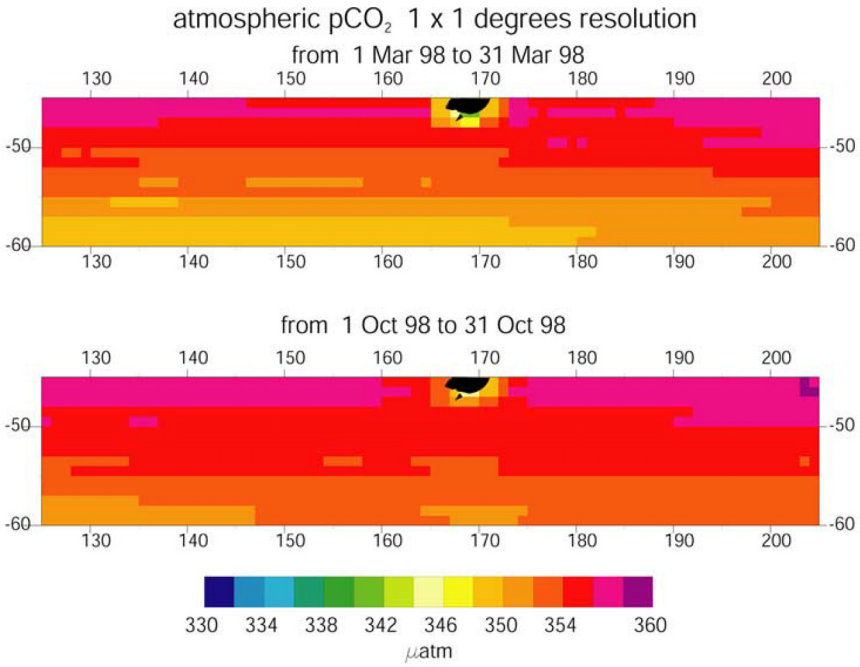

Figure 9. Atmospheric pCO_2 maps (top) in March 1998 and (bottom) in October 1998.

[51] The north–south ΔpCO_2 gradient is also seen on the climatological ΔpCO_2 maps by *Takahashi et al.* [2002] corrected for the atmospheric trend according to their assumptions (Figure 10, bottom), although the longitudinal location of the sinks is different. The spatial distribution of the absolute difference between extrapolated pCO_2 and *Takahashi et al* [2002] climatological pCO_2. is reported below statistical and methodological errors on (Figure 7, bottom). The differences with respect to Takahashi ΔpCO_2 maps are consistent with the imprecision (statistical and methodological) of our extrapolated fields in March, but not in October (pCO_2 differences up to 15 µatm). In March, the two maps exhibit the same regional patterns, in spite of local differences: on the Takahashi ΔpCO_2 map, ΔpCO_2 increases from north to south, with an absorbing region for CO_2 in the north and a slightly absorbing region in the south, whereas on our extrapolated map, ΔpCO_2 increases from absorption in the north to equilibrium to the south. On the other hand, in October, the maps disagree. Our extrapolated map shows a north–south gradient from absorption to outgassing which results in a near-zero mean air–sea flux (see below), while the Takahashi climatological map has a weak north–south gradient, with most of the study area being a sink for CO_2 and a small area close to equilibrium. In our case, the spatial variations are primarily due to north–south variations in Reynolds SST (surface water pCO_2) and in ECMWF Patm (atmospheric pCO_2). This might result from our spring pCO_2–SST regression in zone B which has a negative slope indicating a large mixing effect, whereas the Takahashi climatology was made without taking explicitly into account vertical mixing. In addition, the observed pCO_2 used to build the *Takahashi et al.* [2002] climatological pCO_2 maps vary from ±4 µatm to ±9 µatm within 4 × 5 degree pixels in the study area so that part of the discrepancy between our and Takahashi's approach may be due to small-scale (10–1000 km) variability which the two approaches treat in different ways.

[52] When analyzed over one year, the means of ΔpCO_2 are the closest in April and differ the most in October.

Monthly Net Air–Sea CO_2 Flux Maps

[53] Monthly 1 × 1 degree net air–sea CO_2 flux maps result from the product of monthly K and monthly ΔpCO_2 grids at 1 × 1 degree resolution.

[54] To examine the consequences on the air–sea flux of differences between ΔpCO_2 calculated using different grids, we compare our flux maps to monthly 1 × 1 degree air–sea CO_2 flux maps that are prepared by subsampling the 4 × 5 degree climatological mean ΔpCO_2 fields by *Takahashi et al.* [2002] and recasted onto the 1 × 1 degree ERS-2 K grids. The flux thus calculated is hereafter called the Takahashi climatological CO_2 flux. It must be noted that subgrid scale features are lost by the space-time averaging scheme used for the construction of the 4 × 5 degree field. The lost spatial information cannot be recovered by resampling the original map with a finer 1 × 1 degree resolution. Hence the Takahashi climatological maps give highly smoothed flux distributions. In addition, *Takahashi et al.* [2002] assumed that the annual mean pCO_2 in the southwestern part of the study area (125°E–180° and 50°S–60°S) did not increase with time in response to atmospheric CO_2 due to deep convective mixing, and hence applied no correction for the uptake of atmospheric CO_2. The results of a recent analysis have shown that this is not the case. Hence, in this study, we adjust the Takahashi climatology pCO_2 values from 1995 to 1997–1998 using the atmospheric increase of 1.7 uatm yr^{-1} measured at the Cape Grim station,

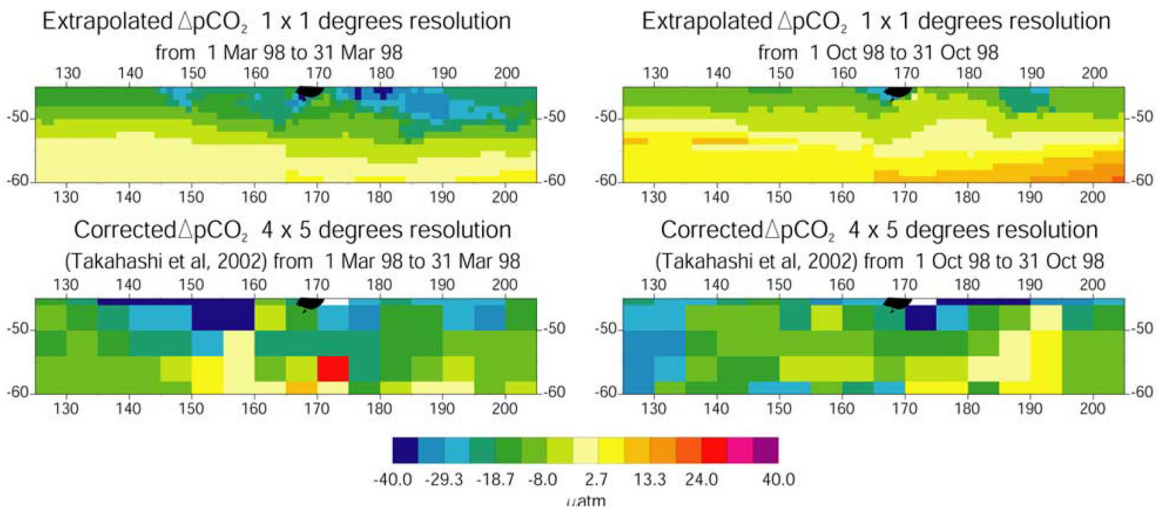

Figure 10. (top) Extrapolated ΔpCO_2 maps and (bottom) *Takahashi et al.* [2002] corrected ΔpCO_2 maps (left) in March 1998 and (right) in October 1998.

Tasmania. This assumption makes the ΔpCO_2 values in the study area less negative and thus leads to smaller ocean uptake flux values (called hereafter without correction for the atmospheric trend) as shown in Figure 12.

[55] The air–sea flux integrated over the whole area, deduced either from our extrapolation method or from the Takahashi climatological ΔpCO_2, is always toward the ocean (Figure 11).

[56] Before analyzing the differences, we need to carefully evaluate the error on each flux estimate; given that the same K were used in all flux computations, only errors on pCO_2 are considered here (uncertainties due to imprecision in K estimates are discussed in section 2.2). Assuming that there are only random errors (no systematic biases) on the Δp fields, the error on the integrated flux, Flux_error, coming from noise on Δp can be deduced from the quadratic sum of the errors in each pixel:

$$Flux\_error = \sqrt{\sum_{i=1}^{npixels} (K_i \cdot \Delta p\_error_i \cdot S_i)^2} \qquad (2)$$

where K_i, Δp_error_i and S_i are the CO_2 exchange coefficient, the error on Δp and the surface of the *i*-th pixel respectively. Concerning our extrapolation, taking the Δp_error_i in 1x1 degree pixels equal to stdfit or to std (in case no fit is used) the flux error is small and ranges between 10^{-3} GtC yr^{-1} (September) and 3 10^{-3} GtC yr^{-1} (March). Concerning the flux derived from *Takahashi et al.* [2002] pCO_2 maps, the variability of pCO_2 observations used to build the extrapolated maps in 4 × 5° pixels (4 to 9 µatm) leads to small errors on the flux as deduced from equation (2), always lower than 10^{-3} GtC yr^{-1}. However, these estimates are optimistic as systematic biases coming from imperfection in the extrapolation method are not taken into account. Hence we also consider the influence of the methodological error on our extrapolation and compare the fluxes to the ones obtained with the alternative methods. The monthly extrapolated net air–sea CO_2 fluxes determined using the 3 schemes (see section 4.2.3) (Figure 12) are very close to each other in the fall (within 0.01 GtC yr^{-1}), whereas they differ by up to 0.085 GtC yr^{-1} (peak to peak) in September and January. In the following, we will consider that the largest difference between the flux retrieved from the standard scheme (continuous line on Figure 12) and from one of the alternative scheme (dots or circles on Figure 12) is indicative of the error on the flux derived from the standard scheme. This leads to an error of 0.03 GtC yr^{-1} on the flux averaged over one year.

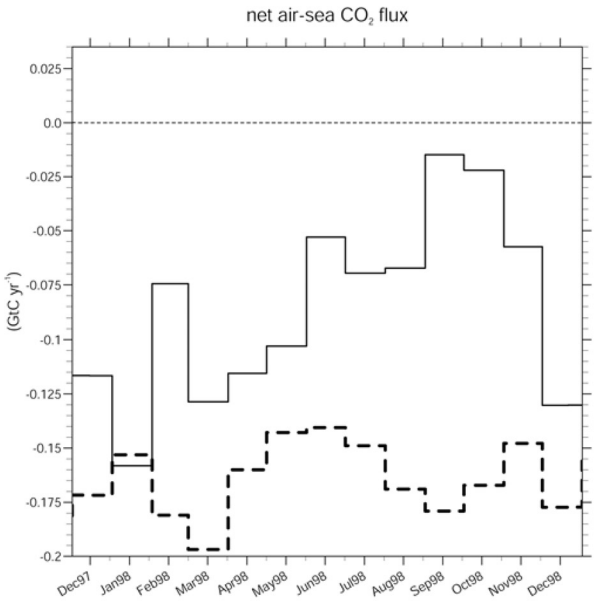

Figure 11. Extrapolated net air–sea CO_2 flux deduced from ERS-2 CO_2 exchange coefficients and pCO_2 standard extrapolation method (solid line), and *Takahashi et al.* [2002] climatological mean ΔpCO_2 fields with correction for the atmospheric trend between 1995 and 1998 (dashed line).

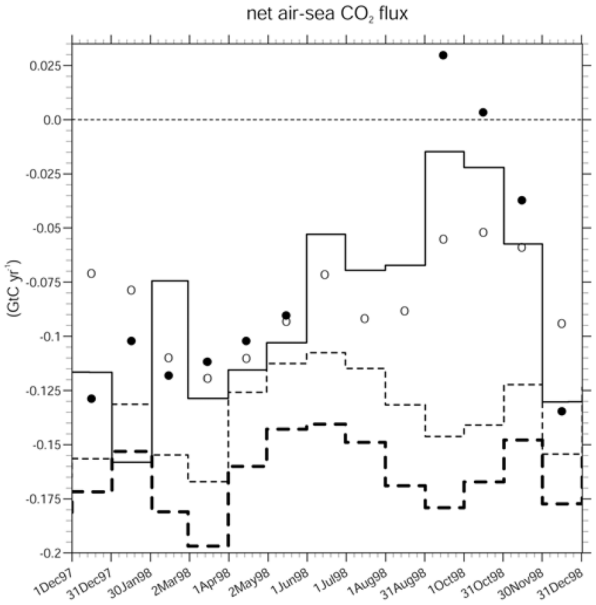

Figure 12. Extrapolated net air−sea CO_2 flux using standard extrapolation (solid line), alternative scheme I (dots) and II (open circles), (the maximum of the absolute difference between the standard extrapolation and the two alternative schemes is taken as the methodological error) and the CO_2 flux derived from the *Takahashi et al.* [2002] climatological mean ΔpCO_2 field with and without correction for the atmospheric trend (thick and thin dashed lines, respectively).

[57] Averaged over one year, the net air−sea CO_2 flux deduced from our extrapolation method is an absorption by the ocean of 0.08 GtC yr^{-1}. Its seasonal variation is large (about 0.14 GtC yr^{-1}) and overcomes the variability between December 1997 and December 1998 (the flux in December 1997 is close to the one in December 1998; the difference is about 0.015 GtC yr^{-1}). On the other hand, the Takahashi climatological flux shows a small seasonal variation (about 0.06 GtC yr^{-1}), and the minimum and the maximum of these fluxes do not occur in the same months. The Takahashi climatological CO_2 flux is maximum in winter (June 1998) and minimum in fall (March 1998), whereas our extrapolated CO_2 flux is minimum in summer (January 1998) and maximum in spring (September 1998). The Takahashi climatological CO_2 flux is always more negative than our monthly extrapolated CO_2 fluxes, except in January 1998 when it is very close (difference less than 0.02 GtC yr^{-1}). The differences are large from June 1998 to November 1998 (between 0.05 and 0.17 GtC yr^{-1}), and are maximum in September 1998 and October 1998 (about 0.15 GtC yr^{-1}). Thence *Takahashi et al.* [2002] climatological mean ΔpCO_2 fields lead to a larger absorbing flux than our extrapolation method (−0.16 GtC yr^{-1}, with correction for the atmospheric trend).

Discussion

[58] It is very challenging to develop an extrapolation method valid over a wide range of longitudes because processes at play may vary in longitude and the knowledge of oceanographic fronts is not sufficient to take these variations into account. For instance, *Metzl et al.* [1999] rely upon transects in two sectors in the Indian Ocean and support the idea of a different pCO_2-SST dependency in the Subantarctic Zone for each sector, with lower pCO_2 (for a given SST) in the eastern sector than in the central one. In our study one challenge is to find relationships valid both on AESOPS transects and on Astrolabe transects without degrading the precision of the fits: this is done in the Subantarctic and Polar zones (Zones A and B) in which we find relationships applicable to both transects. In addition, they are in agreement with the independent SOIREE transects.

[59] We do not extend our extrapolation method over the whole Southern Ocean, because of the lack of time series pCO_2 transects along other tracks at various seasons during the 1997−1999 period that would permit to validate them and eventually to adapt the method to other longitudes. On the other hand, using measurements made over another period would add uncertainty coming from possible interannual variability. Actually, in the Southern Ocean the oceanic trend related to the CO_2 atmospheric trend is poorly known and it may vary spatially because of the presence of upwelled waters in some part of the region: this was the assumption considered by Takahashi et al. and as we will show, such an assumption introduces large pCO_2 variations when several years are considered. Thus, before combining data measured from several years, it is essential to elucidate the interannual pCO_2 variability at the ocean surface and its relation to the atmospheric trend, a difficult exercise (given the sparcity of the data and the large spatial variability of pCO_2 related to oceanic variability), which is outside the scope of this paper. Another issue complicating the use of data from other years is the need for satellite chlorophyll. The information on chlorophyll greatly improves the extrapolation of pCO_2. To illustrate this point, we report in Table 5 the stdfit for pCO_2-SST fits in Zone A and B together. Compared to the stdfit reported in Table 2, it is clear that the use of Chl data to distinguish zones A and B reduces stdfit by a factor between 1.2 and 1.8 in zone B. In addition, pCO_2-Chl fit obtained in Zone A is of better quality than pCO_2-SST fit in Zone A, as was noticed in section 3.1.

[60] With respect to Figure 5 of *Metzl et al.* [1999] who looked at relationships of pCO_2 versus SST in the subantarctic zone of the central and eastern Indian Ocean, the slopes of our pCO_2-SST fits for Zone B are about half of their. This is because in our work pCO_2-SST fits are computed only in low Chl areas, thus excluding the very low pCO_2 values from our regressions. In their Figure 5, *Metzl et al.* [1999] study the region 45°S−46°S 13°5−155°E. From SeaWIFS Chl maps in 1997−1998, it appears that this region is 90% of the time characterized by Chl

Table 5. Statistics of pCO_2-SST Fits Obtained in Zone A and Zone B Together

Time Period	Statistics
Spring	$pCO_2 = -2.86SST + 371$ stdfit = 7.1 μatm
December	$pCO_2 = -2.53SST + 360$ Stdfit = 6.9 μatm
Fall	$pCO_2 = -4.42SST + 378$ stdfit = 4.6 μatm

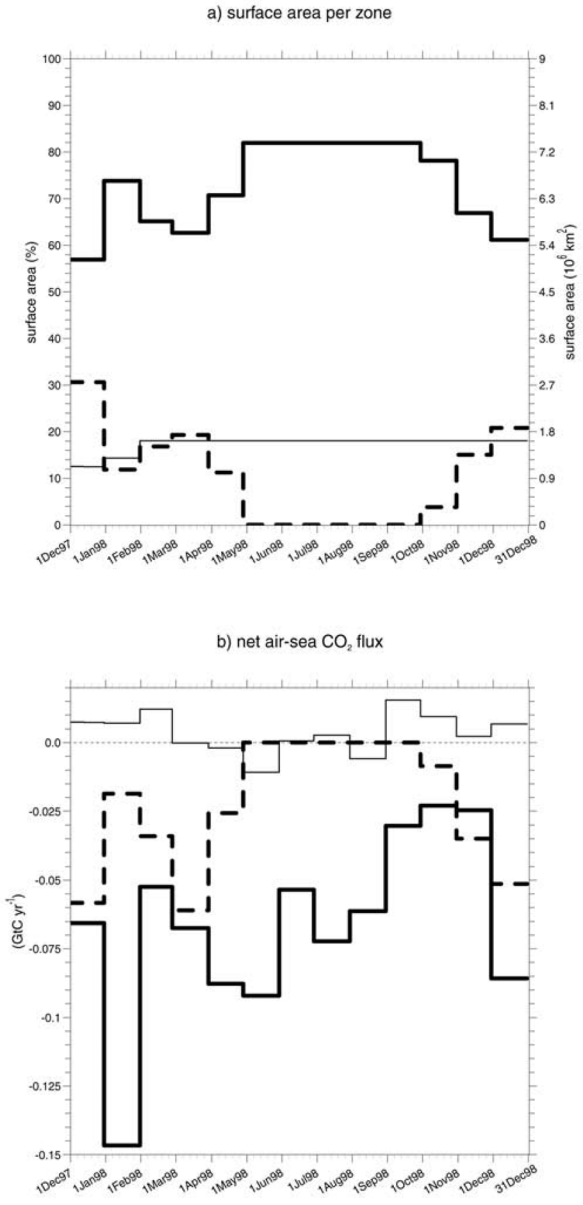

Figure 13. (a) Surface area of zone A (thick dashed line), zone B (thick solid line), and zone C (solid line) from December 1997 to November 1998. (b) Monthly extrapolated flux of CO_2 in zone A (dashed line), in zone B (thick solid line), and in zone C (solid line) from December 1997 to November 1998.

higher than 0.37 mg m^{-3}. Thus Figure 5 of *Metzl et al* [1999] has to be compared with pCO_2 versus SST in our Zone A (Figure 5). Part of the measurements we use appears to be aligned with pCO_2-SST CSIRO measurements. On the other hand, in some cases, relatively high pCO_2 values are observed together with high SST contrary to Metzl el al. study. These relatively high pCO_2 values observed both on AESOPS and Astrolabe transects are always associated with low chlorophyll values.(This is the reason why our pCO_2-Chl fits work better than pCO_2-SST fits in Zone A). These differences may be due to a change in processes driving pCO_2 variability at interannual timescale.

[61] When dealing with an extrapolation method, it is of primary importance to estimate the precision of extrapolated fields. In the present case, this is a difficult task because of the limited number of available measurements for the year 1997–1998. In addition, dividing the set of measurements into two subsets (one for developing the extrapolation, one for validating it) is not sufficient to check the validity of the extrapolation fields. The set of measurements for validation should ideally be acquired during different campaigns, at other locations and other periods than the ones used for developing the extrapolation. In this study only SOIREE transects provide independent data for validation. Thus we estimate the precision of our extrapolation method from the scatter of the pCO_2 residuals with respect to the fit (statistical approach) and from the comparison of pCO_2 extrapolated using alternative extrapolation schemes (methodological approach). The methodological error (which comes from changing the geographical locations of biogeochemical provinces, the parameter chosen as a proxy for pCO_2 variation [SST or chlorophyll], etc.) is in most places larger than the statistical error and is likely to be an upper bound to the true methodological error since the standard scheme was chosen to minimize the residuals of the measurements to the fits, while having the most general approach and being based on a representation of physical and biological phenomena. Nevertheless, the methodological errors are compatible with errors deduced from SOIREE measurements in summer in Zone A and B. In the absence of independent measurements in all zones and in all seasons, we take them as indicative to deduce errors on the air–sea flux. From SOIREE comparisons, it seems that methodological errors in Zone C are underestimated but this has a weak impact on the flux error estimate as the flux is weak in Zone C. In winter, we have no data and extrapolation method is derive as a mean of spring and fall measurements so that error in winter may be underestimated.

[62] Extrapolated ΔpCO_2 are less negative than *Takahashi et al.* [2002] climatological ΔpCO_2 except in small areas (Figure 10). These ΔpCO_2 differences lead to significant differences in the air–sea CO_2 fluxes. Seasonal variation obtained with our extrapolated pCO_2 is larger, although, in the Takahashi climatology maps, space-time variability was smoothed by averaging over the 30 years of time and 4 × 5 degree pixel size. The Takahashi CO_2-corrected fluxes are always more negative than our extrapolated CO_2 flux, as Figure 11 shows. These differences cannot be explained by errors we estimate on our extrapolation method using our methodological approach. Therefore we look at errors linked to the assumptions on interannual variability. We consider the monthly Takahashi climatological CO_2 flux derived either from ΔpCO_2 corrected for the atmospheric trend of 1.7 μatm yr^{-1} between 1995 and 1997–1998, as described in section 5.3, or computed for a reference year (1995). The correction for the atmospheric trend makes the absorbed flux to increase by 0.015 to 0.035 GtC yr^{-1} (depending on the month) with respect to the flux deduced from the 1995 ΔpCO_2 fields. We find that the Takahashi climatological CO_2 flux matches better

our estimates when no correction for the atmospheric trend is applied and that the differences between the two flux estimates cannot be explained by the methodological error in February and March and from June to November. Although the correction for the atmospheric trend is not applied over the whole study area, it is responsible for a decrease in the yearly CO_2 sink of 0.03 GtC yr^{-1} (from -0.13 GtC yr^{-1} to -0.16 GtC yr^{-1}, without and with correction for the atmospheric trend, respectively). This stresses the importance of knowing accurately how the surface ocean pCO_2 is affected by the atmospheric trend.

[63] Part of the disagreement between our and *Takahashi et al.* [2002] pCO_2 estimates may come from the conceptual differences between the two approaches. We use few campaigns (eight north–south transects) and a regression approach to extrapolate pCO_2 measurements over the study area. Thus this analysis is mainly driven by spatial variability (only eight periods of time) and excludes interannual variations. In contrast to this approach, *Takahashi et al.* [2002] computed their global climatological mean estimates using a longest pCO_2 database with campaigns conducted between 1958 and 2000, thus making assumptions on interannual variability, in a larger region and using a lateral two-dimensional advection–diffusion transport equation to extrapolate these measurements.

[64] From the net air–sea CO_2 flux in zone A, B, and C, we observe that most of the areas with strong CO_2 uptake are linked with chlorophyll-rich areas. It is therefore important to know the CO_2 flux in these areas and whether this flux represents a large part of the total flux in the study area. Hence we look at the mean value of our extrapolated flux of CO_2 in each zone (A, B, and C) separately. The surface area of these zones changes each month (see Figure 13a). Zone B represents 60% to 80% of S (S is defined as the total area of the study area and is equal to about 9.10^6 km^2), zone C represents 15% to 20% of S and zone A represents up to 30% of S. Zone A exists only from December 1997 to May 1998 and from October 1998 to December 1998. Our monthly CO_2 flux estimate for each zone is shown in Figure 13b. From January 1998 to December 1998, we find a CO_2 sink equal to $-6.6.10^{-2}$ GtC yr^{-1} in zone B, -2.10^{-2} GtC yr^{-1} in A and $0.35.10^{-2}$ GtC yr^{-1} in C. The mean flux of CO_2 in zone B represents about 80% of the total flux because it is associated with the largest area. The CO_2 flux in zone C is always very small (close to equilibrium). The absolute CO_2 flux in zone A is more than the CO_2 flux in C although A and C have a comparable surface area. In addition, we find that the CO_2 sink in zone A represents about 24% of the total sink. Therefore, at the annual scale, most of the flux is absorbed in zone B. Nevertheless, the monthly flux in zone A is close to monthly flux in zone B during several months (December 1997, March 1998, and November 1998) and is responsible for most of the seasonal variation of the net air–sea flux over the whole area.

Conclusion

[65] We analyze in situ measurements and we develop a method for estimating net air–sea CO_2 fluxes south of Australia and New Zealand (22% of the area of the Southern Ocean between 45°S and 60°S) using remotely sensed measurements. We predict the spatial distribution and temporal variation of the fluxes from satellite data and are able to determine the origin of this variation. We show that the oceanic pCO_2 distribution is mostly controlled by biological activity in regions where the chlorophyll concentration is above a given threshold,, whereas it appears to be primarily driven by water mixing in other parts of the subantarctic and polar zones,. However, the effect of biological activity in these low-chlorophyll regions probably also plays a role in depleting the region in CO_2 and is implicitly taken into account.

[66] We also show that the north–south gradient of atmospheric pressure leads to significant ΔpCO_2 variation.

[67] The study area is always a sink for atmospheric CO_2. The absorbed flux of CO_2 amounts to -0.08 GtC yr^{-1}, which is less than the absorption flux computed from *Takahashi et al.* [2002] climatological pCO_2 maps by a factor of 1.6 to 2, depending on whether or not a correction is applied for the atmospheric trend. This strengthens the need for accurately assessing how pCO_2 at the ocean surface follows or not the pCO_2 increase in the atmosphere. In summer and fall, the fluxes obtained by the two approaches are close. The differences observed in spring and in winter are not easily explained since there are no in situ measurements available: the observed differences depend uniquely on the extrapolation methods used in both approaches. It is therefore essential to gather in situ measurements during these seasons. In order to spatially and temporally extend this kind of extrapolation method confidently, interannual variability of oceanic pCO_2 needs to be addressed such that measurements from several years intervals may be combined. This requires long-term monitoring of pCO_2 in the Southern Ocean.

Appendix A: Computation of pCO_2 From CO_2 Concentration Measurements

[68] In each campaign, sea surface pCO_2 is deduced from in situ measurements of the CO_2 concentration in dry air, xCO_2 in an equilibrator. The CO_2 partial pressure in the equilibrator, pCO_{2eq} is estimated as

$$pCO_{2eq} = xCO_2 \cdot [Peq - pH_2O] \quad (A1)$$

where Peq is the total pressure under which the gas and seawater were equilibrated and pH_2O is the saturated water pressure at equilibrator temperature. pH_2O is derived from the temperature in the equilibrator and from the formulation of *Weiss and Price* [1980]. Then, surface pCO_2 is derived from pCO_{2eq}, by correcting it for the difference between in situ and equilibrator temperature using a temperature effect of $0.0423°C^{-1}$. In the case of the Astrolabe campaigns, Peq was not measured. However, it is expected to be close to the atmospheric pressure (Patm). Patm was also not measured on these campaigns, so ocean pCO_2 has been derived from xCO_2 using Patm inferred from the ECMWF atmospheric model (ECMWF Patm) at high resolution (temporal resolution: 6 hours, spatial resolution: 1 × 1 degree). It should be noticed that in the Southern Ocean, Patm can be very low: on average over the two campaigns, Patm is 1000 mbar and can be as low as 971 mbar (minimum for these campaigns). Hence, when dealing with measurements

made at a pressure close to the atmospheric pressure, one must pay great attention to Peq: an error of 40 mbar in Peq induces an error of 4% in pCO_2 (about 14 μatm).

[69] **Acknowledgments.** We are very much indebted to Cathy Boonne for providing the atmospheric pressure data inferred from the ECMWF atmospheric model and Olivier Coze, Nicolas Martin and Stephanie Contardo for processing support. CERSAT/IFREMER produced the level 2 ERS-2 wind speed data. The SeaWiFS project and DAAC/GSFC produced and distributed the SeaWiFS data. We note sadly that this is a posthumous contribution from our colleague, Michel Frankignoulle, who passed away in March 2005. This study was supported by the following French national programs: CNES/TAOB and CNRS-PROOF/FLAMENCO2.

D. C. E. Bakker, School of Environmental Sciences, University of East Anglia, Norwich NR4 7TJ, UK.
J. Boutin, J. Etcheto, L. Merlivat, and Y. Rangama, Laboratoire d'Océanographie Dynamique et de Climatologie/Institut Pierre Simon Laplace, Université Pierre et Marie Curie, 4 Place Jussieu, 75252 Paris, France. (jb@lodyc.jussieu.fr)
B. Delille, Unité d'Océanographie Chimique, Université de Liège, Allée du 6 Août, 17 4000 Liège, Belgium.
T. Takahashi, Lamont-Doherty Earth Observatory of Columbia University, Palisades, NY 10964, USA.

2.4 Spring and summer air-sea CO_2 fluxes in the Indian sector of the Southern Ocean

2.4.1 Foreword

Building on the approach described in Chapter 0, we assessed air-sea CO_2 fluxes in the Indian sector of the Southern Ocean based on 8 cruises (Table 2-1) carried out in the framework of the BELCANTO projects. However, there are two significant differences with the former study.

- In Chapter 2.3, the interpolation of pCO_2, SST and Chl *a* was performed regardless of the considered area. Here, we computed air-sea CO_2 fluxes per physical zone - defined by the positions of the fronts - rather than per latitude as conventionally done.
- This was the first step towards an assessment of the biological pump, comparing consistently air-sea CO_2 fluxes with C export given per physical zone, rather than per latitude. We used the positions of the fronts derived from SST gradients as described in the chapter 2.1.

This chapter will be published as a section of the report:

Dehairs,F., C. Lancelot, L. André, H. Goosse, M. Frankignoulle, S. Becquevort, A. Borges, D. Cardinal, A.de Montety, B. Delille, M. Elskens, S.H.M. Jacquet, W. Lefebvre, B. Pasquer, N. Savoye, and V. Schoemann. Assessing the sensitivity of the Southern Ocean's Biological pump to climate change. Belgian Science Policy Reports, +pp 124, *in press*

2.4.2 Introduction

Based on underway pCO_2 measurements carried out in the framework of BELCANTO projects in the Indian sector of the Southern Ocean (Figure 2.4-1 and Table 1), we budgeted spring and summer air-sea CO_2 fluxes using SST, SeaWIFS chlorophyll-a concentration (Chl) and wind speed inferred from satellite measurements. We focused on the Indian sector (20°E-150°E; 30°S-60°S) from October 1997 to December 1999. CO_2 fluxes were partitioned according to the main oceanographic provinces of the Southern Ocean, namely the subtropical zone (STZ), both north and south subantarctic zone (denoted as NSAZ and SSAZ respectively), polar frontal zone (PFZ) and polar open oceanic zone (POOZ), using the positions of fronts inferred from SST gradients (chapter 2.1)

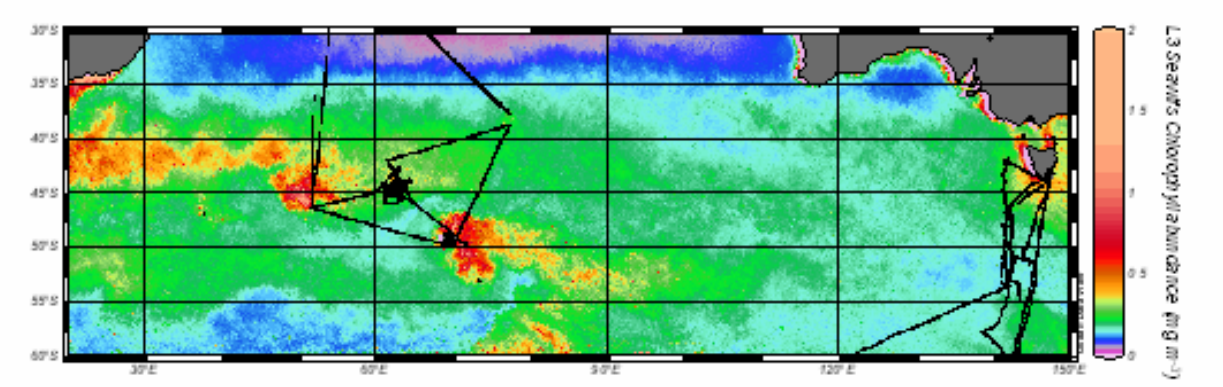

Figure 2.4-1: Underway pCO_2 measurements carried out in the Indian sector of the Southern Ocean in the framework of BELCANTO projects superimposed on SeaWIFS chlorophyll a concentration (average of maps used for the pCO_2 reconstruction, e.g. spring and summer seasons from October 1997 to December 1999).

ship	area	period
R.S.V. Aurora Australis	South of Tasmania - SR3 transect	28-02 to 31-03-1998
R.S.V. Marion Dufresne	Crozet Basin	12-11 to 19-11-1998
R.V. La curieuse	Kerguelen Plateau	02-12 to 5-12-1998
R.S.V. Marion Dufresne	Crozet Basin	21-12 to 29-12-1999
R.S.V. Marion Dufresne	Crozet Basin	06-01 to 20-02-1999
S.V. Astrolabe	South of Tasmania - Adélie Land	22-10 to 28-10-1999
S.V. Astrolabe	South of Tasmania - Adélie Land	21-12 to 27-12-1999
R.S.V. Aurora Australis	South of Tasmania - Eastern Antarctica	31-10 to 12-12-2003

Table 2-1: Campaigns of pCO_2 measurements carried out in the Indian Sector of the Southern Ocean in the framework of BELCANTO projects.

2.4.3 Correlation of oceanic pCO_2 with chlorophyll and SST

Complete description of the experimental set-up of underway pCO_2 measurements is provided in the chapters 2.2 and Variability of the net air–sea CO_2 flux inferred from shipboard and satellite measurements in the Southern Ocean south of Tasmania and New Zealand.2.3. Surface pCO_2 measurements were corrected to a single reference year (arbitrary chosen as 1999) using atmospheric CO_2 concentration measured at Cape Grim station (provided by Globalview –CO_2 http://www.cmdl.noaa.gov/ccgg/globalview/co2/index.html). We collocated corrected pCO_2 measurements with weekly standard maps (resolution of 9×9 km) of Level 3 SeaWIFS Chl (obtained from the National Atmosphere and Space Agency http://oceancolor.gsfc.nasa.gov/). SST was derived from Advanced Very High Resolution Radiometer (AVHRR) data (obtained from the Physical Oceanography Distributed Active Archive Center). Then, we carried out correlations of corrected pCO_2 in spring and summer season with Chl *a* and in situ SST using Surfer® package ("kriging" method - type "block") (Figure 2.4-2). Wind speed was derived form ERS-2 wind products delivered by the Centre ERS d'archivage et de Traitement (CERSAT) of the Institut Français de Recherche pour l'Exploitation de la Mer (IFREMER)

2.4.4 Reconstruction of CO_2 fluxes fields.

The pCO_2 fields were reconstructed following the same rationale of the study conducted south of Tasmania. We used fits between pCO_2, SST and SeaWIFS Chlorophyll shown in the Figure 2.4-2 to reconstruct pCO_2 fields over the Indian sector from October 1997 to December 1999. This time period is covered by SeaWIFS data, our analysis of the positions of fronts and most of the *in situ* pCO_2 measurements. We reconstructed monthly pCO_2 fields with a resolution of 0.2°×0.2° using monthly SeaWIFS and SST maps. SST maps were derived from AVHRR data obtained from the PODAAC. Then we compute CO_2 fluxes. The CO_2 fluxes were computed fromthe gas transfer velocity parameterization of Liss and Merlivat (1986), Wanninkhof (1992) and Wanninkhof and McGillis (1999) using wind speed derived form ERS-2 wind products delivered by the CERSAT.

In spring a strong sink for atmospheric CO_2 is centred on the Crozet Basin (Figure 2.4-3). This is likely due to the intense frontal dynamics specific to this region which promotes large decreases of pCO_2 (Chapter 2.2). In summer, the sink of atmospheric CO_2 spreads over the entire SSAZ and PFZ. The signature on the distribution CO_2 fluxes of the SSTF, SAF and the PF are remarkably well marked. On the whole, the most intense sink of atmospheric CO_2 was encountered in the SSAZ.

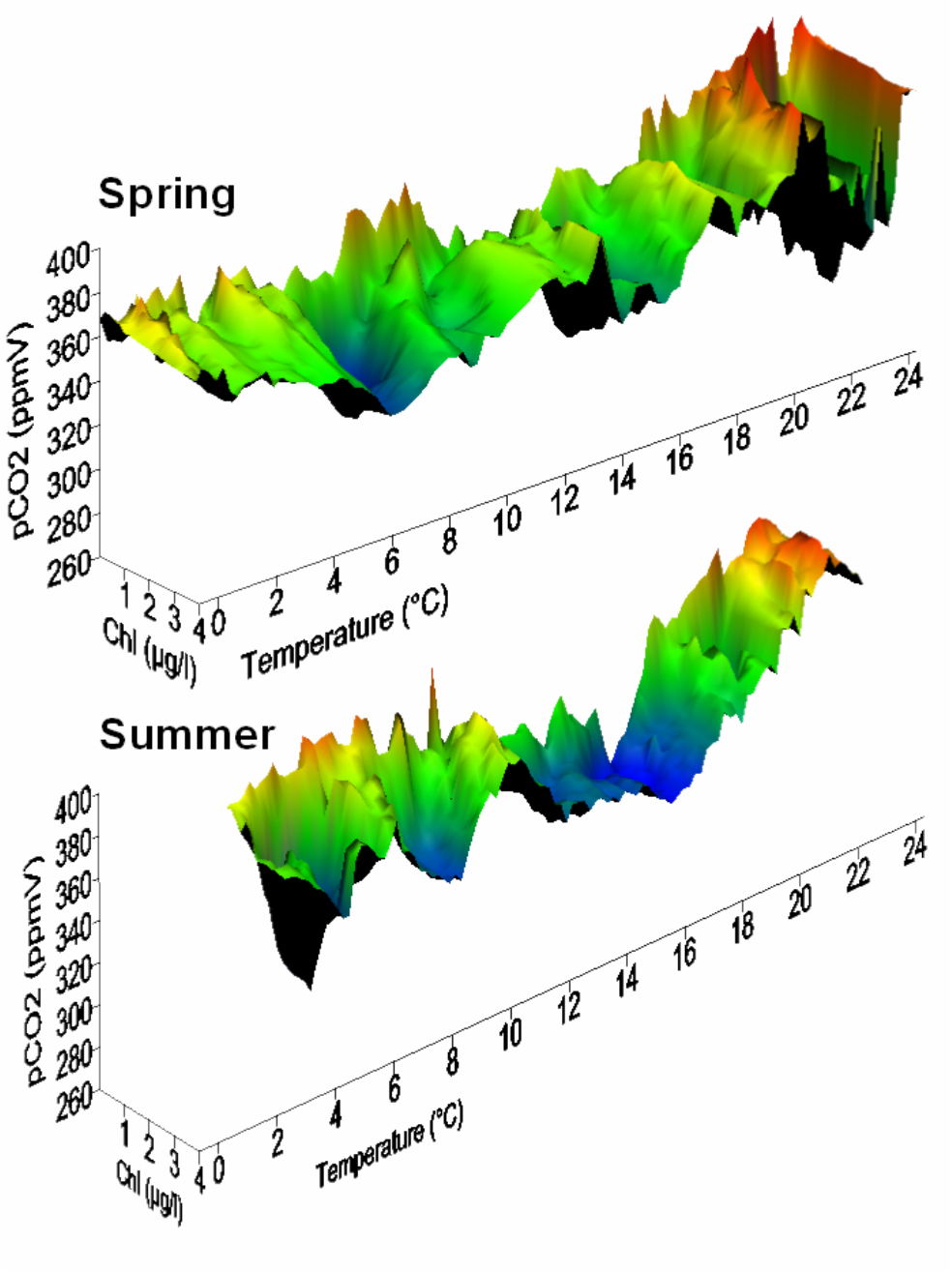

Figure 2.4-2: Cross correlations between pCO_2 , SST and Level3 SeaWIFS chlorophyll-a concentration (Chl) in spring (top) and summer (bottom) in the Indian sector of the Southern ocean used for the reconstruction of pCO_2 fields.

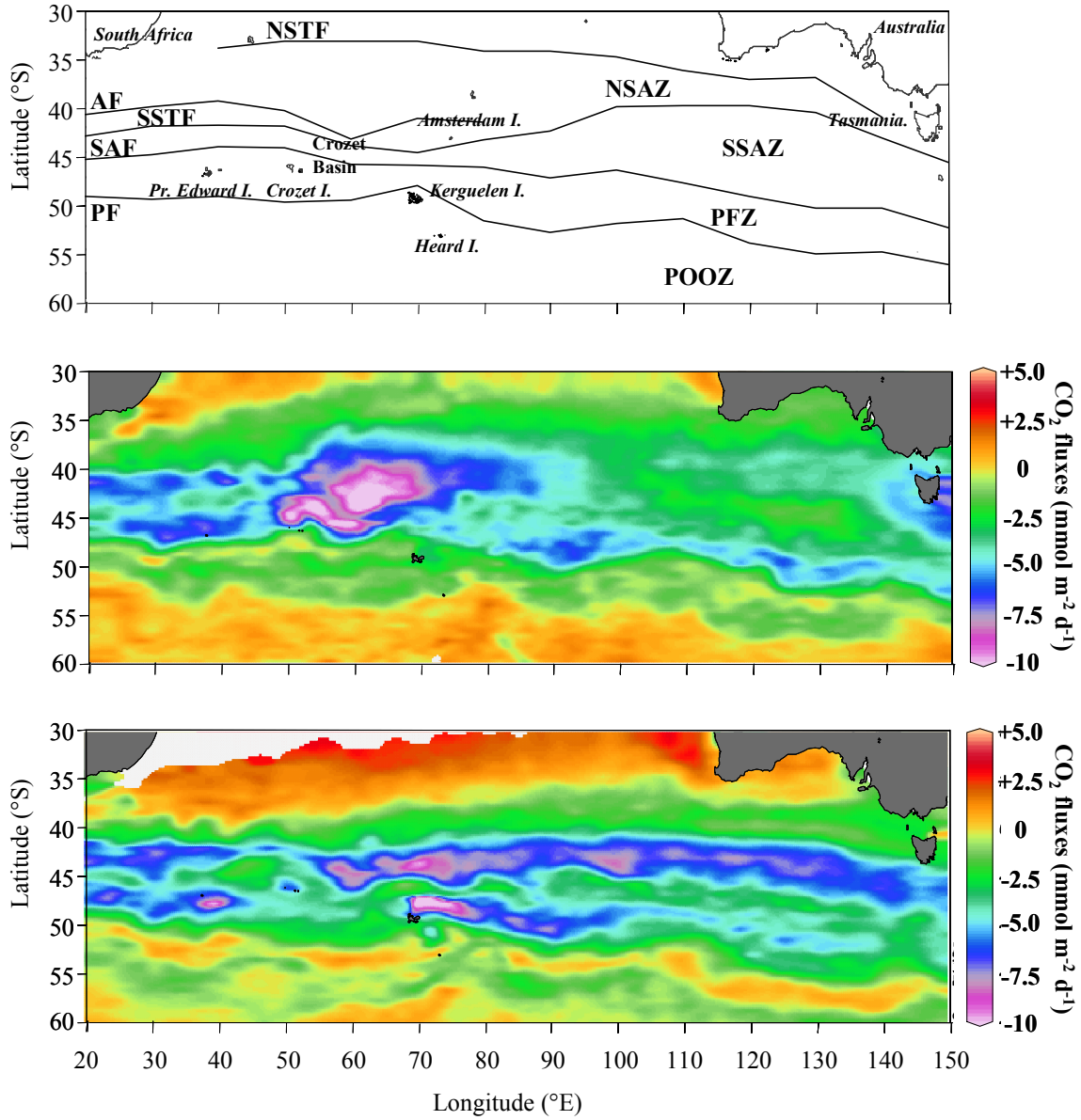

Figure 2.4-3. Mean positions of the fronts inferred from SST gradients (top) and reconstructed air-sea CO_2 fluxes in spring (middle) and summer (bottom) based on the Wanninkhof (1992) gas transfer velocity parameterization.

2.4.5 Budget of air-sea CO_2 fluxes

While budgeting CO_2 fluxes from reconstructed CO_2 fluxes fields, attention was paid to discriminate the different oceanographic provinces of the Southern Ocean delimited by the fronts. Analysis of the positions of these fronts was carried out mainly using SST gradients derived from remote sensing AVHRR data in conjunction with previous work based on XBT and CTD vertical profiles (Chapter 2.1). Monthly maps of the main frontal structures were established over the whole Indian sector of the Southern Ocean from 1997 to 1999. These maps allowed us to budget CO_2 flux per province using different parameterizations of the gas transfer velocity (Table 2-2).

The overall sink of atmospheric CO_2 for the 35°S-50°S band of the Indian sector of the Southern Ocean ranges from -0.039 to -0.110 PgC in spring and from -0.032 to -0.093 PgC in summer (Table 2-2). As expected, large changes in the sink status with respect to the choice of the gas transfer velocity parameterization were obtained. From January 1991 to March 1993, Metzl et al. (1995) computed summer CO_2 fluxes ranging from -2.5 to -5.5 mmol m^{-2} d^{-1}, with an average value around -3.5 mmol m^{-2} d^{-1} in the same area. Metzl et al. (1999) computed average fluxes in this zone of about -5.1 mmol m^{-2} d^{-1} in spring and -11.3 mmol m^{-2} d^{-1} in summer from 1992 to 1995. These fluxes, computed with the gas transfer velocity parameterization of Liss and Merlivat (1986) are higher that our present estimations. Both present study carried out in the Indian sector of the S.O. and previous study carried out in the western Pacific sector of the S.O. (chapter 2.3) exhibit lower estimates than previous ΔpCO_2 based studies (Metzl et al., 1995; Metzl et al., 1999; Takahashi et al., 2002). This might support the conclusions of inverse models that previous ΔpCO_2 based studies overestimate CO_2 fluxes in the Southern Ocean (Gloor et al., 2003; Gurney et al., 2004; Jacobson et al., 2005). However, one can note that the studies of Metzl et al. (1995; 1999) and Takahashi et al (2002) were mostly based on older data than those used in the present budgets. Hence, these differences might also be ascribed to a large inter-annual variability of the magnitude of the fluxes of CO_2 in the Southern Ocean as also recently observed from 1998 to 2002 (Nicolas Metzl, LOCEAN (FR), personal communication).

.

	Liss et Merlivat (1986)		Wanninkhof (1992)		Wanninkhof and McGillis (1999)		Nightingale et al. (2000)	
Average flux (mmol m^{-2} d^{-1})	Spring	Summer	Spring	Summer	Spring	Summer	Spring	Summer
STZ	-0.72	0.48	-1.37	0.94	-1.43	0.84	-0.94	0.67
NSAZ	-2.02	-0.73	-4.01	-1.43	-5.11	-1.77	-2.69	-0.96
SSAZ	-1.96	-2.52	-4.04	-5.15	-5.85	-7.35	-2.67	-3.40
PFZ	-1.52	-2.01	-3.29	-4.36	-5.42	-7.24	-2.13	-2.83
POOZ	-0.10	-0.39	-0.22	-0.82	-0.43	-1.32	-0.14	-0.54
35°~50°S	-1.97	-1.66	-4.00	-3.39	-5.59	-4.87	-2.66	-2.24
Integrated flux (PgC)								
NSAZ	-0.018	-0.006	-0.036	-0.012	-0.046	-0.015	-0.024	-0.008
SSAZ	-0.012	-0.016	-0.025	-0.032	-0.036	-0.045	-0.016	-0.021
PFZ	-0.008	-0.011	-0.017	-0.023	-0.029	-0.038	-0.011	-0.015
35°~50°S	-0.039	-0.032	-0.080	-0.065	-0.110	-0.093	-0.053	-0.043

Table 2-2 Averaged and integrated air-sea CO_2 fluxes over the different provinces of the Indian sector of the Southern Ocean. Fluxes were computed using the gas transfer velocity parameterizations of Liss and Merlivat (1986), Wanninkhof (1992) and Wanninkhof and McGillis (1999). Integrated fluxes are given for a three months period.

3 Subantarctic coastal area

Macrocystis kelp beds in a fjord of the Kerguelen Archipelago (SubAntarctica)

3.1 Seasonal changes of pCO_2 over a subantarctic Macrocystis kelp bed

3.1.1 Foreword

In the framework of the MICROBIOKER program funded by the Institut Polaire Paul-Emile Victor, three over-wintering campaigns were carried out in the Kerguelen Archipelago (Sub-Antarctica). This chapter presents the results from the survey carried from December 1995 to December 1997. To our best knowledge, this was the first long term survey of pCO_2 in a Subantarctic coastal area and the first study of dissolved inorganic carbon dynamics in giant kelp *Macrocystis pyrifera* beds.

This chapter has been published in Polar Biology:

Delille.B, D. Delille, M. Fiala, C. Prevost & M. Frankignoulle, 2000. Seasonal changes of pCO_2 over a subantartic Macrocystis kelp bed. Polar Biology 23, 706-716.

Polar Biol (2000) 23: 706–716

ORIGINAL PAPER

B. Delille · D. Delille · M. Fiala · C. Prevost
M. Frankignoulle

Seasonal changes of pCO_2 over a subantarctic *Macrocystis* kelp bed

Accepted: 1 April 2000

Abstract The partial pressure of carbon dioxide (pCO_2), calculated from pH and total alkalinity measurements, was monitored together with chlorophyll *a* and bacterioplankton biomass in shallow coastal water located inside and outside a giant kelp bed (*Macrocystis pyrifera*) situated in the Kerguelen Archipelago, Southern Ocean. In spite of large changes over a short time-scale, pCO_2 variations over the year are large and exhibit a seasonal pattern in which the different stages of the annual biological turnover are well marked. The overall pattern of pCO_2 variations is related to biological activity (development of both photosynthesis and respiration) during almost the whole year. However, physical and thermodynamical constraints exert a strong influence on pCO_2 at meso time-scale (10 days) and/or when biological activity is weak. *Macrocystis* acts to maintain pCO_2 below saturation almost the whole year and large undersaturations (pCO_2 as low as 20 µatm) were observed within the kelp bed. Furthermore, primary production of *Macrocystis* covers a period of $8 \sim 9$ months a year from winter to late summer and the kelp bed seems to favour the spring phytoplanktonic bloom. The buffer factor β indicates that, outside the kelp bed, inorganic carbon dynamics are mainly influenced by air-sea exchange and photosynthesis without calcification. Inside the kelp bed, β suggests calcification by the epiphytic community.

B. Delille (✉) · M. Frankignoulle
Unité d'Océanographie Chimique,
Mécanique des Fluides Géophysiques,
Institut de Physique, Bât B5, Université de Liège,
4000 Sart Tilman, Belgium
e-mail: Bruno.Delille@ulg.ac.be
Fax: +32-4-3662355

D. Delille · M. Fiala · C. Prevost
Observatoire Océanologique de Banyuls,
Université P. et M. Curie, U.M.R./C.N.R.S. 7621,
66650 Banyuls sur mer, France

Introduction

In coastal areas, many factors play a role in the changes of pCO_2. As in the open ocean, warming and cooling of surface water, wax and wane of plankton blooms, wind velocity and lateral advection all influence pCO_2, but other complex processes, such as exchanges with the shallow sediment, outflows of fresh water, tidal mixing and coastal upwellings may strongly affect the carbon budget of the water column (Wollast 1991; Bakker et al. 1996; Frankignoulle et al. 1996a, 1996b; Borges and Frankignoulle 1999). The role of shelf seas in global cycling is indeed still poorly understood (Inoue and Sugimura 1988; Kempe and Pegler 1991; Wollast 1991; Bakker et al. 1996; Frankignoulle et al. 1996a, 1996b; Gattuso et al. 1998; Wollast 1998; Borges and Frankignoulle 1999).

Because of its inaccessibility, the Southern Ocean is the least documented ocean (Metzl et al. 1995; Bakker et al. 1997). With the exception of the works of Metzl et al. (1991), Poisson et al. (1993) and Louanchi et al. (1999), which gave observations above the Kerguelen Plateau, previous studies of pCO_2 in the Southern Ocean did not investigate subantarctic coastal areas. Recently Delille et al. (1997) carried out measurements of pCO_2 and related parameters over diel cycles inside and outside a kelp bed in the Kerguelen Archipelago. However, there is no other study about dissolved CO_2 in the coastal areas of the Subantarctic Zone (SAZ) and Polar Frontal Zone (PFZ).

A substantial proportion of these coastlines is occupied by highly productive giant kelp bed, *Macrocystis pyrifera*. This marine macroalga is one of the largest and grows up to 50 m in length, forming undersea forests in hard-bottom subtidal areas of subantarctic islands (Sfriso et al. 1987; Lavery and McComb 1991; Hanisak 1993). Macroalgae have a great potential for biomass production and CO_2 uptake (Smith 1981; Wilcox and North 1988; Gao and McKinley 1994). Smith (1981) pointed out that the coastal marine macrophytes

ecosystems, including both macroalgae and seagrasses, occupy only about 2×10^6 km^2 but could act as an effective carbon sink because of their biomass (estimated to be about two-thirds of oceanic plant biomass) and relatively high turnover time (about 1 year) compared to phytoplankton (about 1 week). However, with the exception of works of Frankignoulle and Distèche (1984, 1987) and Frankignoulle and Bouquegneau (1987, 1990), little is known about the influence of macrophytes on pCO_2 and their quantitative significance in the global carbon (Gattuso et al. 1998). Moreover, productivity of *Macrocystis* is high and ranges from 1000 to 1300 gC m^{-2} year^{-1} (Mann 1982; Wheeler and Druehl 1986) but Jackson (1977) also measured productivity up to 3400 gC m^{-2} year^{-1} off southern California. Kelps act to reduce currents within the kelp bed and decrease exchanges with surrounding waters (Jackson and Winant 1983). The authors noticed that residence time of water within the kelp bed may be long compared to some biological processes like nitrate uptake by the kelp, phytoplankton doubling and some larval development time. They also pointed out that such reduced currents would allow nutrients to recycle internally and plankton populations to exist solely within. However, in contrast to the numerous studies on the biology and primary productivity of polar microalgae, high-latitude macroalgae have been little studied, although dense populations of highly productive seaweeds are known from the Southern Ocean (Dunton and Dayton 1995).

The purpose of this paper is to examine the seasonal changes of pCO_2 both outside and inside a *M. pyrifera* giant kelp bed, in order to understand the role of physico-chemical and biological processes with regard to pCO_2 within shallow water of the Kerguelen Archipelago, and the influence of *Macrocystis* kelp bed on pCO_2. The present study was undertaken as a part of a program designed to elucidate the annual pattern of pCO_2 in the coastal area of the northern part of the Southern Ocean, as well as the role played by the *Macrocystis* kelp bed with regard to atmospheric pCO_2.

Materials and methods

Sampling

Measurements were carried out from December 1995 to December 1997 in Morbihan Bay (Fig. 1), Kerguelen Archipelago, Southern Ocean (Indian sector). Usually, the Kerguelen Archipelago is cited in the literature as a subantarctic island (Belkin and Gordon 1996; Delille et al. 1997; Razouls et al. 1997). However, from a strict oceanographic point of view, this archipelago is situated either in the PFZ or in the Antarctic Zone, depending on the position of the Polar Front with regard to the island. One should note that this latter position is still a matter of debate (Belkin and Gordon 1996; Park and Gambéroni 1997). Located in the southeast of the archipelago, Morbihan Bay (about 600 km^2) opens to the ocean through the Royal Pass, which is 12 km wide and 40 m deep. The bay is always free of ice. Satellite data processing has permitted estimation of the biomass (wet weight) of *M. pyrifera* at about 1100 kt, spread over an area of about 190 km^2 in the Morbihan Gulf in 1988 (Belsher and Mouchot 1992). Samples were collected

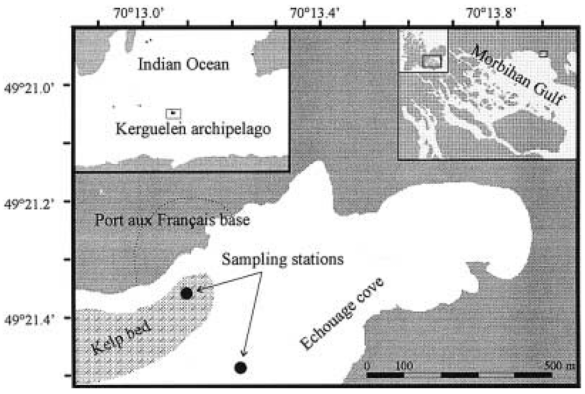

Fig. 1 Location of Morbihan Bay (Kerguelen Archipelago) and sampling sites

in the vicinity of the base of "Port Aux Français" in Echouage Cove (≈400 × 300 m), which is open to dominant winds. Coastlines of the cove are partly surrounded by a *M. pyrifera* kelp bed. Two sampling sites were chosen, one inside and one outside the kelp bed. Both sites were sampled every 10 days, at the same time of the day (between 1.45 p.m. and 2.15 p.m.) in order to reduce the influence of diel cycles. Samples were taken from the surface from the same water mass, and attention was paid to avoid degassing. Analyses were begun in the base laboratory within 30 min after sample collection.

Salinity was determined with a Guildline induction salinometer whose accuracy was 0.003 on the practical salinity scale. Solar radiation and wind velocity measurements were provided by Météo-France.

Inorganic carbon

The inorganic carbon speciation was calculated from pH and total alkalinity (TAlk) measurements. TAlk was measured using the classical Gran electrotitration method on 100-ml GF/F filtered samples. The accuracy of measurements was 4 μeq kg^{-1}. pH was measured using commercial combination electrodes (Ross type, Orion), calibrated according to the NBS scale. The accuracy of pH measurements was 0.01 pH units. CO_2 speciation was calculated using the CO2SYS Package (Lewis and Wallace 1998), the CO_2 acidity constants of Mehrbach et al. (1973) refitted by Dickson and Millero (1987), the CO_2 solubility coefficient of Weiss (1974), the borate acidity constant of Dickson (1990a) and the SO_4^{2-} dissociation constant of Dickson (1990b). The total borate molality was calculated using the Uppström (1974) ratio to chlorinity. As silicates and phosphates concentrations were available in 1996 and partially in 1997, they were included in the calculations. Taking into account uncertainties of pH, TAlk, temperature, salinity, silicate and phosphate concentrations, the errors in pCO_2 and DIC were 14 μatm and 9 μmole kg^{-1}, respectively.

Bacterial abundance

Bacterial abundance was determined by acridine orange direct counts (AODC) (Hobbie et al. 1977). A minimum of 300 fluorescing cells with a clear outline and definite cell shape were counted as bacterial cells in 10 random microscope fields.

Chlorophyll

Phytoplankton was studied using chlorophyll *a* concentration. All samples were prefiltered through a 200-μm mesh to remove detritic

material and larger biota, and then filtered by gentle vacuum filtration of 1 l of seawater through a Whatman GF/F glass-fibre filter. The measurements of chlorophyll a were carried out using the spectrofluorometric method developed by Neveux and Panouse (1987). Fluorescence was measured on a Perkin-Elmer MPF 66 spectrofluorometer.

Nutrients

Water samples were filtered through a Whatman GF/F glass-fibre filter. The filtrates were subsequently frozen at −20 °C until laboratory analysis. Nitrate + nitrite, silicate and phosphate concentrations were assayed using a Skalar AutoAnalyser and the method of Treguer and Le Corre (1975). The accuracy of the analyses was assured by calibration with standard salts in low-nutrient seawater. The analytical accuracies were ± 0.1 μmol l^{-1} for nitrate, ± 0.01 μmol l^{-1} for phosphate and ± 0.1 μmol l^{-1} for silicate.

Results

Water temperature (Fig. 2) ranged from 0.7 °C in austral winter (from June to August) to 8.5 °C in summer (from December to March) outside the kelp bed but could reach 15.3 °C within the kelp in calm weather conditions and high irradiancy (Fig. 3). Salinity (Fig. 2) varied between 31.1 and 33.7 and showed drastic changes between two successive samplings. Moreover, even though variations inside and outside the kelp bed tended to correspond, this was not systematic since we observed differences up to 1 on the practical salinity scale between the two sampling sites.

Unfortunately, biological parameters were not wholly available in 1997 and we present here only the results observed in 1996. Chlorophyll *a* concentration (Fig. 4) showed values ranging from 0.4 to 2.1 μg l^{-1} from February to August. In September, an increase occurred inside the kelp bed followed by another sharp and large increase (up to 71 μg l^{-1} inside the kelp bed) 5 weeks later at both sampling sites, when water temperature and solar irradiation were high. Smaller increases occurred in December and January.

Bacterial abundance (Fig. 4) ranged from 7×10^4 to 2×10^6 cells ml^{-1} in 1996. The overall pattern was similar at both sampling sites. Maximal abundance occurred during late summer and autumn (from February to April), but secondary peaks were still observed during winter, in July and August. Bacterial abundance was at its weakest level in spring and early summer (from September to December).

Outside the kelp bed, the concentration of $NO_3^- + NO_2^-$ (Fig. 4) increased progressively from 12 to 29 μmol l^{-1} during autumn and winter. These concentrations decreased drastically in October corresponding to a sharp increase in phytoplankton biomass and reached a low level (3.6 μmol l^{-1}). Depletion was limited in time and concentration of $NO_3^- + NO_2^-$ began to increase just after the phytoplanktonic bloom.

Inside the kelp bed, the overall seasonal pattern was rather similar; however, some small but significant differences existed. A slight decrease in nutrient concentration was initiated in July when solar irradiancy was beginning to increase. Furthermore, decrease of $NO_3^- + NO_2^-$ inside the kelp bed occurred 2 or 3 weeks earlier than outside the kelp bed. This decrease corresponded to the first peak of chlorophyll *a* observed inside the kelp bed in September. In late summer, another sharp depletion of total nitrate and nitrite occurred inside the kelp bed.

pH ranged from 7.94 to 8.46 outside the kelp bed and from 8.07 to 9.11 inside the kelp bed (Fig. 5). At both sampling sites and for the 2 years, pH exhibited similar seasonal patterns with a minimum in winter (May/June) and a maximum in late spring (November) and summer (March). However, it is worth noting that the seasonal pattern was more marked inside the kelp bed, with sharp peaks in summer.

In contrast, TAlk appeared to be constant all year with slight fluctuations ranging from 2.12 to 2.29 (Fig. 5). No clear differences appeared between the inside and outside of the kelp bed.

pCO_2 ranged from 160 to 640 μatm outside the kelp bed and from 20 to 460 μatm inside the kelp bed (Fig. 2). Magnitudes of yearly variations were high (about 350 μatm in 1996 and 450 μatm in 1997) and similar for both sampling sites. Large changes at short time-scales (10 days) were observed. It was possible to distinguish seasonal tendencies in changes of pCO_2. Furthermore, this seasonal cycle for pCO_2 had roughly similar patterns for both sites and both years with a large offset (about 150 μatm) between both sites. However, significative differences in the overall patterns existed between the sampling sites depending on the time of the year. Outside the kelp bed, pCO_2 increased during late summer and autumn (from January to May) whereas strong decrease and undersaturation – atmospheric CO_2 concentrations were estimated to be around 361 ppmV from Amsterdam Island measurement (V. Kazan, personal communication) – were observed within the kelp bed. Nevertheless, maxima of pCO_2 were observed prior to wintertime (July to August) at both sampling sites. With the exception of an increase observed in July 1996, pCO_2 tended to decrease during winter in good agreement with the decrease of temperature, and reached a minimum in August. At the end of winter, when both temperature and solar irradiancy began to increase, pCO_2 tended to increase also. In September a sharp and large decrease of pCO_2 occurred and led to a pCO_2 minimum. Then, pCO_2 increased outside the kelp bed from November to June while other significant decreases occurred inside the kelp bed until April.

Since salinity presented large variations through the year, attention was paid to normalizing DIC to a constant salinity of 35. In the same way as pCO_2, DIC_{35} exhibited large variations at a short time-scale (Fig. 2). However, seasonal tendencies appeared in the DIC_{35} pattern. At both sampling sites, DIC_{35} reached its maximum values during winter and its weakest values in

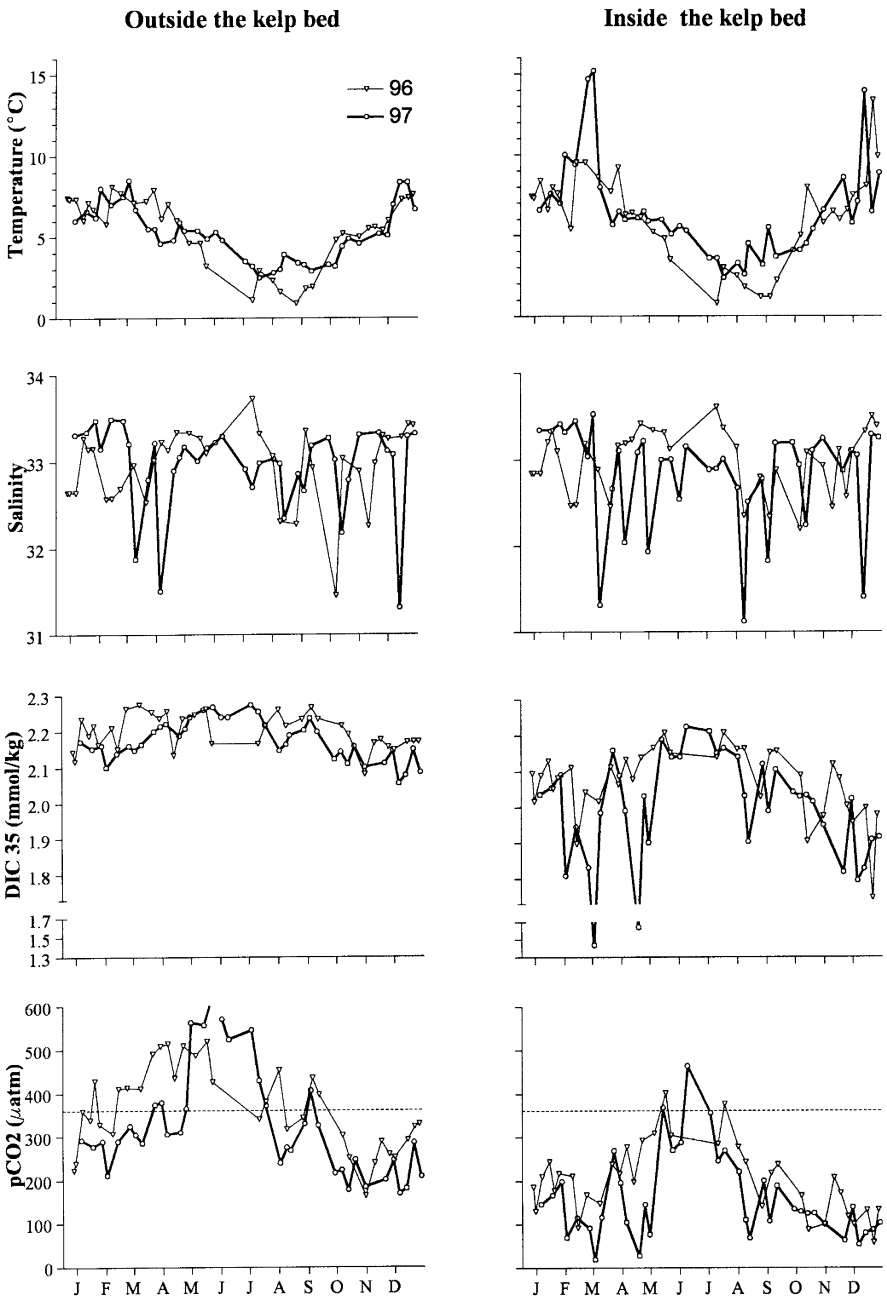

Fig. 2 Seasonal variations of temperature, salinity, DIC_{35} and pCO_2 inside and outside the kelp bed (*thin line with triangles* 1996; *thick line with circles* 1997). The *dotted line* represents the atmospheric pCO_2 value

summer. DIC_{35} exhibited striking differences between the sampling sites. Drawdown of DIC_{35} in spring was larger inside the kelp bed than outside, with a magnitude of yearly variations around 0.2 mmol kg^{-1} outside the kelp bed against 0.5 and 0.7 mmol kg^{-1} inside the kelp bed in 1996 and 1997, respectively. Furthermore, inside the kelp bed variations can be very large, reaching 60 umol kg^{-1} day^{-1}.

Discussion

Short-term variations

Sudden weather changes, heavy rains, and successions of snowfalls and thaws are very common in the Kerguelen Archipelago. In Echouage Cove, these phenomena

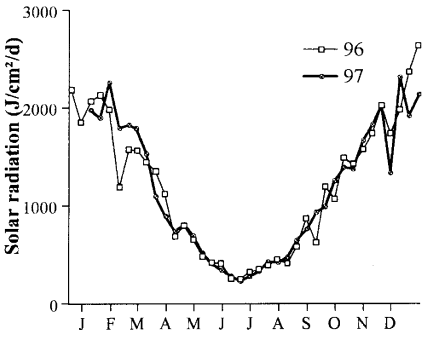

Fig. 3 Solar radiation in Echouage Cove (*thin line with triangles* 1996; *thick line with circles* 1997)

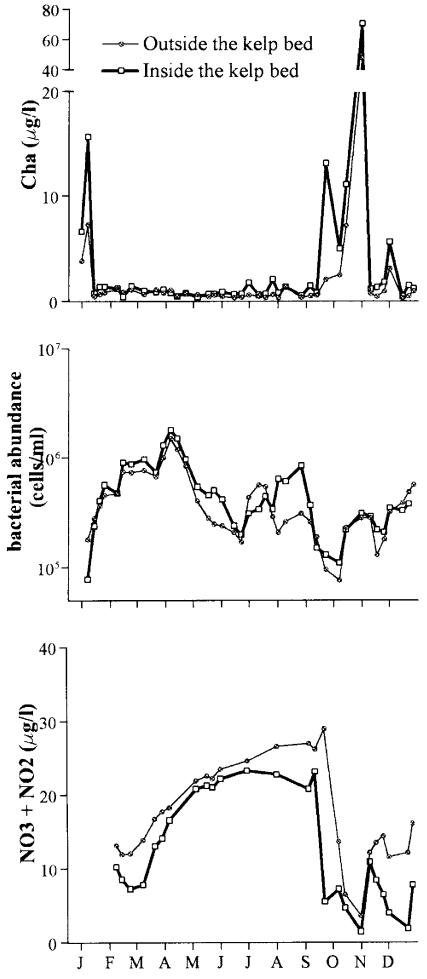

Fig. 4 Seasonal variations of chlorophyll *a*, bacterial abundance and $NO_3^- + NO_2^-$ in 1996 (*thin line with circles* outside the kelp bed; *thick line with squares* inside the kelp bed)

associated with the low rain-water retention of surrounding soils may lead to large and brief inputs of fresh water by rivers and small streams. In contrast, frequent storms and tides favour advection and mixing with offshore water whose salinity is around 33.4 (Razouls et al. 1997). These antagonist processes lead to large short-term variations of salinity. Sudden input of fresh water is responsible for sharp decreases in salinity while mixing with offshore water ensuing storms acts to maintain the salinity of the cove above 33.0.

Furthermore, salinity and temperature differences between inside and outside the kelp bed can reach 1 and 7 °C, respectively. Thus, water within the kelp bed can present a strong heterogeneity with surrounding water in terms of physico-chemical conditions. Some sharp decreases in the salinity patterns occur only inside the kelp bed (Fig. 2), suggesting than after an input of fresh water and subsequent decrease of salinity, the ensuing mixing and increase of salinity are faster outside the kelp bed than inside. This is in accordance with studies by Jackson and Winant (1983), which showed than *Macrocystis* kelp beds counteract advection of surrounding water and slow coastal currents.

The inorganic carbon parameters DIC_{35} and pCO_2 also present large short-term variations and high differences between the sampling sites. Different factors may perceptibly influence inorganic carbon dynamics. Taking into account the TAlk and DIC content of small streams surrounding the cove (TAlk 0.3 meq kg^{-1}, DIC 0.32 mmol kg^{-1}), we calculated that an input of local fresh water corresponding to a decrease in salinity of 1, will decrease pCO_2 and DIC by about 12 µatm and 50 µmol kg^{-1}. Furthermore, physical processes such as exchanges with shallow sediment could have a significative impact on CO_2, but are difficult to assess in the present study.

Furthermore, large short-term variations due to biological activity would not be surprising since biological activity is able to lead to large changes of pCO_2 within a few hours. Poisson et al. (1993) reported pCO_2 daily variations up to 26 µatm in 27 h above the Kerguelen plateau, while Delille et al. (1997) noticed a magnitude of daily pCO_2 variation around 35 µatm in some shallow waters of the Kerguelen Archipelago. In both cases, the authors assumed that biological activity was responsible for such rapid variations. In the same way, previous studies of macrophyte beds showed than water-column pCO_2 may vary greatly over a diel cycle (Smith 1981; Frankignoulle and Distèche 1984, 1987; Frankignoulle and Bouquegneau 1990; Delille et al. 1997).

However, air-sea exchanges tend to maintain pCO_2 near saturation. The effect of air-sea exchanges on the observed pCO_2 is enhanced by the low depth of the cove and by the high wind velocity commonly observed in this area. One can assess the effect of air-sea exchanges on pCO_2 in the cove. The CO_2 air-sea flux (F) can be calculated using the equation $F = \alpha K \Delta pCO_2$ where α is the solubility coefficient of CO_2, ΔpCO_2 the air-sea gradient of CO_2 and K the gas coefficient, which mainly depends on wind speed. Several authors have proposed different algorithms in order to compute K and we applied the two most common algorithms from Liss and Merlivat (1986)

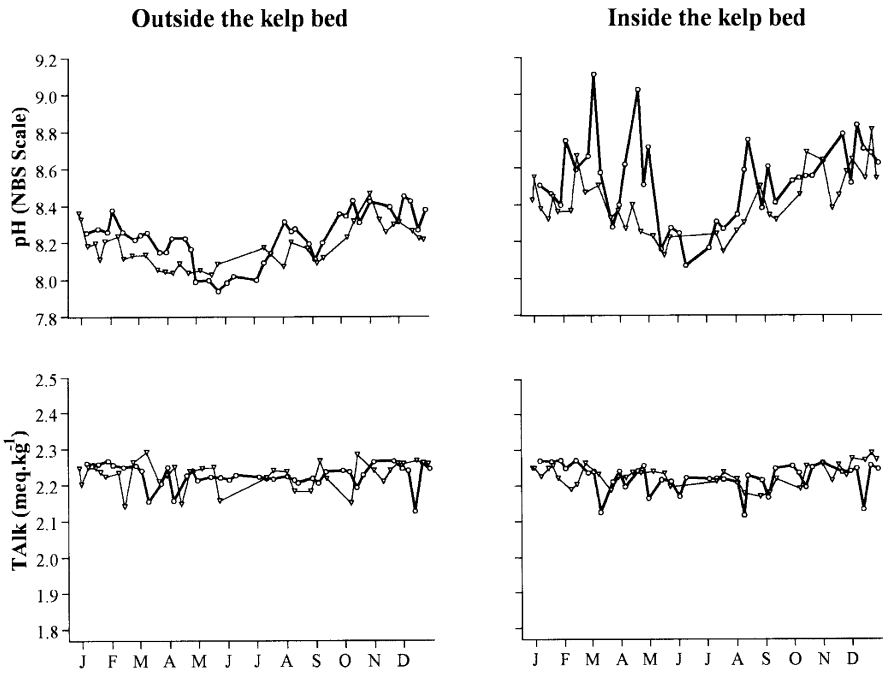

Fig. 5 Seasonal variations of pH and TAlk inside and outside the kelp bed (*thin line with triangles* 1996; *thick line with circles* 1997)

and Wanninkhof (1992). Air-sea flux of CO_2 directly affects the DIC. Taking account of the height of the water column, it is possible to compute the effect of the change of DIC on pCO_2. We computed by iteration (1 day time step) the variation of pCO_2 due to air-sea exchanges in 10 days. In average conditions ($S = 32.9$, $T = 5$ °C, DIC = 2.06 mmol kg^{-1}, wind speed = 9.3 m s^{-1}, water column height = 10 m) with an oversaturation of 100 µatm, air-sea exchanges would lead to a decrease of pCO_2 equal to 29 and 42 µatm, according to the algorithms of Liss and Merlivat (1986) and Wanninkhof (1992), respectively. However, in May 1997 outside the kelp bed, we computed that air-sea exchange would have induced decreases of pCO_2 up to 94 and 127 µatm in 10 days ($S = 33.1$, $T = 5.2$ °C, DIC = 2.14 mmol kg^{-1}, wind speed = 9 m s^{-1}, water column height = 10 m). Thus air-sea exchanges of CO_2 can lead to large changes of pCO_2 over a short time-scale.

In order to explain the large variations in salinity, temperature and inorganic carbon observed at both spatial and short temporal scales, we assume that the shallow water of the cove behaves as follows. Under calm weather conditions advection is weak. Hence, insolation and input of fresh water strongly affect physico-chemical parameters while input of fresh water, exchanges with shallow sediment and biological processes can lead to large changes in DIC_{35} and pCO_2 within the shallow water of the cove. Furthermore, this behaviour is enhanced inside the kelp bed where advection is weaker. When a storm occurs, advection greatly increases. This leads to the homogenization of shallow water, both outside and inside the kelp bed, with offshore water whose physico-chemical parameters, DIC_{35} and pCO_2 are likely to be more constant. Consequently, physico-chemical parameters, DIC_{35} and pCO_2 within the cove tend to mean values. At the same time, air-sea exchange of pCO_2 enhanced by high wind velocity act to maintain pCO_2 near saturation.

Seasonal variations outside the kelp bed

Biological parameters exhibit seasonal patterns, which allow one to distinguish the successive steps of the yearly biological turnover. The phytoplanktonic spring bloom is well marked and leads to a large depletion of $NO_3^- + NO_2^-$ in October. This depletion is limited in time and mineralization starts just after the end of the spring phytoplanktonic bloom. From February to April, bacterial abundance reaches its highest level and the associated strong respiration leads to a large increase of $NO_3^- + NO_2^-$ concentration. This increase is weaker in winter, in good agreement with the decrease of bacterial abundance and subsequent weaker respiration. However, mineralization continues until springtime when the phytoplanktonic spring bloom occurs.

Outside the kelp bed, annual variation of pCO_2 is high (up to 470 µatm). In spite of large variations of pCO_2 over the meso time-scale (10 days), seasonal patterns appear obviously (Fig. 2) and are partly consistent from the 1st year to the next. Hence, although short-term processes exist, they do not mask the seasonal changes.

Considering the merging of the two annual cycles, we discuss the change of CO_2 in June/July 1996 assuming that it was similar to the change in 1997. One can speculate about the effect of physical processes on pCO_2 (fresh water outflow, temperature changes, ventilation). Salinity changes corresponding to inputs of fresh water can induce perceptible changes of pCO_2 (see above) but low salinity events are limited in time and advection with offshore water is likely to quickly counteract the effect of the inputs of fresh water. Therefore, river outflow should have a weak influence on inorganic carbon dynamics over a seasonal scale. For each month, we computed the impact of temperature changes and air-sea exchanges on pCO_2. Impact of temperature changes was calculated using the algorithm of Copin-Montegut (1988, 1989) while effects of air-sea exchanges were computed by iteration (1 day time step) for 30-day periods, taking account of monthly averages of salinity, temperature, DIC, TAlk, atmospheric pCO_2, wind speed, a height of water column equal to 6 m inside the kelp and 10 m outside the kelp and the algorithm of Liss and Merlivat (1986). The use of the algorithm of Wanninkhof (1992) enhances the effect of air-sea exchange but this did not change our analysis. Computation results are presented in Fig. 6. It is worth noting that physical processes (especially air-sea exchange) can potentially exert a strong influence on pCO_2. However, with the exception of late autumn and early winter (May to July) and late spring (November, December), pCO_2 varies in the opposite way with regard to physical constraint. Therefore, the influence of thermodynamical constraints and air-sea exchange on the inorganic carbon system appears to be generally counteracted by other processes during almost the whole year and the explanation of seasonal changes of pCO_2 must be found in the primary influence of biological activity on pCO_2 dynamics.

In fact, the different phases of the yearly biological turnover are distinguishable in pCO_2 patterns. In autumn, pCO_2 increases and reaches its greatest value prior to wintertime. The explanation of the high values reached (520 and 640 µatm) must be the intense mineralization. In early winter, mineralization is weaker, solar radiation reaches its minimum value and, subsequently, photosynthetic activities which are still in process (i.e. kelp bed) are at their weakest. Thus, physical processes are dominant and can exert a strong influence on pCO_2. CO_2 exchanges with the atmosphere, enhanced by strong winter winds, tend to minimize undersaturation or

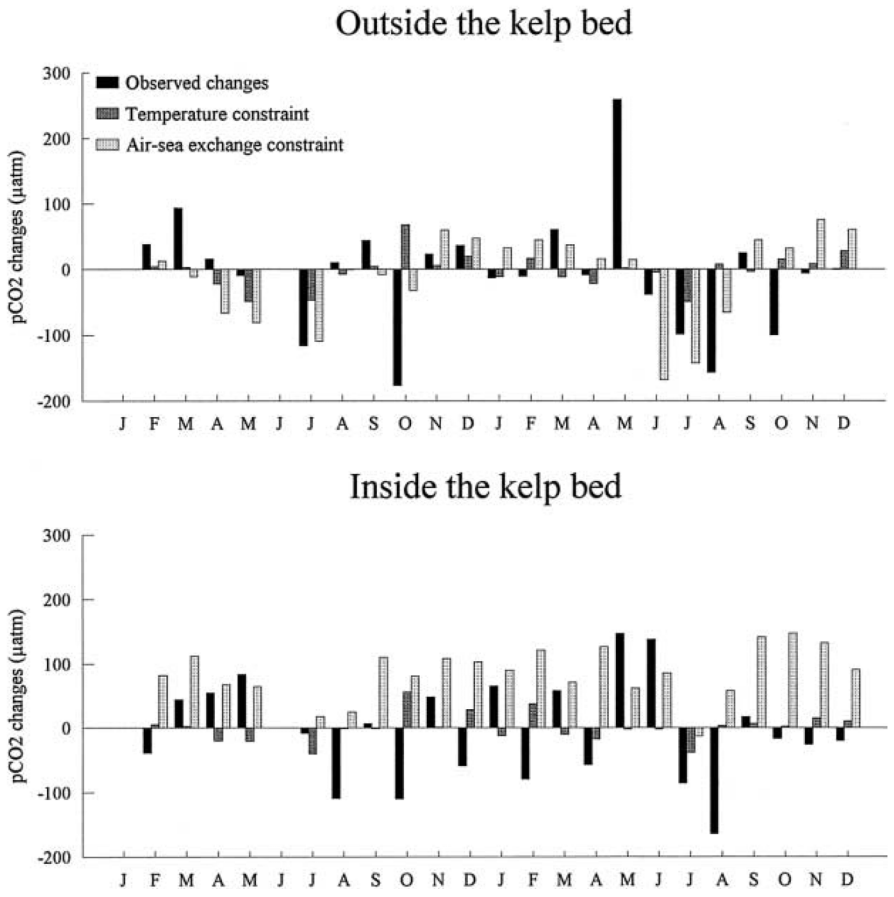

Fig. 6 Monthly pCO_2 changes and assessment of physical forcing (*black bar* observed changes, *dark* and *light grey* pCO_2 changes induced by temperature changes and air-sea exchanges, respectively)

oversaturation and finally reduce pCO_2 during June and July. However, the explanation of ensuing undersaturation at the end of winter 1997 (August) is not obvious. An explanation may be found in the decrease of the temperature of surface water, but the observed decrease of temperature does not account for all the undersaturation. Another reason may lie in the exchange of water of the kelp bed – whose pCO_2 is low – with surrounding water. In September 1997, oversaturation of pCO_2 could be linked to an increase of bacterial abundance. This would suggest a close coupling between bacterial abundance and pCO_2 in the shallow waters of the cove.

In spring, a marked decrease of pCO_2 corresponds with an increase of chlorophyll a biomass and a sharp drawdown of nutrient content. This is the beginning of an intense photosynthetic production, which leads to a minimum value of pCO_2 during the phytoplanktonic bloom. This period is brief, and then pCO_2 starts to increase, with the beginning of mineralization. Furthermore, this increase could be enhanced by air-sea exchange in November and December (Fig. 5).

DIC_{35} shows a consistent pattern with the pCO_2 pattern. Increase of DIC_{35} in autumn can be related to the decay of organic matter. In winter, changes of DIC_{35} are weak in spite of a large decrease of pCO_2. This suggests a low mineralization and a strong influence of some physical processes on pCO_2 (i.e. temperature decrease and advection of offshore water). In summer, as one would expect, the DIC_{35} minimum corresponds to the maximum of chlorophyll a biomass and highlights the influence of primary production on inorganic carbon dynamics.

Influence of the *Macrocystis* kelp bed

Overall patterns of biological parameters are similar at both sampling sites. However, it is interesting to note that the phytoplanktonic bloom and subsequent decrease of $NO_3^- + NO_2^-$ occur 2 or 3 weeks earlier inside the kelp than outside. Thus the kelp bed appears to favour the phytoplanktonic bloom. The reason is not obvious and might lie in lower turbulence inside the kelp bed. However, other explanations cannot be excluded.

The seasonal trend of the CO_2 content of water inside the kelp bed (Fig. 2) shows significant differences with regard to the seasonal pattern of pCO_2 outside the kelp bed. It is essential to pay careful attention to these, taking account of the differences in nutrient contents, since they allow specific biological activity of the kelp bed to be distinguished.

Similarly to outside the kelp bed, Fig. 6 shows that with the exception of autumn (March to June), November 1996 and January 1997, pCO_2 varies in the opposite way to physical constraint. Furthermore, even if pCO_2 varies in the same way as physical constraint, this does not account necessarily for the whole change (May to July 1997). Since the effect of input of fresh water does not exceed a decrease of about 25 µatm (for a salinity decrease of 2), the only explanation for the large undersaturation of CO_2 observed in August ($80 \sim 150$ µatm) must be found in the photosynthetic activity of the *Macrocystis* kelp bed, which would correspond to an increase of solar radiation. Uptake of nutrient attendant to this photosynthetic activity is noticeable in the decrease of nutrient that occurred in July and August despite the high bacterial abundance (Fig. 4). By the end of September, phytoplanktonic blooms begin and induce a strong decrease in pCO_2 and a first depletion of $NO_3^- + NO_2^-$. Photosynthetic production of the kelp bed is then likely to decrease, due to limitation of nutrient (Jackson 1977) and decrease of light availability by phytoplankton and epiphyte communities. Hence, just after the bloom, at a lower photosynthetic activity of the kelp, physical constraints (i.e. air-sea exchange, increase of temperature, advection) lead to a slight increase of CO_2 enhanced by the beginning of mineralization. When $NO_3^- + NO_2^-$ content reaches a sufficient level, together with a high solar irradiation (Fig. 3), photosynthetic activity of the kelp bed increases again and leads to a second marked decrease of pCO_2 and $NO_3^- + NO_2^-$ concentrations. This decrease occurs in contrast with outside the kelp bed where pCO_2 and $NO_3^- + NO_2^-$ continue to increase until winter. It is worth noting that photosynthetic activity of the kelp bed in summer can lead to a value of pCO_2 as low as 20 µatm. On the whole, this photosynthetic activity continues almost all year and maintains pCO_2 inside the kelp bed below saturation from July to May.

Kelp bed primary production yields to substantial decrease of DIC_{35}. Overall decrease of DIC_{35} is initiated in August, suggesting that kelp bed primary productivity begins as soon as solar irradiancy increases. In spite of homogenization with surrounding water, primary production of the *Macrocystis* kelp bed acts to maintain the DIC_{35} value within the kelp bed below the value observed outside the kelp from August to April. This leads to an estimate than primary production of the kelp bed covers a period of $8 \sim 9$ months a year. Moreover, it is worth noting that inorganic carbon uptake by *Macrocystis* was large enough to yield decreases of DIC between 30 and 60 µmol kg^{-1} day^{-1}. Taking into account the depth of the kelp bed ($5 \sim 6$ m), these decreases would correspond to a productivity between 2.2 and 4.2 gC m^{-2} day^{-1}. These rough values are in the range of previous observations of productivity of *Macrocystis* (2.7–3.6 gC m^{-2} day^{-1}) in warmer water (Mann 1982; Wheeler and Druehl 1986). However, our calculations are biased by mixing with surrounding water. In fact, daily uptake of DIC within the *Macrocystis* kelp bed of the Kerguelen Archipelago can be larger – up to 100 µmol kg^{-1} day^{-1} – as was reported by Delille et al. (1997). Therefore, study of DIC_{35} variations over diel cycles – weaker influence of mixing – is needed to improve measurement of *Macrocystis* productivity.

This primary production yields to undersaturation of CO_2 during almost the whole year. Thus, the

Macrocystis kelp bed would act as a strong sink of CO_2. However, accurate study of the role of the kelp bed with regard to the atmosphere would need to take account of the diel cycles of pCO_2 within the kelp bed, as well as computation of CO_2 fluxes.

Buffer factor

The homogeneous factor [$\beta = d\ln(pCO_2)/d\ln(DIC)$] is a useful tool for identifying processes that mainly affect the inorganic carbon dynamics, such as primary production or water mass mixing. It can be obtained by plotting $\ln(pCO_2)$ versus $\ln(DIC)$, and when dissolved CO_2 is the only inorganic species involved in the carbon exchange (e.g. air-sea exchange), β corresponds to the Revelle factor and its value is about 12 for average seawater conditions. However, this value depends also on the processes that induce modifications of the inorganic species involved in the CO_2 system speciation. Thus, if organic matter production/respiration by organic metabolism have a weak effect on β, this value can decrease down to −7 when inorganic metabolisms develop (e.g. uptake or release of bicarbonates and/or carbonates by calcifying organisms). When organic and inorganic carbon metabolisms occur simultaneously, one can use the relation $\beta = -7.02 + 0.186 \times \%C_{org}$ (Frankignoulle 1994) where $\%C_{org}$ is the percentage of change in inorganic carbon concentration due to organic metabolism (photosynthesis and respiration). Hence, we can assess the influence of inorganic metabolism on the inorganic carbon dynamics.

By using this approach, Robertson et al. (1994) studied a coccolithophore bloom in the North Atlantic while Wanninkhof and Feely (1998) discussed the influence of the aging water masses from the Atlantic to the South Indian and South Pacific Oceans. Furthermore, the buffer factor may provide substantial help in assessing inorganic carbon dynamics even in coastal waters where complex processes develop (Frankignoulle et al. 1996b, 1996c).

The data set presented here allows us to estimate β values using the slope of a plot of $\ln(pCO_2)$ versus $\ln(DIC)$. To remove influence of temperature and salinity, pCO_2 were computed from normalized TAlk and DIC ($TAlk_{35}$ and DIC_{35}) for a constant temperature $T = 5$ °C. Then, we plotted this value [$pCO_{2(35,5°)}$] as a function of DIC_{35}. Figure 7 illustrates results obtained using the whole data set from the monitoring and gives the relationship between $\ln[pCO_{2(35,5°)}]$ and $\ln[DIC_{35}]$ for both sampling sites.

It is worth noting that in spite of large variations of physico-chemical conditions (i.e. pH, DIC_{35}, temperature and salinity) and the length of the monitoring (2 years), $\ln[pCO_{2(35,5°)}]$ versus $\ln[DIC_{35}]$ exhibit fairly good linear relationships at both sampling sites. Outside the kelp bed, the slope, β, is calculated to be 12.61 ($r^2 = 0.82$). This value is close to the expected theoretical value ($\beta = 13.2$, with $S = 32.96$, pH = 8.21, TAlk = 2.23 mmol kg^{-1}), obtained from average values observed during the 2 years and calculated assuming that dissolved CO_2 is the only inorganic species involved in CO_2 dynamics. This observation clearly indicates that total inorganic carbon variations measured in this area are mainly driven by changes in the dissolved CO_2 level, e.g. air-sea CO_2 exchanges and/or organic matter production/degradation, without any associated calcification or calcium carbonate precipitation.

Inside the kelp bed, $\ln[pCO_{2(35,5°)}]$ versus $\ln[DIC_{35}]$ exhibit a quite linear relationship. This suggests that some processes within the kelp bed exert a strong constraint on the behaviour of the carbonate system and that the triggering due to hydrodynamic processes is partially hidden over the year. In fact, residence time in the interior of the kelp bed is likely to allow biological processes that develop within the kelp bed to exert a strong influence on characteristics of water masses flowing through the kelp bed, accordingly to the observations of Jackson and Winant (1983).

A preliminary calculation inside the kelp bed gives $\beta = 9.08$ ($r^2 = 0.95$), which differs significantly from the result outside the kelp bed. In spite of a good correlation coefficient in calculation of the relationship, $\ln[pCO_{2(35,5°)}]$ versus $\ln[DIC_{35}]$ displays a slight curve, allowing us to think β is not absolutely constant throughout the year. If one divides the year between

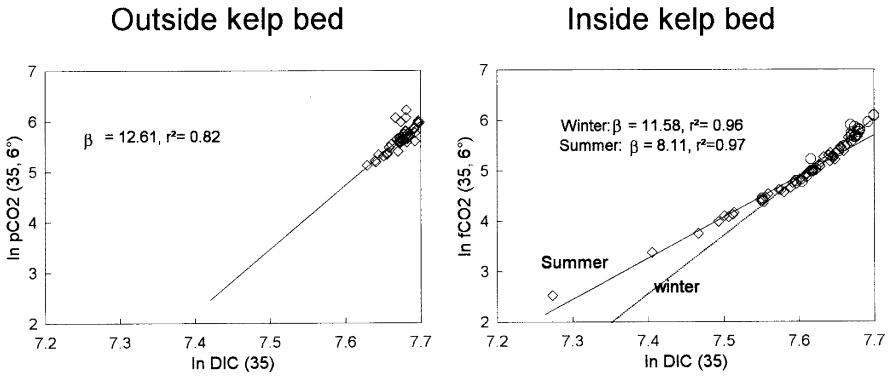

Fig. 7 Plots of $\ln[pCO_{2(35,6°)}]$ versus $\ln[DIC_{35}]$ and regression lines to obtain the homogeneous buffer factors. On the *left* figure, *squares* and *thin line* correspond to both years. On the *right* figure, we distinguish summer (*squares* and *thin line*) and winter (*circles* and *dotted line*) seasons

winter (May to August) and the other seasons, calculations give $\beta = 11.58$ ($r^2 = 0.96$) in winter and $\beta = 8.11$ ($r^2 = 0.97$) for the rest of the year. In winter, β is close to the value outside the kelp bed, indicating that total inorganic carbon variations are mainly driven by changes in the dissolved CO_2 level, e.g. air-sea CO_2 exchanges and/or organic matter production/degradation. Decrease of β in summer lies in the removal of CO_3^{2-} and/or HCO_3^- superimposed on changes of the CO_2 concentration. Two processes might be responsible for such removal: (1) uptake of HCO_3^- by the *Macrocystis*, (2) calcification by the epiphytic community (uptake of CO_3^{2-} and/or HCO_3^-).

A number of macroalgae are reported to be capable of using HCO_3^- (Gao and McKinley 1994). However, if *Macrocystis* uses HCO_3^- for growth, large uptakes of DIC – up to 60 μmol kg^{-1} day^{-1}, which have been observed – would lead to weak changes of pCO_2 (less than 15 μatm day^{-1}) and large changes of TAlk, which are not observed in the present study, and also in the study of Delille et al. (1997), whose reported daily decrease of DIC of 90 μmol kg^{-1} day^{-1} associated with decreases of pCO_2 of 220 μatm above some *Macrocystis* kelp beds of the Kerguelen Archipelago. This leads us to think that *Macrocystis* uptake of HCO_3^- is weak or non-existent. Therefore, the explanation of the decrease of β must be found in the presence of calcifying organisms which develop within the kelp bed. This is in accordance with the presence of small shells on the fronds of *Macrocystis* in the Kerguelen Archipelago. Moreover, other epiphyte species probably remove CO_3^{2-} and/or HCO_3^- in substantial amounts.

Conclusions

In spite of an important temporal variability at meso time-scale, partly due to hydrodynamical processes, pCO_2 in the shallow water of the Kerguelen Archipelago exhibits obviously large seasonal changes. These changes are mainly influenced by biological activity almost the whole year. Photosynthesis in spring and summer is responsible for marked undersaturation of CO_2 while decay of organic matter leads to oversaturations in autumn and winter. Physical processes have a great potential to influence pCO_2 but, with the exception of winter time, influences of temperature variations and air-sea exchanges are hidden by the magnitude of variations due to biological processes. Thermodynamical constraints and air-sea exchanges play a leading role in inorganic carbon dynamics in winter when biological activity is weak, as well as between the end of the phytoplanktonic spring bloom and autumnal mineralization. Furthermore, physical processes (i.e. input of fresh water, advection and air-sea exchanges) exert a strong influence on CO_2 and DIC at meso time-scale.

Primary production of *Macrocystis* appears to cover a period which extends from winter to late summer and favours the development of the spring phytoplanktonic blooms. Growth of macrophytes tends to act as a net sink for atmospheric CO_2 almost the whole year and leads to very low values of pCO_2 (as low as 20 μatm).

In our approach, we used the homogeneous buffer factor (β) to discuss processes responsible for the observed CO_2 variations. Plotting $\ln[pCO_{2(35,6°)}]$ versus $\ln[DIC_{35}]$ yields excellent relationships, even in such a complex system and for a long time (2 years). Outside the kelp bed, inorganic carbon dynamics seem to be mainly driven by air-sea exchanges, physical processes and organic production without calcification. CO_2 uptake is likely to be the major pathway for inorganic carbon assimilation by *Macrocystis* while inorganic epiphytic metabolism appears to develop within the *Macrocystis* kelp bed in summer.

Acknowledgements The authors would like to thank V. Kazan for providing atmospheric CO_2 data, Météo-France for providing meteorological data, G. Abril, A. Borges and K. El Kalay for fruitful discussions, L. Oriol for her technical assistance and anonymous referees for improving significantly the quality of the paper. This research was supported by the "Institut Français pour la Recherche et la Technologie Polaires", the Belgian Federal Office for Scientific, Technical and Cultural Affairs through the Belgian Scientific Programme on the Antarctic (contract A4/DD/B14) and the FNRS (Belgium), with whom Michel Frankignoulle is a research associate.

3.2 Influence of giant kelp beds (Macrocystis pyrifera) on diel cycles of pCO_2 and DIC in Sub-Antarctic coastal area.

3.2.1 Foreword

This study has been conducted in parallel with the survey of the chapter 3.1. It also addresses the influence of *Macrocystis pyrifera* kelp beds on pCO_2 dynamics in shallow waters. However, the sampling sites are different and this chapter address both diel and seasonal variability. In the previous chapter, there were stong indications that the primary production of the kelp beds is significant, compared to primary production of phytoplankton of the surrounding waters. It appears that residence time of water within the kelp is longer than 24 h. This allows to make a tentative estimate of the maximum net ecosystem production of the kelp beds. This latter appears to be significant when compared to temperate sites and other macrophytes species.

This part has been submitted for publication to Estuarine, Coastal and Shelf Science:

Delille B., A.V. Borges & D. Delille. Influence of giant kelp beds (*Macrocystis pyrifera)* on diel cycles of pCO_2 in Sub-Antarctic coastal area.

3.2.2 Abstract

The partial pressure of CO_2 (pCO_2) and dissolved inorganic carbon (DIC) were monitored in shallow coastal waters located inside and outside a giant kelp bed (*Macrocystis pyrifera*) situated in the Kerguelen Archipelago (Southern Ocean). Photosynthesis and respiration by microplankton and kelps are responsible for marked pCO_2 and DIC diel cycles. Daily variations are significant in spring and summer, but absent in winter, reflecting the seasonal cycle of biological activity in the kelp beds. If kelp beds seem to favour the onset of phytoplankton bloom, most of the primary production inside the kelp beds is due to the kelps. Primary production of *Macrocystis* kelp beds in the subantarctic high nutrients-low chlorophyll (HNLC) waters off Kerguelen Archipelago is elevated and is tightly linked to light availability; it is significant from October to April and reaches its climax in December at the solar radiation maximum.

3.2.3 Introduction

Marine macrophytes (seagrasses and macroalgae) can be found in any shallow coastal aquatic system including estuaries. They cover only 2 10^6 km^2 worldwide (Whittaker and Likens, 1973), but could act as an effective carbon sink because of their large biomass (estimated to be about two-thirds of oceanic plant biomass) and relatively high turnover time (1 year) compared to phytoplankton (1 week) (Smith, 1981). It has been pointed out that macrophytes have a great potential for biomass production and CO_2 uptake in a global context (Smith, 1981; Wilcox and North, 1988; Gao and McKinley, 1994; Duarte and Chiscano, 1999; Duarte et al., 2004). Nevertheless, little is known of the influence of macrophytes on dissolved inorganic carbon (DIC) dynamics, and the quantitative significance in the global carbon and CO_2 cycles remains poorly constrained (Gattuso et al., 1998b; Duarte et al., 2004; Borges, 2005; Borges et al., 2005).

Frankignoulle and Distèche (1984; 1987), Frankignoulle and Bouquegneau (1987; 1990) studied the impact of *Posidonia oceanica* seagrass meadows on the partial pressure of CO_2 (pCO_2) and DIC dynamics in the Mediterranean Sea. The *Posidonia* meadows exert a strong influence on the pCO_2 of surrounding waters, driving a diel signal of pCO_2 consistent with the solar radiation cycle. The diel and seasonal variations of the carbon budget show two yearly phases with spring and summer photosynthesis yielding to a drawdown of CO_2 and the winter decay of organic matter which results in a CO_2 release. In the Bay of Palma (Spain), strong decreases of pCO_2 over *Posidonia* meadows has been recently reported due to their higher primary productivity compared to the surrounding oligotrophic waters (Gazeau et al., 2005). In the same area, Barrón et al. (2006) highlighted the strong influence of calcification by epiphythes and calcium carbonate ($CaCO_3$) dissolution on pCO_2

dynamics in *Posidonia* meadows, in agreement with observations in other seagrass ecosystems (Morse et al., 1987; Ku et al., 1999; Delille et al., 2000; Burdige and Zimmerman, 2002; Yates and Halley, 2003; Yates and Halley, 2006). On the whole *Posidonia oceanica* seagrass meadows appear to act as a sink for atmospheric CO_2. In the waters surrounding the Kerguelen Archipelago, it has been previously reported that the DIC and pCO_2 of the waters above *Macrocystis* kelp beds are strongly influenced by the biological activity of the kelps leading to a potential sink of atmospheric CO_2 (Delille et al., 1997; Delille et al., 2000).

The primary production in *Macrocystis* kelp bed is high and generally ranges from 1000 to 1300 gC m-2 y-1 (Mann, 1982; Wheeler and Druehl, 1986) and Jackson (1977) measured primary production up to 3400 gC m-2 y-1 off southern California. The survey of DIC over macrophyte beds allows to assess net ecosystem production by mass balance (Gazeau et al., 2005). This is of particular interest in polar areas and in particular in the Southern Ocean where dense population of highly productive macroalgae are present, but production has seldom been estimated (Dunton and Dayton, 1995).

The purpose of the present paper is to examine the diel changes of pCO_2 and DIC both outside and inside a *Macrocystis pyrifera* giant kelp bed within the shallow waters of the Kerguelen Archipelago, in order to understand the physico-chemical and biological processes controlling pCO_2 dynamics and to follow the seasonal evolution of kelp bed primary production.

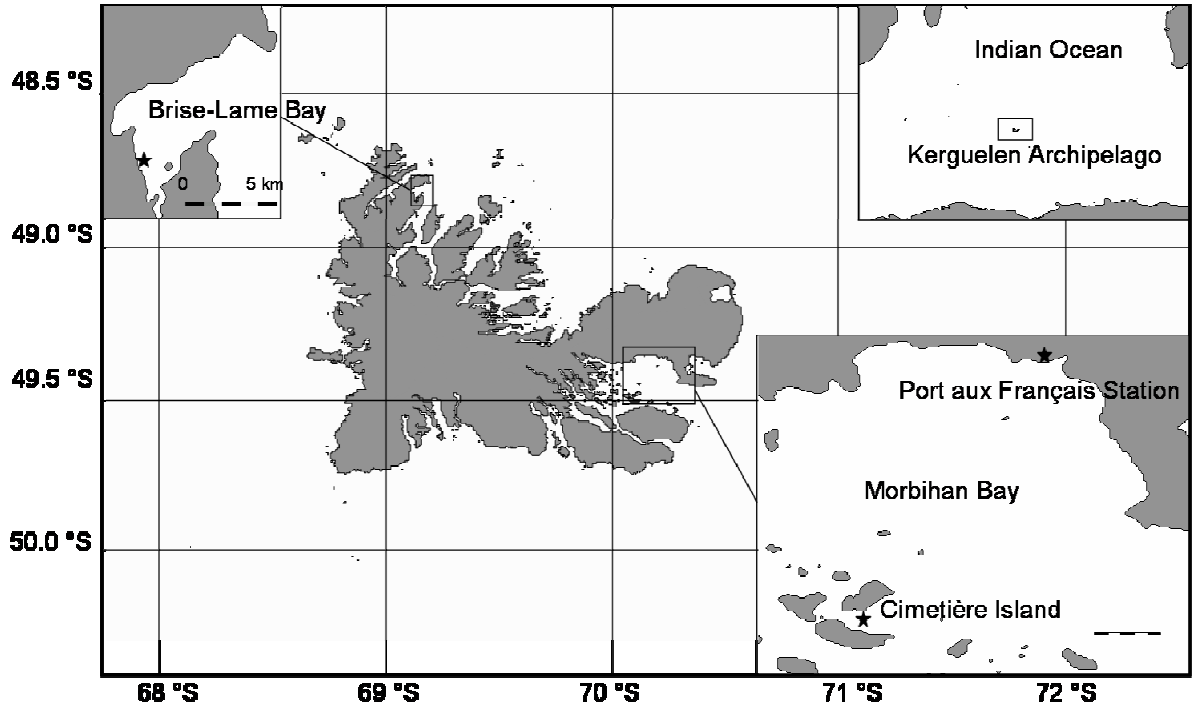

Figure 1. Brise-Lame Bay and Morbihan Bay in the Kerguelen Archipelago. The sampling sites are indicated by stars.

3.2.4 Material and Methods

Sites and sampling. The Kerguelen archipelago (Fig. 1) is usually cited in the literature as a Sub-Antarctic island. From a strict oceanographic point of view, this archipelago is situated either in the Polar Frontal Zone (Sub-Antarctica) or Permanently Open Ocean Zone (Antarctica) depending of the position of the Polar Front with regards to the archipelago (e.g. Delille et al. 2000). A substantial proportion of the coastlines of the archipelago are occupied by *Macrocystis pyrifera* kelp beds.

Samples were collected from January to December 1996 at the vicinity of the Cimetière Island in the Morbihan Bay (MB), and in the Brise-Lame Bay (BLB) in the northern part of the Kerguelen archipelago. Located in the southeast of the archipelago, the Morbihan Bay (about 600 km²) opens to the ocean through the Royal Pass, which is 12 km wide and 40m deep. Biomass (wet weight) of *Macrocystis pyrifera* in the Morbihan Bay was assessed using remote sensing data to be about 1 100 kt, spread over an area of about 190 km² (Belsher and Mouchot, 1992). Average biomass within two-thirds of the area covered by *Macrocystis* kelp beds is 22.5 kg m-2 and can reach 26 kg m-2. Brise-Lame Bay has a surface area of about 12 km² and is widely open. However, sampling sites were chosen in the most sheltered part of the bay that is surrounded by *Macrocystis pyrifera* kelp beds.

Two sampling stations were chosen at each site, one located inside and one outside the kelp beds. Surface waters were sampled at both stations every third hour during 24 hours from 21:00 onwards. Analyses began aboard the *R.V. La Curieuse* within 15 min after sample collection. Diel surveys were numbered chronologically, while BLB and MB denotes, respectively, diel surveys carried out in the Brise-Lame Bay and at the Cimetière Island in the Morbihan Bay.

Dissolved inorganic carbon. The inorganic carbon speciation was calculated from pH and total alkalinity (TA) measurements. TA was measured using the classical Gran electrotitration method on 100ml GF/F filtered samples. The accuracy of measurements was ±4 μeq kg-1. pH was measured using a commercial combination electrode (Ross type, Orion®) calibrated on the U.S. National Bureau of Standards (NBS) scale. The accuracy of pH measurements was ±0.01 pH units. CO_2 speciation was calculated with the CO2SYS Package (Lewis and Wallace, 1998; Pelletier et al., 1998), using the CO_2 acidity constants of Mehrbach et al. (1973) refitted by Dickson and Millero (1987), the CO_2 solubility coefficient of Weiss (1974), the borate acidity constant of Dickson (1990b). The total borate molality was calculated using the Uppström (1974) ratio to salinity. Taking into account uncertainties on pH, TA, temperature, salinity, the errors in pCO_2 and DIC were ±14 μatm and ±9 μmol kg-1, respectively. DIC was normalized to a constant salinity of 33.4, denoted as DICn. Normalized pCO_2 ($pCO_{2\ n}$) was computed at a constant temperature of 5°C from normalized TA and DIC at a constant salinity of 33.4.

Chl*orophyll a* (Chl *a*). Samples were prefiltered through a 200 μm mesh to remove detritic material and larger biota, and then filtered by gentle vacuum filtration of 1 L of seawater through a Whatman® GF/F glass-fibber filter. The measurements of

chlorophyll a were carried out with a Perkin-Elmer® MPF 66 spectrofluorometer using the spectrofluorometric method developed by Neveux and Panouse (1987).

Related parameters. Salinity was determined with a Guildline® induction salinometer with an accuracy of 0.003 on the practical salinity scale. Solar radiation measurements were provided by MétéoFrance from station located at Port aux Français (Morbihan Bay).

3.2.5 Results

Figure 2 shows the seasonal changes of the 24 h averages of each parameter in MB, BLB and in an adjacent station at Port aux Français (Delille et al., 2000). Sea surface temperature (SST) ranged from 1.6°C in austral winter (from June to August) to 8.4°C in summer (from December to March) inside the kelp bed. In winter, the diel temperature changes were small (0.2°C inside and outside the kelp beds) compared to summer (1.5°C outside the kelp beds; 2.6° inside the kelp beds). On repeated occasions - like MB3, MB8, BLB1 and BLB5 cycles - diel cycle of SST is more marked inside the kelp beds than outside (Fig. 3), with a strong daytime increase of SST and a rapid decrease at dusk. In summer, SST difference between inside and outside the kelp bed reached 1.0°C during daytime. Chl *a* concentrations ranged from 1.0 μg L-1 to 2.0 μg L-1 in February and then decreased below 0.3 μg L-1 in July. The increase in September was much larger inside the kelp beds. The yearly maximum of Chl *a* was about 5.3 μg L-1. Diurnal changes of Chl *a* concentration (Fig. 4) were on some occasions large (up to 3.0 μg L-1) but did not exhibit clear or recurrent patterns.

pCO_2 ranged from 170 μatm to 520 μatm outside the kelp bed and from 80 μatm to 530 μatm inside the kelp beds in MB-BLB (Fig. 2). Seasonal changes are similar at both sites in the Morbihan Bay and at BLB. Values were below atmospheric equilibrium in summer (January) and then increased from February to April. CO_2 over-saturation appeared in February outside the kelp bed and in March inside the kelp beds. After a maximum in April, pCO_2 decreased until July to reach values close to atmospheric equilibrium during winter. The decrease of pCO_2 during spring and subsequent CO_2 under-saturation began earlier and was more marked inside the kelp beds (August) than outside (September). Outside the kelp beds, pCO_2 tended to increase during early November, while pCO_2 continued to decrease inside the kelp beds to reach the lowest values by the end of December.

The magnitude of diel variations of pCO2 n were on some occasions high, reaching 180 μatm outside the kelp beds, and 270 μatm inside (Fig. 5). From August to February, pCO_{2n} outside the kelp beds tended to reach minimum values between 12:00 and 18:00, however, recurrent diel cycles were hardly distinguishable, especially during winter. In contrast, diel cycles inside the kelp beds exhibited a clear pattern from November to April, with a strong increase of pCO_{2n} from 18:00 to 00:00 that rapidly led to highest values between 00:00 and 06:00. $pCO_{2\ n}$ started to decrease to reach the lowest values between 12:00 and 18:00. From May to July, no clear trends were observed in the diel changes of pCO_{2n}.

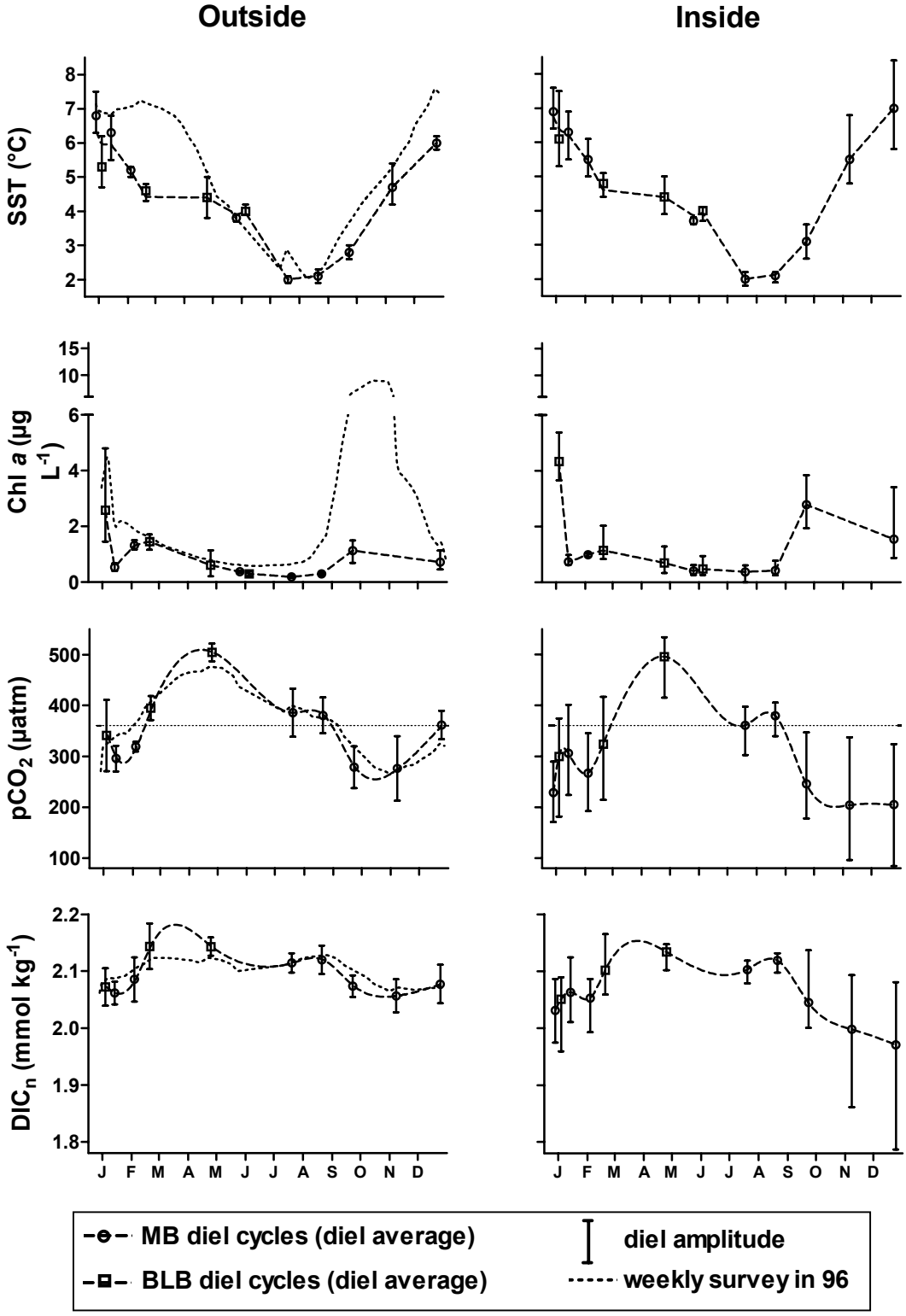
Outside
Inside
SST (°C)
Chl a (µg L-1)
pCO2 (µatm)
DICn (mmol kg-1)
J F M A M J J A S O N D
MB diel cycles (diel average)
BLB diel cycles (diel average)
diel amplitude
weekly survey in 96

Figure 2. Mean and amplitude of diel changes of temperature (SST), chlorophyll *a* (Chl *a*), partial pressure of CO_2 (pCO_2) and dissolved inorganic carbon normalized to a constant salinity of 33.4 (DIC_n). The vertical bars indicate the range of diel change (maximum and minimum values). Average values from the diel cycle inside and outside kelp beds, at the Cimetière Island in the Morbihan Bay (MB) are indicated by circles, and in the Brise-Lame Bay (BLB) by squares. Due to logistical constrains, MB measurements were not carried out during autumn while BLB measurements were carried out mostly during summer and autumn. Averaged values from both sites were merged into a composite annual cycle indicated by the long dash line in order to cover satisfactorily one annual cycle. The dotted line is the annual cycle at the Port aux Français station from Delille et al. (2000)The horizontal dotted line represents the atmospheric pCO_2 at Amsterdam Island (361 µatm, V. Kazan, personal communication).

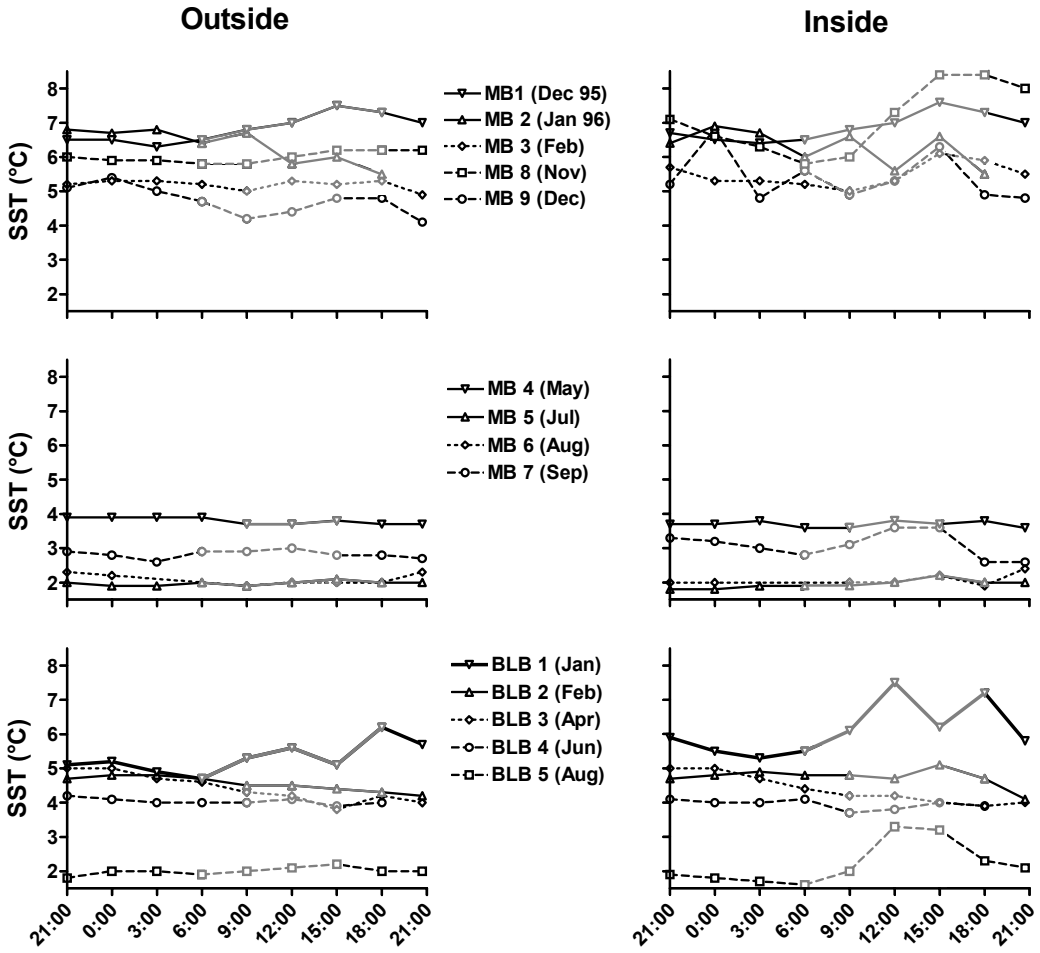

Figure 3. Diel changes of the sea surface temperature (SST) at the Cimetière Island in the Morbihan Bay (MB) and in the Brise-Lame Bay (BLB) inside and outside kelp beds. Daytime is indicated in grey on the lines.

In accordance with $pCO_{2\,n}$, DIC_n exhibited marked seasonal changes ranging from 2.03 mmol kg^{-1} to 2.13 mmol kg^{-1} outside the kelp bed, while values as low as 1.79 mmol kg^{-1} were observed inside the kelp beds (Fig. 2). DICn increased during late summer to reach a maximum in May, and decreased slightly until late August when a sharp decrease of DICn was observed. DICn began to increase outside the kelp bed in November in parallel with pCO2 n, whereas DICn decreased inside the kelp bed until January.

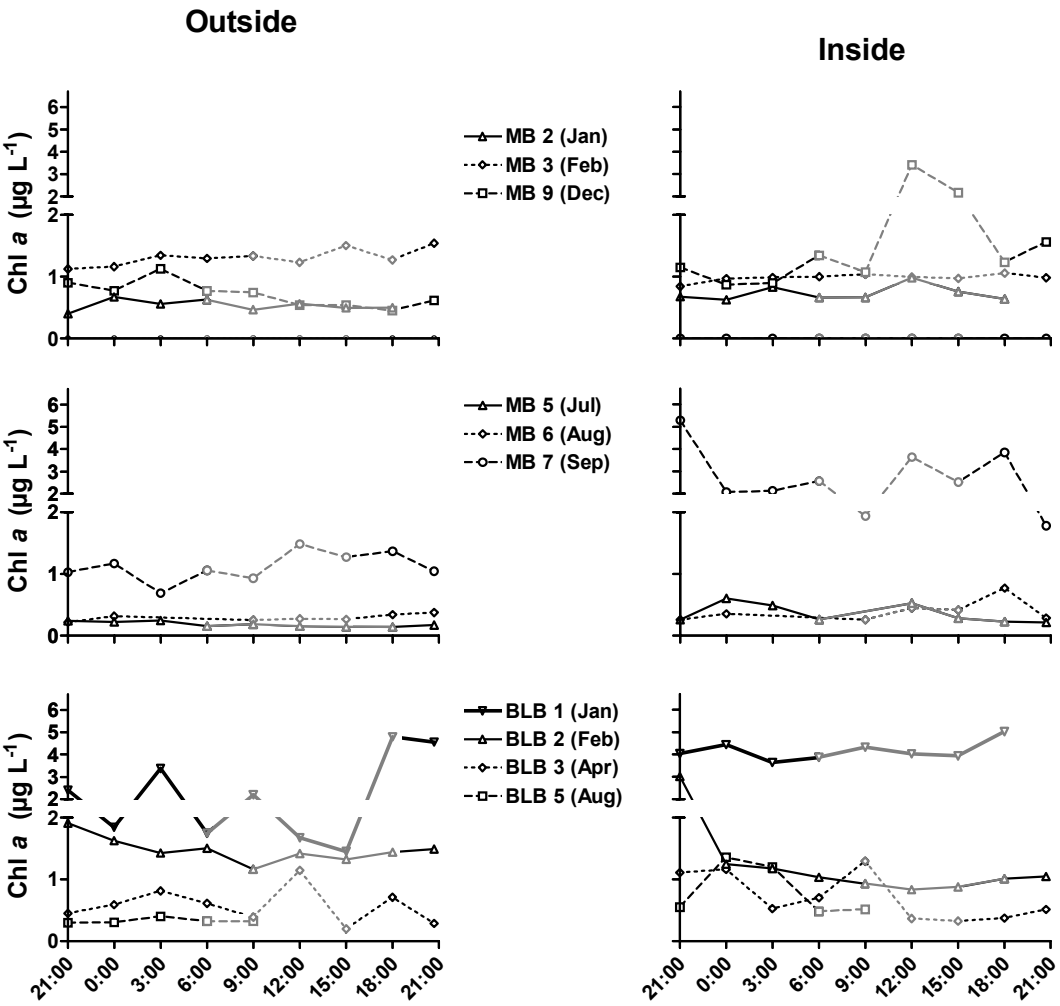

Figure 4. Diel changes of chlorophyll a (Chl a) at the Cimetière Island in the Morbihan Bay (MB) and in the Brise-Lame Bay (BLB) inside and outside kelp beds. Daytime is indicated in grey on the lines.

The magnitude of the diel changes of DIC_n outside the kelp beds did not exceed 0.08 mmol kg^{-1}, while inside the kelp beds diel changes up to 0.30 mmol kg^{-1} were observed. While no obvious recurrent pattern was apparent outside the kelp beds, DIC_n exhibited a clear diel cycle from November to April (Fig. 6). DIC_n increased steadily during night time, to reach a maximum between 03:00 and 09:00. Then, DIC_n decreased during day time to reach the lowest values between 12:00 and 18:00. During winter, diel changes of DIC_n were weak and did not show any obvious pattern, the cycle at MB7 excepted, which exhibited a large decrease at 03:00 and a sharp increase at 18:00.

3.2.6 Discussion

3.2.6.1 Seasonal variations

The overall seasonal changes of SST, pCO_2 and DIC_n outside the kelp bed in BLB-MB are consistent with those in the Port aux Français station based on a weekly monitoring carried out the same year by Delille et al. (2000) (Fig. 2). This suggests that the drivers of the seasonal variations of pCO_2 and DIC_n are similar for both sites. Planktonic photosynthesis in spring and summer is responsible for the marked decreases of both DIC_n and pCO_2, while autumnal decay of organic matter is responsible of a sharp increase of these two quantities, leading to a strong CO_2 over-saturation.

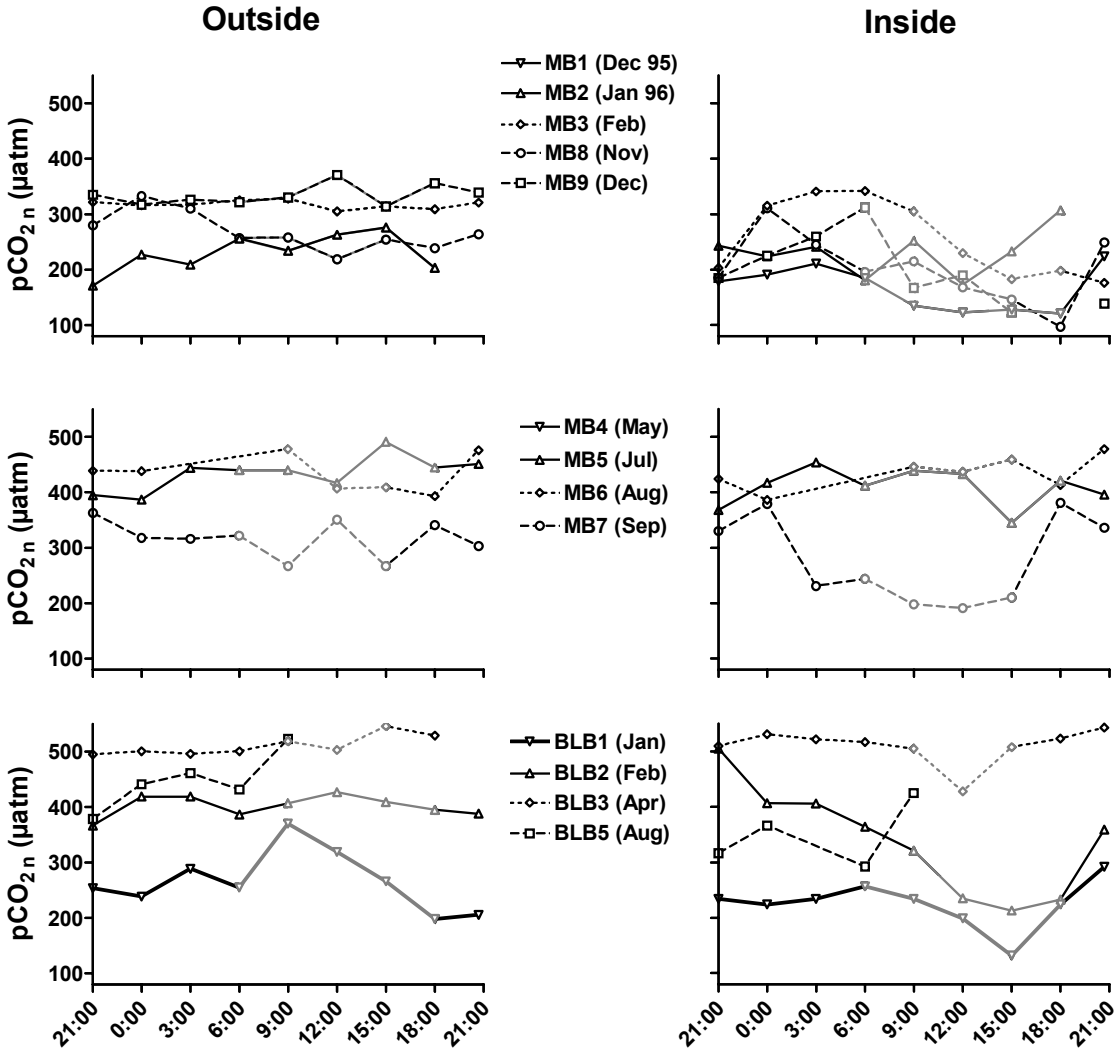

Figure 5. Diel changes of the partial pressure of CO_2 normalised to a constant temperature of 5°C and salinity of 33.4 ($pCO_{2\ n}$) at the Cimetière island in the Morbihan Bay (MB) and in the Brise-Lame Bay (BLB) inside and outside kelp beds. Daytime is indicated in grey on the lines.

In winter, cooling leads to a steady decrease of pCO_2 while air-sea exchanges enhanced by strong winds maintain values close to atmospheric equilibrium. In November and December, pCO_2 increases outside the kelp beds while pCO_2 remains constant inside the kelps, due to the primary production by the macroalgae and enhanced planktonic primary production (Delille et al., 2000). The large difference in Chl *a* concentrations between outside and inside the kelp bed during the MB7 cycle indicates that the kelp bed may enhance phytoplankton growth (Fig. 4). This is consistent with the earlier onset of the spring phytoplanktonic bloom inside the kelp bed, that could be due to the lower turbulence inside the kelp bed compared to outside, but other factors can not be excluded.

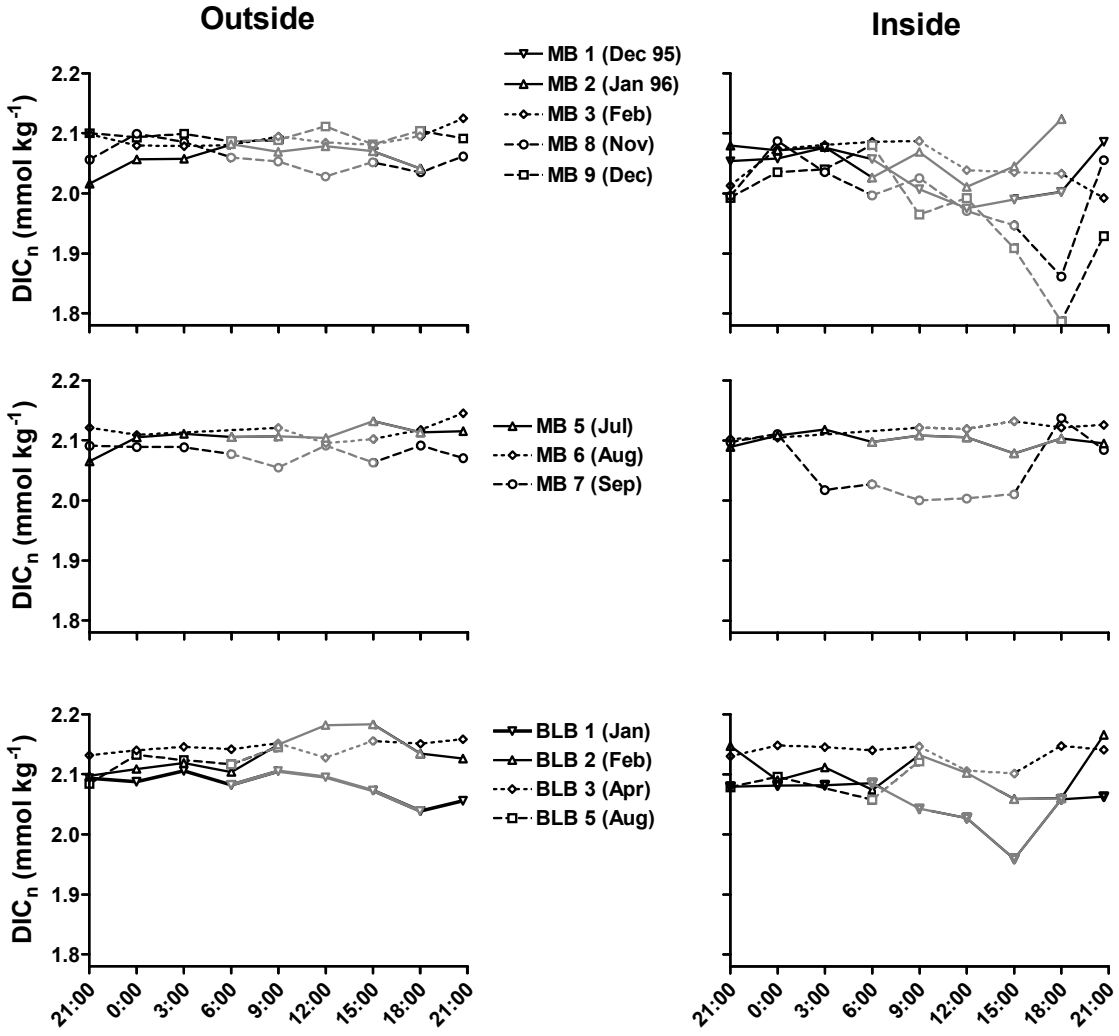

Figure 6. Diel changes of normalized DIC at a constant salinity of 33.4 (DIC_n) at the Cimetière island in the Morbihan Bay (MB) and in the Brise-Lame Bay (BLB) inside and outside kelp beds. Daytime is indicated in grey on the lines.

3.2.6.2 Diel variations

Outside the kelp beds, the magnitude of $pCO_{2\,n}$ and DIC_n diel changes can be as large as 180 μatm and 127 μmol kg^{-1}, respectively, but no clear trends emerge,

except from November to January when a weak decrease of $pCO_{2\ n}$ and DIC_n is observed during day time, due to higher phytoplankton biomass as indicated by the higher Chl *a* concentrations. In contrast, within the *Macrocystis* kelp beds, regular and recurrent diurnal $pCO_{2\ n}$ and DIC_n variations in phase with the solar cycle were observed. After dawn, both $pCO_{2\ n}$ and DIC_n strongly decrease on some occasions until dusk. Since $pCO_{2\ n}$ and DIC_n are independent from temperature or salinity changes, the variations of these quantities are due to the uptake or release of CO_2 from photosynthesis, by macroalgae and plankton. Photosynthesis induces a large decrease of pCO_2 during daytime, up to 270 µatm, especially inside the kelp beds where concentrations of CO_2 can shift from an over-saturation to an under-saturation. The amplitude of the daily changes of $pCO_{2\ n}$ and DIC_n are consistent with previous observations in Kerguelen Archipelago (Delille et al., 1997) and higher than above *Posidonia oceanica* meadows (Frankignoulle and Distèche, 1984; Frankignoulle and Bouquegneau, 1987; Frankignoulle and Bouquegneau, 1990). From spring to autumn, intense CO_2 uptake starts generally at dawn to reach a maximum on average 3 h before dusk. In some occasions, we observed a rapid increase at dusk followed by a plateau throughout the night (MB1, MB8, BLB2), when the expected effect from respiration on $pCO_{2\ n}$ and DIC_n would be a steady increase from dusk to dawn. This could be explained by the fact that during the daytime the kelp bed reduces currents and wind stress, and acts as black body at the surface, promoting an increase of SST (e.g. BLB 5 cycle on figure 3) and, potentially, the stratification of the near-surface water column. This would explain that SST can be 1.0°C higher inside than outside the kelp beds during daytime. At dusk, as temperature drops a rapid destratification of the near-surface water column would lead to a significant and rapid increase of $pCO_{2\ n}$ and DIC_n.

3.2.6.3 DIC uptake by the Macrocystis

Even if kelp beds favour the onset of the spring phytoplankton bloom, the large diel changes of $pCO_{2\ n}$ and $DIC_{\ n}$ are most likely related to the macroalgae primary production. High Chl *a* concentrations are solely observed between November and January whereas large diel cycles of $pCO_{2\ n}$ and DIC_n within the *Macrocystis* kelp beds are conspicuous from September to April (Fig. 2). Furthermore, Chl *a* concentrations are similar inside and outside the kelp bed, except in September. Even if *Macrocystis* kelp beds reduce currents and decrease turbulence (Jackson and Winant, 1983), this positive effect on planktonic primary production is probably counteracted by lower light availability and the competition for nutrients with the macroalgae. We hypothesize that planktonic production is similar inside and outside the kelp bed, and that the five times larger DIC uptake is mainly due to macroalgae primary production.

In order to follow the seasonal changes of primary production of the kelp bed community, we roughly assessed the DIC uptake by the kelp bed community (DIC_{kelp}) from the amplitude of the day time DIC_n decrease and removing the planktonic daytime DIC uptake, according to:

$$\Delta DIC_{kelp} = \Delta DIC_{n\,inside} - \Delta DIC_{n\,outside} \times \frac{chl\,a_{inside}}{chl\,a_{outside}} \qquad (1)$$

where ΔDIC_{inside} and $\Delta DIC_{outside}$ are the amplitude of the day time DIC_n decrease inside and outside the kelp bed, respectively; Cha_{inside} and $Cha_{outside}$ are the mean Chl *a* concentrations inside and outside the kelp bed, respectively.

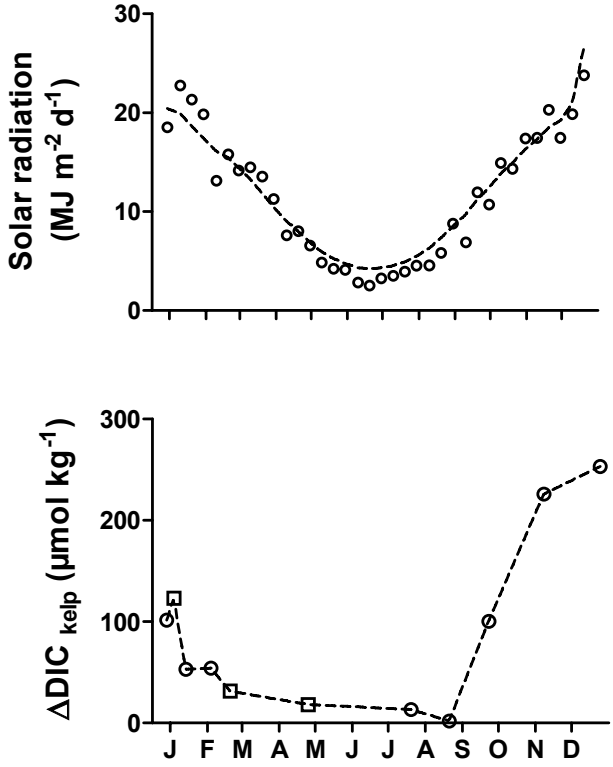

Figure 7. Seasonal variations of solar radiation in the Morbihan Bay and ΔDIC_{kelp} at the Cimetière Island in the Morbihan Bay (circles) and in the Brise-Lame Bay (squares).

This approach is prone to several errors. We assumed that planktonic primary productivity is similar inside and outside the kelp bed. We also hypothesize that phytoplankton primary production inside the kelp bed is correlated linearly with the chlorophyll a, although other factors (stratification, light availability, nutrients availability) are also likely to affect primary production. However, planktonic production outside the kelp beds by planktonic communities seems to be weak with regards to primary production by kelps and thereafter the error of the assessment of primary production by the kelps is weak accordingly. Air-sea exchange of CO_2 was not considered in the calculation, due to difficulty to estimate the gas transfer velocity above a *Macrocystis* kelp bed. The dense canopy of *Macrocystis* kelp bed covers a substantial portion of the air-sea interface preventing air-sea gas exchanges. Furthermore, the dense canopy of *Macrocystis* kelp beds dampens conspicuously waves and the effect of wind stress on the air-sea interface. *Macrocystis* also produce large amounts of biofilms that impede air-sea exchange. Theses effects are likely to decrease drastically air-sea CO_2 exchanges. We assumed that air-sea CO_2 exchange is negligible compared to the changes of CO_2 due to biological activity.

Significant advection at daily scale of waters surrounding the kelp beds can also affect DIC. However, Jackson and Winant (1983) showed that *Macrocystis* kelp beds reduce water currents, exchanges with surrounding waters, and that the residence

time of water within the kelp beds can reach several days. Accordingly, the higher Chl *a* concentrations inside the kelp beds observed during the MB7 cycle suggests that the residence time in the studied kelp beds is at least as long as the time for phytoplankton doubling.

Keeping in mind the potential biases mentioned above, it is possible by integrating ΔDIC_{kelp} over the depth of the water column, to derive the "maximum net kelp community production" during day time. Maximum net kelp community production integrates primary production and respiration of non-planktonic organisms (mainly the kelp and epiphytes communities) during daytime, when gross primary production outweighs community respiration leading to positive and elevated values of production. Maximum net kelp community production is not comparable with conventional measurements which provide either net or gross primary production. Nevertheless, the assessment of ΔDIC_{kelp} allows to consistently follow the seasonal changes of primary production of the kelps.

Figure 7 shows the seasonal changes of ΔDIC kelp. During winter ΔDIC kelp decreases in parallel to the decrease of solar radiation. In autumn and winter ΔDIC kelp is low but still detectable and continues to decrease to reach its minimum in August. The decrease of ΔDIC kelp throughout autumn and winter contrast with the study of Attwood et al. (1991) who observed that net production by *Macrocystis laevis* in the Prince Edward Islands was 50% higher in August than in April. In September, ΔDIC_{kelp} increases sharply together with solar radiation to reach a maximum in December at the time of solar radiation climax. On the whole, significant CO_2 consumption and related primary production occur from September to February while solar radiation is above the threshold of 1000 J cm^{-2} d^{-1}.

By integrating ΔDIC_{kelp} over the depth of the water column (5 m), we derive an assessment of maximum net kelp community production of *Macrocystis* kelp beds around 15 gC m^{-2} d^{-1} at its climax (ΔDIC kelp= 250 µmol kg^{-1}, MB9 cycle). This is two to five times higher than, respectively, maximum daily net and gross primary production by *Macrocystis* kelp bed in California assessed from model simulations (Jackson, 1987). Also, this estimate is above the range of average maximum above-ground production of 29 marine seagrass species from 0.01 gC m^{-2} d^{-1} to 5.0 gC m^{-2} d^{-1} reported by Duarte and Chiscano (1999), and well above the global average of macroalgae production of 0.3 gC m^{-2} d^{-1} reported by Charpy-Roubaud and Sournia (1990). These comparisons should be taken with caution due to the potential biases discussed above, and because our estimates integrate the production of the whole kelp bed community, rather than the only the macroalgae. Nevertheless, this highlights the significance of primary production by *Macrocystis* kelp beds located in high nutrients low chlorophyll (HNLC) Sub-Antarctic region of the Southern Ocean.

3.2.7 Conclusion

Nitrate concentrations in Morbihan Bay can exceed 20 µg L-1 and this nutrient is only briefly exhausted in spring (Delille et al., 2000). Hence, the main limiting factor of *Macrocystis* growth in the HNLC waters of the Kerguelen Archipelago appears to be light availability rather than macronutrients availability, as suggested by the tight link between primary production and light availability we report here, and in agreement with model output of Jackson (1987) of Californian kelp beds. Compared to other kelp

beds, to marine seagrass and to macroalgae, the primary production by sub-antarctic *Macrocystis* kelp beds is elevated. *Macrocystis* kelp beds would therefore act as effective sinks for atmospheric CO_2 by drastically decreasing DIC. However, related air-sea CO_2 transfer occurs outside the kelp bed when surface waters flow outward, rather than within the kelp bed where the dense canopy dampens gas fluxes across the air-sea interface. A rigorous assessment of CO_2 fluxes driven by *Macrocystis* kelp beds would therefore require an extended pCO_2 survey of surrounding waters coupled with assessment of water mass advection.

3.2.8 Acknowledgements

We thank V. Kazan for atmospheric pCO_2 data and MétéoFrance for meteorological data. This work could have not been done without the efficient and enthusiastic help of D. Rochard and J.M. Guédé and the other crew members of the *R.V. La Curieuse* as well as A.Lamalle and the volunteers of the Institut Paul-Emile Victor present in the Kerguelen Archipelago in 1996. This research was supported by the Institut Paul-Emile Victor, the Belgian Science Policy (contract A4/DD/B14, EV/7/12E, SD/CA/03A) and the FNRS with which AVB is a research associate.

3.3 Spatial and temporal variations of bacteria and phytoplankton in a subAntarctic coastal area (Kerguelen Archipelago)

3.3.1 Foreword

Surveys presented in the chapters 3.1 and 3.2 were conducted in near-shore shallow (less than 10 m depth) waters of the Kerguelen Archipelago which are probably influenced in some extent by *Marcosystis pyrifera* giant kelp beds. In order to extend the pCO_2 coverage to deeper waters, other surveys located inside and outside shleltered bay and fjords were conducted. The results of a one year survey have been splitted in two complementary chapters. Present chapter addresses the dynamics of microbial planktonic populations, while the chapter 3.4 addresses the pCO_2 dynamics and related air-sea CO_2 fluxes.

This part as been submitted for publication to Aquatic Microbial Ecology:

Delille D., F. Gleizon and B. Delille. Spatial and temporal variations of bacteria and phytoplankton in a subAntarctic coastal area (Kerguelen Archipelago).

3.3.2 Abstract

Bacterial abundance and production were measured monthly for one year along cross-shore transects (seven stations each) carried out in 3 subAntarctic fjords of the Kerguelen Archipelago. Mean values of the 3 most coastal (inside) and most offshore (outside) stations were used to describe the relationship between temperature, phytoplankton biomass, bacterial abundance and bacterial production over an annual cycle. All the sampling protocol was repeated two times during each cruise: at noon and midnight. During the entire sampling period temperature ranged from 2.1 to 7.4 °C, chlorophyll a concentrations varied by a factor of 10, bacterial abundance by a factor of 12 and bacterial production by a factor of 30. Over one day, all these parameters could vary by a factor of 4 between noon and midnight. A clear seasonality was observed for all the parameters. However, while variations of phytoplankton and bacterial production paralleled those of temperature, bacterial abundance is low in midsummer and maximum in autumn. While no general pattern could be observed from the total data set, spatial gradients could interfere strongly with temporal changes.

Keywords: Phytoplankton, Bacterioplankton, Seasonal changes, Diel changes, Spatial distribution, Kerguelen Archipelago, subAntarctica.

3.3.3 Introduction

Because the oceans are a significant sink for anthropogenic CO_2, a central objective of major biological oceanographic programs is to quantify, model and predict, at global and annual scales, the flux of biogenic carbon to deep waters. Bacterial assemblages have the potential to influence food web and biogeochemical cycles in aquatic systems (Cottrell & Kirchman 2004, Staroscik & Smith 2004). In the coastal area, production, degradation and export of organic matter are disproportionate compared to the open ocean (e.g. Wollast, 1998). Furthermore, phytoplankton primary production to community respiration ratios exhibited high spatio-temporal variability (Gazeau et al., 2004). Indeed, seasonal changes in growth rates and respiratory demands of aerobic heterotrophic bacteria, which dominate total community respiration, can induce changes from autotrophy to heterotrophy (Hopkinson 1985, Cho & Azam 1988, Fuhrman et al., 1989, Griffith et al., 1990, Wiebe et al., 1993, Delille 2003, Delille et al. 1995, 1996). The information available concerning the patterns of energy flow through the lower food web in polar regions is still scarce and often contradictory (Anderson & Rivkin 2001). Bacteria cannot be included convincingly in scenarios describing trophic interactions of plankton communities.

Since high nutrient-low chlorophyll Southern Ocean waters are characterized by high concentrations of inorganic nitrogen and phosphorus, bacterioplankton assemblages seem to be limited by DOC (Karl et al. 1991, Ducklow et al. 2001). Reviewing reports of phytoplankton and bacterial abundance and production, Cole et al. (1988) found significant correlations between bacterial and phytoplankton

parameters suggesting the ubiquity of a functional relationship between bacteria and phytoplankton. Since the latter excrete the organic substrates essential for bacterial metabolism, it can be assumed that bacterial dynamics are essentially controlled by phytoplankton dynamics (Smith et al. 1995). This model may be valid in the oceans, however, in coastal areas the situation is likely to be more complex due to important sources of non-phytoplanktonic substrates (Ducklow & Kirchman 1983, Bouvy et al. 1986, Alber & Valiela 1994, Smith & Benner 2005).

High latitude oceans account for about 10 to 20% of oceanic carbon production (Behrenfeld & Falkowski 1997). Although subAntarctic data are necessary for the construction of a global carbon budget for the Southern Ocean, investigations in the subAntarctic area have been much less numerous than similar Antarctic studies (Friedmannn 1993, Bernard & Froneman 2005). Furthermore most of the previous studies of microbial distribution focused on short-term observations in a limited period of time (Lochte et al. 1997, Duclow et al. 2001, Simon et al. 2004 and references herein). The seasonal variability in plankton biomass is poorly documented due to the scarcity of time series carried out over one or several years (Horne et al. 1969, Delille 1990, 2003 Helbling et al. 1995, Moline & Prézelin 1996). However, seasonal changes have to be understood in order to construct accurate carbon budgets (Platt et al. 1992, Priddle et al. 1992, Tréguer & Jacques 1992). This is particularly true for the Southern Ocean with intense temporal variability, perhaps the most extreme seasonality observed anywhere in the world ocean (Karl 1993). The purpose of the research presented here was to document the spatial and temporal distribution of bacterioplankton and phytoplankton in coastal subAntarctic area during a whole year.

3.3.4 Material and Methods

This survey was carried out from December 1998 to December 1999 in coastal surface waters of the Kerguelen Archipelago (Fig. 1). Usually, the Kerguelen archipelago (69°30'E, 49°30'S) is cited in the literature as a subAntarctic island However, from a strict oceanographic point of view, this archipelago is situated either in the Polar Frontal Zone (Sub-Antarctica) or Permanently Open Ocean Zone (Antarctica) depending of the position of the Polar Front with regards to the archipelago (e.g. Delille et al. 2000). Waters of the archipelago are always free of ice. Cross-shore transects were carried out in two fjords and one large bay. Located in the southeast of the archipelago, the Morbihan Bay (about 600 km²) opens to the ocean through the Royal Pass, which is 12 km wide and 40m deep. The fjords, Recques Bay and Table Bay, are located north and south of the archipelago, respectively. Recques bay is 14.5 km deep and 2 km wide while Table Bay is 10.5 km deep and 3 km wide and receives water from the Cook glacier.

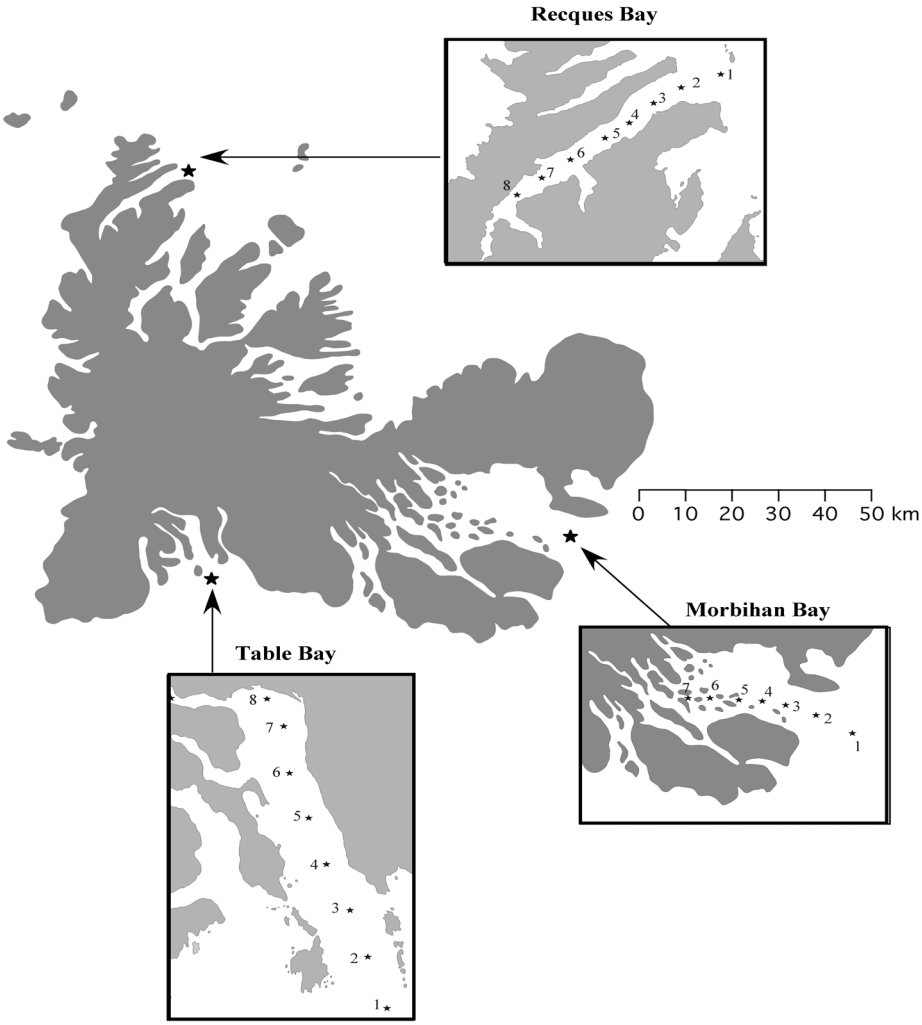

Figure 1. Location of the sampling stations in the Kerguelen Archipelago.

Water samples were collected at 1 m depth using a Niskin bottle. Analysis were performed onboard *R.V. La curieuse* within a few minutes after sample collection.

Water samples for chlorophyll *a* analysis were prefiltered through a 200 µm mesh filter to remove larger detrital material and the larger biota. 1000 mL of seawater were filtered through a Whatman GF/F glass-fibre filters at a vacuum differential < 20 cm Hg. Pigments were extracted in 90 % acetone in the dark at least two hours (Neveux & Panouse, 1987). Chlorophyll *a* concentrations were calculated by measurement of fluorescence using a Turner Designs fluorometer which had been calibrated against purified chlorophyll *a* (Sigma).

Total bacterial abundance were determined by epifluorescence microscopy (Hobbie et al. 1977). Direct counts (AODC) were performed using an Olympus BHA microscope with acridine orange staining onto a 0.2 µm pore size black Nuclepore filter. A minimum of 500 fluorescing cells with a clear outline and definite cell shape were counted under oil immersion (x 1000) in a minimum of 10 randomly chosen fields.

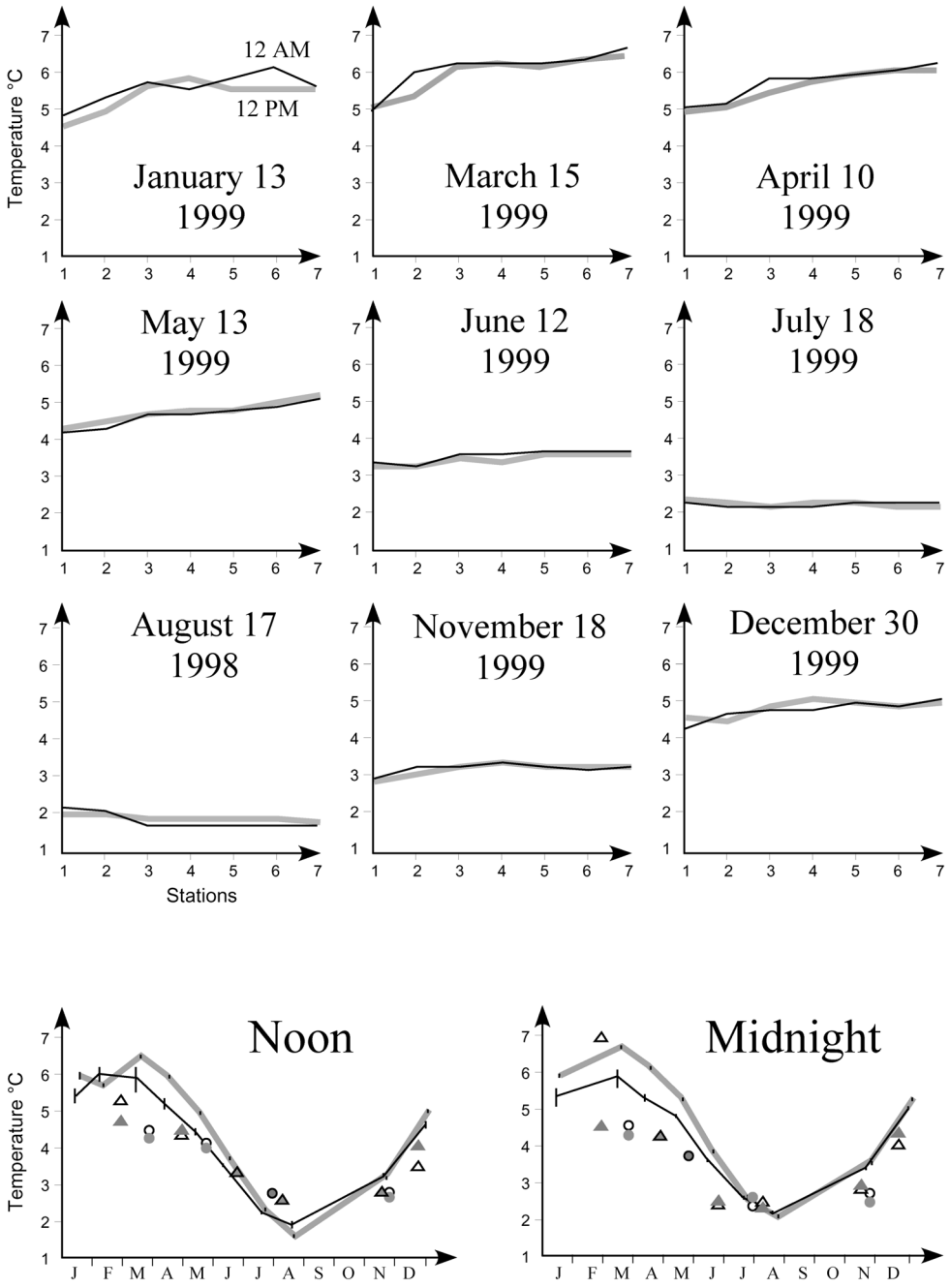

Figure 2. Top : Spatial distribution of surface seawater temperature in Morbihan Bay (thin black line : noon, thick gray line : midnight).

Bottom : Seasonal changes in surface seawater temperature (thin black line : outside stations of Morbihan Bay, thick gray line : inside stations of Morbihan Bay, open triangles : outside stations of Recques Bay, gray triangles : inside stations of Recques Bay, open circles : outside stations of Table Bay, gray circles : inside stations of Table Bay).

Bacterial production was measured via the incorporation of ^{14}C-leucine (Simon & Azam 1989). Sample water (10 mL) was amended with ^{14}C-leucine (final concentration 10 nmol L^{-1}). Aliquots of 5 mL were placed into 4 sterile vials, one of which contained 0.5 mL of 100% TCA as a killed control, and incubated for 4 h in the dark in flowing seawater tables. Incubations were terminated by the addition of TCA to a final concentration of 5%. The results obtained were converted to bacterial carbon production (BCP, g) using the equation :

BCP = $leucine_{inc}$ x (100/7.3) x 131.2 x 0.86

where $leucine_{inc}$ = moles of leucine incorporated, 7.3 = mol% of leucine in protein, 131.2 = formula weight of leucine, and 0.86 = conversion of a gram of protein produced to a gram of carbon. Previous studies showed that this calculation is appropriate in the Southern Ocean (Pedros-Alio et al. 2002, Simon et al. 2004).

After tenfold dilutions in sterile aged seawater, viable heterotrophic platable bacteria were counted using the spread plate method with 2216 E medium (Oppenheimer & ZoBell, 1952, Marine Agar DIFCO). Each dilution were plated in triplicate. After inoculation (0.2 mL) the plates were incubated at 18°C for 10 days (mesophilic/psychrotrophic assemblages) or 4°C for 20 days (psychrotrophic/psychrophilic assemblages).

3.3.5 Results

The temperature ranged from 2.1°C to 7.4 °C over the sampling period (Fig. 2). In the Morbihan Bay, salinity usually ranged from 33.42 to 33.68, but in a given transect maximum range of variation was 33.28 to 33.68 (February 5).

3.3.5.1 Spatial distribution

Spatial distribution of biological parameters of all the transects carried out in the Morbihan Bay are presented in Fig. 3,4,5,6 & 7.

Chlorophyll a could vary 10 fold along a same transect (Fig.3, January 13). The highest values were then observed in the coastal zone (excepted the most coastal station). However opposite gradient were also observed (November 18 and December 30) and the concentrations were roughly low and constant during winter.

Within a given transect total bacterial abundance varied less than 10 fold (Fig.4). Maximum range of variation was observed in autumn (March 15). Total bacterial abundance often decreased with the distance from the coast (February 5, August 17 and November 18) but this is not a general pattern.

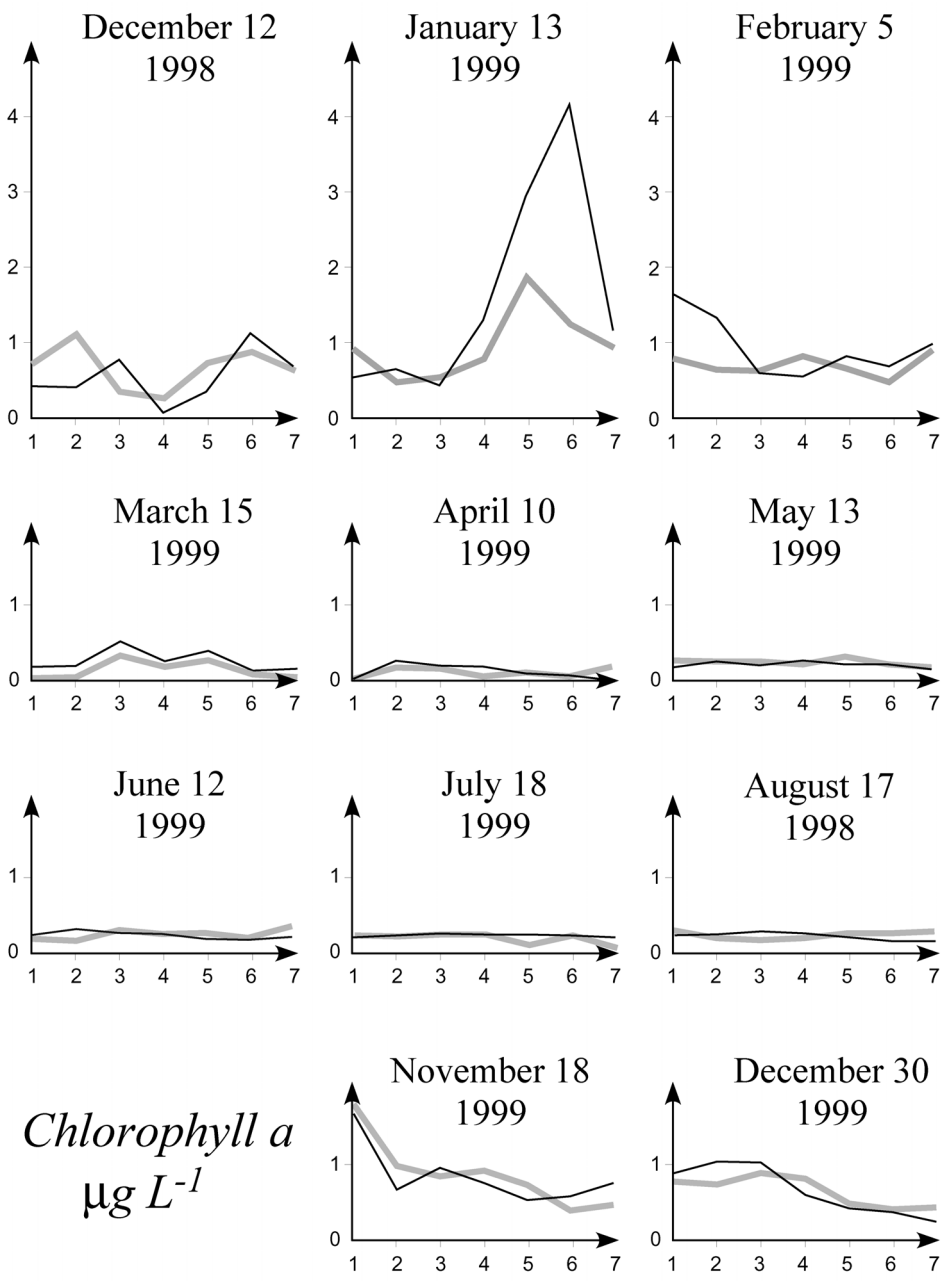

Figure 3. Spatial distribution of chlorophyll *a* concentration in surface seawater of the Morbihan Bay (thin black line : noon, thick gray line : midnight).

Leucine incorporation showed strong spatial variation during the warmer periods (Fig.5). More than ten fold ranges were observed (December 12, January 13, February 5 & November 18). Like for bacterial abundance there was no clear general pattern. However, the greatest values were often observed in the more coastal station.

Within a given transect psychrotrophic heterotrophic bacterial abundance could vary more than 10 fold (Fig. 6). Despite the clear increasing gradient from the outer stations to the more coastal ones observed in February 5, like for other bacterial parameters, there were no general patterns in the spatial distribution. The spatial distributions of the psychrophilic heterotrophic bacterial assemblage (Fig. 7) paralleled those of the psychrotrophic one.

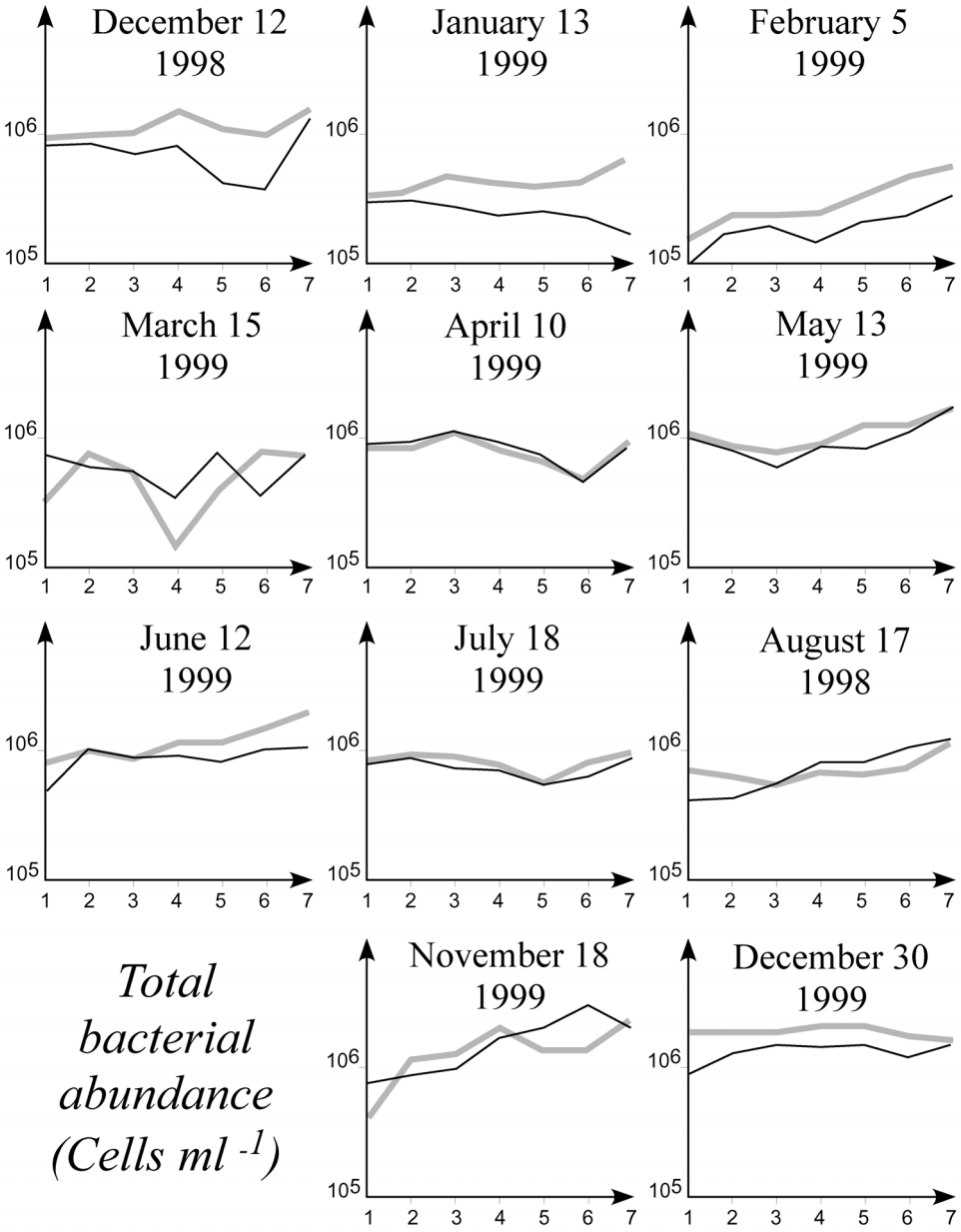

Figure 4. Spatial distribution of total bacterial abundance in surface seawater of the Morbihan Bay (thin black line : noon, thick gray line : midnight).

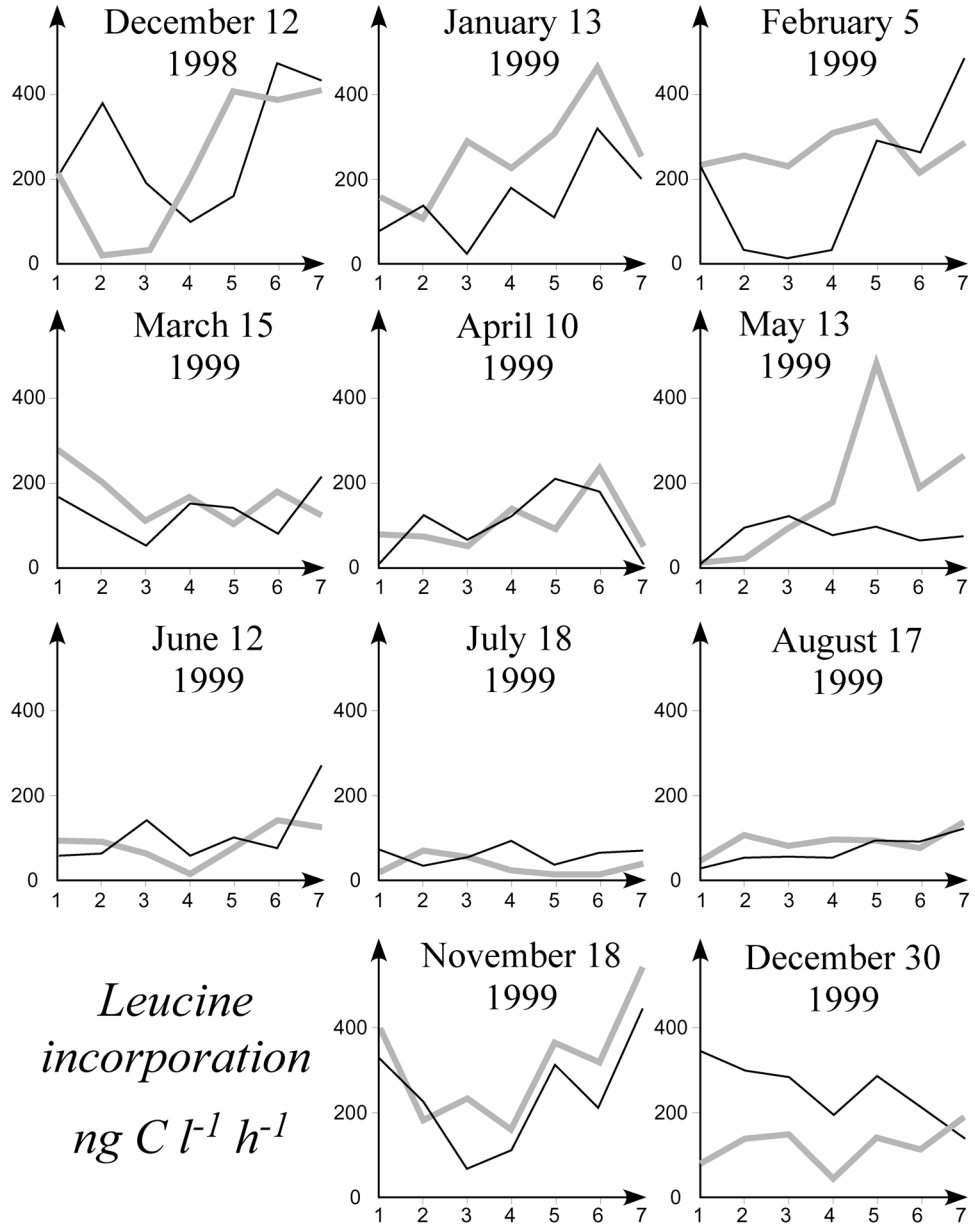

Figure 5. Spatial distribution of bacterial production in surface seawater of the Morbihan Bay (thin black line : noon, thick gray line : midnight).

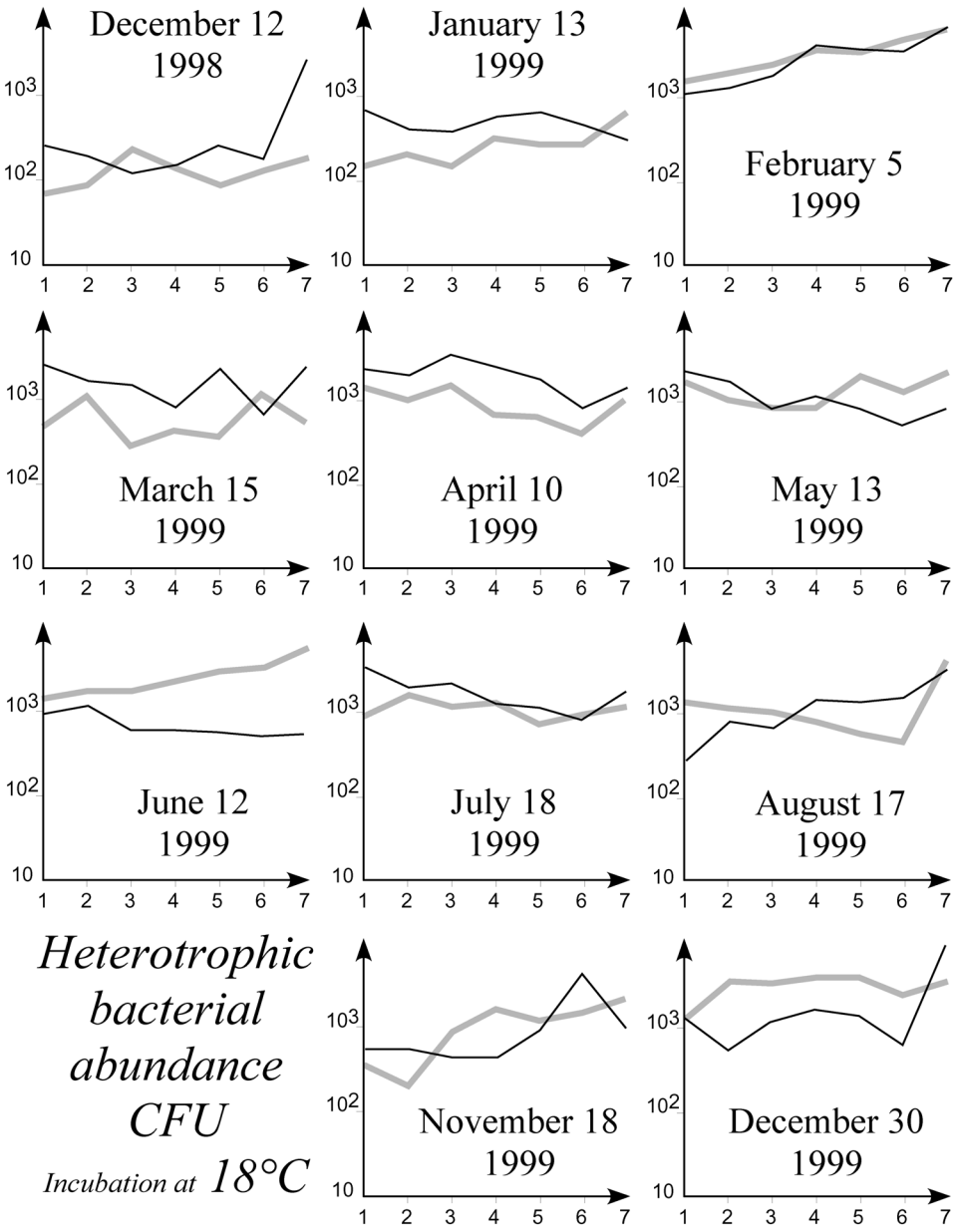

Figure 6. Spatial distribution of "psychrotrophic" heterotrophic bacterial abundance in surface seawater of the Morbihan Bay (thin black line : noon, thick gray line : midnight).

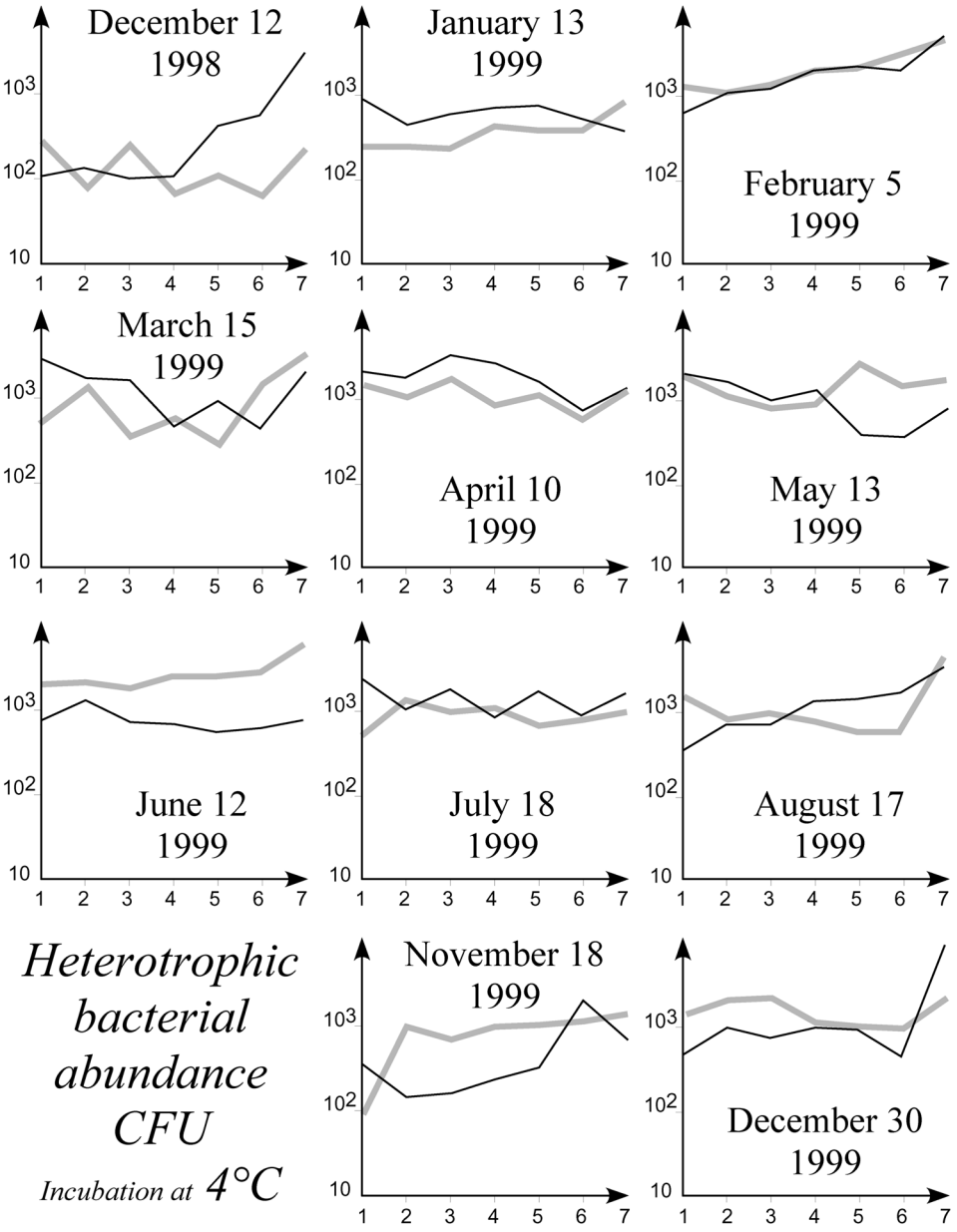

Figure 7. Spatial distribution of "psychrophilic" heterotrophic bacterial abundance in surface seawater of the Morbihan Bay (thin black line : noon, thick gray line : midnight).

3.3.5.2 Diel changes

Chlorophyll *a* could vary 2 fold between night and day (Fig. 3, January 13 & February 5). In both case phytoplankton biomass was lower during the night than during the day.

A comparison of noon and midnight data showed that bacterial abundance tend to be higher during the night relative to daytime at any given station of summer transects (Fig. 4, December to February). Bacterial abundance could be 2 times higher at midnight than at noon as observed in December (December 12, 1998).

Leucine incorporation could varied 5 fold between night and day (Fig.5, February 5 & May 13. Excepted for the two transects realized in December, the stronger differences corresponded to an increase of the bacterial production during the night.

One order of magnitude changes in the more psychrophilic heterotrophic bacterial abundance could occur between night and day (Fig. 7, December 12). The corresponding range was only of 5 fold for less psychrophilic ones (Fig. 6). Despite this difference there was a conspicuous resemblance between the data obtained under the 2 different incubation temperatures. There was no clear general pattern. Heterotrophic bacterial abundance could be higher during the day (April 12) or during the night (June 12). The two data sets were merged to compute seasonal averages.

3.3.5.3 Seasonal changes

For each transect, we have averaged the data of the 3 most coastal stations (inside) and offshore stations (outside) in order to distinguish clear seasonal trends. Results are shown in Fig. 8.

Chlorophyll *a* showed clear seasonal variations with maximal values in summer (January) and minimal values in winter. In the coastal zone, total annual ranges were 0.15 ± 0.03/ 2.77 ± 1.48 $\mu g\ L^{-1}$ at noon and 0.11 ± 0.08 /1.38 ± 0.47 $\mu g\ L^{-1}$ at midnight. Corresponding values were 0.18 ± 0.04/ 1.15 ± 0.47 $\mu g\ L^{-1}$ at noon and 0.20 ± 0.08 /1.19 ± 0.53 $\mu g\ L^{-1}$ at midnight offshore. Thus, chlorophyll *a* varied 18 fold at noon in the coastal zone and only 6.6 fold at midnight in the same area and no more than 6 fold in the offshore zone.

The seasonal pattern of bacterial production was rather similar to the one of chlorophyll *a,* with maximal values in summer and minimal ones in winter. In the coastal zone, total annual ranges were 44 ± 17/ 394 ± 156 ng C L^{-1} h^{-1} at noon and 82 ± 29/648 ± 209 ng C L^{-1} h^{-1} at midnight. Corresponding values were 27 ± 15/307 ± 30 at noon and 45 ± 14/336 ± 106 ng C L^{-1} h^{-1} at midnight in the offshore zone. The seasonal range of fluctuation of bacterial production is thus relatively constant during the day and along the coastal/offshore gradient (about 10 fold in any situation). However the values recorded at the inner stations seemed larger during the night than during the day.

The seasonal pattern of total bacterial abundance was more complex. A first maximum was observed in January then minimal values were measured in late summer (late January/February). A first increase was observed from February to June, followed by a small decrease in July and August. A second peak of abundance was observed in November. In the coastal zone, total annual abundance ranged from $1.8 \times 10^5 \pm 7.3 \times 10^4$ to $2.4 \times 10^6 \pm 2.5 \times 10^5$ cells mL^{-1} at noon and from $4.4 \times 10^5 \pm 1.0 \times 10^5$ to $1.7 \times 10^6 \pm 3.1 \times 10^5$ cells mL^{-1} at midnight. Corresponding values in offshore zone ranged from $1.3 \times 10^5 \pm 6.2 \times 10^4$ to $1.4 \times 10^6 \pm 3.2 \times 10^5$ at noon and from $2.0 \times 10^5 \pm 4.2 \times 10^4$ to $1.8 \times 10^6 \pm 1.0 \times 10^4$ cells mL^{-1} at midnight. Thus, total bacterial abundance varied 13 fold at noon in the coastal zone and only 3.9 fold at midnight in the same area. In the offshore zone total bacterial abundance varied 11 fold at noon and 10 fold at midnight.

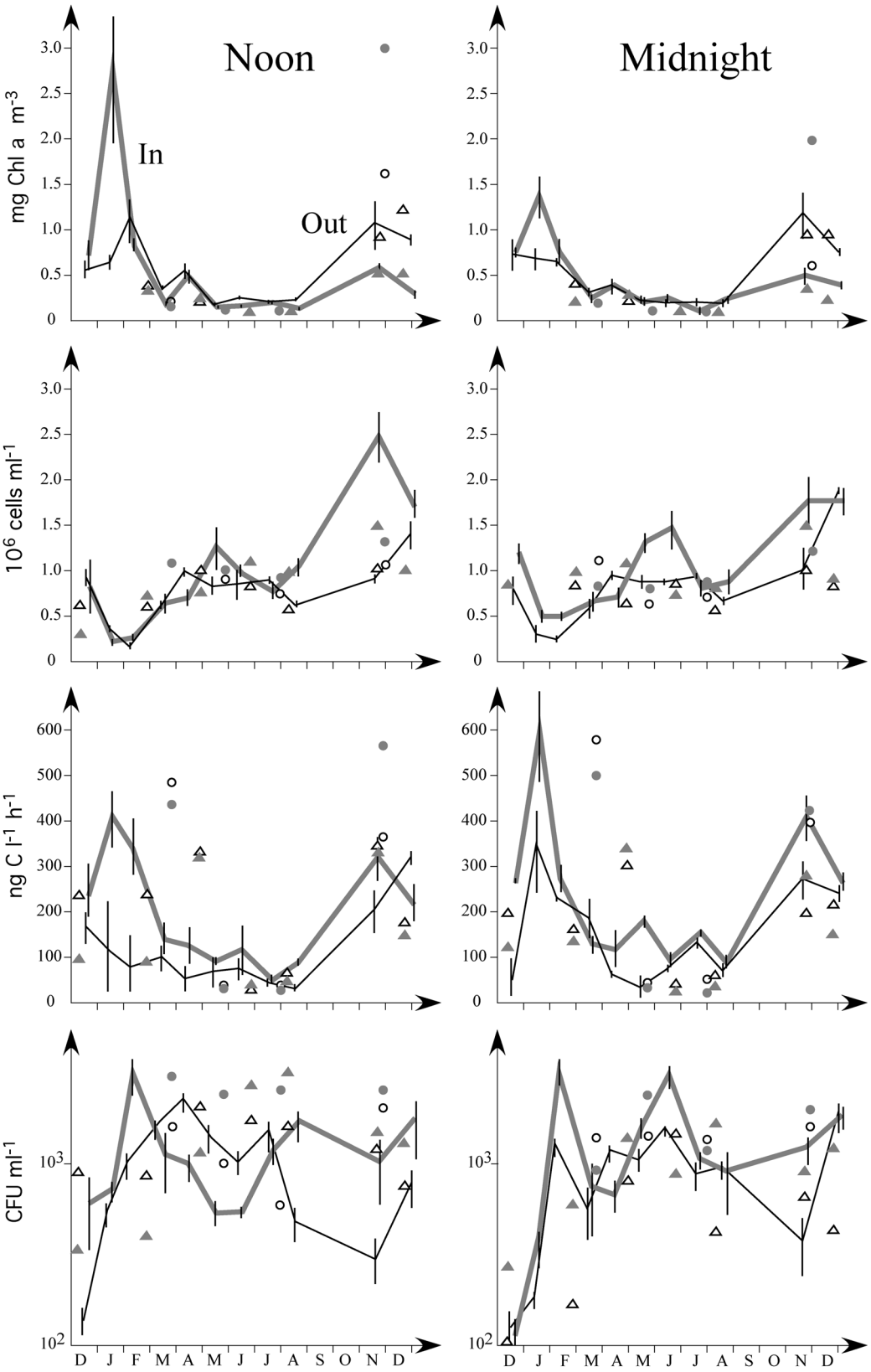

Figure 8. Seasonal changes in chlorophyll *a,* total bacterial abundance, bacterial production and heterotrophic bacterial abundance (thin black line : outside stations of Morbihan Bay, thick gray line : inside stations of Morbihan Bay, open triangles : outside stations of the Recques Bay.

The seasonal pattern of heterotrophic bacterial abundance differed greatly from that of temperature, Chlorophyll *a* and bacterial production. Several small growth phases could be distinguished. However, minimal values were generally observed in summer and maximal values in winter. At noon heterotrophic bacterial abundance varied 16 fold in both coastal and offshore zone while at midnight it varied 28 fold in the coastal zone and 14 fold in the more offshore area.

3.3.6 Discussion

The highest chlorophyll *a* values observed during the survey (2.77 $\mu g\ L^{-1}$) were lower than the values obtained previously during spring blooms in a coastal station of the Morbihan bay (generally between 7 and 20 $\mu g\ L^{-1}$, with a maximum around 50 $\mu g\ L^{-1}$, Delille *et al*. 1996, Delille et al. 2000) but were of the same magnitude as those observed around subAntarctic and Antarctic islands (Perissinotto *et al*. 1992, Whitehouse *et al*. 1993). In contrast, the data collected from 1990 to 1994 at the station Kerfix located in the Indian sector of the Southern Ocean, southwest off Kerguelen Archipelago showed lower concentration of phytoplankton with a maximum of 1.2 $\mu g\ L^{-1}$ (Fiala et al. 1998). In the present study chlorophyll *a* varied 18 fold between winter and summer. This seasonal range is far below that observed in Antarctica by Anderson & Rivkin (2001). They reported a 1000-fold increase of chlorophyll *a* in McMurdo Sound between late August and early January. Even if our data correspond to mean values and thus probably underestimate possible extreme variations, this observation highlights the differences between Antarctic and subAntarctic conditions. Even if the maximum values of chlorophyll *a* concentrations reported in McMurdo Sound (4 to 6 $\mu g\ L^{-1}$) are higher that the values observed around Kerguelen Islands during this study, the major difference lies in the minimal values, which were much lower in Antarctica, probably due to the sea-ice cover that is always absent in Kerguelen region. Using an average C:Chl *a* ratio of 35, the phytoplanktonic biomass ranges from 4 to 100 $\mu g\ C\ L^{-1}$.

Using an average bacterial cell mass of 60 fg C $cell^{-1}$ (Delille 2003) bacterial biomass would range from 8 to 15 $\mu g\ C\ L^{-1}$. This biomass is relatively high compared to the data available for the open Southern Ocean (Hodson et al. 1981, Cota et al. 1990, Goeyens et al. 1991, Delille 1992, 2003) but are consistent with the values reported in the Bransfield Strait (4 to 28 $\mu g\ C\ L^{-1}$, Karl et al. 1991, 8 to 34 $\mu g\ C\ L^{-1}$, Vosjan & Olanczuk-Neyman 1991), the southern Antarctic Pacific zone (9 to 82 $\mu g\ C\ L^{-1}$, Sazhin 1993) and the Terre Adélie coastal area (1 to 30 $\mu g\ C\ L^{-1}$, Delille 1993). Despite the uncertainties related to the use of questionable conversion factors, phytoplanktonic biomass seems to dominate the bacterial one in the coastal waters of the Kerguelen Archipelago. This contrast with the situation observed at Kerfix station in the offshore waters south-western of the archipelago, where bacterial biomass exceed phototrophic biomass (Delille 2003) .

In the Antarctic polar frontal region, Simon et al. (2004) reported bacterial production values ranging between 9 and 40 ng $C\ L^{-1}\ h^{-1}$ during summer and autumn (December to May). The higher values observed in the coastal zone of Kerguelen

Archipelago could be related to both higher temperature and larger availability of nutrients.

Salinity changes were too small to explain the differences observed in biological parameters. Many other factors act to control bacterial activity, two of which are temperature and substrate availability. The relative importance of these two factors is not well understood (Hoch & Kirchman 1993). Temperature has been reported to have only a rather limited influence on Antarctic and subAntarctic bacterioplanktonic populations (Delille et al. 1988, Vincent 1988, Delille & Perret, 1989, Fukunaga & Russell, 1990; Vosjan & Olanczuk-Neyman, 1991, Nedwell & Rutter, 1994). Important regulating factors of the subAntarctic bacterial communities are related to the available trophic sources (Delille & Bouvy 1989, Delille & Perret 1991). The bacterial assemblage in the Kerguelen coastal area showed strong seasonality. Both abundance and production varied with time but their variations were not parallel. Production reaches a maximum in January while bacterial abundance is at the lowest. In a temperate estuary, Coffin & Sharp (1987) observed that while bacterial production remained high over the summer months, bacterial abundance was kept low by microflagellate grazing. In the Arctic Ocean, Anderson & Rivkin reported that even if grazing losses of bacteria were insignificant immediately before and after phytoplankton bloom, microzooplankton could consume 90% of local bacterial production. Bacterivory communities were not quantified in this study, but they may have contributed to the low summer bacterial abundance. In addition to grazing, the reduced rates of fall bacterial production may result from bacterioplankton having consumed enough of the available organic carbon to become substrate limited. Heterotrophic bacterial abundance are only representative of culturable bacteria, however, it is a useful bacterial indicator corresponding to a small group of active bacteria that react immediately to the changes in their nutrient supply (Delille & Bouvy 1989, Rheinheimer et al. 1989). The large development of heterotrophic assemblage during autumn and winter observed in the present study is thus a clear indication of the availability of organic substrates. Temperature is probably the most important regulating factor of bacterial production during this period.

In contrast, the diel variations of temperature were certainly too small to explain the corresponding changes of bacterial biomass and production. Diel vertical migration of zooplankton as been reported in numerous part of the ocean. Such migration could have an impact on bacterivory. Algal metabolism (phytoplankon or macroalgae) obviously change between day and night (Mague et al. 1980). Variation in DOC excretion rate must play an important regulating role in diel variation of bacterial parameters. Diel variability of the growth of heterotrophic planktonic bacteria has been previously related to changes in phytoplankton and zooplankton activity (Riemann & Søndergaard 1984, Wheeler et al. 1989, Delille et al. 1997). No consistent pattern in the diel bacterial activity, however, can be deduced from these studies. This holds true in the present study. This is presumably due to the fact that relationships between diel changes of phytoplankton, zooplankton and bacterioplankton activity are intricate and differ between aquatic environments. Short-term changes in bacterial quantities might be explained by a tight coupling to photosynthetic processes as well as by changes of water masses. Advection during diurnal cycles is a possible explanation for bacterial variability (Karner & Rassoulzadegan 1995, Delille et al. 1997).

Concentrations of particulate and dissolved organic carbon vary spatially. This variation is driven by he inputs from both plankton and terrestrial sources. Plankton-

derived organic matter is enriched in protein and labile polysaccharides, whereas terrestrial organic matter contains humic material and structural polysaccharides, such as cellulose and lignin, which are relatively resistant to mineralization by microbial processes (Delille & Perret 1991, Benner 2002). Terrestrial material would not play a major role because of the complex detrital processing cycle that would largely dissipate the carbon and energy (Peterson et al. 1994) The abundance and composition of POM and DOM could have short-term (days) impacts on bacterial metabolism. Rates of constitutive enzymes can respond quite rapidly, on the order of minutes to hours, whereas days may be required for a rare ribotype to increase sufficiently in abundance before to affect significantly DOM mineralization at the community level (Findlay 2003). Between these two extremes, the induction and synthesis of new enzymes occurs within hours (Kirchman et al. 2004). The response of bacteria to phytoplankton or any other organic matter availability changes is not instantaneous; rather, bacterial activity is dependent upon previous activity of phytoplankton or allochtonous organic inputs. The montly sampling used in the present study would be therefore insufficient to capture all the relationships between bacteria and their trophic sources. Indeed, even a weekly sampling may be insufficient to capture all the relationships between phytoplankton and bacteria (Staroscik & Smith 2004).

3.3.7 Conclusion

Temperature variations are larger in subAntarctic coastal area than in the surrounding open oceanic zone, with obvious consequences on the microbial network. In contrast, the range of seasonal variations of phytoplankton is smaller in the subAntarctic coastal area than in the Antarctic one. This is probably related to the absence of ice cover. In Kerguelen fjords low winter temperature seems to limit bacterial production and in a lesser extend bacterial abundance.

Changes in bacterial abundance are not necessarily related to changes in bacterial growth. Steady-state abundance is the balance between growth and mortality; hence, the loss rates due to bacterivory and viral lysis must be similar to cell growth. Even a small imbalance may result in large oscillations in bacterial populations (Anderson & Rivkin 2001). Short term changes could be as large as long term seasonal changes. Interactive effects of temperature and substrate supply could occur (Pomeroy & Wiebe 2001). The data available do not allow us to decipher the main regulating factor. It is therefore likely that grazing, viral lysis, substrate availability and temperature adaptation all play a role in the regulation of the bacterial communities.

3.3.8 Acknowledgements

We are indebt to the efficient and enthusiast help of the captains and crew members of the *R.V. La Curieuse.* This research was supported by the "Institut Français pour la Recherche et la Technologie Polaires" and the Belgian Science Policy (contract A4/DD/B14, EV/7/12E, SD/CA/03A).

3.4 pCO_2 dynamics and related air-sea CO_2 fluxes in the Kerguelen Archipelago (Sub-Antarctica)

3.4.1 Foreword

In chapters 3.1 and 3.2, we addressed the dynamics of pCO_2 in the shallow waters of the Kerguelen Archiepelago. The impact on air-sea exchange on the CO_2 dynamics is addressed in both chapters, but we did not budget the air-sea CO_2 fluxes *per se*. Surveys of pCO_2 presented in the chapter 3.1 and 3.2 were conducted in near-shore shallow (less than 10 m depth) areas of the Archipelago. Dynamics of pCO_2 was strongly influenced extent by *Marcosystis pyrifera* giant kelp beds. Maximal net community production within the kelp is significant and primary production of the kelp lasts almost all the year 3.2 We therefore conducted other surveys in 1998 and 1999 which aimed to extend our pCO_2 coverage to deeper waters located inside and outside the sheltered bay and fjords. We computed first CO_2 fluxes in a Subantarctic coastal area and budgeted annual air-sea CO_2 fluxes in near-shore water surrounding the archipelago.

This is a companion chapter to the chapter 3.3 that focuses on microbial dynamics.

Some sections of this chapter were published in:

Dehairs F., C. Lancelot, L. André, M. Frankignoulle, E. Dellersnijder, S. Becquevort, D. Cardinal, T. Cattaldo, B. Delille, M. Elskens, N. Fagel, H. Gosse, E. Hannon, G. Probst, V. Schoemann, E. Kopczynska & A. Kostianoy, 2003. An integrated approach to assess carbon dynamics in the Southern Ocean. Belgian Scientific Research Programme on the Antarctic Phase 4, vol 1: Marine biota and Global change, +pp 160 (www.belspo.be/belspo/home/publ/index_en.stm)

This more extended present version will be submitted for publication to Polar Biology:

Delille B., F. Gleizon, A.V. Borges and D. Delille. pCO_2 dynamics and related CO_2 fluxes in Kerguelen Archipelago (Sub-Antarctica).

3.4.2 Introduction

The coastal ocean has been to a large extent ignored in global carbon budgets, owing to its limited surface area. However, the coastal ocean receives inputs of carbon and nutrients disproportionately high in comparison with its surface area, exchanges large amounts of matter and energy with the open ocean and constitutes one of the most biogeochemically active areas of the biosphere (Gattuso et al., 1998; Wollast, 1998). As a consequence, intense air-water CO_2 exchanges are observed (Borges, 2005) and it has been argued that coastal air-sea CO_2 fluxes are significant at regional (Frankignoulle and Borges, 2001; Borges et al., 2003; Borges et al., 2005) and global scales (Tsunogai et al., 1999; Thomas et al., 2004; Borges et al., 2005).

The Subantarctic and Antarctic coastal areas have received little attention in relation to partial pressure of CO_2 (pCO_2) dynamics and related CO_2 fluxes. To our best knowledge, only three studies addressed these issues and pointed out that coastal Antarctic and Subantarctic coastal areas exhibit intense pCO_2 dynamics (Gibson and Trull, 1999- chapters 3.1 and 3.2). The Southern Ocean is a High Nutrient-Low Chlorophyll (HLNC) region owing to several factors and in particular to the limitation of phytoplankton growth by the low concentrations of iron (e.g. de Baar et al. (2005)). Blain et al. (Blain et al., 2001) suggested that natural iron fertilization occurs in the waters surrounding the Kerguelen Archipelago which potentially supports enhanced primary production. However, these authors reported chlorophyll a (Chl a) concentrations of most coastal waters lower than expected according to their iron content. This discrepancy was attributed to high grazing pressure. In contrast, a survey of pCO_2 and related parameters carried out in the shallow waters of the Morbihan Archipelago in 1996 and 1997 showed that pCO_2 reaches significant under-saturation with pCO_2 values down to 160 µatm owing to high Chl *a* concentrations up to 71 µg L^{-1} (chapter 3.1). This suggests that high primary production can occur in the shallow waters of the Archipelago.

Here, we investigate the pCO_2 dynamics of near-shore and offshore waters surrounding the Kerguelen Archipelago, and propose a first annual budget of air-sea CO_2 fluxes in a Subantarctic coastal area.

3.4.3 Material and Methods

Sites and sampling

The Kerguelen Archipelago is usually cited in the literature as a Subantarctic archipelago. From a strict oceanographic point of view, this archipelago is situated either in the Polar Frontal Zone (Sub-Antarctica) or Permanently Open Ocean Zone (Antarctica) depending of the position of the Polar Front (PF) with regards to the archipelago (e.g. Delille et al. 2000). Waters of the archipelago are always free of ice. Cross-shore transects were carried out in three bays (Morbihan Bay, Recques Bay and Table Bay). Located in the southeast of the archipelago, the Morbihan Bay (about 600 km²) opens to the ocean through the Royal Pass (12 km wide and 40m deep). Recques Bay (14.5 m deep and 2 km wide) and Table Bay(10.5 m deep and 3km wide), are located north and south of the archipelago, respectively. Table Bay receives fresh water from the Cook glacier.

This study was carried out in two phases. The first phase lasted from November 1998 to January 1999 and consisted in underway measurements of pCO_2 carried out during opportunity cruises onboard the R.V. Marion Dufresne and R.V. La Curieuse. The second phase lasted from December 1998 to December 1999 and consisted in short cross-shore transects carried out in the three bays (Fig. 3.4-2). Due to logistical constrains, the first cross-shore transect in the northern part of the archipelago was carried out in Rhodes Bay. Results from this transect are reported with the other northern transect carried out in Recques Bay. During these cross-shore transects pCO_2 was computed from pH and total alkalinity (TA) measurements, in parallel with Chl *a* and bacterial abundance. In order to overcome daily variability, cross-shore transects were carried out twice during the same day; one around noon and one around midnight. We present the average of both transects. Samples were collected at 1 m depth using a Niskin bottle, and analysis were carried out onboard within a few minutes after sample collection.

First phase

Underway pCO_2 measurements

The complete description and performance test of the system for pCO_2 measurements have been reported by Frankignoulle et al. (2001). Briefly, pCO_2 was measured continuously from the uncontaminated seawater supply of the ship. A non-dispersive infrared gas analyser (IRGA, Li-cor® LI-6262) was used to measure pCO_2 in air equilibrated with seawater. The IRGA was calibrated daily using two gas standards of 0 ppm and 345.4 ppm. Seawater flows into the equilibrator (3 L min^{-1}) from the top, and a closed air loop (3 L min^{-1}) ensures circulation through the equilibrator (from the bottom to the top), a desiccant (Drierite®), and the IRGA. Temperature at the outlet of the equilibrator was monitored using a platinum resistance thermometer (Metrohm®). The pCO_2 values were corrected for the temperature difference between *in-situ* seawater and water in the equilibrator, using the algorithm proposed by Copin-Montégut (1988,1989).

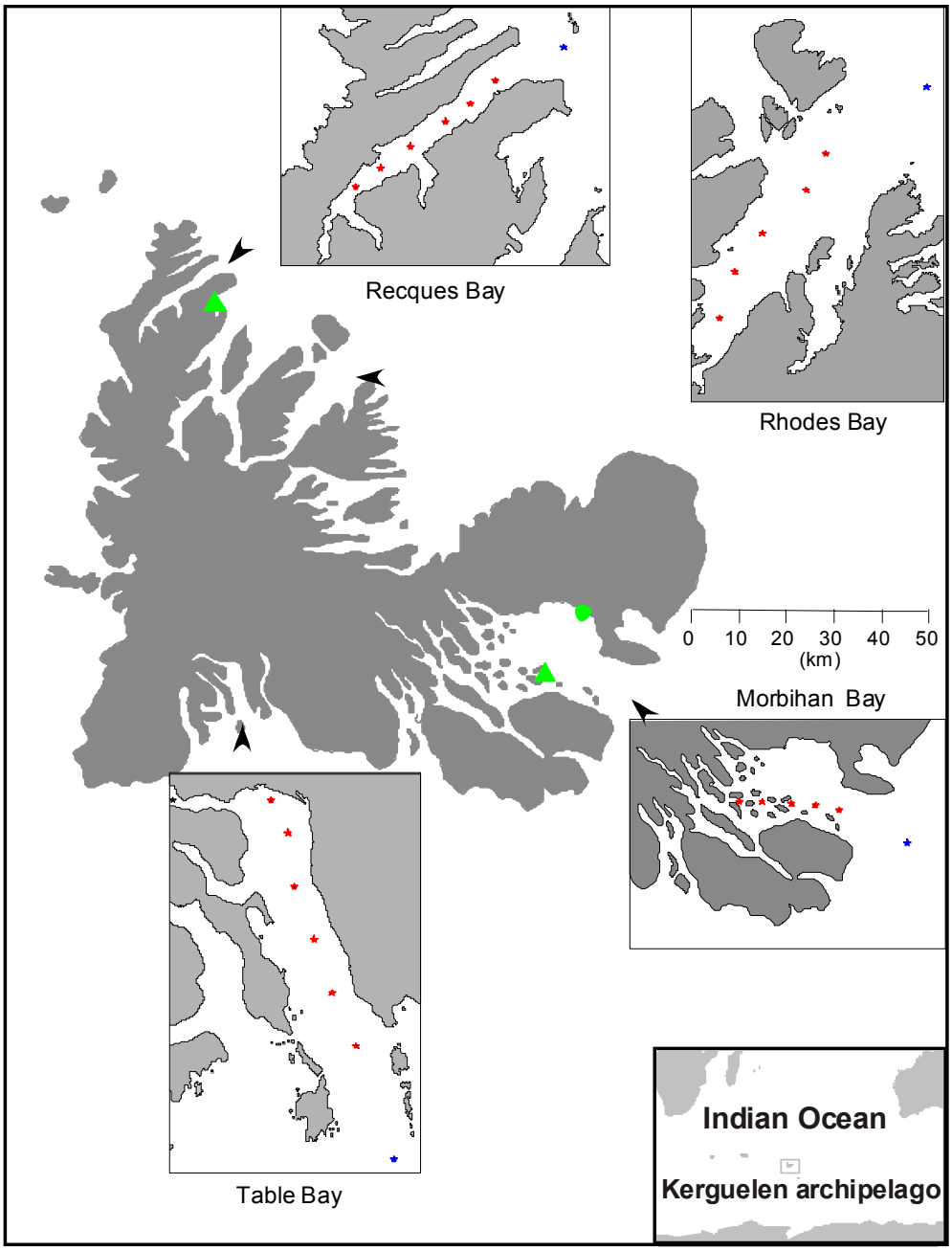

Figure 3.4-1. Sampling stations during the second phase of the present study together with the locations of the surveys carried out in 1996 and 1997 (chapter 3.1 and 3.2).

Stars: location of the stations of the cross-shore transect (blue – outer, red – inner). Green plain circle: location of the weekly survey carried ut from 1996 to 1997. Green triangles, sites of the diel cycles carried out in 1996.

Second phase

Dissolved inorganic carbon

pH was measured using a commercial combination electrode (Ross type, Orion®) calibrated on the total hydrogen ion scale using TRIS (2-amino-2-hydroxymethyl-1,3-propanediol) and AMP (2-aminopyridine) buffers prepared according to Dickson (1993). The accuracy of pH measurements was ±0.01 pH units. TA was measured using the classical Gran electrotitration method on 100ml GF/F filtered samples. The

accuracy of measurements was ±4 µmol kg^{-1}. Dissolved inorganic carbon (DIC) and pCO_2 were computed from pH and TA measurements using the CO2SYS Package (Lewis and Wallace, 1998; Pelletier et al., 1998), with the CO_2 acidity constants of Mehrbach et al. (1973) refitted by Dickson and Millero (1987), the CO_2 solubility coefficient of Weiss (1974), the SO_4^{2-} dissociation constant of Dickson (1990a), the borate acidity constant of Dickson (1990b), and the total borate molality calculated using the Uppström (1974) ratio to salinity.

Chlorophyll a.

Samples were prefiltered through a 200 µm mesh to remove detritic material and larger biota, and then filtered by gentle vacuum of 1 L of seawater through a Whatman® GF/F glass-fibber filter. The measurements of Chl a were carried out with a Perkin-Elmer® MPF 66 spectrofluorometer using the spectrofluorometric method developed by Neveux and Panouse (1987)

Bacterial abundance

Total bacterial abundance was determined by epifluorescence microscopy (Hobbie et al. 1977). Direct counts (AODC) were performed using an Olympus BHA microscope with acridine orange staining onto a 0.2 µm pore size black Nuclepore® filter. A minimum of 500 fluorescing cells with a clear outline and definite cell shape were counted under oil immersion (x 1000) in a minimum of 10 randomly chosen fields.

Related parameters.

Salinity was determined with a Guildline® induction salinometer with an accuracy of ±0.003 on the practical salinity scale. Wind speed was measured at the MétéoFrance station located in the Morbihan Bay. Spatial distribution of Chl a in the Kerguelen offshore waters was derived from sea-viewing wide field-of-view sensor (SEAWFIS) monthly level-3 standard mapped images available from the OceanCoulour website at http://oceancolor.gsfc.nasa.gov/.

3.4.4 Results and Discussion

3.4.4.1 Spring and summer distribution of pCO_2

Western, southern and northern waters

SEAWIFS images (Fig. 3.4-2) provide a synoptic overview of spatial and temporal distribution of Chl a concentration in the waters off the Kerguelen Archipelago. From October 1998 to January 1999, a high-Chl a plume develops eastward of the archipelago above the Kerguelen Plateau and spread southwards to Heard Island (51°S 74°E). The most extensive high-Chl *a* plume was observed in December 1998 and January 1999, while Chl a concentrations peaked in January and February 1999.

The high-Chl *a* plume approximately follows the shape of the continental shelf break westward and extends beyond the continental break eastward. In the vicinity of the archipelago, the plume spreads westward as far as the shelf break and follows approximately the shape of the north-eastern 100 m isobath.

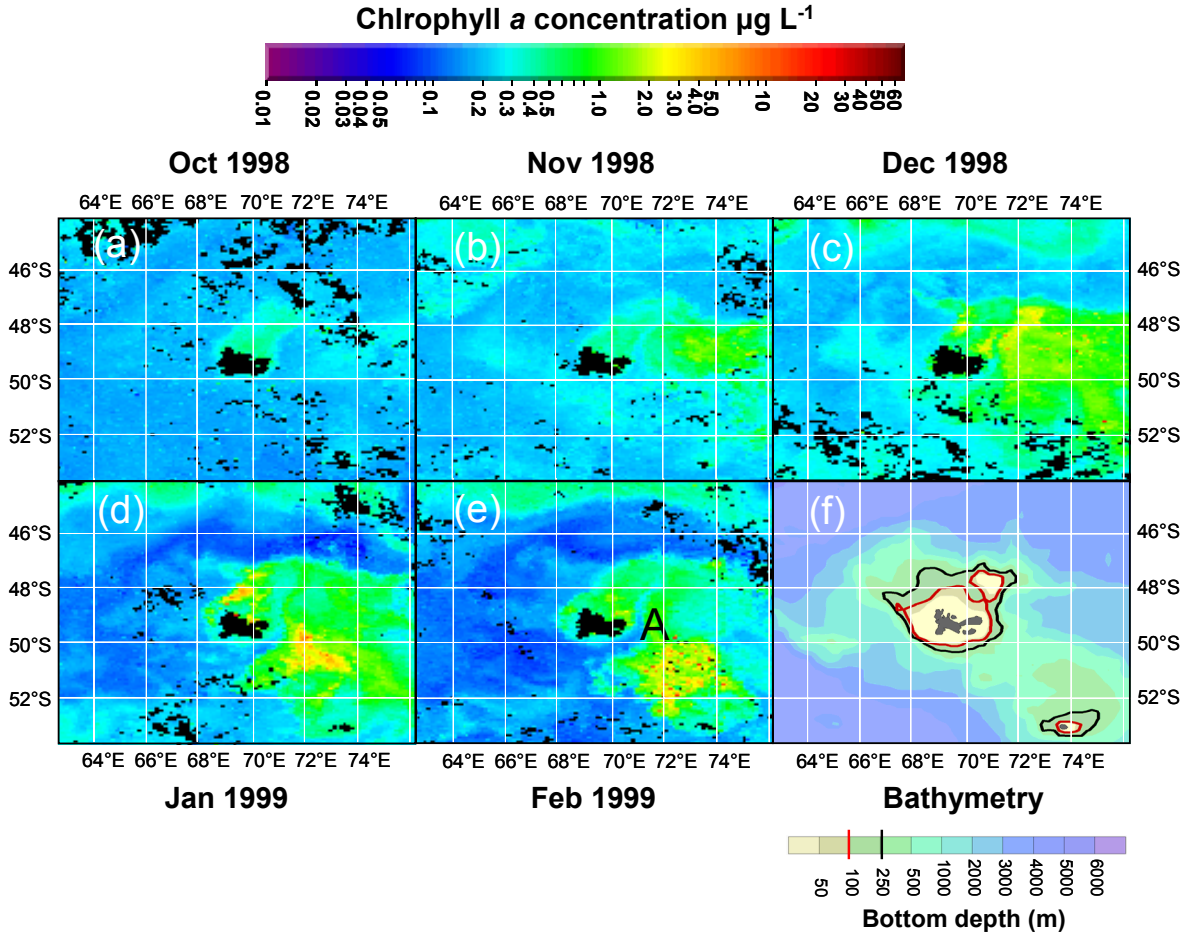

Figure 3.4-2. (a) to (e): Monthly Chl *a* concentration derived from SEAWIFS data from October to Feb 1999 in the water off Kerguelen Archipelago. (f) Bottom topography of the Kerguelen plateau. The A letter denotes a persisting tongue of low-Chl *a* waters which originate south of the archipelago, goes round the south-eastern part of the archipelago and spread northwards.

During the surveys carried out on 11/19/1998 and two months later on 01/15/1999, pCO_2 west of the Archipelago at 68°E was about 370 µatm (Fig. 3.4-3), close to atmospheric PCO_2 (365 µatm). On 19/11/1998, pCO_2 increased by 10 µatm between 68°E and 69°E suggesting that pCO_2 in the coastal waters south of the archipelago were slightly higher that the background values in the open waters west of the archipelago. pCO_2 slightly decreased along the southeastern part of the archipelago, close to the shore, and exhibited a dramatic decrease (down to 330 µatm) in the inner waters of the Morbihan Bay. In the same way, during the survey carried out from 25/11 to 29/11/1998 in the southern part of the archipelago, pCO_2 was close to atmospheric equilibrium 13 km away from shore, increased to 400 µatm 8 km away from shore, and decrease down to 350 µatm in Table Bay, and even lower, down to 270 µatm, in the adjacent Mouche Bay.

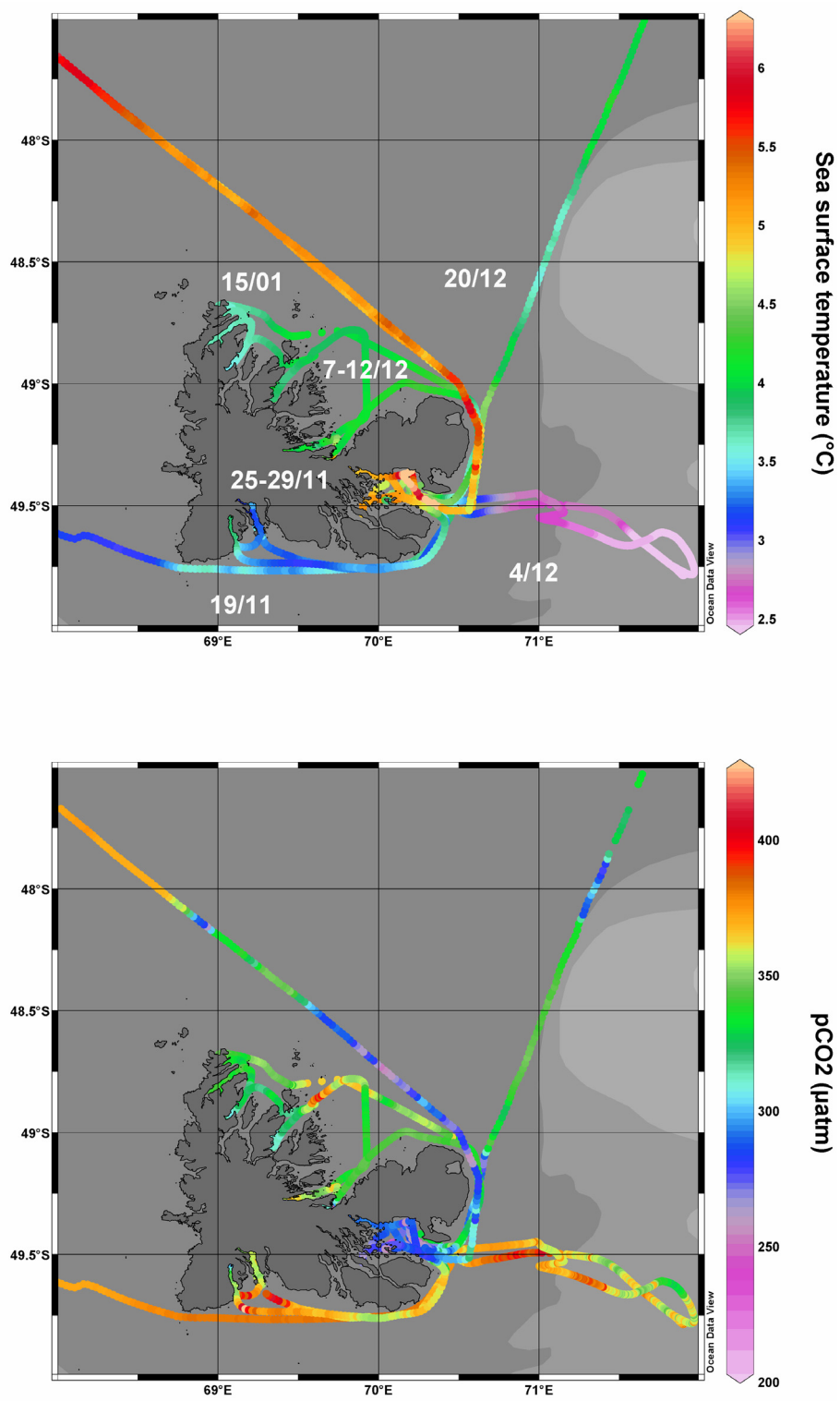

Figure 3.4-3. Sea surface temperature and pCO_2 distribution in the waters surroundin Kerguelen Archipelago observed from 19/11/1998 to 15/01/1999 during the first phase of the study.

In contrast, surveys carried out in the northern part of the archipelago 10 days after, from 7/12 to 12/12/1998, exhibited under-saturation of CO_2 with pCO_2 values ranging from 300 µatm to 350 µatm along the east coast. In the northern part, pCO_2 ranged from 320 µatm close to shore to 350 µatm in the northern part 30 km off shore (with a small patch of over-saturated waters at 69.5°E). This is consistent with the higher Chl a concentration in the northern part compared to the concentration in the southern part of the archipelago (fig. 3.4-2) that is of the same order of magnitude than the open waters west of the archipelago. pCO_2 values decrease in the fords, down to 305 µatm.

The two early summer transects carried out on 12/20/1998 and 15/01/1998, in the high-Chl *a* plume of the archipelago exhibited marked CO_2 undersaturation with pCO_2 values ranging from 290 µatm to 350 µatm, even far away from the shore at the eastern limit of the shelf on 12/20/1998. pCO_2 values in the high-Chl *a* plume were in the same range of values, one month later on 15/01/1998. However, pCO_2 exhibited a sharp increase across the western limit of the plume, which corresponds to the 100 m isobath, to reach values close to PCO_2, corresponding to the background value of the open waters west of the archipelago.

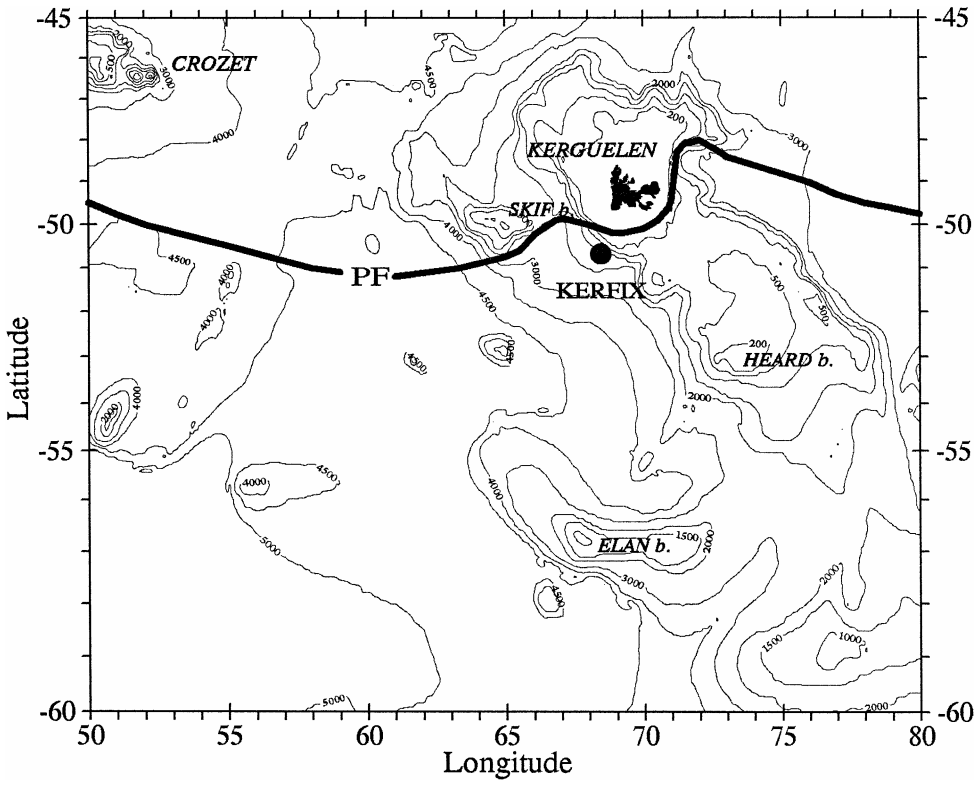

Figure 3.4-4: Location of the time series station KERFIX (black plain circle) with the bathymetry around Kerguelen Islands superimposed. The position of the Polar Front is indicated according to Park et al. (1993) , Park and Gamberoni (1997) and Park et al. 1998 (1998a). After Park et al. (1998b).

In the Chl a-poor coastal waters south of the archipelago, pCO_2 values were slightly higher than the background value of the open waters, while marked CO_2 undersaturation was observed in the high-Chl *a* plume in the northern part of the archipelago. The lowest pCO_2 values were observed in the inner waters of the bays.

The signature of the high-Chl a plume is remarkably well reflected in the pCO_2 mesoscale distribution.

Eastern part

South of the archipelago, a persisting tongue of low-Chl a waters (denoted by the A letter on the figure 3.4-2e) spreads eastwards, rounds up the south-western part of the main island to shift northwards, following the 200 m isobath. This feature is likely to be the signature of the jet associated to the PF, as the tongue closely follows the track of the PF proposed by Park et al. (1998b – Fig. 3.4-4). Such intrusion of Antarctic Surface Water (AASW) appears to be a recurrent feature as it was previously observed in October 1978 and January 1999 by Blain et al. (2001). These authors measured relatively high concentration of iron in the intrusion and ascribed the low Chl a content to an unfavourable light regime.

.

The intrusion of the AASW associated to the jet of the PF is well reflected in the sea surface temperature (SST) distribution (Fig. 3.4-3) observed during the latitudinal transect carried out on 04/12/1998. SST ranges from 2.35°C to 2.80 °C east of 70.5 °E, the lowest value observed during the survey. This intrusion of AASW is well marked in the Chl a concentration distribution, as a clear tongue of low Chl a concentration which follows the 71°E meridian, east of the archipelago. This decrease of Chl a concentration is consistent with an increase of pCO_2 (Fig. 3.4-3) From west to east, pCO_2 values increase sharply out of the Morbihan Bay, up to 406 µatm at 71°E. pCO_2 values decrease westwards down to 327 µatm. West of 71°E, the distribution of pCO_2 is heterogeneous, with patches of CO_2 under-saturation and of CO_2 near-saturation. Such patchy pCO_2 distribution above the Kerguelen plateau was previously reported by Poisson et al. (1993). and was ascribed by these authors to biological activity, since they assumed that surface currents were weak in the area according to Gambéroni et al. (1982) and Park et al. (1991). However, the close vicinity of the PF jet suggests that this mesoscale variability may be due to physical processes related to the jet, since such frontal structures strongly affect the mesoscale distribution of pCO_2 (chapter 2.2).

3.4.4.2 Seasonal pCO_2 variations in near-shore waters

The figure 3.4-5 shows the seasonal changes of Chl a concentration, bacterial abundance and pCO_2 at the stations of the cross-shore transects carried out in 1999, together with daily averages of the diel cycles carried out in 1996 (chapter 3.2), and the weekly surveys carried out from 1996 to 1997 in the near-shore shallow waters of the Morbihan Bay (chapter 3.2).

On a seasonal scale, pCO_2 values around the Kerguelen Archipelago range from 270 µatmn in January and November to 580 µatm in May. In the inner Morbihan Bay, the pCO_2 seasonal pattern is consistent with those observed in 1996 and 1997 in the shallow waters of bay. Outside the bay, the magnitude of pCO_2 variations is slightly weaker and minimum of pCO_2 values occur later in the year outside the Morbihan Bay than inside. This is consistent with the spatial distribution of pCO_2 which shows

an enhanced CO_2 under-saturation inside the Morbihan Bay compared to outside waters (Fig. 3.4-3).

.

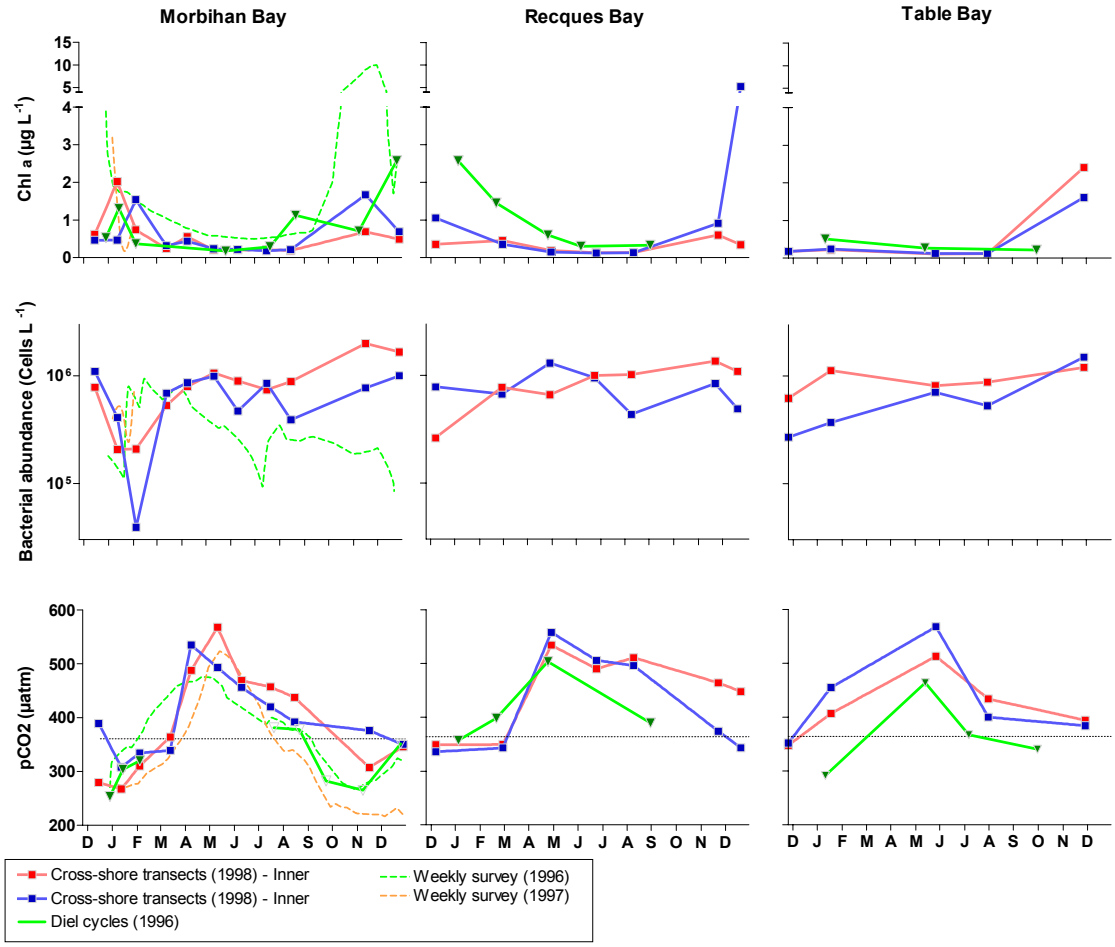

.

Figure 3.4-5 Seasonal changes of Chl *a* concentration, bacterial abundance and pCO_2 in the Morbihan Bay, Recques Bay and Table Bay.

Blue and red solid lines: 1998-99 surveys (blue: outer station; red: average of the 5 inner stations). Green solid line: average of the diel cycles carried out in 1996 outside the *Macrocystis* kelp bed (chapter 3.2). Dashed line: weekly survey carried out in 1996 (green) and 1997 (orange) in the shallow waters of the Morbihan Bay outside *Macrocystis* kelp beds (chapter 3.1.). Diel cycles carried out in the Brise-Lame Bay have been reported together with cross-shore survey of the Recques Bay located 3 km away from Brise-Lame Bay.

pCO_2 changes observed during cross-shore transects are consistent to the Chl *a* pattern. Two phytoplankton blooms with Chl *a* concentration up to 2 µg L^{-1} can be distinguished. Spring bloom occurs in November, which coincides with the bloom observed in 1998 while summer bloom occurs in January. In spring, bacterial abundance was at its climax, indicating an enhanced remineralization which can potentially provides nutrients necessary to the summer bloom. In May, a slight maximum of pCO_2 coincides with the winter maximum of bacterial activity. This suggests that the winter pCO_2 over-saturation could be related to the respiration of the bacterial community. The pCO_2 pattern of the outer station roughly mimics the pattern of the inner stations, with the notable exception of the absence of spring under-saturation, despite the increase of the Chl *a* concentration. This suggests that

the outer station is influenced by other processes, advection of off-shore water for example – which overcomes the influence of the biological activity.

The overall pattern of pCO_2, Chla and bacterial abundance in Recques Bay is similar to the one outside the Morbihan Bay, although with later maximum of Chl a and concomitant decrease of pCO_2. pCO_2 patterns in the inner and outer bay are similar, excepted in spring when enhanced inner Chl a concentration drives a significant pCO_2 decrease and subsequent CO_2 under-saturation. pCO_2 and Chl a patterns derived from the diel cycles are consistent with those from the cross-shore transects, although higher Chla concentration and lower pCO_2 values were observed in September. This is in agreement with the results from the chapter 3.2 that indicate that planktonic and macroalgal primary production in the *Macrocystis* kelp beds increase drastically in September.

Despite the summer increase of Chl a, pCO_2 values are weaker in the Table Bay compared to the other two bays. This suggest that advection of pCO_2 rich outer waters counteracts the decrease of pCO_2 due to phytoplankton growth.

The Morbihan Bay appears to be the most productive site, with an earlier onset of the phytoplankton bloom and lower pCO_2 values. The spring CO_2 undersaturation observed in the inner waters of the Morbihan Bay was not observed in the other two bays. In Recques Bay and Table Bay, CO_2 over-saturation is observed almost all year round.

3.4.5 Annual air-sea exchange of CO_2

Table 3.4-1 and 3.4-2 present the annually integrated air-sea CO_2 fluxes computed from wind speed measurements carried out at the meteorological station of Port aux Français. We derived the fluxes from the interpolated seasonal evolution of pCO_2 and SST. We used atmospheric CO_2 concentration measured at Amsterdam Island (V. Kazan, personal communication). Since the choice of an algorithm to compute the gas transfer velocity (k) is still a matter of debate, air-water CO_2 fluxes were computed using the four frequently cited k-wind parameterizations, i.e. Liss and Merlivat (1986), Wanninkhof (1992), Wanninkhof and McGillis (1999) and Nightingale et al. (2000).

The integration of air-sea CO_2 fluxes allow us to assess that on the whole the near-shore waters (depth < 50 m) surrounding the archipelago behave as a source of CO_2 to the atmosphere, ranging between 0.15 to 0.57 TgC yr^{-1} depending on the k-wind parameterization. Such an emission of CO_2 to the atmosphere contrasts with the model outputs at the KERFIX in the open waters southeast of the archipelago (Fig. 3.4-4) which simulate (Louanchi et al., 2001) a sink for atmospheric CO_2 (Pasquer et al., 2005). Furthermore, based on observational data this Subantarctic area has been considered as a sink for atmospheric CO_2 (Metzl et al., 1995; Metzl et al., 1999).

3.4.6 Conclusions

If we refer to the concept of proximal and distal shelves proposed by (Rabouille et al., 2001), the present study refers to the proximal shelf. Proximal shelves generally act as sources of CO_2 at tropical and temperate latitudes (Borges, 2005) ; Borges et

Site	Year	Liss & Merlivat 86 ($gC\ m^{-2}\ y^{-1}$)	Wanninkhof 92 ($gC\ m^{-2}\ y^{-1}$)	Wanninkhof & McGillis 99 ($gC\ m^{-2}\ y^{-1}$)	Nightingale et al. 00 ($gC\ m^{-2}\ y^{-1}$)
Morbihan Bay					
Cimetary Island - Diel cycles	1996	3.5	1.4	2	1.1
Port aux Français - Weekly sample	1996	0.6	0.2	0	0.1
Port aux Français - Weekly sample	1997	-19	-32	-30.8	-26.3
Deep waters (Inner/Outter)	1999	19.8 / 21.2	40.4 / 43.6	57.7 / 63.3	26.7 / 28.6
Recques Bay (inner/outer)	1999	58.5 / 43.9	120.7 / 90.3	177.9 / 131.8	79.2 / 59.3
Table Bay (inner/outer)	1999	44.8 / 53.4	91.3 / 107.4	130.2 / 148.3	60.1 / 71

Table 3.4-1. Air-sea CO_2 fluxes in the waers surrounding the Kerguelen Archipelago based on cross-shore transects data (1998), weekly survey in shallow waters (1996 and 1997) and diel cycles (1997).

"Cimetray Island –Diel cycles" refers to the diel cycles carried out in the Morbihan Bay (chapter 3.2). "Port aux Français –weekly sample" refers to the weekly survey carried out in the shallow near-shore waters in the close vicinity of Port-aux-Français station (chapter 3.1). Only measurements carried out outside the *Macrocystis* kelp beds are considered.

	Surface area	Liss & Merlivat (1986)	Wanninkhof (1992)	Wanninkhof & McGillis (1999)	Nightingale et al. (2000)
	(km^2)	$TgC\ yr^{-1}$	$TgC\ yr^{-1}$	$TgC\ yr^{-1}$	$TgC\ yr^{-1}$
Morbihan Bay	815	0.012	0.026	0.037	0.017
South	361	0.018	0.036	0.05	0.024
East	465	0.023	0.048	0.068	0.031
North	1838	0.094	0.194	0.285	0.127
West	683	0.014	0.03	0.043	0.02
Kerguelen Archipelago		0.152	0.317	0.468	0.206

Table 3.4-2. Integrated annual air-sea CO_2 fluxes in the waters surrounding Kerguelen Archipelago ranging from 0 m to 50 m depth (the overall surface of the bays have been considered even if the depth can be deeper than 50 m).

Morbihan Bay integration was derived from Morbihan Bay surveys (inner cross-shore transect stations, 1996 diel cycles - chapter 3.2, 1996 and 1997 weekly survey - chapter 3.1. South, East, North, West were derived from, respectively, Table Bay survey (inner and outer), average of Table Bay and Recques Bay surveys (inner and outer), Recques Bay survey (inner and outer), Morbihan Bay cross-shore survey (outer station only).

al. 2005), as they receive large inputs of CO_2-rich riverine waters and terrestrial organic carbon that fuel net heterotrophy. The Kerguelen Archipelago is far from being submitted to anthropogenic pressures and can be considered as a pristine

coastal area. The proximal shelf should therefore receive terrestrial organic matter from the regular land drainage by the heavy precipitation in the area. These inputs seem to drive a net annual source of CO_2 for the atmosphere. Hence, the recurrent observation of the proximal shelf as a source of CO_2 for the atmosphere holds true for Subantarctic pristine environments

3.4.7 Acknowledgements

We thank V. Kazan for atmospheric PCO_2 data and MétéoFrance for meteorological data.

SEAWIFS data was provided by NASA at the OceanColor website (http://oceancolor.gsfc.nasa.gov/). We are indebt to the efficient and enthusiast help of D. Rochard and J.M. Guédé and the other crew members of the *R.V. La Curieuse.* This research was supported by the Institut Paul-Emile Victor, the Belgian Science Policy (contract A4/DD/B14, EV/7/12E, SD/CA/03A) and the FNRS (Belgium) with which AVB is a research associate.

4 Sea ice

Sea-ice sampling in trace clean conditions during Ispol survey (Nov 2004-Jan 2005)

4.1 Air – sea ice exchange of carbon dioxide: the end of a long-lived paradigm ?

4.1.1 Foreword

For decades, sea ice has been considered by the scientific community and biogeochemical modellers involved in assessing oceanic CO_2 uptake as an inert and impermeable barrier to air-sea exchange of gases. However, this assumption is not supported by studies of the permeability of ice to gases and liquids, which show that sea ice is permeable at temperatures above -10°C.

In this chapter we report the first direct measurements of pCO_2 within sea ice and related CO_2 exchanges with the atmosphere. We drew the first comprehensive picture of CO_2 dynamics within sea ice, in particular regarding the sea ice internal biogeochemical drivers of CO_2 fluxes from the atmosphere to sea ice. We show that primary production, although significant, is not the main driver of these fluxes, and that chemical processes coupled with the peculiar physics of the sea ice account for most of the CO_2 uptake. Using remote sensing products, we propose the first conservative estimate of CO_2 fluxes over Antarctic sea ice, which is significant in terms of the CO_2 budget of the Southern Ocean.

In May 2005, we invited the 3 other research groups (Miller and Papadimitriou - CA, Semiletov – USA, Zemmelink –NL) recently involved in CO_2 dynamics within sea ice to meet during the International Liège Colloquium on Gas Transfer at Water surfaces [1, 2] (). We confronted the scientific community interested in gas transfer at the water interfaces with the new observations of air-sea ice gas transfer. The discussions that took place during this Colloquium reinforced our conclusion that sea ice does exchange CO_2 with the atmosphere, as the results from the 4 research groups converged.

This chapter has been submitted as a letter to Nature:

Delille B., Tilbrook B., Lannuzel D., Schoemann V., Becquevort S., Borges A.V., Delille D., Lancelot C., Chou L., Dieckmann G.S. and Tison J.L. Air – sea ice exchange of carbon dioxide: the end of a long-lived paradigm ?

[1] http://www.uea.ac.uk/env/solas/News1/SOLAS%20Newsletter%20Autumn.pdf

[2] http://www.co2.ulg.ac.be/2005.html

4.1.2 Abstract

Climate models often consider sea-ice is an inert barrier preventing air-sea exchange of gases. However, relatively warm sea-ice is permeable to gases and growing evidence supports that gase fluxes between sea-ice and the atmosphere do occur. We report the first direct measurements of the partial pressure of CO_2 (pCO_2) within sea-ice and the related CO_2 fluxes at the air-ice interface for Southern Ocean waters. From late winter to summer, as temperature increases, the CO_2 in brines contained within the ice changes from a large over-saturation to a marked under-saturation, while the underlying oceanic waters remains slightly oversaturated. The decrease from winter to summer of pCO_2 in the brines is driven by net primary production, dilution with melting ice crystals, and dissolution of carbonate minerals. As the ice warms, its permeability increases, allowing greater CO_2 transfer at the air-sea ice interface. The sea-ice turns from a transient source to a sink for atmospheric CO_2. We estimate that over the spring-summer period, the Antarctic sea-ice cover is a sink of atmospheric CO_2, ranging at least from 0.015 to 0.024 PgC, or 5% to 9% of the annual uptake estimates for the Southern Ocean.

4.1.3 Introduction

Sea ice covers about 7% of the Earth surface at its maximal seasonal extent, and represents one of the largest biomes on Earth (Arrigo et al., 1997; Lizotte, 2001). For decades, sea ice has been assumed to be an impermeable and inert barrier to air-sea exchange so that global climate models do not include CO_2 exchanges over ice covered waters (Tison et al., 2002). This paradigm relies on the CO_2 budgets of the water masses of the Weddell Sea, which do not reveal the signature of air-sea exchange of CO_2 in the Winter Surface Water at the time it is subducted and mixed with other water masses, to form Weddell Bottom Water (Weiss et al., 1979; Poisson and Chen, 1987), a major contributor of Antarctic Bottom Water. However, Gosink et al. (1976) stressed that sea ice is a highly permeable medium for gases based on work to estimate permeation constants of SF6 and CO_2 within sea ice. They suggested gas migration through sea ice could be an important factor in winter ocean-atmosphere exchange when the sea ice surface temperature is above -10°C. Semiletov et al. (2004) and Zemmelink et al. (2006) have also reported uptake of atmospheric CO_2 over the sea ice cover in the Arctic and Southern Ocean, respectively.

In order to reconcile these contradictory statements, one must bear in mind there is no evidence of air-sea CO_2 exchange in ice covered water at the time of deep water formation. At this time, in autumn and winter, sea ice is growing – ice growth is one of the main driver of deep water formation - and due to its low surface temperature, is likely impermeable to gas exchange.When sea ice warms and begins to melt in the spring it becomes more permeable and air-sea CO_2 exchange is possible. Spring and summer gas exchanges are unlikely to affect the chemical signatures of deep-water, since deep-water formation is weak at this time of the year. The chemical signature in well-stratified spring surface waters will also be modified

by summer processes prior to winter surface and deep water formation the following winter.

During sea ice growth, most of the impurities (solutes, gases, particulate matter) are expelled from the pure ice crystals at the ice-water interface. However, a small fraction of impurities (~10%) remains trapped in bubbles, brine pockets, tubes or channels that contribute to the overall sea ice porosity and host active auto- and hetero-trophic microbial communities (Arrigo et al., 1997; Lizotte, 2001; Thomas and Dieckmann, 2002a; Arrigo, 2003). Further depletions occur via processes such as brine expulsion, migration, drainage or convection, that are mainly controlled by the history of the thermal regime of the ice (Weeks and Ackley, 1986; Wettlaufer et al., 1997; Eicken, 2003) while brine volume and salinity also depend on thermodynamic equilibrium reactions (Cox and Weeks, 1983). A 5% relative brine volume is a threshold above which sea ice permeability increases drastically (Golden et al., 1998) and is also likely to represent a threshold above which air-ice gas exchange increases (Buckley and Trodahl, 1987). This permeability threshold would occur at a temperature of -10°C for a bulk ice salinity of 10, corroborating the observation that sea ice is a highly permeable medium for gases (Gosink et al., 1976) and consistent with the reported uptake of atmospheric CO_2 over ice covered waters (Semiletov et al., 2004; Zemmelink et al., 2006).

We carried out first measurements of CO_2 concentration within sea ice and related CO_2 fluxes. We drew the first comprehensive picture of CO_2 dynamics within sea ice, and how sea ice internal processes drives CO_2 fluxes from the atmosphere to sea ice. Using remote sensing products, we propose a first conservative estimate of CO_2 fluxes over Antarctic sea ice.

4.1.4 Material and methods

Measurements were carried out during the 2003/V1 cruise on the *R.V. Aurora Australis* from 2003-09-27 to 2003-10-20 in the Indian sector of the Southern Ocean (63.9 to 65.3 °S, 109.4 to 117.7°E) and the ISPOL (Ice Station Polarstern) drifting station experiment onboard the *R.V. Polarstern* from 2004-11-29 to 2005-12-31 in the Weddell Sea (67.35 to 68.43 °S, 55.40 to 54.57 °W). Only first year pack ice was investigated during 2003/V1 cruise, while both first year and multiyear pack ice were sampled during ISPOL experiment. Sampling was only carried out in un-flooded areas, without melting pond or slush surface layers.

Sampling of ice brine was conducted by drilling shallow sackholes (ranging from 15 cm down to almost full ice thickness) through the surface of the ice sheet. The brine from adjacent brine channel and pockets was allowed to seep into the sackhole for 30-60 min, with the hole covered with a plastic lid (Gleitz et al., 1995), reportedly the best current method to sample brines for chemical studies (Papadimitriou et al., 2004). Water was pumped from the hole using a peristaltic pump (Masterflex® - Environmental Sampler) and supplied to the device for measurements of partial pressure of CO_2 (pCO_2). The latter were carried out using a membrane contractor

equilibrator (Membrana® Liqui-cell) coupled to an infrared gas analyzer (IRGA, Li-Cor® 6262). Seawater flowed into the equilibrator at a rate of 2 L min^{-1} and a closed air loop ensured circulation through the equilibrator and the IRGA at a rate of 3 L min^{-1}. Temperature was measured simultaneously i*n situ* and at the outlet of the equilibrator using Li-Cor® sensors. Temperature correction of pCO_2 was applied assuming that the relation from Copin-Montégut (Copin-Montégut, 1988) is valid at low temperature and high salinity. The IRGA was calibrated soon after returning to the ship while the analyser was still cold. For V3/2001, CO_2-in-air standards calibrated on the World Meteorological Organisation X-85 molar scale (mixing ratios of 304.60, 324.65 and 380.03 ppm) were supplied by Commonwealth Scientific and Industrial Research Organisation (CSIRO) Atmospheric Research, Australia. CO_2-in-air standards with mixing rations of 0 ppm and 350 ppm of CO_2 were supplied by Air Liquide Belgium® for the ISPOL cruise. Stable field pCO_2 readings usually occurred within 3 min of flowing gas into the IRGA. The equilibration system ran 6 min before averaging the values given by the IRGA and temperature sensors over 30s and recording the averaged values with a data logger (Li-Cor® Li-1400). All the devices (except the peristaltic pump) were enclosed in an insulated box that contained a 12V power source and was warmed to keep the inside temperature just above 0°C.

A chamber was used to measure air-ice CO_2 fluxes. The accumulation chamber (West system®) is a metal cylinder closed at the top (internal diameter 20 cm; internal height 9.7 cm). A rubber seal surrounded by a serrated-edge iron ring ensured an air-tight connection between the base of the chamber and the ice. For measurement over snow, an iron tube was mounted at the base of the chamber to enclose snow down to the ice and prevent lateral advection of air through the snow. The chamber was connected in a closed loop between the air pump (3 L min^{-1}) and the IRGA. The measurement of pCO_2 in the chamber was recorded every 30 sec for at least 5 min. The flux was computed from the slope of the linear regression of pCO_2 against time ($r^2 \geq 0.99$) according to Frankignoulle (1988). The uncertainty of the flux computation due to the standard error on the regression slope is on average ±3%.

Dissolved Inorganic Carbon (DIC) measurements on 2003/V1 were made using a single operator multiparameter metabolic analyzer (SOMMA) and UIC® 5011 coulometer (Johnson et al., 1998). The system was calibrated by injecting known amounts of pure CO_2 into the system. The number of moles of pure CO_2 injected bracketed the amounts measured in sea-ice brines and showed the measurement calibration did not change over the range of concentrations measured. The measurement precision and accuracy was checked during the analyses using certified reference materials provided by Dr A Dickson, Scripps Institution of Oceanography. Repeat analyses showed an accuracy and precision for the DIC measurements to better than ±0.1%. Total Alkalinity (TA) was computed from pCO_2 and DIC using the CO_2 dissociation constants of Mehrbach et al. (1973) refitted by Dickson and Millero (1987). We assumed a conservative behaviour of dissociation constants during seawater freezing. This assumption is supported by the work of Marion (Marion, 2001) who showed that measurements of carbonate mineral solubilities for subzero temperatures fit with the prediction derived from the four important equilibrium constant of the aqueous carbonate system determined only for positive temperature, namely the first (K_1) and second (K_2) dissociation constants for carbonic acid, the Henry's Law constant for CO_2 (K_H) and the dissociation constant for water (K_W). During the ISPOL experiment, Total Alkalinity (TA) was measured using the classical Gran potentiometric method (Gran, 1952) on 100-mL GF/C filtered

samples, with a reproducibility of ±3 µmol kg^{-1}. DIC was computed from TA and pCO_2 for ISPOL.

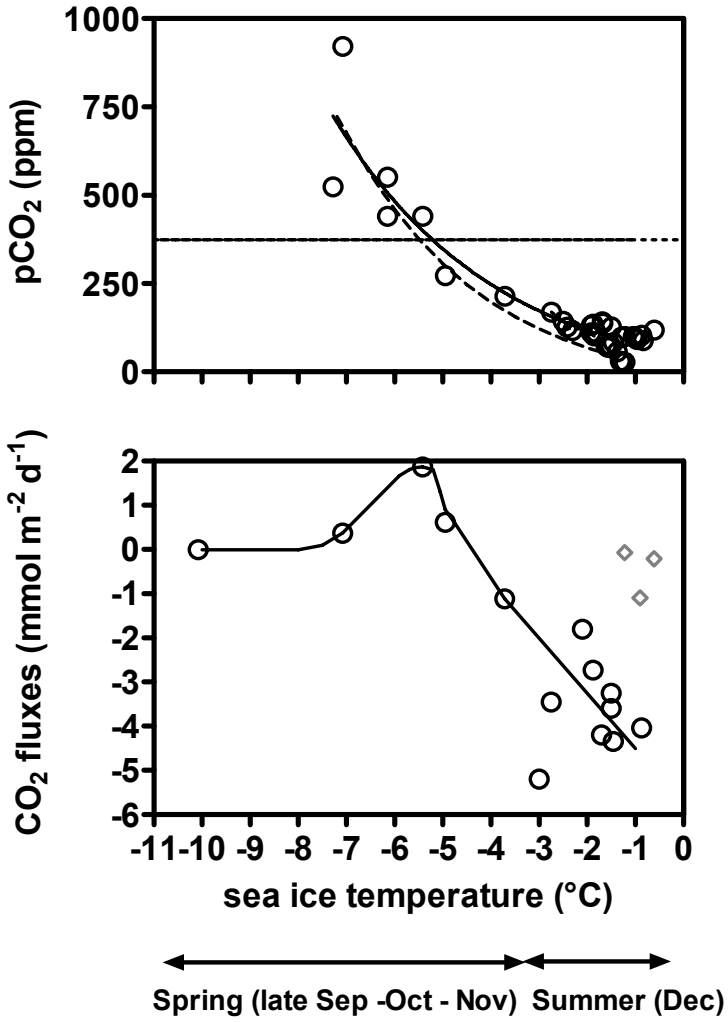

Figure 4.1-1 : (a) pCO_2 within brines ($pCO_{2\ brines}$) and (b) related air-sea ice CO_2 fluxes versus sea ice temperature integrated over the depth of sackholes. Grey diamonds denotes CO_2 flux measurements obtained during superimposed ice events (see 4.1.5.5). Horizontal dotted line and solid curve are $pCO_{2\ air}$ and the mean trend of $pCO_{2\ brines,}$, respectively. The dilution effect largely encompasses the thermodynamic effect of temperature increase on pCO_2 and the pattern of observed pCO_2 matches the theoretical variation related to both processes (dashed curve), suggesting that the increase of temperature and subsequent dilution are among the main drivers of the spring CO_2 drawdown Correspondence between season and ice temperature is only indicative and corresponds to the conditions encountered during our surveys.

4.1.5 Results and discussion

4.1.5.1 pCO_2 changes : Effect of temperature and $CaCO_3$ precipitation

The pCO_2 in brines decreased dramatically as sea-ice warmed (Fig. 4.1-1a) and the pCO_2 shifted from a large over-saturation (ΔpCO_2 = $pCO_{2(water)}$ – $pCO_{2(air)}$ = 525ppm) during early spring (October) to a marked under-saturation (ΔpCO_2 = -335 ppm) during summer (December). At a first glance, the sea-ice brine pCO_2 is inversely correlated to the sea ice temperature, suggesting a large part of the spring pCO_2 drawdown is driven by the dilution of brines associated with the melting of ice crystals as temperature increases (Cox and Weeks, 1983). Conversely, the over-saturation observed at the end of winter can result from brine concentration during sea ice growth and cooling. The precipitation or dissolution of carbonate minerals (Anderson and Jones, 1985), the abiotic release or uptake of gaseous CO_2, primary production and respiration are also likely to influence the CO_2 dynamics.

Calcium carbonate minerals were conspicuously detected in sea-ice off Adélie Land (Fig. 4.1-2).Low values of DIC_{35} and TA_{35} in brines collected in early spring in cold sea-ice (Fig. 4.1-3) indicate that carbonate precipitation also occurred within brines prior to the 2003/V1 cruise further eastwards. The imprint of carbonate precipitation is well marked, leading to a decrease of 65 % of TA_{35} in brines, compared to the underlying water. Carbonate precipitation will reduce the DIC_{35} and increase pCO_2 as the brine salinity increases during ice growth. This will contribute to winter over-saturation of CO_2.

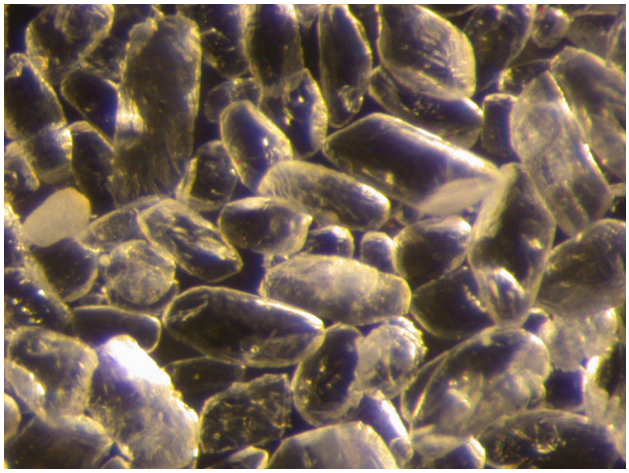

Figure 4.1-2 : Mineral crystals collected in land fast sea-ice in December 2001 off Adélie Land, Antarctica. The photograph was taken through binocular microscope with average crystal size of about 100µm. The crystals were concentrated in melted sea ice core sections by swirling the sample in a beaker and allowing to settle. They were filtered through nucleopore filters and dried in an oven for SEM-Xray combined microanalysis that identified the crystals as calcium carbonate ($CaCO_3$). When left in the melted sea-ice water, the samples disintegrated after several hours.

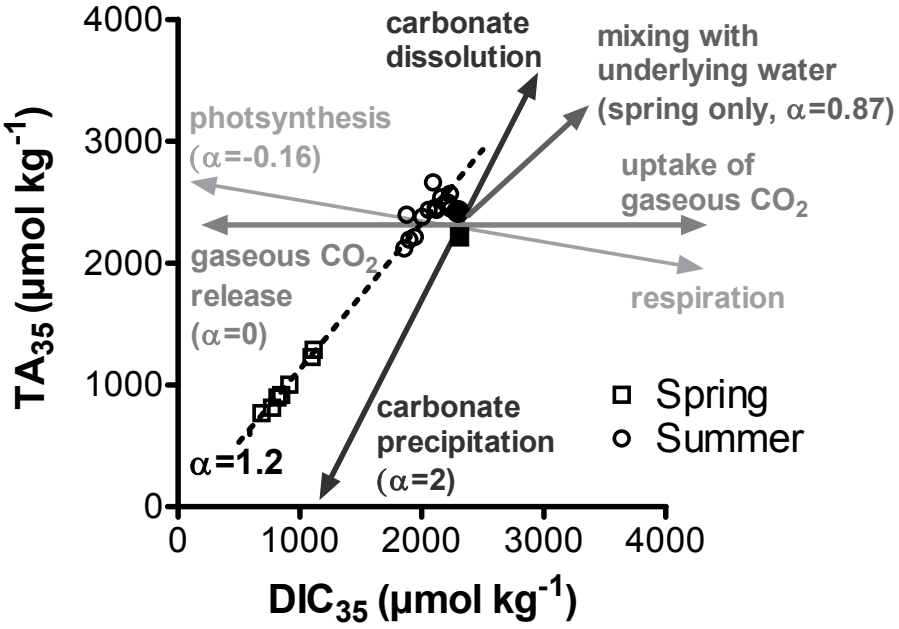

Figure 4.1-3 : The plot of normalized DIC to a constant salinity of 35 (DIC_{35}) against normalized TA (TA_{35}) gives some insights on the processes occurring within sea ice (with the notable exception of temperature change and concentration/dilution of brines that do not affect DIC_{35} and TA_{35}) both prior and during our surveys. Open squares and open circles denote, respectively, spring and summer samples; slope of the corresponding regression line is reported as "α". Solid square and circle denote mean values of the underlying water in spring and summer, respectively (the corresponding average pCO_2 are, respectively, 417 and 390 ppm). Arrows represent the theoretical variation of DIC_{35} and TA_{35} according to specific biogeochemical processes. TA_{35} and DIC_{35} are remarkably well correlated with a slope of 1.2. Carbonate dissolution/precipitation could best explain the observed trend, although the theoretical slope should be 2. Such discrepancy might be ascribed to an uptake of gaseous CO_2 (from bubbles or the atmosphere) combined with carbonate dissolution, or to mixing with underlying water owing to internal convection (Weeks and Ackley, 1986; Golden et al., 1998).

4.1.5.2 Fate of precipitated carbonate minerals and their contribution to the uptake of CO_2

Precipitation of carbonate minerals, mainly calcite and aragonite (Killawee et al., 1998; Marion, 2001; Papadimitriou et al., 2004) in sea ice as a result of the drastic increase of salinity in brines is subject to a long-lived debate. Numerous laboratory experiments have shown carbonate precipitation occurs during sea ice formation (Jones et al., 1983; Tison et al., 2002; Papadimitriou et al., 2004). Some authors have argued it has not been formally verified in the field (Anderson and Jones, 1985; Gleitz et al., 1995). We observed in land fast sea-ice mineral crystals identified as calcium carbonate crystals (figure 4.1-4). The decrease of TA_{35} observed during 2003/V1 cruise is also a conspicuous indication that carbonate precipitation occurred within sea ice prior to the cruise. The fate of the precipitated carbonate minerals remains uncertain. We hypothesize that most of the precipitated carbonate minerals remain within sea ice during winter and dissolves as salinity decreases during spring. Based on field studies, "excess" TA in the water column during sea-ice melting was attributed to the dissolution of calcium carbonate precipitated in brines and released

into the underlying water (Jones et al., 1983). No study has yet investigated carbonate minerals dynamics within natural sea ice. The fate of carbonate minerals is a good illustration of how intricate the links between biogeochemical and physical sea ice processes are. If carbonate precipitation occurs at relatively low salinity and high temperature, these processes would take place in the "skeletal layer" (the lamellar ice-water interface, a relatively open system) during sea ice growth (Fig. 4.1-4, A). This is a logical hypothesis from phase diagram and experimental approaches that show carbonate precipitation occurs from -2.2 to -10° C (Richardson, 1976). Conversely, if carbonate minerals precipitate in high salinity – low temperature conditions, such precipitation would likely take place in late autumn or winter in the upper layers of sea ice while brines channels are closed (Fig. 4.1-4, B). In the latter case, as carbonate minerals dissolve during spring internal melting, this would consume CO_2 in the same proportion as it would have produced during ice cooling and the net uptake of atmospheric/sea water CO_2 related to the production and dissolution of carbonate would be nil over the period.

The precipitation of carbonate minerals in the skeletal layer might have a significant impact on CO_2 concentration in the underlying water or the atmosphere above. The segregation of impurities enhances CO_2 concentration at the ice-water interface during ice growth (Killawee et al., 1998) and acts as a source of CO_2 for the underlying layer (Fig. 4.1-4, C). If carbonate precipitation occurs in the early stages of ice growth, it will further contribute to the increase of pCO_2. A crucial issue is the fate of carbonate minerals. They can either a) sink faster than the CO_2 rich water in the underlying layer (Fig. 4.1-4, D) and act as a net source of CO_2, especially if CO_2 rich brines trapped within sea ice are released to the atmosphere in spring and summer (Fig. 4.1-4, E), b) sink at the same rate than the CO_2 rich water , with negligible impact on DIC budget of the water column, or c) remain trapped in the tortuosity of the skeletal layer while pCO_2 rich brines are expelled to the underlying layer (Fig. 4.1-4, F). The dissolution of these trapped carbonate mineral in spring and summer, triggered by temperature increases and related salinity decreases, would consume CO_2 and drive a net CO_2 uptake within the ice, unless most of the produced CO_2 during precipitation remains also trapped in the ice as bubbles.

Available laboratory experiments using carbon isotope fractionation to trace calcium carbonate precipitation are inconclusive on the timing of precipitation (Papadimitriou et al., 2004). Work by Rysgaard et al. (2006) on "the segregation of DIC versus TA rejection during sea ice growth and related sea ice CO_2 pump" favours hypothesis (c). The carbonate minerals precipitate from -2.2°C, just below the seawater freezing point, to -10°C (Assur, 1958; Richardson, 1976). Within this range, sea ice permeability decreases to the point that brines channels are closed around -5°C for a bulk salinity of 5 (Golden et al., 1998). As the ice forms and the permeability changes, there is likely a stage when fluids still percolate while solid particles are trapped. This should lead to the segregation between carbonate minerals, which remain trapped within sea-ice while CO_2 rich brines are expelled to the underlying water.

Such a mechanism might act as an efficient pump of CO_2 from the atmosphere. The expulsion of brines enriched in CO_2 leads to the formation of dense water that sinks rapidly during sea-ice growth. The sinking of dense water is the main driver of deep-water formation and is potentially an efficient CO_2 sequestration pathway. Numerous vertical distributions profiles of TA below sea ice have revealed the signature of carbonate mineral precipitation (Weiss et al., 1979). While sea ice melts

during spring and summer, trapped carbonate minerals dissolve as the result of the combined increase of temperature and decrease of salinity either within sea ice or in the underlying water. This dissolution of carbonate minerals as observed by Jones et al. (Jones et al., 1983) leads to a decrease of pCO_2 and might act as an efficient and significant sink of CO_2 according to observations and model of Rysgaard et al. (2006). Thus, the precipitation of carbonate minerals, their fate and decoupling with CO_2 enriched brines deserves further investigation.

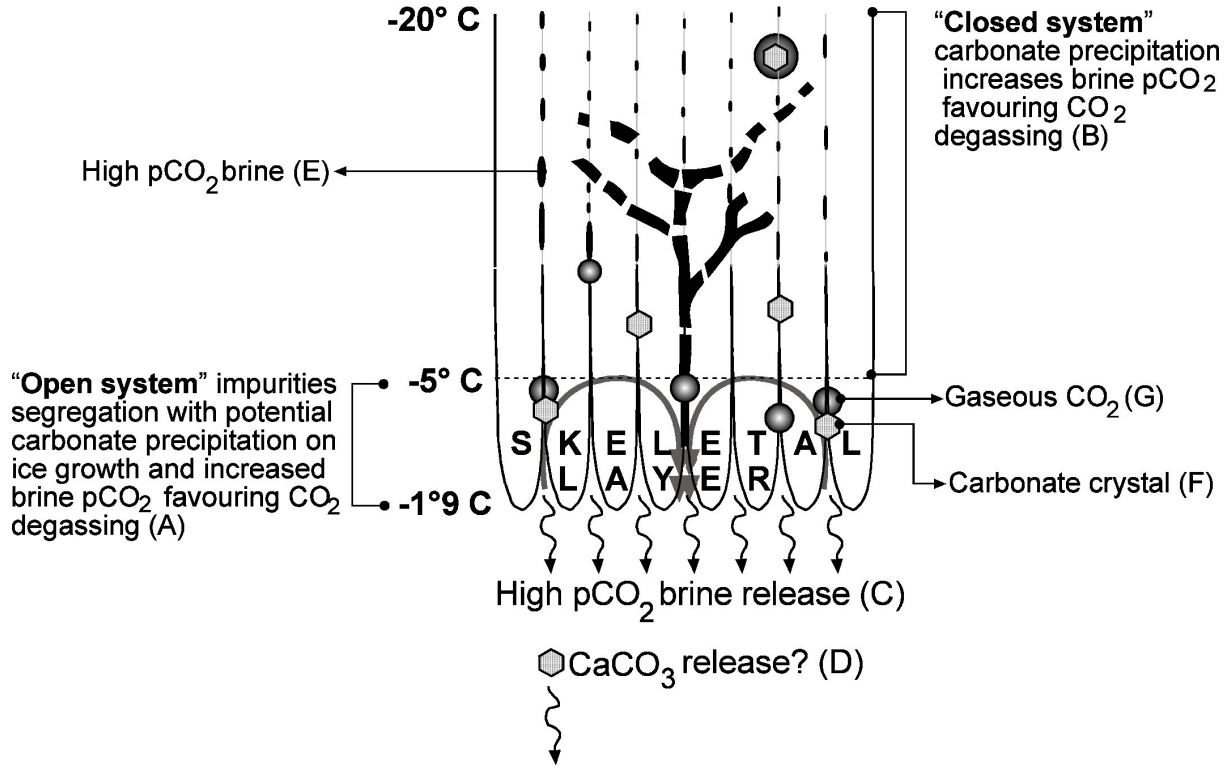

Figure 4.1-4 : Fate of carbonate minerals precipitated within sea ice.

4.1.5.3 Changes of pCO_2 : other processes

However, the observed decrease of TA_{35} due to carbonate precipitation corresponds to a removal of 30 % of $DIC_{35,}$ while the overall decrease of DIC_{35} reaches 70% at the coldest temperature. Thus, about 40% of DIC_{35} reduction has to be ascribed to either autumnal primary production or to CO_2 transfer to the gas phase within the brines (Fig. 3). While sea-ice algae are still active in autumn, their photosynthetic rate is probably limited by light availability and low temperatures (Arrigo et al., 1997; Mock, 2002), so their contribution to the DIC_{35} winter removal is probably small. In contrast, Killawee et al. (Killawee et al., 1998) and Tison et al. (2002) reported that air inclusions within sea ice are mainly composed of CO_2 perhaps issued from carbonate precipitation. The CO_2 can be directly released to the atmosphere during sea ice growth when surface ice is warm enough (~ -7°C, Fig.1b)

to allow transfer of CO_2 during a transient stage as observed during early spring. The elevated sea-ice pCO_2 in autumn therefore results from an intricate superimposition of counteracting processes: those increasing pCO_2 such as brine concentration and carbonate precipitation, and those decreasing pCO_2 such as autumnal primary production, temperature decrease, and CO_2 transfer to the gaseous phase.

4.1.5.4 Relative contribution of thermodynamics, physical, biogeochemical and biological processes to pCO_2 changes

We estimated the potential contribution of thermodynamic, chemical and biological processes (temperature increase and related dilution, carbonate dissolution and primary production) to the spring-summer decrease of pCO_2.

We assessed the potential maximum impact of each main spring and summer physical and biogeochemical processes on pCO_2 (table 4.1-1). The variations are computed from the conditions of temperature, bulk ice salinity, TA_{35} and pCO_2 (-7.2°, 5.4, 791 µmol kg^{-1}, 724 ppm) that corresponded to the average of the two coldest conditions encountered during the 2003/V1 (corresponding to the coldest extremity of the solid curve in figure 1a) and ISPOL cruises. During these cruises, temperature decreased from -7.2 °C to -1.3°C driving melting of ice crystals and dilution of the brines, with a decrease of the brine salinity from 117.1 down to 23.5, according to relationships of Cox and Weeks (1983). The temperature related decrease in salinity also diluted DIC and TA and led to a computed pCO_2 drop of 684 ppm, using the CO_2 dissociation constants of Mehrbach et al. (1973) refitted by Dickson and Millero (1987) (see section 1.1.7.1). The TA normalized to a constant salinity of 35 (TA_{35}) of brines at the lowest observed temperature is only 35% of TA_{35} of the underlying water (Fig. 3) owing to the precipitation of carbonate minerals. Such differences would correspond to the precipitation of carbonate of about 2038 µmol $kg^{-1}$from the brines, assuming the effect of fall and winter microbal activity on TA is negligible. If we assume that the carbonate minerals remain trapped within the ice (see below) and no CO_2 is stored in the gaseous phase within sea ice during the cooling processes, then spring dissolution would reduce pCO_2 by about 583 ppm.

Estimating primary production in sea ice – and the related impact on pCO_2 - is challenging. We assumed the overall sea ice primary production prior to and during the ISPOL cruise corresponded to the autotrophic organic carbon ($OC_{autotroph}$) standing stock in the ice at the end of the ISPOL cruise. This autotrophic organic carbon was estimated from Chl *a* measurements (at 6 depths) and a C:Chla ratio of 83. This ratio was determined by comparing Chl *a* concentration and $OC_{autotroph}$ content derived from abundance and biovolume of autotrophic organisms measured from inverted and epifluorescence microscopy observations, and carbon:volume conversion factors (Hillebrand et al., 1999; Menden-Deuer and Lessard, 2000).

The amount could be underestimated because it does not take into account losses of autotrophic organic carbon (i.e. mortality, exchange with the underlying seawater). In the opposite, we neglected the part of autotrophic community originating from organisms trapped during sea ice growth and autumnal primary production. At the end of the ISPOL cruise, the mean Chl *a* concentration was 3.7 µg kg^{-1} of bulk ice,

which corresponds to an $OC_{autotroph}$ standing stock of 309 µgC kg^{-1} of bulk ice. The build up of the $OC_{autotroph}$ standing stock would correspond to an uptake of DIC of 26 µmol kg^{-1} in bulk ice and an increase of TA of 4 µmol kg^{-1} of bulk ice, according to the Redfield-Ketchum-Richards stoichiometry of biosynthesis (Redfield et al., 1963; Richards, 1965). With the volume of brines derived from the equations of Cox and Weeks (Cox and Weeks, 1975), revised by Eicken (2003), this leads to a decrease of DIC of 669 µmol kg^{-1} and a TA increase of 107 µmol kg^{-1} of brines and subsequent decrease of pCO_2 of brines of 639 ppm (table 4.1-1)**.** The build up of the $OC_{autotroph}$ standing stock would also correspond to a primary production of 0.26 gC m^{-2} considering an ice thickness of 90 cm (average ice thickness during Ispol survey).

			related changes				
	Temperature (°C)	Salinity (of brines)	TA (µmol kg^{-1} of bulk ice)	DIC (µmol kg^{-1} of bulk ice)	TA (µmol kg^{-1} of brines)	DIC (µmol kg^{-1} of brines)	pCO_2 (ppm in brines)
temperature increase and related dilution	5.9	-94	0	0	-2125	-1813	-684
$CaCO_3$ dissolution	0	0	157.2	78.6	4075	2038	-583
Primary production	0	0	4.1	-25.8	107	-669	-639

Table 4.1-1 : Estimates of potential pCO_2 changes related to spring and summer physical and biogeochemical processes observed during the 2003/V1 and ISPOL cruises.

Antarctic pack ice hosts algae communities for which biomass and specific photosynthetic rate can exceed, 500 mg m^{-3} and 8 mg C mgChl a^{-1} h^{-1}, respectively (see Arrigo (2003) for a review). Our calculations suggest that primary production is a significant contributor to CO_2 drawdown although the amount is indubitably difficult to quantify. The dilution of brines with melted ice crystals accounts for a pCO_2 decrease of 660 ppm and could therefore explain most of the observed CO_2 spring drawdown (Fig. 4.1-1b). Carbonate dissolution (see 4.1.5.2) might induce pCO_2 changes comparable to those attributed to primary production and dilution. Finally, it should be noted that uptake of gaseous CO_2 and mixing with underlying water (with pCO_2 values ranging from 380 to 430 ppm) would act to maintain pCO_2 at or above the saturation level rather than promoting the observed decrease (see 4.1.5.7).

4.1.5.5 CO_2 fluxes

Fluxes of CO_2 at the air-ice interface were measured with a chamber and ranged from +1.9 to –5.2 mmol m^{-2} d^{-1} (Fig. 4.1-1b). Higher fluxes have been reported for measurements using eddy correlation over a slush ice - a mixture of melting snow, ice and flooding seawater covering sea ice - in the Antarctic pack (Zemmelink et al., 2006) (-6.6 to -18.2 mmol m^{-2} d^{-1}), and for sea ice melt ponds and open brines channels in fast ice of the North American-Siberian Arctic Ocean shelf zone

(Semiletov et al., 2004), (-19.5 to -38.6 mmol m^{-2} d^{-1}). The differences could result from the occurrence of surface biological communities in the areas investigated by eddy correlation, while the measurements presented here refer to more conventional bare sea-ice. We measured CO_2 fluxes over widespread bare sea-ice without biologically active surface communities. Previous eddy correlation CO_2 fluxes measurements were carried out over areas covered by particular surface environments, namely melt ponds and slush (Semiletov et al., 2004; Zemmelink et al., 2006). Slush – a mixture of melting snow, ice and flooding seawater covering sea ice - is known to berth a highly productive algae community (Legendre et al., 1992). Sea-ice surface communities benefit from high light levels and from nutrients from seawater flooding as snow loading or sea ice rafting depress the ice surface below the freeboard. Such surface flooding occurs over 15-30% of the ice pack in Antarctica (Wadhams et al., 1987). These surface communities exhibit photosynthetic rates comparable to those of open ocean Antarctic phytoplankton (Lizotte and Sullivan, 1992) and might be responsible for the majority of sea surface productivity in Antarctic Sea Ice (Legendre et al., 1992). They easily exchange CO_2 with the atmosphere through the porous snow cover and can potentially enhance significantly the present estimate of CO_2 uptake by sea ice cover.

In a heterogeneous environment like sea-ice, the inherent small spatial resolution of the chamber CO_2 flux measurements allows a consistent comparison with pCO_2 within the ice. The pCO_2 gradient between the atmosphere and the brines in the sea-ice top layer is the main driver of CO_2 fluxes. The CO_2 fluxes are consistent with the saturation level of CO_2 in the brines, with the exception of the transition from upward to downward fluxes at about -5°C. However, the exchanges are modulated by factors like sea ice temperature, and snow and ice structure. At a temperature of about -7°C the CO_2 fluxes are weak despite elevated pCO_2, due to the low permeability of the ice, and no CO_2 flux was detected below -10°C. The permeability of sea-ice for CO_2 decreases at temperatures below - 5°C down to a temperature threshold of -10°C, below which sea ice is virtually impermeable to CO_2 exchange (Fig. 4.1-1b).

While snow allows a rapid exchange of gases with the atmosphere (Massman et al., 1997; Albert et al., 2002; Takagi et al., 2005), very low to nil fluxes were observed after the formation of lenses of superimposed ice above sea ice (diamonds in figure 4.1-1). Superimposed ice forms after a strong snow melt event when percolating freshwater refreezes at the contact of sea ice (Haas et al., 2001). As freshwater ice, the superimposed ice is impermeable to gas transport (Albert and Perron, 2000). The formation of this superimposed ice at the top of sea ice and the subsequent inhibition of air-ice CO_2 fluxes leads to a drastic decrease of brine pCO_2 down to 30 ppm. This highlights the role of CO_2 invasion from the atmosphere that balances the summer pCO_2 drawdown sustained by dilution and primary production, and maintains sea ice pCO_2 above 100 ppm.

4.1.5.6 Upscaling of CO_2 fluxes derived from remote sensing data.

Sea-ice temperature exerts a strong control on both sea-ice pCO_2 and permeability, and ultimately on CO_2 transfer at the air-ice interface (Fig. 1). We derived a relationship between CO_2 flux and sea-ice temperature to allow CO_2 flux fields to be estimated using sea ice temperature and concentration inferred from Advanced Microwave Scanning Radiometer (ASMR) – Earth Observing System data Daily sea-ice concentration and temperature at the air-ice interface with a resolution of 25 km * 25 km, was obtained from ASMR-E L3 data available at http://nsidc.org/data/amsre/)(Cavalieri et al., 2005). The assessment of sea ice temperature from remotely sensed data is still under development, but represent the only available product. We calculated a relationship, flux_{CO_2}, between CO_2 fluxes over both first year and multiyear ice using sea-ice temperature at 5cm depth (Fig. 4.1-5). We then reconstructed weekly CO_2 fluxes fields from September to January, which corresponded to the time period covered by *in situ* measurements, taking into account both AMSR-E sea ice temperature and sea ice concentration, accordingly to:

$$F_{CO_2} = \mathrm{flux}_{CO_2}(T_{ice}) \times 7 \times C_{ice} \times A_{node}$$

where F_{CO_2}, T_{ice}, C_{ice} and A_{node} denote the CO_2 fluxes over a week, AMSR-E L3 temperature and concentration of sea ice, and grid node area, respectively.

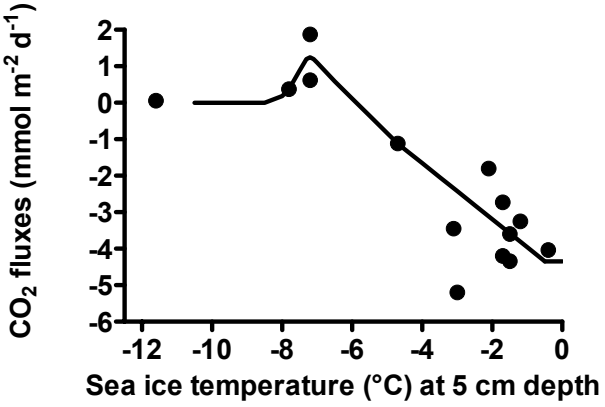

Figure 4.1-5 : Air-sea ice CO_2 fluxes versus sea ice temperature at 5 cm depth. Solid curve represents the relationship (flux_{CO_2}) of air-sea ice CO_2 fluxes to sea ice surface temperature. Fluxes measurements during superimposed ice events were not used in the calculation (see 4.1.5.5).

Spring and summer air-ice CO_2 fluxes (Fig. 4) were estimated from 2002 to 2005 for ice-covered areas with ice concentration above 65%, which corresponded to the range of sea-ice concentration encountered during sampling (Table 4.1-2). This conservative budget suggests Antarctic sea ice cover is pumping between 0.015 and 0.024 PgC during the spring-summer transition, or 6 to 9% of the uptake of the Southern Ocean south of 50°S, based on current assessments of the oceanic uptake of CO_2 south of 50°S of about 0.27 PgC yr^{-1} (Matear and Hirst, 1999; Roy et al., 2003; Takahashi, 2003; Metzl et al., 2006).

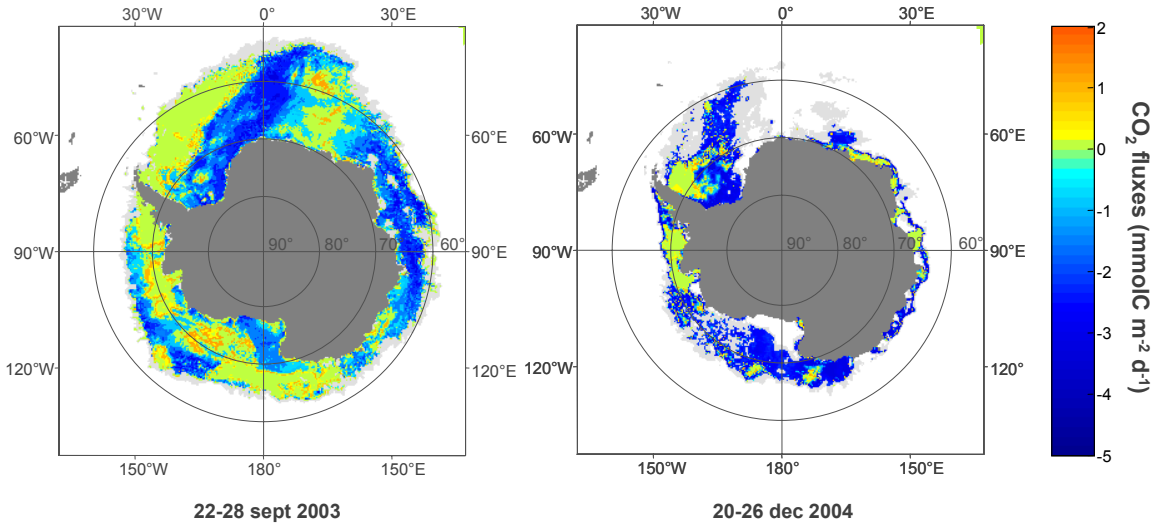

Figure 4.1-6 : Reconstructed air-sea ice CO_2 fluxes over Antarctic sea ice in spring 2003 (22-28 September) and summer 2004 (20-26 September). Light grey areas correspond to regions with sea ice concentration less than 65%. The uptake of atmospheric CO_2 by Antarctic sea ice showed significant seasonal and spatial variability. Spring air-ice CO_2 uptake (September, October and November) ranged from 0.0105 to 0.0184 PgC with summer (December-January) uptake from 0.0042 to 0.0054 PgC.

	CO_2 flux (PgC)
Sep 2002 – Jan 2003	-0.015
Sep 2003 – Jan 2004	-0.017
Sep 2004 – Jan 2005	-0.024
Average	-0.018

Table 4.1-2. Scaled air-sea ice CO_2 fluxes over Antarctic sea-ice in spring and summer provided for regions with sea-ice coverage above 65%.

4.1.5.7 Independent first order assessment of air-ice CO_2 transfers

The potential air-ice CO_2 transfers related to sea-ice physical and biogeochemical processes were assessed by considering a homogeneous 90 cm thick sea-ice cover in equilibrium with the atmosphere and isolated from exchange with the underlying water. The sea-ice thickness value is the mean observed during the ISPOL experiment and is low compared to the values generally observed in the Weddell Sea and elsewhere (Timmermann et al., 2002; Haas, 2003). Temperature, salinity and $\delta^{18}O$ data suggest that low exchanges occurred between sea-ice and the underlying layer during the ISPOL experiment. We assumed that sea-ice was initially in equilibrium with the atmosphere (pCO_2 = 370 ppm), and we applied the

biogeochemically driven DIC and TA changes of the table 4.1-1 (expressed per kilogram of bulk ice), and then computed the air-ice CO_2 transfers required to restore equilibrium. We used the brine volume values computed from the equations of Cox and Weeks (Cox and Weeks, 1975) revisited by Eicken (2003) and mean conditions observed during the two last ISPOL stations (mean sea ice temperature: -1.3°C, mean brine salinity: 24, mean bulk ice salinity: 3.8, mean TA: 1667 µmol kg^{-1} of brines). For the uptake owing to temperature change and related dilution effect, we considered a temperature increase from -7.2 to -1.3 °C corresponding to the range of observations during the 2003/V1 and ISPOL cruises, salinity decrease from 117 to 24 and decrease of TA from 8135 to 1667 µmol $kg^{-1}$of brines so that TA_{35} remains constant.

The CO_2 uptake from the atmosphere related to each process are reported in the table 4.1-3. Taking into account a mean value for the Antarctic sea ice surface area of 16×10^6 km^2 (Comiso, 2003), the corresponding overall CO_2 uptake would be 0.029 PgC which represents an additional CO_2 sink of 11 % to the current consensual assessment of the uptake of CO_2 by the Southern Ocean south of 50°S (0.27 PgC yr^{-1} (Matear and Hirst, 1999; Roy et al., 2003; Takahashi, 2003; Metzl et al., 2006)).

	related CO_2 transfer from the atmosphere ($mmol\ m^{-2}$)
temperature increase and related dilution	-60
$CaCO_3$ dissolution	-57
Primary production	-25

Table 4.1-3 : Estimates of potential air-ice CO_2 fluxes related to spring and summer physical and biogeochemical processes observed during the 2003/V1 and ISPOL cruises. Flux representative of a 4 months period.

4.1.6 Conclusions

The Antarctic sea-ice sustains significant uptake of atmospheric CO_2 due to the combination of primary production and physical and biogeochemical processes occurring within the ice. An independent first order estimate of the potential air-ice CO_2 uptake for Spring-Summer due to thermodynamic, physical and biogeochemical process (4.1.5.7) is about 0.029 PgC, corroborating the above estimate from *in situ* CO_2 flux measurements scaled with remotely sensed ice data (4.1.5.6). Both budgets most probably underestimate the uptake of CO_2 over Antarctic sea-ice as they do not account for surface communities that are likely to enhance significantly CO_2 uptake.

4.1.7 Acknowledgments

We are indebt to Catherine Riaux-Gobin who provided SEM – Xray analysis of $CaCO_3$ crystals carried out in the framework of IPEV- EPONTA 2001. We appreciated the kindness and efficiency of the crews of *R.S.V Aurora Australis* and *R.V. Polarstern*. This research was supported by the Belgian Science Policy (BELCANTO), the Belgian French Community (SIBCLIM), the Australian Climate Change Research Program, and by the Antarctic Climate and Ecosystem Cooperative Research Centre. Author Contributions. All authors significantly contributed to the manuscript. J-LT coordinated the study and with BD constructed crucial thoughts of the paper.

4.2 CO_2 deposition over the multi-year ice of the western Weddell Sea

4.2.1 Foreword

For decades, sea ice has been considered as an inert barrier for gas exchanges, including CO_2. Thus, the air-sea ice CO_2 fluxes measured with the chamber method needed confirmation by other methods to bring confidence in the conclusions of the chapter 4.1. The chamber method allows to measure CO_2 fluxes at small spatial scale and to relate them with the air-ice pCO_2 gradients. However, this method is time-consuming and is not suitable to study temporal variations of CO_2 fluxes throughout the day, or to assess CO_2 at larger spatial scales.

In collaboration with H. Zemmelink from the University of East Anglia (U.K.) we aimed to assess CO_2 fluxes by two other methods:

- pCO_2 profiles above the ice in the air trapped within the snow
- eddy-covariance measurements

These measurements were carried out during the ISPOL cruise at a location close to the sampling sites of the chapter 4.1.

It appeared that to derive CO_2 fluxes from atmospheric pCO_2 profiles within the snow is prone to major difficulties. Accurate high resolution pCO_2 profiles are hardly achievable since a sphere of air with a significant radius is sampled, and also, the air is probably transported over some distance. Also, pCO_2 profiles allow to derive the diffusion controlled flux of CO_2 which does not account for turbulent controlled fluxes, in particular “wind-pumping” events.

Eddy-covariance measurements on the other hand were very useful, as they allowed to follow the daily changes of CO_2 fluxes and to integrate CO_2 fluxes over a large area.

This chapter has been accepted for publication in Geophysical Research Letters:

Zemmelink H.J., B. Delille, J.L. Tison, E.J. Hintsa, L. Houghton & J.W.H. Dacey, 2006. CO_2 deposition over the multi year ice of the western Weddell Sea, *in press*

4.2.2 Abstract

Field measurements by eddy correlation (EC) indicate an average uptake of 0.6 g CO_2 m^{-2} d^{-1} by the ice-covered western Weddell Sea in December 2004. At the same time, snow that covers ice floes of the western Weddell Sea becomes undersaturated with CO_2 relative to the atmosphere during early summer. Gradients of CO_2 from the ice to the atmosphere do not support significant diffusive fluxes and are not strong enough to explain the observed CO_2 deposition. We hypothesize that the transport of air through the snow pack is controlled by turbulence and that undersaturation of CO_2 is caused by biological productivity at the ice-snow and snow-atmosphere interface. The total carbon uptake by the multi-year ice zone of the western Weddell Sea in December could have been as high as 6.6 Tg C y^{-1}.

4.2.3 Introduction

There is no doubt that the ocean plays a major role in regulating the concentration of atmospheric carbon dioxide (CO_2). Takahashi et al. (2002, 2003) analyzed over 940,000 measurements of surface-water pCO_2 and estimated the annual net uptake of CO_2 by the global oceans to be 1.64 Pg C yr^{-1}. The Southern Ocean forms a significant sink for atmospheric CO_2; Takahashi et al. (2002, 2003) estimated an uptake of 0.35 Pg C yr^{-1} south of 50˚S for 1995, which is 21% of the global uptake. However, ice-covered oceanic zones are not taken into account in the current climatology. The role of ice-covered zones was ignored because it was assumed that sea ice precludes gas exchange (Tréguer & Pondaven, 2002). However, recently, Semiletov et al. (2004) showed that invasion of atmospheric CO_2 could be significant over Arctic sea ice. In addition sea ice formation could enhance the uptake of atmospheric CO_2 (Anderson et al., 2004). In this study we present data on CO_2 fluxes over the multi-year ice zone of the western Weddell Sea.

4.2.4 Material and Methods

The study was performed during the 2004 Ice Station Polarstern (ISPOL) cruise, a field experiment designed to improve understanding of physical and biological air-sea-ice interactions in the Weddell Sea through early summer (November-December). ISPOL involved a 37 day drift station on an ice floe (from 68º 15’ S, 54º 45’ W to 67º 22’ S, 55º 25’ W) in the western Weddell Sea, the largest perennial ice-covered zone in the Southern Ocean.

The CO_2 flux was measured at a height of 2.75 m using the eddy correlation (EC) technique. EC is considered to be the most direct technique for measuring gas fluxes

(Fairall et al., 2000), since it utilizes the covariance of scalar concentrations (or mixing ratios) and vertical wind velocity. EC requires measurements at a sufficient rate (10-20 Hz) to adequately capture all turbulence frequencies contributing to the flux. The EC system (Applied Technologies, Inc.) used in this study was battery powered and included a SATI/3K three-axis sonic anemometer and an open-path infrared CO_2/H_2O analyzer (Li-7500, Li-COR, USA). The battery pack and computers of the EC system were placed in a shelter at 20 m distance from the meteorological tower. Data acquisition and processing was to a large extent similar to those of EC measurements conducted in previous experiments as part of slow response techniques to measure DMS fluxes from the oceans (Zemmelink et al., 2004a/b; Hintsa et al., 2004). During ISPOL, post-processing of the data included coordinate rotation followed by application of the Webb et al. (1980) corrections to determine the latent and sensible heat fluxes from the measured mean covariances of vertical wind speed with sonic temperature and with water vapor density. These were then used to compute a density-corrected CO_2 flux with an averaging period of 30 min. Fluxes are indicated according to the micrometeorological convention, i.e. negative when directed downward.

Instrumental failures during snowfall occurred and data during those episodes were discarded from further analysis. The source area of the flux was selected to exclude influence of the ship and the shelter, i.e. measurements were only accepted when the ship and shelter were located downwind from the EC tower. The ice floe in the presumed fetch area was relatively flat (with the exception of some pressure ridges), with an adequate fetch of at least 300 m before the presence of a 10 m wide lead (open water). The 50% source area (determined following Schmid, 1994) for EC measurements at 2.75 m was well within the boundaries of the floe.

(6) The accuracy of the EC system can be derived by comparison of different techniques and sensors that were used during ISPOL to measure latent heat (LH) and sensible heat (SH) fluxes respectively. LH fluxes derived from a bulk aerodynamic approach (using the temperature difference between snow and atmosphere) averaged 10 W m^{-2} (J. Launiainen, pers. Communication, ISPOL meeting Tvärminnen), while our EC measurements resulted in an average LH flux of 14.8 W m^{-2}, a difference of 50%. SH fluxes measured by EC by J. Launiainen averaged 5.9 W m^{-2}; our measurements averaged 4.7 W m^{-2}, a difference of 20%. Although this comparison shows reasonable agreement between independent measurements, it remains difficult to make statements about absolute accuracies. An underlying problem is that the techniques have different source areas with different surface characteristics that influence the flux. We estimate that the uncertainty of the covariance measurements presented in this study is 10-30%, which is comparable to the error estimates of previous experiments conducted at sea (Edson et al. 1998; Hintsa et al., 2004) and slightly higher than the uncertainty of land-based covariance flux measurements, which is typically on the order of 10-15%.

The sonic anemometer was serviced and calibrated by the manufacturer prior to the beginning of the experiment. Zero calibration of wind speed and span calibration of temperature to -30˚C showed that the anemometer was stable in the field. The Li-COR CO_2/H_2O analyzers were serviced and calibrated by the manufacturer at the beginning of the experiment. In the field, zero calibration (by chemical removal of

CO_2 and H_2O) was performed every week and showed no drift. Experience has shown that a change in span is unlikely when zero calibration does not drift. Span calibration in the shore laboratory at the end of the experiment showed that drift of the instruments over the interval of the experiment was negligible.

CO_2 concentrations in the snow were determined daily near the base of a meteorological tower. Two liters of air from a series of inlets at different depths in the snow were sampled through thick-walled Teflon tubing into Vac-U-Chamber airtight boxes (SKC Inc.), into which Tedlar bags were placed for sample accumulation. Several Vac-U-Chamber boxes could be evacuated with a single pump, and a three-way valve on each box allowed switching from purging the tubing to collecting air samples at 100 ml min^{-1} (for more details see Hintsa et al. (2004)). Subsequently, bags were brought back to the ship's laboratory and analyzed for CO_2 using a closed path Li-7000 in absolute mode. Towards the end of December, however, melting and refreezing changed snow conditions and it was decided to use a Li-6262 set up for direct measurements of CO_2 in the field by pumping air through the analyzer at 300 ml min^{-1}.

4.2.5 Results and Discussions

4.2.5.1 Sea ice conditions

Aerial photography and electromagnetic soundings around the selected floe (over a triangle of about 70 km along each side) revealed that the ice floe actually consisted of a mosaic of individual multi-year (probably second-year) ice floes welded together by areas of first-year ice, with frequent occurrences of deformation ridges at the boundaries. Snow thickness near the meteorological tower varied between 0.5 and 1 m, generally higher in the vicinity of ridges. A number of significant changes in the character of the pack ice between 29 November 2004 and 1 January 2005 were observed as described in Zemmelink et al. (2005).

Briefly, during the first three weeks of fieldwork two types of snow were distinguished: snow that covered slush and snow that covered solid ice. Sudden changes in sea ice characteristics occurred towards the end of December, when melting of snow and surface flooding was observed and slush and melt ponds formed at the surface of the snow, in addition to an increase of slush between the snow and underlying ice. Refreezing of water in the snow resulted in the formation of granulated snow (containing small pieces of ice and open spaces) and of superimposed ice (refrozen snow melt as a layer of solid ice at some depth within the snow pack). Snow characteristics became very heterogeneous toward the end of December when the slush turned brown due to the abundance of diatoms.

4.2.5.2 CO_2 fluxes measured by eddy-correlation

The discoloration of slush and melt ponds implies increasing primary production in and at the surface of the snow pack, which would lead to an uptake of CO_2 by the floe. Indeed, the daily flux, as measured by EC, increased from -0.2 g CO_2 m^{-2} d^{-1} in early December, to -0.8 g CO_2 m^{-2} d^{-1} toward the end of December, averaging -0.6 g CO_2 m^{-2} d^{-1} (Figure 1). Fluxes exhibited some variation, probably caused by surface heterogeneity, but also showed a diurnal cycle correlating with the heat flux (data not shown), with maxima around 15:00, especially apparent after year day 350. The observed carbon flux values are lower than fluxes measured by EC over fast ice of the North American-Siberian Arctic Ocean shelf zone (Semiletov et al., 2004), ranging between -0.9 – -1.7 g CO_2 m^{-2} d^{-1}. However, those fluxes were measured over sea-ice melt ponds and open brine channels known to be highly productive (Thomas and Dieckmann, 2002).

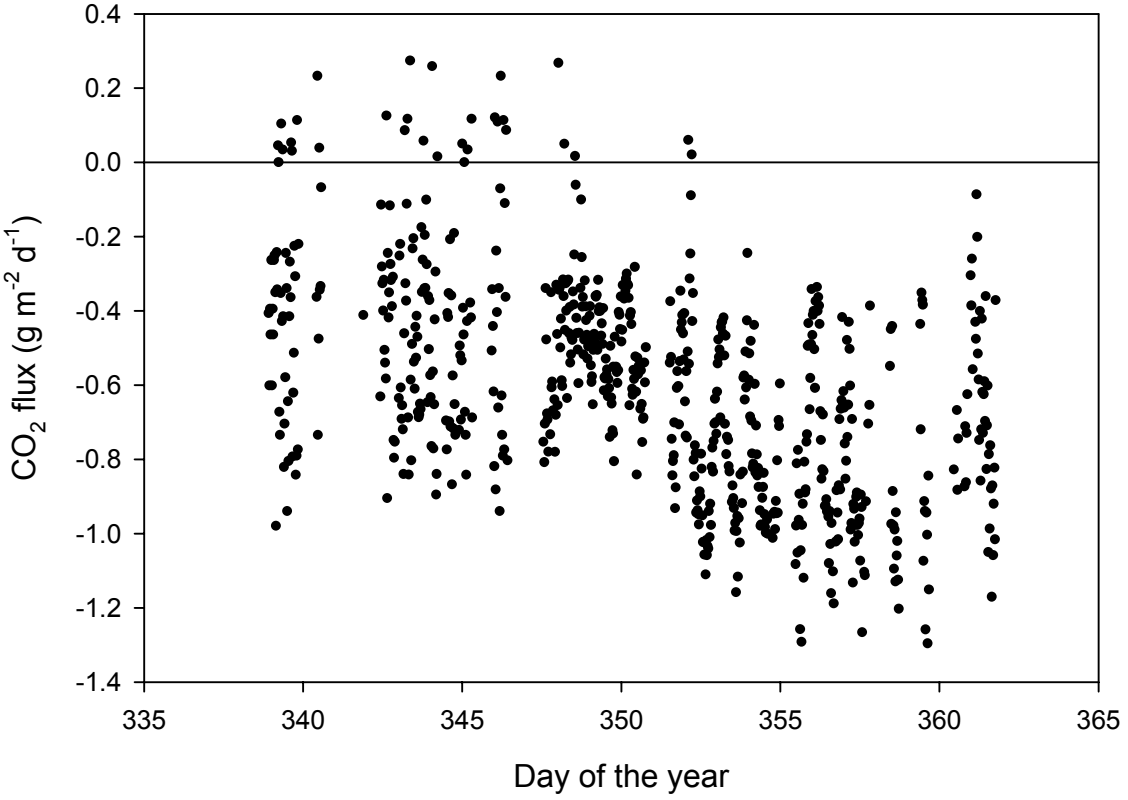

Figure 1: Turbulent CO_2 fluxes (g CO_2 m^{-2} d^{-1}) over the multi-year ice in the western Weddell Sea as measured by eddy correlation in December 2004

From a numerical model Arrigo et al. (1997) concluded that primary production in ice of the Weddell Sea could average 1.4 g C m^{-2} $month^{-1}$ in December, increasing to 1.9 g C m^{-2} $month^{-1}$ in January. This is in agreement with our flux measurements ranging from 1.7 g C $m^{-2}month^{-1}$ (in early December) to 6.8 g C $m^{-2}month^{-1}$ (towards the end of December) with an average of 5.1 g C $m^{-2}month^{-1}$. Maximum growth of "sea ice algae" is reached in first-year ice and is near its peak in December when

surface flooding provides nutrients at the ice-snow interface and within the freeboard layer, near sea level (Arrigo et al. 1997).

Primary production could be hampered by slow replenishment of CO_2 through the snowpack, which tempers atmospheric turbulence. Albert and Shultz (2002) studied in situ transport of SF_6 in undisturbed snow in light (3 m s^{-1}) and moderately strong (9 m s^{-1}) wind conditions. Results indicated that transport in a hoar layer was diffusion-controlled at low wind speed, and more turbulence-controlled at the higher wind speed.

4.2.5.3 pCO_2 gradients within sea ice

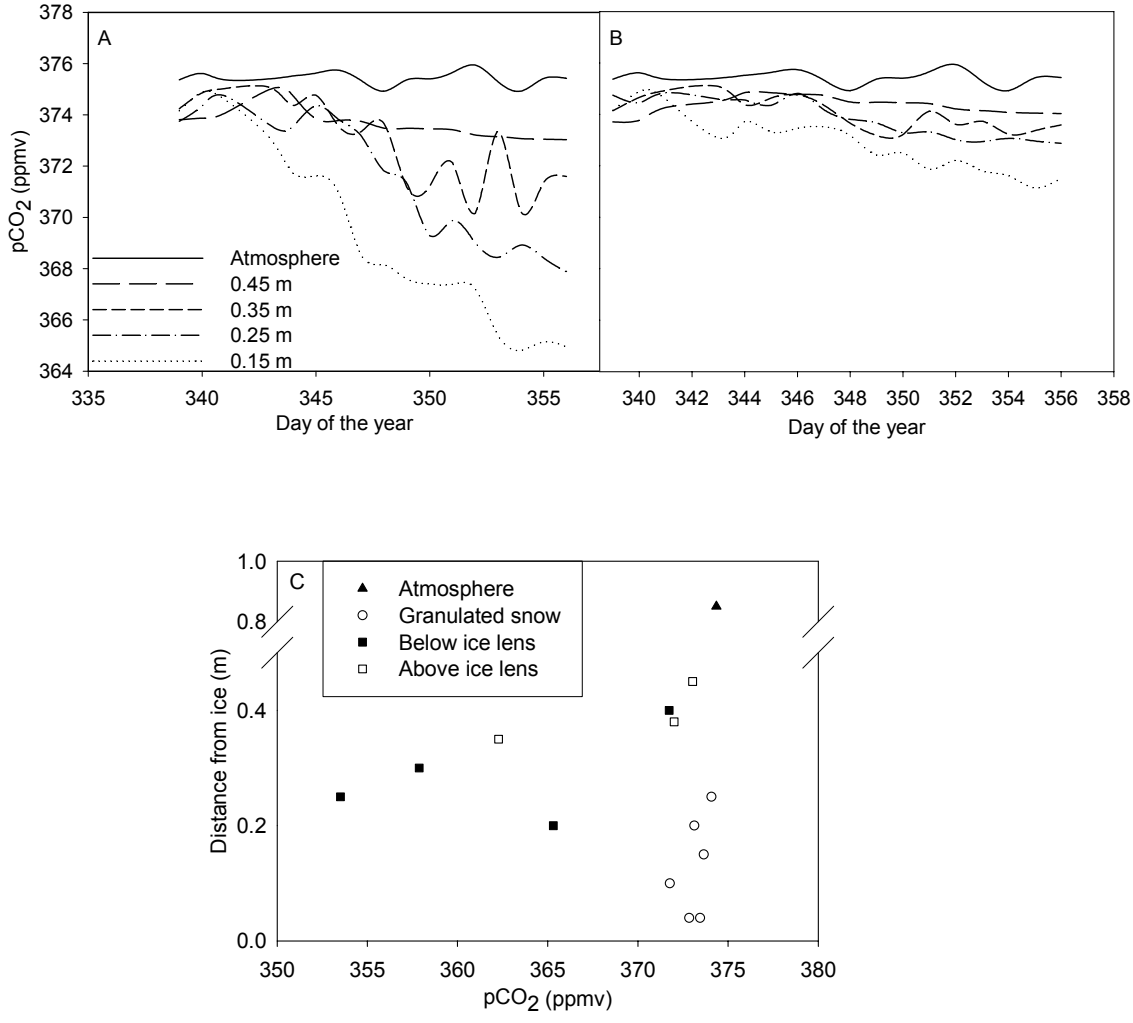

Figure 2A and B: CO_2 concentrations (ppmv) in snow, as a function of distance from the ice surface, and in the atmosphere at 0.85 m from the ice. Figure 2A, profiles over slush. Figure 2B, profiles over solid ice. Figure 2C, CO_2 concentrations (ppmv) at three locations during the last week of December. Melting and freezing resulted in extremely heterogeneous snow characteristics, showing ice formation and inclination of snow layers.

Following Takagi et al., (2005), the diffusion flux (F_d) of CO_2 through the snow layer can be evaluated by Fick's law of diffusion $F_d = D_c\theta\lambda\Delta C/\Delta z$. The binary diffusion constant for CO_2 in air (D; $0.138*10^{-4}$ m^2 s^{-1} at standard temperature (T_0) and pressure (P_0)) was corrected for observed temperature (T) and pressure (P) to determine the diffusion coefficient (D_c) as, $D_c = D\ (P_0/P)(T/T_0)^{1.81}$. A fixed value of the air-filled porosity (θ) of 0.60 cm^3 cm^{-3} (averaged over ISPOL, C. Haas, personal communication) was used to calculate the tortuosity factor λ ($\lambda = (1-(1-\theta)^{2/3})/\theta$). Using a concentration gradient ($\Delta C/\Delta z$) of CO_2 between the ice and atmosphere of 5.24 * 10^{-10} g_{CO2} cm^{-3}_{snow} cm^{-1} (maximum gradient in the snow layer observed during ISPOL), the diffusive flux during ISPOL is about 37.8 mg CO_2 m^{-2} d^{-1}, which is in the same range of values found for diffusive transport through a snowpack as measured in a forest (Takagi et al., 2005). However, it is difficult to interpret our measured gradients and the derived diffusion controlled flux because sampling 2 L of air implies that the sample is pulled from a sphere with a radius of a least 8 cm. It is likely that the air is transported over some distance, depending on the resistance in the snow.

The diffusive flux as found in Takagi et al.'s (2005) study and in this study is significantly lower than the flux measured by EC. Takagi et al. found that CO_2 concentrations in a snow pack fluctuated significantly as wind speeds increased from near zero to 2 m s^{-1}, which shows that wind-pumping strongly affects transport of CO_2 in a snowpack. Wind speeds during ISPOL varied between 1 and 14 m s^{-1}, averaging 5.3 m s^{-1}. It is therefore possible that the observed concentration gradients in the snowpack remained relatively small as a result of airflow within the snowpack, which makes turbulence the dominant transport factor and lowers the estimated influx by Fick's law. However, our study, during which measurements of CO_2 profiles in the snowpack were not made continuously, does not allow a detailed analysis of the dependence between CO_2 concentrations and wind speed as performed in the study of Takagi et al. (2005).

Depletion of CO_2 in snow-encapsulated air is especially apparent above the brown colored slush (Figure 2A, B). Increasing productivity at this interface results in a further decrease of pCO_2 throughout the snow layer over the course of December. In addition, refreezing of meltwater and the formation of ice lenses towards the end of December will hamper turbulence in the snowpack and transport of CO_2. Figure 2C shows the strong undersaturation of CO_2 below an ice lens that impedes exchange with the atmosphere, while CO_2 utilization still occurs. Above another ice lens, uptake of CO_2 also occurs, but it is partially compensated by transfer from the atmosphere. No gradients of CO_2 where observed in coarse-grained granular snow, where turbulent transport of air may not be restricted by the open structure.

4.2.5.4 Budget of CO_2 fluxes

Assuming that the multi-year ice zone in the western Weddell Sea extends to 1.3 * 10^6 km^2 (Gloersen et al. 1992) and an average carbon dioxide flux of -0.6 g CO_2 m^{-2} d^{-1} throughout December; the total carbon uptake in December alone in the multi-year ice zone could be as high as 6.6 Tg C y^{-1}. However, one can not assume that this is going to remain below the ice: part of this carbon might well return to the inorganic carbon pool and atmosphere later in the year. Hoppema et al. (1999) calculated, from estimations of entrainment (introducing 34 Tg C y^{-1} into the 100 m

surface layer) and new production (removing 42 Tg C y^{-1}) , that the total uptake of atmospheric carbon by the Weddell Sea amounted to 8 Tg C y^{-1}. However, Hoppema et al. (1999) discuss that by extrapolating their results from the offshore area to the entire Weddell Sea they probably underestimate the effect of the biological pump. In addition, the budgets presented by Hoppema et al. (1999) are annual estimates; most of the atmospheric exchange will occur in the biologically productive months: December through February. Our calculated carbon uptake is in agreement with the values derived by Hoppema et al. (1999).

4.2.6 Conclusions

The observed fluxes are significant beyond the local scale, as they amount to ~1.8% of the total uptake south of 50˚S as estimated by Takahashi et al. (2002, 2003). Although this is a very crude estimate based on the assumption that the observed ice characteristics are representative of the entire perennial ice zone of the western Weddell Sea (and that biological activity in the flooded snow pack is a common feature), it suggests that this region plays an important role in the Southern Ocean CO_2 budget.

4.2.7 Acknowledgements

This work was financially supported by the Marie Curie Training Site Fellowship (contract number HPMF-CT-2002-01865) and by NERC (award ref. number NER/B/S/2003/00844). This research was also supported in part by Belgian Science Policy (contract EV/12/7E, SD/CA/03A -Belcanto) and Belgian French Community (ARC-contract 02/07-287 - Sibclim), and by the U.S. National Science Foundation (OCE-0327601).This is the MARE contribution 084. We would like to thank WHOI Ocean Life Institute. The authors would like to express their deepest thanks and appreciation to the crew of the R.V. Polarstern for all their efforts in helping us throughout ANT XXII/2. Thanks also the chief scientist Dr. M Spindler and to the AWI for making the cruise possible.

4.3 Biogas (CO2, O2, dimethylsulfide) dynamics in Spring Antarctic fast ice

4.3.1 Foreword

In Spring 1999, prior to the two surveys described in the chapters 4.1 and 4.2, we carried out the very first indirect measurements of pCO_2 in sea ice brines. We also conducted the first survey of temporal changes of the concentration within sea ice brines of dimethylsulfide (DMS), another important climatically active gas.

During this experiment the main processes responsible for CO_2 dynamics documented in the chapter 4.1 are also highlighted. We provide here evidence for the dissolution of carbonate minerals in two stations at the start of the survey, in agreement with the observation of $CaCO_3$ crystals trapped in sea ice in the same area in 2001 (chapters 4.1, Fig. 4.1-2),. In semi-enclosed systems such as sea ice, temporal changes of O_2 allow to estimate primary production with a reasonable accuracy. The theoretical assessment of the effects on pCO_2 of primary production, dissolution of $CaCO_3$ and dilution with ice crystals is consistent with the observations. Hence, the general conclusions of Chapter 4.1 regarding to the main biogeochemical drivers of CO_2 dynamics within pack sea ice hold true in land fast sea ice. This suggests that these conclusions could also hold true for the rest of the Antarctic sea ice cover.

A shortened version of this chapter has been submitted to Limnology and Oceanography:

Delille B., B. Jourdain, A.V. Borges, J.-L. Tison and D. Delille. Biogas (CO_2, O_2 , dimethylsulfide) dynamics in Spring Antarctic fast ice.

4.3.2 Abstract

The study of the temporal variations of CO_2, O_2 and dimethylsulfide (DMS) concentrations within three environments (sea ice brine, platelet ice-like and underlying water) was carried out in the coastal area of Adélie Land, Antarctica, during spring 1999 before ice break-up. Temporal changes were contrasted between the three environments, while similar temporal trends were observed within each environment at all stations. Throughout the experiment, the underlying water exhibited both O_2 under-saturation (around 85%) and high values of the partial pressure of CO_2 (pCO_2) (up to 600 ppm) owing to mixing with deep water. O_2 concentrations increased drastically in sea ice brine as it melted to reach over-saturations up to 160 %, due to the primary production by sea ice algae community (chlorophyll a in the bottom ice increased steadily to reach concentrations up to 160 µg L^{-1} of bulk ice). In parallel, DMS concentrations drastically increased to reach concentration up to 60nmol L^{-1} within sea ice brine and the platelet ice-like layer. High biological activity also consumed CO_2 and promoted the decrease of pCO_2. Other physical and biogeochemical processes, namely melting of pure ice crystals and $CaCO_3$ dissolution, shifted the large CO_2 oversaturation (pCO_2 up to 820 ppm) to a marked CO_2 undersaturation (pCO_2 less than 30 ppm). On the whole, sea ice appeared to act as a sink of CO_2 and a source of DMS for the neighbouring environments, the underlying water or/and the atmosphere.

Keywords: pCO_2, O_2, DMS, fast sea ice, Adélie Land, Southern Ocean

4.3.3 Introduction

Sea ice covers about 7% of the Earth surface at its maximum seasonal extent, representing one of the largest biomes on the planet (Arrigo et al., 1997; Lizotte, 2001). For decades, sea ice was assumed to be an impermeable and inert barrier for air-sea exchanges of CO_2 so that global climate models do not include CO_2 exchanges between this compartment and the atmosphere (Tison et al., 2002). However, there is a growing body of evidence that sea ice exchanges CO_2 with the atmosphere. While estimating permeation constants of SF_6 and CO_2 within sea ice, Gosink et al. (1976) stressed that sea ice is a highly permeable medium for gases. These authors suggested that gas migration through sea ice could be an important factor in winter ocean-atmosphere exchange at sea ice surface temperature above -10°C. More recently, the uptake of atmospheric CO_2 over sea ice cover has been reported (Semiletov et al., 2004; Zemmelink et al., 2006; Semiletov et al., 2006; chapter 4.1), raising the need to further investigate pCO_2 dynamics in the sea ice realm and related CO_2 fluxes.

Very few studies have been carried out on the dynamics of the carbonate system within natural sea ice, and these generally aimed to investigate calcium carbonate ($CaCO_3$) precipitation processes (Gleitz et al., 1995). These studies focused on measurements of dissolved inorganic carbon (DIC) and total alkalinity (TA) (Anderson and Jones, 1985; Rysgaard et al., 2006) rather than on pCO_2. As pointed out by Rysggard et al. (2006), precipitation of carbonate minerals within sea ice could

drive significant CO_2 uptake, but such phenomenon remains to be further investigated and has not yet been systematically observed (Gleitz et al., 1995; Thomas and Dieckmann, 2002a). The observations by Rysggard et al. (2006) suggest that during sea ice formation in fall and winter, carbonate precipitation can occur within sea ice. A significant fraction of CO_2 generated as a by-product of carbonate precipitation appears to be removed during brines expulsion and is partly exported below the pycnocline during deep water formation. While CO_2 enriched brines are expelled from the ice, carbonate minerals could remain trapped in the brines tubes and channels until the spring and summer, when they would dissolve within the sea ice or in the underlying water. Such dissolution consumes CO_2 and therefore acts as a sink for atmospheric CO_2 (Rysgaard et al., 2006). Other processes can potentially act as sink of CO_2. First, sea ice hosts algae community whose primary production has been estimated to account for 10 to 28% of the total production of the Southern Ocean (e.g. Arrigo and Thomas 2004). Second, during sea ice growth, most of the impurities (solutes, gases, particulate matter) are expelled from the pure ice crystals at the ice-water interface (Killawee et al., 1998). The CO_2 rejected into the boundary layer will either diffuse or be convectively driven downwards into the underlying water, removing CO_2 from the surface water. During spring, melting of CO_2-depleted sea ice would decrease pCO_2 of the surface waters. Such mechanism would act as a sink for CO_2 atmospheric. On the whole, spring sea ice appears to act as a CO_2 sink that can be significant in the budget of CO_2 fluxes in the Southern Ocean (Zemmelink et al., 2006; chapter 4.1).

Antarctic sea ice has been shown to contain large amounts of dimethylsulphoniopropionate (DMSP) (Turner et al., 1995; Trevena et al., 2003; Gambaro et al., 2004) a precursor of dimethylsuphide (DMS), another climatically active gas. Marine DMS emissions are involved in climate regulation (Charlson et al., 1987) as atmospheric oxidation products of DMS act as condensation nuclei and therefore directly (as aerosols) and indirectly affect the radiative properties of the atmosphere (Bates et al., 1999). DMS is a by-product of DMSP which is synthesized by a few classes of marine micro- and macroalgae and some higher plants (e.g. Stefels 2000). The physiological role of DMSP in phytoplankton and sea ice algae is poorly understood (Stefels, 2000). It has been suggested that DMSP can act as an active osmolyte and cryoprotectant at the same time (Dickson and Kirst, 1986; Kirst and Wiencke, 1995; Karsten et al., 1996), an antioxidant which protects cells during oxidative stress conditions (U.V. radiation, CO_2 and/or Fe limitation, high Cu^{2+} and H_2O_2 concentration (Sunda et al., 2002)), a grazing-activated chemical defense precursor (Wolfe et al., 1997) or a “trash-can” for reduced compounds and excess energy (Stefels, 2000). DMSP release by the cell occurs during algal growth but significantly increases during cell senescence (Turner et al., 1988; Nguyen et al., 1988)or as a consequence of zooplankton grazing (Wolfe and Steinke, 1996; Dacey et al., 1998), bacterial activity (Kiene and Bates, 1990; Ledyard and Dacey, 1994; Bates et al., 1994) and viral lysis (Hill et al., 1998; Malin et al., 1998). DMS is produced by enzymatic cleavage of released DMSP by bacteria (Kiene and Bates, 1990; Ledyard and Dacey, 1994) and algae (Stefels and Van Boekel, 1993; Steinke and Kirst, 1996; Steinke et al., 1998). During sea ice melting, DMSP and DMS released from the ice can accumulate in surface waters and lead to the occurrence of DMS concentration pulses and hot-spots (Kirst et al., 1991; Levasseur et al., 1994; Trevena and Jones, 2006). Zemmelink et al. (2005) reported that the stratification due to sea ice melting fosters the production of DMSP and DMS in sea ice leads in

such amount that the resulting emission could contribute significantly to the yearly DMS flux from the Southern Ocean to the atmosphere. Hence, sea ice-related processes appears to act as a source of DMS, which could be significant in the budget of DMS fluxes to the atmosphere in the Southern Ocean.

To our best knowledge, there are very few studies on DMS and CO_2 dynamics within natural sea ice. Turner et al. (1995) investigated DMS+DMSP in the Bellingshausen Sea and Drake Passage, Trevena et al. (2006) investigated DMS in Prydz Bay and Kirst et al. (Kirst et al., 1991) and Gambaro et al. (Gambaro et al., 2004) carried out measurements of DMSP in the Weddell Sea and in Terra Nova Bay, respectively. Even less measurements of CO_2 are available: Gleitz et al. (1995) and Delille et al. (chapter 4.1) investigated CO_2 dynamics in, respectively, the Weddell sea and Eastern Antarctica. Here, we present and discuss the first joint temporal survey of DMS, pCO_2 and O_2 concentrations within sea ice brine and the underlying water.

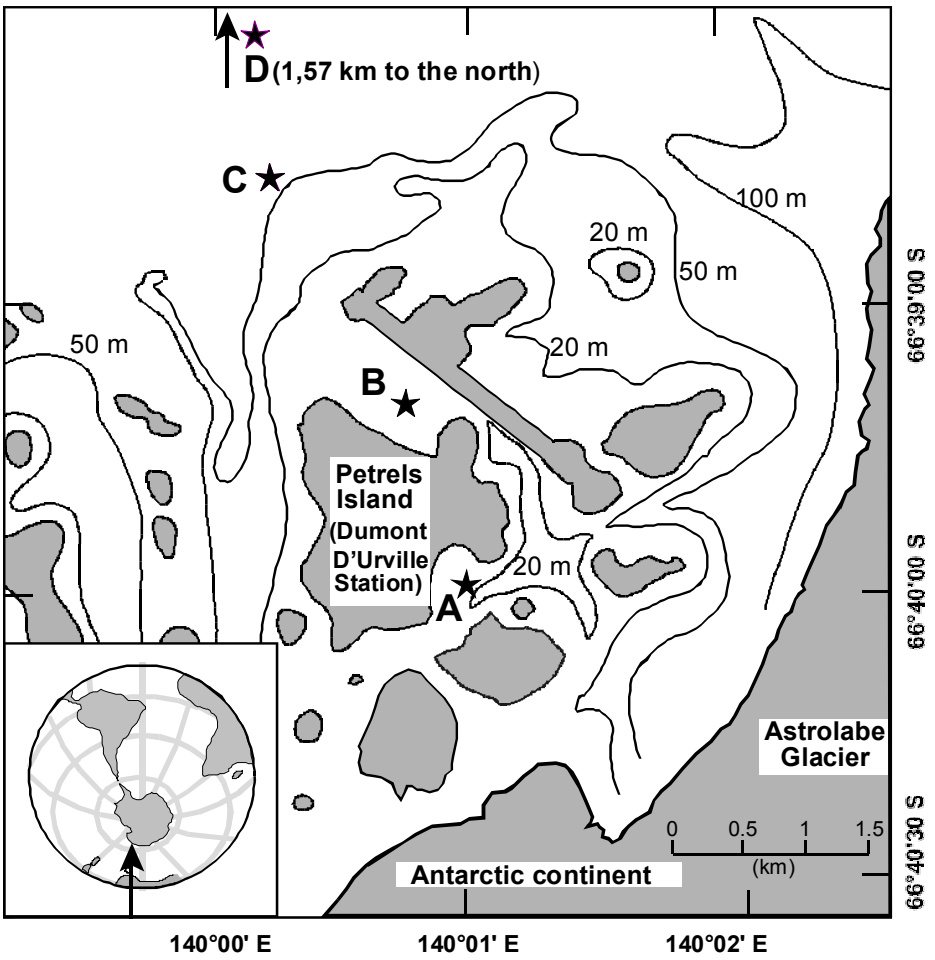

Figure 1: Location of the stations and bottom topography in the vicinity of the French base of Dumont D'Urville located on the Petrels Island – Adélie Land, Antarctica.

4.3.4 Material and Methods

Site and sampling:

The study was carried out from 10-11 to 16-12-1999 just before the sea ice cover break up in the Géologie Archipelago, Adélie Land, Antarctica (66°40' S, 140°01' E). The area is covered from March-April to December by a homogeneous and solid layer of land fast ice. Samples were collected at four contrasting stations along a South-North cross shore transect (Fig. 1). Stations A to C were located in the shallow area close to the Dumont D'Urville Station, Astrolabe Glacier and ground line of the Antarctic continent, and station D was located 3.8 km off the coast. Bottom depth increased from station A to station D and the four stations experienced various snow and ice thickness (table 1) and sheltering conditions, with station A located in a small and well sheltered cove and station D located in an open area.

station	position	bottom depth (m)	ice thickness (cm)	snow thickness (cm)
A	66°39'58"S-140°01'08"E	<10m	168-176	0
B	66°39'38"S-140°01'43"E	<20m	158-171	0-1
C	66°39'28"S-139°59'54"E	~50m	133-153	0-2
D	66°38'09"S-140°00'03"E	~200m	112-113	20

Table 1: Position of stations A to D, approximate bottom depth and ranges of snow and ice thickness.

At each station, all samples were collected within an area of about 40 m² in order to minimize a bias from spatial heterogeneity. Ice brine was sampled by drilling sackholes to a depth of 50 cm using a 10 cm internal diameter ice corer. The brine from adjacent brine channels and pockets was allowed to seep into the sackhole for 10-15 min before collection. One core was sampled for chlorophyll a and stored in a plastic bag. The bottom 10 cm of the core was cut and thawed in the dark. After drilling the ice cover, a loose matrix of water and platelet ice-like (denoted as platelet ice-like) and underlying water were collected at a depth of 0 m and 1 m, respectively. Attention was paid to avoid degassing and freezing during sampling and transportation to the laboratory.

Chlorophyll a

Chlorophyll a (Chl *a*) samples were filtered by gentle vacuum filtration of 1 L of water through Whatman® GF/F glass-fiber filters. The measurements of chlorophyll a were carried out following the recommendations of Arar and Collins (1997). Fluorescence was measured with a Turner Designs® TD 700 fluorometer.

Dissolved inorganic carbon

DIC and pCO_2 were calculated from pH and TA measurements. pH was measured using commercial combination electrodes (Ross type, Orion®) calibrated on the total hydrogen ion scale using TRIS (2-amino-2-hydroxymethyl-1,3-propanediol) and AMP (2-aminopyridine) buffers prepared at salinities of 30, 35, 40 and 80 according to Dickson (1993). pH measurements were carried out as soon as possible after returning to the laboratory (typically less than 3 h after sampling), and samples were maintained at low temperatures (typically between 0°C and 4°C). The pH electrode was calibrated at temperatures ranging from 1°C to 3°C, at salinities of 30, 35, 40 and 80. The accuracy of pH measurements was 0.01 pH units. TA was measured using the classical Gran electrotitration method on 100ml GF/F filtered samples. The accuracy of measurements was ±4 µeq kg^{-1}. The CO_2 speciation was calculated from pH and TA measurements using the CO2SYS Package (Lewis and Wallace, 1998; Pelletier et al., 1998), with the CO_2 acidity constants of Mehrbach et al. (1973) refitted by Dickson and Millero (1987), the CO_2 solubility coefficient of Weiss (1974), the SO_4^{2-} dissociation constant of Dickson (1990a), the borate acidity constant of Dickson (1990b), and the total borate molality calculated using the Uppström (1974) ratio to salinity. We assumed a conservative behaviour of CO_2 dissociation constants at subzero temperature. Indeed, Millero et al. (Millero et al., 2002) reported that the CO_2 acidity constants of Mehrbach et al. (1973) refitted by Dickson and Millero (1987) are valid on a large range of temperature, from -1.6 to 38°C. Furthermore, Marion (Marion, 2001) showed that measurements of carbonate mineral solubilities for subzero temperatures (down to -21.6°C) fit with the prediction derived from the four important equilibrium constant of the aqueous carbonate system determined only for positive temperatures, namely the first (K_1) and second (K_2) dissociation constants for carbonic acid, the Henry's Law constant for CO_2 (K_H) and the dissociation constant for water (K_W). This suggests that equilibrium constants can be assumed valid at subzero temperatures. Taking into account uncertainties on pH, TA, temperature and salinity, the errors on pCO_2 and DIC were ±14 ppm and ±9 µmole kg^{-1}, respectively.

Salinity was determined with a Guildline - Autosal® induction salinometer with an accuracy of ±0.003. Samples above a salinity of 42 were diluted with deionised water prior to measurements.

Oxygen

Dissolved oxygen in brines was measured with the Winkler method, using a potentiometric endpoint determination, with an estimated accuracy of ±2 mmol kg^{-1} (±0.8% of saturation level).

Dimethylsulfide

Dissolved DMS was sampled by flushing seawater or brines through a glass-fiber filter (Whatman GF/F, Ø47 mm) into 20 ml polyethylene vials that were completely filled and stored at 4°C, to prevent DMS loss prior to analysis. DMS analyses were performed in the field within 4 h after sampling, with a gas chromatograph equipped with a flame photometric detector (HP 6890, 393 nm). A few ml of sea-water were introduced into a glass device where DMS was degassed by a helium stream at a flow rate of 180 mL min^{-1}. DMS was then cryogenically trapped at -60°C on a tenax GC 80 loaded tube maintained in a bath of ethanol cooled by a Cryocool CC100

device. DMS was subsequently transferred to the gas chromatograph by thermal desorption of the tenax trap (boiling water) as detailed by Nguyen et al. (1990). Working chromatographic conditions were an oven temperature of 95°C, a detector temperature of 200°C, and a flow rate at the flame of 30 mL min^{-1} of helium (carrier gas), 80 mL min^{-1} of air, and 55 mL min^{-1} of hydrogen. Calibrations were performed just before analysis using a permeation tube (VICI Metronics, Santa Clara, California) placed in a bath thermostated at 30°C. This tube was calibrated against other permeation tubes used as reference for the monitoring of atmospheric DMS at Amsterdam Island (Sciare et al., 1999) and found to produce 1.18 ng of DMS per min, with no detectable shift during one year. Calibration range was typically from 1.18 to 3.54 ng of DMS. The detection limit was close to 0.2 ng of DMS, leading to a DMS detection limit under 0,3 nmol L^{-1} for 10 mL of seawater.

4.3.5 Results

4.3.5.1 Sea ice conditions

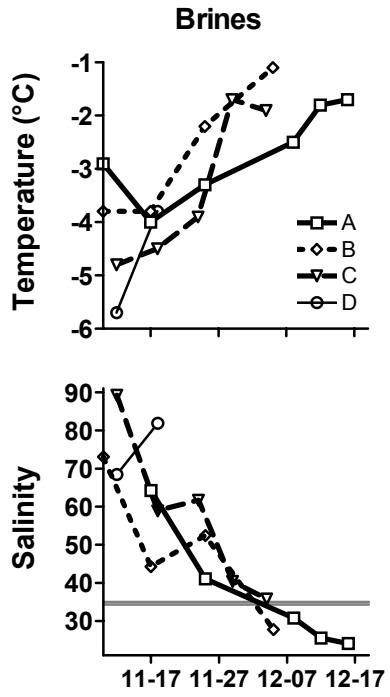

Figure 2: Temporal variation of temperature and salinity of brines. Station A: squares and thick solid line; station B: diamonds and dotted line; station C: triangles and dashed line; station D: circles and thin solid line.

Sea ice broke up progressively in the course of the survey. At the start of the experiment, open water was found approximately at 10-20 km off the coast. Strong katabatic wind took place from 22nd to 25th November and promoted offshore ice break-up that prevented further monitoring of station D, then several strong wind and ice break-up events, detailed by Riaux-Gobin et al. (2005), led to the disappearance of station B and C, while station A remained throughout the survey. In order to

investigate the evolution of pCO_2 after the ice break-up, surface water at the location of stations B, C and D were sampled on 16-12-99.

4.3.5.2 Temperature and salinity of the ice brines

In the course of the survey, brine temperature increased steadily at all stations ranging from -5.7° C at station D to -1.1 °C at station B (Fig. 2). As a consequence, ice crystals melted progressively and salinity of brines drastically decreased from 89.2 at station C down to 24 at station A (Fig. 2). By early December, salinity of brines at stations A and B was lower than the salinity of underlying seawater that ranged from 34.3 to 35.0 (data not shown).

4.3.5.3 Chlorophyll a

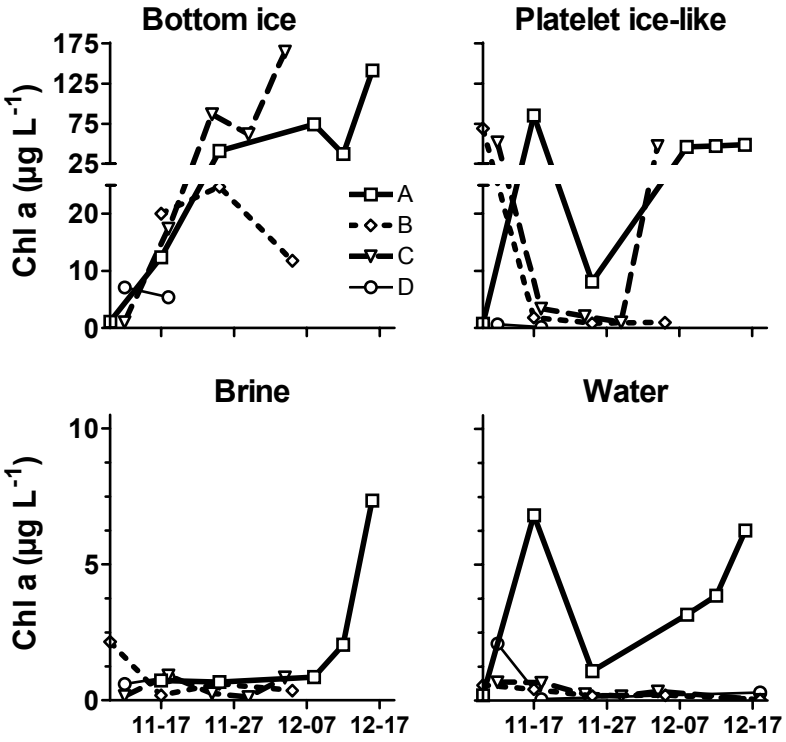

Figure 3: Temporal variation of chlorophyll a concentration (Chl ***a*****), within the underlying water, platelet ice-like and brines. Station A: squares and thick solid line; station B: diamonds and dotted line; station C: triangles and dashed line; station D: circles and thin solid line.**

Chl *a* concentration within the bottom sea ice increased drastically at stations A, B and C (Fig. 3), ranging from 1.0 µg L^{-1} up to 164.0 µg L^{-1} of bulk ice at the station A, in agreement with previous observations by Fiala et al. (2006). In contrast, Chl *a* concentration within brines remained below 2.0 µg L^{-1} except during the last days of the survey at the station A. Chl *a* concentration values in platelet-like ice layer exhibited high temporal and spatial variability, ranging from 0.2 µg L^{-1} to 85 µg L^{-1} of bulk ice. The lowest Chl *a* concentration values were observed in the underlying

water (typically less than 1.0 µg L^{-1}), with the exception of station A, where Chl *a* concentration mimics the pattern observed in the platelet ice, although with a lower magnitude (Chl *a* concentration reached a maximum value of 6.8 µg L^{-1}).

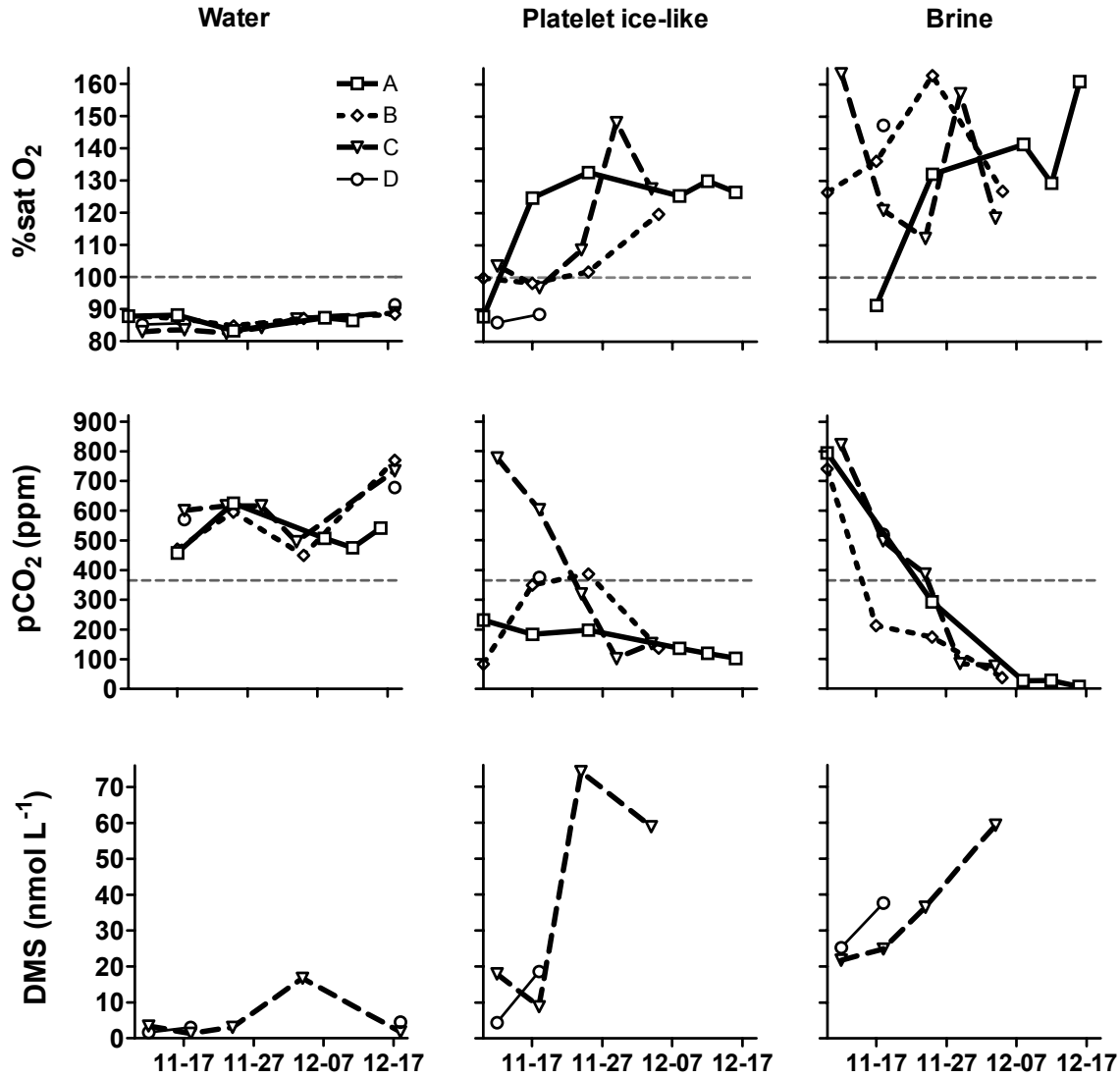

Figure 4: Temporal variation of oxygen saturation level (%O_2), partial pressure of CO2 (pCO_2) and dimethylsufide (DMS) concentration within the underlying water, platelet ice-like and brines. Station A: squares and thick solid line; station B: diamonds and dotted line; station C: triangles and dashed line; station D: circles and thin solid line. Horizontal dashed lines correspond to O_2 and CO_2 saturation levels.

4.3.5.4 Oxygen

Underlying water was under-saturated in oxygen throughout the survey as previously reported in the Weddell Sea (Hoppema et al., 1995). Oxygen saturation level ($\%O_2$) ranged from 82.5 % to 91.4 % (Fig. 4) and slightly increased from November 25 onwards. In contrast, platelet ice exhibited a drastic increase of $\%O_2$, from a slight under-saturation similar to the one in the underlying water, to a marked over-saturation up to 148 % at the station C. Before ice break up, $\%O_2$ at stations A, B and C converged toward a value of 130%. $\%O_2$ in brines showed high temporal and spatial variability, with values ranging from 110 % to 163 %.

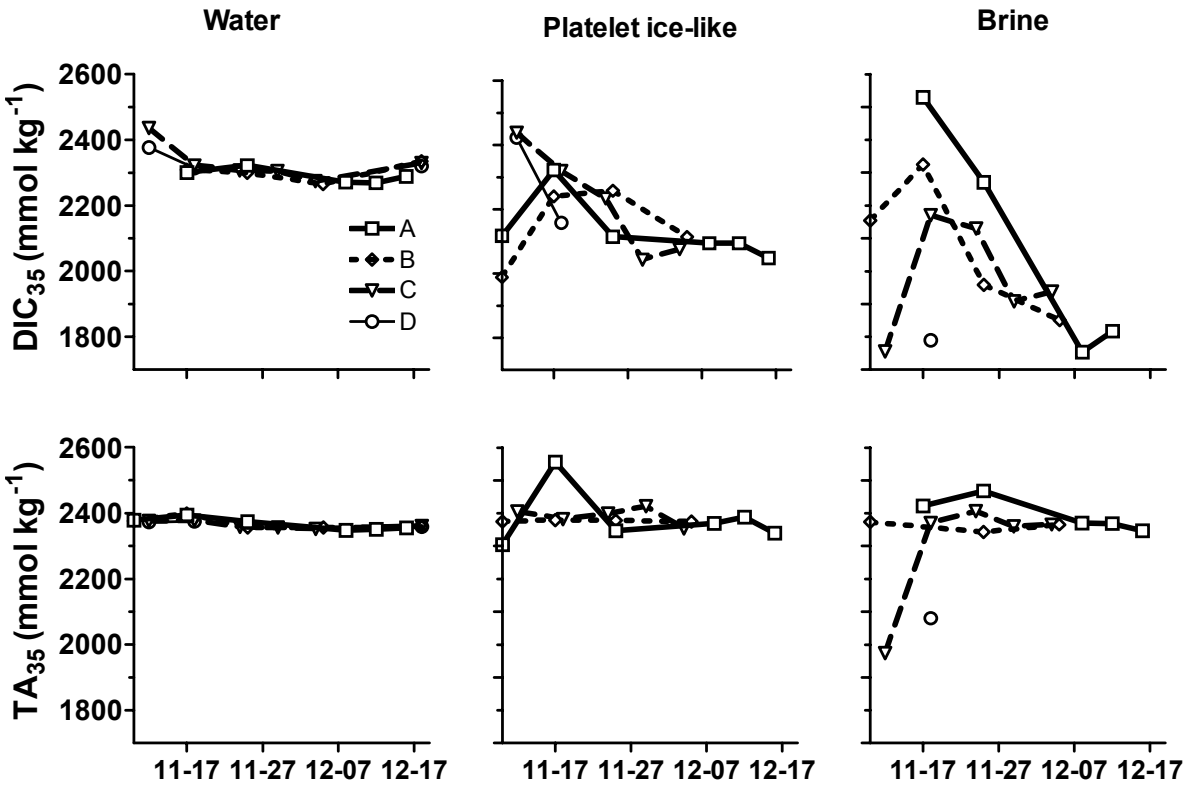

Figure 5: Temporal variation of normalized total alkalinity (TA_{35}) and dissolved inorganic carbon (DIC_{35}) at a constant salinity of 35 within the underlying water, platelet ice layer and brines. Station A: squares and thick solid line; station B: diamonds and dotted line; station C: triangles and dashed line; station D: circles and thin solid line.

4.3.5.5 pCO_2 and carbonate system

Underlying water exhibited a marked over-saturation of CO_2 with respect to atmospheric equilibrium, with pCO_2 values ranging from 450 ppm to 750 ppm (Fig. 4). At stations B and C, pCO_2 decreased to reach a minimum before ice break-up, then increased drastically to reach a maximum after break-up. pCO_2 in the platelet

ice-like showed high spatial and temporal heterogeneity, but tended to decrease to reach values below 200 ppm before the ice break-up. Stations A, B and C brines exhibited a conspicuous and similar decrease of pCO_2 from a significant over-saturation in CO_2, with pCO_2 values ranging from 720 ppm to 820 ppm, to a marked CO_2 under-saturation (pCO_2 values below 30 ppm).

DIC normalized at a constant salinity of 35 (DIC_{35}) mimicked the overall decrease of pCO_2 within platelet ice-like and brines (Fig. 5). TA normalized at a constant salinity of 35 (TA_{35}) remained constant in the underlying layer, while it exhibited a slight increase within brines at stations A and B during the first part of the experiment. This increase was enhanced at station C where, similarly to station D, TA_{35} values in the brines at the start of the survey were significantly lower than those in the underlying water. At the end of the survey, TA_{35} values within sea ice brine converged towards the values observed in sea water.

4.3.5.6 DMS

The largest changes and the highest concentrations of DMS were observed in the platelet ice-like layer where concentrations ranged from 4.4 nmol L^{-1} up to 74.0 nmol L^{-1} (Fig. 4). At station C, DMS concentrations in brines and platelet ice-like converged towards a value of 60 nmol L^{-1}, while values observed in the underlying water ranged between 1.3 nmol L^{-1} and 3.4 nmol L^{-1} and peaked at 16.7 nmol L^{-1}. Values observed in sea water are in the lower end of the range of DMS concentration reported in South Ocean waters (e.g. Trevena and Jones, 2006). DMS concentrations in brines are 4-fold higher than within sea ice. To our best knowledge, no DMS concentrations in sea ice brine have been previously reported, but it has been repeatedly reported that values of DMS, DMSP or DMS+DMSP can be one or two order of magnitude higher in sea ice compared to the underlying water (Kirst et al., 1991; Turner et al., 1995; Gambaro et al., 2004; Trevena and Jones, 2006).

4.3.6 Discussion

4.3.6.1 pCO_2 and O_2 dynamics in the underlying water

Under-saturation of oxygen (Hoppema et al., 1995; Gibson and Trull, 1999) and over-saturation of CO_2 (Weiss 1987; Bakker et al. 1997; Gibson and Trull 1999; Bronte Tilbrook, personnal communication) have been repeatedly reported beneath the ice cover in the Southern Ocean. The CO_2 over-saturation of seawater beneath ice is thought to be related to winter hydrodynamics and/or organic matter decay. To our best knowledge, the only study of under-ice pCO_2 dynamics in near shore waters surrounding Antarctica was carried out in Prydz Bay by Gibson and Trull (1999). Under-ice waters of Prydz Bay exhibited O_2 under-saturation with values ranging from 80% to 85% consistent with our observations in Adélie Land. In Prydz Bay, waters remained CO_2 under-saturated almost throughout the year, but exhibited a marked decrease of pCO_2 before ice break up. This decrease was ascribed to a sharp increase in Chl *a* concentration with values up to 15.0 µg L^{-1}, and related photosynthetic production of oxygen and uptake of CO_2. In contrast, in Adélie Land, with the exception of station A, late spring Chl *a* concentration remained below

values of 1.0 µg L^{-1} and consequently under-ice waters remained under-saturated in O_2 and over-saturated in CO_2. Further investigations are needed to explain such contrasting patterns, but one can note that the strong biological control of the pCO_2 seasonal changes in Prydz Bay is favoured by its shallowness (bottom depth lower than 30 m at a distance of 3 km off the coast) in contrast with the coastal area of Adélie Land which is characterized by a narrow shelf and marked topographic depressions. Bottom topography conjugated to strong catabatic winds, favour Antarctic bottom water formation and deep mixing (Gordon and Tchernia, 1972; Vaillancourt et al., 2003; Marsland et al., 2004) which may subsequently lead to significant upwelling of deep CO_2 rich waters. This may act to sustain CO_2 over-saturation in the Adélie Land near shore waters. Thus, the increase of pCO_2 at the very end of the survey at stations B, C and D, is probably due to wind-driven mixing of the water column that would follow ice break-up, as the water column is no longer sheltered from wind stress.

4.3.6.2 pCO_2 and O_2 dynamics within sea ice brine

While Chl *a* concentration values remained below 2.0 µg L^{-1} in brines, we observed a sustained increase of Chl *a* concentration in the bottom ice from 1.0 µg L^{-1} up to 164.0 µg L^{-1} of bulk ice during the survey. Such build-up of Chl *a* evidenced a large primary production, that consumes CO_2, acting to reduce both DIC_{35} and pCO_2, and produces O_2. We observed in brines a large O_2 over-saturation up to 163 %. Large O_2 over-saturations up to 200% have been previously observed within sea ice (Gleitz et al., 1995; Rysgaard et al., 2001).

At the start of the survey, we observed at stations C and D some TA_{35} values significantly lower than those of the underlying layer. Such patterns can be ascribed to $CaCO_3$ precipitation which would have taken place prior to the sampling period, during autumn or winter. In 2001, mineral crystals were collected within ice in the same area and have been identified as $CaCO_3$ crystals (chapter 4.1).The dissolution of $CaCO_3$ crystals trapped in sea ice can lead to the increase of TA_{35} observed at stations C and D at the start of the survey. Then, TA_{35} within sea ice brine converged to those of the underlying layer likely due to the mixing of brines with the underlying water due to internal convection (Golden et al., 1998) which is likely to occurs until salinity of brines becomes lower than the salinity of the underlying water (~ 34.7) (Fig. 2).

4.3.6.3 Assessment of the individual impact of main internal physical and biogeochemical processes on the brine pCO_2

We estimated the impact of each individual spring physical and biogeochemical sea ice processes on the pCO_2 of brines, taking into account the observed increase of temperature and related dilution of brines, together with $CaCO_3$ dissolution and organic matter production derived, respectively, from TA and O_2 changes.

Dilution Effect

pCO_2 values predicted from the increase of temperature and associated decrease of salinity ($pCO^{d}_{2\,(dil,\,t)}$) were computed on day "d" using the CO_2 dissociation

constants of Mehrbach et al. (1973) refitted by Dickson and Millero (1987) at salinity (S^d) and temperature (t^d) values of day “d”, and from TA and DIC values (denoted as $TA^d_{(dil,\,t)}$ and $DIC^d_{(dil,\,t)}$ respectively) expected from dilution according to:

$$TA^d_{(dil,\,t)} = TA^{d_0} \times \frac{S^d}{S^{d_0}} \quad (1)$$

and

$$DIC^d_{(dil,\,t)} = DIC^{d_0} \times \frac{S^d}{S^{d_0}} \quad (2)$$

where TA^{d_0}, DIC^{d_0} and S^{d_0} denote respectively TA, DIC and salinity on the first day of the time-series “d_0”.

$CaCO_3$ dissolution effect

Dissolution of $CaCO_3$ within sea ice brine is described by:

$$CaCO_3 + CO_2 + H_2O \Leftrightarrow Ca^{2+} + 2\,HCO_3^- \quad (3)$$

Dissolution of 1 mole of $CaCO_3$ transfers CO_2 to the HCO_3^- pool, increases DIC by 1 mole and TA by 2 moles. The DIC and TA changes related to the $CaCO_3$ dissolution denoted as $\Delta DIC^d_{CaCO_3}$ and $\Delta TA^d_{CaCO_3}$, were estimated by considering that the amount of $CaCO_3$ dissolved between day "d_0" and day "d" was directly related to the difference of observed TA on day "d" (TA^d) and the value expected from the dilution of TA on day "d_0" (TA^{d_0}) according to:

$$\Delta TA^d_{CaCO_3} = TA^d - TA^{d_0} \times \frac{S^d}{S^{d_0}} \quad (4)$$

and

$$\Delta DIC^d_{CaCO_3} = 0.5 \times \Delta TA^d_{CaCO_3} \quad (5)$$

Hence:

$$TA^d_{CaCO_3} = TA^{d_0} + \Delta TA^d_{CaCO_3} \quad (6)$$

and

$$DIC^d_{CaCO_3} = DIC^{d_0} + \Delta DIC^d_{CaCO_3} \quad (7)$$

pCO_2 expected from the dissolution of $CaCO_3$ ($pCO^d_{2\,(CaCO_3)}$) on day “d” was computed using the CO_2 dissociation constants of Mehrbach et al. (1973) refitted by

Dickson and Millero (1987) from $TA^{d}_{CaCO_3}$ and $DIC^{d}_{CaCO_3}$ at the initial salinity S^{d_0} and temperature t^{d_0}.

Organic Matter Production

The assessment of organic matter production within sea ice brine is difficult. The evolution of the O_2 concentration can provide a rough assessment of organic matter production by the sea ice microbial communities from the reaction of organic matter production (Redfield et al., 1963; Richards, 1965) that can be expressed as:

$$106\,CO_2 + 16\,NO_3^- + H_2PO_4^- + 17\,H^+ + 122\,H_2O \rightarrow (CH_2O)_{106}(NH_3)_{16}H_3PO_4 + 138\,O_2 \quad (8)$$

where 138 moles of O_2 are produced while 106 moles of CO_2 are consumed. We estimated the production/removal of O_2, taking into account the O_2 dilution by melting ice crystals according to:

$$\Delta O_2^d = [O_2]^d - [O_2]^{d_0} \times \frac{S^d}{S^{d_0}} \quad (9)$$

where ΔO_2^d denotes the amount of O_2 produced/removed on day “d” since day “d_0”, $[O_2]^d$ and $[O_2]^{d_0}$ denote the concentration of O_2 on day "d" and "d_0" respectively (given in µmol kg^{-1}).

DIC changes associated to the production/removal of O_2 through organic matter production is given by:

$$\Delta DIC^d_{bio} = -\frac{106}{138}\Delta O_2^d \quad (10)$$

where ΔDIC^d_{bio} denotes the DIC changes due to organic matter production by sea ice microbial communities between days "d" and "d_0". We used the Redfield ratio rather than the photosynthetic quotient (PQ), since we aimed to account for both primary production and respiration. The Redfield ratio of production of oxygen versus CO_2 consumption is about 1.30 which is close to average PQ observed in sea ice communities of ~1.43 (Glud et al. 2002).

According to (8), 1 mole of H^+ is consumed for each 1 of NO_3^- or $H_2PO_4^-$ incorporated into organic matter, increasing TA by 1 mole.

We estimated the change of TA between day "d" and "d_0", denoted as ΔTA^d_{bio}, due to organic matter production, according to:

$$\Delta TA^d_{bio} = -\frac{17}{106}\Delta DIC^d_{bio} \quad (11)$$

We then derived the values of DIC and TA expected on day “d” from the production of organic matter according to:

$$TA^d_{bio} = TA^{d_0} + \Delta TA^d_{bio} \quad (12)$$

and

$$DIC^{d}_{bio} = DIC^{d_0} + \Delta DIC^{d}_{bio} \quad (13)$$

We computed pCO_2 expected from organic matter production denoted as $pCO^{d}_{2\,(bio)}$, on day "d" from TA^{d}_{bio} and DIC^{d}_{bio} at the initial salinity S^{d_0} and temperature t^{d_0}, using the CO_2 dissociation constants of Mehrbach et al. (1973) refitted by Dickson and Millero (1987).

Finally, we computed TA and DIC derived from the summation of the three processes, respectively, TA^{d}_{all} and DIC^{d}_{all}, according to:

$$TA^{d}_{all} = TA^{d_0} + \Delta TA^{d}_{(dil,\,t)} + \Delta TA^{d}_{CaCO_3} + \Delta TA^{d}_{bio} \quad (14)$$

and

$$DIC^{d}_{all} = DIC^{d_0} + \Delta DIC^{d}_{(dil,\,t)} + \Delta DIC^{d}_{CaCO_3} + \Delta DIC^{d}_{bio} \quad (15)$$

We computed $pCO^{d}_{2\,(all)}$ from TA^{d}_{all} and DIC^{d}_{all} at the temperature t^d and salinity S^d, using the CO_2 dissociation constants of Mehrbach et al. (1973) refitted by Dickson and Millero (1987). Results from these computations at the stations A, B and C are shown in the figure 6 together with the observed pCO_2. Some biases might affect our computations since they address only the gases dissolved in brines and does not account for the amount of O_2 and CO_2 potentially trapped in bubbles. For instance, some part of the oxygen generated by the organic matter formation can accumulate in bubbles and are not accounted for in the estimate of organic matter production, while some part of CO_2 generated as a by-product of winter $CaCO_3$ formation can also be trapped in bubbles. However, despite these potential biases our computations appear to be consistent with the observations.

The temperature increase of ice brine from -5.7°C to -1.1 °C, before the ice break up, drove the melting of ice crystal and subsequent dilution of brines with a salinity decrease from 90 to 24. This dilution decreased drastically both DIC and TA and led to large pCO_2 drawdowns (Fig. 6). The effect of dilution largely outweighed the increase of pCO_2 related to the increase of temperature, and explains a large part of the observed pCO_2 patterns at all three stations.

Organic matter production led to significant changes of pCO_2 at all three stations. At station A, the magnitude of pCO_2 changes due to organic matter production was similar to those related to dilution and $CaCO_3$ dissolution. At stations B and C, the impact of organic matter production on pCO_2 appeared to be slightly lower than the effect of dilution and $CaCO_3$ dissolution. The effect of $CaCO_3$ dissolution was significant, but was only detected at the start of the experiment under relatively cold conditions, for brine temperatures below -4.5°C.

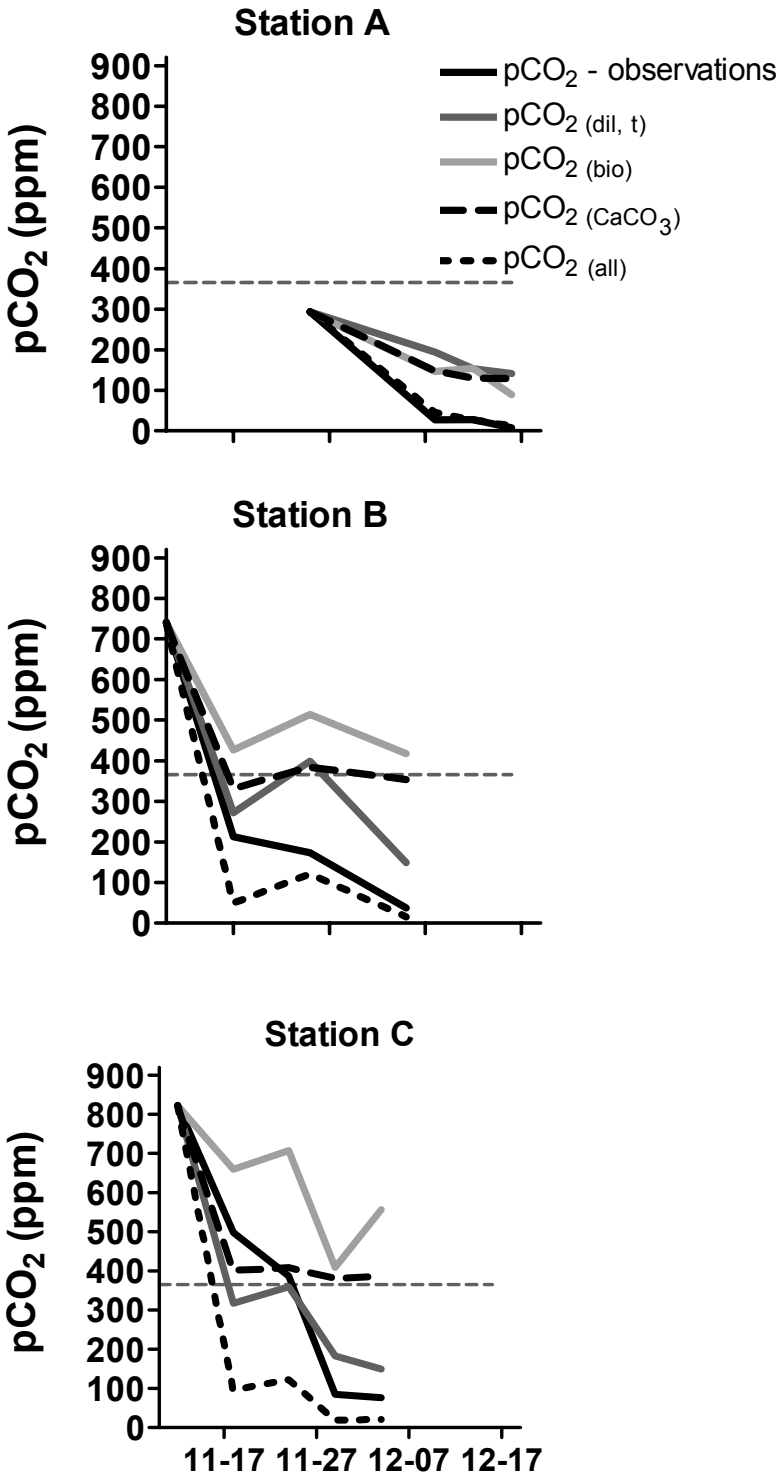

Figure 6: Observed and computed partial pressure of CO_2 (pCO_2) at stations A, B and C. Observed pCO_2: plain black line; pCO_2 computed from temperature and salinity changes (pCO_2 (dil, t)): plain dark grey line; pCO_2 computed from primary production derived from oxygen changes (pCO_2 (bio)): plain light grey line, pCO_2 computed from $CaCO_3$ dissolution derived from total alkalinity changes (pCO_2 ($CaCO_3$)): dashed black line; pCO_2 computed from all three processes (pCO_2 (all)): dotted black line. Due to poor reliability or lack of measurements of salinity of the brines on 10/11/99 at station A, simulations at this station were made from the 25-11-99 onwards. Horizontal grey dashed line corresponds to atmospheric pCO_2.

On the whole, with the exception of station A, temperature increase and related dilution appeared to be the most significant processes affecting pCO_2 during spring,

with a significant contribution from $CaCO_3$ dissolution and organic matter production to the drastic decrease in pCO_2 and subsequent CO_2 under-saturation of the sea ice brine. This CO_2 under-saturation contrasted with the CO_2 over-saturation of the underlying water which was well marked throughout the survey and even increased at the end of the experiment.

With the exception of station A, the summation of the three processes ($pCO^{d}_{2\,(all)}$) shows a predicted pCO_2 decrease which is stronger than the observations (Fig. 6). This discrepancy may be ascribed to the mixing of brines with CO_2 over-saturated underlying water or/and CO_2 transfer from the atmosphere to the ice. Both processes act to maintain pCO_2 close to or above saturation. During the survey, as the temperature of the ice brine was above -5° C the ice was permeable to both gases and liquids (Gosink et al., 1976; Golden et al., 1998) allowing both gas exchanges with the atmosphere and internal convection for brine salinities above seawater salinity. Hence, the difference between the observed and simulated pCO_2 signals corresponds to the CO_2 transfer from the neighboring environments towards the ice that appeared to act as a sink of CO_2 for the underlying water and/or the atmosphere.

4.3.6.4 DMS dynamics

DMS concentrations in the underlying water layer were significantly lower than in sea ice from the very start of the experiment. Taking into account the low and constant Chl *a* concentration in seawater, peak of DMS concentrations in seawater can be due to the input from sea ice rather than in situ production, as it has been previously suggested (e.g. DiTullio et al. 1998; Trevena and Jones 2006). As mentioned above, brine temperature was above -5°C at almost all times, and brine salinity was above the salinity of the underlying water, thus internal convection was likely to drive the transport of DMSP and DMS from the ice brine to the underlying water.

We observed a threefold increase of DMS within sea ice brine which was slightly enhanced in the platelet ice-like. This drastic increase of DMS production was inversely related to the decrease in salinity. The release of DMSP by healthy algal cells may occur in response to decreasing salinity (Stefels and Dijkhuizen, 1996) during sea ice melting as in response to rapidly decreasing osmotic conditions, considering that DMSP acts as an osmolyte (Dickson and Kirst, 1986), or due to the increase of grazing activity subsequent to the widening of brine channels (Archer et al., 1996). As mentioned above, the decrease of salinity was also associated to drastic CO_2 drawdown and O_2 increase. Sunda et al. (2002) suggested that DMSP and DMS, by scavenging hydroxyl radicals and other reactive oxygen species, may serve as antioxidants which protect the cells in case of oxidative stress and among them low CO_2 and high O_2 concentrations. This is supported by recent work of McMinn et al. (2005) which reported that the growth and photosynthesis of sea ice algae communities are adversely affected by increasing external O_2 concentrations. These authors evidenced that ice algae are submitted to an oxic stress thought to be due to the occurrence of toxic O_2 species in high O_2 conditions encountered in sea ice. One can also note that an alternative explanation to the decrease of sea ice algae growth with O_2 increase is the competition between carboxylase and oxygenase reactions at the site of ribulose-1,5-carboxylase/oxygenase. The relative

rates of both reactions depend on the concentrations of the two gases which are anti-correlated during sea ice melting and reach extreme values that potentially favour the release of DMS. On the whole, from this study it is not possible to decipher what is the main factor leading to the rapid release of DMS during sea ice melting, but it is worth noting that the decrease of salinity led to uncommon low CO_2 - high O_2 conditions that potentially favour the release of DMS.

The potentially significant flux of DMS from surface waters to the atmosphere related to sea ice melting has already been pointed out by several authors. Levasseur et al. (1994) suggested that the release following ice melting of sea ice DMSP within sea water could produce a one day pulse of DMS flux ten times higher than the average summer flux. In the same way, Trevena et al. (2006) suggested that the release of DMSP and DMS during sea ice melting may result in "hot spots" of seawater DMS with concentrations of the order of 100 nmol L^{-1}. However, in the light of the growing body of evidence that CO_2 fluxes occur at the air-sea ice interface, we surmise that as sea ice becomes permeable and allows direct gases transfer from the ice to the atmosphere, DMS may also escape from the ice directly to the atmosphere. Such transfer can be potentially significant taking into account the high DMS content of sea ice brine. Thereafter, sea ice-related DMS release to the atmosphere might not be restricted to transient (Levasseur et al., 1994) and sparse (Trevena and Jones, 2006) air-sea fluxes following sea ice melting and further studies of sea ice-related DMS emissions to the atmosphere should investigate potentially long-lasting air-ice transfer.

4.3.6.5 Platelet-ice like

pCO_2, O_2, DIC_{35} and DMS dynamics within the platelet-ice like layer mimicked patterns observed within brines. However, the magnitude of changes of O_2, pCO_2 and DIC_{35} is lower in the platelet ice-like layer than in the brines. This should be ascribed to both mixing with the underlying water and lower Chl *a* concentrations. With the exception of one measurement, TA_{35} remained constant throughout the survey indicating that no dissolution of $CaCO_3$ took place within this layer. This suggests that either $CaCO_3$ dissolution occurred prior to the survey or that in the warmer and less saline conditions (salinity ranged from 29 to 41 during the survey) of the platelet ice-like layer, $CaCO_3$ crystals formation did not occur. Finally, the few DMS measurements carried out during the survey indicated that DMS concentration was enhanced within the platelet ice-like layer compared to the brine and underlying water. This might be due to an enhanced grazing pressure within the platelet ice-like layer, which is more accessible to grazers than the plain ice cover.

4.3.7 Conclusion

Biogases (CO_2, O_2 and DMS) exhibited strong dynamics within land fast sea ice prior to the ice break-up. Elevated O_2 and DMS concentrations were due to high sea ice algae abundance and related primary production, that also decreased pCO_2. Other physical and biogeochemical processes, namely dilution of brines by melting ice crystals and $CaCO_3$ dissolution also played a significant role on pCO_2, DIC and TA dynamics. pCO_2 values expected from salinity, temperature, oxygen, and TA changes are lower than the observations prior to ice break-up, indicating the

occurrence of an additional source of CO_2. This source can be ascribed to the transfer of CO_2 from neighbouring environments, i.e. the underlying layer and the atmosphere, towards sea ice suggesting that sea ice cover was acting as a CO_2 sink for one or both neighbouring environments. In parallel, high DMS concentrations encountered within sea ice brine showed that sea ice could potentially act as a source of DMS for these neighbouring environments. According to salinity and temperature conditions, the sea ice cover was permeable to gases and liquids potentially allowing exchanges with the atmosphere. Although no measurement of DMS and CO_2 fluxes at the ice interfaces were carried out during the experiment, our data set indicates that Spring land fast sea ice can potentially act as a sink of CO_2 and as a source of DMS for the atmosphere.

4.3.8 Acknowledgments

This work could not have been done without the efficient and enthusiastic help of P. David and the other members of the Institut Paul-Emile Victor present on the Dumont D'Urville Station on November and December 1999. This research was supported by the Belgian Science Policy (contract A4/DD/B14, EV/7/12E, SD/CA/03A), the Institut Paul-Emile Victor and the FNRS with which AVB is a research associate.

5 Synthesis

Coinciding with the beginning of this work, Bakker et al. (1997) reviewed current knowledge of CO_2 dynamics in the S.O. and wrote:

The above suggests a mosaic of $fC0_2$-values in surface-water with both oversaturation and undersaturation in austral summer. [..]. From these data it is not clear whether the Southern Ocean constitutes a net sink or source of CO_2 in summer, not to mention that in winter which has hardly been sampled. Mechanisms behind the observed $fC0_2$-values in surface- water often were not identified. Minima of $fC0_2$ frequently did not correlate to elevated Chl*orophyll a levels (Robertson and Watson, 1995), i.e. biological effects were not easily identifiable. Spatial variability of fCO_2 at scales of 10-100 km was ascribed to local primary production as well as to mesoscale dynamic processes reflecting bottom topography (Poisson et al., 1993). An improved understanding of the air-sea exchange of CO_2 and its mechanisms is necessary for the Southern Ocean. Observations of seasonal evolution may improve our understanding of the underlying processes and of their variability in time and space.*

Since then what did we learn?

Bakker et al. (1997) pointed out that significant mesoscale variability of pCO_2 can occur in the S.O.. We addressed these issues in the Crozet Basin, an area that experiences merging of frontal structures (chapter 2.2) and in the vicinity of the Polar Frontal Jet over the Kerguelen Plateau (chapter 3.4). As it could be expected, mesoscale variability in the vicinity of frontal systems is tightly linked to physical processes.

First and second climatology of Takahashi et al. (Takahashi et al., 1997; Takahashi et al., 2002) showed that the S.O. acts as a sink for atmospheric CO_2. Estimation of Takahashi et al. (2002) of the overall air-sea CO_2 flux in the S.O. have been revised and is now about -0.35 PgC yr^{-1} south of 50°S, i.e. 0.21% of the global oceanic CO_2 sink (Takahashi, 2003).

In the chapter 2.4, we budgeted spring and summer air-sea CO_2 fluxes in the Indian sector of the S.O. using measurements of underway partial pressure of CO_2 (pCO_2) and SST, Chl *a* concentration and wind speed inferred from remote sensing. CO_2 fluxes were partitioned according to the main hydrological provinces of the Southern Ocean (STZ, NSAZ, SSAZ, PFZ and POOZ) using the positions of fronts derived from SST distributions (chapter 2.1). The CO_2 sink in the 35-50°S latitudinal bands is centred on the SSAZ and the overall sink strength for this latitudinal band ranges from 0.039 to 0.110 PgC in spring and from 0.032 to 0.093 PgC in summer. A further collaborative effort was carried out applying a similar approach to the western Pacific sector of the Southern Ocean (chapter 2.3). Integrating CO_2 fluxes over the

year shows that the studied area acts as a sink for atmospheric CO_2 of 0.08 PgC yr^{-1}. Both studies exhibit lower estimates than previous ΔpCO_2 - based studies (Metzl et al., 1999), but corroborate(Takahashi et al., 2002) the conclusions of inverse models indicating that ΔpCO_2 - based studies probably overestimate CO_2 fluxes in the Southern Ocean (Jacobson et al., 2005, section 1.3.1.3). Such over-estimate is not a surprise. First, Takahashi et al. (2002) overcame inter-annual variability and gathered together data collected during different years while excluding some others prone to enhanced variability owing to ENSO events. Longer time-series begin to show that interannual variability is significant (section 1.3.1.5). If we take into account the figure 1.3-2, one may ask if a new integration with recent data will not lead to a lower estimate. Second, a recurrent bias in such budget based on in situ pCO_2 measurements is the winter under-sampling. Our estimate of the chapter 2.3 is prone to such bias. OISO program aims to overcome this issue, but there are little doubts that the winter under-sampling issue will remain an obstacle towards a robust assessment of the annual budget of air-sea CO_2 fluxes for some years.

Synoptic survey of the position of these fronts inferred from remote sensing data (chapter 2.1) is a powerful tool which allows to assess CO_2 fluxes per hydrological province rather than latitudinal band. Assessment of air-sea CO_2 fluxes in the Indian sector (chapter 2.4) shows that the maximum summer CO_2 fluxes obviously follow the path of the SSTF. As a consequence, CO_2 fluxes in the PFZ, SAZ and SSTZ of the S.O. are much higher than in the POOZ and are significant contributor to the overall CO_2 uptake by the S.O.. Metzl et al. (1999; 2006) came to the same conclusion. However, in the Indian sector, CO_2 fluxes over this productive area is not accounted for in a budget limited to the region south of 50°S. Hence if the assessment of Takahashi et al. probably overestimate CO_2 fluxes south of the 50°S, considering the assessment south of 50°S as representative of the fluxes over the S.O. lead to underestimate the significance of the S.O. as a sink for CO_2 by excluding one of the most productive area. It is worth noting that if we refer to the simple view of the S.O. limited at the band south of 50°S, most of our work was not carried out in the S.O.!. Considering 44°S as the northern limit of the S.O., in the frame of some recent atmospheric model studies (section 1.3.1.3), appears to be more consistent with the definition of the S.O. as the region south of the Subtropical Front (section 1.2.1.1).

The figure 5-5-1 enlarges the perspective of our work. It presents a compilation of assessment derived from measurement carried out by the Belcanto network. This figure draw a comprehensive and consistent of CO_2 fluxes in the Indian-Australian sector of the S.O. of carbon fluxes from the atmosphere to the bathypelagic zone. Air-sea fluxes were derived from the assessments of the chapter 2.4 and are consistent with the outputs of the SWAMCO model (section 1.4.2.4). Besides, air-sea CO_2 fluxes are similar to the new production. This suggests that biological pump is the main driver of CO_2 fluxes in spring and summer in the SAZ and the PFZ.

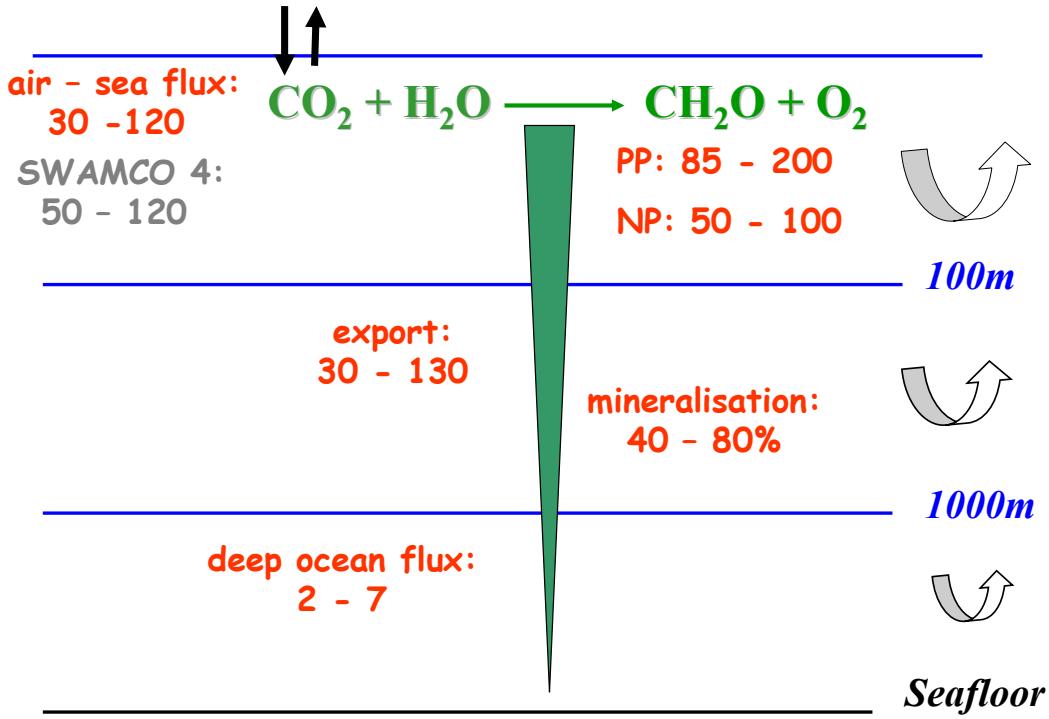

Figure 5-5-1 Synthesis of spring - summer carbon fluxes (mgC m^{-2} d^{-1}) driven by the biological pump (air-sea exchange; photosynthesis; particle export; mineralization; deep ocean particle flux); area between 35°- 54°S (SAZ and PFZ; Indian, Australian sector); PP = Primary Production, NP = New Production; Air-sea fluxes was derived from the assessment of the chapter 2.4.. SWAMCO-4 = Modeled air-sea flux. After Dehairs et al. (2006).

We presented a three years survey of pCO_2 in subantarctic coastal waters surrounding the Kerguelen Archipelago, with a particular attention on the role of *Macrocystis* giant kelp beds. Primary production of *Macrocystis* lasts from early spring to late autumn and is tightly linked to solar irradiance. Maximum net kelp community production can be as high as 15 gC m^{-2} d^{-1} at the solar irradiance climax. Such production strongly affects pCO_2 within kelp bed. Coastal waters of the archipelago experience earlier and more intense phytoplanktonic blooms than offshore waters, which markedly affect pCO_2. However, over the year near-shore waters of the archipelago act as a source of CO_2 of 0.32TgC yr^{-1}. This a modest air-sea CO_2 flux compared to the overall flux of the open waters. Such source contrast with the observation that sheltered bays of the archipelago favours early and significant blooms of phytoplankton. An explanation of this discrepancy could be that riverine inputs of terrestrial organic matter might fuel bacterial activity. This is a common feature on the distal shelf. However, it has not been previously reported for pristine environment as the Kerguelen Archipelago.

The role of sea ice cover in CO_2 budgets of the Southern Ocean has been neglected, since it was assumed as an impermeable and inert cover that prohibited

air-sea fluxes of gases. However, direct measurements of pCO_2 within sea ice and related air-sea ice CO_2 fluxes point out that CO_2 fluxes over the Antarctic sea ice cover may represent a significant additional sink to the CO_2 budget of the S.O. (chapter 4.1and 4.2). Indeed relatively warm sea ice is permeable to gases and liquids, and there is growing evidence for gas exchange between sea ice and the atmosphere. We report the first direct measurements of pCO_2 within first year pack ice, multi-year pack ice and land fast sea ice, and corresponding CO_2 fluxes at the air-sea ice interface. pCO_2 dynamics within sea ice are mostly independent of the pCO_2 in the underlying layer. Internal spring and summer sea ice specific processes (dilution with ice crystals, dissolution of carbonate minerals and primary production), drive drastic decreases of pCO_2 and lead to marked undersaturation of CO_2 with respect to the atmosphere. We observed these interactions in various locations of the S.O. and in different types of sea ice - first year pack ice, multi-year pack ice and land fast sea ice – suggesting that is a ubiquitous behaviour in the S.O. (chapters 4.1 and 4.3). Despite its thinness the Antarctic sea ice edge thus appears to sustain significant uptake of atmospheric CO_2. In parallel, biological activity produces large amounts of DMS, another climatologically active gas, highlighting the potential role of sea ice in the climate change context which have been ignored (chapter 4.3).

We propose a first tentative and conservative estimate of air-ice CO_2 fluxes over Antarctic bare sea ice cover using remote sensing measurement of sea ice surface temperature. In spring and summer, the Antarctic sea ice cover acts as a sink of atmospheric CO_2 ranging from 0.015 PgC to 0.024 PgC which represents 6% to 9% of the annual uptake of the S.O. south of 50°S (0.27 PgC yr^{-1})(chapter 4.1). However, we surmise that the present evaluation of the sea ice CO_2 sink is an underestimate, since it does not account for the uptake of CO_2 by biologically active sea ice surface communities. Eddy-covariance measurements of air-sea ice CO_2 fluxes over slush - a mixture of melting snow, ice and flooding seawater covering sea ice - which hosts abundant surface communities showed 4-fold higher fluxes than over bare sea ice (chapter 4.2). On the whole, sea ice represents an additional significant CO_2 sink that should be taken into account when budgeting exchanges of CO_2 fluxes between the S.O. and the atmosphere.

6 References

GlobalView-CO_2: Cooperative Atmospheric Data Integration Project - Carbon Dioxide. 2003. Boulder, Colorado, available on Internet via anonymous FTP to ftp.cmdl.noaa.gov, Path: ccg/CO_2/GLOBALVIEW, NOAA CMDL.

Ackley, S.F., Sullivan, C.W., 1994. Physical controls on the development and characteristics of antarctic sea-ice biological communities - a review and synthesis. Deep-Sea Research Part I-Oceanographic Research Papers 41**,** 1583-1604

Alber, M., Valiela, I., 1994. Production of microbial aggregates from macrophytes-derived dissolved organic material. Limnology and Oceanography 39**,** 37-50

Albert, M.R., Perron, F.E., 2000. Ice layer and surface crust permeability in a seasonal snow pack. Hydrological Processes 14**,** 3207-3214

Albert, M.R., Shultz, E.F., 2002. Snow and firn properties and air-snow transport processes at Summit, Greenland. Atmospheric Environment 36**,** 2789-2797

Albert, M.R., Grannas, A.M., Bottenheim, J., Shepson, P.B., Perron, F.E., 2002. Processes and properties of snow-air transfer in the high Arctic with application to interstitial ozone at Alert, Canada. Atmospheric Environment 36**,** 2779-2787

Anderson, L.G., Falck, E., Jones, E.P., Jutterstrom, S., Swift, J.H., 2004. Enhanced uptake of atmospheric CO_2 during freezing of seawater: A field study in Storfjorden, Svalbard. Journal of Geophysical Research 109**,**

Anderson, L.G., Holby, O., Lindegren, R., Ohlson, M., 1991. The transport of anthropogenic carbon dioxide into the Weddell sea. Journal of Geophysical Research 96**,** 16,679-16,687

Anderson, L.G., Jones, E.P., 1985. Measurements of total alkalinity, calcium and sulfate in natural sea ice. Journal of Geophysical Research 90**,** 9194-9198

Anderson, M.R., Rivkin, R., 2001. Seasonal patterns in grazing mortality of bacterioplankton in polar oceans : a bipolar comparison. Aquatic Microbial Ecology 25**,** 195-206

Antoine, D., Andre, J.M., Morel, A., 1996. Oceanic primary production .2. Estimation at global scale from satellite (coastal zone color scanner) chlorophyll. Global Biogeochemical Cycles 10**,** 57-69

Arar, E.J., Collins, G.B. Method 445.0: *In vitro* determination of Chlorophyll a and Pheophytin a in marine and freshwater phytoplankton by fluorescence. 1997. Cincinnati, National Exposure Research Laboratory, Office of Research and Development, U.S. Environmental Protection Agency.

Archer, D.E., Eshel, G., Winguth, A., Broecker, W., Pierrehumbert, R., Tobis, M., Jacob, R., 2000. Atmospheric pCO_2 sensitivity to the biological pump in the ocean. Global Biogeochemical Cycles 14**,** 1219-1230

Archer, D.E., Johnson, K., 2000. A Model of the iron cycle in the ocean. Global Biogeochemical Cycles 14**,** 269-279

Archer, S.D., Leakey, R.J.G., Burkill, P.H., Sleigh, M.A., Appleby, C.J., 1996. Microbial ecology of sea ice at a coastal Antarctic site: Community composition, biomass and temporal change. Marine Ecology-Progress Series 135**,** 179-195

Armstrong, R.A., 1999. An optimization-based model of iron-light-ammonium colimitation of nitrate uptake and phytoplankton growth. Limnology and Oceanography 44, 1436-1446

Armstrong, R.A., Lee, C., Hedges, J.I., Honjo, S., Wakeham, S.G., 2001. A new, mechanistic model for organic carbon fluxes in the ocean based on the quantitative association of POC with ballast minerals. Deep-Sea Research Part II 49, 219-236

Arrigo, K.R., 2003. Primary production in sea ice. In: Thomas, D.N., Dieckmann, G. (Eds.), Sea ice: an introduction to its physics, chemistry, biology and geology Blackwell Science, Oxford, pp. 143-183.

Arrigo, K.R., Robinson, D.H., Worthen, D.L., Dunbar, R.B., DiTullio, G., Vanwoert, M., Lizotte, M.P., 1999. Phytoplankton community structure and the drawdown of nutrients and CO_2 in the Southern Ocean. Science 283, 365-367

Arrigo, K.R., Thomas, D.N., 2004. Large scale importance of sea ice biology in the Southern Ocean. Antarctic Science 16, 471-486

Arrigo, K.R., Worthen, D.L., Lizotte, M.P., 1998. Primary production in Southern Ocean waters. Journal of Geophysical Research 103, 15587-15600

Arrigo, K.R., Worthen, D.L., Lizotte, M.P., Dixon, P., Dieckmann, G., 1997. Primary production in antarctic sea ice. Science 276, 394-397

Asher, W.E., Karle, L.M., Higgins, B.J., Farley, P.J., Monahan, E.C., Leifer, I.S., 1996. The influence of bubble plumes on air-seawater gas transfer velocities. Journal of Geophysical Research 101, 12027-12041

Asher, W.E., Wanninkhof, R., 1998. The effect of bubble-mediated gas transfer on purposeful dual-gaseous tracer experiments. Journal of Geophysical Research 103, 10555-10560

Assur, A., 1958. Composition of sea ice and its tensile strength. Arctic Sea Ice National Academy of Sciences-National Research Council, pp. 106-138.

Atkinson, A., Siegel, V., Pakhomov, E., Rothery, P., 2004. Long-term decline in krill stock and increase in salps within the Southern Ocean. Nature 432, 100-103

Attwood, C.G., Lucas, M.I., Probyn, T.A., McQuaid, C.D., Fielding, P.J., 1991. Production and standing stocks of the kelp macrocystis-laevis hay at the prince edward islands, Sub-Antarctic. Polar Biology 11, 129-133

Ayukai, T., Hattori, H., 1992. Production and downward flux of zooplankton fecal pellets in the anticyclonic gyre off Shikoku, Japan. Oceanologica Acta 15, 163-172

Bainbridge, A.E. GEOSECS Atlantic Expedition, volume 2: sections and profiles. 1980. Washington, U.S. Government Printing Office.

Bakker, D.C.E., de Baar, H.J.W., Bathmann, U.V., 1997. Changes of carbon dioxide in surface waters during spring in the Southern Ocean. Deep-Sea Research Part I 44, 91-127

Bakker, D.C.E., Watson, A.J., Law, C.S., 2001. Southern Ocean iron enrichment promotes inorganic carbon drawdown. Deep-Sea Research Part II 48, 2483-2507

Balch, W.M., Gordon, H.R., Bowler, B.C., Drapeau, D.T., Booth, E.S., 2005. Calcium carbonate measurements in the surface global ocean based on Moderate-Resolution Imaging Spectroradiometer data. Journal of Geophysical Research 110, C07001-doi:10.1029/2004JC002560

Bansal, M.K., 1973. Atmospheric rearation in natural streams. Water Research 7, 769-782

Barange, M., Pakhomov, E.A., Perissinotto, R., Froneman, P.W., Verheye, H.M., Taunton-Clark, J., Lucas, M.I., 1998. Pelagic community structure of the subtropical convergence region south of Africa

and in the mid-Atlantic Ocean. Deep-Sea Research Part I-Oceanographic Research Papers 45, 1663-1687

Barrón, C., Duarte, C. M., Frankignoulle, M., and Borges, A., 2006. Organic carbon metabolism and carbonate dynamics in a Mediterranean seagrass (Posidonia oceanica) meadow. Esuaries and Coasts, *in press.*

Bates, N.R., Hansell, D.A., Carlson, C.A., Gordon, L.I., 1998. Distribution of CO_2 species, estimates of net community production, and air-sea CO_2 exchange in the Ross Sea polynya. Journal of Geophysical Research 103 , 2883-2896

Bates, T.S., Charlson, R.J., Gammon, R.H., 1999. Evidence for the climatic role of marine biogenic sulphur. Nature 329, 319-321

Bates, T.S., Kiene, R.P., Wolfe, G.V., Matrai, P.A., Chavez, F.P., Buck, K.R., Blomquist, B.W., CUHEL, R.L., 1994. The cycling of sulfur in surface seawater of the northeast pacific. Journal of Geophysical Research 99, 7835-7843

Bathmann, U., Fischer, G., Muller, P.J., Gerdes, D., 1991. Short-term variations in particulate matter sedimentation off kapp norvegia, Weddell Sea, Antarctica - relation to water mass advection, ice cover, plankton biomass and feeding-activity. Polar Biology 11, 185-195

Bathmann, U.V., Noji, T.T., Voss, M., Peinert, R., 1987. Copepod fecal pellets - abundance, sedimentation and content at a permanent station in the norwegian sea in may june 1986. Marine Ecology-Progress Series 38, 45-51

Bathmann, U.V., Scharek, R., Klaas, C., Dubischar, C.D., Smetacek, V., 1997. Spring development of phytopmankton biomass and composition in major water masses of the Atlantic sector of the Southern Ocean. Deep-Sea Research Part I 44, 51-67

Beaugrand, G., Brander, K.M., Lindley, J.A., Souissi, S., Reid, P.C., 2003. Plankton effect on cod recruitment in the North Sea. Nature 426, 661-664

Behrenfeld, M.J., Falkowski, P.G., 1997. Photosynthetic rates derived from satellite-based chlorophyll concentration. Limnology and Oceanography 42, 1-20

Belkin, I.M., 1989a. Alteration of the front distributions in the Southern Ocean near the Crozet Plateau. Doklady USSR Academy of Sciences, Earth Science Section 308, 265-268English Translation.

Belkin, I.M., 1989b. Thermohaline structure, hydrological fronts, and flux of the Antarctic Circumpolar Current in the central part of the Indian sector of the Southern Ocean. Antarktika 28, 97-112in Russian.

Belkin, I.M., Gordon, A.L., 1996. Southern Ocean fronts from the Greenwich meridian to Tasmania. Journal of Geophysical Research 101, 3675-3696

Bellerby, R.G.J., Turner, D.R., Robertson, J.E., 1995. Surface pH and pCO_2 distributions in the Bellingshausen Sea, Southern Ocean, during the early Austral summer. Deep-Sea Research Part I 42, 1093-1107

Belsher, T., Mouchot, M.-C., 1992. Use of satellite imagery in management of giant kelp resources, Morbihan Gulf, Kerguelen archipelago. Oceanologica Acta 15, 297-307

Benner, R., 2002. Chemical composition and reactivity. In: Hansell DA, Carlson CA (eds) Biogeochemistry of marine dissolved organic matter. Academic Press 59-90

Berger, A., Imbrie, J., Hays, J., Kukla, G., Saltzman, B. Milankovitch and Climate. 1984.

Berger, W.H., 1982. Increase of carbon dioxide in the atmosphere during deglaciation: The coral reef hypothesis. Naturwissenschaften 69**,** 87-88

Berhenfeld, M.J., Falkowski, P.G., 1997. Photosynthetic rates derived from satellite-based chlorophyll concentrations. Limnology and Oceanography 42**,** 1-20

Berman-Frank, I., Cullen, J.T., Shaked, Y., Sherrell, R.M., Falkowski, P.G., 2001. Iron availability, cellular iron quotas, and nitrogen fixation in Trichodesmium. Limnology and Oceanography 46**,** 1249-1260

Bernard, K.S., Froneman, P.W., 2005. Trophodynamics of selected mesozooplankton in the west-Indian sector of the Polar Frontal Zone, Southern Ocean. Polar Biology 28**,** 594-606

Billen, G., Becquevort, S., 1991. Phytoplankton bacteria relationship in the antarctic marine ecosystem. Polar Research 10**,** 245-253

Blain, S., Sedwick, P.N., Griffiths, F.B., Queguiner, B., Bucciarelli, E., Fiala, M., Pondaven, P., Tréguer, P., 2002. Quantification of algal iron requirements in the Subantarctic Southern Ocean (Indian sector). Deep-Sea Research Part II 49**,** 3255-3273

Blain, S., Treguer, P., Belviso, S., Bucciarelli, E., Denis, M., Desabre, S., Fiala, M., Martin Jezequel, V., Le Fevre, J., Mayzaud, P., Marty, J.C., Razouls, S., 2001. A biogeochemical study of the island mass effect in the context of the iron hypothesis: Kerguelen Islands, Southern Ocean. Deep-Sea Research Part I 48**,** 163-187

Bopp, L., Kohfeld, K.E., Le Quere, C., Aumont, O., 2003. Dust impact on marine biota and atmospheric CO_2 during glacial periods. Paleoceanography 18**,** 1046

Bopp, L., Monfray, P., Aumont, O., Dufresne, J.L., Le Treut, H., Madec, G., Terray, L., Orr, J.C., 2001. Potential impact of climate change on marine export production. Global Biogeochemical Cycles 15**,** 81-99

Borges, A.V., 2005. Do we have enough pieces of the jigsaw to integrate CO_2 fluxes in the Coastal Ocean ? Estuaries 28**,** 3-27

Borges, A.V., Delille, B., Frankignoulle, M., 2005. Budgeting sinks and sources of CO_2 in the coastal ocean: Diversity of ecosystems counts. Geophysical Research Letters 32**,** L14601-doi:10.1029/2005GL023053

Borges, A.V., Delille, B., Schiettecatte, L.-S., Gazeau, F., Abril, G., Frankignoulle, M., 2004a. Gas transfer velocities of CO_2 in three European estuaries (Randers Fjord, Scheldt, and Thames). Limnology and Oceanography 49**,** 1630-1641

Borges, A.V., Djenidi, S., Lacroix, G., Théate, J., Delille, B., Frankignoulle, M., 2003. Atmospheric CO_2 flux from mangrove surrounding waters. Geophysical Research Letters 30**,** 1558-doi:10.1029/2003GL017143

Borges, A.V., Vanderborght, J.-P., Schiettecatte, L.-S., Gazeau, F., Ferrón-Smith, S., Delille, B., Frankignoulle, M., 2004b. Variability of the gas transfer velocity of CO_2 in a macrotidal estuary (the Scheldt). Estuaries 27**,** 593-603

Both, C., Bouwhuis, S., Lessells, C.M., Visser, M.E., 2006. Climate change and population declines in a long-distance migratory bird. Nature 441**,** 81-83

Bousquet, P., Peylin, P., Ciais, P., Le Quere, C., Friedlingstein, P., Tans, P.P., 2000. Regional Changes in Carbon Dioxide Fluxes of Land and Oceans Since 1980. Science 290**,** 1342-1346

Boutin, J., Etcheto, J., Merlivat, L., Rangama, Y., 2002. Influence of gas exchange coefficient parameterisation on seasonal and regional variability of CO_2 air-sea fluxes. Geophysical Research Letters 29**,**

Boutin, J., Rangama, Y., Etcheto, J., Merlivat, L., Takahashi, T., Delille, B., Frankignoulle, M. Variability of the air-sea CO_2 fluxes inferred from in situ and remotely sensed parameteres in the Southern Ocean. 2000. Sendai, Sixth International Carbon Dioxide Conference, Sendai 1-5 October 2001 (Japan).

Bouvy, M., Le Romancer, M., Delille, D., 1986. Significance of microheterotrophs in relation to the degradation process of sub-Antarctic kelp beds (*Macrocystis pyrifera*). Polar Biology 5**,** 249-253

Boyd, P.W., Abraham, E.R., 2001. Iron-mediated changes in phytoplankton photosynthetic competence during SOIREE. Deep-Sea Research Part II 48**,** 2529-2550

Boyd, P.W., Crossley, A.C., DiTullio, G.R., Griffiths, F.B., Hutchins, D.A., Queguiner, B., Sedwick, P.N., Trull, T.W., 2001. Control of phytoplankton growth by iron supply and irradiance in the subantarctic Southern Ocean: Experimental results from the SAZ Project. Journal of Geophysical Research 106**,** 31573-31583

Boyd, P.W., Law, C.S., 2001. The Southern Ocean Iron RElease Experiment (SOIREE)--introduction and summary. Deep-Sea Research Part II 48 **,** 2425-2438

Boyd, P.W., Watson, A.J., Law, C.S., Abraham, E.R., Trull, T., Murdoch, R., Bakker, D.C.E., Bowie, A.R., Buesseler, K.O., Chang, H., Charette, M., Croot, P., Downing, K., Frew, R., Gall, M., Hadfield, M., Hall, J., Harvey, M., Jameson, G., LaRoche, J., Liddicoat, M., Ling, R., Maldonado, M.T., McKay, R.M., Nodder, S., Pickmere, S., Pridmore, R., Rintoul, S., Safi, K., Sutton, P., Strzepek, R., Tanneberger, K., Turner, S., Waite, A., Zeldis, J., 2000. A mesoscale phytoplankton bloom in the polar Southern Ocean stimulated by iron fertilization. Nature 407**,** 695-702

Bradford-Grieve, J.M., Boyd, P.W., Chang, F.H., Chiswell, S., Hadfield, M., Hall, J.A., James, M.R., Nodder, S.D., Shushkina, E.A., 1999. Pelagic ecosystem structure and functioning in the Subtropical Front region east of New Zealand in austral winter and spring 1993. Journal of Plankton Research 21**,** 405-428

Bradford-Grieve, J.M., Chang, F.H., Gall, M., Pickmere, S., Richards, F., 1997. Size-fractionated phytoplankton standing stocks and primary production during austral winter and spring 1993 in the Subtropical Convergence region near New Zealand. New-Zealand Journal of Marine and Freshwater Research 31**,** 201-224

Brévière, E., Poisson, A., Tilbrook, B., Metzl, N., Lenton, A., Schauer, B., Pretty, M., Brunet, C. Seasonal and interannual air-sea CO_2 exchange between Tasmania and Antarctica: a high variability. 2005. Gas trasfert at water surfaces, 37th International Liège Colloquium on Ocean Dynamics, 2-6 May, Liège, Belgium.

Broecker, H.C., Peterman, J., Siems, W., 1978. The influence of wind on CO_2 exchanges in a wind-wave tunnel, including the effets of mono-layers. Journal of Marine Research 36**,** 595-610

Broecker, H.C., Siems, W., 1984. The roles of bubbles for gas transfer from water to air at higher windspeeds: experiments in wind-wave facility in Hamburg. In: Brutsaert, W., Jirka, G.H. (Eds.), Gas transfer at water surfaces Reidel, pp. 229-238.

Broecker, W., Peng, T.-H., Ostlund, G., Stuiver, M., 1985. The distribution of bomb radiocarbon in the ocean. Journal of Geophysical Research 90**,** 6953-6970

Broecker, W.S., 1982. Ocean chemistry during glacial time. Geochim. Cosmochim. Acta 46**,** 1689-1706

Brown, C.W., Yoder, J.A., 1994. Cocolithophorid blooms in the global ocean. Journal of Geophysical Research 99**,** 7467-7482

Bryan, F., 1986. High-latitude salinity effects and interhemispheric thermohaline circulations. Nature 323**,** 301-304

Brzezinski, M.A., Pride, C.J., Franck, V.M., Sigman, D.M., Sarmiento, J.L., Matsumoto, K., Gruber, N., Rau, G.H., Coale, K.H., 2002. A switch from Si(OH)(4) to NO3- depletion in the glacial Southern Ocean. Geophysical Research Letters 29**,**

Buckley, R.G., Trodahl, H.J., 1987. Thermally driven changes in the optical properties of sea ice. Cold Regions Science and Technology 14**,** 201-204

Buesseler, K.O., Andrews, J.E., Pike, S.M., Charette, M.A., 2004. The Effects of Iron Fertilization on Carbon Sequestration in the Southern Ocean. Science 304**,** 414-417

Buitenhuis, E.T., Van der Wal, P., De Baar, H.J.W., 2001. Blooms of Emiliania huxleyi are sinks of atmospheric carbon dioxide: a field and mesocosm study derived simulation. Global Biogeochemical Cycles 15**,** 577-587

Buma, A.G.J., De Baar, H.J.W., Nolting, R.F., Van Bennekom, A.J., 1991. Metal enrichment experiments in the Weddell-Scotia Seas: Effects of Fe and Mn on various plankton communities. Limnology and Oceanography 36**,** 1865-1878

Burdige, D.J., Zimmerman, R.C., 2002. Impact of sea grass density on carbonate dissolution in Bahamian sediments. Limnology and Oceanography 47**,** 1751-1763

Butler, A., 1998. Acquisition and utilization of transition metal ions by marine organisms. Science 281**,** 207-210

Caldeira, K. and Wickett, M. E., 2005. Ocean model predictions of chemistry changes from carbon dioxide emissions to the atmosphere and ocean. Journal of Geophysical Research, *in press.*

Capella, J.E., Quetin, L.B., Hofmann, E.E., Ross, R.M., 1992. Models of the early life-history of Euphausia-superba .2. Lagrangian calculations. Deep-Sea Research Part A-Oceanographic Research Papers 39**,** 1201-1220

Carstens, M. Zur ÿkologie von Schmelzwassertümpeln auf arktischem Meereis - Charakteristika, saisonale Dynamik und Vergleich mit anderen aquatischen Lebensraümen polarer Regionen. Alfred-Wegener-Institut für Polar-und Meeresforschung. 409, -325. 2002. Bremerhaven, Christian-Albrechts-Universität zu Kiel. Berichte zur Polar- und Meeresforschung.

Cavalieri, D.J., Comiso, J.C., Markus, T. *AMSR-E/Aqua Daily L3 25 km Tb, Sea Ice Temperature, and Sea Ice Conc. Polar Grids V001, September 2002 to January 2005*. [V001]. 2005. Boulder, CO, USA, National Snow and Ice Data Center.

Cember, R., 1989. Bomb radiocarbon in the red sea: Medium-scale gas exchange experiment. Journal of Geophysical Research 94**,** 2111-2123

Charette, M., Buesseler, K.O., 2000. Does iron fertilisation lead to rapid carbon export in the Southern Ocean? Geochemistry, Geophysics, Geosystems (G3)2000GC000069.

Charlson, R.J., Lovelock, J.E., Andrea, M.O., Warren, S.G., 1987. Oceanic phytoplankton atmospheric sulphur, cloud albedo and climate. Nature 326**,** 655-661

Charpy-Roubaud, C., Sournia, A., 1990. The comparative estimation of phytoplanktonic,microphytobenthic and macrophytobenthic primary production in the ocean. Marine microbial food webs 4**,** 31-57

Chen, C.T.A., 1982. On the distribution of anthropogenic CO_2 in the Atlantic and Southern ocean. Deep-Sea Research Part I 29**,** 563-580

Chen, C.Y., Durbin, E.G., 1994. Effects of pH on the growth and carbon uptake of marine phytoplankton. Marine Ecology-Progress Series 109**,** 83-94

Chierici, M., Miller, L.A., Whitney, F.A., Johnson, K.W., Wong, C.S., 2005. Biogeochemical evolution of the carbon dioxide system in the waters of long-lived mesoscale eddies in the Northeast Pacific Ocean. Deep-Sea Research II 52, 955-974

Cho, B.C., Azam, F., 1988. Major role of bacteria in biogeochemical fluxes in the ocean's interior. Nature 332, 441-443

Clarke, A., Leakey, R.J.G., 1996. The seasonal cycle of phytoplankton, macronutrients, and the microbial community in a nearshore Antarctic marine ecosystem. Limnology and Oceanography 41, 1281-1294

Clementson, L.A., Parslow, J.S., Griffiths, F.B., Lyne, V.D., Mackey, D.J., Harris, G.P., McKenzie, D.C., Bonham, P.I., Rathbone, C.A., Rintoul, S., 1998. Controls on phytoplankton production in the Australasian sector of the subtropical convergence. Deep-Sea Research Part I 45, 1627-+

Coale, K.H., Fitzwater, S.E., Gordon, R.M., Johnson, K.S., Barber, R.T., 1996a. Control of community growth and export production by upwelled iron in the equatorial Pacific Ocean. Nature 379, 621-624

Coale, K.H., Johnson, K.S., Fitzwater, S.E., Gordon, R.M., Tanner, S., Chavez, F.P., Ferioli, L., Sakamoto, C., Rogers, P., Millero, F., Steinberg, P., Nightingale, P., Cooper, D., Cochlan, W.P., Landry, M.R., Constantinou, J., Rollwagen, G., Trasvina, A., Kudela, R., 1996b. A massive phytoplankton bloom induced by an ecosystem-scale iron fertilization experiment in the equatorial Pacific Ocean. Nature 383, 495-501

Coffin, R.B., Sharp, J.H., 1987. Microbial trophodynamics in the Delaware Estuary. Marine Ecology-Progress Series 41, 253-266

Cole, J.J., Caraco, N.F., 1998. Atmospheric exchange of carbon dioxide in a low-wind oligotrophic lake measured by the addition of SF6. Limnology and Oceanography 43, 647-656

Cole, J.J., Finlay, S., Pace, M.L., 1988. Bacterial production in fresh and saltwater: a cross-system overview. Marine Ecology-Progress Series 43, 1-10

Colton, M.T., Chase, R.R.P., 1983. Interaction of the Antarctic Circumpolar Current with bottom topography: an investigation using satellite altimetry. Journal of Geophysical Research 88, 1825-1843

Comiso, J.C., 2003. Large-scale characteristics and variability of the global sea ice cover. In: Thomas, D.N., Dieckmann, G. (Eds.), Sea ice: an introduction to its physics, chemistry, biology and geology Blackwell Science, Oxford, pp. 112-142.

Conway, T.J., Tans, P.P., Waterman, L.S., Thoning, K.W., 1994. Evidence for interannual variability of the carbon-cycle from the national-oceanic-and-atmospheric-administration climate-monitoring-and-diagnostics-laboratory global-air-sampling-network. Journal of Geophysical Research-Atmospheres 99, 22831-22855

Copin-Montégut, C., 1988. A new formula for the effect of temperature on the partial pressure of carbon dioxide in seawater. Marine Chemistry 25, 29-37

Copin-Montégut, C., 1989. A new formula for the effect of temperature on the partial pressure of carbon dioxide in seawater, Corrigendum. Marine Chemistry 27, 143-144

Cota, G.F., Kottmeier, S.T., Robinson, D.H., Smith Jr, W.O., Sullivan, C.W., 1990. Bacterioplankton in the marginal ice zone of the Weddell Sea: biomass, production and metabolic activities during austral autumn. Dee-Sea Res. 37, 1145-1167

Cottrell, M.T., Kirchman, D.L., 2004. Single-cell analysis of bacterial growth, cell size, and community structure in the Delaware estuary. Aquatic Microbial Ecology 34, 139-149

Cox, G.F.N., Weeks, W.F. Brine drainage and initial salt entrapment in sodium chloride ice. 345, -85pp. 1975. CRREL research report.

Cox, G.F.N., Weeks, W.F., 1983. Equations for determining the gas and brine volumes in sea-ice samples. Journal of Glaciology 29**,** 306-316

Crosta, X., Shemesh, A., Etourneau, J., Yam, R., Billy, I., Pichon, J.J., 2005. Nutrient cycling in the Indian sector of the Southern Ocean over the last 50,000 years. Global Biogeochemical Cycles 19**,**

Culkin, F., 1965. The major constituents of seawater. In: Riley, J.P., Skirrow, G. (Eds.), Chemical Oceanography (Vol.2) Acadamic Press, London, pp. 121-161.

Dacey, J.W.H., Howse, F.A., Michaels, A.F., Wakeham, S.G., 1998. Temporal variability of dimethylsulfide and dimethylsulfoniopropionate in the Sargasso Sea. Deep-Sea Research Part I-Oceanographic Research Papers 45**,** 2085-+

Dafner, E.V., Mordasova, N.V., 1994. Influence of biotic factors on the hydrochemical structure of surface water in the Polar Frontal Zone of the Atlantic Antarctic. Marine Chemistry 45**,** 137-148

Danckwerts, P.V., 2006. Significance of liquid-film coefficient in gas absorption. Industrial Engineering Chemistry 43**,** 1460-1467

Davidson, A.T., Marchant, H.J., 1992. Protist abundance and carbon concentration during a phaeocystis-dominated bloom at an antarctic coastal site. Polar Biology 12**,** 387-395

De Baar, H.J.W., Boyd, P.W., Coale, K.H., Landry, M.R., Tsuda, A., Assmy, P., Bakker, D.C.E., Bozec, Y., Barber, R.T., Brzezinski, M.A., Buesseler, K.O., Boye, M., Croot, P.L., Gervais, F., Gorbunov, M.Y., Harrison, P.J., Hiscock, W.T., Laan, P., Lancelot, C., Law, C.S., Levasseur, M., Marchetti, A., Millero, F.J., Nishioka, J., Nojiri, Y., van Oijen, T., Riebesell, U., Rijkenberg, M.J.A., Saito, H., Takeda, S., Timmermans, K.R., Veldhuis, M.J.W., Waite, A.M., Wong, C.S., 2005. Synthesis of iron fertilization experiments: From the iron age in the age of enlightenment. Journal of Geophysical Research 110**,**

de Baar, H.J.W., de Jong, J.T.M., Bakker, D.C.E., Loscher, B.M., Veth, C., Bathmann, U., Smetacek, V., 1995. Importance of iron for plankton blooms and carbon dioxide drawdown in the Southern Ocean. Nature 373**,** 412-415

Deacon, G.E.R., 1982. Physical and biological zonation in the Southern Ocean. Deep-Sea Research Part I 29**,** 1-15

Deacon, G.E.R., 1983. Kerguelen, Antarctic and subantarctic. Deep-Sea Research Part I 30**,** 77-81

DeBaar, H.J.W., Buma, A.G.J., Nolting, R.F., Cadée, G.C., Jacques, G., Tréguer, P.J., 1990. On iron limitation of the Southern Ocean experimental observations in the Weddell and Scotia Seas. Marine Ecology-Progress Series 65**,** 105-122

Dehairs, F., Lancelot, C., André, L., Frankignoulle, M., Cattaldo, T., Elskens, M., Kopczynska, E.E., Becquevort, S., Schoemann, V., Hannon, E., Fagel, N., Cardinal, D., Navez, J., Delille, B., Kostianoy, A.G. An integrated approach to assess carbon dynamics in the Southern Ocean, Final Report. -161. 2001. Belgium, Office for Technichal, Scientifical and technical affairs.

Dehairs, F., Lancelot, C., André, L., Goosse, H., Frankignoulle, M., Becquevort, S., Borges, A., Cardinal, D., de Montety, A., Delille, B., Elskens, M., Jacquet, S.H.M., Lefebvre, W., Pasquer, B., Savoye, N., Schoemann, V. Assessing the sensitivity of the Southern Ocean's Biological pump to climate change. -+124. 2006. Belgium, Belgium Science Policy. Belcanto II - Final Report.

Delille, B., Delille, D., Fiala, M., Prevost, C., Frankignoulle, M., 2000. Seasonal changes of pCO_2 over a subantarctic Macrocystis kelp bed. Polar Biology 23**,** 706-716

Delille, B., Harlay, J., Zondervan, I., Jacquet, S., Chou, L., Wollast, R., Bellerby, R.G.J., Frankignoulle, M., Borges, A.V., Riebesell, U., Gattuso, J.-P., 2005. Response of primary production and calcification to changes of pCO_2 during experimental blooms of the coccolithophorid *Emiliania huxleyi.* Global Biogeochemical Cycles 19**,**doi:10.1029/2004GB002318.

Delille, B., Tilbrook, B., Lannuzel, D., Schoemann, V., Borges, A., Lancelot, C., Chou, L., Dieckmann, G., Tison, J.-L., 2006. Air – sea ice exchange of carbon dioxide: the end of a long-lived paradigm ? submitted to. Nature

Delille, D., 1990. Seasonal changes of subantarctic heterotrophic bacterioplankton. Archiv für Hydrobiologie 119**,** 267-277

Delille, D., 1992. Marine bacterioplankton at the Weddell Sea ice edge: distribution of psychrophilic and psychrotrophic populations. Polar Biology 12**,** 205-210

Delille, D., 1993. Seasonal changes in the abundance and composition of marine bacterial communities in an Antarctic coastal area. Polar Biology 13**,** 463-470

Delille, D., Bouvy, M., 1989. Bacterial responses to natural organic inputs in a marine subantarctic area. Hydrobiologia 182**,** 225-238

Delille, D., Bouvy, M., Cahet, G., 1988. Short term variations of bacterio-plankton in Antarctic zone: Terre Adélie area. Microbial Ecology 15**,** 293-309

Delille, D., Fiala, M., Razouls, S., 1996. Seasonal changes in bacterial and phytoplankton biomass in a subantarctic coastal area (Kerguelen Islands). Hydrobiologia 330**,** 143-150

Delille, D., Fiala, M., Rosiers, C., 1995. Seasonal changes in phytoplankton and bacterioplankton distribution at the ice-water interface in the Antarctic neritic area. Marine Ecology-Progress Series 123**,** 225-233

Delille, D., Marty, G., Cansemi-Soullard, M., Frankignoulle, M., 1997. Influence of subantarctic Macrocystis bed in diel changes of marine bacterioplankton and CO_2 fluxes. Journal of Plankton Research 19**,** 1251-1264

Delille, D., Perret, E., 1989. Influence of temperature on the growth potential of southern polar marine area. Microbial Ecology 18**,** 117-123

Delille, D., Perret, E., 1991. The influence of giant kelp Macrocystis pyrifera, on the growth of subAntarctic marine bacteria. Journal of Experimental Marine Biology and Ecology 153**,** 227-239

Delille, D., 2003. Seasonal and inter-annual variability of bacterioplankton biomass at station Kerfix, off Kerguelen Islands, Antarctica. Oceanologica Acta 26**,** 225-229

DelValls, T.A., Dickson, A.G., 1998. The pH of buffers based on 2-amino-2hydroxymetyl-1,3-propanediol ('tris') in synthetic sea water. Deep-Sea Research Part I 45**,** 1541-1554

Dickson, A.G., 1981. An exact definition of the total alkalinity and a procedure for the estimation of alkalinity and total inorganic carbon from titration data. Deep-Sea Research Part I 28**,** 609-623

Dickson, A.G., 1984. pH scales and proton-transfer reactions in saline media such as sea water. Geochimica et cosmochimica acta 48**,** 2299-2308

Dickson, A.G., 1990a. Standard potential of the reaction: $AgCl(s) + 1/2H_2(g) = Ag(s) + HCl(aq)$, and the standard acidity constant of the ion HSO_4^- in synthetic seawater from 273.15 to 318.15 K. Journal of Chemical Thermodynamics 22**,** 113-127

Dickson, A.G., 1990b. Thermodynamics of the dissociation of boric acid in synthetic seawater from 273.15 to 318.15 K. Deep-Sea Research Part I 37**,** 755-766

Dickson, A.G., 1993. pH buffers for sea water media based on the total hydrogen ion concentration scale. Deep-Sea Research Part I 40**,** 107-118

Dickson, A.G., Millero, F.J., 1987. A comparison of the equilibrium constants for the dissociation of carbonic acid in seawater media. Deep-Sea Research Part I 34**,** 1733-1743

Dickson, D.M.J., Kirst, G.O., 1986. The role of DMSP, glycine betaine and hoarine in the osmoacclimation of *Platymonas subcordiformis*. Planta 167**,** 536-543

DiTullio, G., Garrison, D.L., Mathot, S., 1998. Dimethylsulfoniopropoinate in sea ice algae from the Ross Sea Polynya. In: Lizotte, M., Arrigo, K. (Eds.), Antartcic sea ice biological processes, interactions and variability pp. 139-146.

DiTullio, G.R., Grebmeier, J.M., Arrigo, K.R., Lizotte, M.P., Robinson, D.H., Leventer, A., Barry, J.P., VanWoert, M.L., Dunbar, R.B., 2000. Rapid and early export of Phaeocystis antarctica blooms in the Ross Sea, Antarctica. Nature 404**,** 595-598

Djenidi, S., Kostianoy, A.G., Sheremet, N.A., Elmoussaoui, A. Seasonal and Interannual SST variability of the North-East Atlantic Ocean. 99-105. 2000. UNESCO. Oceanic Fronts and Related Phenomena, (Konstantin Fedorov International Memorial Symposium), IOC Workshop Report Series, n°159.

DOE, 1994. Handbook of methods for the anlysis of the various parameters of the carbon dioxide system in sea water.

Dower, K.M., Lucas, M.I., 1993. Photosynthesis-irradiance relationships and production associated with a warm-core ring shed from the agulhas retroflection south of africa. Marine Ecology-Progress Series 95**,** 141-154

Duarte, C.M., Chiscano, C.L., 1999. Seagrass biomass and production: a reassessment. Aquatic Botany 65**,** 159-174

Duarte, C.M., Middelburg, J.J., Caraco, N., 2004. Major role of marine vegetation on the oceanic carbon cycle. Biogeosciences Discussions 1**,** 659-679

Ducklow, H., Carlson, C.A., Church, M., Kirchman, D.L., Smith, D., Steward, G., 2001. The seasonal development of the bacterioplankton bloom in the Ross Sea, Antarctica, 1994–1997. Deep-Sea Research Part II 48**,** 4199-4221

Ducklow, H.W., Kirchman, D.L., 1983. Bacterial dynamics and distribution during a spring diatom bloom in the Hudson River plume, USA. Journal of Plankton Research 5**,** 333-356

Dunton, K.H., Dayton, P.K., 1995. The biology of high latitude kelp. In: Skjoldal, H.R., Hopkins, C., Erikstad, K.E., Leinaas, H.P. (Eds.), Ecology of Fjords and Coastal Waters Elsevier Science B.V., pp. 499-507.

Edson, J.B., Hinton, A.A., Prada, K.E., Hare, J.E., Fairall, C.W., 1998. Direct covariance flux estimates from mobile platforms at sea. Journal of Atmospheric and Oceanic Technology 15**,** 547-562

Edwards, M., Richardson, A.J., 2004. Impact of climate change on marine pelagic phenology and trophic mismatch. Nature 430**,** 881-884

Edwards, R.J., Emery, W.J., 1982. Australasian Southern Ocean frontal structure during summer 1976-77. Australian Journal of Marine and Freshwater Research 33**,** 3-22

Eicken, H., 2003. From the microscopic, to the macroscopic, to the regional scale: grwoth, microstructure and properties of sea ice. In: Thomas, D.N., Dieckmann, G. (Eds.), Sea ice: an introduction to its physics, chemistry, biology and geology Blackwell Science, Oxford, pp. 22-81.

Eilersten, H.C., Sandberg, S., Tollesen, H., 1995. Photoperiodic control of diatom spore growth - a theory to explain the onset of phytoplankton blooms. Marine Ecology-Progress Series 116**,** 303-307

El-Sayed, S.Z., Taguchi, S., 1981. Primary production and standing crop of phytoplankton along the ice-edge in the Weddell Sea. Dee-Sea Res. 28**,** 1017-1032

El-Sayed, S.Z., Turner, J.T., 1977. Productivity of the Antarctic and tropical/subtropical regions: a comparative study. In: Dunbar, M.J. (Ed.), Polar Oceans Arctic Institute of North America, Calgary, pp. 403-463.

El-Sayed, S.Z., Weber, L.H., 1998. Spatial and temporal variations in phytoplankton biomass and primary productivity in the southwest Atlantic and Scotia Sea. Polar Biology 1**,** 83-90

Engel, A., Delille, B., Jacquet, S., Riebesell, U., Rochelle-Newall, E., Terbrüggen, A., Zondervan, I., 2004a. Transparent exopolymer particles and dissolved organic carbon production by Emiliania huxleyi exposed to different CO_2 concentrations: a mesocosm experiment. Aquatic Microbial Ecology 34**,** 93-104

Engel, A., Thoms, U., Riebesell, U., Rochelle-Newall, E., Zondervan, I., 2004b. Polysaccharid aggregation as a potential sink of marine dissolved organic carbon. Nature 428**,** 929-932

Engel, A., Zondervan, I., Aerts, K., Beaufort, I., Benthien, A., Chou, L., Delille, B., Gattuso, J.P., Harlay, J., Heemann, C., Hoffmann, L., Jacquet, S., Nejstgaard, J., Pizay, M.D., Rochelle-Newall, E., Schneider, U., Terbrueggen, A., Riebesell, U., 2005. Testing the direct effect of CO_2 concentration on a bloom of the coccolithophorid Emiliania huxleyi in mesocosm experiments. Limnology and Oceanography 50**,** 493-507

Etcheto, J., Merlivat.L, 1988. Satellite determination of the carbon dioxide exchange coefficient at ocean-atmosphere interface:a first step. Journal of Geophysical Research 93**,** 669-678

Fairall, C.W., Hare, J.E., Edson, J.B., McGillis, W., 2000. Parameterization and micrometeorological measurement of air-sea gas transfer. Boundary-Layer Meteorology 96**,** 63-105

Falkowski, P., Scholes, R.J., Boyle, E., Canadell, J., Canfield, D., Elser, J., Gruber, N., Hibbard, K., Hogberg, P., Linder et, a., 2000. The global carbon cycle: a test of our knowledge of earth as a system. Science 290**,** 291-296

Fasham, M.J.R., Flynn, K.J., Pondaven, P., Anderson, T.R., Boyd, P.W., 2006. Development of a robust marine ecosystem model to predict the role of iron in biogeochemical cycles: A comparison of results for iron-replete and iron-limited areas, and the SOIREE iron-enrichment experiment. Deep-Sea Research Part I 53**,** 333-366

Fedorov, K.N., 1986. The Physical Nature and Structure of Oceanic Fronts. Springer-Verlag, Berlin, Heidelberg, New York, London, Paris, Tokyo.

Fedorov, K.N., Ginsburg, A.I., 1992. The Near-Surface Layer of the Ocean. Utrecht, The Netherlands.

Feely, R.A., Boutin, J., Cosca, C.E., Dandonneau, Y., Etcheto, J., Inoue, H.Y., Ishii, M., Quere, C.L., Mackey, D.J., McPhaden, M., 2002. Seasonal and interannual variability of CO_2 in the equatorial Pacific. Deep-Sea Research II 49**,** 2443-2469

Fiala, M., Delille, B., Dubreuil, C., Kopczynska, E.E., Leblanc, K., Morvan, J., Quéguiner, B., Blain, S., Cailliau, C., Conan, P., Corvaisier, R., Denis, M., Frankignoulle, M., Oriol, L., Roy, S., 2003. Mesoscale surface distribution of biogeochemical characteristics associated with a frontal system in the Crozet Basin (Southern Indian Ocean) during austral summer 1999. Marine Ecology-Progress Series 249**,** 1-14

Fiala, M., Kopczynska, E.E., Jeandel, C., Oriol, L., Vetion, G., 1998a. Seasonal and interannual variability of size-fractionated phytoplankton biomass and community structure at station Kerfix, off the Kerguelen Islands, Antarctica. Journal of Plankton Research 20**,** 1341-1356

Fiala, M., Kuosa, H., Kopczynska, E. E., Oriol, L., and Delille, D., 2006. Spatial and seasonal heterogeneity of sea ice microbial communities in the first-year ice of Terre Adélie area (Antarctica). Aquatic Microbial Ecology, *in press.*

Fiala, M., Machado, M.-C., Oriol, L., 2002. Phytoplankton distribution in the Indian sector of the Southern Ocean during spring. Deep-Sea Research Part II 49**,** 1867-1880

Fiala, M., Semeneh, M., Oriol, L., 1998b. Size-fractionated phytoplankton biomass and species composition in the Indian sector of the Southern Ocean during austral summer. Journal of Marine Systems 17**,** 179-194

Findlay, S.E.G., 2003. Bacterial response to variation in dissolved organic matter. Findlay SEG, Sinsabaugh RL (eds) Aquatic ecosystems: interactivity of dissolved organic matter Academic Press, San Diego, pp. 366-379.

Fortier, L., Le Fevre, J., Legendre, L., 1994. Export of biogenic carbon to fish and to the deep ocean: the role of large planktonic microphages. Journal of Plankton Research 16**,** 809-839

Fouilland, E., Descolas-Gros, C., Courties, C., Pons, V., 1999. Autotrophic carbon assimilation and biomass from size-fractionated phytoplankton in the surface waters across the subtropical frontal zone (Indian Ocean). Polar Biology 21**,** 90-96

Foxton, P., 1966. The distribution and life history of Salpa thompsoni Foxton with observations on a related species, Salpa gerlachei. Discovery Rep. 34**,** 1-116

Frankignoulle, M., 1988. Field measurements of air-sea CO_2 exchange. Limnology and Oceanography 33**,** 313-322

Frankignoulle, M., 1994. A complete set of buffer factors for acid/base CO_2 system in seawater. Journal of Marine Systems 5**,** 111-118

Frankignoulle, M., Borges, A.V., 2001a. Direct and indirect pCO_2 measurements in a wide range of pCO_2 and salinity values (the Scheldt estuary). Aquatic Geochemistry 7**,** 267-273

Frankignoulle, M., Borges, A.V., 2001b. European continental shelf as a significant sink for atmospheric carbon dioxide. Global Biogeochemical Cycles 15**,** 569-576

Frankignoulle, M., Borges, A.V., Biondo, R., 2001. A new design of equilibrator to monitor carbon dioxide in highly dynamic and turbid environments. Water Research 35**,** 1344-1347

Frankignoulle, M., Bouquegneau, J.-M., 1987. Seasonal variations of the diel carbon budget of a marine macrophytes ecosystem. Marine Ecology-Progress Series 38**,** 197-199

Frankignoulle, M., Bouquegneau, J.-M., 1990. Daily and yearly variations of total inorganic carbon in a productive coastal area. Estuarine, Coastal and Shelf Science 30**,** 79-89

Frankignoulle, M., Bourge, I., Wollast, R., 1996a. Atmospheric CO_2 fluxes in a highly polluted estuary (The Scheldt). Limnology and Oceanography 41**,** 365-369

Frankignoulle, M., Canon, C., Gattuso, J.-P., 1994. Marine calcification as a source of carbon dioxide: positive feedback to increasing atmospheric CO_2. Limnology and Oceanography 39**,** 458-462

Frankignoulle, M., Distèche, A., 1984. CO_2 chemistry in the water column above a *Posidonia* seagrass bed and related air-sea exchanges. Oceanologica Acta 7**,** 209-219

Frankignoulle, M., Distèche, A., 1987. Study of the transmission of the diurnal CO_2 concentration changes observed above a *Posidonia* seagrass bed. A method to determine the turbulent diffusion coefficient in a 8 meters water column. Continental Shelf Research 7**,** 67-76

Frankignoulle, M., Gattuso, J.-P., Biondo, R., Bourge, I., Copin-Montégut, G., Pichon, M., 1996b. Carbon fluxes in coral reefs. II. Eulerian study of inorganic carbon dynamics and measurement of air-sea CO_2 exchanges. Marine Ecology-Progress Series 145**,** 123-132

Franks, P.J.S., 1992. Phytoplankton blooms at fronts: patters, scales, and physical forcing mechanisms. Rev. Aquat. Sci. 6**,** 121-137

Frew, N.M., 1997. The Role of Organic Films in Air-Sea Gas Exchange. In: Liss, P.S., Duce, R. (Eds.), The Sea Surface and Global Change Cambridge University Press, Cambridge, pp. 121-172.

Frew, N.M., Bock, E.J., Schimpf, U., Hara, T., Haussecker, H., Edson, J.B., McGillis, W.R., Nelson, R.K., McKenna, S.P., Uz, B.M., Jahne, B., 2004. Air-sea gas transfer: Its dependence on wind stress, small-scale roughness, and surface films. Journal of Geophysical Research 109**,**

Friedmann, E.I., 1993. Antarctic Microbiology. Wiley, New York.

Friis, K., Körtzinger, A., Wallace, D.W.R., 2003. The salinity normalization of marine inorganic carbon chemistry data. Geophysical Research Letters 30**,**

Froneman, P.W., Laubscher R.K., McQuaid, C.D., 2001. Size-fractionated primary production in the south Atlantic and Atlantic sectors of the Southern Ocean. Journal of Plankton Research 23**,** 611-622

Froneman, P.W., McQuaid, C.D., Laubscher R.K., 1999. Size-fractionated primary production studies in the vicinity of the Subtropical Front and an adjacent warm-core eddy south of Africa in austral winter. Journal of Plankton Research 21**,** 2019-2035

Froneman, P.W., McQuaid, C.D., Perissinotto, R., 1995. Biogeographic structure of the microphytoplankton assemblages of the south Atlantic and Southern Ocean during austral summer. Journal of Plankton Research 17**,** 1791-1802

Fuhrman, J.A., Sleeter, T.D., Carlson, C.A., 1989. Dominance of bacterial biomass in the Sargasso Sea and its ecological implications. Marine Ecology-Progress Series 57**,** 207-217

Fukunaga, N., Russell, N.J., 1990. Membrane lipid composition and glucose uptake in two psychrotolerant bacteria from Antarctica. J. Gen. Microbiol. 136**,** 1669-1673

Furuya, K., Hasumoto, H., Nakai, T., Nemoto, T., 1986. Phytoplankton in the Subtropical Convergence during the austral summer: community structure and growth activity. Dee-Sea Res. 33**,** 621-630

Gall, M., Hawes, I., 1999. Predicting rates of primary production in the vicinity of the Subtropical Convergence east of New Zealand. New-Zealand Journal of Marine and Freshwater Research 33**,** 443-455

Gambaro, A., Moret, I., Piazza, R., Andreoli, C., Da Rin, E., Capodaglio, G., Barbante, C., Cescon, P., 2004. Temporal evolution of DMS and DMSP in Antarctic coastal sea water. International Journal of Environmental Analytical Chemistry 84**,** 401-412

Gambéroni, L., Géronimi, J., Jeanin, P.F., Murail, J.F., 1982. Study of frontal zones in the Crozet-Kerguelen region. Oceanologica Acta 5**,** 289-299

Gao, K., Aruga, Y., Asada, K., Kiyohara, M., 1993. Influence of enhanced $C0_2$ on growth and photosynthesis of the red algae gracilaria sp and g-chilensis. Journal of Applied Phycology 5**,** 563-571

Gao, K., McKinley, K.R., 1994. Use of macroalgae biomass production and CO_2 remediation: a review. Journal of Applied Phycology 6**,** 45-60

Garabato, A.C.N., Polzin, K.L., King, B.A., Heywood, K.J., Visbeck, M., 2004. Widespread intense turbulent mixing in the Southern Ocean. Science 303**,** 210-213

Garrison, D.L., Close, A.R., Reimnitz, E., 1989. Algae concentrated by frazil ice - evidence from laboratory experiments and field-measurements. Antarctic Science 1**,** 313-316

Gattuso, J.-P., Frankignoulle, M., Bourge, I., Romaine, S., Buddemeier, R.W., 1998a. Effect of calcium carbonate saturation of seawater on coral calcification. Global an Planetary Change 18**,** 37-46

Gattuso, J.-P., Frankignoulle, M., Wollast, R., 1998b. Carbon and carbonate metabolism in coastal aquatic ecosystems. Annual Review Ecology Systematics 29**,** 405-433

Gazeau, F., Duarte, C.M., Gattuso, J.-P., Barrón, C., Navarro, N., Ruíz, S., Prairie, Y.T., Calleja, M., Delille, B., Frankignoulle, M., Borges, A.V., 2005. Whole-system metabolism and CO_2 fluxes in a Mediterranean Bay dominated by seagrass beds (Palma Bay, NW Mediterranean). Biogeosciences 2**,** 87-96

Gazeau, F., Smith, S.V., Gentili, B., Frankignoulle, M., Gattuso, J.-P., 2004. The European coastal zone: characterization and first assessment of ecosystem metabolism. Estuarine, Coastal and Shelf Science 60**,** 673-694

Gibson, J.A.E., Garrick, R.C., Burton, H.R., 1990. Seasonal fluctuation of bacterial numbers near the Antarctic continent. Proc Natl Inst Polar Res (NIPR) Symp Polar Biol 3**,** 16-22

Gibson, J.A.E., Trull, T.W., 1999. Annual cycle of fCO_2 under sea-ice and in open water in Prydz Bay, East Antarctica. Marine Chemistry 66**,** 187-200

Gleitz, M., v.d.Loeff, M.R., Thomas, D.N., Dieckmann, G.S., Millero, F.J., 1995. Comparison of summer and winter in organic carbon, oxygen and nutrient concentrations in Antarctic sea ice brine. Marine Chemistry 51**,** 81-91

Gloersen, P., Campbell, W.J., Cavalieri, D.J., Comiso, J.C., Parkinson, C.L., Zwally, H.J., 1992. Arctic and Antarctic sea ice, 1978-1987: Satellite passive-microwave observations and analysis. Washington, DC.

Gloor, M., Gruber, N., Sarmiento, J.L., Sabine, C.L., Feely, R.A., Rödenbeck, C., 2003. A first estimate of present and preindustrial air-sea CO_2 flux patterns based on ocean interior carbon measurements and models. Geophysical Research Letters 30**,**doi:10.1029/2002GL015594.

Glud, R.N., Rysgaard, S., Kuhl, M., 2002. A laboratory study on O-2 dynamics and photosynthesis in ice algal communities: quantification by microsensors,O-2 exchange rates, C-14 incubations and a PAM fluorometer. Aquatic Microbial Ecology 27**,** 301-311

Goeyens, L., Tréguer, P., Lancelot, C., Mathot, S., Becquevort, S., Morvan, J., Dehairs, F., Bayens, W., 1991. Ammonium regeneration in the Scotia-Weddell confluence area during spring 1988. Marine Ecology-Progress Series 78**,** 141-252

Golden, K.M., Ackley, S.F., Lytle, V.I., 1998. The percolation phase transition in sea ice. Science 282**,** 2238-2241

Goosse, H., Fichefet, T., 1999. Importance of ice-ocean interactions for the global ocean circulation: A model study. Journal of Geophysical Research 104**,** 23337-23355

Gordon, A.L., Tchernia, P., 1972. Waters of the continental margin off Adélie coast, Antarctica. In: Hayes, D.E. (Ed.), Antarctic Oceanology 2: The Australian-New Zealand sector American Geophysical Union, pp. 59-69.

Gosink, T.A., Pearson, J.G., Kelley, J.J., 1976. Gas movement through sea ice. Nature 263**,** 41-42

Goyet, C., Beauverger, C., Brunet, C., Poisson, A., 1991. Distribution of carbon dioxide partial pressure in surface waters of the Southwest Indian Ocean. Tellus 43B**,** 1-11

Goyet, C., Poisson, A., 1989. New determination of carbonic acid dissociation constants in seawater as a function of temperature and salinity. Deep-Sea Research Part I 36**,** 1635-1654

Gradinger, R., Meiners, K., Plumley, G., Zhang, Q., Bluhm, B.A., 2005. Abundance and composition of the sea-ice meiofauna in off-shore pack ice of the Beaufort Gyre in summer 2002 and 2003. Polar Biology 28**,** 171-181

Gradinger, R., Nürnberg, D. Snow algal communities on arctic ack ice floes dominated by Chlamydomonas Nivalis (Bauer) wille. 9, 35-43. 1996. Proc. NIPR Symp. Polar Biol.

Gran, G., 1952. Determination of the equivalence point in potentiometric titration, part II. Analyst 77**,** 661-671

Granskog, M.A., Kaartokallio, H., Shirasawa, K., 2003. Nutrient status of Baltic Sea ice: Evidence for control by snow-ice formation, ice permeability, and ice algae. Journal of Geophysical Research 108**,**

Griffith, P.C., Douglas, D.J., Wainright, S.C., 1990. Metabolic activity of size-fractionated microbial plankton in estuarine, nearshore, and continental shelf waters of Georgia. Marine Ecology-Progress Series 59**,** 263-270

Griffiths, R.W., Pearce, A.F., 2002. Instability and eddy pairs on the Leeuwin Current south of Australia. Deep-Sea Research Part I 32**,** 1511-1534

Gruber, N., Friedlingstein, P., Field, C.B., Valentini, R., Heimann, M., Richey, J.E., Romero-Lankao, P., Schulze, D., Chen, C.T.A., 2004. The vulnerability of the carbon cycle in the 21st century: An assessment of carbon-climate-human interactions. In: Field, C.B., Raupach, M.R. (Eds.), The Global Carbon Cycle: Integrating Humans, Climate, And The Natural World. Island Press, Washington, D.C., pp. 45-76.

Gruber, N., Mikaloff Fletcher, S.E., Jacobson, A.R., Gloor, M., Sarmiento, J.L., Takahashi, T., OIP Members. Oceanic sources and sinks for atmospheric CO_2. 2005. Seventh International Carbon Dioxide Conference, Boulder, Colorado, U.S.A., September 25-30.

Grundlingh, M.L., 1978. Drift of a satellite-tracked buoy in the southern Agulhas Current and Agulhas Return Current. Deep-Sea Research Part I 25**,** 1209-1224

Gualtieri, C., Gualtieri, P., Doria, G.P., 2006. Dimensional analysis of reaeration rate in streams. Journal of the Environmental Engineering 128**,** 12-18

Guérin, F., Abril, G., Serça, D., Delon, C., Richard, S., Delmas, R., Tremblay, A., and Varfalvy, L., 2006. Gas transfer velocities of CO_2 and CH4 in a tropical reservoir and its river downstream. Journal of Marine Systems, *in press.*

Guilderson, T.P., Fairbanks, R.G., Rubenstone, J.L., 1994. Tropical temperature variations since 20,000 years ago: modulating interhemispheric climate change. Science 263**,** 663-665

Gurney, K.R., Law, R.M., Denning, A.S., Rayner, P.J., Pak, B.C., Baker, D., Bousquet, P., Bruhwiler, L., Chen, Y.H., Ciais, P., Fung, I.Y., Heimann, M., John, J., Maki, T., Maksyutov, S., PEYLIN, P., Prather, M., Taguchi, S., 2004. Transcom 3 inversion intercomparison: Model mean results for the estimation of seasonal carbon sources and sinks. Global Biogeochemical Cycles 18**,**doi:10.1029/2003GB002111.

Haas, C., 2003. Dynamics versus thermodynamics: the sea ice thickness distribution. In: Thomas, D.N., Dieckmann, G. (Eds.), Sea ice: an introduction to its physics, chemistry, biology and geology Blackwell Science, Oxford, pp. 82-111.

Haas, C., Thomas, D.N., Bareiss, J., 2001. Surface properties and processes of perennial Antarctic sea ice in summer. Journal of Glaciology 47**,** 613-625

Hall, A., Visbeck, M., 2002. Synchronous variability in the southern hemisphere atmosphere, sea ice, and ocean resulting from the annular mode. Journal of Climate 15**,** 3043-3057

Hall, J.A., Safi, K., 2001. The impact of in situ Fe fertilisation on the microbial food web in the Southern Ocean. Deep-Sea Research Part II 48**,** 2591-2613

Hannon, E., Boyd, P.W., Silvoso, M., Lancelot, C., 2001. Modeling the bloom evolution and carbon flows during SOIREE: Implications for future in situ iron-enrichments in the Southern Ocean. Deep-Sea Research Part II 48**,** 2745-2773

Hansson I, 1973. A new set of acidity constants of carbonic acid and boric acid in seawater. Deep-Sea Research Part I 20**,** 461-478

Hartmann, D.L., Lo, F., 1998. Wave-driven zonal flow vacillation in the Southern Hemisphere. Journal of the Atmospheric Sciences 55**,** 1303-1315

Hasle, G.R., 1969. An analysis ofthe phytoplankton of the Pacific Southern Ocean; abundance, composition and distribution during the Bratteg Exp. 1947-48. Hvalräd Skr. 52**,** 1-168

Hays, J.D., Imbrie, J., Shackleton, N.J., 1976. Variations in the Earth's orbit: Pacemaker of the Ice Ages. Science 194**,** 1121-1132

Heimdal, B.R., 1997. Modern coccolithophorids. In: Tomas, C.R. (Ed.), Identifying marien phytoplankton. San Diego, pp. 731-831.

Helbling, E.W., Villafane, V.E., Holm-Hansen, O., 1995. Variability of phytoplankton distribution and primary production around Elephant Island, Antarctica, during 1990-1993. Polar Biology 15**,** 233-246

Hennessey, J.P., 1977. Some aspects of wind speed statistics. Journal of Applied Meteorology 16**,** 119-128

Hense, I., Bathmann, U.V., Timmermann, R., 2000. Plankton dynamics in frontal systems of the Southern Ocean. Journal of Marine Systems 27**,** 235-252

Hesshaimer, V., Heimann, M., Levin, I., 1994. Radiocarbon evidence for a smaller oceanic carbon dioxide sink than previously believed. Nature 370**,** 201-203

Heywood, K.J., Naveira Garabato, A.C., Stevens, D.P., 2002. High mixing rates in the abyssal Southern Ocean. Nature 415**,** 1011-1014

Higbie, R., 1935. The role of a pure gas into a still liquid during short priod of exposure. Transm. Am. Inst. Chem. Engr 35**,** 365-373

Hill, R.W., White, B.A., Cottrell, M.T., Dacey, J.W.H., 1998. Virus-mediated total release of dimethylsulfoniopropionate from marine phytoplankton: a potential climate process. Aquatic Microbial Ecology 14**,** 1-6

Hillebrand, H., Durselen, C.D., Kirschtel, D., Pollingher, U., Zohary, T., 1999. Biovolume calculation for pelagic and benthic microalgae. Journal of Phycology 35**,** 403-424

Hintsa, E.J., Dacey, J.W.H., McGillis, W.R., Edson, J.B., Zappa, C.J., Zemmelink, H.J., 2004. Sea-to-air fluxes from measurements of the atmospheric gradient of dimethylsulfide and comparison with

simultaneous relaxed eddy accumulation measurements. Journal of Geophysical Research 109, doi:10.1029/2002JC001617

Hirst, A.C., 1999. The Southern Ocean response to global warming in the CSIRO coupled ocean-atmosphere model. Environmental Modelling and Software 14, 227-241

Hiwatari, T., Yuzawa, A., Okazaki, M., Yamamoto, M., Akano, T., Kiyohara, M., 1995. Effects of CO_2 concentrations on growth in the coccolithophorids (haptophyta). Energy Conversion and Management 36, 779-782

Ho, D.T., Asher, W.E., Bliven, L.F., Schlosser, P., Gordan, E.L., 2000. On mechanisms of rain-induced air-water gas exchange. Journal of Geophysical Research 105, 24045-24057

Ho, D.T., Bliven, L.F., Wanninkhof, R., Schlosser, P., 1997. The effect of rain on air-water gas exchange. Tellus B 49, 149-158

Ho, D. T., Veron, F., Harrison, E., Bliven, L. F., scott, N., and McGillis, W., 2006. The combined effect of rain and wind on air-water gas exchange: A feasibility study. Journal of Marine Systems, *in press.*

Ho, D.T., Zappa, C.J., McGillis, W.R., Bliven, L.F., Ward, B., Dacey, J.W.H., Schlosser, P., Hendricks, M.B., 2004. Influence of rain on air-sea gas exchange: Lessons from a model ocean. Journal of Geophysical Research 109,doi:10.1029/2003JC001806.

Hobbie, J.E., Daley, R.J., Jasper, S., 1977. Use of nuclepore filters for counting bacteria by fluorescence microscopy. Applied Environmental Microbiology 33, 1225-1228

Hoch, M.P., Kirchman, D.L., 1993. Seasonal and inter-annual variability in bacterial production and biomass in a temperate estuary. Marine Ecology-Progress Series 98, 283-295

Hodson, R.E., Azam, F., Carlucci, A.F., Fuhrman, J.A., Karl, D.M., Holm-Hansen, O., 1981. Microbial uptake of dissolved organic matter in McMurdo Sound, Antarctica. Marine Biology 61, 89-94

Holliday, N.P., Read, J.F., 1998. Surface oceanic fronts between Africa and Antarctica. Deep-Sea Research Part I 45, 217-238

Holm-Hansen, O., El-Sayed, S.Z., Francheschini, G.A., CUHEL, R.L., 1977. Primary production and the factors controlling phytoplankton growth in the Southern Ocean. In: Llano, G.A. (Ed.), Adaptation within the Antarctic ecosystem Gulf, Houston, pp. 11-50.

Holm-Hansen, O., Mitchell, B.G., 1991. Spatial and temporal distribution of phytoplankton and primary production in the western Bransfield Strait region. Dee-Sea Res. 38, 961-980

Hong, Y., Smith, W.O., White, A.M., 1997. Studies of transparent exopolymer particles (TEP) produced in the Ross Sea (Antarctica) and by Phaeocystis antarctica (Prymnesiophyceae). Journal of Phycology 33, 368-376

Hope, D., Palmer, S.M., Billett, M.F., Dawson, J.J.C., 2004. Variations in dissolved CO_2 and CH4 in a first-order stream and catchment: an investigation of soil-stream linkages. Hydrological Processes 18, 3255-3275

Hopkinson, C.S., 1985. Shallow-water benthic and pelagic metabolism: evidence of heterotrophy in the nearshore Georgia Bight. Marine Biology 87, 19-32

Hoppema, M., 1999. Annual uptake of atmospheric CO_2 by the Weddell Sea derived from a surface layer balance, including estimations of entrainment and new production. Journal of Marine Systems 19, 219-233

Hoppema, M., 2004a. Weddell Sea turned from source to sink for atmospheric CO_2 between pre-industrial time and present. Global an Planetary Change 40, 219-231

Hoppema, M., Fahrbach, E., Richter, K.U., de Baar, H.J.W., Kattner, G., 1998. Enrichment of silicate and CO_2 and circulation of the bottom water in the Weddell Sea. Deep-Sea Research Part I 45, 1797-1817

Hoppema, M., Fahrbach, E., Schröder, M., Wistotzki, A., de Baar, H.J.W., 1995. Winter-summer differences of carbon dioxide and oxygen in the Weddel Sea surface layer. Marine Chemistry 51, 177-192

Hoppema, M., Roether, W., Bellerby, R.G.J., De Baar, H.J.W., 2001. Direct measurements reveal insignificant storage of anthropogenic CO_2 in the abyssal Weddell Sea. Geophysical Research Letters 28, 1747-1750

Hoppema, M., 2004b. Weddell Sea is a globally significant contributor to deep-sea sequestration of natural carbon dioxide. Deep-Sea Research Part I 51, 1169-1177

Hoppema, M., Stoll, M.H.C., de Baar, H.J.W., 2000. CO_2 in the Weddell Gyre and Antarctic Circumpolar Current: austral autumn and early winter. Marine Chemistry 72, 203-220

Horne, A.J., Fogg, G.E., Eagle, D.J., 1969. Studies in situ of the primary production of an area of inshore Antarctic sea. Journal of the Marine Biological Association of the United Kingdom 49, 393-405

Houghton, J.T., Ding, Y., Griggs, D.J., Noguer, M., van der Linden, P.J., Dai, X., Maskell, K., Johnson, C.A., 2001. Climate Change 2001: The Scientific Basis. Cambridge University Press, New York.

Huntley, M.E., Sykes, P.F., Marin, V., 1989. Biometry and trophodynamics of Salpa-thompsoni foxton (tunicata, thaliacea) near the antarctic peninsula in austral summer, 1983-1984. Polar Biology 10, 59-70

Hutchins, D.A., Sedwick, P.N., DiTullio, G.R., Boyd, P.W., Queguiner, B., Griffiths, F.B., Crossley, C., 2001. Control of phytoplankton growth by iron and silicic acid availability in the subantarctic Southern Ocean: Experimental results from the SAZ Project. Journal of Geophysical Research 106, 31559-31572

Hwang, P.A., 2005. Comparison of Ocean Surface Wind Stress Computed with Different Parameterization Functions of the Drag Coefficient. Journal of Oceanography 61, 91-107

Iglesias-Rodriguez, M.D., Armstrong, R.A., Feely, R.A., Hood, R., Kleypas, J.A., Milliman, J.D., Sabine, C., Sarmiento, J.L., 2002. Progress made in study of ocean's calcium carbonate budget. Eos 83, 374-375

Inoue, H., Sugimura, Y., 1986. Distribution of pCO_2 and δ^{13} in the air and surface sea water in the Southern ocean of australia. Mem. natl. polar res. ,spec. 40, 454-461

Inoue, H., Sugimura, Y., 1988. Distribution and variations of oceanic carbon dioxide in the western North Pacific, eastern Indian, and Southern Ocean south of Australia. Tellus 40, 308-320

Ishimatsu, A., Hayashi, M., Lee, K.-S., Kikkawa, T., Jita, J., 2005. Physiological effects on fishes in a high-CO_2 world. Journal of Geophysical Research 110,doi:10.1029/2004JC002564.

Ivchenko, V.O., Zalesny, V.B., Drinkwater, M.R., 2004. Can the equatorial ocean quickly respond to Antarctic sea ice/salinity anomalies? Geophysical Research Letters 31,

Jabaud-Jan, A., Metzl, N., Brunet, C., Poisson, A., Schauer, B., 2004. Interannual variability of the carbon dioxide system in the southern Indian Ocean (20 degrees S-60 degrees S): The impact of a warm anomaly in austral summer 1998. Global Biogeochemical Cycles 18,

Jackson, G.A., 1977. Nutrients and production of giant kelp, *Macrocystis pyrifera*, off southern California. Limnology and Oceanography 22**,** 979-995

Jackson, G.A., 1987. Modeling the growth and harvest yield of the giant kelp Macrocystis pyrifera. Marine Bioloy 95**,** 611-624

Jackson, G.A., Winant, C.D., 1983. Effect of a kelp forest on coastal currents. Continental Shelf Research 2**,** 75-80

Jacobson, A.R., Sarmiento, J., Gloor, M., Gruber, N., Mikaloff Fletcher, S.E. Oceanic constraints on the size of the Terrestrial CO_2 fertilization sink. 2005. Seventh International Carbon Dioxide Conference, Boulder, Colorado, U.S.A., September 25-30.

Jacques, G., Panouse, M., 1991. Biomass and composition of size fractionated phytoplankton in the Weddell-Scotia confluence area. Polar Biology 11**,** 315-328

Jacquet, S., Heldal, M., Iglesias-Rodriguez, D., Larsen, A., Wilson, W., Bratbak, G., 2002. Flow cytometric analysis of an *Emiliana huxleyi* bloom terminated by viral infection. Aquatic Microbial Ecology 27**,** 111-124

Jähne, B., Haussecker, H., 1998. Air-water gas exchange. Annual Review of Fluid Mechanics 30**,** 443-468

Jean-Baptiste, P., Poisson, A., 2000. Gas transfer experiment on a lake (Kerguelen Islands) using He- 3 and SF6. Journal of Geophysical Research 105**,** 1177-1186

JGOFS Synthesis group. Meeting of the Southern Ocean synthesis group, Year 1998. 32, 1-75. 2001. JGOFS Synthesis report.

Johnson, K.M., Dickson, A.G., Eischeid, G., Goyet, C., Guenther, P., Key, R.M., Millero, F.J., Purkerson, D., Sabine, C.L., Schottle, R.G., Wallace, D.W.R., Wilke, R.J., Winn, C.D., 1998. Coulometric total carbon dioxide analysis for marine studies: assessment of the quality of total inorganic carbon measurements made during the US Indian Ocean CO_2 Survey 1994-1996. Marine Chemistry 63**,** 21-37

Jones, E.P., Coote, A.R., Levy, E.M., 1983. Effect of sea ice meltwater on the alkalinity of sewater. Journal of Marine Research 41**,** 43-52

Karl, D.M., 1993. Microbial processes in the southern oceans. In: Friedmann E.I. (Ed.), Antarctic Microbiology Wiley-Liss, Inc., New York, pp. 1-63.

Karl, D.M., Holm-Hansen, O., Taylor, G.T., Tien, G., Bird, D.F., 1991. Microbial biomass and productivity in the western Bransfield Strait, Antarctica during the 1986-87 summer. Dee-Sea Res. 89**,** 1029-1055

Karner, M., Rassoulzadegan, F., 1995. Extracellular enzyme activity: indicationss for high short-term variability in a coastal marine ecosystem. Microbial Ecology 30**,** 143-156

Karsten, U., Kuck, K., Vogt, C., Kirst, G.O., 1996. Dimethylsulphoniumpropionate production in phototrophic organisms and its physiological function as a cryoprotectant. In: Kiene, R.P., Visscher, P.T., Keller, M.D., Kirst, G.O. (Eds.), Biological and environmental chemistry of DMSP and related sulfonium compounds Plenum Press, New York, pp. 143-153.

Kazmin, A.S., Rienecker, M.M., 1996. Variability and frontogenesis in the large-scale oceanic frontal zones. Journal of Geophysical Research 104**,** 20963-20970

Kester, D.R., 1986. Equilibrium models in seawater: applications and limitations. In: Bernhard, M., Brinckman, F.E., Sadler, P.J. (Eds.), The importance of chemical 'speciation' in environmental processes. Springer Vrlag, Berlin, pp. 337-363.

Kiene, R.P., Bates, T.S., 1990. Biological removal of dimethyl sulfide from sea-water. Nature 345, 702-705

Killawee, J.A., Fairchild, I.J., Tison, J.-L., Janssens, L., Lorrain, R., 1998. Segregation of solutes and gases in experimental freezing of dilute solutions: Implications for natural glacial systems. Geochimica et cosmochimica acta 62, 3637-3655

Kirchman, D.L., Dittel, A.I., Findlay, S.E.G., Fischer, D., 2004. Changes in bacterial activity and community structure in response to dissolved organic matter in the Hudson River, New York. Aquatic Microbial Ecology 35, 243-257

Kirst, G.O., Thiel, C., Wolff, H., Nothnagel, J., Wanzek, M., Ulmke, R., 1991. Dimethylsulfoniopropionate (DMSP) in ice-algae and its possible biological role. Marine Chemistry 35, 381-388

Kirst, G.O., Wiencke, C., 1995. Ecophysiology of polar algae. Journal of Phycology 31, 181-199

Klaas, C., Archer, D.E., 2002. Association of sinking organic matter with various types of mineral ballast in the deep sea: Implications for the rain ratio. Global Biogeochemical Cycles 16,

Kleypas, J.A., Buddemeier, R.W., Archer, D., Gattuso, J.-P., Langdon, C., Opdyke, B.N., 1999. Geochemical consequences of increased atmospheric carbon dioxide on coral reefs. Science 284, 118-120

Kohfeld, K.E., Le Quere, C., Harrison, S.P., Anderson, R.F., 2005. Role of marine biology in glacialΓÇôinterglacial CO_2 cycles. Science 308, 74-78

Kopczynska, E.E., Dehairs, F., Elskens, M., Wright, S., 2001. Phytoplankton and microzooplankton variability between the Subtropical and Polar Fronts south of Australia: thriving under regenerative and new production in late summer. Journal of Geophysical Research 106, 31597-31610

Kopczynska, E.E., Weber, L.H., El-Sayed, S.Z., 1986. Phytoplankton species composition and abundance in the Indian sector of the Antarctic Ocean. Polar Biology 6, 161-169

Kortzinger, A., Mintrop, L., Wallace, D.W.R., Johnson, K.M., Neill, C., Tilbrook, B., Towler, P., Inoue, H.Y., Ishii, M., Shaffer, G., Saavedra, R.F.T., Ohtaki, E., Yamashita, E., Poisson, A., Brunet, C., Schauer, B., Goyet, C., Eischeid, G., 2000. The international at-sea intercomparison of fCO(2) systems during the R/V Meteor Cruise 36/1 in the North Atlantic Ocean. Marine Chemistry 72, 171-192

Kostianoy, A.G., Ginzburg, A.I., Frankignoulle, M., Delille, B., 2004. Fronts in the Southern Indian Ocean as inferred from satellite sea surface temperature data. Journal of Marine Systems 45, 55-73

Kostianoy, A.G., Ginzburg, A.I., Lebedev, S.A., Frankignoulle, M., Delille, B., 2003. Fronts and mesoscale variability in the southern Indian Ocean as inferred from the TOPEX/POSEIDON and ERS-2 altimetry data. Oceanology 43, 632-642

Kostianoy, A.G., Lutjeharms, J.R.E., 1999. Atmospheric effects in the Angola-Benguela Frontal Zone. Journal of Geophysical Research 104, 20963-20970

Ku, T.C.W., Walter, L.M., Coleman, M.L., Blake, R.E., Martini, A.M., 1999. Coupling between sulfur recycling and syndepositional carbonate dissolution: evidence from oxygen and sulfur isotope composition of pore water sulfate, South Florida Platform, U.S.A. Geochimica et cosmochimica acta 63, 2529-2546

Kumar, N., Anderson, R.F., Mortlock, R.A., Froelich, P.N., Kubik, P., Dittrich-Hannen, B., Suter, M., 1995. Increased biological productivity and export production in the glacial Southern Ocean. Nature 378, 675-680

Lampitt, R.S., Noji, T., von Bodungen, B., 1990. What happens to zooplankton faecal pellets? Implications for material flux. Marine Biology 104, 15-23

Lancelot, C., Hannon, E., Becquevort, S., Veth, C., de Baar, H.J.W., 2000. Modelling phytoplankton blooms and carbon export production in the Southern Ocean: Dominant controls by light and iron of the Atlantic sector in Austral spring 1992. Deep-Sea Research Part I 47**,** 1621-1662

Lancelot, C., Keller, M.D., Rousseau, V., Smith Jr, W.O., Mathot, S., 2006. Autecology of the marine haptophyte Phaeocystis. In: Anderson, D.M., Cembella, A.D., Hallegraeff, G.M. (Eds.), Physiological Ecology of Harmful Algal Blooms Springer-Verlag, Berlin, pp. 209-224.

Lancelot, C., Mathot, S., Becquevort, S., Dandois, J.-M., Billen, G. Carbon and nitrogen cycling through the micrtobial network of the marginal ice zone of the Southern Ocean with particular emphasis on the northwestern Weddell Sea. Cashetto, S. 1-190. 1993. Brussel, Belgian Science Policy Office. Belgian Scientific Research Programme on the Antarctic. Scientific Results of Phase Tow (10/1988-05/1992). Vol. I. Plankton Ecology and Marine Biogeochemistry.

Langdon, C., Broecker, W.S., Hammond, D.E., Glenn, E., Fitzsimmons, K., Nelson, S.G., Peng, T.-H., Hajdas, I., Bonani, G., 2003. Effect of elevated CO_2 on the community metabolism of an experimental coral reef. Global Biogeochemical Cycles 17**,**

Lannuzel, D., Schoemann, V., de Jong, J., Tison, J.-L., Chou, L., 2006. Distribution and Biogeochemical Behaviuos of Iron in the East Antarctic Sea Ice, submitted to. Marine Chemistry

LaRoche, J., Breitbarth, E., 2005. Importance of the diazotrophs as a source of new nitrogen in the ocean. Journal of Sea Research 53**,** 67-91

Laubscher R.K., Perissinotto, R., McQuaid, C.D., 1993. Phytoplankton production and biomass at frontal zones in the Atlantic sector of the Southern Ocean. Polar Biology 13**,** 471-481

Le Fevre, J., Legendre, L., Rivkin, R.B., 1998. Fluxes of biogenic carbon in the Southern Ocean: roles of large microphagous zooplankton. J. Mar. Syst. 17**,** 325-34510.1016/S0924-7963(98)00047-5.

Leblanc, K., Quéguiner, B., Fiala, M., Blain, S., Morvan, J., Corvaisier, R., 2002. Particulate biogenic silica and carbon production rates and particulate matter distribution in the Indian sector of the Subantarctic Ocean. Deep-Sea Research Part II 49**,** 3189-3206

Ledyard, K.M., Dacey, J.W.H., 1994. Dimethylsulfide production from dimethylsulfoniopropionate by a marine bacterium. Marine Ecology-Progress Series 110**,** 95-103

Lee, K., Millero, F.J., Byrne, R.H., Feely, R.A., Wanninkhof, R., 2000. The recommended dissociation constants for carbonic acid in seawater. Geophysical Research Letters 27**,** 229-232

Legeckis, R., Cresswell, G., 1981. Satellite observations of sea-surface temperature fronts off the coast of western and southern Australia. Deep-Sea Research Part I 28**,** 297-306

Legendre, L., Ackley, S.F., Dieckmann, G.S., Gulliksen, B., Horner, R., Hoshiai, T., Melnikov, I.A., Reeburgh, W.S., Spindler, M., Sullivan, C.W., 1992. Ecology of sea ice biota .2. Global significance. Polar Biology 12**,** 429-444

Levasseur, M., Gosselin, M., Michaud, S., 1994. A new source of dimethylsulfide (DMS) for the arctic atmosphere - ice diatoms. Marine Biology 121**,** 381-387

Lewis, E., Wallace, D. CO_2sys Program Developed for CO_2 System Calculations, ORNL/CDIAC-105. 1998. Oak Ridge, Tennessee, Carbon Dioxide Information Analysis Center, Oak Ridge National Laboratory, U.S. Department of Energy.

Li, W.K.W., 1994. Primary production of prochlorophytes, cyanobacteria, and eukaryotic ultraphytoplankton: measurements from flow cytometric sorting. Limnology and Oceanography 39**,** 169-175

Liss, P.S., Merlivat, L., 1986. Air-sea exchange rates: introduction and synthesis. In: Buat-Ménard, P. (Ed.), The role of air-sea exchanges in geochemical cycling Reidel, pp. 113-118.

Liss, P.S., Slater, P.G., 1974. Flux of Gases across the Air-Sea Interface. Nature 247**,** 181-184

Liu, Z.Y., Shin, S.-L., Webb, R.S., Lewis, W., Otto-Bliesner, B.L., 2005. Atmospheric CO_2 forcing on glacial thermohaline circulation and climate. Geophysical Research Letters 32**,**

Lizotte, M.P., 2001. The contributions of sea ice algae to Antarctic marine primary production. American Zoologist 41**,** 57-73

Lizotte, M.P., Sullivan, C.W., 1992. Biochemical-composition and photosynthate distribution in sea ice microalgae of mcmurdo-sound, antarctica - evidence for nutrient stress during the spring bloom. Antarctic Science 4**,** 23-30

Lo Monaco, C., Goyet, C., Metzl, N., Poisson, A., Touratier, F., 2005a. Distribution and Inventory of Anthropogenic CO_2 in the Southern Ocean: Comparison of three Data-based Methods. Journal of Geophysical Research 110**,**doi:10.1029/2004JC002571.

Lo Monaco, C., Metzl, N., Poisson, A., Brunet, C., Schauer, B., 2005b. Anthropogenic CO_2 in the Southern Ocean : distribution and inventory at thindo-Atlantic boundary (WOCE line I6). Journal of Geophysical Research 110**,**doi:10.1029/2004JC002643.

Lochte, K., Bjornsen, P.K., Giesenhagen, H., Weber, A., 1997. Bacterial standing stock and production and their relation to phytoplankton in the Southern Ocean. Deep-Sea Research Part II 44**,** 321-340

Louanchi, F., Hoppema, M., Bakker, D.C.E., Poisson, A., Stoll, M.H.C., de Baar, H.J.W., Schauer, B., Ruiz-Pino, D., Wolf-Gladrow, D.A., 2001. Modelled and observed sea surface fCO_2 in the Southern Ocean: a comparative study. Tellus 51**,** 541-559

Louanchi, F., Metzl, N., Poisson, A., 1996. Modelling the monthly sea surface fCO_2 fields in the Indian Ocean. Marine Chemistry 55**,** 265-279

Lueker, T.J., Dickson, A.G., Keeling, C.D., 2000. Ocean ${}_PCO_2$ calculated from dissolved inorganic carbon,alkalinity, and equations for K_1 and K_2 : validation based on laboratory measurements of CO_2 in gas and seawater at equilibrium. Marine Chemistry 70**,** 105-119

Lutjeharms, J.R.E., 1981. Spatial scales and intensities of circulation in the ocean areas adjacent to South Africa. Deep-Sea Research Part I 28**,** 1289-1302

Lutjeharms, J.R.E., Valentine, H.R., 1984. Southern Ocean thermal fronts south of Africa. Deep-Sea Research Part I 31**,** 1461-1475

Lutjeharms, J.R.E., van Ballegooyen, R.C., 1984. Topographic control in the Agulhas Current system. Deep-Sea Research Part I 31**,** 1321-1337

Lutjeharms, J.R.E., van Ballegooyen, R.C., 1988. The retroflection of the Agulhas Current. Journal of Physical Oceanography 18**,** 1570-1583

Mague, T.H., Friberg, E., Hughes, D.J., Morris, I., 1980. Extracellular release of carbon by marine phytoplankton; a physiological approach. Limnology and Oceanography 25**,** 262-279

Malin, G., Wilson, W.H., Bratbak, G., Liss, P.S., Mann, N.H., 1998. Elevated production of dimethylsulfide resulting from viral infection of cultures of Phaeocystis pouchetii. Limnology and Oceanography 43**,** 1389-1393

Manabe, S., Stouffer, R.J., 1997. Coupled ocean-atmosphere model response to freshwater input: Comparison to Younger Dryas event. Paleoceanography 12**,** 321-336

Mann, K.H., 1982. Ecology of coastal waters. Blackwell, Oxford.

Marion, G.M., 2001. Carbonate mineral solubility at low temperatures in the Na-K-Mg-Ca-H-Cl-SO4-OH-HCO3-CO3-CO_2-H2O system. Geochimica et cosmochimica acta 65**,** 1883-1896

Marsland, S.J., Bindoff, N.L., Williams, G.D., Budd, W.F., 2004. Modeling water mass formation in the Mertz Glacier Polynya and Adelie Depression, East Antarctica. Journal of Geophysical Research 109**,**

Martin-Jezequel, V., Huonnic, P., Delille, B., Riebesell, U. Impact of the pCO_2 level on microalgae. Comparison of past, present & future situations during mesocosms experiments. I: phytoplanktonic development. 2004. SOLAS open science conference, 13-16 October 2004, SOLAS, Halifax, Canada.

Martin, J.H., 1990. Glacial to interglacial CO_2 changes: The Iron hypothesis. Paleoceanography 5**,** 1-13

Martin, J.H., Coale, K.H., Johnson, K.S., Fitzwater, S.E., Gordon, R.M., Tanner, S.J., Hunter, C.N., Elrod, V.A., Nowicki, J.L., Coley, T.L., Barber, R.T., Lindley, S., Watson, A.J., Van Scoy, K., Law, C.S., Liddicoat, M.I., Ling, R., Stanton, T., Stockel, J., Collins, C., Anderson, A., Bidigare, R., Ondrusek, M., Latasa, M., Millero, F.J., Lee, K., Yao, W., Zhang, J.Z., Friederich, G., Sakamoto, C., Chavez, F., Buck, K., Kolber, Z., Greene, R., Falkowski, P., Chisholm, S.W., Hoge, F., Swift, R., Yungel, J., Turner, S., Nightingale, P., Hatton, A., Liss, P., Tindale, N.W., 1994. Testing the iron hypothesis in ecosystems of the equatorial Pacific Ocean. Nature 371**,** 123-129

Martin, J.H., Gordon, R.M., Fitzwater, S.E., 1990. Iron in antarctic waters. Nature 345**,** 156-158

Martin, J.H., Fitzwater, S.E., 1988. Iron deficiency limits phytoplankton growth in the north-east Pacific subarctic. Nature 331**,** 341-343

Martineau, C., Vincent, W.F., Frenette, J.-J., Dodson, J.J., 2004. Primary consumers and particulate organic matter : isotopic evidence of strong selectivity in the estuarine transition zone. Limnology and Oceanography 49**,** 1679-1686

Massman, W.J., Sommerfeld, R.A., Mosier, A.R., Zeller, K.F., Hehn, T.J., Rochelle, S.G., 1997. A model investigation of turbulence-driven pressure-pumping effects on the rate of diffusion of CO_2, N2O, and CH4 through layered snowpacks. Journal of Geophysical Research-Atmospheres 102**,** 18851-18863

Matear, R.J., Hirst, A.C., 1999. Climate change feedback on the future oceanic CO_2 uptake. Tellus 51**,** 722-733

Matsumoto, K., Sarmiento, J.L., Brzezinski, M.A., 2002. Silicic acid leakage from the Southern Ocean: A possible explanation for glacial atmospheric pCO(2). Global Biogeochemical Cycles 16**,**

McElroy, M.B., 1983. Marine biological controls on atmospheric CO_2 and climate. Nature 302**,** 328-329

McGillis, W.R., Edson, J.B., Zappa, C.J., Ware, J.D., McKenna, S.P., Terray, E.A., Hare, J.E., Fairall, C.W., Drennan, W., Donelan, M., Degrandpre, M.D., Wanninkhof, R., Feely, R.A., 2004. Air-sea CO_2 exchange in the equatorial Pacific. Journal of Geophysical Research 109**,** C08S02-doi:10.1029/2003JC002256

McKenzie, C.H., Cox, E.R., 1991. Spatial and seasonal changes in the species composition of armoured dinoflagellates inthe Southwestern Atlantic Ocean. Polar Biology 11**,** 139-144

McMinn, A., Pankowski, A., Delfatti, T., 2005. Effect of hyperoxia on the growth and photosynthesis of polar sea ice microalgae. Journal of Phycology 41**,** 732-741

McNeil, B.I., Metzl, N., Key, R.M., Matear, R.J. An empirical estimate of the Southern Ocean air-sea CO_2 flux. 2005. Seventh International Carbon Dioxide Conference, Boulder, Colorado, U.S.A., September 25-30.

McNeil, B.I., Tilbrook, B., Matear, R.J., 2001. Accumulation and uptake of anthropogenic CO_2 in the Southern Ocean, south of Australia between 1968 and 1996. Journal of Geophysical Research 106, 31431-31445

Mehrbach, C., Culberson, C.H., Hawley, J.E., Pytkowicz, R.M., 1973. Measurements of the apparent dissociation constants of carbonic acid in seawater at atmospheric pressure. Limnology and Oceanography 18, 897-907

Melching, C.S., Flores, H.E., 1999. Reaeration equations derived from U.S. Geological Survey Database. Journal of the Environmental Engineering 125, 407-414

Menden-Deuer, S., Lessard, E.J., 2000. Carbon to volume relationships for dinoflagellates, diatoms, and other protist plankton. Limnology and Oceanography 45, 569-579

Metzl, N. Air-sea CO_2 fluxes in the Southern Ocean: natural and methodological variabilities. 2004. SOLAS Open Conference, 13-16 October, Halifax, Canada.

Metzl, N. Air-sea CO_2 flux variations in the Southern Ocean: new observations, new questions. 61, 7-11. 2005. Global Change Newsletter.

Metzl, N., Beauverger, C., Brunet, C., Goyet, C., Poisson, A., 1991. Surface water carbon dioxide in the southwest Indian Sector of the Southern Ocean: A highly variable CO_2 source/sink region in summer. Marine Chemistry 35, 85-95

Metzl, N., Brunet, C., Jabaud-Jan, A., Poisson, A., and Schauer, B. Summer and winter air-sea CO_2 fluxes in the Southern Ocean. Submitted to Deep-Sea Research Part I.

Metzl, N., Louanchi, F., Poisson, A., 1998. Seasonal and interannual variations of sea surface carbon dioxide in the subtropical Indian Ocean. Marine Chemistry 60, 131-146

Metzl, N., Poisson, A., Louanchi, F., Brunet, C., Schauer, B., Brès, B., 1995. Spatio-temporal distribution of air-sea fluxes of CO_2 in the Indian and Antarctic Ocean. Tellus 47B, 56-69

Metzl, N., Tilbrook, B., Poisson, A., 1999. The annual fCO_2 cycle and the air-sea CO_2 flux in the sub-Antarctic Ocean. Tellus 51, 849-861

Mikaloff Fletcher, S.E., Gruber, N., Jacobson, A.R., Doney, S.C., Dutkiewicz, S., Gerber, M., Follows, M., Joos, F., Lindsay, K., Menemenlis, D., Mouchet, A., Muller, S.A., Sarmiento, J.L., 2006. Inverse estimates of anthropogenic CO_2 uptake, transport, and storage by the ocean. Glob. Biogeochem. Cycles GB2002,doi:10.1029/2005GB002530.

Millero, F.J., 1979. The thermodynamics of the carbonate system in seawater. Geochimica et cosmochimica acta 43, 1651-1661

Millero, F.J., 1995. Thermodynamics of the carbon dioxide system in the oceans. Geochimica et cosmochimica acta 59, 661-677

Millero, F.J., Pierrot, D., Lee, K., Wanninkhof, R., Feely, R., Sabine, C.L., Key, R.M., Takahashi, T., 2002. Dissociation constants for carbonic acid determined from field measurements. Deep-Sea Research Part I 49, 1705-1723

Miyake, Y., Sugimura, Y., Saruhashi, K., 1974. The Carbon Dioxide content in the Surface Waters in the Pacific Ocean . Rec. of Ocean. Works in Japan 12, 45-52

Mock, T., 2002. In situ primary production in young Antarctic sea ice. Hydrobiologia 470, 127-132

Moline, M., Prezelin, B.B., Schofield, O., 1997. Palmer LTER: stable interannual successional patterns of phytoplankton communities in the coastal waters of Palmer Station Antarctica. Antarctic journal of the United States 32**,** 151-153

Moline, M.A., Prézelin, B.B., 1996. Long-term monitoring and analyses of physical factors regulating variability in coastal Antarctic phytoplankton biomass, in situ productivity and taxonomic composition over subseasonal, seasonal and interannual time scales. Marine Ecology-Progress Series 145**,** 143-160

Moore, J.K., Abbott, M.R., 2000. Phytoplankton chlorophyll distributions and primary production in the Southern Ocean. Journal of Geophysical Research 105**,** 28709-28722

Moore, J.K., Abbott, M.R., Richman, J.G., 1997. Variability in the location of the Antarctic Polar Front (90DG-20DGW) from satellite sea surface temperature data. Journal of Geophysical Research 102**,** 27825-27833

Moore, J.K., Abbott, M.R., Richman, J.G., 1999. Location and dynamics of the Antarctic Polar Front from satellite sea surface temperature data. Journal of Geophysical Research 104**,** 3059-3073

Moore, J.K., Abbott, M.R., 2002. Surface chlorophyll concentrations in relation to the Antarctic Polar Front: seasonal and spatial patterns from satellite observations. Journal of Marine Systems 37**,** 69-86

Morel, F.M.M., Milligan, A.J., Saito, M.A., 2005. Marine bioinorganic chemistry: the role of trace metals in the oceanic cycles. In: Holland, H.D., Turekian, K.K. (Eds.), The Oceans and Marine Geochemistry - Treatise on Geochemistry Elsevier-Pergamon, Oxford, UK.

Morrison, J.M., Gaurin, S., Codispoti, L.A., Takahashi, T., Millero, F.J., Gardner, W.D., Richardson, M.J., 2001. Seasonal evolution of hydrographic properties in the Antarctic Circumpolar Current at 170°W during 1997-1998. Deep-Sea Research Part II 48**,** 3943-3972

Morse, J.W., Zullig, J.J., Iverson, R.L., Choppin, G.R., Mucci, A., Millero, F.J., 1987. The influence of seagrass beds on carbonate sediments in the Bahamas. Marine Chemistry 22**,** 71-83

Munhoven, G. Modelling glacial-interglacial atmsopheric CO_2 variations: The role of continental weathering. -pp 273. 1997. Université de Liège.

Murphy, L.S., Haugen, E.M., 1985. The distribution and abundance of phototrophic ultraplankton in the North Atlantic. Limnology and Oceanography 30**,** 47-58

Murphy, P.P., Feely, A., Gammon, H., Harrison, D.E., Kelly, K.C., Waterman, L.S., 1991a. Assessment of the air-sea exchange of CO_2 in the South Pacific during Austral autumn. Journal of Geophysical Research 96**,** 20445-20465

Murphy, P.P., Feely, A., Gammon, H., Kelly, K.C., Waterman, L.S., 1991b. Autumn air-sea disequilibrium of CO_2 in the South Pacific Ocean. Marine Chemistry 35**,** 77-84

Nedwell, D.B., Rutter, M., 1994. Influence of temperature on growth rate and competition between two psychrotolerant antarctic bacteria: temperature diminishes affinity for substrate uptake. Applied Environmental Microbiology 60**,** 1984-1992

Neiman, V.G., Scherbinin, A.D., 1997. Dynamics of the Indian Ocean. Moscow: Scientific World (231 pp.) (in Russian). Moscow.

Nelson, D.M., Smith Jr, W.O., Muench, R.D., Gordon, L.I., Sullivan, C.W., Husby, A., 1989. Particulate matter and nutrient distributions in the ice-edge zone of the weddel Sea: Relationship to hydrography during late summer. Deep-Sea Research Part I 36**,** 191-209

Nelson, D.M., Smith, W.O., 1991. Sverdrup revisited - critical depths, maximum chlorophyll levels, and the control of Southern-Ocean productivity by the irradiance-mixing regime. Limnology and Oceanography 36, 1650-1661

Nelson, D.M., Tréguer, P., Brzezinski, M.A., Leynaert, A., Queguiner, B., 1995. Production and dissolution of biogenic silica in the ocean - revised global estimates, comparison with regional data and relationship to biogenic sedimentation. Global Biogeochemical Cycles 9, 359-372

Neveux, J., Panouse, M., 1987. Spectrofluorometric determination of chlorophylls and pheophytins. Archiv für Hydrobiologie 109, 567-581

Nguyen, B.C., Mihalopoulos, N., Belviso, S., 1990. Seasonal variation of atmospheric dimethysulfide at Amsterdam Island in the Southern Indian Ocean. Journal of atmospheric chemistry 11, 123-141

Nguyen, B.C., Belviso, S., Mihalopoulos, N., Gostan, J., Nival, P., 1988. Dimethyl sulfide production during natural phytoplanktonic blooms. Marine Chemistry 24, 133-141

Nicol, S., 2000. Ocean circulation off east Antarctica affects ecosystem structure and sea-ice extent. Nature 406, 504-507

Nightingale, P.D., Liss, P.S., Schlosser, P., 2000a. Measurements of air-sea gas transfer during an open ocean algal bloom. Geophysical Research Letters 27, 2117-2120

Nightingale, P.D., Malin, G., Law, C.S., Watson, A.J., Liss, P.S., Liddicoat, M.I., Boutin, J., Upstill-Goddard, R.C., 2000b. In situ evaluation of air-sea gas exchange parameterizations using novel conservative and volatile tracers . Global Biogeochemical Cycles 14, 373-387

Nimer, N.A., Merrett, M.J., 1993. Calcification rate in *Emiliania huxleyi* Lohmann in respose to light, nitrate and availability of inorganic carbon. New Phytologist 123, 673-677

Nodder, S.D., Waite, A.M., 2001. Is Southern Ocean organic carbon and biogenic silica export enhanced by iron-stimulated increases in biological production? Sediment trap results from SOIREE. Deep-Sea Research Part II 48, 2681-2701

Nowlin, W.D.J., Klinck, J.M., 1986. The physics of the Antartic Circumpolar Current. Reviews of Geophysics 24, 469-491

O'Connor, D.J., Dobbins, W.E., 1958. Mechanism of reaeration in natural streams. Trans. Am. Soc. Civ. Eng. 123, 641-684

Oke, P.R., England, M.H., 2004. Oceanic response to changes in the latitude of the Southern Hemisphere subpolar westerly winds. Journal of Climate 17, 1040-1054

Opdyke, B.N., Walker, J.C.J., 1992. Return of the coral reef hypothesis: basin to shelf partitioning of $CaCO_3$ and its effect on atmospheric CO_2. Geology 20, 733-736

Oppenheimer, M., 1998. Global warming and the stability of the West Antarctic Ice Sheet. Nature 393, 325-332

Oppenheimer, M., Alley, R.B., 2004. The West Antarctic ice sheet and long term climate policy - An editorial comment. Climatic change 64 , 1-10

Orr, J.C., Fabry, V.J., Aumont, O., Bopp, L., Doney, S.C., Feely, R.A., Gnanadesikan, A., Gruber, N., Ishida, A., Joos, F., Key, R.M., Lindsay, K., Maier-Reimer, E., Matear, R., Monfray, P., Mouchet, A., Najjar, R.G., Plattner, G.K., Rodgers, K.B., Sabine, C.L., Sarmiento, J.L., Schlitzer, R., Slater, R.D., Totterdell, I.J., Weirig, M.F., Yamanaka, Y., Yool, A., 2005. Anthropogenic ocean acidification over the twenty-first century and its impact on calcifying organisms. Nature 437, 681-686

Orsi, A.H., Whitworth, T.I., Nowlin, W.D.J., 1995. On the meridional extent and fronts of the Antarctic Circumpolar Current. Deep-Sea Research Part I 42, 641-673

Paasche, E., 1973. Silicon and the ecology of marine plankton datoms. I. Thalassiosira pseudonana (Cyclotella nana) grown ina chemostat with the silicate as limiting nutrient. Marine Biology 19, 117-126

Pakhomov, E.A., 1998. The Prince Edward Islands pelagic ecosystem, south Indian Ocean: a review of achievements, 1976--1990. Journal of Marine Systems 16, 297-310

Pakhomov, E.A., Froneman, P.W., Ansorge, I.J., Lutjeharms, J.R.E., 2000. Temporal variability in the physico-biological environment of the Prince Edward Islands (Southern Ocean). Journal of Marine Systems 26, 75-95

Pakhomov, E.A., Froneman, P.W., Perissinotto, R., 2002. Salp/krill interactions in the Southern Ocean: spatial segregation and implications for the carbon flux. Deep-Sea Research Part II 49, 1881-1907

Pakhomov, E.A., McQuaid, C.D., 1996. Distribution of surface zooplankton and seabirds across the Southern Ocean. Polar Biology 16, 286

Papadimitriou, S., Kennedy, H., Kattner, G., Dieckmann, G.S., Thomas, D.N., 2004. Experimental evidence for carbonate precipitation and CO_2 degassing during sea ice formation. Geochimica et cosmochimica acta 68, 1749-1761

Park, P.K., Charriaud, E., Craneguy, P., Kartavtseff, A., 2001. Fronts, transport, and Weddell Gyre at 30°E between Africa and Antarctica. Journal of Geophysical Research 106, 2857-2898

Park, Y.H., Charriaud, E., Fieux, M., 1998a. Thermohaline structure of the Antarctic Surface Water/Winter Water in the Indian sector of the Southern Ocean. Journal of Marine Systems 17, 5-23

Park, Y.H., Charriaud, E., Pino, D.R., Jeandel, C., 1998b. Seasonal and interannual variability of the mixed layer properties and steric height at station KERFIX, southwest of Kerguelen. Journal of Marine Systems 17, 571-586

Park, Y.H., Gambéroni, L., 1995. Large-scale circulation and its variability in the south Indian Ocean from TOPEX/Poseidon altimetry. Journal of Geophysical Research 100, 24911-24929

Park, Y.H., Gambéroni, L., 1997. Cross-frontal exchange of Antarctic Intermediate Water and Antarctic Bottom Water in the Crozet Basin. Deep-Sea Research Part I 4, 963-986

Park, Y.H., Gambéroni, L., Charriaud, E., 1991. Frontal structure and transport of the Antarctic Circumpolar Current in the south Indian Ocean sector, 40-80°E. Marine Chemistry 35, 45-62

Park, Y.H., Gambéroni, L., Charriaud, E., 1993. Frontal structure, water masses, and circulation in the Crozet basin. Journal of Geophysical Research 98, 12361-12385

Park, Y.H., Pollard, R.T., Read, J.F., Leboucher, V., 2002. A quasi-synoptic view of the frontal circulation in the Crozet Basin during the Antares-4 cruise. Deep-Sea Research Part II 49, 1823-1842

Pasquer, B., Laruelle, G., Becquevort, S., Schoemann, W., Goosse, H., Lancelot, C., 2005. Linking ocean biogeochemical cycles and ecosystem structure and function: results of the complex SWAMCO-4 model. Journal of Sea Research 53, 93-108

Passow, U., 1991. Species-specificsedimentation and sinking velocities of diatoms. Marine Biology 108, 449-455

Peacock, S., 2004. Debate over the ocean bomb radiocarbon sink: Closing the gap. Global Biogeochemical Cycles 18, GB2022-doi:10.1029/2003GB002211

Pedros-Alio, C., Vasqué, D., Guixa-Boixereu, N., Gasol, J.M., 2002. Prokaryotic plankton biomass and heterotrophic production in western Antarctic waters during the 1995-1996 austral summer. Deep-Sea Research Part II 49, 825

Peers, G., Quenel, S.-A., Price, N., 2005. Copper requirements for iron acquisition and growth of coastal and oceanic diatoms. Limnology and Oceanography 50, 1149-1158

Pelletier, G., Lewis, E., Wallace, D. CO_2sys.xls: A calculator for the CO_2 system in seawater for Microsoft Excel/VBA. 1998. Olympia, WA, Washington State Department of Ecology.

Peng, T.-H., Takahashi, T., Broecker, W.S., Olafsson, J., 1987. Seasonal variability of carbon dioxide,nutrients and oxygen in the Northern North Atlantic surface water: observations and a model. Tellus 39B, 439-458

Perissinotto, R., Lutjeharms, J.R.E., van Ballegooyen, R.C., 2000. Biological-physical interactions and pelagic productivity at the Prince Edward Islands, Southern Ocean. Journal of Marine Systems 24, 327-341

Perissinotto, R., McQuaid, C.D., Laubscher R.K., 1992. Marine productivity enhancement around Bouvet and the South Sandwich Islands (Southern Ocean). Marine Ecology-Progress Series 88, 41-53

Perrin, R.A., Lu, P., Marchant, H.J., 1987. Seasonal-variation in marine-phytoplankton and ice algae at a shallow antarctic coastal site. Hydrobiologia 146, 33-46

Perry, A.L., Low, P.J., Ellis, J.R., Reynolds, J.D., 2005. Climate Change and Distribution Shifts in Marine Fishes. Science 308, 1912-1915

Peterson, B.J., Fry, B., HULLAR, M., SAUPE, S., WRIGHT, R., 1994. The distribution and stable carbon isotopic composition of dissolved organic carbon in estuaries. Estuaries 17, 111-121

Piola, A.R., Matano, R.P., Palma, E.D., Möller Jr., O.O., Campos, E.J.D., 2005. The influence of the Plata River discharge on the western South Atlantic shelf. Geophysical Research Letters 32, L01603-doi:10.1029/2004GL021638

Platt, T., Sathendranath, S., Ulloa, O., Harrison, W.G., Hoepffner, N., Goes, J., 1992. Nutrient control of phytoplankton photosynthesis in the western North Atlantic. Nature 356, 229-231

Poisson, A., Chen, C.T.A., 1987. Why is there little anthropogenic CO_2 in the Antarctic bottom water? Deep-Sea Research Part A 34, 1255-1275

Poisson, A., Metzl, N., Brunet, C., Schauer, B., Brès, B., Ruiz-Pino, D., Louanchi, F., 1993. Variability of sources and sinks of CO_2 in the Western Indian and Southern Oceans During the Year 1991. Journal of Geophysical Research 98, 22 759-22 778

Pollard, R.T., Read, J.F., 2001. Circulation pathways and transports of the Southern Ocean in the vicinity of the Southwest Indian ridge. Journal of Geophysical Research 106, 2881-2898

Pomeroy, L.R., Wiebe, W.J., 2001. Temperature and substrates as interactive limiting factors for marine heterotrophic bacteria. Aquatic Microbial Ecology 23, 187-204

Pondaven, P., Ragueneau, O., Treguer, P., Hauvespre, A., Dezileau, L., Reyss, J.L., 2000. Resolving the 'opal paradox' in the Southern Ocean. Nature 405, 168-172

Priddle, J., Smetacek, V., Bathmann, U., 1992. Antarctic marine production, biogeochemical carbon cycles and climatic change. Phil. Trans. R. Soc. Lond. 338, 289-297

Prieur, L., Sournia, A., 1994. Processes and fluxes in the geostrophic Almeria-Oran front. Journal of Marine Systems 5, 187-203

Project Members Climap, 1976. The surface of the ice-age earth. Science 191, 1131-1144

Qiu, B.S., Gao, K.S., 2002. Effects of CO_2 enrichment on the bloom-forming cyanobacterium Microcystis aeruginosa (Cyanophyceae): Physiological responses and relationships with the availability of dissolved inorganic carbon. Journal of Phycology 38**,** 721-729

Quéguiner, B., Brzezinski, M.A., 2002. Biogenic silica production rates and particulate organic matter distribution in the Atlantic sector of the Southern Ocean during austral spring 1992. Deep-Sea Research Part II 49**,** 1765-1786

Rabouille, C., Mackenzie, F.T., Ver, L.M.B., 2001. Influence of the human perturbation on carbon, nitrogen, and oxygen biogeochemical cycles in the global coastal ocean. Geochimica et cosmochimica acta 65**,** 3615-3641

Ragueneau, O., 1994. Determination of biogenic silica in coastal waters: applicability and limits of the alkaline digestion method. Marine Chemistry 45**,** 43-51

Raven, J.A., Caldeira, K., Elderfield, H., Hoegh-Guldberg, O., Liss, P.S., Riebesell, U., Shepherd, R., Turley, C., Watson, A.J. Ocean acidification due to increasing atmospheric carbon dioxide. Policy document 12/05. 2005. The Royal Society.

Read, J.F., Lucas, M.I., Holley, S.E., Pollard, R.T., 2000. Phytoplankton, nutrients and hydrography in the frontal zone between the Southwest Indian Subtropical gyre and the Southern Ocean. Deep-Sea Research Part I 47**,** 2341-2368

Read, J.F., Pollard, R.T., 1993. Structure and transport of the Antarctic Circumpolar Current and Agulhas Return Current at 40°E. Journal of Geophysical Research 98**,** 12281-12295

Redfield, A.C., Ketchum, B.H., Richards, F.A., 1963. The influence of organisms on the composition of sea-water. In: Hill, M.N. (Ed.), The composition of sea-water and comparative and descriptive oceanography Wiley-Intersciences, New York, pp. 26-87.

Revelle, R., Suess, E., 1957. Carbon dioxide exchange between atmosphere and ocean and the question of increase of atmospheric CO_2 during the past decades. Tellus 9**,** 18-27

Reynolds, R.W., Smith, T.M., 1994. Improved global sea surface temperature analyses using interpolation. J. Clim. 7**,** 929-948

Rheinheimer, G., Gocke, K., Hoppe, H.G., 1989. Vertical distribution of microbiological and hydrographic-chemical parameters in different areas of the Baltic Sea. Marine Ecology-Progress Series 52**,** 55-70

Riaux-Gobin, C., Tréguer, P., Dieckmann, G., Maria, E., Vetion, G., Poulin, M., 2005. Land-fast ice off Adelie Land (Antarctica): short-term variations in nutrients and chlorophyll just before ice break-up. Journal of Marine Systems 55**,** 235-248

Richards, F.A. Anoxic basins and fjords. Riley, J. P. and Skirrow, G. [1], 611-645. 1965. New York, Academic Press. Chemical Oceanography.

Richardson, C., 1976. Phase relatioships in sea ice as a function of temperature. Journal of Glaciology 17**,** 507-519

Richardson, G., Wadley, M.R., Heywood, K.J., Stevens, D.P., Banks, H.T., 2005. Short-term climate response to a freshwater pulse in the Southern Ocean. Geophysical Research Letters 32**,**

Riebesell, U., Wolf-Gladrow, D.A., Smetacek, V., 1993. Carbon dioxide limitation of marine phytoplankton growth rates. Nature 361**,** 249-251

Riebesell, U., Zondervan, I., Rost, B., Tortell, P.D., Zeebe, R., Morel, F.M.M., 2000. Reduced calcification of marine plankton in response to increased atmospheric CO_2. Nature 407**,** 364-367

Riemann, B., Sondergaard, M., 1984. Measurements of diel rates of bacterial secondary production in aquatic environments. Applied Environmental Microbiology 47**,** 632-638

Rintoul, S., Trull, T.W., 2001. Seasonal evolution of the mixed layer in the Subantarctic Zone south of Australia. Journal of Geophysical Research 106**,** 31447-31462

Rintoul, S.R., Bullister, J.L., 1999. A late winter hydrographic section from Tasmania to Antarctica. Deep-Sea Research Part I 46**,** 1417-1454

Rintoul, S.R., Donguy, J.R., Roemmoch, D.H., 1997. Seasonal evolution of upper thermal structure between Tasmania and Antarctica. Deep-Sea Research Part I 44**,** 1185-1202

Rintoul, S.R., Sokolov, S., 2001. Baroclinic transport variability of the Antarctic Circumpolar Current south of Australia (WOCE repeat section SR3). Journal of Geophysical Research 106**,** 2815-2832

Roberts, P.E., 1980. Surface distribution of albacore tuna, Thunnus alalunga Bonaterre, in relation to the Subtropical Convergence Zone east of New Zealand. New-Zealand Journal of Marine and Freshwater Research 14**,** 373-380

Robertson, J.E., Robinson, C., Turner, D.R., Holligan, P., Watson, A.J., Boyd, P., Fernandez, E., Finch, M., 1994. The impact of a coccolithophorid bloom on oceanic carbon uptake in the NE Atlantic during summer 1991. Deep-Sea Research Part I 41**,** 297-314

Robertson, J.E., Watson, A.J., 1995. A summer-time sink for atmospheric carbon dioxide in the Southern Ocean between 88°W and 80°E. Deep-Sea Research Part I 45**,** 1081-1091

Rochelle-Newall, E., Delille, B., Frankignoulle, M., Gattuso, J.-P., Jacquet, S., Riebesell, U., Terbrüggen, A., Zondervan, I., 2004. CDOM in experimental mesocosms maintained under different pCO_2 levels. Marine Ecology-Progress Series 272**,** 25-31

Rodionov, V.B., Kostianoy, A.G., 1998. Oceanic Fronts in the Seas of the North European Basin. GEOS, Moscow.

Rothlisberger, R., Bigler, M., Wolff, E.W., Joos, F., Monnin, E., Hutterli, M.A., 2004. Ice core evidence for the extent of past atmospheric CO_2 change due to iron fertilisation. Geophysical Research Letters 31**,**

Roy, R., Roy, L., Vogel, J.C., Porter-Moore, C., Pearson, T., Good, C.E., Millero, F.J., Campbell, D.M., 1993. The dissociation constants of carbonic acid in seawater at salinities 5 to 45 and temperatures 0 to 45°C. Marine Chemistry 44**,** 249-267

Roy, T., Rayner, P.J., Matear, R., Francey, R.J., 2003. Southern hemisphere ocean CO_2 uptake: reconciling atmospheric and oceanic estimates. Tellus B 55**,** 701-710

Rubin, S.I., 2003. Carbon and nutrient cycling in the upper water column across the Polar Frontal Zone andAntarctic Circumpolar Current along 170°W. Global Biogeochemical Cycles 17**,** 1087

Rueter, J.G., 1988. Iron stimulation of photosynthesis and nitrogen-fixation in anabaena-7120 and *Trichodesmium* (cyanophyceae). Journal of Phycology 24**,** 249-254

Rueter, J.G., Ohki, K., Fujita, Y., 1990. The effect of iron nutrition on photosynthesis and nitrogen-fixation in cultures of Trichodesmium (cyanophyceae). Journal of Phycology 26**,** 30-35

Rysgaard, S., Glud, R., Sejr, M. K., Bendtsen, J., and Christensen, P. B., 2006. Inorganic carbon transport during sea ice growth and decay: A carbon pump in polar seas. submitted to Journal of Geophysical Research.

Rysgaard, S., Kuhl, M., Glud, R.N., Hansen, J.W., 2001. Biomass, production and horizontal patchiness of sea ice algae in a high-Arctic fjord (Young Sound, NE Greenland). Marine Ecology-Progress Series 223**,** 15-26

Sabine, C., Heimann, M., Artaxo, P., Bakker, D., Chen, C.T.A., Field, C.B., Gruber, N., Le Quéré, C., Prinn, R.G., Richey, J.E., Lankao, P.R., Sathaye, J.A., Valentini, R., 2004a. Current Status and Past Trends of the Global Carbon Cycle. In: Field, C.B., Raupach, M.R. (Eds.), The Global Carbon Cycle: Integrating Humans, Climate, And The Natural World. Island Press, Washington, D.C., pp. 17-41.

Sabine, C.L., Feely, R.A., Key, R.M., Lee, K., Bullister, J.L., Wanninkhof, R., Wong, C.S., Wallace, D.W.R., Tilbrook, B., Millero, F.J., Peng, T.-H., Kozyr, A., Ono, T., Rios, A.F., 2004b. The oceanic sink for anthropogenic CO_2. Science 305**,** 367-371

Saji, N.H., Goswami, B.N., Vinayachandran, P.N., Yamagata, T., 1999. A dipole mode in the tropical Indian Ocean. Nature 401**,** 360-363

Sarmiento, J., Gruber, N., 2002. Sinks for Anthropogenic Carbon. Physics Today August 2000**,** 30-36

Sarmiento, J.L., Gruber, N., Brzezinski, M.A., Dunne, J.P., 2004. High-latitude controls of thermocline nutrients and low latitude biological productivity. Nature 427**,** 56-60

Sarthou, G., Timmermans, K.R., Blain, S., Tréguer, P., 2005. Growth physiology and fate of diatoms in the ocean: a review. Journal of Sea Research 53**,** 25-42

Sarukhanian, E.I., Smirnov, N.P., 1986. Water Masses and Circulation of the Southern Ocean. Gidrometeoizdat, Leningrad.

Savoye, N., Dehairs, F., Elskens, M., Cardinal, D., Kopczynska, E.E., Trull, T.W., Wright, S., Baeyens, W., Griffiths, F.B., 2004. Regional variation of spring N-uptake and new production in the Southern Ocean. Geophysical Research Letters 31**,**

Sazhin, A.F., 1993. Bacterioplankton of surface waters in Antarctic zone of the Pacific. Russ. J. Aquat. Ecol. 2**,** 103-109

Schmid, H.P., 1994. Source areas for scalars and scalar fluxes. Boundary-Layer Meteorology 67**,** 293-318

Schoemann, W., Becquevort, S., Stefels, J., Rousseau, W., Lancelot, C., 2005. Phaeocystis blooms in the global ocean and their controlling mechanisms: a review. Journal of Sea Research 53**,** 43-66

Schulz, K.G., Zondervan, I., Gerringa, L.J.A., Timmermans, K.R., Veldhuis, M.J.W., Riebesell, U., 2004. Effect of trace metal availability on coccolithop^horid calcification. Nature 430**,** 673-676

Sciare, J., Mihalopoulos, N., Nguyen, B.C., 1999. Summertime seawater concentrations of dimethylsulfide in the western Indian Ocean: reconciliation of fluxes and spatial variability with long-term atmospheric observations. Journal of atmospheric chemistry 32**,** 357-373

Sedwick, P.N., Blain, S., Quéguiner, B., Griffiths, F.B., Fiala, M., Bucciarelli, E., Denis, M., 2002a. Chemical limitation on phytoplankton growth in the Crozet Basin, Subantarctic Southern Ocean. Deep-Sea Research Part II 49**,** 3327-3349

Sedwick, P.N., Blain, S., Quéguiner, B., Griffiths, F.B., Fiala, M., Bucciarelli, E., Denis, M., 2002b. Resource limitation of phytoplankton growth in the Crozet Basin, Subantarctic Southern Ocean. Deep-Sea Research Part II 49**,** 3327-3349

Sedwick, P.N., DiTullio, G.R., Hutchins, D.A., Boyd, P.W., Griffiths, F.B., Crossley, A.C., Trull, T.W., Queguiner, B., 1999. Limitation of algal growth by iron deficiency in the Australian Subantarctic region. Geophysical Research Letters 26**,** 2865-2868

Seidov, D., Barron, E., Haupt, B.J., 2001. Meltwater and the global ocean conveyor: northern versus southern connections. Global and Planetary Change 30, 257-270

Semiletov, I., Makshtas, A., Akasofu, S.I., Andreas, E.L., 2004. Atmospheric CO_2 balance: The role of Arctic sea ice. Geophysical Research Letters 31, L05121-doi:10.1029/2003GL017996

Semiletov, I., Pipko, I.I., Makshtas, A., Repina, I., Shakhova, N., 2006. Carbonate chemistry dynamics and carbon dioxide fluxes across the atmosphere-ice-water interfaces in the Arctic ocean: Pacific sector of the Arctic. submitted to. Journal of Marine Systems

Shin, S.-L., Liu, Z., Otto-Bliesner, B.L., Kutzbach, J.E., Vavrus, S.J., 2003. Southern Ocean sea-ice control of the glacial North Atlantic thermohaline circulation. Geophysical Research Letters 30,

Siegenthaler, U., Stocker, T.F., Monnin, E., Luthi, D., Schwander, J., Stauffer, B., Raynaud, D., Barnola, J.M., Fischer, H., Masson-Delmotte, V., Jouzel, J., 2005. Stable Carbon Cycle-Climate Relationship During the Late Pleistocene. Science 310, 1313-1317

Sigman, D.M., Boyle, E.A., 2000. Glacial/interglacial variations in atmospheric carbon dioxide. Nature 407, 859-869

Simon, M., Azam, F., 1989. Protein content and protein synthesis rates of planktonic marine bacteria. Marine Ecology-Progress Series 364 , 114-118

Simon, M., Rosenstock, B., Zwisler, W., 2004. Coupling of epipelagic and mesopelagic heterotrophic picoplankton production to phytoplankton biomass in the Antarctic polar frontal region. Limnology and Oceanography 49 , 1035-1043

Skirrow, G., Whitfield, M., 1975. The effect of increases in the atmospheric carbon dioxide content on the carbonate ion concentration of surface ocean water at 25°C. Limnology and Oceanography 20, 103-108

Smetacek, V., Scharek, R., Nothig, E.M., 1990. Seasonal and regional variation in the pelagial and its relationship to the life history cycle of krill. In: Kerry, K.R., Hempel, G. (Eds.), Antarctic Ecosystems. Ecological Change and Conservation Springer, Berlin, pp. 103-114.

Smith Jr, W.O., Nelson, D.M., 1985. Phytoplankton bloom produced by a receding ice edge in the Ross Sea: spatial coherence with the density field. Science 227, 163-166

Smith Jr, W.O., Nelson, D.M., 1990. Phytoplankton growth and new production in the Weddell Sea marginal ice zone in austral spring and autumn. Limnology and Oceanography 35, 809-821

Smith, D.C., Steward, G.F., Long, R.A., Azam, F., 1995. Bacterial mediation of carbon fluxes during a diatom bloom in a mesocosm. Deep-Sea Research Part II 42, 75-97

Smith, E.M., Benner, R., 2005. Photochemical transformations of riverine dissolved organic matter: effects on estuarine bacterial metabolism and nutrient demand. Aquatic Microbial Ecology 40, 37-50

Smith, S.V., 1981. Marine macrophytes as global carbon sink. Science 211, 838-840

Smith, W.O., Gordon, L.I., 1997. Hyperproductivity of the Ross Sea (Antarctica) polynya during austral spring. Geophysical Research Letters 24, 233-236

Smythe-Wright, D., Chapman, P., Duncombe Rae, C., Shannon, L.V., Boswell, S.M., 1998. Characteristics of the South Atlantic subtropical frontal zone between 15°W and 5°E. Deep-Sea Research Part I 45, 167-192

Solomon, D.K., Cerling, T.E., 1987. The annual carbon dioxide cycle in montane soil: observation, modeling, and implications for weathering. Water Resources Research 23, 2257-2265

Staroscik, A.M., Smith, D.S., 2004. Seasonal patterns in bacterioplankton abundance and production in Narragansett Bay, Rhode Island, USA. Aquatic Microbial Ecology 35**,** 275-282

Stefels, J., 2000. Physiological aspects of the production and conversion of DMSP in marine algae and higher plants. Journal of Sea Research 43**,** 183-197

Stefels, J., Dijkhuizen, L., 1996. Characteristics of DMSP-lyase in Phaeocystis sp (Prymnesiophyceae). Marine Ecology-Progress Series 131**,** 307-313

Stefels, J., Van Boekel, W.H.M., 1993. Production of dms from dissolved dmsp in axenic cultures of the marine-phytoplankton species *Phaeocystis sp*. Marine Ecology-Progress Series 97**,** 11-18

Steinke, M., Kirst, G.O., 1996. Enzymatic cleavage of dimethylsulfoniopropionate (DMSP) in cell-free extracts of the marine macroalga Enteromorpha clathrata (Roth) Grev, (Ulvales, Chlorophyta). Journal of Experimental Marine Biology and Ecology 201**,** 73-85

Steinke, M., Wolfe, G.V., Kirst, G.O., 1998. Partial characterisation of dimethylsulfoniopropionate (DMSP) lyase isozymes in 6 strains of Emiliania huxleyi. Marine Ecology-Progress Series 175**,** 215-225

Stephens, B.B., Keeling, R.F., 2000. The influence of Antarctic sea ice on glacial-interglacial CO_2 variations. Nature 404**,** 171-174

Steyaert, J., 1973. Distribution of plankton diatorms along an African-Antarctic transect. Invest. Pesq. (Barc) 37**,** 295-328

Stocker, T.F., Wright, W.S., Broecker, W., 1992. Influence of high-latitude surface forcing on the global thermohaline circulation. Paleoceanography 7**,** 529-541

Stoll, M.H.C., De Baar, H.J.W., Hoppema, M., Fahrbach, E., 1999. New early winter fCO_2 data reveal continuous uptake of CO_2 by the Weddell Sea. Tellus, Series B: Chemical and Physical Meteorology 51**,** 679-687

Sullivan, C.W., Arrigo, K.R., McClain, C.R., Comiso, J.C., Firestone, J., 1993. Distributions of phytoplankton blooms in the Southern Ocean. Science 262**,** 1382-1387

Sunda, W., Kieber, D.J., Kiene, R.P., Huntsman, S., 2002. An antioxidant function for DMSP and DMS in marine algae. Nature 418**,** 317-320

Sundquist, E.T., Plummer, L.N., 1981. Carbon dioxide in the ocean surface: the homogenous buffer factor. Science 204**,** 1203-1205

Sverdrup, H.U., Johnson, M.W., Fleming, R.H., 1942. The oceans: their physics, chemistry and general biology. Prentice-Hall, Englewood Cliffs.

Sweeney, C., 2003. The annual cycle of surface CO_2 and O2 in the Ross Sea: A model for gas exchange on the continental shelves of Antarctica. Biogeochemistry of the Ross Sea pp. 295-312.

Sweeney, C. Estimating air-sea gas exchanges using bomb ^{14}C. 2004. Halifax, Nova Scotia, Canada, Surface Ocean-Lower Atmos. SOLAS Science 2004.

Takagi, K., Nomura, M., Ashiya, D., Takahashi, H., Sasa, K., Fujinuma, Y., Shibata, H., Akibayashi, Y., Koike, T., 2005. Dynamic carbon dioxide exchange through snowpack by wind-driven mass transfer in a conifer-broadleaf mixed forest in northernmost Japan. Global Biogeochemical Cycles 19**,**

Takahashi, T. Ocean basin summations of sea-air flux computed using the 10 meter height winds - http://www.ldeo.columbia.edu/res/pi/CO_2/carbondioxide/text/10m_wind.prn. 2003.

Takahashi, T., Feely, A., Weiss, R.F., Wanninkhof, R., Chipman, D.W., Sutherland, S.C., 1997. Global air-sea flux of CO_2: An estimate based on measurements of sea–air pCO_2 difference. Proceedings of the National Academy of Sciences of the United States of America 94**,** 8292-8299

Takahashi, T., Sutherland, S.C., Sweeney, C., Poisson, A., Metzl, N., Tilbrook, B., Bates, N.R., Wanninkhof, R., Feely, R.A., Sabine, C., Olafsson, J., Nojiri, Y., 2002. Global sea-air CO_2 flux based on climatological surface ocean pCO_2, and seasonal biological and temperature effects. Deep-Sea Research Part II 49**,** 1601-1622

Takahashi, T., Sweeney, C., Sutherland, S.C., Chipman, D.W., Goddard, J., Rubin, S.I. Method of underway pCO_2 measurements in surface waters and the atmosphere during the AESOPS Expeditions,
1996- 1998 in the Pacific sector of the Southern Ocean and the Ross Sea. 2000. Woods Hole Oceanographic Insitution., Woods Hole, Massachusetts, U.S. JGOFS Data Cent.

Talbot, V. Activité protéolytique et dynamique bactérienne en Océan Austral. 1995. Université Aix-Marseille II.

Taylor, F.J.R., 1976. Dinoflagellates from the international Indian Ocean expedition. Bibl. Bot. 132**,** 1-234

Thomas, D.N., Dieckmann, G.S., 2002a. Biogeochemistry of Antarctic sea ice. Oceanography and Marine Biology 40**,** 143-169

Thomas, D.N., Dieckmann, G.S., 2002b. Ocean science - Antarctic Sea ice - a habitat for extremophites. Science 295**,** 641-644

Thomas, D.N., Dieckmann, G.S., 2003. Sea ice: an introduction to its physics, chemistry, biology and geology. Blackwell Science, Oxford.

Thomas, H., Bozec, Y., Elkalay, K., De Baar, H.J.W., 2004. Enhanced open ocean storage of CO_2 from shelf sea pumping. Science 304**,** 1005-1008

Thompson, D.W.J., Wallace, J.M., 2000. Annular modes in the extratropical circulation. Part I: Month-to-month variability. Journal of Climate 13**,** 1000-1016

Timmermann, R., Beckmann, A., Hellmer, H.H., 2002. Simulations of ice-ocean dynamics in the Weddell Sea 1. Model configuration and validation. Journal of Geophysical Research 107**,**

Timmermans, K.R., Van der Wagt, B., De Baar, H.J.W., 2006. Growth rates, half-saturation constants, and silicate, nitrate, and phosphate depletion in relation to iron availability of four large, open-ocean diatoms from the Southern Ocean. Limnology and Oceanography 49**,** 2141-2151

Tison, J.-L., Haas, C., Gowing, M.M., Sleewaegen, S., Bernard, A., 2002. Tank study of physico-chemical controls on gas content and composition during growth of young sea ice. Journal of Glaciology 48**,** 177-191

Toggweiler, J.R., 1999. Variation of atmospheric CO_2 by ventilation of the ocean's deepest water. Paleoceanography 14**,** 571-588

Toggweiler, J.R., Gnanadesikan, A., Carson, S., Murnane, R., Sarmiento, J.L., 2003a. Representation of the carbon cycle in box models and GCMs: 1. Solubility pump. Global Biogeochemical Cycles 17**,**

Toggweiler, J.R., Murnane, R., Carson, S., Gnanadesikan, A., Sarmiento, J.L., 2003b. Representation of the carbon cycle in box models and GCMs - 2. Organic pump. Global Biogeochemical Cycles 17**,**

Tomczak, M., Godfrey, J.S., 1994. Regional Oceanography: An Introduction. Pergamon, New York.

Tortell, P.D., DiTullio, G.R., Sigman, D.M., Morel, F.M.M., 2002. CO_2 effects on taxonomic composition and nutrient utilization in an Equatorial Pacific phytoplankton assemblage. Marine Ecology-Progress Series 236, 37-43

Tortell, P.D., Maldonado, M.T., Price, N.M., 1996. The role of heterotrophic bacteria in iron-limited ocean ecosystems. Nature 383, 330-332

Trevena, A.J., Jones, G.B., Wright, S.W., van den Enden, R.L., 2003. Profiles of dimethylsulphoniopropionate (DMSP), algal pigments, nutrients, and salinity in the fast ice of Prydz Bay, Antarctica. Journal of Geophysical Research 108,

Trevena, A.J., Jones, G.B., 2006. Dimethylsulphide and dimethylsulphoniopropionate in Antarctic sea ice and their release during sea ice melting. Marine Chemistry 98, 210-222

Tréguer, P., Jacques, G., 1992. Dynamics of nutrients and phytoplankton, and fluxes of carbon, nitrogen and silicon in the Antarctic Ocean. Polar Biology 12, 149-162

Tréguer, P., Le Corre, P. Manuel d'analyses des sels nutritifs dans l'eau de mer. Utilisation de l'Auto-analyzer II Technicon. 2° edn. 1975. Brest, U.B.O.

Tréguer, P., Pondaven, P., 2002. Climatic changes and the carbon cycle in the Southern Ocean: a step forward. Deep-Sea Research Part II 49, 1597-1600

Trousselier, M., Courties, C., Zettlemaier, S., 1995. Flow cytometric analysis of coastal lagoon bacterioplankton and picoplankton: fixation and storage effects. Estuarine, Coastal and Shelf Science 40, 621-623

Trull, T.W., Armand, L., 2001. Insights into Southern Ocean carbon export from the [delta]13C of particles and dissolved inorganic carbon during the SOIREE iron release experiment. Deep-Sea Research Part II 48, 2655-2680

Tsunogai, S., Watanabe, S., Sato, T., 1999. Is there a "continental shelf pump" for the absorption of atmospheric CO_2? Tellus Series B 5, 701-712

Turner, S.M., Malin, G., Liss, P.S., Harbour, D.S., Holligan, P.M., 1988. The seasonal-variation of dimethyl sulfide and dimethylsulfoniopropionate concentrations in nearshore waters. Limnology and Oceanography 33, 364-375

Turner, S.M., Nightingale, P.D., Broadgate, W., Liss, P.S., 1995. The distribution of dimethyl sulphide and dimethylsulphoniopropionate in Antarctic waters and sea ice. Deep-Sea Research Part II 42, 1059-1080

Uppström.L., 1974. The boron-chlorinity ratio of deep seawater from the Pacific Ocean. Deep-Sea Research Part I 21, 161-163

Utermöhl, H., 1958. Zur Vervollkommnung der quantitativen Phytoplankton-Methodik. Mitt. Int. Ver. Theor. Angew. Limnol. 9, 1-38

Vaillancourt, R.D., Sambrotto, R.N., Green, S., Matsuda, A., 2003. Phytoplankton biomass and photosynthetic competency in the summertime Mertz Glacier Region of East Antarctica. Deep-Sea Research Part II 50, 1415-1440

van Ballegooyen, R.C., Grundlingh, M.L., Lutjeharms, J.R.E., 1994. Eddy fluxes of heat and salt from the southwest Indian Ocean into the southeast Atlantic Ocean: a case study. Journal of Geophysical Research 99, 14053-14070

Veldhuis, M.J.W., Kraay, G.W., Gieskes W.W.C., 1993. Growth and fluorescence characteristics of ultraplankton on a north-south transect in the eastern North Atlantic. Deep-Sea Research Part II 40, 609-626

Verbeke, V. Concentrations en gaz ds la glace de mer: développements techniques et implications environmentales. +pp 305. 2005. Université Libre de Bruxelles.

Vincent, W.F., 1988. Microbial Ecosystems of Antarctica. Cambridge University Press, London.

von Bodungen, B., 1986. Phytoplankton growth and krill grazing during spring in the Bransfield Strait, Antarctica - implications from sediment trap collections. Polar Biology 6**,** 153-160

von Bodungen, B., Fisher, G., Nothig, E.M., Wefer, G., 1987. Sedimentation of krill faeces during spring development of phytoplankton in Brans field Strait Antarctica. Mitteilung Geologische Palaontologische Institut Universitat Leipzig 62**,** 243-257

von Bodungen, B., Nothig, E.M., Sui, Q., 1988. New production of phytoplankton and sedimentation during summer 1985 in the southeastern Weddell Sea. Comparative Biochemistry and Physiology B-Biochemistry & Molecular Biology 90**,** 475-487

von Brockel, K., 1985. Primary production data from the southeastern Weddell Sea. Polar Biology 4**,** 75-80

Voronina, N.M., 1998. Comparative abundance and distribution of major filter-feeders in the Antarctic pelagic zone. Journal of Marine Systems 17**,** 375-390

Vosjan, J.H., Olanczuk-Neyman, K.M., 1991. Influence of temperature on respiratory ETS-Activity of micro-organisms from Admiralty Bay, King George Island, Antarctica. Netherlands Journal of Sea Research 28**,** 225

Wadhams, P., Lange, M.A., Ackley, S.F., 1987. The ice thickness distribution across the atlantic sector of the antarctic ocean in midwinter. Journal of Geophysical Research 92**,** 14535-14552

Walsh, J.J., Dieterle, D.A., Lenes, J., 2001. A numerical analysis of carbon dynamics of the Southern Ocean phytoplankton community: the roles of light and grazing in effecting both sequestration of atmospheric CO_2 and food availability to larval krill. Deep-Sea Research Part I 48**,** 1-48

Wanninkhof, R., Asher, W., Weppernig, R., Chen, H., Schlosser, P., Langdon, C., SAMBROTTO, R., 1993. Gas transfer experiment on Georges bank using 2 volatile deliberate tracers. Journal of Geophysical Research 98**,** 20237-20248

Wanninkhof, R., Feely, R.A., 1998. fCO_2 dynamics in the Atlantic, South Pacific and South Indian Ocean. Marine Chemistry 60**,** 15-31

Wanninkhof, R., Hitchcock, G., Wiseman, W.J., Vargo, G., Ortner, P.B., Asher, W., Ho, D.T., Schlosser, P., Dickson, M.L., Masserini, R., Fanning, K., Zhang, J.Z., 1997. Gas exchange, dispersion, and biological productivity on the west Florida shelf: Results from a Lagrangian tracer study. Geophysical Research Letters 24**,** 1767-1770

Wanninkhof, R., Knox, M., 1996. Chemical enhancement of CO_2 exchange in natural waters. Limnology and Oceanography 41**,** 689-697

Wanninkhof, R., Ledwell, J.R., Broecker, W.S., 1985. Gas exchange-wind speed relation measured with sulfur hexafluoride on a lake. Science 227**,** 1224-1226

Wanninkhof, R., Lewis, E., Feely, A., Millero, F.J., 1999. The optimal carbonate dissociation constants for determining surface water pCO_2 from alkalinity and total inorganic carbon. Marine Chemistry 65**,** 291-301

Wanninkhof, R., McGillis, W.R., 1999. A cubic relationship between air-sea CO_2 exchange and wind speed. Geophysical Research Letters 26**,** 1889-1892

Wanninkhof, R., Sullivan, K.F., Top, Z., 2004. Air-sea gas transfer in the Southern Ocean. Journal of Geophysical Research 109, C08S19-doi:10.1029/2003JC001767

Wanninkhof, R., Thoning, K., 1993. Measurement of fugacity of CO_2 in surface water using continuous and discrete sampling methods. Marine Chemistry 44, 189-204

Wanninkhof, R.H., 1992. Relationship between wind speed and gas exchange over the ocean. Journal of Geophysical Research 97, 7373-7382

Watson, A.J., Bakker, D.C.E., Ridgwell, A.J., Boyd, P.W., Law, C.S., 2000. Effect of iron supply on Southern Ocean CO_2 uptake and implications for glacial atmospheric CO_2. Nature 407, 730-733

Watson, A.J., Upstill-Goddard, R.C., 1991. Air-sea gas exchange in rough and stormy seas measured by a dual-tracer technique. Nature 349 , 145-147

Watterson, I.G., 2000. Southern midlatitude zonal wind vacillation and its interaction with the ocean in GCM simulations. Journal of Climate 13, 562-578

Weaver, A.J., Hillaire-Marcel, C., 2004. Global warming and the next ice age. Science 304, 400-402

Webb, E.K., Pearman, G.I., Leuning, R., 1980. Corrections of flux measurements for density effects due to heat and water vapour transfer. Quart. J. Meteorol. Soc. 106, 85-100

Weeks, S.J., Shillington, F.A., 1996. Phytoplankton pigment distribution and frontal structure in the subtropical convergence region south of Africa. Deep-Sea Research Part I 43, 739-768

Weeks, W.F., Ackley, S.F. The growth, structure and properties of sea ice. Utersteiner, N. [146], 9-164. 1986. New York, Plenum Press. NATO ASI Series B: Physics.

Wefer, G., Fisher, G., 1991. Annual primary production and export flux in the Southern Ocean from sediment trap data. Marine Chemistry 35, 597-613

Weiss, R.F., 1974. Carbon dioxide in water and seawater: the solubility of a non-ideal gas. Marine Chemistry 2, 203-215

Weiss, R.F., 1987. Winter Weddell Sea Project 1986: Trace gas studies during legs ANT V/2 and ANT V/3 of Polarsten. Antarctic journal of the United States 22, 99-100

Weiss, R.F., Ostlund, H.G., Craig, H., 1979. Geochemical studies of the Weddell sea. Deep-Sea Research Part I 26, 1093-1120

Weiss, R.F., Price, B.A., 1980. Nitrous oxide solubility in water and seawater. Marine Chemistry 8, 347-359

Weissenberger, J., Grossmann, S., 1998. Experimental formation of sea ice: importance of water circulation and wave action for incorporation of phytoplankton and bacteria. Polar Biology 20, 178-188

Wentz, F.J., Peteherych, S., Thomas, L.A., 1984. A model function for ocean radar cross sections at 14.6 GHz. Journal of Geophysical Research 3704

Wettlaufer, J.S., Worster, M.G., Huppert, H.E., 1997. Natural convection during solidification of an alloy from above with application to the evolution of sea ice. Journal of Fluid Mechanics 344, 291-316

Wheeler, P.A., Kirchman, D.L., Landry, M.R., Kokkinakis, S.A., 1989. Diel periodicity in ammonium uptake and regeneration in the oceanic subarctic Pacific: implications for interactions in microbial food webs. Limnology and Oceanography 34, 1025-1033

Wheeler, W.N., Druehl, L.D., 1986. Seasonal growth and productivity of *Macrocystis integrifolia* in British Columbia, Canada. Marine Biology 90**,** 181-186

Whitaker, T.M. Primary production of phytoplankton of Signy Island, South Orkneys, the Antarctic. 214, 169-189. 1982. Proceedings of the Royal Society of London. Series B.

Whitehouse, M.J., Symon, C., Priddle, J., 1993. Variations in the distribution of chlorophyll *a* and inorganic nutrients around South Georgia, South Atlantic. Antarctic Science 5**,** 367-376

Whitman, W.G., 2006. The two-film theory of gas absorption. Chem. Metall. Engineering 29**,** 146-148

Whittaker, R.H., Likens, G.E., 1973. Carbon in the biota. In: Woodwell, G.M., Pecan, E.V. (Eds.), Carbon and the biosphere U.S. National Technical Information Service, Springfield, Virginia, U.S.A, pp. 281-302.

Wiebe, W.J., Sheldon, W.M., Pomeroy, L.R., 1993. Evidence for an enhanced substrate requirement by marine mesophilic bacterial isolates at minimal growth temperatures. Microbial Ecology 25**,** 151-159

Wilcox, H.A., North, W.J., 1988. CO_2 Reduction and Reforestation. Science 242**,** 1493-1494

Winter, A., Elbrachter, M., Krause, G., 1999. Subtropical coccolithophores in the Weddell Sea. Deep-Sea Research Part I 46**,** 439-449

Wolfe, G.V., Steinke, M., 1996. Grazing-activated production of dimethyl sulfide (DMS) by two clones of *Emiliania huxleyi*. Limnology and Oceanography 41**,** 1151-1160

Wolfe, G.V., Steinke, M., Kirst, G.O., 1997. Grazing-activated chemical defence in a unicellular marine alga. Nature 387**,** 894-897

Wolff, E.W., Fischer, H., Fundel, F., Ruth, U., Twarloh, B., Littot, G.C., Mulvaney, R., R+Âthlisberger, R., de Angelis, M., Boutron, C.F., Hansson, M., Jonsell, U., Hutterli, M.A., Lambert, F., Kaufmann, P., Stauffer, B., Stocker, T.F., Steffensen, J.P., Bigler, M., Siggaard-Andersen, M.L., Udisti, R., Becagli, S., Castellano, E., Severi, M., Wagenbach, D., Barbante, C., Gabrielli, P., Gaspari, V., 2006. Southern Ocean sea-ice extent, productivity and iron flux over the past eight glacial cycles. Nature 440**,** 491-496

Wollast, R., 1998. Evaluation and comparison of the global carbon cycle in the coastal zone and in the open ocean. In: Brink, K.H., Robinson, A.R. (Eds.), The Global Coastal Ocean John Wiley & Sons, pp. 213-252.

Woolf, D.K., 1997. Bubbles and their role in air-sea gas exchange. In: Liss, P., Duce, R. (Eds.), The sea surface and global change Cambridge University Press, pp. 173-205.

Woolf, D. K., Leifer, I. S., Nightingale, P., Rhee, T. S., Bowyer, P., Caulliez, G., de Leeuw, G., Larsen, S., Liddicoat, M., Baker, J., and Andreae, M. O., 2006. Modelling of bubble-mediated gas transfer; fundamental principles and a laboratory test. Journal of Marine Systems, *in press.*

Xu, Y., Shaked, Y., Tang, D.G., Morel, F.M.M., 2005. Physiological effects of Zn, Cd and Co in Emiliana huxleyi. Abstracts of Papers of the American Chemical Society 229**,** U893

Yager, P.L., Wallace, D.W.R., Johnson, K.M., Smith Jr, W.O., Minnett, P.J., Deming, J.W., 1995. The Northeast Polynya as an atmospheric CO_2 sink: A seasonal rectification hypothesis. Journal of Geophysical Research 100**,** 4389-4398

Yates, K.K., Halley, R.B., 2003. Measuring coral reef community metabolism using new benthic chamber technology. Coral reefs 22**,** 247-255

Yates, K.K., Halley, R.B., 2006. Diurnal variation in rates of calcification and carbonate sediment dissolution in Florida Bay. Esuaries and Coasts 29**,** 24-39

Yoshikawa-Inoue, H., Ishii, M., 2005. Variations and trends of CO_2 in the surface seawater in the Southern Ocean south of Australia between 1969 and 2002. Tellus B 57**,** 58-69

Zappa, C.J., Raymond, P.A., Terray, E.A., McGillis, W.R., 2003. Variation in surface turbulence and the gas transfer velocity over a tidal cycle in a macro-tidal estuary. Estuaries 26**,** 1401-1415

Zeebe, R.E., Wolf-Gladrow, D., 2001. CO_2 in seawater: Equilibrium, Kinetics, Isotopes. Elsevier.

Zemmelink, H.J., Dacey, J.W.H., Hintsa, E.J., McGillis, W.R., Gieskes W.W.C., Klaassen, W., de Groot, H.W., De Baar, H.J.W., 2004a. Fluxes and gas transfer rates of the biogenic trace gas DMS derived from atmospheric gradients. Journal of Geophysical Research 109**,** doi:10.1029/2003JC001795

Zemmelink, H. J., Delille, B., Tison, J.-L., Hintsa, E. J., Houghton, L., and Dacey, J. W. H., 2006. CO_2 deposition over the multiyear ice of the western Weddell Sea. Geophysical Research Letters, *in press.*

Zemmelink, H.J., Gieskes W.W.C., Klaassen, W., Beukemma, W.J., Groot, H.K., De Baar, H.J.W., Hintsa, E.J., McGillis, W.R., Dacey, J.W.H., 2004b. Relaxed eddy accumulation measurements of the sea-to-air transfer of dimethylsulfide over the northeastern Pacific. Journal of Geophysical Research 109 **,** doi:10.1029/2002JC001616

Zemmelink, H.J., Houghton, L., Dacey, J.W.H., Worby, A.P., Liss, P.S., 2005. Emission of dimethylsulfide from Weddell Sea leads. Geophysical Research Letters 32**,**

Zimmerman, R.C., Kohrs, D.G., Steller, D.L., Alberte, R.S., 1997. Impacts of CO_2 enrichment on productivity and light requirements of Eelgrass. Plant Physiology 115**,** 599-607

Zondervan, I., Zeebe, R.E., Rost, B., Riebesell, U., 2001. Decreasing marine biogenic calcification: A negative feedback on rising atmospheric pCO_2. Global Biogeochemical Cycles 15**,** 507-516

7 List of publications

7.1.1 Part of the main manuscript

Delille.B, D. Delille, M. Fiala, C. Prevost & M. Frankignoulle, 2000. Seasonal changes of pCO_2 over a subantartic Macrocystis kelp bed. *Polar Biology* 23, 706-716. [1]

Fiala M., **B. Delille**, C. Dubreuil, E. Kopczynska, K. Leblanc, J. Morvan, B. Quéguiner, S. Blain, C. Cailliau,P. Conan, R. Corvaisier, M. Denis, M. Frankignoulle, L. Oriol, S. Roy. 2003. Mesoscale surface distribution of biogeochemical characteristics associated with a frontal system in the Crozet Basin (Southern Indian Ocean) during austral summer 1999. *Marine Ecology Progress Series* 249, 1–14 [2]

Kostianoy A.G., A.I. Ginzburg, M. Frankignoulle & **B. Delille,** 2004. Fronts in the Southern Indian Ocean as inferred from satellite sea surface temperature data *Journal of Marine Systems* 45(1-2): 55-73. doi:10.1016/j.jmarsys.2003.09.004 [3]

Rangama Y., J. Boutin,.J. Etcheto, L. Merlivat, T. Takahashi, **B. Delille**, M. Frankignoulle, & D.C.E. Bakker, 2005. Variability of net air-sea CO_2 flux inferred from in situ and satellite measurements in the Southern Ocean south of Tasmania and New Zealand, *Journal of Geophysical Research,* 110(C9), C09005, doi:10.1029/2004JC002619 [4]

Zemmelink H.J., **B. Delille**, J.L. Tison, E.J. Hintsa, L. Houghton & J.W.H. Dacey, 2006. CO_2 deposition over the multi year ice of the western Weddell Sea, *Geophysical Research Letters, in press* [5]

Delille B., A.V. Borges & D. Delille, Influence of giant kelp beds (Macrocystis pyrifera) on diel cycles of pCO_2 and DIC in Sub-Antarctic coastal area., *submitted to Estuarine, Coastal and Shelf Science* [6]

Delille B., B. Jourdain, A.V. Borges, J.-L. Tison and D. Delille. Biogas (CO_2, O_2 , dimethylsulfide) dynamics in Spring Antarctic fast ice. *submitted to Limnology and Oceanoraphy* [7]

Delille D., F. Gleizon and **B. Delille**. Spatial and temporal variations of bacteria and phytoplankton in a subAntarctic coastal area (Kerguelen Archipelago). s*ubmitted to Aquatic Microbial Ecology* [8]

Delille B., B. Tilbrook B., D. Lannuzel, V. Schoemann, S. Becquevort, A.V. Borges, D. Delille, C. Lancelot, L. Chou, G.S. Dieckmann and J.-L. Tison, Air – sea ice exchange of carbon dioxide: the end of a long-lived paradigm ? *submitted to Nature* [9]

Dehairs,F., C. Lancelot, L. André, H. Goosse, M. Frankignoulle, S. Becquevort, A. Borges, D. Cardinal, A.de Montety, **B. Delille**, M. Elskens, S.H.M. Jacquet, W. Lefebvre, B. Pasquer, N. Savoye, and V. Schoemann. Assessing the sensitivity of the Southern Ocean's Biological pump to climate change. Belgian Science Policy Reports, +pp 124, *in press.*

Dehairs F., C. Lancelot, L. André, M. Frankignoulle, E. Dellersnijder, S. Becquevort, D. Cardinal, T. Cattaldo, **B. Delille**, M. Elskens, N. Fagel, H. Gosse, E. Hannon, G. Probst, V. Schoemann, E. Kopczynska & A. Kostianoy, 2003. An integrated approach to assess carbon dynamics in the Southern Ocean. Belgian Scientific Research Programme on the Antarctic Phase 4, vol 1: Marine biota and Global change, +pp 160 (www.belspo.be/belspo/home/publ/index_en.stm)

7.1.2 Related to this work

Kostianoy A.G., A.I. Ginzburg, M. Frankignoulle & **B. Delille**, 2003. Fronts and Mesoscale Variability in the Southern Indian Ocean as Inferred from the TOPEX/POSEIDON and ERS-2 Altimetry Data. *Oceanology* 43(5):632-642 [10]

Jacquet S.H.M., F. Dehairs, D.B. Cardinal, J. Navez & **B. Delille,** 2005. Barium distribution controlled by hydrological and biogeochemical processes: results from a Southern Ocean Frontal System [Crozet-Kerguelen Basin], *Marine Chemistry* 95(3-4): 149-162 [11]

Den Ouden G., M. Vanderstraeten & 90 other authors, 2005, Belgian global change research 1990-2002: Assessment and integration report, Belgian Science Policy, +pp 209 (http://www.belspo.be/belspo/home/publ/presBGC_en.stm).

7.1.3 Adaptation of phytoplankton communities to ocean acidification

Delille B., J. Harlay, I. Zondervan, S. Jacquet, L. Chou, R. Wollast, R.G.J Bellerby, M. Frankignoulle, A.V. Borges, U. Riebesell & J-P. Gattuso, 2005. Response of primary production and calcification to changes of pCO_2 during experimental blooms of the coccolithophorid *Emiliania huxleyi*, *Global Biogeochemical Cycles,* 19, GB2023, doi:10.1029/2004GB002318 [12]

Engel A., **B. Delille**, S. Jacquet,U. Riebesell, E. Rochelle-Newall, A. Terbrüggen & I. Zondervan, 2004. Transparent exopolymer particles and dissolved organic carbon production by Emiliania huxleyi exposed to different CO2 concentrations: A mesocosm experiment. *Aquatic Microbial Ecology* 34:93-104 [13]

Rochelle-Newall E, **B. Delille**, M. Frankignoulle, J-P. Gattuso, S. Jacquet, U. Riebesell , A. Terbruggen and I. Zondervan, 2004. Chromophoric dissolved organic matter in experimental mesocosms maintained under different pCO_2 levels. *Marine Ecology Progress Series* 272:25-31 [14]

Engel A., I. Zondervan, K. Aerts, L. Beaufort, A. Benthien, L. Chou, **B. Delille**, J-P. Gattuso, J. Harlay, C. Heemann, L. Hoffmann, S. Jacquet, J. Nejstgaard, M.-D. Pizay, E. Rochelle-Newall, U. Schneider, Terbrueggen A. and Riebesell U, 2005. Testing the direct effect of CO_2 concentration on marine phytoplankton: A mesocosm experiment with the coccolithophorid *Emiliania huxleyi*. *Limnology and Oceanography* 50(2): 493-507 [15]

7.1.4 Inorganic carbon dynamics in the coastal ocean

M. Frankignoulle, G. Abril, A. Borges, I. Bourges, C. Canon, **B. Delille**, E. Libert & J.-M. Théate, 1998. Carbon dioxide emission from European estuaries *Science* 282, 434-436. [16]

Abril G., H. Etcheber, **B. Delille**, M. Frankignoulle & A.V. Borges, 2003. Calcite dissolution and atmospheric CO_2 fluxes in the eutrophised Loire. *Marine Ecology Progress Series* 259:129-138 [17]

Borges, A.V., S. Djenidi, G. Lacroix, J. Théate, **B. Delille** & M. Frankignoulle, 2003. CO_2 atmospheric flux from mangrove surrounding waters. *Geophysical Research Letters* 30(11) 1558, doi:10.1029/2003GL017143 [18]

Borges, A.V., **B. Delille**, L.-S. Schiettecatte, F. Gazeau, G. Abril & M. Frankignoulle, 2004. Gas transfer velocities of CO_2 in three European estuaries (Randers Fjord, Scheldt and Thames). *Limnology and Oceanography* 49(5):1630-1641 [19]

Borges A.V., J.-P. Vanderborght, L.-S. Schiettecatte, F. Gazeau, S. Ferrón-Smith, **B. Delille** & M. Frankignoulle, 2004. Variability of the gas transfer velocity of CO_2 in a macrotidal estuary (The Scheldt). *Estuaries* 27(4): 595-605 [20]

Gazeau F., C. M. Duarte, J.- P. Gattuso, C. Barrón, N. Navarro, S. Ruíz, Y.T. Prairie, M. Calleja, **B. Delille**, M. Frankignoulle & A.V. Borges, 2005. Whole-system metabolism and CO_2 fluxes in a Mediterranean Bay dominated by seagrass beds (Palma Bay, NW Mediterranean), *Biogeoscience*s 2: 43-60 [21]

Borges A.V., **B. Delille** & M. Frankignoulle, 2005. Budgeting sinks and sources of CO_2 in the coastal ocean: Diversity of ecosystems counts, *Geophysical Research Letters,* 32, L14601, doi:10.1029/2005GL023053 [22]

Gazeau F., A.V. Borges, C. Barrón, C.M. Duarte, N. Iversen, J.J. Middelburg, **B. Delille**., M.-D Pizay, M. Frankignoulle & J.-P. Gattuso, 2005. Net ecosystem production in an estuary estimated by different methods (The Randers Fjord, Denmark) *Marine Ecology Progress Series,* 301:23-41 [23]

Borges A.V., L.-S. Schiettecatte, G. Abril, **B. Delille** & F. Gazeau, 2006, Carbon dioxide in european coastal waters, *Estuarine, Coastal and Shelf Science, in press* [24]

7.1.5 Bioremediation of hydrocarbons

Delille.D & **B. Delille**, 2000. Field observati.ons on the variability of crude oil impact on bacterial assemblages from subAntarctic intertidal sediments. *Marine Environmental Research* 49, 403-417. [25]

Delille. D, **B. Delille** & E Pelletier. 2002. Effectiveness of bioremediation of crude oil contaminated subAntarctic intertidal sediment the microbial response. *Microbial Ecology* 44, 118-126. [26]

Delille D., E. Pelletier, **B. Delille** & F. Coulon, 2003. Effect of nutrient enrichments on the bacterial assemblage of diesel or crude oil contaminated Antarctic soils. *Polar Record* 39, 1–10. doi:10.1017/S0032247402002863 [27]

Pelletier E., D. Delille & **B. Delille,** 2004. Effectiveness of crude oil bioremediation in sub-Antarctic intertidal sediments: chemistry and toxicity of oiled residues. *Marine Environmental Research* 57(4):311-327, doi:10.1016/j.marenvres.2003.07.001 [28]

8 Annexes

8.1.1.1 Alternative carbonic acid dissociation constants

Based on the Mehrbach et al. (1973) data set, Lueker et al. (2000) reformulated apparent equilibrium constants K_1^* and K_2^* consistent with the "total hydrogen ion" pH scale.

It comes:

$$pK_1^* = \frac{3633.86}{T_{(K)}} - 61.2172 + 9.67770 \times \ln(T_{(K)}) - 0.011555 \times S + 0.0001152 \times S^2 \quad (77)$$

and

$$pK_2^* = \frac{471.78}{T_{(K)}} + 25.9290 - 3.16967 \times \ln(T_{(K)}) - 0.01781 \times S + 0.0001122 \times S^2 \quad (78)$$

where K_b^* is given in mol kg^{-1} and $T_{(K)}$ and S denote the absolute temperature (given in Kelvin) and salinity, respectively.

8.1.1.2 Effect of pressure on carbonic acid dissociation constants

The effect of pressure on the dissociation constants K_i can be corrected using the equation of Millero (1979):

$$\ln(K_i^P) = \ln(K_i^0) - \frac{a_0 + a_1(S - 34.8) + a_2 \times T_{(C)} + a_3 \times (T_{(C)})^2)}{R \times (T_{(C)} + 273.15)} \times P + 0.5 \frac{b_0 + b_1(S - 34.8) + b_2 \times T_{(K)})}{R \times (T_{(C)} + 273.15)} \times P^2 \quad (79)$$

where, K_i^P (mol kg^{-1}) is a dissociation constant at a given pressure P (bar), K_i^0 (mol kg^{-1}) is the same dissociation constant at the atmospheric pressure, a given pressure P (bar) and $T_{(C)}$ is the temperature (°C), S the salinity, R is the gas constant (83.1451 bar cm^3 mol^{-1} K^{-1}), and a_i and b_i are the coefficient given in the table

	a_0	a_1	a_2	a_3	b_0	b_1	b_2
K_1	-25.50	-0.151	0.1271	-	-0.00308	-0.000578	-0.0000877
K_2	-15.82	0.321	-0.0219	-	0.00113	-0.000314	-0.0001475
K_B	-29.48	0.295	0.1622	-0.002608	-0.00284	0.000354	-

Table 8-1 Pressure dependence coefficiens for the first and second dissociation constants of carbonic acid and for the dissociation constant of boric acid (Millero, 1979)

8.1.1.3 Dissociation constant of boric acid

According to the DOE (DOE, 1994), dissociation constants of boric acid from Dickson (Dickson, 1990b) should be used in the computations based on the total pH scale:

$$\ln(K_B^*) = \frac{-8966.9 - 280.53 \times S^{0.5} - 77.942 \times S + 1.728 \times S^{3/2} - 0.0996 \times S^2}{T_{(K)}} + 148.0248 + 137.1942 \times S^{0.5} + 1.62142S + (24.4344 - 25.085 \times S^{0.5} - 0.2474 \times S) \times \ln(T_{(K)}) + 0.053105 \times S^{0.5} \times T \quad (80)$$

where K_b^* is given in mol kg^{-1} and $T_{(K)}$ and S denote the absolute temperature (given in Kelvin) and salinity, respectively.

On the NBS scale, the dissociation constant of boric acid, K_b', from Lyman (1957) refitted by Millero (1979) should be used accordingly to:

$$\ln(K_B') = 148.0248 - \frac{8966.9}{T_{(K)}} - 24.4344\ln(T_{(K)}) + \left(0.0473 + \frac{49.1}{T_{(K)}}\right) \times \sqrt{S} \quad (81)$$

where K_b' is given in mol kg^{-1} and $T_{(K)}$ and S denote the absolute temperature (given in Kelvin) and salinity, respectively.

Total borate B_T (mmol L^{-1}) is conservative and a function of salinity (Culkin, 1965):

$$B_T = [B(OH)_3] + [B(OH)_4^-] = 1.21210^{-2} \times S \quad (82)$$

where S is the salinity.

8.1.1.4 Dissociation constant of HSO_4^-

While considering the dissociation constant K_S of the reaction:

$$HSO_4^- \leftrightarrow H^+ + SO_4^{2-} \tag{83}$$

i.e.

$$K_S = \frac{\left[H^+\right]_F \left[SO_4^{2-}\right]}{\left[HSO_4^-\right]} \tag{84}$$

Based on the equation from Dickson (1990a), DOE (1994) proposed the following equation to compute K_S (mol kg^{-1}) on the free scale:

$$\begin{aligned} pK_S = & -\frac{4276.1}{T_{(K)}} + 141.328 - 23.093 \ln\left(T_{(K)}\right) \\ & + \left(-\frac{13856}{T_{(K)}} + 324.57 - 47.986 \ln T_{(K)} \right) \times I^{0.5} \\ & + \left(\frac{35474}{T_{(K)}} - 771.54 + 114.723 \ln\left(T_{(K)}\right) \right) \times I - \left(\frac{2698}{T_{(K)}} \right) \times I^{1.5} + \left(\frac{1776}{T_{(K)}} \right) \times I^2 \\ & + \ln(1 - 0.001005 \times S) \end{aligned} \tag{85}$$

where $T_{(K)}$ is the absolute temperature (given in Kelvin), Sis the salinity and I is the ionic strength I . The ionic strength I is given by (Millero, 1982):

$$I = \frac{19.924 \times S}{1000 - 1.005 \times S} \tag{86}$$

where S is the Salinity.